THE DESIGN OF MOLECULAR TOOLS IN RELATION TO PRIONS AND THEIR BIOSAFETY

EDITED BY: Maria Lurdes Pinto, Maria Anjos Pires, Leonor Orge and Jesus R. Requena

PUBLISHED IN: Frontiers in Bioengineering and Biotechnology

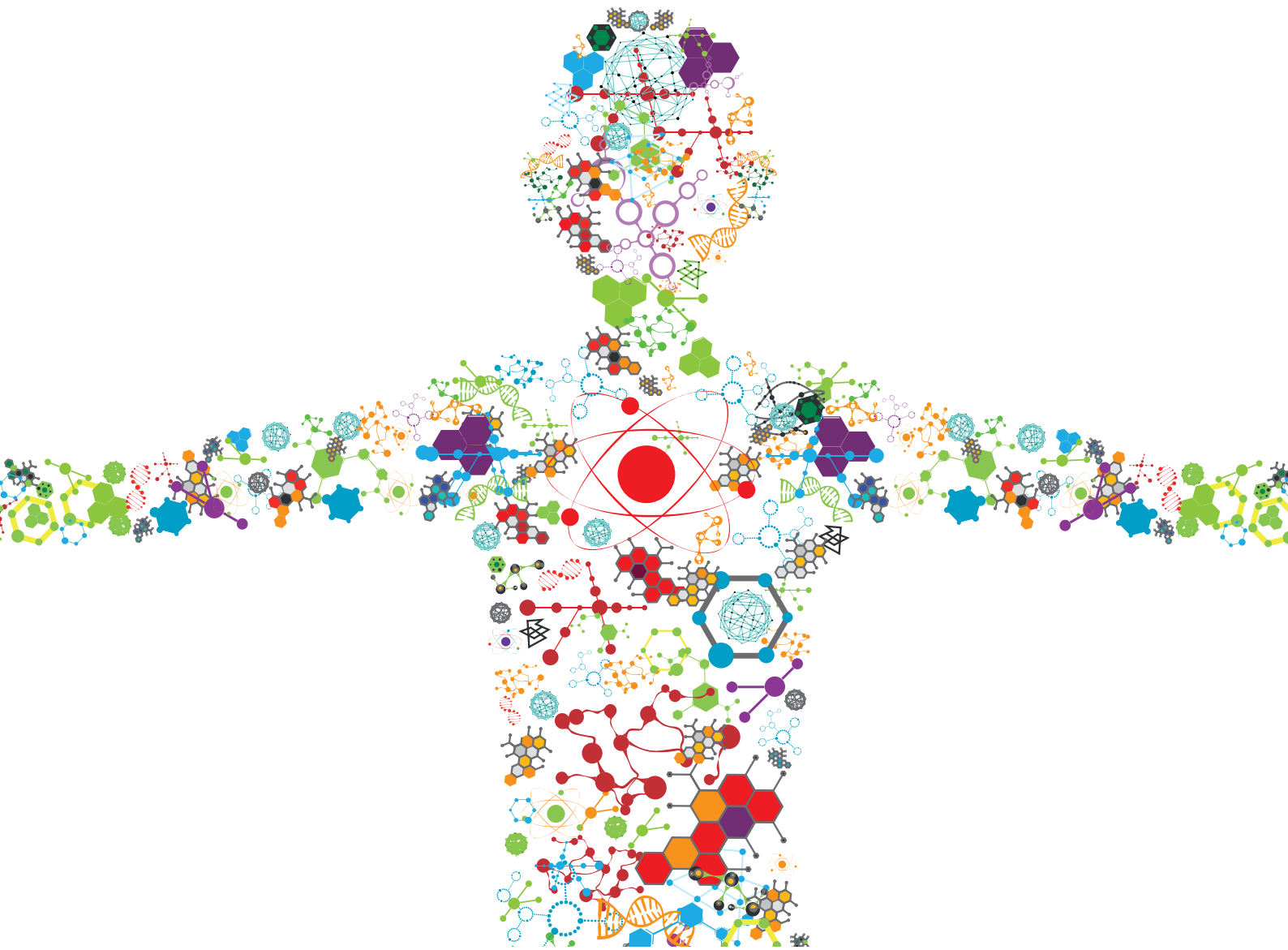

frontiers Research Topics

ISSN 1664-8714
ISBN 978-2-88966-519-8
DOI 10.3389/978-2-88966-519-8

About Frontiers

Frontiers is more than just an open-access publisher of scholarly articles: it is a pioneering approach to the world of academia, radically improving the way scholarly research is managed. The grand vision of Frontiers is a world where all people have an equal opportunity to seek, share and generate knowledge. Frontiers provides immediate and permanent online open access to all its publications, but this alone is not enough to realize our grand goals.

Frontiers Journal Series

The Frontiers Journal Series is a multi-tier and interdisciplinary set of open-access, online journals, promising a paradigm shift from the current review, selection and dissemination processes in academic publishing. All Frontiers journals are driven by researchers for researchers; therefore, they constitute a service to the scholarly community. At the same time, the Frontiers Journal Series operates on a revolutionary invention, the tiered publishing system, initially addressing specific communities of scholars, and gradually climbing up to broader public understanding, thus serving the interests of the lay society, too.

Dedication to Quality

Each Frontiers article is a landmark of the highest quality, thanks to genuinely collaborative interactions between authors and review editors, who include some of the world's best academicians. Research must be certified by peers before entering a stream of knowledge that may eventually reach the public - and shape society; therefore, Frontiers only applies the most rigorous and unbiased reviews.
Frontiers revolutionizes research publishing by freely delivering the most outstanding research, evaluated with no bias from both the academic and social point of view. By applying the most advanced information technologies, Frontiers is catapulting scholarly publishing into a new generation.

What are Frontiers Research Topics?

Frontiers Research Topics are very popular trademarks of the Frontiers Journals Series: they are collections of at least ten articles, all centered on a particular subject. With their unique mix of varied contributions from Original Research to Review Articles, Frontiers Research Topics unify the most influential researchers, the latest key findings and historical advances in a hot research area! Find out more on how to host your own Frontiers Research Topic or contribute to one as an author by contacting the Frontiers Editorial Office: frontiersin.org/about/contact

THE DESIGN OF MOLECULAR TOOLS IN RELATION TO PRIONS AND THEIR BIOSAFETY

Topic Editors:
Maria Lurdes Pinto, University of Trás-os-Montes and Alto Douro, Portugal
Maria Anjos Pires, University of Trás-os-Montes and Alto Douro, Portugal
Leonor Orge, Instituto Nacional Investigaciao Agraria e Veterinaria (INIAV), Portugal
Jesus R. Requena, University of Santiago de Compostela, Spain

Citation: Pinto, M. L., Pires, M. A., Orge, L., Requena, J. R., eds. (2021). The Design of Molecular Tools in Relation to Prions and their Biosafety. Lausanne: Frontiers Media SA. doi: 10.3389/978-2-88966-519-8

Table of Contents

frontiers in Bioengineering and Biotechnology

EDITORIAL
published: 20 January 2021
doi: 10.3389/fbioe.2020.638513

Editorial: The Design of Molecular Tools in Relation to Prions and Their Biosafety

Maria Lurdes Pinto[1]*, *Leonor Orge*[2], *Maria dos Anjos Pires*[3] and *Jesús R. Requena*[4]

[1] University of Trás-os-Montes and Alto Douro, Vila Real, Portugal, [2] Instituto Nacional de Investigação Agrária e Veterinária, Oeiras, Portugal, [3] Departamento de Ciências Veterinárias, Universidade de Trás os Montes e Alto Douro, Vila Real, Portugal, [4] CIMUS Biomedical Research Institute, University of Santiago de Compostela-IDIS, Santiago, Spain

Keywords: prions and related diseases, biosafety, biosecurity, misfolding and aggregation, central nervous system

Editorial on the Research Topic

The Design of Molecular Tools in Relation to Prions and Their Biosafety

On the 24th and 25th of October of 2019, the 8th Iberian Prion Meeting took place in the beautiful town of Castelo Branco, in central Portugal. The Iberian Prion Meetings have attracted, since their first edition, prion researchers not just from the Iberian Peninsula but from all over Europe and beyond. Much smaller than their "bigger sisters," the Annual International Prion Meetings, they never aimed at counter-programming them, much to the contrary, they have been a complement to them, focused on fostering regional collaborations and providing a valuable learning experience for novice prion researchers. In the last edition, the organizers coordinated with Frontiers in Bioengeneering and Biotechnology to publish a special issue that, originating from the communications to the meeting, would stretch beyond them to present a view of the state of the art in "the design of molecular tools in relation to prions and their biosafety."

Little we knew 1 year ago that our reflections on a zoonotic agent would have to be conducted under the shadow of another one. SARS-CoV-2 has changed everything. The Iberian Prion and International Prion meetings of 2020, that should have been held in Corunna and Goettingen, respectively, have been canceled, and it is unlikely that they will take place in 2021, either. During the last Iberian Prion Meeting we discussed the potential dangers of a new prion zoonosis in the wake of the first cases of Chronic Wasting Disease (CWD) in Scandinavia (Benestad et al., 2016; Koutsoumanis et al., 2019), keeping in mind that Castelo Branco is located near the Serra da Estrela, home of the largest population of deer in Portugal. CWD does not seem to be transmissible to humans, but what if it is passaged to sheep or cattle sharing grazing lands with the deer? Does this context sound familiar? Bat coronaviruses passaged to dromedaries, pangolins or civets…Bovine spongiform encephalopathy (BSE) prions, HIV, Ebola, coronaviruses…all the major health crises of the last decades are zoonoses. We therefore have to maintain research on all these agents, because it is not "if" but "when" new outbreaks, perhaps of more infectious and/or more deadly versions of them will strike.

In this special issue of Frontiers in Bioengeneering and Biotechnology, 11 articles from 83 authors describe and explore an array of tools to identify, diagnose, study and fight prions. Unfortunately, diagnosis of prion diseases is often done post mortem, impairing the management of disease in the individual and preventing early screening. Early detection methods are thus of pivotal importance in this research field. Two articles (Zerr et al.; Pires Barbosa et al.) focus wholly and one (Ascari et al.) partially on the Second-Generation real-time quaking-induced conversion (RT-QuIC), a technique that is revolutionizing diagnostic of prion diseases. Recent advances in its

OPEN ACCESS

Edited and reviewed by:
Alan Raybould,
University of Edinburgh,
United Kingdom

***Correspondence:**
Maria Lurdes Pinto
lpinto@utad.pt

Specialty section:
This article was submitted to Biosafety and Biosecurity, a section of the journal Frontiers in Bioengineering and Biotechnology

Received: *07 December 2020*
Accepted: *18 December 2020*
Published: *20 January 2021*

Citation:
Pinto ML, Orge L, Pires MdA and Requena JR (2021) Editorial: The Design of Molecular Tools in Relation to Prions and Their Biosafety. Front. Bioeng. Biotechnol. 8:638513. doi: 10.3389/fbioe.2020.638513

optimization and application to cerebrospinal fluid are presented and discussed. Additional ante-mortem diagnostic methods are reviewed by Ascari et al. and Konold et al. reveal the importance to reassure the current tools for TSE screening in animals, namely in asymptomatic goats. They point out to the need of reviewing current European surveillance regulations for scrapie screening, by testing other tissues than central nervous tissue, in order to keep an accurate surveillance and control of animal prion diseases. The article by Konold et al. sheds also light on the pathology of prion diseases, a subject particularly addressed by López-Pérez et al. In their article, regarding autophagy, the authors review the data from *in vivo* and *in vitro* studies that suggest a decrease of autophagic activity or a deterioration of the lysosomal degradation process in prion diseases. Whether these features are a prerequisite or consequence of prion-induced toxicity still remains unclear. del Río and Ferrer report on cutting edge technology to study neurodegenerative and metabolic diseases, in which the accumulation of misfolded proteins are a key-factor. They explain that microfluidics and lab-on-chip platforms may be valuable methods to improve understanding of the seeding and spreading processes of these "prion-like" amyloids and constitute an important alternative to unnecessary animal experimentation following the 3Rs of biological research. A *sine qua non* step on the developing of the disease is prion replication, and in an original research article, Spagnolli et al. describe the use of computational methods to address the molecular underpinnings of the heretofore enigmatic "deformed templating" conversion of different propagative PrP conformers. Also taking advantage of a biotechnological approach applied to the study of basic aspects of prion structural biology, Silva et al. describe the design of extremely sensitive, quantitative nanoLC mass-spectrometry methods to probe the structure of PrP^{Sc}. By treating PrP^{Sc} with lysine-specific chemical probes and measuring the extent of modification of each individual one, they were able to scan the correlation of each one of them with abrogation of infectivity. Only one K_{220} had a reactivity that is consistent with the loss of infectivity, which the authors discuss in the context of recent PrP^{Sc} models.

While understanding prion propagation is of an intrinsic biological interest, of course the ultimate goal of prion biology and biotechnology is to develop therapies for prion diseases. Peña-Díaz et al. describe the use of a High Throughput Screening protocol based on Thioflavin-T fluorescence, light-scattering measurements and Transmission Electron Microscopy. This pipeline was used by the authors to discover and characterize a small molecule that acts as potent inhibitors of α-Synuclein amyloid formation. This article, besides showcasing the application of bioengeneering approaches to the search of prion therapies, highlights the interconnection of prion diseases with other protein misfolding-related (prion, prion-like of prionoid…) diseases.

Regarding prion biosafety and biosecurity, Eraña et al. used a method based on cyclic amplification of a starting PrP^{Sc} pool of molecules, protein misfolding shaking amplification (PMSA) to develop a sensitive and ingenious method to evaluate prion decontamination procedures. Moudjou et al. also present new data on the application of PrP^{Sc} amplification techniques, RT-QuIC (again…) and protein misfolding cyclic amplification (PMCA) to solve the problem of procedures for decontamination of surgical instruments.

As guest editors of this special issue of Frontiers in Bioengeneering and Biotechnology, we hope that readers will enjoy this collection of articles that highlight the importance of technological advances, from computational methods to mass spectrometry to microfluidics in the quest to understand, detect and decontaminate prions. However, as investigators search at the molecular level, we must never forget the great importance of the broader relationships occurring at the interfaces of humans, animals, and the environment in the pursuit of global health.

AUTHOR CONTRIBUTIONS

All authors listed have made a substantial, direct and intellectual contribution to the work, and approved it for publication.

REFERENCES

Benestad, S. L., Mitchell, G., Simmons, M., Ytrehus, B., and Vikoren, T. (2016). First case of chronic wasting disease in Europe in a Norwegian free-ranging reindeer. *Vet. Res.* 47:88. doi: 10.1186/s13567-016-0375-4

Koutsoumanis, K., Allende, A., Alvarez-Ordóñez, A., Bolton, D., Bover-Cid, S., Chemaly, M., et al. (2019). Scientific Opinion on the update on chronic wasting disease (CWD) III. *EFSA J.* 17:5863. doi: 10.2903/j.efsa.2019.5863

Conflict of Interest: The authors declare that the research was conducted in the absence of any commercial or financial relationships that could be construed as a potential conflict of interest.

frontiers in Bioengineering and Biotechnology

ORIGINAL RESEARCH
published: 12 March 2020
doi: 10.3389/fbioe.2020.00164

The Scrapie Prevalence in a Goat Herd Is Underestimated by Using a Rapid Diagnostic Test

Timm Konold[1], John Spiropoulos[1], Jemma Thorne[1], Laura Phelan[1], Louise Fothergill[2], Brenda Rajanayagam[3], Tobias Floyd[1], Beatriz Vidana[1], Judith Charnley[4], Nadya Coates[5] and Marion Simmons[1]*

[1] Pathology Department, Animal and Plant Health Agency Weybridge, Addlestone, United Kingdom, [2] Central Sequencing Unit, Animal and Plant Health Agency Weybridge, Addlestone, United Kingdom, [3] Department of Epidemiological Sciences, Animal and Plant Health Agency Weybridge, Addlestone, United Kingdom, [4] Animal and Plant Health England Field Delivery, Skipton, United Kingdom, [5] TSE/BVDV Testing Laboratory, Eurofins Forensic Services, Risley, United Kingdom

OPEN ACCESS

Edited by:
Maria Leonor Dos Santos Diniz Orge, National Institute of Agricultural and Veterinary Research (INIAV), Portugal

Reviewed by:
Maria Lurdes Pinto, University of Trás-os-Montes and Alto Douro, Portugal
Rita Payan-Carreira, University of Trás-os-Montes and Alto Douro, Portugal

***Correspondence:**
Timm Konold
Timm.Konold@apha.gov.uk

Specialty section:
This article was submitted to Biosafety and Biosecurity, a section of the journal Frontiers in Bioengineering and Biotechnology

Received: *17 December 2019*
Accepted: *18 February 2020*
Published: *12 March 2020*

Citation:
Konold T, Spiropoulos J, Thorne J, Phelan L, Fothergill L, Rajanayagam B, Floyd T, Vidana B, Charnley J, Coates N and Simmons M (2020) The Scrapie Prevalence in a Goat Herd Is Underestimated by Using a Rapid Diagnostic Test. Front. Bioeng. Biotechnol. 8:164. doi: 10.3389/fbioe.2020.00164

Current European surveillance regulations for scrapie, a naturally occurring transmissible spongiform encephalopathy (TSE) or prion disease in sheep and goats, require testing of fallen stock or healthy slaughter animals, and outline measures in the case of confirmation of disease. An outbreak of classical scrapie in a herd with 2500 goats led to the culling of the whole herd, providing the opportunity to examine a subset of goats, take samples, and examine them for the presence of disease-associated prion protein (PrP^{Sc}) to provide further information on scrapie test sensitivity, pathology, and association with prion protein genotype. Goats were examined clinically prior to cull, and the brains examined post mortem by Bio-Rad ELISA, a rapid screening test used for active surveillance in sheep and goats, and two confirmatory tests, Western blot and immunohistochemistry. Furthermore, up to 10 lymphoid tissues were examined by immunohistochemistry. Of 151 goats examined, three (2.0%) tested positive for scrapie by ELISA on brain, confirmed by confirmatory tests, and a further five (3.3%) were negative by ELISA but positive by at least one of the confirmatory tests. Only two of these, both positive by ELISA, displayed evident signs of scrapie. In addition, 10 (6.6%) goats, which also included two clinical suspects, were negative on brain examination but had detectable PrP^{Sc} in lymphoid tissue. PrP^{Sc} was detected most frequently in the medial retropharyngeal lymph node (LN; 94.4% of all 18 cases) and palatine tonsil (88.9%). Abnormal behavior and circling or loss of balance when blindfolded were the best clinical discriminators for scrapie status. None of the goats that carried a single allele in the prion protein gene associated with increased resistance to scrapie (Q_{211}, K_{222}, S_{146}) were scrapie-positive, and the percentage of goats with these alleles was greater than expected from previous surveys. Significantly more goats that were scrapie-positive were isoleucine homozygous at codon 142 (I_{142}). The results indicate that the sensitivity of the applied screening test is poor in goats compared to the confirmatory tests as gold standard, particularly for asymptomatic animals. Sensitivity of surveillance could be improved by testing retropharyngeal LN or palatine tonsil in addition to brain.

Keywords: transmissible spongiform encephalopathy, prion, classical scrapie, goat, clinical diagnosis, immunohistochemistry, ELISA

INTRODUCTION

Scrapie is a naturally occurring transmissible spongiform encephalopathy (TSE) in sheep and goats, which causes neurological signs and ultimately leads to death. The disease is caused by misfolding of the prion protein, which makes the physiological, cellular form (PrP^{C}) resistant to enzymatic digestion with proteinases (Prusiner, 1995). In the absence of a reliable and quick test in a live animal, disease suspicion is currently based on clinical examination, which needs to be confirmed in the dead animal by examination of the brain. The majority of diagnostic tests are based on the detection of the misfolded scrapie prion protein (PrP^{Sc}) (Gavier-Widén et al., 2005). Two scrapie types exist, atypical and classical scrapie, which are epidemiologically distinct and produce different disease phenotypes. Contrary to classical scrapie, atypical scrapie usually affects single and older animals, the agent is less resistant to proteolytic digestion with proteinase K, PrP^{Sc} is not detectable in lymphoid tissue by immunohistochemical examination (IHC) and relatively absent in the brainstem. Different biochemical profiles are also identified on Western blot examination of brain (Benestad et al., 2008). Scrapie is a World Organization for Animal Health (OIE) listed disease, although management of the animal health risks associated with the scrapie agent in the OIE's Terrestrial Animal Health Code (OIE, 2018) only applies to classical scrapie, due to the known contagious nature of this disease type. In Europe, rules for the prevention, control, and eradication of classical scrapie are laid down in European Parliament and Council Regulation (EC) No 999/2001. In addition to the examination of reported clinical suspects, this requires active surveillance for TSEs by testing brain tissue from healthy slaughter animals or animals that died or were killed on farm (fallen stock), where surveillance stream and minimum number of tested animals is dependent on the animal population in each member state. In the United Kingdom, a minimum of 500 fallen goats over 18 months of age need to be tested. Regulation (EC) No 999/2001 currently lists four rapid TSE tests that can be used for brain examination. In case of a positive result, the sample requires examination by confirmatory tests, such as Western immunoblot (WB) or immunohistochemistry (European Parliament Council of the European Union, 2001).

If classical scrapie is confirmed in a holding, there are different options for disease eradication: complete herd cull, cull of susceptible animals only (in sheep), or no cull provided that animals, at the end of their productive lives, are slaughtered in the country of origin and those over 18 months of age are tested for scrapie.

Susceptibility to scrapie is influenced by polymorphisms in the prion protein gene (*PRNP*), principally at codons 136, 154, and 171, and selection for resistant genotypes has led to a great reduction in classical scrapie cases in sheep within the European Union (EFSA, 2014). Recent research has shown that there are also polymorphisms associated with lower risk toward classical scrapie in the caprine *PRNP*: at codon 142 [methionine (M) instead of isoleucine (I)], at codon 146 [serine (S) or aspartate (D) instead of asparagine (N)], at codon 154 [histidine (H) instead of arginine (R)], at codon 211 [glutamine (Q) instead of R] and 222 [lysine (K) instead of Q] (Barillet et al., 2009). Based on current scientific evidence, the K_{222}, D_{146}, and S_{146} alleles have been shown to confer genetic resistance to classical scrapie strains known to occur in the EU goat population [EFSA Panel on Biological Hazards (BIOHAZ) et al., 2017] although genotype-based scrapie eradication is currently not an approved option for goats in the EU regulation.

There are only a few reports on classical scrapie outbreaks in large goat herds, where goats were subject to clinical examinations (González et al., 2009) and postmortem examinations, which included assessment of PrP^{Sc} distribution in lymphoid tissue (González et al., 2009, 2010; Corbière et al., 2013a,b; Ortiz-Pelaez et al., 2015). These demonstrated that up to 50% of goats might be infected, even though the brain examination was negative. It has also been shown that brain examination by immunohistochemistry may be superior to testing by rapid tests in goats with classical scrapie (González et al., 2009; Ortiz-Pelaez et al., 2015).

Following an outbreak of classical scrapie in a goat farm in Great Britain in 2012, the decision was made to cull the whole herd (more than 2000 goats) which required the testing of a minimum subset of 150 goats over 18 months of age, according to Regulation (EC) No 999/2001. The study reported here describes the outcome of further investigations of this subset.

MATERIALS AND METHODS

Herd and Case History

The affected farm was a dairy goat herd with 2500 goats. It was established in 2007 by purchasing 600 female goats from one farm and five male goats from another farm. More goats were subsequently purchased from eight different farms to increase herd size, and female and male goats from other farms were added to the herd annually. According to the owner, all goats were purchased from herds that had been monitored for scrapie. The main breeds were Saanen, Toggenburg, and Alpine. Pregnant does gave birth indoors. Adult does were routinely vaccinated against clostridial disease (Heptavac Plus, MSD Animal Health, Milton Keynes, United Kingdom) and enzootic abortion (Cevac Chlamydia, Ceva Animal Health, Amersham, United Kingdom). The farm had a history of sheep occupancy, although there was no known history of scrapie in these sheep. Classical scrapie was first detected in a fallen stock goat in March 2012, which resulted in TSE monitoring of all slaughtered or dead animals over 18 months of age. The scrapie prevalence based on postmortem test examination of the brain from clinical suspects and fallen stock over a 4-year period (2012–2015) was 2.8% in 2012, 3.6% in 2013, 2.7% in 2014, and 2.4% in 2015 (mean 2.9%; 95% confidence interval: 2.06, 3.69).

In 2014, the farmer took part in the survey of the national goat population to determine the proportion of goats with a scrapie resistant K_{222} allele of the *PRNP* (Goldmann et al., 2016) but none of the 16 billies and 14 does used for breeding carried this allele.

The farmer reported the first clinical suspect in March 2015, which was confirmed positive. Eleven further cases were reported as clinical suspects up to January 2016, of which

five tested positive for scrapie based on examination of the brain. One goat that tested negative in brain had lymphoid tissue tested retrospectively, and presented with PrP^{Sc} by immunohistochemistry in medial retropharyngeal lymph node (LN), mesenteric LN, spleen, distal ileum, and recto-anal mucosa-associated lymphoid tissue (RAMALT).

In February 2016, after it was decided to cull the herd, 151 female goats were transported to APHA Weybridge for clinical examination and more extensive investigation by postmortem tests. Goats were to some degree selected randomly from 920 lactating and 25 non-lactating goats (the farmer was asked to pick the goats randomly), but the group included any goats with possible clinical signs of scrapie, and all the goats selected were at least 24 months old (minimum age of previous confirmed scrapie cases) and born on the farm, even though at least five of 56 previously confirmed scrapie cases were born on a different farm.

Herd cull was carried out under Regulation (EC) No. 999/2001 and the relevant national Transmissible Spongiform Encephalopathies (England) Regulations to eradicate scrapie and no licensed procedures were undertaken in animals that would have required ethical approval. However, the same standard for animal care and housing that is generally applied to animals used for scientific procedures under the Animal (Scientific Procedures) Act 1986 was applied.

Clinical Assessment

Although goats were assessed at least twice daily by animal technicians during normal husbandry procedures, specific clinical examinations for signs of scrapie were only done once prior to cull and provided the clinical data for analysis. Goats were group-housed and examined in their pen for between 1 and 51 days after arrival (median 22 days) and up to 50 days (median 5 days) prior to cull. Cull had to be scheduled over 63 days due to availability of staff and postmortem room, and goats with clinical disease (not necessarily scrapie) or those that were heavily lactating were culled first. All goats were female with a median age of 36 months (range: 24–72 months) based on the farmer's records. There were 102 (68%) lactating goats, which were milked daily and dried off depending on cull date and milk volume generated. A short examination protocol was used to assess body condition, posture and movement, behavior, pruritus, and vision (Konold and Phelan, 2014), which differed from the one used previously (Konold et al., 2010) in that it also included blindfolding to assess vestibular system function. Animal handling was limited to the assessment of the menace response, scratch test, body condition, and response to blindfolding, and the animal was visually inspected in the pen to assess behavior, locomotion, tremor, hair or skin changes, and response to a hand clap. Based on the observed signs, an animal was regarded as "showing no evidence of scrapie", "inconclusive with regards to scrapie", or "clinical suspect" prior to cull. To be inconclusive, the animal had to display one of the signs: repeatable response to scratching (positive scratch test), tremor, abnormal behavior, circling, collapsing episodes, ataxia/dysmetria, or a uni- or bilateral absent menace response, whereas a suspect had to clearly and consistently display more than one of these signs (Konold and Phelan, 2014).

The clinical diagnosis was compared with the postmortem diagnosis (see below) to establish diagnostic sensitivity (percentage of animals with scrapie that have disease suspicion based on clinical signs) and specificity (percentage of animals without scrapie that do not have suspicious signs of scrapie).

Postmortem Examination

Goats were euthanized by intravenous barbiturate overdose (10 ml Somulose, Dechra, Shrewsbury, United Kingdom) and exsanguination. The following tissues were collected: brain, lateral and medial retropharyngeal LN, submandibular LN, palatine tonsil, pre-scapular LN, pre-femoral LN, mesenteric LN, spleen, distal ileum, and rectal tissue containing RAMALT. The brain was cut sagittally, the right side fixed with 10% formol saline and the left side frozen. Lymphoid tissue was fixed in 10% buffered formalin. The right side of the obex was submitted to an approved TSE testing site (Eurofins Forensic Services, Risley, United Kingdom) for rapid testing (TeSeE ELISA, Bio-Rad Laboratories, Watford, United Kingdom) to detect the proteinase-resistant prion protein PrP^{res}. Tissue processing for IHC with monoclonal antibody R145 (APHA Weybridge, New Haw, United Kingdom) was as described previously for brain (Dustan et al., 2008). R145 is a rat monoclonal antibody, which recognizes the epitope 231-RESQA-235 of the bovine prion protein and was applied to sections for 60 min at a dilution of 1:150. Brain sections for IHC included the medulla oblongata at the level of the obex (all cases), rostral medulla at the level of the cerebellar peduncles, cerebellum, thalamus, and cerebrum at the level of frontal cortex (all cases with no detectable PrP^{Sc} in the obex). All obex samples that were tested by rapid test were also tested by discriminatory WB using the methodology described previously (Simmons et al., 2016), with the exception of two goats where caudal medulla was tested instead due to lack of remaining obex. The WB is based on the Bio-Rad TeSeE Universal Western Blot using the manufacturer's instructions. Two replicate gels were run with 18.75 mg tissue equivalent per well. Primary antibodies were Sha31 (Bio-Rad Laboratories, directed against the 148-YEDRYYRE-155 epitope), which was prepared according to the manufacturer's kit instructions, and the N-terminal antibody P4 (R-Biopharm Rhône Ltd., Glasgow, United Kingdom, directed against the 93-WGQGGSH-99 epitope), which was used in a dilution 1:5000 of a stock solution of 1 mg/ml. Incubation times for the Sha31 and P4 antibodies were 30 and 60 min, respectively. Additional investigations were requested for clinical suspects with neurological signs in which scrapie was not confirmed, which included staining of brain sections with hematoxylin-eosin (Dustan et al., 2008) and gram-staining in cases with inflammatory changes (Stevens and Bancroft, 1982).

A 1 g piece of frontal cortex was submitted fresh from each goat to determine the full open reading frame of the caprine *PRNP* using the same equipment, reagents, primers, and protocol as published previously (Konold et al., 2010). For the purpose of this study, polymorphisms are reported for codons 142, 146, 154, 211, 222, and 240.

Statistical Calculations

All calculations were carried out using Statistica (version 13.5, TIBCO, Dublin, Ireland).

To find retrospectively the best clinical markers for disease suspicion using confirmatory tests on brain as gold standard (see below), classification and regression tree analysis was used (Breiman et al., 1984). Categorical dependent variables were the TSE status based on brain examination (positive, negative), and factor codes were the clinical variables tremor (yes, no), mental status (normal, abnormal), behavior resting/approached/handled (normal, abnormal), menace response (normal, impaired, exaggerated), scratch test (negative, positive, inconclusive), body condition (good, poor), ataxia (no, yes), circling or loss of balance when blindfolded (yes, no), skin lesions (yes, no), skin lesion frequency (none, one, more than one), hair loss (yes, no), hair loss frequency (none, one, more than one), short hair (yes, no), and short hair frequency (none, one, more than one). Equivocal signs (e.g., inconsistent menace response, temporary circling when blindfolded or possibly ataxia) were still classified as abnormal.

To compare the age of goats between groups (scrapie-negative, scrapie-positive in lymphoid tissue only, scrapie-positive in brain), age distribution was assessed for normality in box and whisker plots and an appropriate test used (ANOVA or the non-parametric Kruskall–Wallis if data were not normally distributed).

To assess whether false negative results in the screening ELISA test were associated with higher optical density (OD) values than true negative results, OD values for each sample were divided by the cut-off specified for each test run to calculate an OD cut-off ratio (multiplied by 100). The ratios were grouped by *PRNP* genotype at codon 142 based on recent findings that *PRNP* polymorphisms may affect test sensitivity in goats (Simmons et al., 2020), and the data compared by non-parametric Mann–Whitney *U*-test. This test was also used to compare the ages of goats with a false negative and true negative ELISA result, grouped by genotype at codon 142.

To determine whether scrapie status was associated with particular genotypes, the proportion of scrapie-positive and negative animals carrying each polymorphism was compared by Fisher's exact test; $P < 0.05$ was indicative of an association of genotype with scrapie status.

RESULTS

All data can be found as a supplementary file (**Supplementary Table S1**). Animal data, test results, and clinical status of these scrapie cases are displayed in **Table 1**.

Following the clinical examination, 12 goats (8%) were classified as clinical suspects, 32 (21%) were inconclusive with regard to scrapie, and 107 (71%) showed no evidence of scrapie.

The pathological examination identified 18 goats (11.9%) with PrP^{Sc} indicative of infection with the scrapie agent.

Three goats (2.0%) tested positive on brain examination by the rapid test, confirmed by IHC and WB. Five goats (3.3%) were rapid test-negative but positive on the confirmatory tests.

In addition, there were 10 goats (6.6%), which had PrP^{Sc} in lymphoid tissue, but brain examination was negative. The WB profile (see **Figure 1** for examples) or presence of PrP^{Sc} in

TABLE 1 | Scrapie case data.

Goat ID	Breed	Age [m]	*PRNP* Genotype	ELISA (obex)	IHC obex	WB (obex or caudal medulla)	IHC (lymphoid tissue)	Clinical status
2113	TO	60	II_{142} PP_{240}	**P**	**P**	**P**	**P**	**Suspect**[I]
2135	SA	36	II_{142} PP_{240}	**P**	**P**	**P**	**P**	**Suspect**
2073	TO	60	II_{142} SP_{240}	**P**	**P**	**P****	**P**	Inconclusive
2146	SA	24	II_{142} PP_{240}	N	**P***	N**	**P**	Inconclusive
2165	AL	24	II_{142} SP_{240}	N	**P***	Inconclusive	**P**	No evidence
2176	TO	24	II_{142} SS_{240}	N	**P**	**P**	**P**	No evidence
2078	AL	72	II_{142} PP_{240}	N	**P**	**P**	**P**	No evidence
2117	SA	24	IM_{142} PP_{240}	N	N	**P**	**P**	No evidence
2191	TO	60	II_{142} SP_{240}	N	N	N	**P**	**Suspect**
2169	SA	60	IM_{142} PP_{240}	N	N	N	**P**	**Suspect**[II]
2179	AL	24	II_{142} SP_{240}	N	N	N	**P**	Inconclusive
2112	SA	60	II_{142} PP_{240}	N	N	N	**P**	Inconclusive
2166	TO	24	IM_{142} SP_{240}	N	N	N	**P**	No evidence
2201	TO	60	IM_{142} PP_{240}	N	N	N	**P**	No evidence
2126	SA	60	II_{142} PP_{240}	N	N	N	**P**	No evidence
2182	SA	24	II_{142} PP_{240}	N	N	N	**P**	No evidence
2143	TO	60	II_{142} SP_{240}	N	N	N	**P**	No evidence
2155	TO	24	II_{142} SP_{240}	N	N	N	**P**	No evidence

*AL = Alpine, SA = Saanen, TO = Toggenburg. All goats were GG_{127}, RR_{211}, and QQ_{222}. *Minimal immunolabeling; **caudal medulla was tested; P = positive, N = negative; one WB result was classified as inconclusive because of an extremely weak band at approximately 27 kDa (the PrP^{res} region), [I]video clip "classical scrapie in goats" of this animal available to view at https://www.youtube.com/watch?v=Kkhak9yJ3H0 (Konold and Vallino Costassa, 2018); [II]see **Supplementary Video File S1**.*

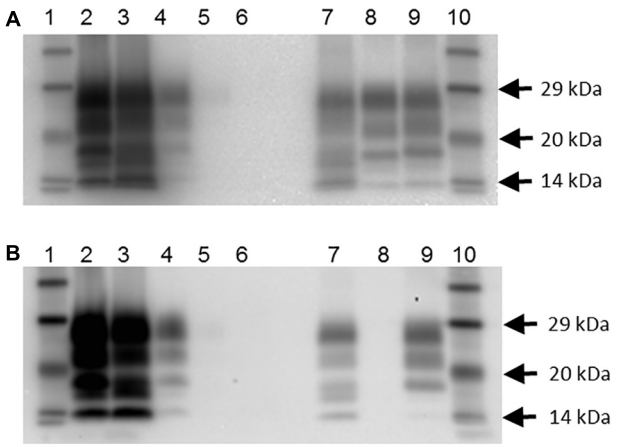

FIGURE 1 | Western blot profile of digested brain samples from selected goats using two monoclonal antibodies. **(A)** Sha31 antibody. **(B)** P4 antibody. Lanes 1 and 10: molecular mass marker; lane 2: goat 2135 (clinical suspect, positive on brain by IHC and ELISA); lane 3: goat 2113, clinical suspect, positive on brain by IHC and ELISA); lane 4: goat 2078 (no clinical signs of scrapie, positive on brain by IHC, negative by ELISA); lane 5: goat 2117 (no clinical signs of scrapie, negative on brain by IHC and ELISA, positive on lymphoid tissue by IHC; scrapie profile difficult to discern with the picture contrast used); lane 6: goat 2102 (clinical suspect, negative on brain by ELISA and on all tissues by IHC); lane 7: caprine classical scrapie control (RSCRAP 17/00006, $I I_{142} QQ_{222}$); lane 8: bovine classical BSE control (RBSE 98/00291); lane 9: ovine classical scrapie control (PG1903/97).

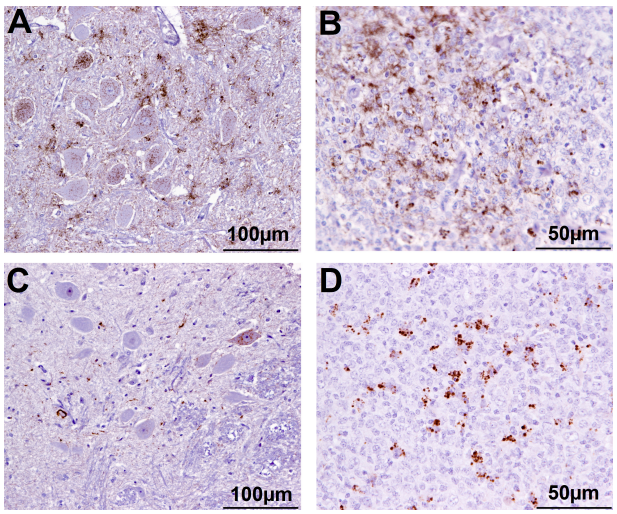

FIGURE 2 | Immunohistochemical examination of brain and lymphoid tissue from selected goats. Obex **(A)** and medial retropharyngeal LN **(B)** from clinical suspect goat 2135, positive on brain by ELISA and WB; obex **(C)** from goat 2146 with inconclusive signs with regard to scrapie, negative on brain by ELISA and WB and pre-scapular LN **(D)** from clinical suspect goat 2169, negative by all tests on brain, PrP^{Sc} detected in pre-scapular LN only. Note the comparatively sparser PrP^{Sc} accumulation in the obex in **C** (immunolabeling visible in only one neuron) compared to **A**. Immmunolabeling is restricted to tingible body macrophages in the pre-scapular LN in **D** whereas macrophages and follicular dendritic cells are both immunolabeled in **B**.

lymphoid tissue (see **Figure 2** for examples) was suggestive of classical scrapie in all cases.

Two goats (2153—scrapie-negative and 2179—scrapie-positive in lymphoid tissue only) had encephalitic lesions in the brain suggestive of listeriosis, and gram-staining identified gram-positive rods in 2153. Goat 2153, which presented with multifocal severe suppurative encephalitis, developed neurological signs 7 days after being examined for scrapie, which included inability to stand unaided, head tilt and turn to the right and vertical nystagmus suggestive of a vestibular disease, and was euthanized. It had been clinical unremarkable with no evidence of scrapie at the time of the examination for scrapie. Goat 2179, which presented with moderate focal necrotizing, granulomatous encephalitis, was euthanized 5 days after the examination and considered inconclusive with regard to scrapie because of the display of a head tremor and temporary anti-clockwise circling when blindfolded. It presented with PrP^{Sc} in lymphoid tissue. By contrast, a goat (2102) that displayed a head tremor and ataxia with hind limb weakness, which was considered a scrapie suspect, had neither scrapie confirmed nor any other noticeable lesions in the brain.

All cases that were positive by examination of the brain also had PrP^{Sc} in lymphoid tissue. A total of 144 goats (95%) had the whole range of lymphoid tissue suitable for examination. The tissue that presented with PrP^{Sc} most frequently was the medial retropharyngeal LN, the least frequent the spleen (see **Table 2**). PrP^{Sc} was detected in all 10 lymphoid tissues in the three cases with a positive brain ELISA result and in one case with a negative ELISA but positive confirmatory brain test result. It was more variable in the other scrapie cases and one goat (2169) had detectable PrP^{Sc} only in the pre-scapular LN.

TABLE 2 | PrP^{Sc} accumulation in ten peripheral issues in the 18 scrapie-positive goats.

Tissue (N examined)	PrP^{Sc} positive (% of scrapie-affected goats)
Medial retropharyngeal LN (151)	17 (94.4%)
Palatine tonsil (151)	16 (88.9%)
Submandibular LN (149)	13 (72.2%)
Mesenteric LN (151)	13 (72.2%)
Pre-scapular LN (151)	13 (72.2%)
Distal ileum (151)	12 (66.7%)
Pre-femoral LN (151)	11 (61.1%)
Lateral retropharyngeal LN (148)	9 (50.0%)
RAMALT (149)	9 (50.0%)
Spleen (151)	7 (38.9%)

The mean age of animals positive for scrapie in brain (N = 8, mean 41 months, range 24–72 months), positive in lymphoid tissue only (N = 10, mean 46 months, range 24–60 months), and scrapie-negative animals (N = 133, mean 39 months, range 24–72 months) was not significantly different (P = 0.67, Kruskall–Wallis test on not normally distributed ages).

Sensitivity and specificity of the clinical examination were 25 and 93%, respectively, using brain examination as the gold standard and only clinical suspects as scrapie-affected. Inclusion

of clinically inconclusive cases as also scrapie-affected would double sensitivity but reduce specificity to 72% with the brain examination as gold standard.

The results from the classification and regression tree analysis are displayed in **Figure 3**.

Using the clinical discriminators "behavior resting/approached/handled" and "circling or loss of balance when blindfolded" 143 goats were correctly identified as brain-negative (100% specificity), two were correctly identified as brain-positive and six were falsely identified as brain-negative (25% sensitivity).

A list of the clinical signs displayed by scrapie-positive and negative goats is shown in **Table 3**.

A significantly higher proportion of lymphoid tissue only-positive goats displayed tremor, and a significantly higher proportion of brain-positive goats displayed abnormal behavior, compared to the scrapie-negative group (two-tailed Fisher's exact test, $P = 0.046$ after applying Bonferroni's correction for multiple comparisons).

Table 4 lists the number and percentage of scrapie-positive and negative goats with polymorphisms associated with resistance to classical scrapie. A significantly higher proportion of homozygous I_{142} goats compared to heterozygous or homozygous M_{142} goats were affected by scrapie [two-tailed Fisher's exact test, $P = 0.008$ (II_{142} versus IM_{142}) and 0.017 (II_{142} versus MM_{142}) after applying Bonferroni's correction for multiple comparisons]. None of the goats carried an H_{154} allele.

When the OD value ratios were compared between four rapid test-negative but confirmatory test positive and 39 rapid and confirmatory test negative II_{142} goats, there was no significant difference in the OD ratios: median 8.4% (range: 8.1–12.6%) and median 9.4% (range: 3.0–18.7%), respectively; $P = 0.95$. The single IM_{142} goat with a false negative ELISA result had a ratio of 9.1%, which was close to the median of 64 goats with a true negative result (median: 9.4%, range: 5.5–29.9%). All these goats were RR_{211}, QQ_{222} and PP_{240}, SP_{240} or SS_{240}.The median age of the four II_{142} ELISA-false negative goats was 24 months (range 24–72 months), which was not significantly different to the 39 true negative goats (median 36, range: 24–72 months) with the same genotype ($P = 0.41$). Similarly, the single ELISA-false-negative IM_{142} goat was 24 months of age, which was close to the median of the 64 true-negative IM_{142} goats (median 36, range 24–72 months).

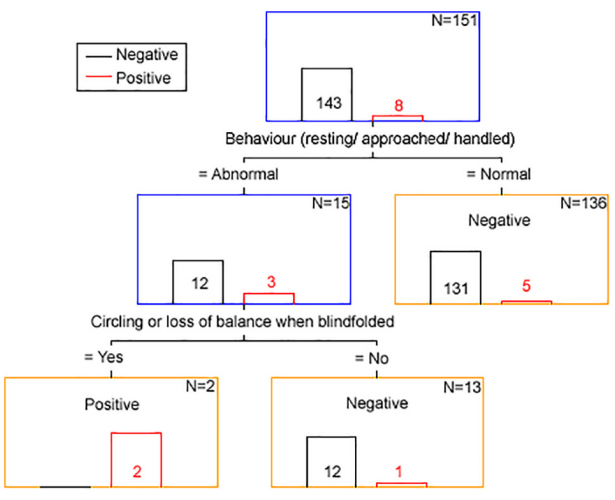

FIGURE 3 | Clinical discriminator for scrapie status based on classification and regression tree analysis. The number in or above each bar is the number of animals with a positive (red font and bar) and negative (black font and bar) scrapie status based on examination of brain tissue by all confirmatory tests. *N* is the number of animals remaining in each node (blue box = intermediary node, yellow box = final node). The term "Negative" of "Positive" in each node corresponds to the clinical scrapie status.

DISCUSSION

Continued monitoring by postmortem tests and whole herd cull are currently the only options in case of a classical scrapie outbreak in goats, although they are unlikely to succeed in the eradication of classical scrapie in a country (EFSA, 2014). Both options are costly (compensation for culled goats *versus* costs for continuing monitoring for scrapie of fallen stock and healthy slaughter goats over 18 months) and both have considerable emotional impact on the farmer (herd cull versus continuous restrictions and animal welfare implications due to scrapie). In our case, whole herd cull was selected, which provided an opportunity for more information about classical scrapie in goats, complimentary to previous studies of a different goat herd in Great Britain (González et al., 2009; Konold et al., 2010), to compare the test sensitivity of clinical examinations and screening TSE postmortem tests with confirmatory tests and assess distribution of PrP^{Sc} in various tissues.

Based on the scrapie prevalence in this farm in the previous 4 years, which was below 4% and had declined over the previous 3 years, it was unexpected to find 5.3% of goats to be scrapie-affected based on brain examination alone. The selection of goats for transport was not completely random, and bias may have occurred because clinical suspects were included. Thus, the percentage of confirmed scrapie cases within the 151 goats may not reflect the true prevalence in the whole herd. However, this bias effect was likely to be small because of the high proportion of clinical suspects previously in this herd that were not confirmed pathologically.

Most striking was the finding that the ELISA, a postmortem screening test approved for TSE testing by the European Union, considerably underestimated the number of scrapie cases, with only three cases (2%) being positive whereas a further five cases were diagnosed by the confirmatory tests, IHC or WB, when testing the same brain region (obex). The 2% detection rate is in agreement with the estimated herd prevalence in previous years, which was also based on the ELISA as an initial screening test, but underestimates the real scrapie prevalence in this herd. Previous studies have demonstrated that caprine scrapie cases may be missed by reliance on the screening test alone (González et al., 2009; Ortiz-Pelaez et al., 2015) but misdiagnosis of more than 50% of cases in our study was unexpected, and it contradicts results from another study where ELISA and IHC performed

TABLE 3 | Individual signs in 151 goats assessed by the short protocol.

	Scrapie-positive (brain) *N* = 8	Scrapie-positive (LRS only) *N* = 10	Scrapie-negative *N* = 133
Abnormal behavior	3 (37.5%)	2 (20.0%)	10 (7.5%)
Circling when blindfolded	2 (25.0%)	3 (30.0%)	3 (2.3%)
Menace response			
Impaired	2 (25.0%)	0	26 (19.5%)
Exaggerated	1 (12.5%)	3 (30.0%)	16 (12.0%)
Tremor	1 (12.5%)	4 (40.0%)	14 (10.5%)
Abnormal mental status	1 (12.5%)	0	2 (1.5%)
Disequilibrium when blindfolded	1 (12.5%)	0	0
Ataxia or dysmetria	1 (12.5%)	1 (10.0%)	2 (1.5%)
Poor body condition (BCS $\leq$ 2)	0	3 (30.0%)	8 (6.0%)
Scratch test			
Positive or inconsistent	0	0	8 (6.0%)
Inconclusive	0	0	1 (0.8%)
Hair loss			
Poll	4 (50.0%)	5 (50.0%)	68 (51.1%)
Nose	1 (12.5%)	0	10 (7.5%)
Neck	0	1 (10.0%)	2 (1.5%)
Side abdomen/chest	0	1 (10.0%)	1 (0.8%)
Rump	0	1 (10.0%)	1 (0.8%)
Tail base	0	1 (10.0%)	0
Eyelid	0	0	7 (5.3%)
Shoulder	0	0	2 (1.5%)
Back	0	0	1 (0.8%)
Hair short			
Shoulder	1 (12.5%)	0	4 (3.0%)
Neck	0	2 (20.0%)	11 (8.3%)
Rump	0	1 (10.0%)	9 (6.8%)
Poll	0	1 (10.0%)	5 (3.8%)
Side abdomen/chest	0	1 (10.0%)	1 (0.8%)
Tail base	0	0	16 (12.0%)
Eyelid	0	0	1 (0.8%)
Back	0	0	1 (0.8%)

similarly in the detection of scrapie in French goats (Corbière et al., 2013a). A recent study in goats demonstrated that rapid screening tests performed well in clinically affected animals but were less sensitive in the pre-clinical phase, which was dependent on *PRNP* polymorphisms. In particular, the presence of the M_{142} allele appeared to compromise to some extent the sensitivity of the Bio-Rad screening tests (Simmons et al., 2020). In the present study, however, four were II_{142} and only one was M_{142} heterozygous. There was no evidence that the ELISA-false negative cases had a higher OD value than the true negative cases, and it also did not seem to be influenced by breed and age. It confirmed disease in clinical suspects when PrP^{Sc} accumulation in the brain appears to be moderate to high as judged by IHC (Konold et al., 2010; Niedermeyer et al., 2016) but its reliability appears to be poor in asymptomatic cases, even goats that do not carry an M_{142} allele. Asymptomatic animals are likely to represent the majority of goats targeted by this screening test as part of the active scrapie surveillance. Of the two confirmatory tests used, WB and IHC, both performed equally well, with only one sample each classified as positive by one but not the other test. The WB-negative but IHC-positive sample was caudal medulla because obex was not available for WB testing in this animal, and testing

TABLE 4 | Number and frequency of goats with selected allele variants.

	Number of goats with allele variants (proportion)	
Polymorphism at codon	**Scrapie-positive (18)**	**Scrapie-negative (133)**
II_{142}	14 (78%)	44 (33%)
IM_{142}	4 (22%)	67 (50%)
MM_{142}	0	22 (17%)
IM_{142} PP_{240}	2 (4%)	53 (96%)
IM_{142} SP_{240}	1 (6%)	15 (94%)
NN_{146}	18 (100%)	131 (98%)
NS_{146}	0	2 (2%)
RR_{211}	18 (100%)	128 (96%)
RQ_{211}	0	5 (4%)
QQ_{222}	18 (100%)	130 (98%)
QK_{222}	0	3 (2%)

of tissue caudal to the target area may explain a negative test result in the Western blot.

A further 10 goats presented with PrP^{Sc} in lymphoid tissue only, indicating infection with the scrapie agent and suggestive of an earlier stage of disease. This was expected from previous studies in goats where lymphoid tissue in addition to brain was tested (González et al., 2009; Corbière et al., 2013b; Ortiz-Pelaez et al., 2015; Niedermeyer et al., 2016; Georgiadou et al., 2017). Also in agreement with previous studies where at least five different lymphoid tissues were tested (González et al., 2009; Niedermeyer et al., 2016), the medial retropharyngeal LN was the tissue that most consistently presented with PrP^{Sc} by IHC, followed by palatine tonsil but there was no consistent hierarchy at an individual animal level. RAMALT was positive in 50% of the cases, which is similar to the 42% reported in an earlier study (González et al., 2009), but considerably lower compared to sheep with more than 85% (González et al., 2006), and, if used as *ante mortem* test, sensitivity may even be lower because of the considerably smaller amount of tissue that can be collected in a live animal.

One animal (2169) had detectable PrP^{Sc} only in the pre-scapular (superficial cervical) LN, which has previously been reported for a different scrapie-affected farm in the United Kingdom (González et al., 2010). As observed in this previous study for cases with limited lymphoid tissue involvement, immunolabeling was restricted to tingible body macrophages in this LN. It may indicate an earlier stage of infection as demonstrated for sheep with classical scrapie (van Keulen et al., 2002). Why only this LN was affected is not known; the same phenomenon was not observed in two other scrapie-affected goats with the same *PRNP* genotype. This may represent a different pathogenesis, for example, iatrogenic infection by subcutaneous injection with a contaminated needle in the neck region, of which afferent lymph vessels drain in this LN (Tanudimadja, 1973). It may also be caused by a different scrapie strain or some genetic or animal factors that led to limited PrP^{Sc} accumulation in peripheral LNs. This LN is generally not tested in scrapie studies so it is not known how often it occurs in scrapie outbreaks. Additional, deeper section examined from this LN by IHC were negative, which suggested that PrP^{Sc} accumulation was limited, possibly because of a very early stage of infection, and could easily be missed. Surprisingly, this goat was a clinical scrapie suspect displaying tremor, hair loss, mild ataxia, poor body condition, and clockwise circling when blindfolded. Histologically, there was diffuse mild vacuolation of the white matter tracts in thalamus, cerebrum, and cerebellum, occasionally accompanied by astrocytes with mild swollen vesicular astrocytes, which was interpreted as artifactual change although could have also been the result of a toxic or metabolic insult to the brain, but neither liver not kidney was available for further investigation.

None of the goats in the affected herd presented with PrP^{Sc} in brain only, without detectable PrP^{Sc} in lymphoid tissue, whereas in a previously reported outbreak of scrapie in British goats this was the case in four of 72 scrapie cases (6%), of which all were homo- or heterozygous M_{142} (González et al., 2009). This may be explained by the lower number of scrapie cases having these *PRNP* polymorphisms in the present study (three versus 32 in the other outbreak) or the scrapie strains were different.

A significantly greater proportion of goats with scrapie was homozygous for I_{142}. There is some evidence that the scrapie risk is reduced in goats homozygous for M_{142} but also in goats heterozygous for M_{142} and homozygous for P_{240} (Barillet et al., 2009; Corbière et al., 2013b). However, in the current study, there were actually two goats with the IM_{142} PP_{240} combination that had scrapie compared to one goat with the IM_{142} SP_{142} combination. Indeed, a review of the literature concluded that the M_{142} allele is only associated with incomplete resistance to classical scrapie [EFSA BIOHAZ Panel (EFSA Panel on Biological Hazards (BIOHAZ) et al., 2017)]. None of the goats that carried a single allele associated with increased resistance (Q_{211}, K_{222}, S_{146}) were scrapie-positive, which was expected from previous studies [EFSA Panel on Biological Hazards (BIOHAZ) et al., 2017] but the number of goats with these polymorphisms in the selected herd subpopulation was unexpected. The billies used on this farm did not carry a K_{222} allele, and to our knowledge artificial insemination was not used, which suggests that this allele must have been present in the female population and would have only been detected by genotyping more goats if a scrapie eradication program by genotype selection was considered. Given that the most recent national survey in the United Kingdom detected a QK_{222} genotype frequency of only 0.6% in Saanen, Toggenburg, and their crossbreds (Goldmann et al., 2016), which were the breeds present on the farm, finding 2% out of 151 goats with this polymorphism was unexpected. Similarly, the frequency of the NS_{146} genotype was mostly limited to Boer goats and in dairy goats was estimated to be 0.2% or less (Goldmann et al., 2011, 2016), whereas 2% (two Toggenburg goats) had this polymorphism in the study reported here.

Sensitivity of the clinical examination was expectedly poor although better than in a previous study where sensitivity was 3.9% (only clinical suspects considered scrapie-affected) and 11.7% (including clinically inconclusive goats) using brain examination as gold standard (Konold et al., 2010). This may be due to the inclusion of blindfolding in the short examination protocol, which as the classification tree suggested, was an important clinical discriminator. However, by including response to blindfolding, specificity, which was 99.6% (clinical suspects only) and 88.5% (with clinically inconclusive included) in the previous study, decreased slightly. Classification tree analysis indicated that only two clinical signs, abnormal behavior (nervousness or dullness) and abnormal responses to blindfolding (loss of balance or circling), were important for a suspect clinical diagnosis of scrapie with similar sensitivity although more examinations of goats with and without scrapie are necessary to confirm this. In general, circling is a sign more often observed in sheep with atypical scrapie (Onnasch et al., 2004; Konold et al., 2006; Simmons et al., 2010) than sheep or goats with classical scrapie (Laven, 1990; Ulvund, 2006; Konold et al., 2010) but blindfolding, which may elicit circling, is rarely used as part of the examination protocol.

None of the goats that tested positive for scrapie on brain showed signs of pruritus. Hair loss suggestive of pruritus was found in scrapie-positive and negative goats and the scratch

test was only positive in scrapie-negative goats, which implied that scrapie goats displayed the non-pruritic form of the disease (Konold et al., 2010). It is possible that some of the scrapie-negative goats suffered from other conditions leading to hair loss and pruritus, such as mite or lice infestation (Jackson, 1986), which we did not investigate. Hair loss may also have non-infectious causes, such as friction due to poorly designed feeding stations. Indeed, a study in the United Kingdom has identified skin lesions, including hair loss, and pruritus as one of the major welfare issues in commercial dairy goat farms (Anzuino et al., 2010). It was surprising that neurological signs such as ataxia, tremor, and loss of balance or circling were not observed significantly more frequently in goats with PrP^{Sc} in brain. This may be due to other conditions that may have been present in the brain-negative population. For example, tremor in large animals as single sign may have no obvious cause and can even be a sign in frightened animals (Mayhew, 2009). It is also possible that some scrapie-affected goats were in an earlier stage of clinical disease when clear neurological signs may be more subtle, or absent, as demonstrated in a study where scrapie goats were monitored over time (Konold et al., 2010).

Listeriosis was diagnosed in two goats. In one goat neurological signs developed after the clinical examination and the clinical findings of nystagmus and head tilt were consistent with a vestibular system dysfunction as seen in listeriosis (Braun et al., 2002), which is unlike scrapie. Ideally, all clinical examinations should have been carried out within a few days prior to cull as clinical signs may develop after the clinical examination. This was not always possible for logistical reasons, but 87% of examinations were carried out within 14 days prior to cull. The other goat with listeriosis was clinically inconclusive because of the display of a head tremor and inconsistent circling when blindfolded. It implied that a neurological disease was present and a more thorough neurological examination might have detected other abnormalities associated with listeriosis, such as facial asymmetry and reduced sensory perception (Braun et al., 2002), or more signs developed over the 5 days between examination and cull.

CONCLUSION

The results of this study continue to highlight the limitations of the Bio-Rad ELISA as brain screening test to diagnose classical scrapie in goats, and other or additional tests should be considered. It is recommended to include testing of the medial retropharyngeal LN or palatine tonsil, which are also located at the head that is generally submitted for testing and are less prone to rapid autolysis, to increase the sensitivity of goat scrapie surveillance.

DATA AVAILABILITY STATEMENT

This manuscript contains previously unpublished data. The name of the repository and accession number(s) are not available.

ETHICS STATEMENT

Ethical review and approval was not required for the animal study because herd cull was carried out under Regulation (EC) No. 999/2001 and the relevant national Transmissible Spongiform Encephalopathies (England) Regulations to eradicate scrapie and no licensed procedures were undertaken in animals that would have required ethical approval. However, the same standard for animal care and housing that is generally applied to animals used for scientific procedures under the Animal (Scientific Procedures) Act 1986 was applied. Written informed consent for participation was not obtained from the owners because all animals were culled to eradicate disease and the owner compensated as per national TSE legislation. A subset of these animals were transported live to APHA Weybridge for culling and formed the basis for this study.

AUTHOR CONTRIBUTIONS

TK examined the goats and analyzed the data, supported by LP, and drafted the manuscript. JS, TF, BV, and MS carried out the histopathologic and immunohistochemical examinations. MS also managed the project. JT was responsible for Western immunoblotting, LF for genotyping, and NC for interpretation of the rapid test result. BR and JC provided historical data. All authors read, contributed to, and approved the final manuscript.

FUNDING

This study was funded by the Department for Environment, Food and Rural Affairs (Projects SE1960 and SE1961).

ACKNOWLEDGMENTS

We are grateful to husbandry staff at the Animal Sciences Unit who transported and cared for the animals and to staff at the Pathology Department who carried out the necropsies and contributed to the examination of tissues. We thank the TSE lead scientist for the support and help to carry out this study. This study would not have been possible without the farmer's consent.

SUPPLEMENTARY MATERIAL

The Supplementary Material for this article can be found online at: https://www.frontiersin.org/articles/10.3389/fbioe.2020.00164/full#supplementary-material

TABLE S1 | List of animal data with clinical signs and postmortem test results for each individual goat.

VIDEO FILE S1 | Goat with PrP^{Sc} in pre-scapular lymph node only. This goat displays a whole body tremor, has extensive hair loss with skin lesions, suspected hind limb ataxia, and circles anti-clockwise when blindfolded.

REFERENCES

Anzuino, K., Bell, N. J., Bazeley, K. J., and Nicol, C. J. (2010). Assessment of welfare on 24 commercial UK dairy goat farms based on direct observations. *Vet. Rec.* 167, 774–780. doi: 10.1136/vr.c5892

Barillet, F., Mariat, D., Amigues, Y., Faugeras, R., Caillat, H., Moazami-Goudarzi, K., et al. (2009). Identification of seven haplotypes of the caprine PrP gene at codons 127, 142, 154, 211, 222 and 240 in french alpine and saanen breeds and their association with classical scrapie. *J. Gen. Virol.* 90, 769–776. doi: 10.1099/vir.0.006114-0

Benestad, S. L., Arsac, J. N., Goldmann, W., and Nöremark, M. (2008). Atypical/Nor98 scrapie: properties of the agent, genetics, and epidemiology. *Vet. Res.* 39:19. doi: 10.1051/vetres:2007056

Braun, U., Stehle, C., and Ehrensperger, F. (2002). Clinical findings and treatment of listeriosis in 67 sheep and goats. *Vet. Rec.* 150, 38–42. doi: 10.1136/vr.150.2.38

Breiman, L., Friedman, J., Stone, C., and Olshen, R. A. (1984). *Classification and Regression Trees*. New York, NY: Chapman & Hall.

Corbière, F., Chauvineau-Perrin, C., Lacroux, C., Lugan, S., Costes, P., Thomas, M., et al. (2013a). The limits of test-based scrapie eradication programs in goats. *PLoS One* 8:e54911. doi: 10.1371/journal.pone.0054911

Corbière, F., Perrin-Chauvineau, C., Lacroux, C., Costes, P., Thomas, M., Brémaud, I., et al. (2013b). PrP-associated resistance to scrapie in five highly infected goat herds. *J. Gen. Virol.* 94, 241–245. doi: 10.1099/vir.0.047225-0

Dustan, B. H., Spencer, Y. I., Casalone, C., Brownlie, J., and Simmons, M. M. (2008). A histopathologic and immunohistochemical review of archived UK caprine scrapie cases. *Vet. Pathol.* 45, 443–454. doi: 10.1354/vp.45-4-443

EFSA (2014). Scientific opinion on the scrapie situation in the EU after 10 years of monitoring and control in sheep and goats. *EFSA J.* 12:3781. doi: 10.2903/j.efsa.2014.3781

EFSA Panel on Biological Hazards (BIOHAZ), Ricci, A., Allende, A., Bolton, D., Chemaly, M., and Obert Davies, R. (2017). Scientific opinion on genetic resistance to transmissible spongiform encephalopathies (TSE) in goats. *EFSA J.* 15:4962. doi: 10.2903/j.efsa.2017.4962

European Parliament Council of the European Union (2001). *Regulation (EC) No 999/2001 of the European Parliament and of the Council of 22 May 2001 Laying Down Rules for the Prevention, Control And Eradication of Certain Transmissible Spongiform Encephalopathies*. Brussels: European Union.

Gavier-Widén, D., Stack, M. J., Baron, T., Balachandran, A., and Simmons, M. (2005). Diagnosis of transmissible spongiform encephalopathies in animals: a review. *J. Vet. Diagn. Invest.* 17, 509–527. doi: 10.1177/104063870501700601

Georgiadou, S., Ortiz-Pelaez, A., Simmons, M. M., Windl, O., Dawson, M., Neocleous, P., et al. (2017). Goats with aspartic acid or serine at codon 146 of the PRNP gene remain scrapie-negative after lifetime exposure in affected herds in Cyprus. *Epidemiol. Infect.* 145, 326–328. doi: 10.1017/s0950268816002272

Goldmann, W., Marier, E., Stewart, P., Konold, T., Street, S., Langeveld, J., et al. (2016). Prion protein genotype survey confirms low frequency of scrapie-resistant K222 allele in British goat herds. *Vet. Rec.* 178:168. doi: 10.1136/vr.103521

Goldmann, W., Ryan, K., Stewart, P., Parnham, D., Xicohtencatl, R., Fernandez, N., et al. (2011). Caprine prion gene polymorphisms are associated with decreased incidence of classical scrapie in goat herds in the United Kingdom. *Vet. Res.* 42:110. doi: 10.1186/1297-9716-42-110

González, L., Dagleish, M. P., Bellworthy, S. J., Sisó, S., Stack, M. J., Chaplin, M. J., et al. (2006). Postmortem diagnosis of preclinical and clinical scrapie in sheep by the detection of disease-associated PrP in their rectal mucosa. *Vet. Rec.* 158, 325–331. doi: 10.1136/vr.158.10.325

González, L., Martin, S., Hawkins, S. A., Goldmann, W., Jeffrey, M., and Sisó, S. (2010). Pathogenesis of natural goat scrapie: modulation by host PRNP genotype and effect of co-existent conditions. *Vet. Res.* 41:48. doi: 10.1051/vetres/2010020

González, L., Martin, S., Sisó, S., Konold, T., Ortiz-Peláez, A., Phelan, L., et al. (2009). High prevalence of scrapie in a dairy goat herd: tissue distribution of disease-associated PrP and effect of PRNP genotype and age. *Vet. Res.* 40:65. doi: 10.1051/vetres/2009048

Jackson, P. (1986). Skin diseases in goats. *Practice* 8, 5–10. doi: 10.1136/inpract.8.1.5

Konold, T., Bone, G. E., Phelan, L. J., Simmons, M. M., González, L., Sisó, S., et al. (2010). Monitoring of clinical signs in goats with transmissible spongiform encephalopathies. *BMC Vet. Res.* 6:13. doi: 10.1186/1746-6148-6-13

Konold, T., Davis, A., Bone, G. E., Simmons, M. M., Kahn, J., Blake-Dyke, M. C., et al. (2006). Atypical scrapie cases in the UK. *Vet. Rec.* 158:280. doi: 10.1136/vr.158.8.280

Konold, T., and Phelan, L. (2014). Clinical examination protocol to detect atypical and classical scrapie in sheep. *J. Vis. Exp.* 19:e51101. doi: 10.3791/51101

Konold, T., and Vallino Costassa, E. (2018). "Scrapie," in *Infectious Diseases of Livestock*, eds J. A. W. Coetzer, G. R. Thomson, N. J. Maclachlan, and M. L. Penrith, (South Africa: Anipedia).

Laven, R. (1990). Scrapie in a four year old goat. *Goat Vet. Soc. J.* 11, 77–79.

Mayhew, I. G. (2009). *Large Animal Neurology*. Chichester: Wiley-Blackwell.

Niedermeyer, S., Eiden, M., Toumazos, P., Papasavva-Stylianou, P., Ioannou, I., Sklaviadis, T., et al. (2016). Genetic, histochemical and biochemical studies on goat TSE cases from Cyprus. *Vet. Res.* 47:99. doi: 10.1186/s13567-016-0379-0

OIE (2018). "Chapter 14.8. Scrapie," in *Terrestrial Animal Health Standards Commission*, eds E. Bonbon, G. Maria Funes, M. Okita, L. I. Carbajo Goñi, S. Hammami, and B. Todeschini (Paris: World Organisation for Animal Health), 1–6.

Onnasch, H., Gunn, H. M., Bradshaw, B. J., Benestad, S. L., and Bassett, H. F. (2004). Two Irish cases of scrapie resembling Nor98. *Vet. Rec.* 155, 636–637. doi: 10.1136/vr.155.20.636

Ortiz-Pelaez, A., Georgiadou, S., Simmons, M. M., Windl, O., Dawson, M., Arnold, M. E., et al. (2015). Allelic variants at codon 146 in the PRNP gene show significant differences in the risk for natural scrapie in Cypriot goats. *Epidemiol. Infect.* 143, 1304–1310. doi: 10.1017/s0950268814002064

Prusiner, S. B. (1995). The prion diseases. *Sci. Am.* 272, 48–57.

Simmons, M., Thorne, L., Ortiz-Pelaez, A., Spiropoulos, J., Georgiadou, S., Papasavva-Stylianou, P., et al. (2020). Transmissible spongiform encephalopathy in goats: is PrP rapid test sensitivity affected by genotype? *J. Vet. Diagn. Invest.* 32, 87–93. doi: 10.1177/1040638719896327

Simmons, M. M., Chaplin, M. J., Konold, T., Casalone, C., Beck, K. E., Thorne, L., et al. (2016). L-BSE experimentally transmitted to sheep presents as a unique disease phenotype. *Vet. Res.* 47:112. doi: 10.1186/s13567-016-0394-1

Simmons, M. M., Konold, T., Thurston, L., Bellworthy, S. J., Chaplin, M. J., and Moore, S. J. (2010). The natural atypical scrapie phenotype is preserved on experimental transmission and sub-passage in PRNP homologous sheep. *BMC Vet. Res.* 6:14. doi: 10.1186/1746-6148-6-14

Stevens, A., and Bancroft, J. D. (1982). *Theory and Practice of Histological Techniques*. Edinburgh: Churchill Livingstone.

Tanudimadja, K. (1973). *Morphology of the lymph drainage of the head, neck, thoracic limb and Thorax Of The Goat (Capra Hircus)*. Ames: Iowa State University.

Ulvund, M. J. (2006). "Clinical findings in scrapie," in *Prions in Humans and Animals*, eds B. Hörnlimann, D. Riesner, and H. Kretzschmar, (Berlin: de Gruyter), 398–407.

van Keulen, L. J., Vromans, M. E., and van Zijderveld, F. G. (2002). Early and late pathogenesis of natural scrapie infection in sheep. *APMIS* 110, 23–32. doi: 10.1034/j.1600-0463.2002.100104.x

Conflict of Interest: NC is employed by the company Eurofins.

The remaining authors declare that the research was conducted in the absence of any commercial or financial relationships that could be construed as a potential conflict of interest.

frontiers in Bioengineering and Biotechnology

CASE REPORT
published: 06 August 2020
doi: 10.3389/fbioe.2020.00929

Second-Generation RT-QuIC Assay for the Diagnosis of Creutzfeldt-Jakob Disease Patients in Brazil

Breno José Alencar Pires Barbosa[1], Bruno Batitucci Castrillo[1], Ricardo Pires Alvim[1], Marcelo Houat de Brito[1], Helio R. Gomes[1], Sônia M. D. Brucki[1], Jerusa Smid[1], Ricardo Nitrini[1], Michele C. Landemberger[2], Vilma R. Martins[2], Jerson L. Silva[3] and Tuane C. R. G. Vieira[3]**

[1] Department of Neurology, Hospital das Clínicas, University of São Paulo Medical School, São Paulo, Brazil, [2] Tumor Biology and Biomarkers Group, International Research Center, A.C. Camargo Cancer Center, São Paulo, Brazil, [3] National Center of Nuclear Magnetic Resonance Jiri Jonas, Institute of Medical Biochemistry Leopoldo de Meis, National Institute of Science and Technology for Structural Biology and Bioimaging, Federal University of Rio de Janeiro-UFRJ, Rio de Janeiro, Brazil

OPEN ACCESS

Edited by:
Maria Dos Anjos Pires, University of Trás-os-Montes and Alto Douro, Portugal

Reviewed by:
Assia Angelova, German Cancer Research Center (DKFZ), Germany
Sumit Ghosh, The Research Institute at Nationwide Children's Hospital, United States

***Correspondence:**
Breno José Alencar Pires Barbosa
brenojb@gmail.com
Tuane C. R. G. Vieira
tuane@bioqmed.ufrj.br

Specialty section:
This article was submitted to Biosafety and Biosecurity, a section of the journal Frontiers in Bioengineering and Biotechnology

Received: 22 May 2020
Accepted: 20 July 2020
Published: 06 August 2020

Citation:
Barbosa BJAP, Castrillo BB, Alvim RP, de Brito MH, Gomes HR, Brucki SMD, Smid J, Nitrini R, Landemberger MC, Martins VR, Silva JL and Vieira TCRG (2020) Second-Generation RT-QuIC Assay for the Diagnosis of Creutzfeldt-Jakob Disease Patients in Brazil. Front. Bioeng. Biotechnol. 8:929. doi: 10.3389/fbioe.2020.00929

The recent development of IQ-CSF, the second generation of real-time quaking-induced conversion (RT-QuIC) using cerebrospinal fluid (CSF), for the diagnosis of Creutzfeldt-Jakob Disease (CJD) represents a major diagnostic advance in the field. Highly accurate results have been reported with encouraging reproducibility among different centers. However, availability is still insufficient, and only a few research centers have access to the method in developing countries. In Brazil, we have had 603 suspected cases of CJD since 2005, when surveillance started. Of these, 404 were undiagnosed. This lack of diagnosis is due, among other factors, to the lack of a reference center for the diagnosis of these diseases in Brazil, resulting in some of these samples being sent abroad for analysis. The aim of this research study is to report the pilot use of IQ-CSF in a small cohort of Brazilian patients with possible or probable CJD, implementing a reference center in the country. We stored CSF samples from patients with possible, probable or genetic CJD (one case) during the time frame of December 2016 through June 2018. All CSF samples were processed according to standardized protocols without access to the clinical data. Eight patients presented to our team with rapidly progressive dementia and typical neurological signs of CJD. We used CSF samples from seven patients with other neurological conditions as negative controls. Five out of seven suspected cases had positive tests; two cases showed inconclusive results. Among controls, there was one false-positive (a CSF sample from a 5-year-old child with leukemia under treatment). The occurrence of a false positive in one of the negative control samples raises the possibility of the presence of interfering components in the CSF sample from patients with non-neurodegenerative pathologies. Our pilot results illustrate the feasibility of having CJD CSF samples tested in Brazilian centers and highlight the importance of interinstitutional collaboration to pursue a higher diagnostic accuracy in CJD in Brazil and Latin America.

Keywords: Creutzfeldt-Jakob disease, prion, rapidly progressive dementia, real-time quaking-induced conversion, biomarkers

INTRODUCTION

Prion diseases, also known as transmissible spongiform encephalopathies (TSEs), encompass a group of rare neurodegenerative conditions secondary to abnormal conversion of a constitutively expressed cellular glycoprotein, the prion protein (PrP^{C}), into an abnormally folded isoform (PrP^{sc}) (Geschwind, 2016; Zanusso et al., 2016). Sporadic Creutzfeldt-Jakob disease (sCJD) is the most common prion disease in humans and usually presents as rapidly progressive dementia in combination with variable degrees of multisystem neurological impairment (Zerr and Hermann, 2018). Since its clinical and molecular manifestations are heterogeneous and non-specific, early diagnosis of prion diseases remains challenging in clinical practice (Geschwind and Murray, 2018).

Brain histopathological evaluation and/or detection of PrP^{Sc} are still the standard criteria for establishing a definitive diagnosis for CJD (CDC, 2018). However, invasiveness when performing this type of analysis *antemortem* brings very little benefit to the patient, since these diseases are still incurable. Clinical signs and paraclinical tests are the most commonly used approaches during the course of the disease and can be used to classify it as a possible or probable prion disease (Brown et al., 2003; CDC, 2018).

Among the paraclinical tests, brain diffusion weighted-MRI (DW-MRI) and cerebrospinal fluid (CSF) analysis have increased diagnostic accuracy (Eisenmenger et al., 2016; Staffaroni et al., 2019; Bizzi et al., 2020). The presence of 14-3-3 protein, Tau protein, neuron-specific enolase (NSE), the astroglial protein S100B and PrP^{Sc} itself are used as biomarkers in CFS for TSE diagnosis (Schmitz et al., 2016; Connor et al., 2019). Overall, the only protein that is a specific biomarker for TSE is PrP^{Sc}. PrP^{Sc} can be detected in CSF based on its self-propagating ability: converting and seeding the aggregation of the non-pathogenic PrP^{C} into PrP^{Sc}.

The real-time quaking-induced conversion (RT-QuIC) assay was developed in 2010, and since then, its experimental conditions have been improved and tested on a large number of samples in several laboratories worldwide (Wilham et al., 2010; Green, 2019). It ultrasensitively detects limited amounts of PrP^{Sc} in CSF and other tissue samples (Wilham et al., 2010). The recent development of the second-generation (IQ-CSF) RT-QuIC assay using CSF for the diagnosis of CJD represents a major diagnostic advance in the field (Wilham et al., 2010; Orrú et al., 2014). In humans, RT-QuIC analysis showed a sensitivity of 97.2% and specificity of 100%, with encouraging reproducibility among different centers (Franceschini et al., 2017).

RT-QuIC started to be clinically used in 2015 and became a criterion of the Centers for Disease Control and Prevention (CDC) to diagnose CJD as probable (CDC, 2018). Its high sensitivity and specificity make it an important clinical laboratory test for widespread use, but its global availability is still insufficient; only a few research centers have access to the method, especially in developing countries.

Surveillance of TSE cases has been compulsory in Brazil since 2005 (Martins et al., 2007), and 603 suspected CJD cases were reported up to June 2018. Of these, 404 were undiagnosed (de Oliveira Cardoso et al., 2015; Ministério da Saúde, 2018). Difficulties in performing imaging examinations and neuropathological analyses are found in several medical units in the country, making diagnosis problematic. Some diagnosed patients had samples sent to centers outside the country for biomarker analysis, allowing for greater coverage of the diagnostic criteria. The implementation of a specific test in Brazil, such as RT-QuIC, which can provide diagnosis for different TSEs with ease and confidence, is urgent to have notification and differential diagnosis for these diseases. This is also important to guide medical decisions. Here, we report the pilot use of the second-generation (IQ-CSF) RT-QuIC assay in a small cohort of Brazilian patients with possible or probable CJD to implement a reference center for this analysis in the country.

MATERIALS AND METHODS

Clinical Investigation

Patients with suspected CJD were admitted for investigation under a protocol for rapidly progressive dementia (RPD) as previously reported (Studart Neto et al., 2017). Following a full neurological examination, all patients underwent complete blood cell count, serum electrolytes, blood glucose, acute C-reactive protein, liver, renal and thyroid function tests, antithyroid and antinuclear antibody testing, as well as treponemal and HIV serology. Patients also underwent brain magnetic resonance imaging [T1, T2, fluid-attenuated inversion recovery (FLAIR), gradient echo, and diffusion weighted imaging sequences], EEG, and CSF (cell count, biochemistry, and g globulin levels). CSF 14-3-3 protein was assessed in cases of suspected prion diseases, as required by Brazilian norms. Selected patients underwent chest and abdomen computed tomography, mammography (for women), testicular ultrasound (for men), and thyroid ultrasound to rule out paraneoplastic RPD. In addition, we obtained onconeural and/or neuronal surface antigen antibody testing when paraneoplastic or autoimmune encephalitis was suspected. A flowchart for patient inclusion is provided in **Figure 1**.

Three cases had access to molecular analysis of the PRNP gene for polymorphisms in the 129 codon. Samples were analyzed using denaturing high-performance liquid chromatography. Technical details about this procedure as well as amplification reactions and DNA extraction have been previously described (Castro et al., 2004; Smid et al., 2013).

CSF Samples

We analyzed eight CSF samples from seven patients with possible, probable or genetic CJD referred to the Department of Neurology at University of São Paulo from December 2016 to June 2018. One patient (named ABT) had her CSF tested twice at different times. We used CSF samples from seven patients with other neurological conditions as negative controls. CSF samples (10 mL) were collected by lumbar puncture (LP) following a standard procedure. Two milliliters of the CSF sample were then centrifuged at 1000 × g for 10 min and stored in polypropylene tubes at −80°C until blind analysis by researcher TCRGV at UFRJ.

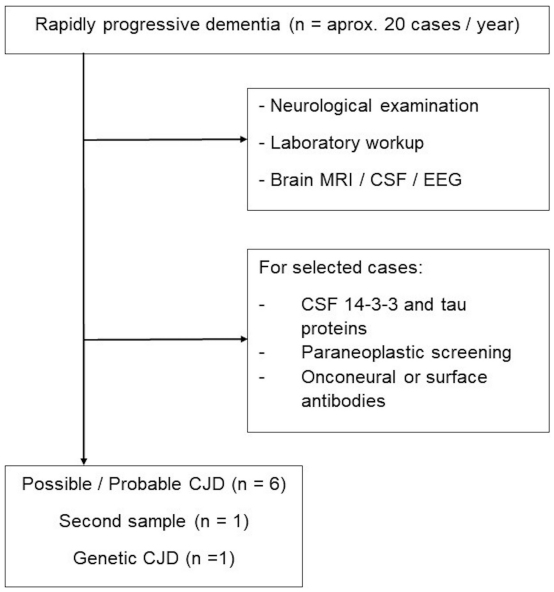

FIGURE 1 | Flowchart of samples included for RT-QuIC analysis.

RT-QuIC

The RT-QuIC assay was performed using the improved QuIC-CSF (IQ-CSF) conditions as published (Orrú et al., 2015). Briefly, 20 μL of CSF was added to 80 μL of reaction mixture in each well of a black 96 well plate with a clear bottom (Nunc). The final solution contained 10 mM phosphate buffer at pH 7.4, 1 mM ethylenediaminetetraacetic acid tetrasodium salt dihydrate (EDTA) at pH 8.0, 300 mM NaCl, 10 μM thioflavin-T (ThT), 0.002% sodium dodecyl sulfate (SDS) and 0.1 mg/mL recombinant Syrian hamster truncated form of prion protein (Ha rPrP 90–231). Samples were tested in quadruplicate three or four times independently, generating a total of 12 or 16 wells evaluated for each sample. The plates were sealed and incubated in a FLUOstar OMEGA plate reader (BMG Labtech, Germany) at 55°C with intermittent cycles of shaking (60 s, double-orbital, 700 rpm) and rest (60 s). ThT fluorescence was collected every 45 min using 450 ± 10 nm (excitation) and 480 ± 10 nm (emission) wavelengths. The threshold was defined as the average fluorescence for all samples within the first 10 h of incubation plus 10 standard deviations (SD). A sample was considered positive when at least two of four replicate wells crossed this threshold. All IQ-CSF RT-QuIC analyses were performed at the Federal University of Rio de Janeiro.

Unseeded reaction (not shown) and random CSF samples from patients with other neurological conditions (**Table 1**) were selected as negative controls. Given the descriptive nature of this study, no statistical analyses were performed.

RESULTS

In the referred time frame, seven patients presented to our team with rapidly progressive dementia and typical neurological signs of CJD. The patient named ABT had her CSF tested twice at different times (ABT1 and ABT2 samples), therefore rendering a total of eight CSF samples. ABT patient results will be better reported in Case 1 description.

We randomly used CSF samples from seven patients with other neurological conditions as negative controls. Five out of eight suspected samples had positive RT-QuIC results in our hands (**Figure 2A**). Clinical diagnosis, CSF analysis and RT-QuIC results are summarized in **Table 1**.

Samples from patients LRC and DAS were used as positive controls, given that they were previously analyzed using RT-QuIC in a reference center outside the country (The National Prion Disease Pathology Surveillance Center, Cleveland, OH, United States). Our RT-QuIC analyses were also positive, corroborating this result (**Figure 2A**). Patient ASM was a genetic CJD positive for the E200K mutation, and in our analysis, this patient was also positive, presenting a very short lag phase and a high fluorescence signal (**Figure 2A**).

Among the negative controls, there was one false positive, sample CT2 (**Figure 2A**). The false-positive case was a 5-year-old child with leukemia who was receiving intrathecal chemotherapy (GBTLI protocol with methotrexate, aracitin, citrabin, dexamethasone) during the time frame of the study.

In the following, two cases are presented in which the results obtained with RT-QuIC show interesting aspects related to RT-QuIC sensitivity and disease progression.

Case 1

ABT was a 72-year-old woman with 7 years of formal education. She had an atypical presentation characterized by a 4-month history of rapidly progressive cognitive impairment associated with visual hallucinations and gait disturbances with repeated falls. She had no relevant past medical history or family history of any neurological conditions. On neurological examination, she scored 17/30 on the Mini-Mental State Examination (MMSE), and physical tests revealed only a prominent axial syndrome as she could not sit or stand up without bilateral support. There were no pyramidal signs, parkinsonism or visuospatial impairment. A comprehensive investigation with metabolic, inflammatory, paraneoplastic, and infectious tests was unremarkable. Brain magnetic resonance imaging (MRI) revealed symmetric diffusion weighted image (DWI) hyperintensities in the basal ganglia (**Figure 3**), a finding that raised the suspicion of CDJ. The CSF analysis was unremarkable with elevated tau protein levels and negative 14-3-3. The RT-QuIC results were inconclusive; once from 16 wells, only two crossed the threshold (ABT1 sample in **Figure 2B**). Electroencephalogram (EEG) revealed disorganized electrical brain activity with no periodic waves. Three months later, she developed a significant worsening, with the need for aid for most activities of daily living, severe cognitive impairment (she could not be tested with the MMSE), myoclonus and the presence of prominent frontal reflexes on neurological examination. At this point, a prolonged EEG eventually showed bilateral periodic sharp waves, and another lumbar puncture was performed with a second sample sent for RT-QuIC analysis, with a positive result with a high fluorescence (ABT2 sample in **Figure 2B**). She eventually died of clinical complications

TABLE 1 | Results of diagnostic investigations in the tested patient cohort.

Sample, age	Diagnosis[a]	CSF analysis					RT-QuIC status
		WBC/μ L	Prot (mg/dL)	Glu (mg/dL)	Tau[b] (pg/mL)	14-3-3	
CT1, 55	Control (chronic meningitis)	23	192	30	–	–	Negative
CT2, 5	Control (leukemia)	2	22	45	–	–	Positive
CT3, 62	Control (cranial nerves syndrome)	1	71	102	–	–	Negative
HCS, 63	Control (multiple sclerosis)	1	43	80	–	–	Negative
HBV, 41	Control (HIV)	3	35	66	–	–	Negative
RMC, 64	Control (SAH/ventriculitis)	25	134	54	–	–	Negative
ABS, 43	Control (chronic meningitis)	9	62	40	–	–	Negative
LRC, 69	RPD (probable CJD)	1	27	61	2279	Negative	Positive[d]
DAS, 69	RDP (probable CJD)	5	32	63	2109	Positive	Positive[d]
ABT1, 74	RPD (possible CJD)	1[c]	39	71	908	Negative	Negative
ABT2, 74	RPD (possible CJD)	1	32	61	NA	NA	Positive
ASM, NA	RPD (genetic CJD)			NA			Positive
JJN, 65	RPD (probable CJD)	1	66	61	519	NA	Positive
GMT, 75	RPD (possible CJD)	4	97	61	115	NA	Negative
TN, 73	RPD (probable CJD)	1	79	96	NA	Negative	Positive

WBC, white blood cells; Prot, protein levels; Glu, glucose levels; RPD, rapidly progressive dementia; SAH, subarachnoid hemorrhage; NA, not available. [a]Controls and their suspected diagnosis/investigation. [b]Reference value for total tau levels was <450 pg/mL. [c]This sample had 33 red blood cells. [d]These patients also had their CSF samples sent abroad with positive results (The National Prion Disease Pathology Surveillance Center, Cleveland, OH, United States).

11 months after the first symptoms appeared. PRNP gene analysis revealed codon 129 heterozygous MV.

Case 2

JJN was a 65-year-old male who presented to our clinic with an 8-month history of behavioral changes. He had 4 years of education and a medical history of hypertension and gouty arthritis. There was no family history of any neurological conditions. His wife described the first symptoms as prominent changes in his food preferences with an unusual demand for rice and chicken. Two months later, he developed visual hallucinations, mostly described as the presence of spiders in the ceiling. In the first evaluation, he was independent of instrumental activities of daily living. Neurological examination revealed an MMSE of 20/30 with an unremarkable physical examination. A laboratory work-up including metabolic, inflammatory and serology studies was negative. At this point, we were surprised by the finding of brain MRI diffusion weighted imaging revealing marked bilateral hypersignal in the frontotemporoparieto-occipital cortex, basal ganglia, thalamus and – less markedly – in the hippocampus, raising the suspicion of sporadic Creutzfeldt-Jakob Disease (sCJD) (**Figures 4A,B**). The patient was hospitalized for further investigation. The EEG study revealed bilateral and synchronous slow waves. A brain 18-FDG PET showed hypometabolism in the temporal and frontal lobes, caudate nuclei and temporoparietal cortex (**Figure 4C**). The CSF study was initially unremarkable, except for the high total tau protein levels, whereas 14-3-3, p-tau and beta-amyloid values were within the normal range. A CSF sample was sent for autoantibodies and RT-QuIC testing. The patient was empirically treated with intravenous methylprednisolone for 5 days and was discharged for outpatient follow-up. At this point, we received CSF results negative for autoantibodies with an inconclusive RT-QuIC response; from 12 wells, only two crossed the threshold (**Figure 2C**). In the following months, he eventually developed cognitive deterioration and parkinsonism, with the presence of more complex visual hallucinations. He eventually died of clinical complications approximately 28 months after initial symptoms. PRNP gene analysis revealed codon 129 heterozygous MV.

DISCUSSION

The present study reports the results of pilot second-generation RT-QuIC testing in a small patient cohort referred for rapidly progressive neurological syndromes of suspected prion nature. Our center previously reported 61 cases of rapidly progressive dementia among 1648 patients in a 3-year interval. Immune-mediated encephalopathies represented the majority of the samples (46%), followed by CJD (11.5%) (Studart Neto et al., 2017). All cases from that study were diagnosed with CJD according to the University of California San Francisco Modified Criteria (Vitali et al., 2011), which does not include CSF testing.

As we described here, IQ-CSF RT-QuIC proved to be an extremely important tool in the diagnosis of ABT and JJN cases (Cases 1 and 2). Both patients presented with rapidly progressive neurological syndromes and could not initially be classified with possible or probable CJD, according to the most recent criteria (CDC, 2018). Both ABT and JJN showed slightly elevated levels of total Tau protein, but although this biomarker has 87–90% sensitivity, it is only 67–75% specific for CJD (Connor et al., 2019). 14-3-3 protein was not elevated in both cases, despite their genetic subtype MV, which is often associated with positive 14-3-3 protein levels (Manix et al., 2015).

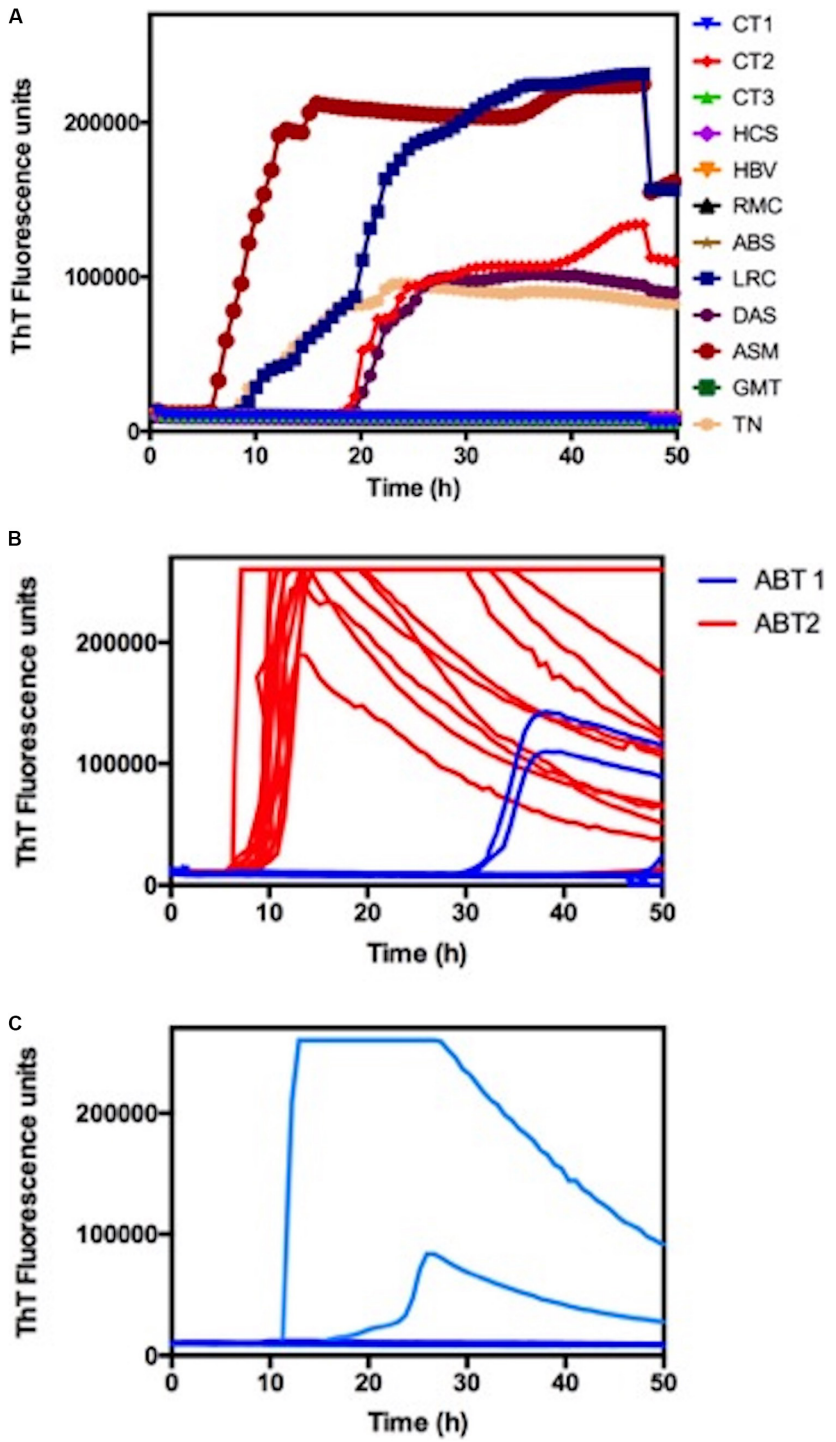

FIGURE 2 | Blind RT-QuIC analysis of CSF samples. **(A)** RT-QuIC responses from reactions seeded with 20 μl of CSF from suspected CJD cases (LRC; DAS; ASM; JJN; GMT, TN). The RT-QuIC responses from reactions seeded with CSF samples from patients with other neurological disorders (CT1; CT2; CT3; HCS; HBV; RMC; ABS) were used as a negative control. Each curve represents the mean of four replicate readings of three or four repetitions. **(B)** Single-well analysis of CSF samples from patient ABT. ABT1 and ABT2 refer to the first and second collections, respectively. **(C)** Single-well analysis of CSF samples from patient JJN.

In the case of ABT patient, the clinical presentation of rapid cognitive impairment with visual hallucinations and gait impairment was considered atypical. In this case, the brain MRI was an important diagnostic clue, with DWI hyperintensities in the basal ganglia leading to a differential diagnosis with metabolic encephalopathies, hypoxic-ischemic lesions or toxic

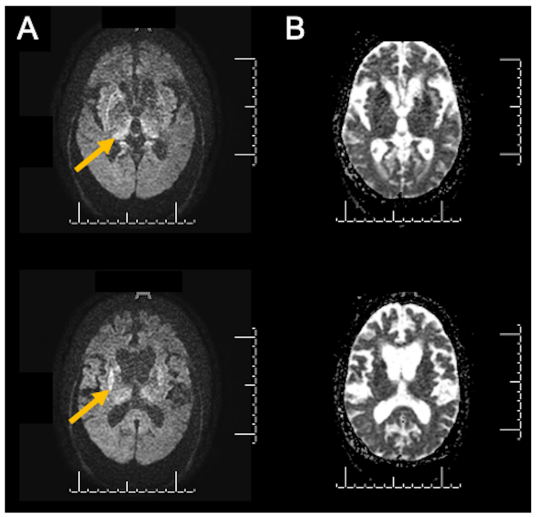

FIGURE 3 | Diffusion-weighted images (DWI) from ABT (case 1) revealing enlarged ventricles and symmetric hyperintensities in the basal ganglia (**A**, yellow arrows). **(B)** shows corresponding apparent diffusion coefficient (ADC) hypointensities in the same territory.

lesions (i.e., carbon monoxide intoxication) (Finelli and DiMario, 2003). A careful clinical assessment made all possibilities less likely, and CJD became our main hypothesis. Despite an inconclusive RT-QuIC result for the first collected sample, the patient eventually evolved with a more typical impairment, and the second CSF sample with a 3-month interval yielded positive RT-QuIC.

The different results obtained with the ABT patient samples were very intriguing. We hypothesize that this difference could be attributed to higher loads of PrP^{sc} following disease progression. Although disease duration does not seem to be related to RT-QuIC results (McGuire et al., 2012), it is not yet clear whether there is a change in the presence of seeds in CSF according to disease progression. To our knowledge, this approach performed with samples of a patient collected at different times has not yet been tested, and this is the first report suggesting that RT-QuIC results change according to disease evolution. A more feasible hypothesis would be that the first sample had some interference, such as blood that could mask the positive result (Cramm et al., 2016), despite a only modest presence of red blood cells in this particular sample (33 cells/μL, see **Table 1**).

Atypical features for sCJD in JJN (Case 2) included (1) a presentation with mild behavioral changes; (2) the initial sparing of motor systems, with evidence of motor findings in the neurological examination only almost 12 months after first symptoms; (3) an unremarkable EEG with 7–8 months of evolution; and (4) the presence of a bilateral T2 hypersignal in the hippocampus. The RT-QuIC was inconclusive, but together with MRI, it could suggest early diagnosis of probable CJD. Perhaps with disease progression, JJN's CSF sample would obtain a positive RT-QuIC result, as observed for ABT patient.

The occurrence of one false-positive case in our RT-QuIC test weakens our diagnostic accuracy and underscores the need for improvements in the protocol. Despite having an extremely high specificity, IQ-CSF RT-QuIC false-positive results have been reported in the literature. Hayashi et al. (2017) reported the case of a 61-year-old man who presented with rapid cognitive impairment, myoclonus and recurrent seizures. A brain MRI revealed cortical hyperintensities, and the CSF analysis showed elevated 14-3-3 and tau levels, with a positive RT-QuIC. Despite aggressive treatment with corticotherapy, the patient died, and post-mortem assessment revealed only pathological changes after convulsion, with no signs of prion disease. The authors conclude that convulsion may cause false-positive RT-QUIC results and that a post-mortem evaluation remains the gold standard for diagnosing similar cases. The shaking effect was analyzed *in vitro* by Orrú et al. (2016), and they showed that long shaking periods reduced scrapie-seeded reaction times, but continuous shaking promoted false-positive reactions.

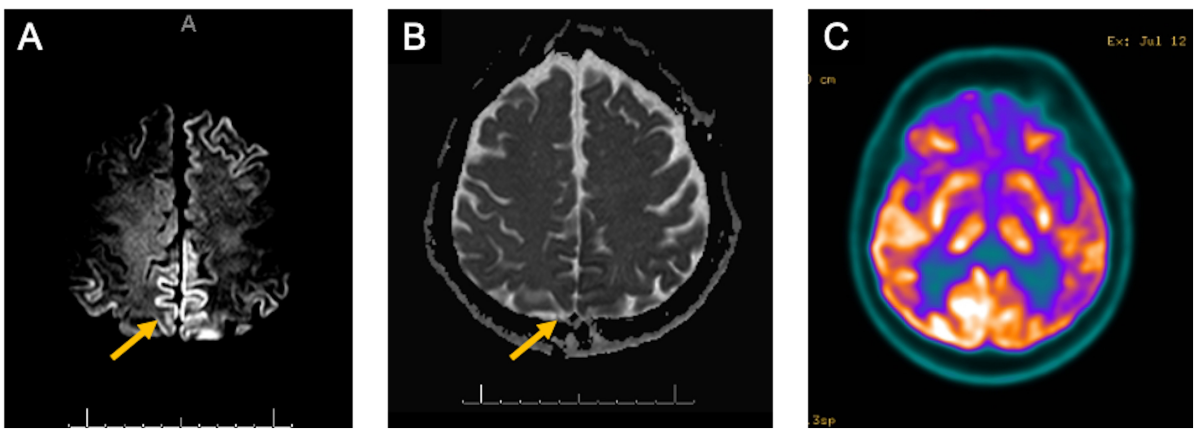

FIGURE 4 | (A) MRI diffusion-weighted images from JJN (case 2) revealing hyperintensities on frontal, temporoparietal and posterior cingulate cortical areas (**A**, yellow arrow); **(B)** MRI apparent diffusion coefficient maps with corresponding hypointensities in the same regions above (**B**, yellow arrow); **(C)** 18-FDG PET/CT shows hypometabolism on the bilateral temporoparietal cortex, posterior cingulate, precuneus, and caudate nucleus.

Regarding our false-positive case, we did not find any similar cases reporting the use of intrathecal medications as a possible reason for a positive RT-QuIC result. A positive case in a 5-year-old child without any neurological symptoms would never be expected; an 18-year-old woman was the youngest person diagnosed with probable sCJD using RT-QuIC (Yao et al., 2017). Therefore, this sample was selected as a negative control, although infant CSF was never RT-QuIC analyzed. Despite optimized protocols, sample processing issues can always be a possibility for such unexpected results.

The present study is limited by its pilot nature, with a modest sample size. Improvements in the establishment of the protocol are necessary, requiring a greater number of analyses. The use of nasal brushes to collect patient samples for RT-QuIC analysis is also valid to improve protocol sensitivity and specificity. However, this is the first study to our knowledge to report specific biomarker-based feasible results performed in a developing country for prion diagnosis, in addition to pointing out new possible interferences in the protocol, and the need to understand how the different current diagnostic approaches can reveal disease progression.

CONCLUSION

The cases reported here illustrate the importance of using RT-QuIC for patients with neurological syndromes, enabling the diagnosis of probable CJD, while no other method was sufficient to support this diagnosis, even with atypical clinical presentation. In addition, the identification of a false positive in a sample from a leukemic pediatric patient undergoing intrathecal treatment with chemotherapy suggests new possible interferences in the method. This will require future investigation of the effect of these chemotherapeutic agents for inclusion or not as a limitation for carrying out the assay.

CSF samples are often evaluated only once, due to the invasiveness of CSF collection and the absence of curative treatment for TSEs, in addition to rapid disease progression. One of the cases we report points out the importance of carrying out studies that evaluate the progression of the disease and that RT-QuIC is a useful approach for such studies. In this case, the use of nasal brushes might be prioritized over CSF analysis, since this provides greater sensitivity and enables more frequent sample collection, given the less invasive nature of the procedure.

Finally, our study illustrates the feasibility of having CJD CSF samples tested in Brazilian centers, and highlights the importance of inter-institutional collaboration in order to pursue a greater diagnostic accuracy for CJD in developing countries. It also demonstrates that RT-QuIC can be clinically available for testing patients from Brazil and other Latin American countries, and points to the need and feasibility of establishing a national reference center for the diagnosis of these rare but devastating diseases.

DATA AVAILABILITY STATEMENT

All datasets generated for this study are included in the article/supplementary material.

ETHICS STATEMENT

Ethical review and approval was not required for the study on human participants in accordance with the local legislation and institutional requirements. Written informed consent to participate in this study was provided by the participants' legal guardian/next of kin. Written informed consent was obtained from the individual(s), and minor(s)' legal guardian/next of kin, for the publication of any potentially identifiable images or data included in this article.

AUTHOR CONTRIBUTIONS

BB: study design, patient data collection, and manuscript writing. BB, BC, RA, MB, HG, and SB: patient data collection and interpretation. JS and RN: study design, data interpretation, and manuscript critical revision. ML and VM: genetic analysis. JLS and TV: RT-QuIC facility implementation. TV: study design, RT-QuIC evaluations, RT-QuIC data analysis, and manuscript writing. All authors contributed to the article and approved the submitted version.

FUNDING

This work was supported by research grants from the Carlos Chagas Filho Foundation for Research Support in the State of Rio de Janeiro (FAPERJ) and the National Council of Technological and Scientific Development (CNPq) to JLS and TV.

ACKNOWLEDGMENTS

We would like to acknowledge all the patients and their families for their contributions to this study.

REFERENCES

Bizzi, A., Pascuzzo, R., Blevins, J., Grisoli, M., Lodi, R., Moscatelli, M. E. M., et al. (2020). Evaluation of a new criterion for detecting prion disease with diffusion magnetic resonance imaging. *JAMA Neurol.* doi: 10.1001/jamaneurol.2020.1319 [Epub ahead of print].

Brown, P., Brunk, C., Budka, H., Cervenakova, L., Collie, D., Green, A., et al. (2003). *WHO Manual for Surveillance of Human Transmissible Spongiform Encephalopathies, Including Variant Creutzfeldt-Jakob Disease*. Geneva: World Health Organization.

Castro, R. M. R. P. S., Landemberger, M. C., Walz, R., Carlotti, C. G., Huang, N., Cunha, D. R., et al. (2004). High capacity and low cost detection of prion protein gene variant alleles by denaturing HPLC.

J. Neurosci. Methods 139, 263–269. doi: 10.1016/j.jneumeth.2004.05.001

CDC (2018). *CDC's Diagnostic Criteria for Creutzfeldt-Jakob Disease (CJD) [Internet]*. Atlanta: Centers for Disease Control and Prevention.

Connor, A., Wang, H., Appleby, B. S., and Rhoads, D. D. (2019). Clinical laboratory tests used to aid in diagnosis of human prion disease. *J. Clin. Microbiol.* 57:e00769-19.

Cramm, M., Schmitz, M., Karch, A., Mitrova, E., Kuhn, F., Schroeder, B., et al. (2016). Stability and reproducibility underscore utility of RT-QuIC for diagnosis of Creutzfeldt-Jakob disease. *Mol. Neurobiol.* 53, 1896–1904. doi: 10.1007/s12035-015-9133-2

de Oliveira Cardoso, C. A., de Albuquerque Navarro, M. B. M., Soares, B. E. C., and Oliveira Cardoso, T. A. (2015). Avaliação epidemiológica dos óbitos por doenças priônicas no Brasil sob o enfoque da biossegurança. *Cadernos Saúde Coletiva* 23, 2–10. doi: 10.1590/1414-462x201500010002

Eisenmenger, L., Porter, M.-C., Carswell, C. J., Thompson, A., Mead, S., Rudge, P., et al. (2016). Evolution of diffusion-weighted magnetic resonance imaging signal abnormality in sporadic creutzfeldt-jakob disease, with histopathological correlation. *JAMA Neurol.* 73, 76–84.

Finelli, P. F., and DiMario, F. J. (2003). Diagnostic approach in patients with symmetric imaging lesions of the deep gray nuclei. *Neurologist* 9, 250–261. doi: 10.1097/01.nrl.0000087718.55597.6a

Franceschini, A., Baiardi, S., Hughson, A. G., McKenzie, N., Moda, F., Rossi, M., et al. (2017). High diagnostic value of second generation CSF RT-QuIC across the wide spectrum of CJD prions. *Sci. Rep.* 7:10655.

Geschwind, M. D. (2016). Rapidly progressive dementia. *Continuum* 22, 510–537. doi: 10.1212/con.0000000000000319

Geschwind, M. D., and Murray, K. (2018). Differential diagnosis with other rapid progressive dementias in human prion diseases. *Handb. Clin. Neurol.* 153, 371–397. doi: 10.1016/b978-0-444-63945-5.00020-9

Green, A. J. E. (2019). RT-QuIC: a new test for sporadic CJD. *Pract. Neurol.* 19, 49–55. doi: 10.1136/practneurol-2018-001935

Hayashi, Y., Iwasaki, Y., Yoshikura, N., Asano, T., Mimuro, M., Kimura, A., et al. (2017). An autopsy-verified case of steroid-responsive encephalopathy with convulsion and a false-positive result from the real-time quaking-induced conversion assay. *Prion* 11, 284–292. doi: 10.1080/19336896.2017.1345416

Manix, M., Kalakoti, P., Henry, M., Thakur, J., Menger, R., Guthikonda, B., et al. (2015). Creutzfeldt-Jakob disease: updated diagnostic criteria, treatment algorithm, and the utility of brain biopsy. *Neurosurg. Focus* 39:E2.

Martins, V. R., Gomes, H. R., Chimelli, L., Rosemberg, S., and Landemberger, M. C. (2007). Prion diseases are under compulsory notification in Brazil: surveillance of cases evaluated by biochemical and/or genetic markers from 2005 to 2007. *Dement. Neuropsychol.* 1, 347–355. doi: 10.1590/s1980-57642008dn10400004

McGuire, L. I., Peden, A. H., Orrú, C. D., Wilham, J. M., Appleford, N. E., Mallinson, G., et al. (2012). Real time quaking-induced conversion analysis of cerebrospinal fluid in sporadic Creutzfeldt-Jakob disease. *Ann. Neurol.* 72, 278–285. doi: 10.1002/ana.23589

Ministério da Saúde (2018). *Protocol for Notification and Investigation of Creutzfeldt-Jakob Disease with a Focus on the Identification of the New Variant [Internet]*. Brazil: Ministério da Saúde.

Orrú, C. D., Bongianni, M., Tonoli, G., Ferrari, S., Hughson, A. G., Groveman, B. R., et al. (2014). A test for Creutzfeldt-Jakob disease using nasal brushings. *N. Engl. J. Med.* 371, 519–529. doi: 10.1056/nejmoa1315200

Orrú, C. D., Groveman, B. R., Hughson, A. G., Zanusso, G., Coulthart, M. B., and Caughey, B. (2015). Rapid and sensitive RT-QuIC detection of human creutzfeldt-jakob disease using cerebrospinal fluid. *mBio* 6:e02451-14.

Orrú, C. D., Hughson, A. G., Groveman, B. R., Campbell, K. J., Anson, K. J., Manca, M., et al. (2016). Factors that improve RT-QuIC detection of prion seeding activity. *Viruses* 8:140. doi: 10.3390/v8050140

Schmitz, M., Ebert, E., Stoeck, K., Karch, A., Collins, S., Calero, M., et al. (2016). Validation of 14-3-3 protein as a marker in sporadic creutzfeldt-jakob disease diagnostic. *Mol. Neurobiol.* 53, 2189–2199.

Smid, J., Landemberger, M. C., Bahia, V. S., Martins, V. R., Nitrini, R., Smid, J., et al. (2013). Codon 129 polymorphism of prion protein gene in is not a risk factor for Alzheimer's disease. *Arquivos Neuro Psiquiatr.* 71, 423–427. doi: 10.1590/0004-282x20130055

Staffaroni, A. M., Kramer, A. O., Casey, M., Kang, H., Rojas, J. C., Orrú, C. D., et al. (2019). Association of blood and cerebrospinal fluid tau level and other biomarkers with survival time in sporadic creutzfeldt-jakob disease. *JAMA Neurol.* 76, 969–977.

Studart Neto, A., Soares Neto, H. R., Simabukuro, M. M., Solla, D. J. F., Gonçalves, M. R. R., Fortini, I., et al. (2017). Rapidly progressive dementia: prevalence and causes in a neurologic unit of a tertiary hospital in Brazil. *Alzheimer Dis. Assoc. Disord.* 31, 239–243. doi: 10.1097/wad.0000000000000170

Vitali, P., Maccagnano, E., Caverzasi, E., Henry, R. G., Haman, A., Torres-Chae, C., et al. (2011). Diffusion-weighted MRI hyperintensity patterns differentiate CJD from other rapid dementias. *Neurology* 76, 1711–1719. doi: 10.1212/wnl.0b013e31821a4439

Wilham, J. M., Orrú, C. D., Bessen, R. A., Atarashi, R., Sano, K., Race, B., et al. (2010). Rapid end-point quantitation of prion seeding activity with sensitivity comparable to bioassays. *PLoS Pathog.* 6:e1001217. doi: 10.1371/journal.ppat.1001217

Yao, Y., Dong, X., Guan, H., and Lu, Q. (2017). Cerebrospinal fluid real-time quaking-induced conversion test for sporadic Creutzfeldt–Jakob disease in an 18-year-old woman: a case report. *Medicine* 96:e8699. doi: 10.1097/md.0000000000008699

Zanusso, G., Monaco, S., Pocchiari, M., and Caughey, B. (2016). Advanced tests for early and accurate diagnosis of Creutzfeldt-Jakob disease. *Nat. Rev. Neurol.* 12:427. doi: 10.1038/nrneurol.2016.92

Zerr, I., and Hermann, P. (2018). Diagnostic challenges in rapidly progressive dementia. *Expert Rev. Neurother.* 18, 761–772. doi: 10.1080/14737175.2018.1519397

Conflict of Interest: The authors declare that the research was conducted in the absence of any commercial or financial relationships that could be construed as a potential conflict of interest.

frontiers in Bioengineering and Biotechnology

REVIEW
published: 27 August 2020
doi: 10.3389/fbioe.2020.00975

An Update on Autophagy in Prion Diseases

Óscar López-Pérez[1,2,3,4], Juan José Badiola[2], Rosa Bolea[2], Isidro Ferrer[3,4,5], Franc Llorens[3,4,6] and Inmaculada Martín-Burriel[1,2,7]*

[1] Laboratorio de Genética Bioquímica (LAGENBIO), Instituto Agroalimentario de Aragón-IA2, Instituto de Investigación Sanitaria Aragón-IISA, Universidad de Zaragoza, Zaragoza, Spain, [2] Centro de Encefalopatías y Enfermedades Transmisibles Emergentes (CEETE), Instituto Agroalimentario de Aragón-IA2, Instituto de Investigación Sanitaria Aragón-IISA, Universidad de Zaragoza, Zaragoza, Spain, [3] Centro de Investigación Biomédica en Red de Enfermedades Neurodegenerativas (CIBERNED), Instituto Carlos III, L'Hospitalet de Llobregat, Barcelona, Spain, [4] Instituto de Investigación Biomédica de Bellvitge (IDIBELL), L'Hospitalet de Llobregat, Barcelona, Spain, [5] Departamento de Patología y Terapéutica Experimental, Universidad de Barcelona, L'Hospitalet de Llobregat, Barcelona, Spain, [6] Department of Neurology, Clinical Dementia Center and National Reference Center for CJD Surveillance, University Medical School, Göttingen, Germany, [7] Centro de Investigación Biomédica en Red de Enfermedades Neurodegenerativas (CIBERNED), Instituto Carlos III, Zaragoza, Spain

OPEN ACCESS

Edited by:
Jesus R. Requena, University of Santiago de Compostela, Spain

Reviewed by:
Neil A. Mabbott, University of Edinburgh, United Kingdom
Bruno Jorge Antunes Colaço, University of Trás-os-Montes and Alto Douro, Portugal
Ina Maja Vorberg, Deutsches Zentrum für Neurodegenerative, Helmholtz-Gemeinschaft Deutscher Forschungszentren (HZ), Germany

****Correspondence:***
Óscar López-Pérez
oscarlzpz@gmail.com

Specialty section:
This article was submitted to Biosafety and Biosecurity, a section of the journal Frontiers in Bioengineering and Biotechnology

Received: *15 May 2020*
Accepted: *27 July 2020*
Published: *27 August 2020*

Citation:
López-Pérez Ó, Badiola JJ, Bolea R, Ferrer I, Llorens F and Martín-Burriel I (2020) An Update on Autophagy in Prion Diseases. Front. Bioeng. Biotechnol. 8:975. doi: 10.3389/fbioe.2020.00975

Autophagy is a dynamic intracellular mechanism involved in protein and organelle turnover through lysosomal degradation. When properly regulated, autophagy supports normal cellular and developmental processes, whereas defects in autophagic degradation have been associated with several pathologies, including prion diseases. Prion diseases, or transmissible spongiform encephalopathies (TSE), are a group of fatal neurodegenerative disorders characterized by the accumulation of the pathological misfolded isoform (PrP^{Sc}) of the physiological cellular prion protein (PrP^{C}) in the central nervous system. Autophagic vacuoles have been described in experimental models of TSE and in the natural disease in humans. The precise connection of this process with prion-related neuropathology, or even whether autophagy is completely beneficial or pathogenic during neurodegeneration, is poorly understood. Thus, the biological role of autophagy in these diseases is still open to debate. During the last years, researchers have used a wide range of morphological, genetic and biochemical methods to monitor and manipulate the autophagic pathway and thus determine the specific role of this process in TSE. It has been suggested that PrP^{C} could play a crucial role in modulating the autophagic pathway in neuronal cells, and the presence of abnormal autophagic activity has been frequently observed in several models of TSE both *in vitro* and *in vivo*, as well as in human prion diseases. Altogether, these findings suggest that autophagy is implicated in prion neuropathology and points to an impairment or failure of the process, potentially contributing to the pathogenesis of the disease. Additionally, autophagy is now emerging as a host defense response in controlling prion infection that plays a protective role by facilitating the clearance of aggregation-prone proteins accumulated within neurons. Since autophagy is one of the pathways of PrP^{Sc} degradation, and drug-induced stimulation of autophagic flux (the dynamic process of autophagic degradation activity) produces anti-prion effects, new treatments based on its activation have been tested to develop therapeutic strategies for prion diseases. In this review, we summarize previous and recent findings concerning the role of autophagy in TSE.

Keywords: autophagy, LC3, p62, neurodegenerative diseases, prion diseases, Creutzfeldt-Jakob disease, scrapie, therapies

INTRODUCTION

Transmissible spongiform encephalopathies (TSE), or prion diseases, are a group of fatal neurodegenerative disorders that affect both humans and animals (Prusiner, 1982). Human prion diseases include kuru, the various forms of Creutzfeldt-Jakob disease (CJD), Gerstmann-Sträussler-Scheinker (GSS) syndrome, fatal familial insomnia, sporadic fatal insomnia, and the variably protease-sensitive prionopathy (Imran and Mahmood, 2011a). In animals, they include, but are not limited to, bovine spongiform encephalopathy (BSE) in cattle, classical and atypical scrapie in sheep and goats, and chronic wasting disease in cervids (Imran and Mahmood, 2011b). Ovine scrapie was the first TSE described and constitutes one of the most widely studied models of these pathologies (Pattison and Jones, 1967).

Prion diseases are characterized by a long asymptomatic incubation period and a rapidly progressing pathology that leads inevitably to death. According to the protein-only hypothesis (Prusiner, 1982), TSE are caused by the conformational conversion of native cellular prion protein (PrP^{c}), which is encoded by the prion protein (*PRNP*) gene, into an infectious misfolded isoform named scrapie-associated prion protein (PrP^{Sc}). Accumulation of PrP^{Sc} in the central nervous system (CNS), which is believed to be the main pathogenic event responsible for the pathological changes produced in TSE patients, induces spongiform degeneration, glial activation and neuronal loss (Wells and McGill, 1992; Wood et al., 1997). Hence, prion diseases share profound similarities with other neurodegenerative disorders associated with the accumulation of misfolded protein aggregates like Alzheimer's disease, Parkinson's disease and Huntington's disease (Soto, 2003). Despite the similarities between these diseases, prions remain unique since epidemiological data support their ability to transmit under natural and experimental conditions between individuals and, to a certain extent, between species (Mays and Soto, 2016).

For years, TSE research field has focused on characterizing the underlying molecular mechanisms of the basic pathological processes involved in prion pathogenesis and neurodegeneration. Unfortunately, despite the great efforts of the researchers, these mechanisms are not completely understood. Recent evidence has emerged implicating impaired protein homeostasis as a major cause of toxicity common to prion diseases (Goold et al., 2015). Cellular homeostasis requires a proper balance between the protein degradation and synthesis to eliminate and replace proteins, respectively. In this regard, cells employ various biological mechanisms that control protein degradation, which include lysosomal routes such as the autophagic pathway (Majeski and Dice, 2004). Existing data suggest that neurons fail to recover homeostasis after exposure to PrP^{Sc}, which ultimately leads to neuronal dysfunction and death by mechanisms that originate as a survival response to intracellular PrP^{Sc} accumulation (Mays and Soto, 2016). Indeed, many studies have identified autophagic dysregulation in TSE models (Boellaard et al., 1989, 1991; Liberski et al., 2004; Sikorska et al., 2004; Mok et al., 2007; Xu et al., 2012; Homma et al., 2014; Moon et al., 2016c; Llorens et al., 2017; Thellung et al., 2018; Lopez-Perez et al., 2019a,b, 2020), although the casual relationship between these observations and disease pathogenesis is currently unknown. Considering the impact of autophagy in other neurodegenerative disorders (Bursch and Ellinger, 2005; Rubinsztein, 2006), in this review we summarize, evaluate and discuss previous and recent findings concerning the role of this process, as well as the therapeutic effects of its modulation, in prion diseases.

AUTOPHAGY

Autophagy is a fundamental pathway of cellular catabolism and recycling, in which nonessential cytoplasm and unwanted or damaged components are sequestered in vesicles and delivered to lysosomes for degradation, thus maintaining homeostatic balance (Rubinsztein, 2006). There are three different types of autophagy in mammalian cells classified according to their method of delivery to the lysosome: macroautophagy, microautophagy and chaperone-mediated autophagy (CMA) (Mizushima et al., 2008). As macroautophagy is the most prevalent and best characterized form, it is often referred to as autophagy. During macroautophagy (hereafter autophagy), portions of the cytoplasm are surrounded by an isolation membrane of unknown origin named phagophore. Elongation and fusion of the edges of the phagophore engulf the cytoplasmic material inside a double-membrane vesicle, with about 1 μm diameter, called autophagic vacuole or autophagosome. Sequestered contents can include individual, aggregated and misfolded proteins, whole organelles such as parts of the endoplasmic reticulum (ER), mitochondria and peroxisomes, and even invading pathogens. The outer membrane of the autophagosome then docks and fuses with the lysosome to form an autophagolysosome or autolysosome, where the autophagic cargo, together with the inner membrane, is degraded by lysosomal hydrolases. Eventually, the resulting macromolecules are released back into the cytosol and recycled by the cell (Yoshimori, 2004; Rubinsztein et al., 2012; Feng et al., 2014).

MOLECULAR MECHANISMS

Autophagy is a highly conserved process from yeast to human (Reggiori and Klionsky, 2002). To date, independent genetic screens in yeast model systems, mainly in *Saccharomyces cerevisiae*, have allowed the identification of about 30 autophagy-related (*ATG*) genes, many of which have known homologs in higher eukaryotes (Bednarczyk et al., 2018). Among these *ATG* genes, one subset is required for autophagosome formation, whose corresponding encoded proteins are known as the "core autophagy machinery" (Xie and Klionsky, 2007). Autophagosome formation can be summarized in several distinct stages: induction, nucleation, expansion, fusion, and cargo degradation/recycling (Yin et al., 2016). For simplicity, we will use in this section of the review the unified yeast nomenclature when describing autophagy-related proteins.

Induction

Initiation of the autophagic process is carried out by the Atg1 kinase complex, composed of the serine/threonine kinase Atg1, its regulatory subunit Atg13, and the Atg17-Atg31-Atg29 scaffolding subcomplex (**Figure 1A**; Kamada et al., 2010). The stimuli necessary to induce autophagy are detected by nutrient-sensing pathways such as the target of rapamycin complex 1 (TORC1; mTORC1 in mammals), which is considered the main negative regulator of autophagy (Laplante and Sabatini, 2012). Under normal conditions, TORC1 maintains autophagy at a basal level by phosphorylating certain proteins including Atg1 and Atg13, which impedes activation of the Atg1 kinase complex. During starvation, or treatments with chemical compounds such as rapamycin, an intracellular signaling cascade inhibits TORC1, resulting in the dephosphorylation of Atg1 and Atg13. In this situation, Atg1 auto-phosphorylates, increases its kinase activity, and recruits and activates other Atg proteins, allowing them to be localized to the phagophore assembly site (PAS) and begin nucleation (Ariosa and Klionsky, 2016).

Nucleation of the Phagophore

In autophagy, nucleation refers to the process of mobilizing and recruitment of proteins needed for phagophore expansion to the PAS (Yin et al., 2016). The autophagy-specific class III phosphatidylinositol 3-kinase complex I (PtdIns3K-C1), which is comprised of the lipid kinase Vps34, the regulatory kinase Vps15, Vps30/Atg6 (BECN1 in mammals) and Atg14, is the nucleation machinery that is recruited to the PAS upon induction of autophagy (**Figure 1B**; Birgisdottir et al., 2019). The function of this set of proteins is to catalyze the conversion of phosphatidylinositol (PtdIns) to phosphatidylinositol 3-phospate (PtdIns3P). This molecule then serves as a signal that recruits other Atg proteins that recognize and preferentially bind PtdIns3P at the nucleation site (Ariosa and Klionsky, 2016). Another important negative regulator of autophagy is the Atg6-Bcl-2 interaction complex. Under normal conditions, Bcl-2 directly inhibits autophagy by binding to Atg6, while during starvation, Bcl-2 dissociates from Atg6, allowing Atg6 to associate with the PtdIns3K-C1 complex and perform its function in PtdIns3P formation (Ariosa and Klionsky, 2016).

Expansion and Maturation Into an Autophagosome

Autophagy employs the use of two ubiquitin-like (Ubl) conjugation systems to extend and elongate the phagophore. These systems involve the Ubl proteins Atg12 and Atg8 [microtubule-associated protein 1 light chain 3 (MAP1LC3, or LC3) in mammals] (**Figure 1C**; Ohsumi, 2001). During the first Ubl conjugation reaction, Atg12 associates with Atg5, which depends on the E1 activating and E2 conjugating enzymes Atg7 and Atg10 (Mizushima et al., 2003b). The Atg12-Atg5 conjugate subsequently forms a multimeric complex with Atg16 (Mizushima et al., 2003a). In the second Ubl reaction, Atg8 is first cleaved off by the protease Atg4, and then recognized and processed by the E1 activating and E2 conjugating enzymes Atg7 and Atg3. The proteolyzed protein Atg8 (LC3-I in mammals) is then covalently attached to phosphatidylethanolamine (PE) to form Atg8-PE (LC3-II in mammals), a reaction that is facilitated by the E3-like Atg12-Atg5-Atg16 complex (Feng et al., 2014; Ariosa and Klionsky, 2016). Although these two conjugates are essential for autophagy and localize at the PAS, how their covalent modification reactions contribute to phagophore expansion and maturation is unknown (Ariosa and Klionsky, 2016). To further expand the phagophore, the membrane necessary is delivered from peripheral sites to the PAS by the shuttling of the transmembrane protein Atg9 (Mari et al., 2010).

Fusion, Degradation, and Recycling

Upon completion of the autophagosome, it targets to, docks and then fuses with the degradative organelle (Yin et al., 2016). The Atg12-Atg5-Atg16 complex is mainly localized on the outer side of the autophagosome and is released into the cytosol before or after autophagosome completion (Yang and Klionsky, 2009). In contrast, Atg8-PE is present both on inner and outer autophagosome membranes (Kabeya et al., 2000). The Atg8-PE that resides on the outer side is released by a second Atg4-dependent cleavage, a deconjugation necessary to initiate the fusion stage, whereas the inner population remains inside the vesicle and is degraded in the degradative organelle (Yang and Klionsky, 2009; Nair et al., 2012). This protein is currently the most widely used marker to monitor autophagic activity because the amount of the membrane-associated LC3-II form in mammals reflects the number of autophagosomes (Mizushima and Yoshimori, 2007). After fusion, the cargo is delivered inside the degradative organelle and degraded by resident hydrolases. Metabolites generated in the proteolytic process are released back into the cytosol through various permeases located in the membrane and reutilized by the cell (Ariosa and Klionsky, 2016).

PHYSIOLOGICAL ROLES OF AUTOPHAGY

Autophagy is an essential survival mechanism that primarily acts as an adaptive catabolic response to environmental adversity. This process rapidly increases its activity when cells are exposed to extreme conditions of metabolic stress, especially during nutrient deprivation, but also in the absence of growth factors, oxygen or energy (Levine and Kroemer, 2008; Kroemer et al., 2010). The basic response of autophagy is to serve as a source of energy during starvation: when there is a lack of nutrients or resources become limited, the cell is forced to break down and recycle part of its own reserves, including pre-existing material such as proteins, lipids and carbohydrates, to meet demands for metabolic substrates and stay alive until the situation improves (Levine and Kroemer, 2008).

However, constitutive turnover of cytoplasmic material by basal autophagy, even during favorable growth conditions, is also essential for proper cell physiology (Yin et al., 2016). In this regard, cells employ several quality control mechanisms aimed at degrading and recycling intracellular proteins and components to maintain normal internal homeostasis and

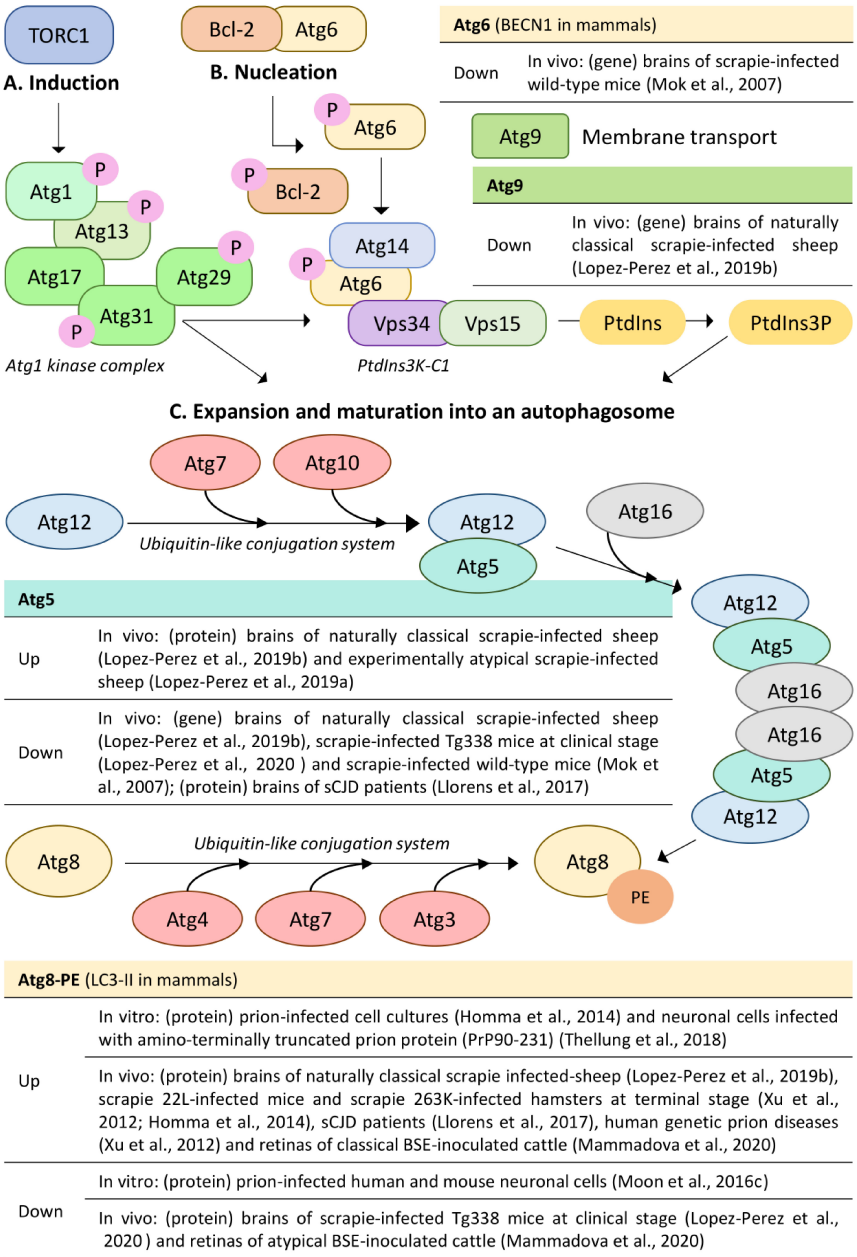

Atg6 (BECN1 in mammals)	
Down	In vivo: (gene) brains of scrapie-infected wild-type mice (Mok et al., 2007)

Atg9	Membrane transport

Atg9	
Down	In vivo: (gene) brains of naturally classical scrapie-infected sheep (Lopez-Perez et al., 2019b)

Atg5	
Up	In vivo: (protein) brains of naturally classical scrapie-infected sheep (Lopez-Perez et al., 2019b) and experimentally atypical scrapie-infected sheep (Lopez-Perez et al., 2019a)
Down	In vivo: (gene) brains of naturally classical scrapie-infected sheep (Lopez-Perez et al., 2019b), scrapie-infected Tg338 mice at clinical stage (Lopez-Perez et al., 2020) and scrapie-infected wild-type mice (Mok et al., 2007); (protein) brains of sCJD patients (Llorens et al., 2017)

Atg8-PE (LC3-II in mammals)	
Up	In vitro: (protein) prion-infected cell cultures (Homma et al., 2014) and neuronal cells infected with amino-terminally truncated prion protein (PrP90-231) (Thellung et al., 2018)
	In vivo: (protein) brains of naturally classical scrapie infected-sheep (Lopez-Perez et al., 2019b), scrapie 22L-infected mice and scrapie 263K-infected hamsters at terminal stage (Xu et al., 2012; Homma et al., 2014), sCJD patients (Llorens et al., 2017), human genetic prion diseases (Xu et al., 2012) and retinas of classical BSE-inoculated cattle (Mammadova et al., 2020)
Down	In vitro: (protein) prion-infected human and mouse neuronal cells (Moon et al., 2016c)
	In vivo: (protein) brains of scrapie-infected Tg338 mice at clinical stage (Lopez-Perez et al., 2020) and retinas of atypical BSE-inoculated cattle (Mammadova et al., 2020)

FIGURE 1 | Molecular mechanisms of the core autophagy machinery and alterations (up/down) of autophagy-related genes and proteins involved in autophagosome formation in prion disease models. Figure shows the molecular mechanisms of **(A)** induction, **(B)** nucleation of the phagophore, and **(C)** expansion and maturation into an autophagosome. The unified yeast nomenclature has been used for simplicity. P, phosphate; PtdIns3K-C1, phosphatidylinositol 3-kinase complex I; PtdIns, phosphatidylinositol; PtdIns3P, phosphatidylinositol 3-phospate; PE, phosphatidylethanolamine; sCJD, sporadic Creutzfeldt-Jakob disease; BSE, bovine spongiform encephalopathy. Based on (Ariosa and Klionsky, 2016).

preserve viability, which include the ubiquitin-proteasome system (UPS) and lysosomal routes such as the endocytic and autophagic pathways (Majeski and Dice, 2004). The UPS fundamentally breaks down short-lived proteins after they have executed their function in the cell (Hochstrasser, 1995), while autophagy is responsible for the degradation of long-lived proteins and whole organelles (Yoshimori, 2004). These proteolytic systems also confer a protective effect against misfolded or damaged proteins. Under normal conditions, cells efficiently control misfolded proteins by enzyme- and chaperone-mediated folding. However, when chaperone refolding fails, misfolded proteins are targeted for degradation through combined proteolytic activity of the UPS and autophagy, making interaction between these systems essential for protein quality control (Zheng et al., 2009). Existing data indicate that UPS inhibition by genetic

or pharmacological manipulation induces autophagy as a protective cell response (Pandey et al., 2007) and, conversely, inhibition of autophagy increases proteasomal activity (Zhu et al., 2007), suggesting that both systems act as compensatory mechanisms in protein quality control. There are several signaling proteins that connect the UPS with the autophagic pathway, including p62 protein, or sequestosome 1 (SQSTM1), a selective autophagy receptor that recognizes and shuttles ubiquitinated proteins to the autophagosomes for degradation (Bjorkoy et al., 2005, 2006). p62 can be degraded by autophagy, since the levels of this protein decrease after treatment with autophagy inducers such as rapamycin, but increase after autophagy inhibition (Bjorkoy et al., 2005; Yue, 2007). Therefore, p62 accumulation is considered a sign of autophagic malfunction (Bjorkoy et al., 2009).

While cytosolic components and organelles are directed to lysosomes for degradation via the autophagic pathway, extracellular material and membrane proteins are directed via the endocytic pathway, thus both autophagosomes and endosomes converge in the lysosome to deliver their cargo. However, in some situations, cells relieve intracellular stress conditions by selective secretion of deleterious or damaged material, such as proteins and RNA, to the extracellular environment through exosomes (Baixauli et al., 2014). These vesicles play a crucial role in intercellular communication and, in coordination with autophagy, are essential to maintain cell homeostasis, since modulation of autophagy allows regulation of exosome biogenesis and release (Fader and Colombo, 2006). Although autophagosomes generally fuse with lysosomes, they can also fuse with multivesicular bodies containing exosomes, forming a vesicle called amphisome which subsequently fuses with lysosomes (Hessvik and Llorente, 2018). Under induction of autophagy, the multivesicular bodies target the autophagic pathway, which restrains secretion of exosomes from the cell (Fader et al., 2008).

Autophagy is also involved in other physiological processes, such as cell remodeling during development, cell differentiation, innate and adaptive immunity, genomic stability, longevity, and cell death (Levine and Yuan, 2005; Lum et al., 2005; Maiuri et al., 2007; Yorimitsu and Klionsky, 2007; Levine and Kroemer, 2008; Mizushima et al., 2008). Through all these functions, autophagy protects the organism against diverse pathologies, and when it does not work correctly, promotes the development of these. Defective autophagy has been linked to a broad range of human and animal diseases, including cardiomyopathies, infections, cancer, and protein misfolding disorders that lead to neuronal, muscle and liver degeneration (Levine and Kroemer, 2008).

AUTOPHAGY IN NEURODEGENERATIVE DISEASES

Although autophagy physiologically occurs at basal level in cells, the demand for basal autophagy is tissue-specific. Those tissues whose cells do not divide after differentiation, such as neurons, myocytes or hepatocytes, are highly dependent on basal autophagy degradation, since they are predisposed to accumulation of misfolded proteins and damaged organelles that could be diluted through cell division (Komatsu et al., 2005, 2007; Hara et al., 2006; Komatsu et al., 2006; Nakai et al., 2007). In neurons, the efficient transport of proteins, organelles and autophagosomes at significant distances from the cell body through axons and dendrites (collectively known as neurites) could be altered by a defective autophagic mechanism, which would affect intercellular communication and, subsequently, contribute to neurite degeneration and neuronal cell death (Chu et al., 2009; Son et al., 2012). Additionally, neuronal autophagy has been implicated in regulation of neurite length, synapse growth and plasticity required for learning and memory (Son et al., 2012). Compared to other systems, the CNS displays low levels of autophagosomes under basal conditions and even during starvation, probably because neurons remove autophagosomes faster, or because they do not require a substantial level of autophagy due to their susceptibility to autophagic flux imbalance (Ariosa and Klionsky, 2016). The described evidence shows that basal autophagy plays a critical role in maintaining neuronal health and function, and is controlled more tightly in these cells than that of non-neuronal cells, since the intense sensitivity of the CNS to accumulation of protein aggregates and damaged organelles could easily lead to the development of neurodegenerative diseases, even in absence of expression of disease-associated mutant proteins (Frake et al., 2015; Kiriyama and Nochi, 2015).

A common feature of various neurodegenerative diseases is the intracellular accumulation of aggregates of toxic proteins that by some means escape the degradation process, which inevitable leads to dysfunction and neuronal death (Nixon, 2005; Shibata et al., 2006). The mere existence of these aggregates is a sign of malfunction of neuronal degradative mechanisms (Chu, 2011). Although most of these diseases are age-related, several *in vivo* studies have provided a direct correlation between defective autophagy and neurodegeneration. Neural-tissue deletion of *Atg* genes in mice results in accumulation of ubiquitin-positive protein aggregates in neurons, neurodegeneration, neuronal loss, progressive motor deficits and abnormal reflexes, which resemble the clinical and pathological characteristics of neurodegenerative diseases (Hara et al., 2006; Komatsu et al., 2006). Indeed, abnormal autophagic activity has frequently been observed in specific neuronal populations in Alzheimer's disease (AD), Parkinson's disease (PD), Huntington's disease (HD), and prion diseases (Boellaard et al., 1989, 1991; Ravikumar et al., 2002; Qin et al., 2003; Webb et al., 2003; Liberski et al., 2004; Sikorska et al., 2004; Iwata et al., 2005; Nixon et al., 2005; Rubinsztein et al., 2005; Berger et al., 2006; Mizushima and Hara, 2006; Ventruti and Cuervo, 2007).

Autophagic vacuoles are abundant in AD brains, mainly within dystrophic neurites, but also in the cell body of affected neurons (Nixon et al., 2005). Intracellular amyloid-β (Aβ) increases autophagic activity and, in turn, autophagic vacuoles may contribute to generate the pathogenic peptide, since they are a major reservoir of intracellular Aβ and the crucial elements for its formation (Yu et al., 2005;

Ling et al., 2009; Pajak et al., 2009a,b; Lipinski et al., 2010). In AD, retrograde transport of autophagosomes along microtubules and their maturation into autophagolysosomes are impaired, leading to ineffective degradation and excessive accumulation of immature autophagic vacuoles in degenerate neurites (Nixon, 2007; Boland et al., 2008). Increase or hyperphosphorylation of tau protein, which controls the stability of microtubules, may affect the activity of these tubular structures, disrupting neuronal functions of autophagic transport through neurites and synapses (Funderburk et al., 2010). In addition, the expression of ATG5, ATG12, LC3, and BECN1 decrease in AD brains as the disease progresses (Pickford et al., 2008; Ma et al., 2010). This combination of autophagy induction, defective maturation and clearance of Aβ-generating autophagosomes, and progressive reduction of key autophagy proteins, suggests an impairment of autophagic activity, which probably impedes the degradation of Aβ and creates the appropriate circumstances for its aggregation and accumulation in AD (Nixon, 2007; Boland et al., 2008; Jaeger et al., 2010).

Similarly, PD patients display characteristics of autophagy in degenerating neurons of the substantia nigra (Anglade et al., 1997). Inhibition of both CMA and macroautophagy leads to accumulation of α-synuclein (Webb et al., 2003; Cuervo et al., 2004; Vogiatzi et al., 2008), while autophagic activation through BECN1 stimulation reduces α-synuclein levels in the limbic system and improves synaptic and dendritic pathology (Spencer et al., 2009). In addition, overexpression of several familial PD-associated molecules, such as the wild-type form and the mutant forms of α-synuclein, disrupts the autophagic machinery, suggesting that autophagy may play a relevant role in the pathogenesis of PD (Cuervo et al., 2004; Xilouri et al., 2009; Winslow et al., 2010). Endosomal membranes and vacuoles with ultrastructural characteristics of autophagosomes are also increased in several experimental models of HD (Kegel et al., 2000). While wild-type huntingtin (HTT) regulates autophagy in response to ER stress, expression of its mutant form disrupts ER function and increases autophagic vacuoles (Atwal and Truant, 2008). In HD, autophagosomes form at normal rates and are adequately eliminated by lysosomes, but they fail to efficiently recognize and trap cytosolic cargo in their lumen, leading to mutant HTT accumulation in cells (Martinez-Vicente et al., 2010). Moreover, recruitment of BECN1 by accumulated mutant HTT and mutations that affect the dynein motor machinery also reduce autophagic clearance of the toxic protein (Ravikumar et al., 2005; Shibata et al., 2006).

All these observations have generated controversy regarding whether the increase of autophagosomes in degenerating neurons plays a protective homeostatic role, or instead contributes to pathogenic neuronal death (Son et al., 2012). Early studies showing accumulation of autophagosomes in brains affected with neurodegenerative diseases initially suggested that autophagy may contribute to the pathogenesis of these disorders (Levine and Kroemer, 2008). However, there is wide evidence that both Aβ peptide and the mutant forms of α-synuclein and HTT are substrates for autophagic degradation (Ravikumar et al., 2002; Webb et al., 2003; Shin et al., 2014). Induction of autophagy by pharmacological or genetic manipulation has beneficial effects and reduces the toxic protein levels in several models of neurodegenerative diseases, while its inhibition produces an opposite response (Rubinsztein et al., 2007). Therefore, the prevailing explanation is that autophagy protects against neurodegenerative diseases and the accumulation of autophagosomes produced by the expression of mutant proteins primarily represents an attempt to eliminate those proteins from the cell (Levine and Kroemer, 2008). The development of the disease implies that autophagy may reach a saturation point in which its capacity to degrade aggregated mutant proteins is exceeded, or that there are defects in the autophagic pathway produced by the same pathological factors that trigger the disease (Levine and Kroemer, 2008). In either case, impairment of autophagy likely contributes to accumulation of damaged organelles and toxic proteins, leading to the neurodegenerative conditions observed in these diseases (Son et al., 2012).

AUTOPHAGY IN PRION DISEASES

Until three decades ago, data on autophagy in TSE were very limited and consisted mostly of ultrastructural studies of electron microscopy. Autophagic vacuoles in prion diseases were first described by Boellard et al. in experimental models of CJD and scrapie in mice and hamsters (Boellaard et al., 1989, 1991). Thereafter, the presence of multivesicular bodies and autophagic vacuoles was also observed in prion-infected neuronal cell cultures that displayed characteristics of neurodegeneration (Schatzl et al., 1997). Numerous large multivesicular bodies, autophagolysosomes and autophagosomes at different stages of formation have subsequently been described in neuronal cell bodies, dystrophic neurites and synapsis in brain biopsies from patients with various forms of human prion disease and in experimentally induced scrapie, CJD and GSS (Liberski et al., 2004, 2011; Sikorska et al., 2004). These findings suggest a crucial role for autophagy in TSE, which encouraged many researchers to analyze in detail this process in prion infection-related conditions. However, up to date, the role of autophagy in prion diseases is still controversial. Authors have used different approaches to quantify or monitor autophagy. Results are different *in vitro* and *in vivo* and, even in the same species, regulation can be dissimilar in different anatomical areas of the CNS. We will try to identify and discuss hereafter the origin of these discrepancies to get a global vision of autophagy studies in prion diseases.

Is the Cellular Prion Protein Involved in Autophagy Regulation?

Although a functional role for PrP^c in modulating the autophagic pathway has been suggested (Shin et al., 2013), PrP^c deficiency does not affect basal autophagy flux of *Prnp*-knockout mice hippocampal neurons under normal culture conditions. However, under stress conditions such as serum deprivation, these cells show higher levels of LC3-II than neurons of wild-type mice (Oh et al., 2008). It was subsequently reported that autophagy regulation by PrP^c might be related to its known protective role against oxidative stress as the deficiency of PrP^c

impair autophagy flux via hydrogen peroxide (H_2O_2)-induced oxidative stress (Oh et al., 2012), and that PrP^c expression increases autophagic activity through modulation of alpha7 nicotinic acetylcholine receptor (α7nAchR) to protect neurons against PrP106-126 toxicity (Jeong and Park, 2015). Thus, PrP^c seems to regulate autophagy only under stress conditions. Similar properties have been attributed to HTT regulating autophagy in response to ER stress (Atwal and Truant, 2008).

Dysregulation of Autophagy in Prion Diseases

Expression studies of genes and proteins involved in the autophagic pathway have been performed in order to decipher the implication of autophagy in the neuropathology associated to TSE. Thus, the expression levels of several of these molecules are altered in several prion disease models both *in vivo* and *in vitro* (**Figure 1** and **Table 1**). However, reported changes and their interpretation are different, and even contradictory, depending on the experimental model used.

Downregulation of mRNA transcripts of positive gene regulators of autophagy such as *BECN1*, *ATG5*, *ATG9*, *FBXW7* (F-box and WD repeat domain containing 7) and *GAS5* (growth arrest-specific 5) has been observed in the CNS of scrapie-infected wild-type or transgenic mice and sheep naturally affected with classical scrapie (Mok et al., 2007; Lopez-Perez et al., 2019b, 2020). These changes were associated with an impairment of autophagy at late stages of the disease, as only animals displaying clinical signs showed altered expression profiles. On the contrary, the encoded protein of *FBXW7* is upregulated at the early stage of infection in the scrapie murine brain cell line SMB-S15 and in brains of scrapie-agent 263K-infected hamsters, leading to degradation of mTORC1 and increase of autophagic flux (Xu et al., 2016). In these cells, knockdown of *ATG5* and *FBXW7* inhibited autophagic flux and increased PrP^{Sc} accumulation. Both *in vivo* and *in vitro* models suggest that downregulation of autophagy regulator genes could inhibit the process and favor/stimulate prion accumulation.

However, studies analyzing other molecular pathways related to autophagy report an increase of autophagy activity at late stages of the disease. For example, mitochondrial dysfunction is a common and prominent feature of prion diseases (Zhu et al., 2018). Mitophagy, which is the specific autophagic elimination of defective mitochondria, is activated in prion-infected SMB-S15 cells and in mice infected with scrapie strains 139A and ME7 at the terminal stage of the disease, represented by the transcriptional and protein increase of the two essential elements regulating mitophagy activity: PINK1 (PTEN-induced kinase 1) and Parkin (Gao et al., 2020). Transcripts of *SCRG1* (scrapie-responsive gene 1), whose encoded protein has been linked to the presence of autophagic vacuoles in neurons of scrapie-infected mice at terminal stage, are also enhanced in sporadic CJD (sCJD) and murine models of scrapie and BSE (Dandoy-Dron et al., 1998, 2000; Dron et al., 1998, 2005, 2006). Similarly, autophagy activator genes *HSPA8* [heat shock protein family A (Hsp70) member 8] and *HSPB8* [heat shock protein family B (small) member 8] are upregulated in the CNS of sCJD-infected Tg340-*PRNP*129MM mice at clinical stage, sCJD patients (Llorens et al., 2017), and naturally scrapie-infected sheep (Serrano et al., 2011). Upregulation of these genes involved in autophagy regulation may reflect an attempt of the cell to induce autophagy, although over time, this process may become impaired, resulting in the accumulation of autophagic vacuoles as observed in other neurodegenerative diseases (Polajnar and Zerovnik, 2014).

Nevertheless, drawing conclusions from expression changes of genes involved in the complex autophagy machinery is complicated. Universal autophagy markers could help in this analysis. The study of p62 protein, in combination with other assays such as the monitoring of LC3-II conversion, is widely used to evaluate autophagic activity (Klionsky et al., 2016; Zhang et al., 2016). Downregulation of the amount of both LC3-II and p62 in human and mouse neuronal cells infected with human prions was related to an activation of the autophagic flux in response to prion infection (Moon et al., 2016c). Interestingly, overexpression of LC3-II and p62 in prion-infected cell cultures and in brains of 263K-infected hamsters and 22L-infected mice was also associated with an activation of autophagy to promote PrP^{Sc} degradation (Homma et al., 2014). Similarly, the increment of these proteins was also observed in neuronal cells treated with amino-terminally truncated prion protein (PrP90-231), which suggested that PrP stimulates autophagic flux but leads progressively to the accumulation of autophagolysosomes with impaired resolution ability (Thellung et al., 2018). The opposite results about LC3/p62 regulation could be the consequence of analyzing different points of autophagy kinetics, or maybe TSE models are reacting differently to different prion strains. In addition, most of these studies were performed using neuronal cells and very few have focused on analyzing autophagic changes in glial cells. In fact, astrocyte reactivity resulting from activation of the unfolded protein response has been shown to be crucial in mediating prion neuropathology (Smith et al., 2020). We observed p62 immunolabeling in both neuronal and glial cells in scrapie-infected sheep and mice (Lopez-Perez et al., 2019b, 2020), but more studies including these cell populations are needed in order to deciphering the biological relevance of these findings.

Murine models allow the investigation of preclinical stages of the disease. Using mice overexpressing the highly sensitive VRQ/VRQ variant of the ovine *PRNP* gene, we described a downregulation of LC3 and upregulation of p62 in highly prion-affected brain areas of scrapie-infected Tg338 mice at clinical stage (Lopez-Perez et al., 2020). The absence of changes in scrapie-infected mice at preclinical stage indicates that impairment of autophagy takes place at the last stage of prion infection and is not the result of depletion or exhaustion of the autophagic machinery. In accordance to this hypothesis, the expression of autophagy related genes was neither altered at early stages of the disease. However, these results differ from those observed in other murine models. Conversion of LC3-I into LC3-II and downregulation of p62 have been reported in the terminal stage of scrapie 263K-infected hamsters (Xu et al., 2012). Changes reported in hamsters were similar to those observed in patients with genetic prion diseases (Xu et al., 2012). As PrP^c

TABLE 1 | Alterations (up/down) of autophagy-related genes and proteins not involved in autophagosome formation in prion disease models.

Molecule	Regulation	Prion disease model	References
p62	Up	*In vitro*: (protein) prion-infected cell cultures and neuronal cells infected with amino-terminally truncated prion protein (PrP90-231)	Homma et al., 2014; Thellung et al., 2018
		In vivo: (protein) brains of naturally classical scrapie-infected sheep, experimentally atypical scrapie-infected sheep, scrapie-infected Tg338 mice at clinical stage, scrapie 22L-infected mice and scrapie 263K-infected hamsters	Homma et al., 2014; Lopez-Perez et al., 2019a,b, 2020
	Down	*In vitro*: (protein) prion-infected human and mouse neuronal cells	Moon et al., 2016c
		In vivo: (protein) brains of scrapie 263K-infected hamsters at terminal stage and human genetic prion diseases	Xu et al., 2012
FBXW7	Up	*In vitro*: (protein) prion-infected SMB-S15 cells at early stage	Xu et al., 2016
		In vivo: (protein) brains of scrapie 263K-infected hamsters	Xu et al., 2016
	Down	*In vivo*: (gene) brains of scrapie-infected Tg338 mice at clinical stage	Lopez-Perez et al., 2020
GAS5	Down	*In vivo*: (gene) brains of scrapie-infected Tg338 mice at clinical stage	Lopez-Perez et al., 2020
SCRG1	Up	*In vivo*: (gene) brains of scrapie- and BSE-infected mice and sCJD patients; (protein) brains of scrapie-infected mice at terminal stage	Dandoy-Dron et al., 1998, 2000; Dron et al., 1998, 2005, 2006
HSPA8, HSPB8	Up	*In vivo*: (gene) brains of sCJD-infected Tg340 mice at clinical stage, sCJD patients and naturally classical scrapie-infected sheep	Serrano et al., 2011; Llorens et al., 2017
PINK1, Parkin	Up	*In vitro*: (gene and protein) prion-infected SMB-S15 cells	Gao et al., 2020
		In vivo: (protein) brains of scrapie 139A- and ME7-infected mice at terminal stage	

BSE, bovine spongiform encephalopathy; sCJD, sporadic Creutzfeldt-Jakob disease.

seems to have a role in autophagy regulation under stress conditions, overexpression of PrP^{c} in transgenic mice could alter the response.

Models can react differently to prion infection, but could autophagy also be regulated differently depending on the prion strain? Analyzing the CNS of sheep naturally infected with classical scrapie at clinical stage, we observed changes compatible with induction of autophagy in brain regions with low levels of prion-related lesions, such as basal ganglia and cerebellar Purkinje cells, which displayed an upregulation of both p62 and LC3 proteins (Lopez-Perez et al., 2019b). In these animals, p62 was overexpressed in most of the CNS areas. However, in brains from sheep experimentally infected with atypical scrapie at clinical stage, LC3 levels did not change and p62 was only increased in the areas most affected by prion toxicity (Lopez-Perez et al., 2019a). In addition, p62 positively correlated both with histopathological lesions and PrP^{Sc} deposits in the latter model. Considering the accumulation of p62 as a marker for autophagy malfunction, these results indicate that impairment of autophagy is limited to brain areas displaying high levels of prion-related lesions in atypical scrapie, unlike the classical form of the disease where this impairment seems to occur along the brain. The differences observed between the two forms of scrapie could reflect differences in the toxicity of both prions, as atypical scrapie displays longer incubation periods than the classical form. In line with these findings, a recent study reported that strain-dependent incubation period is negatively correlated with PrP^{Sc} deposition and neuroinflammation, but positively with autophagy (Mammadova et al., 2020). Retinas from cattle inoculated with classical BSE displayed an upregulation of autophagy indicated by the increase of LC3-II, whereas those inoculated with atypical BSE displayed a downregulation, which suggests that autophagic dysfunction contributes to increased PrP^{Sc} accumulation in atypical BSE, leading to greater neuroinflammation, shorter incubation periods and, therefore, an accelerated disease progression when compared to classical BSE.

Autophagic impairment has also been suggested in sCJD cases, where LC3-II and DJ-1 (protein deglycase DJ-1) proteins are overexpressed, while ATG5 is downregulated and LAMP2 (lysosome-associated membrane protein 2) is unaltered (Llorens et al., 2017). These alterations, along with the accumulation of autophagic vacuoles, abnormal lysosomes and autophagolysosomes observed in neurons of sCJD patients, suggest that, although autophagy mechanisms may be activated in sCJD, this process is not fully functional. Therefore, autophagic impairment does occur in prion diseases. Despite the discrepancies observed between the different TSE models, most of the reported results suggest a dysfunction of autophagy at the last stage of the disease, although it is still unknown whether such dysregulation is cause or consequence of prion toxicity.

Autophagy in Prion Neuropathology

Despite the numerous studies reporting an abnormal autophagic activity, the biological role of this process in prion diseases, as in most neurodegenerative diseases, is currently unclear. Initially, it was suggested its participation in prion neuropathology by contributing to formation of spongiform changes (Liberski et al., 2002, 2004, 2008, 2011). Although the histogenesis of typical TSE vacuoles has yet to be explained, it has been proposed that vacuolization is by some means related to tissue destruction by autophagy, thus these vacuoles may

originate abruptly from autophagic vacuoles with no detectable transition stages (Liberski et al., 2008, 2011). Excessive PrP^{Sc} accumulation could lead to overload of the catabolic machinery, phagocytosis of neuronal cytoplasm and, finally, massive elimination of damaged neurons by autophagy (Jeffrey et al., 1992). The pathogenesis of dystrophic neurites, another constant neurodegenerative alteration in TSE, is also unclear. It has been suggested that autophagic vacuoles originate in the neuronal cell body, flow down with axonal transport along the neurites, and then, in the presence of an impairment of that transport, are accumulated forming dystrophic neurites (Liberski et al., 2011; Liberski, 2019), a reasoning which resembles that described in AD (Nixon, 2007; Boland et al., 2008).

Autophagy could also be a positive factor for prion propagation. A moderate basal level of autophagy may promote prion spreading during certain stages of infection by generating smaller PrP^{Sc} seeds (Heiseke et al., 2010), which are more efficient templates for the conversion of PrP^{c} into PrP^{Sc} than larger aggregates (Silveira et al., 2005). In addition, proteasome impairment in prion-infected neuronal cells results in formation of large cytosolic perinuclear aggresomes containing PrP^{Sc} (Kristiansen et al., 2005). Similar structures were found in brains of prion-infected mice. PrP^{Sc} aggresomes may generate prion seeds (Cohen and Taraboulos, 2003), trigger autophagy (Kopito, 2000; Garcia-Mata et al., 2002) and, in turn, be sequestered by autophagosomes that fuse with lysosomes containing PrP^{Sc}, where the nucleation process of forming more PrP^{Sc} can be initiated or perpetuated (Liberski et al., 2008).

In contrast to this disease-promoting role, it is also likely that the increment of autophagic vacuoles observed in prion disease models is due to the activation of the autophagic machinery as a defense mechanism that reflects the effort of neurons to survive in the harmful environment produced by PrP^{Sc} accumulation, leading even to degradation of prions (Heiseke et al., 2010). PrP^{c} is a plasma membrane-anchored glycoprotein that cycles between the cell surface and intracellularly via endosomal vesicles (Vey et al., 1996; Peters et al., 2003). After internalization, PrP^{c} traffics to early endosomes where it is directed to recycling endosomes to be returned to the plasma membrane or to multivesicular bodies to be degraded by lysosomes (Campana et al., 2005). PrP^{Sc} also appears to traffic along the same endo-lysosomal pathway (Yim et al., 2015). There are two main PrP^{Sc} populations within the infected cell: a population on the cell surface consisting of newly formed PrP^{Sc}, which is highly labile, metabolizes rapidly and is a substrate for non-autophagic lysosomal degradation (Caughey and Raymond, 1991; Goold et al., 2013), and an internalized population comprising most of total cellular PrP^{Sc}, which is more aggregated, is relatively stable and is subject to autophagic and proteasomal degradation (Boellaard et al., 1991; Caughey and Raymond, 1991; Heiseke et al., 2010; Goold et al., 2013; Yao et al., 2013). While implicated in the clearance of disease-associated proteins, including PrP^{Sc}, degradation by the UPS may be restricted to soluble misfolded proteins or smaller oligomeric forms (Li et al., 2010; Goold et al., 2013, 2015; Bhat et al., 2014). For larger, more insoluble aggregates, the catalytic chamber of the proteasome may remain inaccessible, preventing their effective degradation (Qin et al., 2003; Scotter et al., 2014). In fact, PrP^{Sc} does not seem to be ubiquitinated to a significant degree and its status as a proteasome substrate remains controversial (Goold et al., 2015). Several studies have shown that prion infection inhibits UPS activity, likely by direct interaction between PrP^{Sc} and the 20 S proteasome core particle (Kristiansen et al., 2007; Deriziotis et al., 2011; McKinnon et al., 2016). In the context of UPS impairment, an upregulation of autophagy has been described, which may facilitate the clearance of larger aggregates (Korolchuk et al., 2010; Goold et al., 2015). Indeed, PrP^{Sc} colocalizes with lysosomal markers *in vivo* (Dearmond and Bajsarowicz, 2010) and, despite PrP^{Sc} deposits do not colocalize with autophagosomes in brains of scrapie infected hamsters, they do colocalize in prion-infected SMB-S15 cells after treatment with bafilomycin A_1 (Xu et al., 2012). In addition, although the more usual places of PrP^{Sc} accumulation are the plasma membrane and the endosomal vesicles (Mays and Soto, 2016), and the majority of intracellular PrP^{Sc} is found within the endo-lysosomal system (Goold et al., 2015), some PrP misfolded forms harboring similarities with infectious PrP^{Sc} also appear to be present at the ER and cytosol (Mays and Soto, 2016). Since the ER lumen lacks degradation machinery, misfolded proteins are retro-translocated to the cytosol for degradation and, eventually, irreversibly aggregated ER proteins are targeted for lysosomal degradation via autophagic pathways (Goold et al., 2015). Hence, it is assumed that autophagy may be used by the cell to control or counteract prion infection providing a neuroprotective effect, while lysosomal dysfunction in combination with reduced autophagy may contribute to the development of the disease (Mok et al., 2007; Yao et al., 2013).

Autophagy in the Treatment of Prion Diseases

At present there are no effective therapeutic or prophylactic treatments for prion diseases, nor any useful drugs are available. Existing data indicate that neurons do not recover cell homeostasis after exposure to PrP^{Sc}, which eventually leads to cell damage and neuronal cell death (Mays and Soto, 2016). Considering the complex pathogenesis of TSE, with many factors contributing to toxicity (Aguzzi and Falsig, 2012), treatments aimed at the basic toxic cause, that is, PrP^{Sc} accumulation, should be effective in improving all aspects of toxicity (Goold et al., 2015). There is wide experimental evidence that induction of autophagy by chemical compounds has beneficial effects and results in decreased PrP^{Sc} both *in vitro* and *in vivo*, indicating that the stimulation of this degradative pathway is sufficient to overcome the apparent stability of internal PrP^{Sc} levels, whereas inhibition of the process by pharmacological blocking or gene silencing leads to prion accumulation (Heiseke et al., 2010; Goold et al., 2015; Abdelaziz et al., 2019).

Imatinib increases lysosomal clearance of PrP^{Sc} in cultured prion-infected cells by activating the autophagic machinery (Ertmer et al., 2004, 2007). Both lithium and trehalose also

improve PrP^{Sc} clearance in prion-infected neuroblastoma and neuronal cells, respectively, by inducing autophagy (Aguib et al., 2009; Heiseke et al., 2009). Treatment with lithium not only decreases PrP^{Sc} levels, but also those of PrP^{c}, which indirectly contributes to PrP^{Sc} reduction by limiting the amount of substrate available for prion conversion (Heiseke et al., 2010). Both rapamycin and metformin, which are known to inhibit mTORC1 signaling, also decrease the PrP^{Sc} load in prion-infected neuroblastoma and neuronal cells, respectively, by enhancing autophagy, suggesting that both mTORC1-dependent and independent autophagy induction pathways are involved in prion degradation (Heiseke et al., 2009; Ishibashi et al., 2015; Abdelaziz et al., 2020). In addition, both PrP^{c} and PrP^{Sc} are actively released into the extracellular environment in association with exosomes, contributing to the spread of prion infectivity between cells (Fevrier et al., 2004). Autophagy stimulation with rapamycin strongly inhibits exosomal prion release and hence the intercellular prion dissemination, while its inhibition promotes the release of exosomes and exosome-associated prions (Abdulrahman et al., 2018). Natural compounds such as hinokitiol and Ginsenoside-RG3, and other chemical compounds such as AR-12, spermine, resveratrol, FK506 and astemizole, also have anti-prion effects *in vitro* by induction of autophagy (Jeong et al., 2012; Karapetyan et al., 2013; Nakagaki et al., 2013; Moon et al., 2016a,b; Wang et al., 2016; Abdulrahman et al., 2017; Phadwal et al., 2018).

Some of these treatments are effective also *in vivo* both in terms of PrP^{Sc} reduction and beneficial clinical effects. Intraperitoneal or oral application of trehalose, rapamycin, imatinib, astemizole, AR-12 or FK506 to prion-infected mice during the early stage of infection produces anti-prion effects, such as extension of incubation period and survival time, and delay of PrP^{Sc} neuroinvasion and the onset of clinical signs, by induction of autophagosome formation and autophagy (Yun et al., 2007; Aguib et al., 2009; Heiseke et al., 2009; Cortes et al., 2012; Karapetyan et al., 2013; Nakagaki et al., 2013; Abdelaziz et al., 2019). However, the administration of some of these drugs when neuroinvasion has already accomplished does not cause an evident clearance of PrP^{Sc} in the CNS, probably because they do not efficiently cross the blood-brain barrier or because their effective pharmacological concentrations *in vivo* need to be higher (Yun et al., 2007; Heiseke et al., 2010; Goold et al., 2015).

The molecular mechanisms that explain how autophagy protects against neurodegeneration have not yet been determined, although there are several hypotheses. In addition to reducing the basic toxic protein that causes the disease, autophagy has been proposed to eliminate damaged organelles, such as the mitochondria, and attenuate the apoptotic response to various forms of stress (Ravikumar et al., 2006; Zhu et al., 2007). In general, it is reasonable to assume that reducing PrP^{Sc} accumulation by stimulating autophagy could represent an effective therapeutic strategy for prion diseases in the near future, but additional and more complex studies are necessary.

CONCLUSION

Although it is unknown whether the accumulation of autophagic vacuoles in the CNS of several neurodegenerative diseases reflects a proper response to deposition of misfolded proteins or an impaired autophagosome clearance, there is direct evidence indicating a decrease of autophagic activity or a deterioration of the lysosomal degradation process. Dysregulation of autophagy-related genes and proteins in various TSE models, along with the abnormal accumulation of autophagic vacuoles, fully supports the impairment of autophagy in prion diseases, which will probably impede the clearance of protein aggregates and damaged organelles from neurons and will contribute to prion replication, neurodegeneration, and the development of the disease. Altogether, research performed in this subject indicates that autophagy is involved in prion neuropathology *in vivo* and may be a potential target for therapeutic intervention. Unfortunately, the analysis of autophagy in TSE is currently incomplete. At the level of the whole organism, the therapeutic effectiveness of manipulating autophagy may depend on particular complex factors of the disease. More research involving appropriate experimental *in vivo* models, late preclinical animals, and different prion strains, will be necessary to earn more detailed information on the molecular mechanisms underlying autophagic impairment in prion diseases. Other challenges include clarifying whether dysregulated autophagy is a prerequisite or consequence of prion-induced toxicity, or whether increased autophagy may have deleterious effects. It is important to keep in mind that a certain level of autophagy may be a positive modifier of prion infection and susceptibility, so it cannot be ruled out that autophagy plays a dual role combining pro- and anti-prion effects. A better understanding of the role of autophagy in the specific conditions of prion infection and its consequences for neurodegeneration will benefit the development of innovative and effective therapeutic strategies based on the manipulation of this process.

AUTHOR CONTRIBUTIONS

ÓL-P collected the literature and drafted the original manuscript. RB, FL, and IM-B conceptualized, designed the study, and revised the content of the manuscript. JB and IF revised the manuscript critically for intellectual content. All authors read and approved the final version of the manuscript for publication.

FUNDING

This study has been funded by the Instituto Carlos III grant PI19/00144 to FL and also by the project EFA148/16 REDPRION, 65% subsidized by the Fondo Europeo de Desarrollo Regional (FEDER) through the Interreg V-A España-Francia-Andorra (POCTEFA 2014-2020) program.

REFERENCES

Abdelaziz, D. H., Abdulrahman, B. A., Gilch, S., and Schatzl, H. M. (2019). Autophagy pathways in the treatment of prion diseases. *Curr. Opin. Pharmacol.* 44, 46–52. doi: 10.1016/j.coph.2019.04.013

Abdelaziz, D. H., Thapa, S., Abdulrahman, B., Vankuppeveld, L., and Schatzl, H. M. (2020). Metformin reduces prion infection in neuronal cells by enhancing autophagy. *Biochem. Biophys. Res. Commun.* 523, 423–428. doi: 10.1016/j.bbrc.2019.12.074

Abdulrahman, B. A., Abdelaziz, D., Thapa, S., Lu, L., Jain, S., Gilch, S., et al. (2017). The celecoxib derivatives AR-12 and AR-14 induce autophagy and clear prion-infected cells from prions. *Sci. Rep.* 7:17565. doi: 10.1038/s41598-017-17770-8

Abdulrahman, B. A., Abdelaziz, D. H., and Schatzl, H. M. (2018). Autophagy regulates exosomal release of prions in neuronal cells. *J. Biol. Chem.* 293, 8956–8968. doi: 10.1074/jbc.RA117.000713

Aguib, Y., Heiseke, A., Gilch, S., Riemer, C., Baier, M., Schatzl, H. M., et al. (2009). Autophagy induction by trehalose counteracts cellular prion infection. *Autophagy* 5, 361–369. doi: 10.4161/auto.5.3.7662

Aguzzi, A., and Falsig, J. (2012). Prion propagation, toxicity and degradation. *Nat. Neurosci.* 15, 936–939. doi: 10.1038/nn.3120

Anglade, P., Vyas, S., Javoy-Agid, F., Herrero, M. T., Michel, P. P., Marquez, J., et al. (1997). Apoptosis and autophagy in nigral neurons of patients with Parkinson's disease. *Histol. Histopathol.* 12, 25–31.

Ariosa, A. R., and Klionsky, D. J. (2016). Autophagy core machinery: overcoming spatial barriers in neurons. *J. Mol. Med.* 94, 1217–1227. doi: 10.1007/s00109-016-1461-9

Atwal, R. S., and Truant, R. (2008). A stress sensitive ER membrane-association domain in Huntingtin protein defines a potential role for Huntingtin in the regulation of autophagy. *Autophagy* 4, 91–93. doi: 10.4161/auto.5201

Baixauli, F., Lopez-Otin, C., and Mittelbrunn, M. (2014). Exosomes and autophagy: coordinated mechanisms for the maintenance of cellular fitness. *Front. Immunol.* 5:403. doi: 10.3389/fimmu.2014.00403

Bednarczyk, M., Zmarzly, N., Grabarek, B., Mazurek, U., and Muc-Wierzgon, M. (2018). Genes involved in the regulation of different types of autophagy and their participation in cancer pathogenesis. *Oncotarget* 9, 34413–34428. doi: 10.18632/oncotarget.26126

Berger, Z., Ravikumar, B., Menzies, F. M., Oroz, L. G., Underwood, B. R., Pangalos, M. N., et al. (2006). Rapamycin alleviates toxicity of different aggregate-prone proteins. *Hum. Mol. Genet.* 15, 433–442. doi: 10.1093/hmg/ddi458

Bhat, K. P., Yan, S., Wang, C. E., Li, S., and Li, X. J. (2014). Differential ubiquitination and degradation of huntingtin fragments modulated by ubiquitin-protein ligase E3A. *Proc. Natl. Acad. Sci. U.S.A.* 111, 5706–5711. doi: 10.1073/pnas.1402215111

Birgisdottir, A. B., Mouilleron, S., Bhujabal, Z., Wirth, M., Sjottem, E., Evjen, G., et al. (2019). Members of the autophagy class III phosphatidylinositol 3-kinase complex I interact with GABARAP and GABARAPL1 via LIR motifs. *Autophagy* 15, 1333–1355. doi: 10.1080/15548627.2019.1581009

Bjorkoy, G., Lamark, T., Brech, A., Outzen, H., Perander, M., Overvatn, A., et al. (2005). p62/SQSTM1 forms protein aggregates degraded by autophagy and has a protective effect on huntingtin-induced cell death. *J. Cell Biol.* 171, 603–614. doi: 10.1083/jcb.200507002

Bjorkoy, G., Lamark, T., and Johansen, T. (2006). p62/SQSTM1: a missing link between protein aggregates and the autophagy machinery. *Autophagy* 2, 138–139. doi: 10.4161/auto.2.2.2405

Bjorkoy, G., Lamark, T., Pankiv, S., Overvatn, A., Brech, A., and Johansen, T. (2009). Monitoring autophagic degradation of p62/SQSTM1. *Methods Enzymol.* 452, 181–197. doi: 10.1016/S0076-6879(08)03612-4

Boellaard, J. W., Kao, M., Schlote, W., and Diringer, H. (1991). Neuronal autophagy in experimental scrapie. *Acta Neuropathol.* 82, 225–228. doi: 10.1007/bf00294449

Boellaard, J. W., Schlote, W., and Tateishi, J. (1989). Neuronal autophagy in experimental Creutzfeldt-Jakob's disease. *Acta Neuropathol.* 78, 410–418. doi: 10.1007/bf00688178

Boland, B., Kumar, A., Lee, S., Platt, F. M., Wegiel, J., Yu, W. H., et al. (2008). Autophagy induction and autophagosome clearance in neurons: relationship to autophagic pathology in Alzheimer's disease. *J. Neurosci.* 28, 6926–6937. doi: 10.1523/JNEUROSCI.0800-08.2008

Bursch, W., and Ellinger, A. (2005). Autophagy–a basic mechanism and a potential role for neurodegeneration. *Folia Neuropathol.* 43, 297–310.

Campana, V., Sarnataro, D., and Zurzolo, C. (2005). The highways and byways of prion protein trafficking. *Trends Cell Biol.* 15, 102–111. doi: 10.1016/j.tcb.2004.12.002

Caughey, B., and Raymond, G. J. (1991). The scrapie-associated form of PrP is made from a cell surface precursor that is both protease- and phospholipase-sensitive. *J. Biol. Chem.* 266, 18217–18223.

Chu, C. T. (2011). Autophagy in different flavors: dysregulated protein degradation in neurological diseases. *Neurobiol. Dis.* 43, 1–3. doi: 10.1016/j.nbd.2011.03.020

Chu, C. T., Plowey, E. D., Dagda, R. K., Hickey, R. W., Cherra, S. J. III, and Clark, R. S. (2009). Autophagy in neurite injury and neurodegeneration: *in vitro* and *in vivo* models. *Methods Enzymol.* 453, 217–249. doi: 10.1016/S0076-6879(08)04011-1

Cohen, E., and Taraboulos, A. (2003). Scrapie-like prion protein accumulates in aggresomes of cyclosporin A-treated cells. *EMBO J.* 22, 404–417. doi: 10.1093/emboj/cdg045

Cortes, C. J., Qin, K., Cook, J., Solanki, A., and Mastrianni, J. A. (2012). Rapamycin delays disease onset and prevents PrP plaque deposition in a mouse model of Gerstmann-Straussler-Scheinker disease. *J. Neurosci.* 32, 12396–12405. doi: 10.1523/JNEUROSCI.6189-11.2012

Cuervo, A. M., Stefanis, L., Fredenburg, R., Lansbury, P. T., and Sulzer, D. (2004). Impaired degradation of mutant alpha-synuclein by chaperone-mediated autophagy. *Science* 305, 1292–1295. doi: 10.1126/science.1101738

Dandoy-Dron, F., Benboudjema, L., Guillo, F., Jaegly, A., Jasmin, C., Dormont, D., et al. (2000). Enhanced levels of scrapie responsive gene mRNA in BSE-infected mouse brain. *Brain Res. Mol. Brain Res.* 76, 173–179. doi: 10.1016/s0169-328x(00)00028-0

Dandoy-Dron, F., Guillo, F., Benboudjema, L., Deslys, J. P., Lasmezas, C., Dormont, D., et al. (1998). Gene expression in scrapie. Cloning of a new scrapie-responsive gene and the identification of increased levels of seven other mRNA transcripts. *J. Biol. Chem.* 273, 7691–7697. doi: 10.1074/jbc.273.13.7691

Dearmond, S. J., and Bajsarowicz, K. (2010). PrPSc accumulation in neuronal plasma membranes links Notch-1 activation to dendritic degeneration in prion diseases. *Mol. Neurodegener.* 5:6. doi: 10.1186/1750-1326-5-6

Deriziotis, P., Andre, R., Smith, D. M., Goold, R., Kinghorn, K. J., Kristiansen, M., et al. (2011). Misfolded PrP impairs the UPS by interaction with the 20S proteasome and inhibition of substrate entry. *EMBO J.* 30, 3065–3077. doi: 10.1038/emboj.2011.224

Dron, M., Bailly, Y., Beringue, V., Haeberle, A. M., Griffond, B., Risold, P. Y., et al. (2005). Scrg1 is induced in TSE and brain injuries, and associated with autophagy. *Eur. J. Neurosci.* 22, 133–146. doi: 10.1111/j.1460-9568.2005.04172.x

Dron, M., Bailly, Y., Beringue, V., Haeberlé, A. M., Griffond, B., Risold, P. Y., et al. (2006). SCRG1, a potential marker of autophagy in transmissible spongiform encephalopathies. *Autophagy* 2, 58–60. doi: 10.4161/auto.2228

Dron, M., Dandoy-Dron, F., Guillo, F., Benboudjema, L., Hauw, J. J., Lebon, P., et al. (1998). Characterization of the human analogue of a Scrapie-responsive gene. *J. Biol. Chem.* 273, 18015–18018. doi: 10.1074/jbc.273.29.18015

Ertmer, A., Gilch, S., Yun, S. W., Flechsig, E., Klebl, B., Stein-Gerlach, M., et al. (2004). The tyrosine kinase inhibitor STI571 induces cellular clearance of PrPSc in prion-infected cells. *J. Biol. Chem.* 279, 41918–41927. doi: 10.1074/jbc.M405652200

Ertmer, A., Huber, V., Gilch, S., Yoshimori, T., Erfle, V., Duyster, J., et al. (2007). The anticancer drug imatinib induces cellular autophagy. *Leukemia* 21, 936–942. doi: 10.1038/sj.leu.2404606

Fader, C. M., and Colombo, M. I. (2006). Multivesicular bodies and autophagy in erythrocyte maturation. *Autophagy* 2, 122–125. doi: 10.4161/auto.2.2.2350

Fader, C. M., Sanchez, D., Furlan, M., and Colombo, M. I. (2008). Induction of autophagy promotes fusion of multivesicular bodies with autophagic vacuoles in k562 cells. *Traffic* 9, 230–250. doi: 10.1111/j.1600-0854.2007.00677.x

Feng, Y., He, D., Yao, Z., and Klionsky, D. J. (2014). The machinery of macroautophagy. *Cell Res.* 24, 24–41. doi: 10.1038/cr.2013.168

Fevrier, B., Vilette, D., Archer, F., Loew, D., Faigle, W., Vidal, M., et al. (2004). Cells release prions in association with exosomes. *Proc. Natl. Acad. Sci. U.S.A.* 101, 9683–9688. doi: 10.1073/pnas.0308413101

Frake, R. A., Ricketts, T., Menzies, F. M., and Rubinsztein, D. C. (2015). Autophagy and neurodegeneration. *J. Clin. Invest.* 125, 65–74. doi: 10.1172/JCI73944

Funderburk, S. F., Marcellino, B. K., and Yue, Z. (2010). Cell "self-eating" (autophagy) mechanism in Alzheimer's disease. *Mt Sinai J. Med.* 77, 59–68. doi: 10.1002/msj.20161

Gao, L. P., Xiao, K., Wu, Y. Z., Chen, D. D., Yang, X. H., Shi, Q., et al. (2020). Enhanced mitophagy activity in prion-infected cultured cells and prion-infected experimental Mice via a Pink1/Parkin-dependent mitophagy pathway. *ACS Chem. Neurosci.* 11, 814–829. doi: 10.1021/acschemneuro.0c00039

Garcia-Mata, R., Gao, Y. S., and Sztul, E. (2002). Hassles with taking out the garbage: aggravating aggresomes. *Traffic* 3, 388–396. doi: 10.1034/j.1600-0854.2002.30602.x

Goold, R., McKinnon, C., Rabbanian, S., Collinge, J., Schiavo, G., and Tabrizi, S. J. (2013). Alternative fates of newly formed PrPSc upon prion conversion on the plasma membrane. *J. Cell Sci.* 126(Pt 16), 3552–3562. doi: 10.1242/jcs.120477

Goold, R., McKinnon, C., and Tabrizi, S. J. (2015). Prion degradation pathways: potential for therapeutic intervention. *Mol. Cell. Neurosci.* 66(Pt A), 12–20. doi: 10.1016/j.mcn.2014.12.009

Hara, T., Nakamura, K., Matsui, M., Yamamoto, A., Nakahara, Y., Suzuki-Migishima, R., et al. (2006). Suppression of basal autophagy in neural cells causes neurodegenerative disease in mice. *Nature* 441, 885–889. doi: 10.1038/nature04724

Heiseke, A., Aguib, Y., Riemer, C., Baier, M., and Schatzl, H. M. (2009). Lithium induces clearance of protease resistant prion protein in prion-infected cells by induction of autophagy. *J. Neurochem.* 109, 25–34. doi: 10.1111/j.1471-4159.2009.05906.x

Heiseke, A., Aguib, Y., and Schatzl, H. M. (2010). Autophagy, prion infection and their mutual interactions. *Curr. Issues Mol. Biol.* 12, 87–97.

Hessvik, N. P., and Llorente, A. (2018). Current knowledge on exosome biogenesis and release. *Cell. Mol. Life Sci.* 75, 193–208. doi: 10.1007/s00018-017-2595-9

Hochstrasser, M. (1995). Ubiquitin, proteasomes, and the regulation of intracellular protein degradation. *Curr. Opin. Cell Biol.* 7, 215–223. doi: 10.1016/0955-0674(95)80031-x

Homma, T., Ishibashi, D., Nakagaki, T., Satoh, K., Sano, K., Atarashi, R., et al. (2014). Increased expression of p62/SQSTM1 in prion diseases and its association with pathogenic prion protein. *Sci. Rep.* 4:4504. doi: 10.1038/srep04504

Imran, M., and Mahmood, S. (2011a). An overview of human prion diseases. *Virol. J.* 8:559. doi: 10.1186/1743-422X-8-559

Imran, M., and Mahmood, S. (2011b). An overview of animal prion diseases. *Virol. J.* 8:493.

Ishibashi, D., Homma, T., Nakagaki, T., Fuse, T., Sano, K., Takatsuki, H., et al. (2015). Strain-dependent effect of macroautophagy on abnormally folded prion protein degradation in infected neuronal cells. *PLoS One* 10:e0137958. doi: 10.1371/journal.pone.0137958

Iwata, A., Riley, B. E., Johnston, J. A., and Kopito, R. R. (2005). HDAC6 and microtubules are required for autophagic degradation of aggregated huntingtin. *J. Biol. Chem.* 280, 40282–40292. doi: 10.1074/jbc.M508786200

Jaeger, P. A., Pickford, F., Sun, C. H., Lucin, K. M., Masliah, E., and Wyss-Coray, T. (2010). Regulation of amyloid precursor protein processing by the Beclin 1 complex. *PLoS One* 5:e11102. doi: 10.1371/journal.pone.0011102

Jeffrey, M., Scott, J. R., Williams, A., and Fraser, H. (1992). Ultrastructural features of spongiform encephalopathy transmitted to mice from three species of bovidae. *Acta Neuropathol.* 84, 559–569. doi: 10.1007/bf00304476

Jeong, J. K., Moon, M. H., Bae, B. C., Lee, Y. J., Seol, J. W., Kang, H. S., et al. (2012). Autophagy induced by resveratrol prevents human prion protein-mediated neurotoxicity. *Neurosci. Res.* 73, 99–105. doi: 10.1016/j.neures.2012.03.005

Jeong, J. K., and Park, S. Y. (2015). Neuroprotective effect of cellular prion protein (PrPC) is related with activation of alpha7 nicotinic acetylcholine receptor (alpha7nAchR)-mediated autophagy flux. *Oncotarget* 6, 24660–24674. doi: 10.18632/oncotarget.4953

Kabeya, Y., Mizushima, N., Ueno, T., Yamamoto, A., Kirisako, T., Noda, T., et al. (2000). LC3, a mammalian homologue of yeast Apg8p, is localized in autophagosome membranes after processing. *EMBO J.* 19, 5720–5728. doi: 10.1093/emboj/19.21.5720

Kamada, Y., Yoshino, K., Kondo, C., Kawamata, T., Oshiro, N., Yonezawa, K., et al. (2010). Tor directly controls the Atg1 kinase complex to regulate autophagy. *Mol. Cell Biol.* 30, 1049–1058. doi: 10.1128/MCB.01344-09

Karapetyan, Y. E., Sferrazza, G. F., Zhou, M., Ottenberg, G., Spicer, T., Chase, P., et al. (2013). Unique drug screening approach for prion diseases identifies tacrolimus and astemizole as antiprion agents. *Proc. Natl. Acad. Sci. U.S.A.* 110, 7044–7049. doi: 10.1073/pnas.1303510110

Kegel, K. B., Kim, M., Sapp, E., McIntyre, C., Castano, J. G., Aronin, N., et al. (2000). Huntingtin expression stimulates endosomal-lysosomal activity, endosome tubulation, and autophagy. *J. Neurosci.* 20, 7268–7278. doi: 10.1523/jneurosci.20-19-07268.2000

Kiriyama, Y., and Nochi, H. (2015). The function of autophagy in neurodegenerative Diseases. *Int. J. Mol. Sci.* 16, 26797–26812. doi: 10.3390/ijms161125990

Klionsky, D. J., Abdelmohsen, K., Abe, A., Abedin, M. J., Abeliovich, H., Acevedo Arozena, A., et al. (2016). Guidelines for the use and interpretation of assays for monitoring autophagy (3rd edition). *Autophagy* 12, 1–222. doi: 10.1080/15548627.2015.1100356

Komatsu, M., Waguri, S., Chiba, T., Murata, S., Iwata, J., Tanida, I., et al. (2006). Loss of autophagy in the central nervous system causes neurodegeneration in mice. *Nature* 441, 880–884. doi: 10.1038/nature04723

Komatsu, M., Waguri, S., Ueno, T., Iwata, J., Murata, S., Tanida, I., et al. (2005). Impairment of starvation-induced and constitutive autophagy in Atg7-deficient mice. *J. Cell Biol.* 169, 425–434. doi: 10.1083/jcb.200412022

Komatsu, M., Wang, Q. J., Holstein, G. R., Friedrich, V. L. Jr., Iwata, J., Kominami, E., et al. (2007). Essential role for autophagy protein Atg7 in the maintenance of axonal homeostasis and the prevention of axonal degeneration. *Proc. Natl. Acad. Sci. U.S.A.* 104, 14489–14494. doi: 10.1073/pnas.0701311104

Kopito, R. R. (2000). Aggresomes, inclusion bodies and protein aggregation. *Trends Cell Biol.* 10, 524–530. doi: 10.1016/s0962-8924(00)01852-3

Korolchuk, V. I., Menzies, F. M., and Rubinsztein, D. C. (2010). Mechanisms of cross-talk between the ubiquitin-proteasome and autophagy-lysosome systems. *FEBS Lett.* 584, 1393–1398. doi: 10.1016/j.febslet.2009.12.047

Kristiansen, M., Deriziotis, P., Dimcheff, D. E., Jackson, G. S., Ovaa, H., Naumann, H., et al. (2007). Disease-associated prion protein oligomers inhibit the 26S proteasome. *Mol. Cell* 26, 175–188. doi: 10.1016/j.molcel.2007.04.001

Kristiansen, M., Messenger, M. J., Klohn, P. C., Brandner, S., Wadsworth, J. D., Collinge, J., et al. (2005). Disease-related prion protein forms aggresomes in neuronal cells leading to caspase activation and apoptosis. *J. Biol. Chem.* 280, 38851–38861. doi: 10.1074/jbc.M506600200

Kroemer, G., Marino, G., and Levine, B. (2010). Autophagy and the integrated stress response. *Mol. Cell* 40, 280–293. doi: 10.1016/j.molcel.2010.09.023

Laplante, M., and Sabatini, D. M. (2012). mTOR signaling in growth control and disease. *Cell* 149, 274–293. doi: 10.1016/j.cell.2012.03.017

Levine, B., and Kroemer, G. (2008). Autophagy in the pathogenesis of disease. *Cell* 132, 27–42. doi: 10.1016/j.cell.2007.12.018

Levine, B., and Yuan, J. (2005). Autophagy in cell death: an innocent convict? *J. Clin. Invest.* 115, 2679–2688. doi: 10.1172/JCI26390

Li, X., Wang, C. E., Huang, S., Xu, X., Li, X. J., Li, H., et al. (2010). Inhibiting the ubiquitin-proteasome system leads to preferential accumulation of toxic N-terminal mutant huntingtin fragments. *Hum. Mol. Genet.* 19, 2445–2455. doi: 10.1093/hmg/ddq127

Liberski, P. P. (2019). Axonal changes in experimental prion diseases recapitulate those following constriction of postganglionic branches of the superior cervical ganglion: a comparison 40 years later. *Prion* 13, 83–93. doi: 10.1080/19336896.2019.1595315

Liberski, P. P., Brown, D. R., Sikorska, B., Caughey, B., and Brown, P. (2008). Cell death and autophagy in prion diseases (transmissible spongiform encephalopathies). *Folia Neuropathol.* 46, 1–25.

Liberski, P. P., Gajdusek, D. C., and Brown, P. (2002). How do neurons degenerate in prion diseases or transmissible spongiform encephalopathies (TSEs): neuronal autophagy revisited. *Acta Neurobiol. Exp.* 62, 141–147.

Liberski, P. P., Sikorska, B., Bratosiewicz-Wasik, J., Gajdusek, D. C., and Brown, P. (2004). Neuronal cell death in transmissible spongiform encephalopathies (prion diseases) revisited: from apoptosis to autophagy. *Int. J. Biochem. Cell Biol.* 36, 2473–2490. doi: 10.1016/j.biocel.2004.04.016

Liberski, P. P., Sikorska, B., Gibson, P., and Brown, P. (2011). Autophagy contributes to widespread neuronal degeneration in hamsters infected with the Echigo-1 strain of Creutzfeldt-Jakob disease and mice infected with the Fujisaki strain of Gerstmann-Straussler-Scheinker (GSS) syndrome. *Ultrastruct. Pathol.* 35, 31–36. doi: 10.3109/01913123.2010.527038

Ling, D., Song, H. J., Garza, D., Neufeld, T. P., and Salvaterra, P. M. (2009). Abeta42-induced neurodegeneration via an age-dependent autophagic-lysosomal injury in Drosophila. *PLoS One* 4:e4201. doi: 10.1371/journal.pone.0004201

Lipinski, M. M., Zheng, B., Lu, T., Yan, Z., Py, B. F., Ng, A., et al. (2010). Genome-wide analysis reveals mechanisms modulating autophagy in normal brain aging and in Alzheimer's disease. *Proc. Natl. Acad. Sci. U.S.A.* 107, 14164–14169. doi: 10.1073/pnas.1009485107

Lopez-Perez, O., Bolea, R., Marin, B., Badiola, J. J., and Martin-Burriel, I. (2019a). Autophagy impairment in highly prion-affected brain areas of sheep experimentally infected with atypical scrapie. *Vet. Microbiol.* 233, 78–84. doi: 10.1016/j.vetmic.2019.04.026

Lopez-Perez, O., Otero, A., Filali, H., Sanz-Rubio, D., Toivonen, J. M., Zaragoza, P., et al. (2019b). Dysregulation of autophagy in the central nervous system of sheep naturally infected with classical scrapie. *Sci. Rep.* 9:1911. doi: 10.1038/s41598-019-38500-2

Lopez-Perez, O., Toivonen, J. M., Otero, A., Solanas, L., Zaragoza, P., Badiola, J. J., et al. (2020). Impairment of autophagy in scrapie-infected transgenic mice at the clinical stage. *Lab. Invest.* 100, 52–63. doi: 10.1038/s41374-019-0312-z

Lum, J. J., DeBerardinis, R. J., and Thompson, C. B. (2005). Autophagy in metazoans: cell survival in the land of plenty. *Nat. Rev. Mol. Cell Biol.* 6, 439–448. doi: 10.1038/nrm1660

Llorens, F., Thune, K., Sikorska, B., Schmitz, M., Tahir, W., Fernandez-Borges, N., et al. (2017). Altered Ca(2+) homeostasis induces Calpain-Cathepsin axis activation in sporadic Creutzfeldt-Jakob disease. *Acta Neuropathol. Commun.* 5:35. doi: 10.1186/s40478-017-0431-y

Ma, J. F., Huang, Y., Chen, S. D., and Halliday, G. (2010). Immunohistochemical evidence for macroautophagy in neurones and endothelial cells in Alzheimer's disease. *Neuropathol. Appl. Neurobiol.* 36, 312–319. doi: 10.1111/j.1365-2990.2010.01067.x

Maiuri, M. C., Zalckvar, E., Kimchi, A., and Kroemer, G. (2007). Self-eating and self-killing: crosstalk between autophagy and apoptosis. *Nat. Rev. Mol. Cell Biol.* 8, 741–752. doi: 10.1038/nrm2239

Majeski, A. E., and Dice, J. F. (2004). Mechanisms of chaperone-mediated autophagy. *Int. J. Biochem. Cell Biol.* 36, 2435–2444. doi: 10.1016/j.biocel.2004.02.013

Mammadova, N., West Greenlee, M. H., Moore, S. J., Sakaguchi, D. S., and Greenlee, J. J. (2020). Experimental study using multiple strains of prion disease in cattle reveals an inverse relationship between incubation time and misfolded prion accumulation, neuroinflammation and autophagy. *Am. J. Pathol.* 190, 1461–1473. doi: 10.1016/j.ajpath.2020.03.006

Mari, M., Griffith, J., Rieter, E., Krishnappa, L., Klionsky, D. J., and Reggiori, F. (2010). An Atg9-containing compartment that functions in the early steps of autophagosome biogenesis. *J. Cell Biol.* 190, 1005–1022. doi: 10.1083/jcb.200912089

Martinez-Vicente, M., Talloczy, Z., Wong, E., Tang, G., Koga, H., Kaushik, S., et al. (2010). Cargo recognition failure is responsible for inefficient autophagy in Huntington's disease. *Nat. Neurosci.* 13, 567–576. doi: 10.1038/nn.2528

Mays, C. E., and Soto, C. (2016). The stress of prion disease. *Brain Res.* 1648(Pt B), 553–560. doi: 10.1016/j.brainres.2016.04.009

McKinnon, C., Goold, R., Andre, R., Devoy, A., Ortega, Z., Moonga, J., et al. (2016). Prion-mediated neurodegeneration is associated with early impairment of the ubiquitin-proteasome system. *Acta Neuropathol.* 131, 411–425. doi: 10.1007/s00401-015-1508-y

Mizushima, N., and Hara, T. (2006). Intracellular quality control by autophagy: how does autophagy prevent neurodegeneration? *Autophagy* 2, 302–304. doi: 10.4161/auto.2945

Mizushima, N., Kuma, A., Kobayashi, Y., Yamamoto, A., Matsubae, M., Takao, T., et al. (2003a). Mouse Apg16L, a novel WD-repeat protein, targets to the autophagic isolation membrane with the Apg12-Apg5 conjugate. *J. Cell Sci.* 116(Pt 9), 1679–1688. doi: 10.1242/jcs.00381

Mizushima, N., Levine, B., Cuervo, A. M., and Klionsky, D. J. (2008). Autophagy fights disease through cellular self-digestion. *Nature* 451, 1069–1075. doi: 10.1038/nature06639

Mizushima, N., Yoshimori, T., and Ohsumi, Y. (2003b). Role of the Apg12 conjugation system in mammalian autophagy. *Int. J. Biochem. Cell Biol.* 35, 553–561. doi: 10.1016/s1357-2725(02)00343-6

Mizushima, N., and Yoshimori, T. (2007). How to interpret LC3 immunoblotting. *Autophagy* 3, 542–545. doi: 10.4161/auto.4600

Mok, S. W., Riemer, C., Madela, K., Hsu, D. K., Liu, F. T., Gultner, S., et al. (2007). Role of galectin-3 in prion infections of the CNS. *Biochem. Biophys. Res. Commun.* 359, 672–678. doi: 10.1016/j.bbrc.2007.05.163

Moon, J. H., Lee, J. H., Lee, Y. J., and Park, S. Y. (2016a). Autophagy flux induced by ginsenoside-Rg3 attenuates human prion protein-mediated neurotoxicity and mitochondrial dysfunction. *Oncotarget* 7, 85697–85708. doi: 10.18632/oncotarget.13730

Moon, J. H., Lee, J. H., Lee, Y. J., and Park, S. Y. (2016b). Hinokitiol protects primary neuron cells against prion peptide-induced toxicity via autophagy flux regulated by hypoxia inducing factor-1. *Oncotarget* 7, 29944–29957. doi: 10.18632/oncotarget.8670

Moon, J. H., Lee, J. H., Nazim, U. M., Lee, Y. J., Seol, J. W., Eo, S. K., et al. (2016c). Human prion protein-induced autophagy flux governs neuron cell damage in primary neuron cells. *Oncotarget* 7, 29989–30002. doi: 10.18632/oncotarget.8802

Nair, U., Yen, W. L., Mari, M., Cao, Y., Xie, Z., Baba, M., et al. (2012). A role for Atg8-PE deconjugation in autophagosome biogenesis. *Autophagy* 8, 780–793. doi: 10.4161/auto.19385

Nakagaki, T., Satoh, K., Ishibashi, D., Fuse, T., Sano, K., Kamatari, Y. O., et al. (2013). FK506 reduces abnormal prion protein through the activation of autolysosomal degradation and prolongs survival in prion-infected mice. *Autophagy* 9, 1386–1394. doi: 10.4161/auto.25381

Nakai, A., Yamaguchi, O., Takeda, T., Higuchi, Y., Hikoso, S., Taniike, M., et al. (2007). The role of autophagy in cardiomyocytes in the basal state and in response to hemodynamic stress. *Nat. Med.* 13, 619–624. doi: 10.1038/nm1574

Nixon, R. A. (2005). Endosome function and dysfunction in Alzheimer's disease and other neurodegenerative diseases. *Neurobiol. Aging* 26, 373–382. doi: 10.1016/j.neurobiolaging.2004.09.018

Nixon, R. A. (2007). Autophagy, amyloidogenesis and Alzheimer disease. *J. Cell Sci.* 120(Pt 23), 4081–4091. doi: 10.1242/jcs.019265

Nixon, R. A., Wegiel, J., Kumar, A., Yu, W. H., Peterhoff, C., Cataldo, A., et al. (2005). Extensive involvement of autophagy in Alzheimer disease: an immuno-electron microscopy study. *J. Neuropathol. Exp. Neurol.* 64, 113–122. doi: 10.1093/jnen/64.2.113

Oh, J. M., Choi, E. K., Carp, R. I., and Kim, Y. S. (2012). Oxidative stress impairs autophagic flux in prion protein-deficient hippocampal cells. *Autophagy* 8, 1448–1461. doi: 10.4161/auto.21164

Oh, J. M., Shin, H. Y., Park, S. J., Kim, B. H., Choi, J. K., Choi, E. K., et al. (2008). The involvement of cellular prion protein in the autophagy pathway in neuronal cells. *Mol. Cell. Neurosci.* 39, 238–247. doi: 10.1016/j.mcn.2008.07.003

Ohsumi, Y. (2001). Molecular dissection of autophagy: two ubiquitin-like systems. *Nat. Rev. Mol. Cell Biol.* 2, 211–216. doi: 10.1038/35056522

Pajak, B., Songin, M., Strosznajder, J. B., and Gajkowska, B. (2009a). Alzheimer's disease genetic mutation evokes ultrastructural alterations: correlation to an intracellular Abeta deposition and the level of GSK-3beta-P(Y216) phosphorylated form. *Neurotoxicology* 30, 581–588. doi: 10.1016/j.neuro.2009.05.008

Pajak, B., Songin, M., Strosznajder, J. B., Orzechowski, A., and Gajkowska, B. (2009b). Ultrastructural evidence of amyloid beta-induced autophagy in PC12 cells. *Folia Neuropathol.* 47, 252–258.

Pandey, U. B., Nie, Z., Batlevi, Y., McCray, B. A., Ritson, G. P., Nedelsky, N. B., et al. (2007). HDAC6 rescues neurodegeneration and provides an essential link between autophagy and the UPS. *Nature* 447, 859–863. doi: 10.1038/nature05853

Pattison, I. H., and Jones, K. M. (1967). The possible nature of the transmissible agent of scrapie. *Vet. Rec.* 80, 2–9. doi: 10.1136/vr.80.1.2

Peters, P. J., Mironov, A. Jr., Peretz, D., van Donselaar, E., Leclerc, E., Erpel, S., et al. (2003). Trafficking of prion proteins through a caveolae-mediated endosomal pathway. *J. Cell Biol.* 162, 703–717. doi: 10.1083/jcb.200304140

Phadwal, K., Kurian, D., Salamat, M. K. F., MacRae, V. E., Diack, A. B., and Manson, J. C. (2018). Spermine increases acetylation of tubulins and facilitates autophagic degradation of prion aggregates. *Sci. Rep.* 8:10004. doi: 10.1038/s41598-018-28296-y

Pickford, F., Masliah, E., Britschgi, M., Lucin, K., Narasimhan, R., Jaeger, P. A., et al. (2008). The autophagy-related protein beclin 1 shows reduced expression

in early Alzheimer disease and regulates amyloid beta accumulation in mice. *J. Clin. Invest.* 118, 2190–2199. doi: 10.1172/JCI33585

Polajnar, M., and Zerovnik, E. (2014). Impaired autophagy: a link between neurodegenerative and neuropsychiatric diseases. *J. Cell. Mol. Med.* 18, 1705–1711. doi: 10.1111/jcmm.12349

Prusiner, S. B. (1982). Novel proteinaceous infectious particles cause scrapie. *Science* 216, 136–144. doi: 10.1126/science.6801762

Qin, Z. H., Wang, Y., Kegel, K. B., Kazantsev, A., Apostol, B. L., Thompson, L. M., et al. (2003). Autophagy regulates the processing of amino terminal huntingtin fragments. *Hum. Mol. Genet.* 12, 3231–3244. doi: 10.1093/hmg/ddg346

Ravikumar, B., Acevedo-Arozena, A., Imarisio, S., Berger, Z., Vacher, C., O'Kane, C. J., et al. (2005). Dynein mutations impair autophagic clearance of aggregate-prone proteins. *Nat. Genet.* 37, 771–776. doi: 10.1038/ng1591

Ravikumar, B., Berger, Z., Vacher, C., O'Kane, C. J., and Rubinsztein, D. C. (2006). Rapamycin pre-treatment protects against apoptosis. *Hum. Mol. Genet.* 15, 1209–1216. doi: 10.1093/hmg/ddl036

Ravikumar, B., Duden, R., and Rubinsztein, D. C. (2002). Aggregate-prone proteins with polyglutamine and polyalanine expansions are degraded by autophagy. *Hum. Mol. Genet.* 11, 1107–1117. doi: 10.1093/hmg/11.9.1107

Reggiori, F., and Klionsky, D. J. (2002). Autophagy in the eukaryotic cell. *Eukaryot. Cell* 1, 11–21. doi: 10.1128/ec.01.1.11-21.2002

Rubinsztein, D. C. (2006). The roles of intracellular protein-degradation pathways in neurodegeneration. *Nature* 443, 780–786. doi: 10.1038/nature05291

Rubinsztein, D. C., DiFiglia, M., Heintz, N., Nixon, R. A., Qin, Z. H., Ravikumar, B., et al. (2005). Autophagy and its possible roles in nervous system diseases, damage and repair. *Autophagy* 1, 11–22. doi: 10.4161/auto.1.1.1513

Rubinsztein, D. C., Gestwicki, J. E., Murphy, L. O., and Klionsky, D. J. (2007). Potential therapeutic applications of autophagy. *Nat. Rev. Drug Discov.* 6, 304–312. doi: 10.1038/nrd2272

Rubinsztein, D. C., Shpilka, T., and Elazar, Z. (2012). Mechanisms of autophagosome biogenesis. *Curr. Biol.* 22, R29–R34. doi: 10.1016/j.cub.2011.11.034

Schatzl, H. M., Laszlo, L., Holtzman, D. M., Tatzelt, J., DeArmond, S. J., Weiner, R. I., et al. (1997). A hypothalamic neuronal cell line persistently infected with scrapie prions exhibits apoptosis. *J. Virol.* 71, 8821–8831. doi: 10.1128/jvi.71.11.8821-8831.1997

Scotter, E. L., Vance, C., Nishimura, A. L., Lee, Y. B., Chen, H. J., Urwin, H., et al. (2014). Differential roles of the ubiquitin proteasome system and autophagy in the clearance of soluble and aggregated TDP-43 species. *J. Cell Sci.* 127(Pt 6), 1263–1278. doi: 10.1242/jcs.140087

Serrano, C., Bolea, R., Lyahyai, J., Filali, H., Varona, L., Marcos-Carcavilla, A., et al. (2011). Changes in HSP gene and protein expression in natural scrapie with brain damage. *Vet. Res.* 42:13. doi: 10.1186/1297-9716-42-13

Shibata, M., Lu, T., Furuya, T., Degterev, A., Mizushima, N., Yoshimori, T., et al. (2006). Regulation of intracellular accumulation of mutant Huntingtin by Beclin 1. *J. Biol. Chem.* 281, 14474–14485. doi: 10.1074/jbc.M600364200

Shin, H. Y., Oh, J. M., and Kim, Y. S. (2013). The Functional Role of Prion Protein (PrPC) on Autophagy. *Pathogens* 2, 436–445. doi: 10.3390/pathogens2030436

Shin, J. Y., Park, H. J., Kim, H. N., Oh, S. H., Bae, J. S., Ha, H. J., et al. (2014). Mesenchymal stem cells enhance autophagy and increase beta-amyloid clearance in Alzheimer disease models. *Autophagy* 10, 32–44. doi: 10.4161/auto.26508

Sikorska, B., Liberski, P. P., Giraud, P., Kopp, N., and Brown, P. (2004). Autophagy is a part of ultrastructural synaptic pathology in Creutzfeldt-Jakob disease: a brain biopsy study. *Int. J. Biochem. Cell Biol.* 36, 2563–2573. doi: 10.1016/j.biocel.2004.04.014

Silveira, J. R., Raymond, G. J., Hughson, A. G., Race, R. E., Sim, V. L., Hayes, S. F., et al. (2005). The most infectious prion protein particles. *Nature* 437, 257–261. doi: 10.1038/nature03989

Smith, H. L., Freeman, O. J., Butcher, A. J., Holmqvist, S., Humoud, I., Schatzl, T., et al. (2020). Astrocyte unfolded protein response induces a specific reactivity state that causes non-cell-autonomous neuronal degeneration. *Neuron* 105, 855–866.e5. doi: 10.1016/j.neuron.2019.12.014

Son, J. H., Shim, J. H., Kim, K. H., Ha, J. Y., and Han, J. Y. (2012). Neuronal autophagy and neurodegenerative diseases. *Exp. Mol. Med.* 44, 89–98. doi: 10.3858/emm.2012.44.2.031

Soto, C. (2003). Unfolding the role of protein misfolding in neurodegenerative diseases. *Nat. Rev. Neurosci.* 4, 49–60. doi: 10.1038/nrn1007

Spencer, B., Potkar, R., Trejo, M., Rockenstein, E., Patrick, C., Gindi, R., et al. (2009). Beclin 1 gene transfer activates autophagy and ameliorates the neurodegenerative pathology in alpha-synuclein models of Parkinson's and Lewy body diseases. *J. Neurosci.* 29, 13578–13588. doi: 10.1523/JNEUROSCI.4390-09.2009

Thellung, S., Scoti, B., Corsaro, A., Villa, V., Nizzari, M., Gagliani, M. C., et al. (2018). Pharmacological activation of autophagy favors the clearing of intracellular aggregates of misfolded prion protein peptide to prevent neuronal death. *Cell Death Dis.* 9:166. doi: 10.1038/s41419-017-0252-8

Ventruti, A., and Cuervo, A. M. (2007). Autophagy and neurodegeneration. *Curr. Neurol. Neurosci. Rep.* 7, 443–451.

Vey, M., Pilkuhn, S., Wille, H., Nixon, R., DeArmond, S. J., Smart, E. J., et al. (1996). Subcellular colocalization of the cellular and scrapie prion proteins in caveolae-like membranous domains. *Proc. Natl. Acad. Sci. U.S.A.* 93, 14945–14949. doi: 10.1073/pnas.93.25.14945

Vogiatzi, T., Xilouri, M., Vekrellis, K., and Stefanis, L. (2008). Wild type alpha-synuclein is degraded by chaperone-mediated autophagy and macroautophagy in neuronal cells. *J. Biol. Chem.* 283, 23542–23556. doi: 10.1074/jbc.M801992200

Wang, J., Zhang, B. Y., Zhang, J., Xiao, K., Chen, L. N., Wang, H., et al. (2016). Treatment of SMB-S15 Cells with Resveratrol Efficiently Removes the PrP(Sc) accumulation *in vitro* and prion infectivity *in vivo*. *Mol. Neurobiol.* 53, 5367–5376. doi: 10.1007/s12035-015-9464-z

Webb, J. L., Ravikumar, B., Atkins, J., Skepper, J. N., and Rubinsztein, D. C. (2003). Alpha-Synuclein is degraded by both autophagy and the proteasome. *J. Biol. Chem.* 278, 25009–25013. doi: 10.1074/jbc.M300227200

Wells, G. A., and McGill, I. S. (1992). Recently described scrapie-like encephalopathies of animals: case definitions. *Res. Vet. Sci.* 53, 1–10. doi: 10.1016/0034-5288(92)90076-e

Winslow, A. R., Chen, C. W., Corrochano, S., Acevedo-Arozena, A., Gordon, D. E., Peden, A. A., et al. (2010). alpha-Synuclein impairs macroautophagy: implications for Parkinson's disease. *J. Cell Biol.* 190, 1023–1037. doi: 10.1083/jcb.201003122

Wood, J. L., McGill, I. S., Done, S. H., and Bradley, R. (1997). Neuropathology of scrapie: a study of the distribution patterns of brain lesions in 222 cases of natural scrapie in sheep, 1982-1991. *Vet. Rec.* 140, 167–174. doi: 10.1136/vr.140.7.167

Xie, Z., and Klionsky, D. J. (2007). Autophagosome formation: core machinery and adaptations. *Nat. Cell Biol.* 9, 1102–1109. doi: 10.1038/ncb1007-1102

Xilouri, M., Vogiatzi, T., Vekrellis, K., Park, D., and Stefanis, L. (2009). Abberant alpha-synuclein confers toxicity to neurons in part through inhibition of chaperone-mediated autophagy. *PLoS One* 4:e5515. doi: 10.1371/journal.pone.0005515

Xu, Y., Tian, C., Sun, J., Zhang, J., Ren, K., Fan, X. Y., et al. (2016). FBXW7-Induced MTOR degradation forces autophagy to counteract persistent prion infection. *Mol. Neurobiol.* 53, 706–719. doi: 10.1007/s12035-014-9028-7

Xu, Y., Tian, C., Wang, S. B., Xie, W. L., Guo, Y., Zhang, J., et al. (2012). Activation of the macroautophagic system in scrapie-infected experimental animals and human genetic prion diseases. *Autophagy* 8, 1604–1620. doi: 10.4161/auto.21482

Yang, Z., and Klionsky, D. J. (2009). An overview of the molecular mechanism of autophagy. *Curr. Top. Microbiol. Immunol.* 335, 1–32. doi: 10.1007/978-3-642-00302-8_1

Yao, H., Zhao, D., Khan, S. H., and Yang, L. (2013). Role of autophagy in prion protein-induced neurodegenerative diseases. *Acta Biochim. Biophys. Sin.* 45, 494–502. doi: 10.1093/abbs/gmt022

Yim, Y. I., Park, B. C., Yadavalli, R., Zhao, X., Eisenberg, E., and Greene, L. E. (2015). The multivesicular body is the major internal site of prion conversion. *J. Cell Sci.* 128, 1434–1443. doi: 10.1242/jcs.165472

Yin, Z., Pascual, C., and Klionsky, D. J. (2016). Autophagy: machinery and regulation. *Microb. Cell* 3, 588–596. doi: 10.15698/mic2016.12.546

Yorimitsu, T., and Klionsky, D. J. (2007). Eating the endoplasmic reticulum: quality control by autophagy. *Trends Cell Biol.* 17, 279–285. doi: 10.1016/j.tcb.2007.04.005

Yoshimori, T. (2004). Autophagy: a regulated bulk degradation process inside cells. *Biochem. Biophys. Res. Commun.* 313, 453–458. doi: 10.1016/j.bbrc.2003.07.023

Yu, W. H., Cuervo, A. M., Kumar, A., Peterhoff, C. M., Schmidt, S. D., Lee, J. H., et al. (2005). Macroautophagy–a novel Beta-amyloid peptide-generating

pathway activated in Alzheimer's disease. *J. Cell Biol.* 171, 87–98. doi: 10.1083/jcb.200505082

Yue, Z. (2007). Regulation of neuronal autophagy in axon: implication of autophagy in axonal function and dysfunction/degeneration. *Autophagy* 3, 139–141. doi: 10.4161/auto.3602

Yun, S. W., Ertmer, A., Flechsig, E., Gilch, S., Riederer, P., Gerlach, M., et al. (2007). The tyrosine kinase inhibitor imatinib mesylate delays prion neuroinvasion by inhibiting prion propagation in the periphery. *J. Neurovirol.* 13, 328–337. doi: 10.1080/13550280701361516

Zhang, Z., Singh, R., and Aschner, M. (2016). Methods for the detection of autophagy in mammalian cells. *Curr. Protoc. Toxicol.* 69, 20.12.1–20.12.26. doi: 10.1002/cptx.11

Zheng, Q., Li, J., and Wang, X. (2009). Interplay between the ubiquitin-proteasome system and autophagy in proteinopathies. *Int. J. Physiol. Pathophysiol. Pharmacol.* 1, 127–142.

Zhu, H., Tannous, P., Johnstone, J. L., Kong, Y., Shelton, J. M., Richardson, J. A., et al. (2007). Cardiac autophagy is a maladaptive response to hemodynamic stress. *J. Clin. Invest.* 117, 1782–1793. doi: 10.1172/JCI27523

Zhu, T., Chen, J. L., Wang, Q., Shao, W., and Qi, B. (2018). Modulation of mitochondrial dynamics in neurodegenerative diseases: an insight Into Prion Diseases. *Front. Aging Neurosci.* 10:336. doi: 10.3389/fnagi.2018.00336

Conflict of Interest: The authors declare that the research was conducted in the absence of any commercial or financial relationships that could be construed as a potential conflict of interest.

frontiers in Bioengineering and Biotechnology

REVIEW
published: 08 September 2020
doi: 10.3389/fbioe.2020.570692

Potential of Microfluidics and Lab-on-Chip Platforms to Improve Understanding of "*prion-like*" Protein Assembly and Behavior

Jose A. del Rio[1,2,3,4]* *and Isidre Ferrer*[3,4,5,6,7]*

[1] Molecular and Cellular Neurobiotechnology, Institute for Bioengineering of Catalonia, Barcelona Institute of Science and Technology, Barcelona, Spain, [2] Department of Cell Biology, Physiology and Immunology, Faculty of Biology, University of Barcelona, Barcelona, Spain, [3] Center for Networked Biomedical Research on Neurodegenerative Diseases (Ciberned), Barcelona, Spain, [4] Institute of Neuroscience, University of Barcelona, Barcelona, Spain, [5] Department of Pathology and Experimental Therapeutics, University of Barcelona, Barcelona, Spain, [6] Bellvitge University Hospital, Hospitalet de Llobregat, Barcelona, Spain, [7] Bellvitge Biomedical Research Institute (IDIBELL), Hospitalet de Llobregat, Barcelona, Spain

OPEN ACCESS

Edited by:
Maria Lurdes Pinto,
University of Trás-os-Montes and Alto Douro, Portugal

Reviewed by:
Byron Caughey,
Rocky Mountain Laboratories (NIAID), United States
Vincent Beringue,
Institut National de Recherche pour l'Agriculture, l'Alimentation et l'Environnement (INRAE), France

***Correspondence:**
Jose A. del Rio
jadelrio@ibecbarcelona.eu;
jadelrio@ub.edu
Isidre Ferrer
8082ifa@gmail.com

Specialty section:
This article was submitted to Biosafety and Biosecurity, a section of the journal Frontiers in Bioengineering and Biotechnology

Received: 08 June 2020
Accepted: 18 August 2020
Published: 08 September 2020

Citation:
del Rio JA and Ferrer I (2020) Potential of Microfluidics and Lab-on-Chip Platforms to Improve Understanding of "prion-like" Protein Assembly and Behavior. Front. Bioeng. Biotechnol. 8:570692. doi: 10.3389/fbioe.2020.570692

Human aging is accompanied by a relevant increase in age-associated chronic pathologies, including neurodegenerative and metabolic diseases. The appearance and evolution of numerous neurodegenerative diseases is paralleled by the appearance of intracellular and extracellular accumulation of misfolded proteins in affected brains. In addition, recent evidence suggests that most of these amyloid proteins can behave and propagate among neural cells similarly to infective prions. In order to improve understanding of the seeding and spreading processes of these "prion-like" amyloids, microfluidics and 3D lab-on-chip approaches have been developed as highly valuable tools. These techniques allow us to monitor changes in cellular and molecular processes responsible for amyloid seeding and cell spreading and their parallel effects in neural physiology. Their compatibility with new optical and biochemical techniques and their relative availability have increased interest in them and in their use in numerous laboratories. In addition, recent advances in stem cell research in combination with microfluidic platforms have opened new humanized *in vitro* models for myriad neurodegenerative diseases affecting different cellular targets of the vascular, muscular, and nervous systems, and glial cells. These new platforms help reduce the use of animal experimentation. They are more reproducible and represent a potential alternative to classical approaches to understanding neurodegeneration. In this review, we summarize recent progress in neurobiological research in "prion-like" protein using microfluidic and 3D lab-on-chip approaches. These approaches are driven by various fields, including chemistry, biochemistry, and cell biology, and they serve to facilitate the development of more precise human brain models for basic mechanistic studies of cell-to-cell interactions and drug discovery.

Keywords: lab-on-chip, amyloid propagation, microfluidics, fibril, seeding, spreading, prion-like, prionoid

INTRODUCTION

The formation of β-sheet enriched misfolded protein aggregates (also termed amyloids) via self-assembly of proteins or polypeptides, with intrinsic or induced amyloidogenic properties, is the hallmark of numerous protein misfolding diseases (PMD) affecting humans (Greenfield et al., 2008). These include neural diseases such as Alzheimer's disease (AD), Parkinson's disease (PD), multiple system atrophy (MSA), amyotrophic lateral sclerosis (ALS), and prionopathies [i.e., Creutzfeldt–Jakob disease (CJD)], as well as non-neural diseases such as pancreatic amyloidosis, systemic amyloidosis, and type II diabetes, among others (see Skinner et al., 2005; Ramirez-Alvarado et al., 2010; Sigurdsson et al., 2012; Otzen, 2013 for references). For several years, considerable effort has been made to uncover the molecular basis of the aggregation process and the different strains of specific amyloids with aggregative and infective properties. As a recent example of this interest, a published study of R. Nonno's lab reveals that a small autocatalytic, but non-fibrillar, 7 kDa fragment of the pathogenic prion currently observed in Gerstmann-Sträussler-Scheinker disease (GSS) patients is also infective (Vanni et al., 2020). In fact, all these studies share as their goal the development of appropriate and specific methods to inhibit their aggregation in real biosafety and clinical scenarios (Giles et al., 2017).

Focusing on neuronal PMDs, several assays for amyloid detection, aggregation, and amplification have been developed in recent years to address the demand for reliable and sensitive *in vitro* detection of the various amyloid species (from oligomers to fibrils) in human samples. These procedures are mainly based on detecting the presence or monitoring the self-aggregation process of pathogenic amyloids using *in situ* or *ex situ* approaches. *In situ* assays are straightforward but they require direct introduction of probe molecules into the aggregation assay and in some cases interference in the process can be observed. Interference of the aggregation process by probe molecules can be avoided in *ex situ* assays, where small samples of an aggregating protein solution are extracted and diluted at specified time points into a buffered solution containing an appropriate dye molecule. Another alternative is to promote the amplification of very small quantities of the active pathological species up to significantly detectable levels, as the polymerase chain reaction (PCR) does for nucleotides. In the first group, available techniques range from classic fluorometric assays [i.e., Thioflavin T (ThT) (Saeed and Fine, 1967), Congo red (Yakupova et al., 2019)], and benzofuranone (for α-synuclein (Lengyel-Zhand et al., 2020), to new biosensor-based methods.

In addition, alternative classical optical detection methods for ThT staining (the most used fluorometric method) include the use of colorimetry techniques using, among others, gold nanoparticles (i.e., Zhou et al., 2015) or FRET methods on CdTe quantum dots (Xia et al., 2016).

Of these, numerous electrochemical biosensing methods based on antibodies {i.e., (Prabhulkar et al., 2012; Li et al., 2016), aptamers (Ylera et al., 2002; Zhao et al., 2020), coupling peptides (Li et al., 2013), and peptides with affinity regions [e.g., for β-amyloid the PrP(95-110)] (Rushworth et al., 2014)} were developed as reliable alternatives for conventional amyloid detection (see also Kaushik et al., 2016; Zhang et al., 2020 for review). These offer advantages compared to conventional methods due to their portability, relatively easy handling, and greater sensitivity. Among the huge number of emerging strategies, of particular interest is the application of new materials such as graphene oxide as a reliable alternative to fluorometric assays (e.g., ThT) to detect β-amyloid in label-free systems (e.g., Huang H. et al., 2017). Their use allows researcher to achieve simultaneous detection of oligomeric and fibrillar structures in the same sample (a challenging problem in classical fluorometric assays) and in other higher sensitivity studies, or the recently developed electrochemical determination of β-amyloid oligomers using a graphene and reduced graphene oxide dual-layer biosensor (Sethi et al., 2020). These are just some examples of the tremendous progress that has been made in the development of sensors for detection of amyloids (mainly β-amyloid). Readers interested in the emerging biosensors and electrochemical detection of amyloids may obtain more details in recent reviews (e.g., Serafin et al., 2020; Zhang et al., 2020).

A second strategy is amplification of the pathogenic amyloid in the presence of its monomeric counterparts using biochemical reactions, such as the protein misfolding cyclic amplification (PMCA) method (Saborio et al., 2001; Soto et al., 2002), real-time quaking-induced conversion (RT-QuIC) assay (Wilham et al., 2010; Sano et al., 2018), and ASA assay (Colby et al., 2007). These methods have evolved and have been adapted for the reliable detection of the presence and aggregative stage of various amyloids (i.e., Orru et al., 2017; Saijo et al., 2019) in different biological samples (i.e., Fairfoul et al., 2016; Haley et al., 2016; Bongianni et al., 2017). In parallel to these biochemical methods, other engineering laboratories have developed ultrasensitive methods based on graphene oxide and entropy-driven strand displacement reaction (ESDR) with LOD of 20 pM (Zhou et al., 2018), or graphene field-effect transistor (G-FET) for β-amyloid formation (Kuo et al., 2018). Unfortunately, these methods are not currently used in patient-derived studies.

Neurodegenerative progression in PMDs runs in parallel with disease-specific characteristic intra- or extra-cellular accumulation of misfolded amyloids. In fact, cellular, molecular, biophysical, and biochemical studies have revealed that most PMDs are progressive disorders, and that amyloid-associated pathologies spread from diseased to healthy cells affecting different brain areas in a sequential basis (see Costanzo and Zurzolo, 2013; Goedert et al., 2017; Holmes and Diamond, 2017; Del Rio et al., 2018; Vilette et al., 2018; Meisl et al., 2020; Peng et al., 2020 for reviews). The spatiotemporal progression of these diseases seems to correlate, with some controversy (see below), with the brain propagation of the amyloid-associated neuropathology between anatomical pathways specific to each disorder, suggesting a cell-to-cell spreading of the disease (Saper et al., 1987; Bertrand et al., 2004; Braak and Del Tredici, 2009; Costanzo and Zurzolo, 2013; Goedert et al., 2017; Peng et al., 2020; **Figure 1**). However, this "connectome" view of the seeding and progression of the amyloid accumulation between connected areas is under debate for some PMDs [i.e., PD, please see Surmeier et al. (2017) for review]. In PD, when comparing the

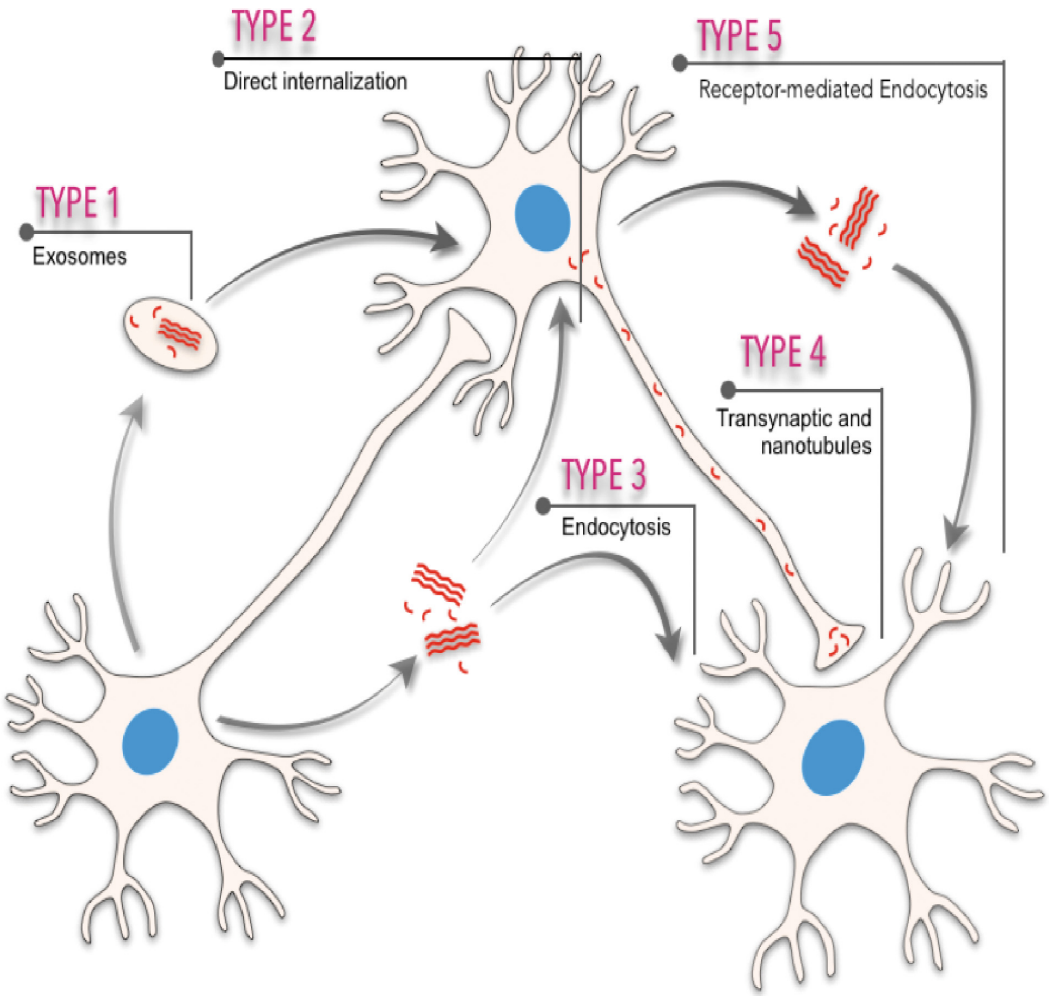

FIGURE 1 | Scheme illustrating the different spreading pathways of a "hypothetical" pathogenic seed between different cells. Five different means of transmission are illustrated: (i) from exosomes or multivesicular bodies, (ii) direct internalization by interacting with plasma membranes, (iii) endocytosis or micropinocytosis processes, (iv) transsynaptic transmission and tunneling nanotubules, and (v) receptor-mediated uptake of the amyloid.

appearance and progression of the Lewy pathology in affected individuals with experimental mouse models of the disease, it seems to correlate better with cell- or region-autonomous mechanisms rather than connectivity (Surmeier et al., 2017). Nevertheless, several routes of inter-cellular amyloid spreading have been proposed such us membrane binding, receptor-mediated, and non-mediated endocytosis (i.e., Holmes et al., 2013; Mao et al., 2016; Aulic et al., 2017; Urrea et al., 2018; Rauch et al., 2020), multivesicular bodies (i.e., exosomes) (Sardar Sinha et al., 2018; Perez et al., 2019; Winston et al., 2019), or tunneling nanotubes (TNTs) (Costanzo and Zurzolo, 2013; Abounit et al., 2016; Zeinabad et al., 2016; Peng et al., 2020; **Figure 1**). Understanding the intercellular formation and transmission of these amyloids, also termed "pathogenic seeds" in some studies, has become a challenging issue in recent years (i.e., Vilette et al., 2018; Erana, 2019; Peng et al., 2020). Relevantly, the participation of neurons, astroglia, and oligodendrocytes also displaying insoluble amyloid inclusions in particular neurodegenerative diseases during seeding and spreading is still unknown and warrants further study (i.e., Kovacs et al., 2017; Ferrer, 2018).

In addition, considering the evidence demonstrating the ability of these amyloids to disseminate protein misfolding as "pathologic seeds" from sick to healthy cells, a "*prion-like*" or "*prionoid*" hypothesis has been proposed (Ashe and Aguzzi, 2013; Aguzzi and Lakkaraju, 2016; Collinge, 2016; Woerman et al., 2018). Indeed, cell-spread of amyloid seeds can act as a self-propagating template disrupting cell viability and leading to both the death of recipient cells and the progression of the neurodegenerative disorder (Ashe and Aguzzi, 2013; Aguzzi and Lakkaraju, 2016; Collinge, 2016; Holmes and Diamond, 2017). However, some criticisms appeared with this terminology [i.e., for tau (Polanco and Gotz, 2015), β-amyloid (Watts and Prusiner, 2018), and MSA-derived α-synuclein (Woerman et al., 2020)]. We suggest to the reader interested in this topic examining the reports of Castilla's and Requena's laboratories (i.e., Castilla and Requena, 2015; Erana et al., 2017) and the recent review of

Wells et al. (2019). In fact, prion diseases (e.g., CJD) are the only neurodegenerative disorders showing an infectious transmissible protein species, the pathogenic prion, capable of recapitulating a clinical disease (e.g., Prusiner, 1998a,b; Moore et al., 2009). Moreover, the prion strain also plays a crucial role in dictating the type (i.e., punctate vs. plaques) and anatomical distribution of the lesions of pathogenic PrP deposition in affected brains (see for example Fraser and Dickinson, 1973; Lasmezas et al., 1996; Scialo et al., 2019 for a recent review).

In this challenging scenario, microfluidics and lab-on-chip (LOC) technologies have emerged in the last 15–20 years as a plausible strategy to monitor some aspects of amyloid aggregation and amyloid-biological interactions, as well as a being a valuable, reproducible tool to analyze cell-to-cell seeding and spreading of pathogenic seeds from "*prion-like*" or "*prionoid*" proteins (Aguzzi and Rajendran, 2009; Scheckel and Aguzzi, 2018). In fact, the use of microfluidics and LOC technology has extended from technical fields (i.e., engineering, physics, and electronics) into a wide variety of biomedical scientific fields including pharmacology, oncology, immunology, and neurobiology.

An Overview of Microfluidics and Lab-on-Chip (LOC) Platforms

Microfluidics platforms are devices containing microchannels with a height/width scale between 100 nm and 100 μm (Tabeling, 2005; Folch i Folch, 2013). Although for neuroscience, pioneer microfluidic studies were developed by Campenot (1977, 1982), (see also Taylor and Jeon, 2010; Neto et al., 2016 for reviews), from the electronics point of view, its origins begin in parallel to microelectronics by micro-fabrication techniques from the semiconductor industry in the 1970s and 1980s (please see Tabeling, 2005). After this, in the 1990s the concept of μTAS (miniaturized total chemical analysis systems) was developed to describe a microfluidic platform that could carry out all the functions required for analysis of an analyte: sample preparation including transport, and chemical reactions as well as selective analyte detection. From this, in terms of manufacture, terms like MEMs (microelectromechanical systems) and LOC devices emerged in the microelectronics and biomedical fields (Folch i Folch, 2013). As indicated in the introduction, LOC might include biosensors/electrochemical/optochemical sensors that have been developed in recent years. In fact, there is a parallel development of the complexity of the LOC devices (i.e., in terms of manufacture) directed to amyloid screening and monitoring with the development of new detection methods.

Today, although with some exceptions (Kamande et al., 2019), the vast majority of microfluidic LOC devices utilized in neurobiology are generated using the silicone elastomer polydimethyl-siloxane (PDMS) (McDonald et al., 2000; McDonald and Whitesides, 2002; Ng et al., 2002; Kuncova-Kallio and Kallio, 2006). PDMS is an economically cheap, biocompatible, soft, flexible, and easy-to-handle elastomer, with an index of refraction of 1.43 (similar to a glass coverslip ≈1.52), and good gas diffusion. Relevant electrical and thermal isolation are highly suitable for biological research (i.e., cell culture) and fluorescent microscopy (McDonald et al., 2000; McDonald and Whitesides, 2002; Ng et al., 2002; Kuncova-Kallio and Kallio, 2006). This new PDMS-based microfluidic application using the elastomer directing microfluidic, micropatterning, and microfabrication technologies to neurobiological experiments was developed 2003–2006 by Jeon's lab (Taylor et al., 2003, 2005; Rhee et al., 2005; Park et al., 2006) with great development in recent years (see Neto et al., 2016 for review). These pioneer studies follow the experiments of Campenot (1977, 1982) in generating a simple, reproducible, and tunable culture platform for compartmentalized neural growth and differentiation. Most of the experiments designed to explore the cell dynamics of different amyloids are currently based on their pioneer microfluidic designs.

PDMS-based manufacture of LOC devices is mainly based on "soft-lithography" protocols (McDonald et al., 2000; Whitesides et al., 2001). Today, PDMS manufacture has evolved to multilayer LOCs as well as more complex platforms. In fact, due to their physical characteristics, different PDMS microfluidic chips can be bounded using plasma reactions (Tran H. T. et al., 2014) to generate multilayered LOCs (i.e., Saar et al., 2016). In fact, some of these multilayered LOCs are used today to analyze amyloid formation *ex situ* (i.e., Saar et al., 2016). Additional methods ranging from hot-embossing lithography (Jeon et al., 2011) to 3D printing methods (Au et al., 2016) have been developed to generate new LOC devices. Readers may obtain more information about LOC platform manufacturing strategies in reference microfabrication books (Minteer, 2006; Herold and Rasooly, 2009; Lee and Sundararajan, 2010; Folch i Folch, 2013). In this review we will focus on the PDMS-derived LOC devices with the greatest impact on the study of amyloids associated with neurodegeneration.

Why Use LOC Devices and Microfluidics in Amyloid-Related Studies?

Microfluidics and LOC devices hold a number of advantages for amyloid-related research at different levels: (1) most LOC devices reduce the use of reagents due to small reaction volumes; (2) some LOC devices can produce a large number of independent but repetitive compartments to allow protein-protein interactions (i.e., micro/nanodroplets, see below); (3) in most LOC platforms we have complete control over spatial and temporal parameters in the reaction conditions; (4) most LOC devices are compatible with several detection methods (i.e., optical or electrical sensors); and (5) some LOC devices allow for the differential culture of different cell types (i.e., neurons, astroglia, oligodendroglia, microglia, etc.) in the same platform in an interactive way – for example in: (i) microfluidically isolated chambers, (ii) cells growing on molecular or chemical gradients, (iii) cells growing under flows, and (iv) cells growing inside 3D structures [cellular aggregation (i.e., neurospheres, neurospheroids, and organoids) or biomaterial-derived scaffolds].

In the large bibliography focused on microfluidics with more than 3000 published reviews reported in Pubmed™, we will focus in this review on first describing the use of LOC platforms to monitor amyloid seeding and aggregation, and second whether

LOCs help researchers understand cell-to-cell amyloid spreading and how LOC devices can help us analyze amyloid effects in neural network physiology. However, in order to understand their potential, first we will broadly summarize the most basic physical concepts of microfluidics that play crucial roles in the design of some of the approaches and devices that will then be further described. In addition, some specific references are included for those readers interested in particular aspects of microfluidics.

Some Basic Physical Concepts in Microfluidics

In biotechnology and bioengineering, microfluidics and LOC are present in various forms depending on the application and end use. The most usual form is single-phase microflows inside channels or capillary tubes. This is the typical case of a physiological buffer or a culture medium that contains a molecule or analyte that should be detected or analyzed using an LOC device. However, for different studies we need to use multiphase flows. This implies the use of two different non-miscible fluids (for example in micro/nanodroplet formation or cell encapsulation). However, in both single and multiphase flows, fluids are often moved by applying hydraulic pressure to the fluid inside the channel/s depending on the LOC design. In some cases, the applied force is a gravitational force but in other cases syringe pumps are used to move the fluid. In order to understand fluid dynamics in single-phase microflows inside small microchannels, first we need to focus our attention briefly on their behavior. In microfluidics one of the most frequently used key values is the Reynolds number (*Re*). This is a dimensionless number expressed as a function of the density of the fluid (ρ), the velocity of the fluid inside the channel (u), the length of the channel (L), and the dynamic viscosity of the fluid (η)

$$Re = \frac{\rho u L}{\eta}$$

At the microscale (as happens in most LOC devices) the *Re* number is very low and the fluids behave like a laminar non-turbulent fluid. In fact, very few microfluidic devices used turbulent flows (with *Re* values $>$ 2,000), but a differential range of fluid flows can be used in a laminar regime. Those microflows that show an *Re* value $<$0.5 follow the multiparametric Navier-Stokes formulation (see Tabeling, 2005; Bruus, 2008 for details). In these cases, aqueous fluids are considered Newtonian fluids which belong to the category of incompressible, uniform, and viscous fluids. However, for micro/nanodroplet or digital microdroplet approaches (see below) the use of two fluids (water and oil) with different behaviors is typical. In these cases, the LOC device can use non-Newtonian fluids that do not follow the formulation below. We refer the reader to classical reference books for specific formulation for non-Newtonian fluids (i.e., Böhme, 1987; Bruus, 2008; Berthier and Silberzan, 2010).

In addition to the Reynolds number, the interfacial tension also plays a role. It states the elastic tendency of a fluid in a surface to contract the surface-air interface in order to reduce its free energy (Sackmann et al., 2014). Interfacial tension is relevant in two immiscible fluids. In this situation and at this scale, interfacial tension dominates the gravitational force (Sackmann et al., 2014). Another dimensionless number is the capillary number. This number compares surface tension forces with viscous forces. Where σ is the interfacial tension, u is the velocity and η is the viscosity.

$$Ca = \frac{\eta\, u}{\sigma}$$

In addition to these values, the Bond number or the Weber number are also described. We refer the reader to Tabeling (2005), Bruus (2008), and Grimmer and Wille (2020) for more details. The factors are relevant for droplet formation. In this review we will consider the droplet formation in a T-junction system in detail (**Figure 2**; Teh et al., 2008). The reader can obtain current information on droplet LOC designs in Grimmer and Wille (2020). In the scheme, the fluid flows are determined as *Qc* and *Qd* and the dimension of the channels *Wd* and *Wc*. In this LOC, the *Ca* is one of the most important parameters in droplet generation. For example, when the *Ca* number is low, the incoming dispersed phase fluid tends to occupy the full section of the channel and droplet formation occurs at the downstream side of the T-junction corner. However, if *Ca* is higher the dispersed phase fluid occupies only a part of the channel and smaller droplets are formed. Practically, when a droplet is generated it continues to grow for a time t_n for necking due to the continuous injection of the dispersed phase fluid. At the end, the final droplet volume V can be predicted (in an easiest vision) with this scaling law.

$$V = Vc + t_n Qd$$

Where *Vc* depends on *Ca* and the duration of necking t_n and decreases as Ca increases. Another relevant factor in droplet formation is the flow rate radio *Q (Q = Qd/Qc)* (from dispersed and C for continuous phases). For example, for small *Q* the droplet is pinched off at the T-junction corner regardless of the *Ca* number. However, for large *Q*, increasing *Ca* will force the detachment point to move from the corner downstream. Due to the large surface-to-volume ratio, fluid/surface interactions largely affect droplet dynamics in the microchannels. In parallel, the presence of the droplet changes the hydrofluidic resistance of the microchannel. If fact, we can assume that the overall flow resistance of a channel can be estimated by:

$$R^* = R + n\, Rd$$

Where R is the resistance of the channel, n is the number of droplets inside the channel, and *Rd* is the single droplet resistance. The value of *Rd* has been studied in several reports and is dependent of several factors such as the viscosity of the dispersed phase and the continuous phase, and the length of the droplet, as well as the geometry of the microchannel (see below). Considering these parameters today we can generate microdroplets for amyloid aggregation in micro/nanodroplets in a controlled space.

For non-bioengineering researchers, and considering Newtonian fluids, the third relevant aspect is that following microfluidic rules, we can correlate the behavior of a pressure-driven microfluidic laminar flow inside a channel with Ohm's law

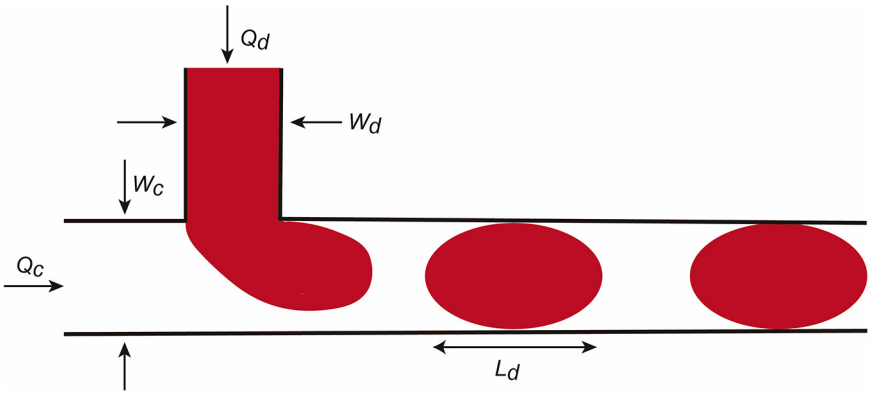

FIGURE 2 | Scheme illustrating micro/nanodroplet formation in a classical T-junction LOC. Please see the main text for details concerning the *Q* and *W* values. In this configuration, the dispersed phase is pumped into the continuous phase orthogonally. As the dispersed phase enters the continuous, shear forces elongate the head of the dispersed phase until a segment eventually separates and relaxes into a sphere or plug shape as a result of interfacial tension.

of electricity ($R = V/I$). Thus, the ratio of the fluid pressure (P) ≈ V (voltage) and the volumetric fluid flow rate Q is the electrical current I (**Figure 2**). This occurs since under laminar flow, the pressure drop inside the microchannel is proportional to the flow rate: $\Delta P = R_Q{}^*Q$. The hydraulic resistance R_Q (also termed R_H in some references) is dependent on microchannel geometry: the cross-section area (s) but also the length (L) of the microchannel. Thus, for an arbitrary section of the microchannel (with equal x and y dimensions) the value of R_Q may be expressed as follows:

$$R_Q = 2\,\mu\,L\frac{p^2}{s^2}$$

Where μ is the dynamic viscosity of the fluid and p is the perimeter of the microchannel. Thus, in this situation the Hagen-Poiseuille equation can be used in a channel with circular section to determine the ΔP as follows (reviewed in Shah and London, 1978):

$$\Delta P = R_Q\,Q = \frac{8\mu L}{\pi r^4}\,Q$$

In the case of a channel with square section [height (h) = width (w)] or rectangular section (when $w/h > 1$), the hydraulic resistance of the channel (R_Q) can be calculated respectively as follows (see Grimmer and Wille, 2020 for details):

$$R_Q = \frac{28.3\,\mu\,L}{h^2} \qquad \text{and} \qquad R_Q \approx \frac{a\,\mu\,L}{w\,h^3}$$

where a denotes (in rectangular section) a dimensionless parameter defined as

$$a = 12\left[1 - \frac{192\,h}{\pi^5\,w}\tanh\left(\frac{\pi\,w}{2\,h}\right)\right]^{-1}$$

However, in a presence of a droplet (see above) the resistance of the microchannel dynamically changes. In fact, the values for the Rd of the droplet are described by this formulation

$$Rd = (\mu_d - \mu_{cont})\,\frac{L_d\,a}{w\,h^3}$$

Where L_d is the length of the droplet, μ_d the viscosity of the dispersed phase, and μ_{cont} the viscosity of the continuous phase and the other parameters described above. Consider that the Hagen-Poiseuille law is similar to Ohm's law (see above). Thus, these calculations are very useful to modulate and determine flow, pressures, and channel geometry as well as to simulate the behavior of our microfluidic flows (i.e., culture media, droplet formation) inside a particular LOC. As examples, we will describe two different microfluidic devices with wide use in neurobiology using correlative microfluidics as well as electric circuit modeling (please see Oh et al., 2012 and Robertson et al., 2014 for additional details).

The Hydrodynamic Focusing/Mixing LOC Device

Hydrodynamic focusing is a method to control continuous flow for solution mixing of fluids or droplets. The basis is the formation by confining fluid streams or flows to small geometries or microchannels. The main advantage of this strategy is the achievement of very short complete mixing times while maintaining a highly controllable system which can be precisely modeled. In the basic system (**Figure 3A**), there are three inlet streams: one central stream to be focused and two streams that converge perpendicularly on the central stream (**Figures 3A–C**). In the example, we consider, in **Figure 3B**, the electric model in which the section of all channels is identical (α) and the value β is the distance between the reference point P_0 and the end of the mixing channel. Following Kirchhoff's two laws, we can approximately define the Wf size in the mixing channel by applying the following equation based in fluid dynamics:

$$\frac{Wf}{W} = \frac{1}{g\ (\lambda)}\,\frac{Q1}{Q1 + Q2 + Q3}$$

where g (λ) is a factor depending on the aspect ratio of the channel h/W, h being the height and W the weight of the microchannel, if $h << W$; λ $\to$ 0, but more commonly $h < 1$ and the formula is more complex (please see Berthier and Silberzan, 2006; Rodriguez-Villarreal et al., 2010 for details). Alternatively, and as first described by Knight et al. (1998),

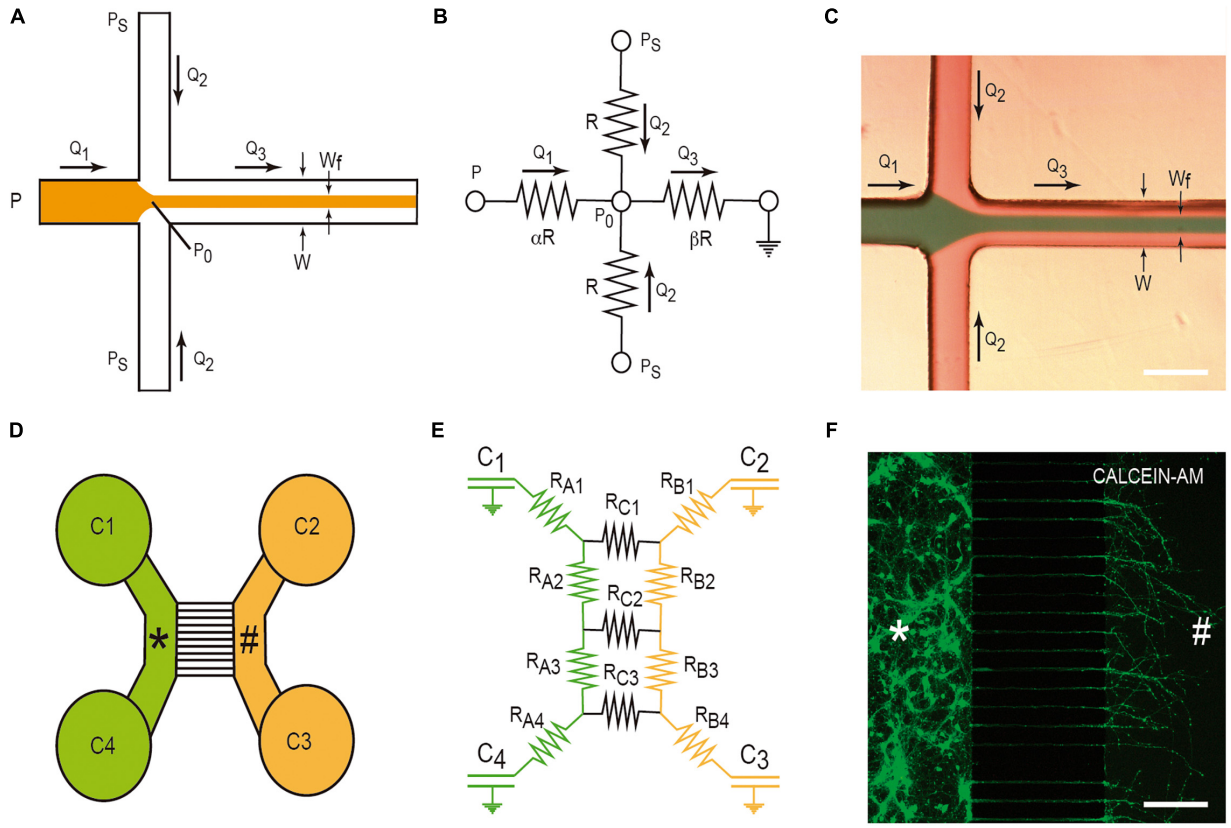

FIGURE 3 | Examples of LOC devices and microfluidic platforms. Microfluidic hydrofluidic mixing device **(A–C)** and compartmentalized LOC device **(D–F)**. For each device, the correlative fluidic and electric model is included. In **(C,F)**, we provide two examples of the generation of hydrodynamic focusing **(C)** and the growth of axons labeled with Calcein^{TM}. The two different compartments are labeled with * and # in **(D–F)**. Please see manuscript section "Some Basic Physical Concepts in Microfluidics" for details of the correlation between fluidics laws and electric laws in LOC devices.

considering Ohm's law and the electric model (**Figure 3B**), the summary of the calculation is the following:

$$r = \frac{Ps}{P} = \frac{\beta Q1 + (2\beta + 1)\, Q2}{(\beta + \alpha)\, Q1 + 2\beta Q2} \quad \text{and} \quad Wf = \frac{1 + 2\beta - 2\beta r}{1 + 2\alpha r}$$

Thus, using these parameters we can control the interaction between two different fluids by modulating *Q1* and *Q2*. In fact, this was used in a large number of experiments (see Kirby, 2010; Badilescu and Packirisamy, 2011 for reference books). In a laminar flow regime mixing only occurs by diffusion. Thus, the mixing of the analytes depends only on their intrinsic diffusion coefficient (see Arter et al., 2020 for a recent review). After this, the diffusion parameters of the different elements (i.e., oligomers) can be controlled and analyzed during amyloid aggregation. In fact, these systems can also include several detection systems such as electrodes (stimulating or recording) as well as optical measurement. In this respect, the Peclét number (Pe) describes the relative rates of molecular convection relative to diffusion. Classically, the LOCs retain large values of Pe to prevent complete diffusional mixing over the timescale. Thus, LOCs are well suited to the study of protein-protein interactions. Typically, this is achieved through quantification of changes in the size or charge of proteins and complexes as they participate in the interaction. Due to the above-mentioned basis, the mixing rate of analytes under microfluidic flow can be measured by analyzing their diffusion coefficient and the hydrodynamic ratios of the biomolecules. With these approaches, the diffusion of α-synuclein (Zhang Y. et al., 2016) and β-amyloid (Scheidt et al., 2019) were analyzed. However, and as an alternative, these experiments have also been developed in droplets from fento to nanoliter volumes. These droplets can be generated at different frequencies (from 0.1 to 1 MHz). In contrast to bulk-phase studies in which aggregation reactions are dominated by secondary effects that rapidly amplify the rate of protein misfolding, masking primary nucleation events (i.e., Knowles et al., 2009), in LOCs droplets single nucleation events can be observed on a drop-by-drop basis, an approach that also enables observation of the spatial and temporal propagation of some fibrillar proteins (e.g., insulin; Knowles et al., 2011; Pfammatter et al., 2017).

Compartmentalized Cell Culture With Microchannels Growing Under Microfluidic Isolation in Two or More Chambers

This microfluidic device was developed to culture two or more different cell types (**Figure 3D**). In fact, their original goal was to

compartmentalize cultured neurons in order to microfluidically isolate the somato-dendritic domain from the axonal domain for axonal RNA isolation for axotomy purposes (**Figure 3D**). This was achieved by using four open chambers with two channels that were interconnected by a variable number of microchannels (up to ∼100). These microchannels showed (in the original model) a small rectangular section with a high fluidic resistance due to its length. This largely reduced the fluidic flow between the two chambers. A more detailed description of the original microfluidic device can be found in Taylor et al. (2005). In order to isolate axons, although depending on the cultured neuron, the length of the microchannels should be more than 400–450 μm since dendrites or immature neurites are able to enter inside microchannels, but for cortical neurons, they only extend for a distance ≈150–250 μm in contrast to growing axons that might extend for distances longer than 1 mm inside the microchannels (Taylor et al., 2005; **Figure 3F**). Taking into account Ohm's law, Robertson et al. (2014) developed an electric model of the device (**Figures 3D,E**). With this, we can model the volumetric transport of the media between the different chambers. In the modeled LOC device, the platform contains a network of resistances R_{A-C}, linking four chambers C_1-C_4 (currently of 7–8 mm Ø). Considering the volume of each chamber (acting as an electronic capacitator), the hydrodynamic pressures (electrical voltage) and the volumetric flow rates (electric current) can be predicted over time as follows:

$$V(t) = \frac{\Delta V}{2}\left(1 - e^{-\frac{2t}{RC}}\right) \quad \text{and} \quad P(t) = R\,\frac{dV}{dt}$$

where the flow rate *V(t)* is the differential volume between wells over time and *P(t)* is the differential hydrostatic pressure between wells over time. Depending on the values of *C* and *R* and the initial conditions of volume of each chamber, the time constant $t = RC/2$ provides us data to estimate the rate of change of the hydraulic pressure, and consequently allows us to estimate the time needed to reach a volume equilibrium in the chambers of the LOC device. In addition, this procedure is a very useful tool during device design, empowering optimization of the relationship between the assay to be performed and design of the microchannel geometry (i.e., length, cross-sectional dimensions, etc.) (Robertson et al., 2014). On a practical basis, we can modulate the volume of each chamber to generate small but controlled media flows that will impair, in parallel with the fluidic resistance inside the small microchannels, the unwanted diffusion of a putative analyte or amyloid through the medium based on a differential concentration. This will be very useful to determine cell-to-cell prion/amyloid transmission; furthermore, we can determine whether an amyloid is taken up by specific domains of the healthy or unhealthy neuron or glial cell (see below). From the numerical data evaluation, the authors analyzed two putative configurations (flow paths): a pressure gradient between wells connecting a culture chamber (i.e., C2 and C3) and a pressure gradient across the microchannels. Using these numerical simulation, the estimated time constants for the pressure to equilibrate were 189 s across each chamber (t_B) and 39,956 s across the microchannels (t_C), respectively (Robertson et al., 2014). As t_C is two orders of magnitude greater than t_B, the two chambers can be considered fluidically isolated over short periods of time. However, the authors do not provide additional data concerning longer times. This is usually solved by increasing the volume of the culture medium in one part of the device with respect to the other. Another relevant aspect in these LOCs is the maintenance and survival of cultured cells. In our experience, we were unable to maintain cultured neurons for more than 20 days. This impairs a putative long-term experiment on infectivity and only specific processes can be analyzed. Furthermore, this limits the use of induced pluripotent stem cells (IPSc), with large differentiation protocols, in these devices. In order to avoid this, pre-differentiated neurospheroids are currently used in similar LOCs and some of these are commercially available (Osaki et al., 2020).

AMYLOID AGGREGATION STUDIES IN LOC DEVICES

Although most amyloid species were initially identified within the context of neurodegenerative diseases and their transmission (see Peng et al., 2020 for a recent review), several proteins have also been found to form amyloid-like fibrils [e.g., islet amyloid polypeptide (amylin) (Zheng et al., 2020) or insulin (Zheng et al., 2020)] outside the nervous system. Furthermore, increasing evidence has pointed toward amyloid formation being a generic self-aggregation property of proteins and polypeptide chains, with many polymeric species having been identified during the process (see Morris et al., 2009 for review). In fact, a key aspect in evaluating the aggregation kinetics of biomolecular species is the ability to monitor fibrillar growth as a function of time (see above). The monitoring of this process can be developed in LOC [e.g., in hydrodynamic focusing systems (i.e., Fitzpatrick et al., 2013; Arosio et al., 2016)], or using electrophoretic approaches in these systems (i.e., Saar et al., 2018).

However, it is well-known that the amyloid aggregation process is largely dependent on the interaction of the protein with several ions (i.e., Kim et al., 2018; Metrick et al., 2019), membranes (i.e., Terakawa et al., 2018; Alghrably et al., 2019), and other surfaces (e.g., water; Schladitz et al., 1999). Thus, researchers used different methods to avoid or control these in some cases unwanted interactions. One of the most widely used methods is the aggregation study inside micelles or micro/nanodroplets (water-oil) of different proteins (i.e., Shim et al., 2007; Teh et al., 2008; Casadevall i Solvas et al., 2012; Shembekar et al., 2016; **Figure 4**). Using microdroplets, many independent reactions can be monitored simultaneously in identical volumes which are several orders of magnitude smaller than what has been common in biochemical assays. On a practical level, the formation of the droplets, mainly by microfluidic focusing devices, is followed by their harvesting and maintenance, trapped or retained in reaction chambers to be further analyzed (i.e., Shim et al., 2007; Teh et al., 2008; Casadevall i Solvas et al., 2012; Shembekar et al., 2016; **Figure 4B**). In these cases (especially for sessile droplets exposed to air) (Casadevall i Solvas et al., 2012), the decrease in droplet volume over time due to the evaporation of water molecules

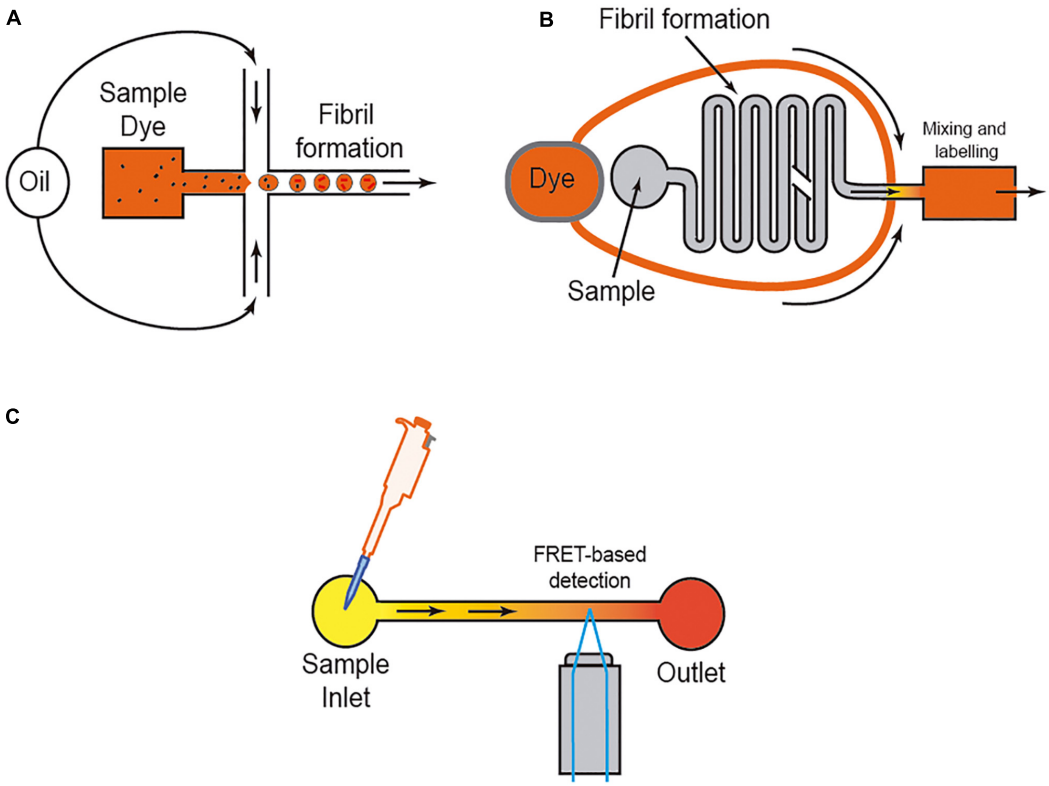

FIGURE 4 | Scheme of three different approaches to analyzing amyloid formation under fluidic flow. In **(A)**, the micro/nanodroplet formation (water-oil) is illustrated. In **(B)** a mixing LOC device is illustrated, and in **(C)** the use of FRET derived protein sensors to monitor protein-protein interaction is illustrated. In each example, the presence of the dye (usually ThT) is displayed.

increases the analyte/protein concentration inside the generated droplet, thereby increasing protein-protein interaction and, more relevantly, amplifying signal(s) associated with the aggregation that can be monitored with several methods, including Förster resonance energy transfer (FRET) (**Figure 4**). Other alternatives to enhance the process of reduction of the microdroplet volume using PDMS-derived microflows to enhance the reactions were also recently reported (i.e., DroMiCo; Kopp et al., 2020). This recently published method generates and traps the microdroplets, the aqueous flow rate is stopped in the LOC, and the oil flow rate is kept minimal at 2 μL/min to accelerate droplet shrinking and prevent entry of air into the device, in order to further analysis.

In fact, amyloid fibril formation typically displays sigmoidal growth kinetics (i.e., Ferrone et al., 1985; Knowles et al., 2009; Morris et al., 2009; Prusiner, 2017). Indeed, changes in the aggregation of fibrils make up a three-phase curve that can be monitored easily using ThT-fluorescence or, depending on the protein sequence, intrinsic amino-acidic residues (i.e., tryptophan) with particular fluorescence properties after aggregation (i.e., Knowles et al., 2009; Meisl et al., 2016; Toprakcioglu et al., 2019). In current aggregation kinetics, the first stage is a "lag-phase" also termed "nucleation-phase" displaying a very small increase in the amount of fluorescence over time (i.e., Arosio et al., 2015), followed by a fast-growing phase and the last phase or "steady state" equilibrium with higher fluorescence values. However, we should consider that this is a dynamic process that includes fibrillar fragmentation, nucleation, and other processes during all the phases. In fact, the duration of the "lag-phase" is highly dependent not only on the monomer concentration and seed formation, but also on physical parameters as well as the presence of molecular chaperones. For example, when sarkosyl-insoluble fractions from AD patients or other tauopathies are analyzed in bulk experiments, the lag-phase cannot be clearly distinguished due to the high concentration of preformed fibrils and "amyloid seeds" (i.e., Ferrer et al., 2020b) in the sample and the curve is almost logarithmic. In fact, the time evolution of the "lag-phase" is also of interest for the characterization of some amyloids (i.e., MSA-derived synuclein vs. PD-derived synuclein) with different seeding as well as propagative properties (i.e., Shahnawaz et al., 2020). Additionally, in most studies the molecular events that occur in this "lag-phase" of amyloid formation are not fully ascertained using classical analytical methods. However, LOC devices and microdroplet formation were very useful in describing, in greater detail, the sequential events during this fibril formation for different amyloids (i.e., Aβ; Arosio et al., 2014), silk fibroin, β-lactoglobulin, lysozyme (Toprakcioglu et al., 2019), human islet amyloid polypeptide (Marek et al., 2010), and sickle hemoglobin (Ferrone et al., 1985). In fact, the events that occur during this lag-phase are of special interest in the effort to understand

amyloid dynamics during neurodegeneration (Orru et al., 2015; Masujin et al., 2016).

In neurodegeneration, although with some discrepancy, it is well-established that lower aggregative amyloid species are more relevant species (i.e., toxic) compared to large amyloid species in different diseases [i.e., for Aβ (Deshpande et al., 2006; Hepler et al., 2006) and α-synuclein (Conway et al., 2000; Winner et al., 2011; Chen and Cremades, 2018; Prots et al., 2018)]. More relevantly, researchers aim to determine the properties of the "propagative seeds" or "propagons" for particular amyloids. This is a challenging question, especially for "*prion-like*" proteins (Aguzzi and Lakkaraju, 2016). Over time, classical bulk methods have been modified to match those that include an amplification step. For example, using a new method, Arosio et al. (2014) detected Aβ propagons in a "lag-phase" of aggregation by sample filtration during the phase, followed by an amplification method with fresh Aβ monomer. This was followed by the quantification of the original propagon concentration using a calibration curve based on controlled seed concentration (Arosio et al., 2014). Using this method, the authors improved by two orders of magnitude the bulk technical approaches to allow the concentration of fibrillar Aβ (Arosio et al., 2014). However, the recent development of "digital microfluidics" which combines the use of microfluidics and high-throughput biological assays (Guo et al., 2012) has helped researchers to develop a digital amyloid quantitative assay (d-AQuA) aimed at allowing absolute quantification of single replicative units, the "propagons," in the proof-of-concept manuscript of insulin (Pfammatter et al., 2017). In fact, the authors used a dilution method of nanodroplets with picolitres of volume containing (or not) "propagon" molecules that were further evaluated using ThT staining, following a Poisson distribution probabilistic model (Pfammatter et al., 2017). This method, although not developed for other amyloids, is faster than currently available methods (e.g., microplate assays) and will be of relevance for fast diagnosis of the presence of "pathological-seeds" for different PMDs. Parallel to these approaches, other groups have developed more automatic methods such as the microchannel-connected multiwell plate (μCHAMP) device (Park et al., 2016) that uses microdroplet formation and microfluidic transport to 96-well plates. The amount of Aβ (at a range of ≈ 10 pg/mL) is detected using a droplet-based magnetic bead immunoassay (Park et al., 2016). Thus, LOC devices are of relevance not only for the reduced sample volume required, but also for automatization and high-throughput assays of amyloid detection. In addition, recent reports illustrate the relevance of the use of aggregation-induced emission (AIE) dyes as a preferential strategy to identify protein fibrillogenesis, particularly the light up characteristic associated with binding events during the aggregation process. These dyes feature high emission efficiency in the aggregate state, strong photo-stability, and excellent biocompatibility (Wurthner, 2020). Examples of their use can be found in the analysis of insulin (Hong et al., 2012; Huang Q. et al., 2017) and of β-amyloid aggregation (Zhang J. D. et al., 2016; Fu et al., 2019; Yang et al., 2019). Readers may find a general survey of these techniques in Wurthner (2020).

LOC AS TOOL TO ANALYZE CELL-TO-CELL TRANSPORT AND BEHAVIOR OF AMYLOIDS

As indicated above, studies of seeding and spreading of different amyloids *in vitro* must be complemented by complex cellular systems mimicking *in vivo* situation as well as animal experimentation. Indeed, several groups have developed *in vitro* cellular models to monitor seeding properties and their associated effects in cell survival. However, for some amyloids (e.g., tau) their overexpression in cells resists aggregation instead of hyperphosphorylation, and additional methods are needed to increase their intracellular content, avoiding phosphorylation. One of the alternatives is a commercially available BioPORTER QuikEase Protein Delivery Kit which can deliver active proteins intracellularly. This method was used by Guo and Lee (2011) to demonstrate that the seeding of normal tau induced by pathological tau led to the formation of NFL-like structures in treated cells (Guo and Lee, 2011). In other approaches, cell lines overexpressing mutated protein with aggregative properties fused with a flag (fluorescence) sequence (i.e., P301L-V5; Xu et al., 2016) have been used for high-throughput assays of tau aggregation. In the presence of an aggregating amyloid species (e.g., tau) the aggregation process can be followed by analyzing the emitted fluorescence. Some of these approaches have also included FRET methods (Shin et al., 2019). These cellular "biosensors," mainly developed in HEK293 or H4 cells, have been adapted for fluorescence detection of other amyloids such as α-synuclein (Prusiner et al., 2015; Holmes and Diamond, 2017). In fact, these methods are already being supported by the use of ultra-resolution confocal microscopy (Kaminski and Kaminski Schierle, 2016) to monitor the amyloid seeding and aggregation processes in cell cultures at the nanoscale level. Today the use of these biosensors is mainly focused on drug screening. However, in a putative scenario the use of these cells in LOCs could be of relevance in determining key factors involved in the seeding process of amyloids (e.g., the relevance of a specific receptor in the process).

However, as indicated, researchers aimed to determine cell-to-cell mechanisms implicated in amyloid seeding and spreading (see introduction). In this respect, several studies reported using LOC devices, with two or more consecutive chambers: Aβ (i.e., Deleglise et al., 2014; Song et al., 2014), α-synuclein (i.e., Volpicelli-Daley et al., 2011; Freundt et al., 2012; Brahic et al., 2016; Urrea et al., 2018; Wang et al., 2018), tau (i.e., Wu et al., 2013; Dujardin et al., 2014; Calafate et al., 2015; Takeda et al., 2015; Usenovic et al., 2015; Congdon et al., 2016; Polanco et al., 2018), TDP-43 (i.e., Feiler et al., 2015), and dipeptide repeat proteins (DPRs) of the *C9orf72* gene product associated with ALS and frontotemporal dementia (FTD). Westergard et al. (2016) were able to perform cell-to-cell transmission by navigating intracellularly along axons allowing seeding and propagation of the amyloid (reviewed in Urrea et al., 2018; Peng et al., 2020; Uemura et al., 2020). These studies reported the sequential transport of the "pathogenic seeds" as free seeds or in exosomes between different cell populations

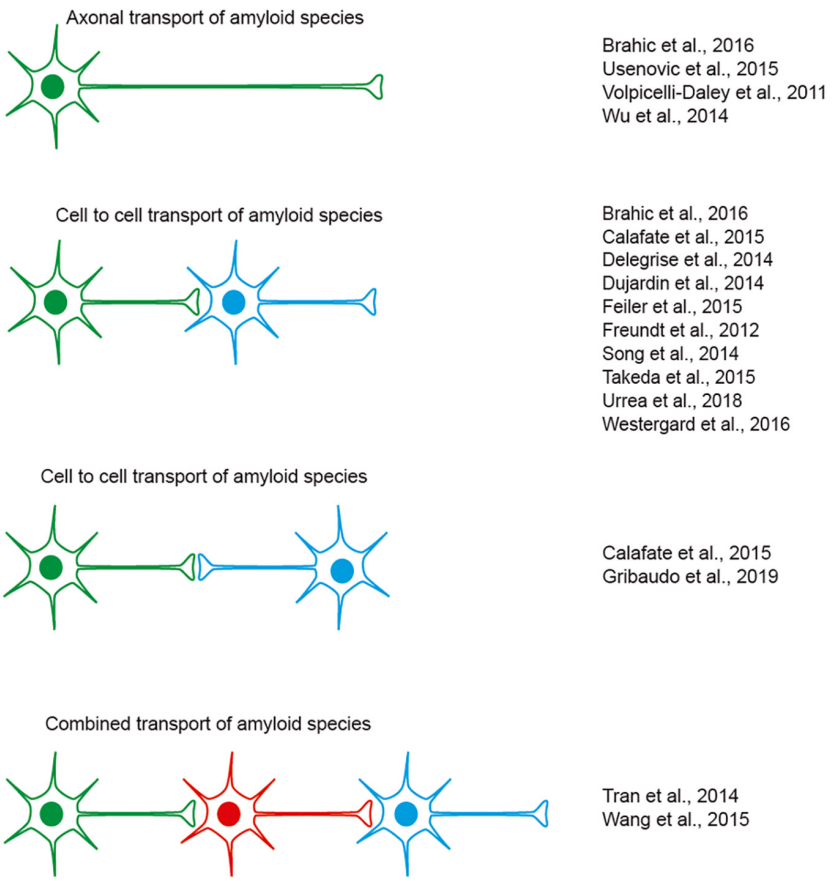

FIGURE 5 | Examples of experiments designed to explore amyloid transport in axons as well as cell-to-cell transmission. The different colors of the illustrated cells represent the cells cultured in different reservoirs of compartmentalized LOC devices and their orientation. In addition, some references are included as examples of their exponential use in neurodegenerative neuroscience.

cultured in different chambers (**Figure 5**). In these experiments a differential volume between reservoirs is established to avoid diffusion transfer by the media between reservoirs. In fact, different LOCs have been designed for specific studies (e.g., co-culture of microglia, astroglia, and neurons (3D hNeuroGliAD) (Park et al., 2018). More relevantly, in several studies neurons derived from IPSc or neuronal progenitors are included to mimic specific neurodegenerative diseases (i.e., Choi et al., 2014; Ruiz et al., 2014; Park et al., 2018). These LOC approaches help researchers to ascertain the role of non-neuronal cells in the seeding and propagation process for particular amyloids (e.g., Aβ roles of microglia reactivity and migration (Cho et al., 2013; Park et al., 2018) and the role of astrocytes in α-synuclein seeding (Cavaliere et al., 2017). However, the emerging role of oligodendrocytes as non-neighboring cells during some amyloid transmission [i.e., α-synuclein (Tu et al., 1998; Uemura et al., 2019), tau (Ferrer et al., 2019, 2020a) see also (Ferrer, 2018) for recent review] has yet to be described in LOC devices. This is in contrast to the different LOC devices aimed at exploring myelination (Park et al., 2009; Yang et al., 2012; Lee et al., 2016). Further studies will help neuroscientists to determine their putative role in PMD.

LOC AS A TOOL TO ANALYZE THE NEURAL CONSEQUENCES OF AMYLOID TRANSMISSION

From the early development of the PDMS compartmentalized LOC, several groups combined electrical and optical measurements of neuronal activity with its compartmentalization (among others, Morales et al., 2008; Gladkov et al., 2017; Lassus et al., 2018; Lopes et al., 2018; Moutaux et al., 2018). And in some studies these LOCs devices were used as platforms to determine drug screening and cytotoxicity (i.e., Meissner et al., 2011; Du et al., 2016). As noted, the seeding and spreading of different amyloids is associated with an increase in progressive cell death. This was determined in classical cell cultures in single

chambers but particularly in LOC with different chambers: (i.e., Aβ Deleglise et al., 2014; Ruiz et al., 2014; Li et al., 2017), α-synuclein (i.e., Tran H. T. et al., 2014; Prots et al., 2018; Gribaudo et al., 2019) and Tau (Wu et al., 2016) by direct exposure of cultured neurons to the pathogenic form of the amyloid. Cytotoxicity was measured with biochemical methods, multielectrode arrays (MEA), or changes in calcium transients [i.e., with Fluo4-AM or genetically encoded calcium indicators (GECIs)]. In this respect, several authors included microflows in 3D-derived cultures in LOC devices to determine the effects of exposure to amyloids. For example, Choi et al. (2013) developed a microfluidic platform capable of generating a gradient of Aβ oligomeric assemblies within microchannels to investigate their neurotoxicity. Two years later, Park et al. (2015) developed a pioneering microfluidic chip containing 3D-neurospheroids by providing an interstitial constant fluid flow. Using this 3D platform, the effect of the fluid flow on the neural proliferation, differentiation, and survival was investigated. The authors compared their results with similar Aβ treatments under static conditions, and the main conclusion was that treatment with Aβ under interstitial flow is more deleterious and largely reduces the viability of neural aggregates (Teller et al., 2015).

However, although effects of the pathogenic seeds have been evaluated in numerous manuscripts, little attention has been paid to elucidating the putative changes in neural networks during seeding and cell-to-cell progression between different areas. Due to the relevance of this issue, LOCs could be a relevant tool to ascertain this progressive neurodegeneration between different cell populations. This is of particular relevance for drug discovery, if our final goal is to block amyloid seeding, aggregation and progression. For most cases, a putative drug treatment (i.e., an inhibiting peptide) could be useful *in silico*, and probably non-cytotoxic in yeast, worm, fruit flies, or mammalian cells, but it could carry collateral effects in modifying the function of neuronal networks. To solve this, in our opinion, we need first to understand the changes induced by pathogenic amyloid during the seeding and aggregation process from both the cellular viewpoint and a system-wide perspective. One example can be seen in a pioneer study developed by Teller et al., in which primary cortical neurons were confined into groups using a homemade PDMS mask (**Figure 6**). In the study, the authors determined the synaptic activity and the development of neuronal networks by using calcium fluorescence probes (Fluo4-AM) and the analysis of the intracellular calcium changes to determine firing rate, coordination between different neurons, and the appearance and maturation of different connectivity "hubs" in the culture. After several days in culture to allow the maturation of connections between these neuronal groups, the authors incubated the culture with different aggregated forms of Aβ (with magnetite). Changes in neural network activity and the correlated neuronal interactions after the treatments were evaluated, and the effects of Aβ treatment in the destabilization of the generated network was determined in detail. In order to analyze this the authors used homemade calcium fluorescence analysis software NetCal^{TM} (Orlandi et al., 2014; Teller et al., 2015; **Figure 6**). The data were also corroborated in our laboratory using mic2net software (Smedler et al., 2014).

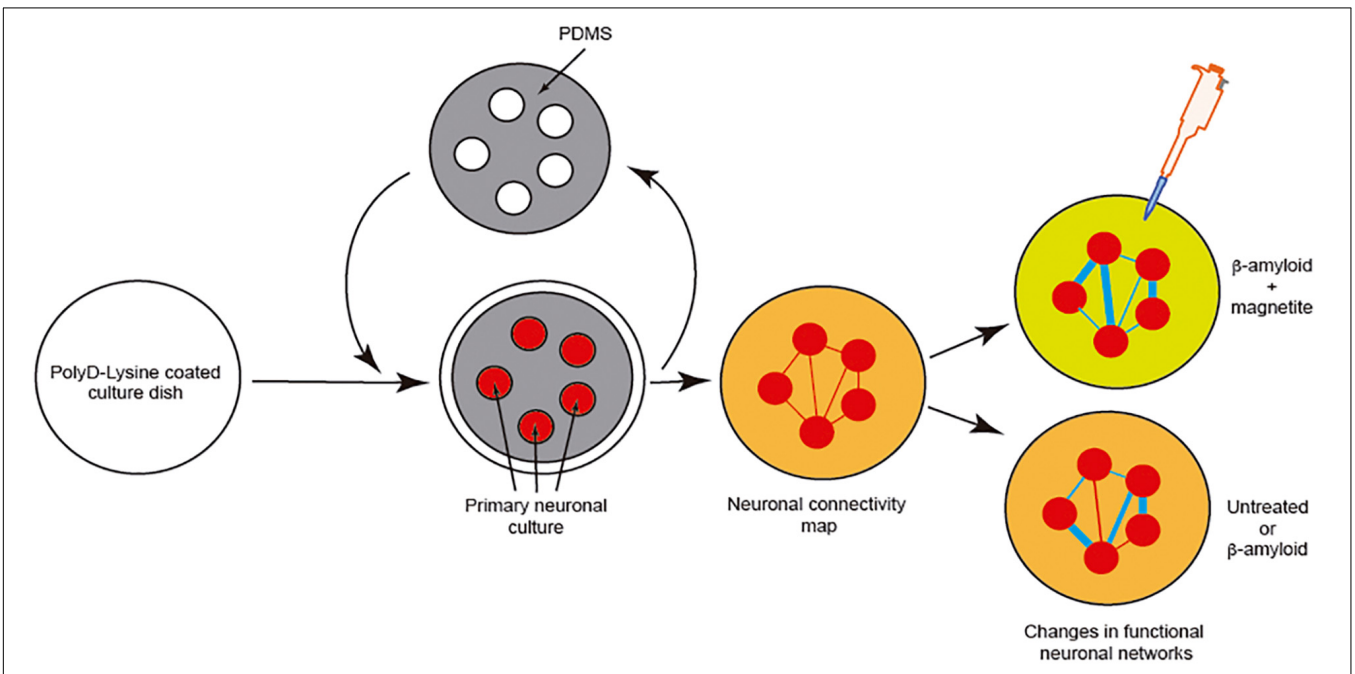

FIGURE 6 | Example of the analysis of neuronal network changes mediated by amyloids (Aβ). We describe the experiment developed by Teller et al. (2015). In the experiment, the authors generated clusters of cells further interconnected in a network like the Atomium attraction in Brussels. After treatment with Aβ alone or Aβ-magnetite, the changes in the neural network were analyzed using NetCal^{TM} software.

Thus, the group developed an *in vivo*-like platform for drug screening in the presence of progressive amyloid generation. Today the use of GECIs (i.e., GCaMP6) instead of classical fluorescence reporters (Fluo4-AM or Fluo8-AM) of neuronal activity and different analysis methods allow us to analyze the network activity of the same culture or neuronal network for longer time periods (Chen et al., 2013). These experiments will help researchers working in drug discovery to avoid the seeding and progression of the amyloids without perturbing neuronal activity.

CONCLUDING REMARKS

In this review we have tried to summarize only a part of the state of the art concerning the use of some microfluidics and LOC devices in amyloid or "*prion-like*" seeding, aggregation, and cell-to-cell transmission research. Unfortunately, for prion infection other strategies would be more appropriate due to the time needed to develop a reliable prion infection. In fact, our lab studied the putative prion formation in IPSc cultured in 2D cultures for more than 150 days with negative results (Matamoros-Angles et al., 2018). Considering this, most probably a 3D culture is needed to develop prion infection, while LOCs will help us in other experimental situations. In this review, we have focused, on a practical basis, on those aspects that we consider relevant for biomedical researchers. In fact, most of the new techniques and proof-of-concept experiments involving aggregation, protein-protein interaction, and analyte detection are not fully described in this review, since, in some cases, they are not yet widely accepted by researchers. We refer the reader to some of the references of this review for additional information. In fact, here we have focused on two types of LOC that could be of interest and which are commonly used in laboratories. For example, micro/nanodroplets LOCs, compared to conventional microtiter plate assays, are an attractive platform for high-throughput studies. LOC devices derived from the compartmentalized culture of neurons or glial cells can help answer key questions in determining cell-specific differences in various disorders, revealing the participation of different cell types, uncovering the differing behaviors of the different "strains" of amyloid, etc. In addition, emerging technologies such as the use of graphene and other materials such as electrochemical and optochemical "biosensors" offer new opportunities to determine amyloid seeding and aggregation in more detail. As indicated, the bioengineering approaches have evolved in recent years, and today, some of them are tools for neurobiological laboratories, as an alternative to unnecessary animal experimentation following the 3Rs of biological research. Although we cannot assume that the use of LOC and microfluidics in neuroscience will follow Moore's law of semiconductors, which suggests doubling of semiconductor numbers in a microprocessor every year, we believe that their use helps and will continue to help neuroscientists. Combined efforts from different disciplines—bioengineering, neurobiology, and clinical practice – in the face of new challenges will be mandatory for future biomedical research.

AUTHOR CONTRIBUTIONS

JR and IF: drafting of manuscript, study conception and design, analysis and interpretation of data, critical revision, and final approval of the version to be published. Both authors contributed to the article and approved the submitted version.

FUNDING

This research was supported by the *PRPSEM* Project with ref. RTI2018-099773-B-I00 from the Spanish Ministry of Science, Innovation and Universities (MCIU/FEDER/AEI), the CERCA Programme, and by the Commission for Universities and Research of the Department of Innovation, Universities, and Enterprise of the Generalitat de Catalunya (SGR2017-648 to JR) and CIBERNED (CMED2018-2) to IF and JR. The project leading to these results received funding from "la Caixa" Foundation (ID 100010434) under the agreement LCF/PR/HR19/52160007 to JR and IF, and the María de Maeztu Unit of Excellence (Institute of Neurosciences, University of Barcelona) MDM-2017-0729 to JR. IF was funded by the Ministry of Economy and Competitiveness, Institute of Health Carlos III (ISCIII–Fondos FEDER, a way to build Europe: FIS PI17/00809).

ACKNOWLEDGMENTS

We thank Tom Yohannan for editorial advice and all members of the Del Rio and Ferrer labs for their comments.

REFERENCES

Abounit, S., Wu, J. W., Duff, K., Victoria, G. S., and Zurzolo, C. (2016). Tunneling nanotubes: a possible highway in the spreading of tau and other prion-like proteins in neurodegenerative diseases. *Prion* 10, 344–351. doi: 10.1080/19336896.2016.1223003

Aguzzi, A., and Lakkaraju, A. K. K. (2016). Cell biology of prions and prionoids: a status report. *Trends Cell Biol* 26, 40–51. doi: 10.1016/j.tcb.2015.08.007

Aguzzi, A., and Rajendran, L. (2009). The transcellular spread of cytosolic amyloids, prions, and prionoids. *Neuron* 64, 783–790. doi: 10.1016/j.neuron.2009.12.016

Alghrably, M., Czaban, I., Jaremko, L., and Jaremko, M. (2019). Interaction of amylin species with transition metals and membranes. *J. Inorg. Biochem.* 191, 69–76. doi: 10.1016/j.jinorgbio.2018.11.004

Arosio, P., Cukalevski, R., Frohm, B., Knowles, T. P., and Linse, S. (2014). Quantification of the concentration of Abeta42 propagons during the lag phase by an amyloid chain reaction assay. *J. Am. Chem. Soc.* 136, 219–225. doi: 10.1021/ja408765u

Arosio, P., Knowles, T. P., and Linse, S. (2015). On the lag phase in amyloid fibril formation. *Phys. Chem. Chem. Phys.* 17, 7606–7618. doi: 10.1039/c4cp05563b

Arosio, P., Muller, T., Rajah, L., Yates, E. V., Aprile, F. A., Zhang, Y., et al. (2016). Microfluidic diffusion analysis of the sizes and interactions of proteins under

native solution conditions. *ACS Nano* 10, 333–341. doi: 10.1021/acsnano.5b04713

Arter, W. E., Levin, A., Krainer, G., and Knowles, T. P. J. (2020). Microfluidic approaches for the analysis of protein-protein interactions in solution. *Biophys. Rev.* 12, 575–585. doi: 10.1007/s12551-020-00679-4

Ashe, K. H., and Aguzzi, A. (2013). Prions, prionoids and pathogenic proteins in Alzheimer disease. *Prion* 7, 55–59. doi: 10.4161/pri.23061

Au, A. K., Huynh, W., Horowitz, L. F., and Folch, A. (2016). 3D-Printed Microfluidics. *Angew. Chem. Int. Ed. Engl.* 55, 3862–3881.

Aulic, S., Masperone, L., Narkiewicz, J., Isopi, E., Bistaffa, E., Ambrosetti, E., et al. (2017). alpha-Synuclein Amyloids Hijack Prion Protein to Gain Cell Entry. Facilitate Cell-to-Cell Spreading and Block Prion Replication. *Sci. Rep.* 7:10050.

Badilescu, S., and Packirisamy, M. (2011). *BioMEMS : Science and Engineering Perspectives*. Boca Raton, FL: CRC Press.

Berthier, J., and Silberzan, P. (2006). *Microfluidics for Biotechnology*. Boston, MA: Artech House.

Berthier, J., and Silberzan, P. (2010). *Microfluidics for Biotechnology*. Boston, MA: Artech House.

Bertrand, E., Lechowicz, W., Szpak, G. M., Lewandowska, E., Dymecki, J., and Wierzba-Bobrowicz, T. (2004). Limbic neuropathology in idiopathic Parkinson's disease with concomitant dementia. *Folia Neuropathol.* 42, 141–150.

Bongianni, M., Orru, C., Groveman, B. R., Sacchetto, L., Fiorini, M., Tonoli, G., et al. (2017). Diagnosis of human prion disease using real-time quaking-induced conversion testing of olfactory mucosa and cerebrospinal fluid samples. *JAMA Neurol.* 74, 155–162. doi: 10.1001/jamaneurol.2016.4614

Böhme, G. (1987). *Non-Newtonian Fluid Mechanics*. Amsterdam: Elsevier.

Braak, H., and Del Tredici, K. (2009). Neuroanatomy and pathology of sporadic Parkinson's disease. *Adv. Anat. Embryol. Cell Biol.* 201, 1–119. doi: 10.1007/978-3-540-79850-7_1

Brahic, M., Bousset, L., Bieri, G., Melki, R., and Gitler, A. D. (2016). Axonal transport and secretion of fibrillar forms of alpha-synuclein, Abeta42 peptide and HTTExon 1. *Acta Neuropathol.* 131, 539–548. doi: 10.1007/s00401-016-1538-0

Bruus, H. (2008). *Theoretical Microfluidics*. Oxford: Oxford University Press.

Calafate, S., Buist, A., Miskiewicz, K., Vijayan, V., Daneels, G., De Strooper, B., et al. (2015). Synaptic Contacts enhance cell-to-cell Tau pathology propagation. *Cell Rep.* 11, 1176–1183. doi: 10.1016/j.celrep.2015.04.043

Campenot, R. B. (1977). Local control of neurite development by nerve growth factor. *Proc. Natl. Acad. Sci. U.S.A.* 74, 4516–4519. doi: 10.1073/pnas.74.10.4516

Campenot, R. B. (1982). Development of sympathetic neurons in compartmentalized cultures. Il Local control of neurite growth by nerve growth factor. *Dev. Biol.* 93, 1–12. doi: 10.1016/0012-1606(82)90232-9

Casadevall i Solvas, X., Turek, V., Prodromakis, T., and Edel, J. B. (2012). Microfluidic evaporator for on-chip sample concentration. *Lab Chip* 12, 4049–4054. doi: 10.1039/c2lc40746a

Castilla, J., and Requena, J. R. (2015). Prion-like diseases: looking for their niche in the realm of infectious diseases. *Virus Res.* 207, 1–4. doi: 10.1016/j.virusres.2015.06.001

Cavaliere, F., Cerf, L., Dehay, B., Ramos-Gonzalez, P., De Giorgi, F., Bourdenx, M., et al. (2017). In vitro alpha-synuclein neurotoxicity and spreading among neurons and astrocytes using Lewy body extracts from Parkinson disease brains. *Neurobiol. Dis.* 103, 101–112. doi: 10.1016/j.nbd.2017.04.011

Chen, S. W., and Cremades, N. (2018). Preparation of alpha-synuclein amyloid assemblies for toxicity experiments. *Methods Mol. Biol.* 1779, 45–60. doi: 10.1007/978-1-4939-7816-8_4

Chen, T. W., Wardill, T. J., Sun, Y., Pulver, S. R., Renninger, S. L., Baohan, A., et al. (2013). Ultrasensitive fluorescent proteins for imaging neuronal activity. *Nature* 499, 295–300. doi: 10.1038/nature12354

Cho, H., Hashimoto, T., Wong, E., Hori, Y., Wood, L. B., Zhao, L., et al. (2013). Microfluidic chemotaxis platform for differentiating the roles of soluble and bound amyloid-beta on microglial accumulation. *Sci. Rep.* 3:1823.

Choi, S. H., Kim, Y. H., Hebisch, M., Sliwinski, C., Lee, S., D'Avanzo, C., et al. (2014). A three-dimensional human neural cell culture model of Alzheimer's disease. *Nature* 515, 274–278.

Choi, Y. J., Chae, S., Kim, J. H., Barald, K. F., Park, J. Y., and Lee, S. H. (2013). Neurotoxic amyloid beta oligomeric assemblies recreated in microfluidic platform with interstitial level of slow flow. *Sci. Rep.* 3:1921.

Colby, D. W., Zhang, Q., Wang, S., Groth, D., Legname, G., Riesner, D., et al. (2007). Prion detection by an amyloid seeding assay. *Proc. Natl. Acad. Sci. U.S.A.* 104, 20914–20919. doi: 10.1073/pnas.0710152105

Collinge, J. (2016). Mammalian prions and their wider relevance in neurodegenerative diseases. *Nature* 539, 217–226. doi: 10.1038/nature20415

Congdon, E. E., Lin, Y., Rajamohamedsait, H. B., Shamir, D. B., Krishnaswamy, S., Rajamohamedsait, W. J., et al. (2016). Affinity of Tau antibodies for solubilized pathological Tau species but not their immunogen or insoluble Tau aggregates predicts *in vivo* and *ex vivo* efficacy. *Mol. Neurodegener.* 11:62.

Conway, K. A., Lee, S. J., Rochet, J. C., Ding, T. T., Williamson, R. E., and Lansbury, P. T. Jr. (2000). Acceleration of oligomerization, not fibrillization, is a shared property of both alpha-synuclein mutations linked to early-onset Parkinson's disease: implications for pathogenesis and therapy. *Proc. Natl. Acad. Sci. U.S.A.* 97, 571–576. doi: 10.1073/pnas.97.2.571

Costanzo, M., and Zurzolo, C. (2013). The cell biology of prion-like spread of protein aggregates: mechanisms and implication in neurodegeneration. *Biochem. J.* 452, 1–17. doi: 10.1042/bj20121898

Del Rio, J. A., Ferrer, I., and Gavin, R. (2018). Role of cellular prion protein in interneuronal amyloid transmission. *Prog. Neurobiol.* 165-167, 87–102. doi: 10.1016/j.pneurobio.2018.03.001

Deleglise, B., Magnifico, S., Duplus, E., Vaur, P., Soubeyre, V., Belle, M., et al. (2014). beta-amyloid induces a dying-back process and remote trans-synaptic alterations in a microfluidic-based reconstructed neuronal network. *Acta Neuropathol. Commun.* 2:145. doi: 10.1186/preaccept-4848873741397798

Deshpande, A., Mina, E., Glabe, C., and Busciglio, J. (2006). Different conformations of amyloid beta induce neurotoxicity by distinct mechanisms in human cortical neurons. *J. Neurosci.* 26, 6011–6018. doi: 10.1523/jneurosci.1189-06.2006

Du, G., Fang, Q., and Den Toonder, J. M. (2016). Microfluidics for cell-based high throughput screening platforms - A review. *Anal. Chim. Acta* 903, 36–50. doi: 10.1016/j.aca.2015.11.023

Dujardin, S., Lecolle, K., Caillierez, R., Begard, S., Zommer, N., Lachaud, C., et al. (2014). Neuron-to-neuron wild-type Tau protein transfer through a trans-synaptic mechanism: relevance to sporadic tauopathies. *Acta Neuropathol. Commun.* 2:14.

Erana, H. (2019). The Prion 2018 round tables (II): Abeta, tau, alpha-synuclein.. are they prions, prion-like proteins, or what?. *Prion* 13, 41–45. doi: 10.1080/19336896.2019.1569451

Erana, H., Venegas, V., Moreno, J., and Castilla, J. (2017). Prion-like disorders and Transmissible Spongiform Encephalopathies: an overview of the mechanistic features that are shared by the various disease-related misfolded proteins. *Biochem. Biophys. Res. Commun.* 483, 1125–1136. doi: 10.1016/j.bbrc.2016.08.166

Fairfoul, G., Mcguire, L. I., Pal, S., Ironside, J. W., Neumann, J., Christie, S., et al. (2016). Alpha-synuclein RT-QuIC in the CSF of patients with alpha-synucleinopathies. *Ann. Clin. Transl. Neurol.* 3, 812–818. doi: 10.1002/acn3.338

Feiler, M. S., Strobel, B., Freischmidt, A., Helferich, A. M., Kappel, J., Brewer, B. M., et al. (2015). TDP-43 is intercellularly transmitted across axon terminals. *J. Cell Biol.* 211, 897–911. doi: 10.1083/jcb.201504057

Ferrer, I. (2018). Oligodendrogliopathy in neurodegenerative diseases with abnormal protein aggregates: the forgotten partner. *Prog. Neurobiol.* 169, 24–54. doi: 10.1016/j.pneurobio.2018.07.004

Ferrer, I., Aguilo Garcia, M., Carmona, M., Andres-Benito, P., Torrejon-Escribano, B., Garcia-Esparcia, P., et al. (2019). Involvement of Oligodendrocytes in Tau Seeding and Spreading in Tauopathies. *Front. Aging Neurosci.* 11:112. doi: 10.3389/fnagi.2019.00112

Ferrer, I., Andres-Benito, P., Zelaya, M. V., Aguirre, M. E. E., Carmona, M., Ausin, K., et al. (2020a). Familial globular glial tauopathy linked to MAPT mutations: molecular neuropathology and seeding capacity of a prototypical mixed neuronal and glial tauopathy. *Acta Neuropathol.* 139, 735–771. doi: 10.1007/s00401-019-02122-9

Ferrer, I., Zelaya, M. V., Aguilo Garcia, M., Carmona, M., Lopez-Gonzalez, I., Andres-Benito, P., et al. (2020b). Relevance of host tau in tau seeding and spreading in tauopathies. *Brain Pathol.* 30, 298–318. doi: 10.1111/bpa.12778

Ferrone, F. A., Hofrichter, J., and Eaton, W. A. (1985). Kinetics of sickle hemoglobin polymerization. I. Studies using temperature-jump and laser photolysis techniques. *J. Mol. Biol.* 183, 591–610.

Fitzpatrick, A. W., Debelouchina, G. T., Bayro, M. J., Clare, D. K., Caporini, M. A., Bajaj, V. S., et al. (2013). Atomic structure and hierarchical assembly of a cross-beta amyloid fibril. *Proc. Natl. Acad. Sci. U.S.A.* 110, 5468–5473.

Folch i Folch, A. (2013). *Introduction to bioMEMS*. Boca Raton, FL: CRC Press.

Fraser, H., and Dickinson, A. G. (1973). Scrapie in mice. Agent-strain differences in the distribution and intensity of grey matter vacuolation. *J. Comp. Pathol.* 83, 29–40.

Freundt, E. C., Maynard, N., Clancy, E. K., Roy, S., Bousset, L., Sourigues, Y., et al. (2012). Neuron-to-neuron transmission of alpha-synuclein fibrils through axonal transport. *Ann. Neurol.* 72, 517–524. doi: 10.1002/ana.23747

Fu, W., Yan, C., Guo, Z., Zhang, J., Zhang, H., Tian, H., et al. (2019). Rational design of near-infrared aggregation-induced-emission-active probes: *in situ* mapping of amyloid-beta plaques with ultrasensitivity and high-fidelity. *J. Am. Chem. Soc.* 141, 3171–3177. doi: 10.1021/jacs.8b12820

Giles, K., Woerman, A. L., Berry, D. B., and Prusiner, S. B. (2017). Bioassays and Inactivation of Prions. *Cold Spring Harb. Perspect. Biol.* 9:a023499. doi: 10.1101/cshperspect.a023499

Gladkov, A., Pigareva, Y., Kutyina, D., Kolpakov, V., Bukatin, A., Mukhina, I., et al. (2017). Design of cultured neuron networks in vitro with predefined connectivity using asymmetric microfluidic channels. *Sci. Rep.* 7:15625.

Goedert, M., Masuda-Suzukake, M., and Falcon, B. (2017). Like prions: the propagation of aggregated tau and alpha-synuclein in neurodegeneration. *Brain* 140, 266–278. doi: 10.1093/brain/aww230

Greenfield, J. G., Love, S., Louis, D. N., and Ellison, D. (2008). *Greenfield's Neuropathology*. London: Hodder Arnold.

Gribaudo, S., Tixador, P., Bousset, L., Fenyi, A., Lino, P., Melki, R., et al. (2019). Propagation of alpha-synuclein strains within human reconstructed neuronal network. *Stem Cell Rep.* 12, 230–244. doi: 10.1016/j.stemcr.2018.12.007

Grimmer, A., and Wille, R. (2020). *Designing Droplet Microfluidic Networks : A Toolbox for Designers*. Berlin: Springer.

Guo, J. L., and Lee, V. M. (2011). Seeding of normal Tau by pathological Tau conformers drives pathogenesis of Alzheimer-like tangles. *J. Biol. Chem.* 286, 15317–15331. doi: 10.1074/jbc.m110.209296

Guo, M. T., Rotem, A., Heyman, J. A., and Weitz, D. A. (2012). Droplet microfluidics for high-throughput biological assays. *Lab Chip* 12, 2146–2155. doi: 10.1039/c2lc21147e

Haley, N. J., Siepker, C., Hoon-Hanks, L. L., Mitchell, G., Walter, W. D., Manca, M., et al. (2016). Seeded amplification of chronic wasting disease prions in nasal brushings and recto-anal mucosa-associated lymphoid tissues from elk by real-time quaking-induced conversion. *J. Clin. Microbiol.* 54, 1117–1126. doi: 10.1128/jcm.02700-15

Hepler, R. W., Grimm, K. M., Nahas, D. D., Breese, R., Dodson, E. C., Acton, P., et al. (2006). Solution state characterization of amyloid beta-derived diffusible ligands. *Biochemistry* 45, 15157–15167. doi: 10.1021/bi061850f

Herold, K. E., and Rasooly, A. (2009). *Lab on a Chip Technology*. Norfolk: Caister Academic Press.

Holmes, B. B., Devos, S. L., Kfoury, N., Li, M., Jacks, R., Yanamandra, K., et al. (2013). Heparan sulfate proteoglycans mediate internalization and propagation of specific proteopathic seeds. *Proc. Natl. Acad. Sci. U.S.A.* 110, E3138–E3147.

Holmes, B. B., and Diamond, M. I. (2017). Cellular models for the study of prions. *Cold Spring Harb. Perspect. Med.* 7:a024026. doi: 10.1101/cshperspect.a024026

Hong, Y., Meng, L., Chen, S., Leung, C. W., Da, L. T., Faisal, M., et al. (2012). Monitoring and inhibition of insulin fibrillation by a small organic fluorogen with aggregation-induced emission characteristics. *J. Am. Chem. Soc.* 134, 1680–1689. doi: 10.1021/ja208720a

Huang, H., Li, P., Zhang, M., Yu, Y., Huang, Y., Gu, H., et al. (2017). Graphene quantum dots for detecting monomeric amyloid peptides. *Nanoscale* 9, 5044–5048. doi: 10.1039/c6nr10017a

Huang, Q., Xie, J., Liu, Y., Zhou, A., and Li, J. (2017). Detecting the Formation and Transformation of Oligomers during Insulin Fibrillation by a Dendrimer Conjugated with Aggregation-Induced Emission Molecule. *Bioconjug. Chem.* 28, 944–956. doi: 10.1021/acs.bioconjchem.6b00665

Jeon, J. S., Chung, S., Kamm, R. D., and Charest, J. L. (2011). Hot embossing for fabrication of a microfluidic 3D cell culture platform. *Biomed. Microdevices* 13, 325–333. doi: 10.1007/s10544-010-9496-0

Kamande, J. W., Nagendran, T., Harris, J., and Taylor, A. M. (2019). Multi-compartment microfluidic device geometry and covalently bound Poly-D-Lysine influence neuronal maturation. *Front. Bioeng. Biotechnol.* 7:84. doi: 10.3389/fbioe.2019.00084

Kaminski, C. F., and Kaminski Schierle, G. S. (2016). Probing amyloid protein aggregation with optical superresolution methods: from the test tube to models of disease. *Neurophotonics* 3:041807. doi: 10.1117/1.nph.3.4.041807

Kaushik, A., Jayant, R. D., Tiwari, S., Vashist, A., and Nair, M. (2016). Nano-biosensors to detect beta-amyloid for Alzheimer's disease management. *Biosens. Bioelectron.* 80, 273–287. doi: 10.1016/j.bios.2016.01.065

Kim, A. C., Lim, S., and Kim, Y. K. (2018). Metal ion effects on abeta and Tau aggregation. *Int. J. Mol. Sci.* 19:128. doi: 10.3390/ijms19010128

Kirby, B. J. (2010). *Micro- and Nanoscale Fluid Mechanics : Transport in Microfluidic Devices*. New York, NY: Cambridge University Press.

Knight, J. B., Vishwanath, A., Brody, J. P., and Austin, R. H. (1998). Hydrodynamic focusing on a silicon chip: mixing nanoliters in microseconds. *Phys. Rev. Lett.* 80, 3863–3866. doi: 10.1103/physrevlett.80.3863

Knowles, T. P., Waudby, C. A., Devlin, G. L., Cohen, S. I., Aguzzi, A., Vendruscolo, M., et al. (2009). An analytical solution to the kinetics of breakable filament assembly. *Science* 326, 1533–1537. doi: 10.1126/science.1178250

Knowles, T. P., White, D. A., Abate, A. R., Agresti, J. J., Cohen, S. I., Sperling, R. A., et al. (2011). Observation of spatial propagation of amyloid assembly from single nuclei. *Proc. Natl. Acad. Sci. U.S.A.* 108, 14746–14751. doi: 10.1073/pnas.1105555108

Kopp, M. R. G., Linsenmeier, M., Hettich, B., Prantl, S., Stavrakis, S., Leroux, J. C., et al. (2020). Microfluidic shrinking droplet concentrator for analyte detection and phase separation of protein solutions. *Anal. Chem.* 92, 5803–5812. doi: 10.1021/acs.analchem.9b05329

Kovacs, G. G., Lee, V. M., and Trojanowski, J. Q. (2017). Protein astrogliopathies in human neurodegenerative diseases and aging. *Brain Pathol.* 27, 675–690. doi: 10.1111/bpa.12536

Kuncova-Kallio, J., and Kallio, P. J. (2006). PDMS and its suitability for analytical microfluidic devices. *Conf. Proc. IEEE Eng. Med. Biol. Soc.* 2006, 2486–2489.

Kuo, C. J., Chiang, H. C., Tseng, C. A., Chang, C. F., Ulaganathan, R. K., Ling, T. T., et al. (2018). Lipid-modified graphene-transistor biosensor for monitoring amyloid-beta aggregation. *ACS Appl. Mater. Interfaces* 10, 12311–12316. doi: 10.1021/acsami.8b01917

Lasmezas, C. I., Deslys, J. P., Demaimay, R., Adjou, K. T., Hauw, J. J., and Dormont, D. (1996). Strain specific and common pathogenic events in murine models of scrapie and bovine spongiform encephalopathy. *J. Gen. Virol.* 77(Pt 7), 1601–1609. doi: 10.1099/0022-1317-77-7-1601

Lassus, B., Naude, J., Faure, P., Guedin, D., Von Boxberg, Y., Mannoury La Cour, C., et al. (2018). Glutamatergic and dopaminergic modulation of cortico-striatal circuits probed by dynamic calcium imaging of networks reconstructed in microfluidic chips. *Sci. Rep.* 8:17461.

Lee, H. U., Nag, S., Blasiak, A., Jin, Y., Thakor, N., and Yang, I. H. (2016). Subcellular optogenetic stimulation for activity-dependent myelination of axons in a novel microfluidic compartmentalized platform. *ACS Chem. Neurosci.* 7, 1317–1324. doi: 10.1021/acschemneuro.6b00157

Lee, S.-J. J., and Sundararajan, N. (2010). *Microfabrication for Microfluidics*. Boston, MA: Artech House.

Lengyel-Zhand, Z., Ferrie, J. J., Janssen, B., Hsieh, C. J., Graham, T., Xu, K. Y., et al. (2020). Synthesis and characterization of high affinity fluorogenic alpha-synuclein probes. *Chem. Commun.* 56, 3567–3570. doi: 10.1039/c9cc09849f

Li, H., Xie, H., Cao, Y., Ding, X., Yin, Y., and Li, G. (2013). A general way to assay protein by coupling peptide with signal reporter via supermolecule formation. *Anal. Chem.* 85, 1047–1052. doi: 10.1021/ac302906c

Li, S. S., Lin, C. W., Wei, K. C., Huang, C. Y., Hsu, P. H., Liu, H. L., et al. (2016). Non-invasive screening for early Alzheimer's disease diagnosis by a sensitively immunomagnetic biosensor. *Sci. Rep.* 6:25155.

Li, W., Xu, Z., Xu, B., Chan, C. Y., Lin, X., Wang, Y., et al. (2017). Investigation of the subcellular neurotoxicity of amyloid-beta using a device integrating microfluidic perfusion and chemotactic guidance. *Adv. Healthc. Mater.* 6:1600895. doi: 10.1002/adhm.201600895

Lopes, C. D. F., Mateus, J. C., and Aguiar, P. (2018). Interfacing microfluidics with microelectrode arrays for studying neuronal communication and axonal signal propagation. *J. Vis. Exp.* 142:e58878.

Mao, X., Ou, M. T., Karuppagounder, S. S., Kam, T. I., Yin, X., Xiong, Y., et al. (2016). Pathological alpha-synuclein transmission initiated by binding lymphocyte-activation gene 3. *Science* 353:aah3374. doi: 10.1126/science.aah3374

Marek, P., Mukherjee, S., Zanni, M. T., and Raleigh, D. P. (2010). Residue-specific, real-time characterization of lag-phase species and fibril growth during amyloid formation: a combined fluorescence and IR study of p-cyanophenylalanine analogs of islet amyloid polypeptide. *J. Mol. Biol.* 400, 878–888. doi: 10.1016/j.jmb.2010.05.041

Masujin, K., Orru, C. D., Miyazawa, K., Groveman, B. R., Raymond, L. D., Hughson, A. G., et al. (2016). Detection of atypical H-type bovine spongiform encephalopathy and discrimination of bovine prion strains by real-time quaking-induced conversion. *J. Clin. Microbiol.* 54, 676–686. doi: 10.1128/jcm.02731-15

Matamoros-Angles, A., Gayosso, L. M., Richaud-Patin, Y., Di Domenico, A., Vergara, C., Hervera, A., et al. (2018). iPS Cell Cultures from a Gerstmann-Straussler-Scheinker Patient with the Y218N PRNP Mutation Recapitulate tau Pathology. *Mol. Neurobiol.* 55, 3033–3048. doi: 10.1007/s12035-017-0506-6

McDonald, J. C., Duffy, D. C., Anderson, J. R., Chiu, D. T., Wu, H., Schueller, O. J., et al. (2000). Fabrication of microfluidic systems in poly(dimethylsiloxane). *Electrophoresis* 21, 27–40. doi: 10.1002/(sici)1522-2683(20000101)21:1<27::aid-elps27>3.0.co;2-c

McDonald, J. C., and Whitesides, G. M. (2002). Poly(dimethylsiloxane) as a material for fabricating microfluidic devices. *Acc. Chem. Res.* 35, 491–499. doi: 10.1021/ar010110q

Meisl, G., Kirkegaard, J. B., Arosio, P., Michaels, T. C., Vendruscolo, M., Dobson, C. M., et al. (2016). Molecular mechanisms of protein aggregation from global fitting of kinetic models. *Nat. Protoc.* 11, 252–272. doi: 10.1038/nprot.2016.010

Meisl, G., Knowles, T. P., and Klenerman, D. (2020). The molecular processes underpinning prion-like spreading and seed amplification in protein aggregation. *Curr. Opin. Neurobiol.* 61, 58–64. doi: 10.1016/j.conb.2020.01.010

Meissner, R., Eker, B., Kasi, H., Bertsch, A., and Renaud, P. (2011). Distinguishing drug-induced minor morphological changes from major cellular damage via label-free impedimetric toxicity screening. *Lab Chip* 11, 2352–2361. doi: 10.1039/c1lc20212j

Metrick, M. A. II, Do Carmo Ferreira, N., Saijo, E., Hughson, A. G., Kraus, A., Orru, C., et al. (2019). Million-fold sensitivity enhancement in proteopathic seed amplification assays for biospecimens by Hofmeister ion comparisons. *Proc. Natl. Acad. Sci. U.S.A.* 116, 23029–23039. doi: 10.1073/pnas.1909322116

Minteer, S. D. (2006). *Microfluidic Techniques : Reviews and Protocols*. Totowa, NJ: Humana Press.

Moore, R. A., Taubner, L. M., and Priola, S. A. (2009). Prion protein misfolding and disease. *Curr. Opin. Struct. Biol.* 19, 14–22.

Morales, R., Riss, M., Wang, L., Gavin, R., Del Rio, J. A., Alcubilla, R., et al. (2008). Integrating multi-unit electrophysiology and plastic culture dishes for network neuroscience. *Lab Chip* 8, 1896–1905. doi: 10.1039/b802165a

Morris, A. M., Watzky, M. A., and Finke, R. G. (2009). Protein aggregation kinetics, mechanism, and curve-fitting: a review of the literature. *Biochim. Biophys. Acta* 1794, 375–397. doi: 10.1016/j.bbapap.2008.10.016

Moutaux, E., Charlot, B., Genoux, A., Saudou, F., and Cazorla, M. (2018). An integrated microfluidic/microelectrode array for the study of activity-dependent intracellular dynamics in neuronal networks. *Lab Chip* 18, 3425–3435. doi: 10.1039/c8lc00694f

Neto, E., Leitao, L., Sousa, D. M., Alves, C. J., Alencastre, I. S., Aguiar, P., et al. (2016). Compartmentalized microfluidic platforms: the unrivaled breakthrough of *in vitro* tools for neurobiological research. *J. Neurosci.* 36, 11573–11584. doi: 10.1523/jneurosci.1748-16.2016

Ng, J. M., Gitlin, I., Stroock, A. D., and Whitesides, G. M. (2002). Components for integrated poly(dimethylsiloxane) microfluidic systems. *Electrophoresis* 23, 3461–3473. doi: 10.1002/1522-2683(200210)23:20<3461::aid-elps3461>3.0.co;2-8

Oh, K. W., Lee, K., Ahn, B., and Furlani, E. P. (2012). Design of pressure-driven microfluidic networks using electric circuit analogy. *Lab Chip* 12, 515–545. doi: 10.1039/c2lc20799k

Orlandi, J. G., Stetter, O., Soriano, J., Geisel, T., and Battaglia, D. (2014). Transfer entropy reconstruction and labeling of neuronal connections from simulated calcium imaging. *PLoS One* 9:e98842. doi: 10.1371/journal.pone.0098842

Orru, C. D., Favole, A., Corona, C., Mazza, M., Manca, M., Groveman, B. R., et al. (2015). Detection and discrimination of classical and atypical L-type bovine spongiform encephalopathy by real-time quaking-induced conversion. *J. Clin. Microbiol.* 53, 1115–1120. doi: 10.1128/jcm.02906-14

Orru, C. D., Groveman, B. R., Hughson, A. G., Manca, M., Raymond, L. D., Raymond, G. J., et al. (2017). RT-QuIC assays for prion disease detection and diagnostics. *Methods Mol. Biol.* 1658, 185–203. doi: 10.1007/978-1-4939-7244-9_14

Osaki, T., Uzel, S. G. M., and Kamm, R. D. (2020). On-chip 3D neuromuscular model for drug screening and precision medicine in neuromuscular disease. *Nat. Protoc.* 15, 421–449. doi: 10.1038/s41596-019-0248-1

Otzen, D. E. (2013). *Amyloid Fibrils and Prefibrillar Aggregates : Molecular and Biological Properties*. Weinheim: Wiley-VCH Verlag GmbH & Co.

Park, J., Koito, H., Li, J., and Han, A. (2009). Microfluidic compartmentalized co-culture platform for CNS axon myelination research. *Biomed. Microdevices* 11, 1145–1153. doi: 10.1007/s10544-009-9331-7

Park, J., Lee, B. K., Jeong, G. S., Hyun, J. K., Lee, C. J., and Lee, S. H. (2015). Three-dimensional brain-on-a-chip with an interstitial level of flow and its application as an in vitro model of Alzheimer's disease. *Lab Chip* 15, 141–150. doi: 10.1039/c4lc00962b

Park, J., Wetzel, I., Marriott, I., Dreau, D., D'avanzo, C., Kim, D. Y., et al. (2018). A 3D human triculture system modeling neurodegeneration and neuroinflammation in Alzheimer's disease. *Nat. Neurosci.* 21, 941–951. doi: 10.1038/s41593-018-0175-4

Park, J. W., Vahidi, B., Taylor, A. M., Rhee, S. W., and Jeon, N. L. (2006). Microfluidic culture platform for neuroscience research. *Nat. Protoc.* 1, 2128–2136. doi: 10.1038/nprot.2006.316

Park, M. C., Kim, M., Lim, G. T., Kang, S. M., An, S. S., Kim, T. S., et al. (2016). Droplet-based magnetic bead immunoassay using microchannel-connected multiwell plates (muCHAMPs) for the detection of amyloid beta oligomers. *Lab Chip* 16, 2245–2253. doi: 10.1039/c6lc00013d

Peng, C., Trojanowski, J. Q., and Lee, V. M. (2020). Protein transmission in neurodegenerative disease. *Nat. Rev. Neurol.* 16, 199–212.

Perez, M., Avila, J., and Hernandez, F. (2019). Propagation of Tau via extracellular vesicles. *Front. Neurosci.* 13:698. doi: 10.3389/fnins.2019.00698

Pfammatter, M., Andreasen, M., Meisl, G., Taylor, C. G., Adamcik, J., Bolisetty, S., et al. (2017). Absolute quantification of amyloid propagons by digital microfluidics. *Anal. Chem.* 89, 12306–12313. doi: 10.1021/acs.analchem.7b03279

Polanco, J. C., and Gotz, J. (2015). No full admission for tau to the exclusive prion club yet. *EMBO J.* 34, 2990–2992. doi: 10.15252/embj.201593311

Polanco, J. C., Li, C., Durisic, N., Sullivan, R., and Gotz, J. (2018). Exosomes taken up by neurons hijack the endosomal pathway to spread to interconnected neurons. *Acta Neuropathol. Commun.* 6:10.

Prabhulkar, S., Piatyszek, R., Cirrito, J. R., Wu, Z. Z., and Li, C. Z. (2012). Microbiosensor for Alzheimer's disease diagnostics: detection of amyloid beta biomarkers. *J. Neurochem.* 122, 374–381. doi: 10.1111/j.1471-4159.2012.07709.x

Prots, I., Grosch, J., Brazdis, R. M., Simmnacher, K., Veber, V., Havlicek, S., et al. (2018). alpha-Synuclein oligomers induce early axonal dysfunction in human iPSC-based models of synucleinopathies. *Proc. Natl. Acad. Sci. U.S.A.* 115, 7813–7818. doi: 10.1073/pnas.1713129115

Prusiner, S. B. (1998a). The prion diseases. *Brain Pathol.* 8, 499–513.

Prusiner, S. B. (1998b). Prions. *Proc. Natl. Acad. Sci. U.S.A.* 95, 13363–13383.

Prusiner, S. B. (2017). *Prion Biology : A Subject Collection from Cold Spring Harbor Perspectives in Biology*. Cold Spring Harbor, NY: Cold Spring Harbor Laboratory Press.

Prusiner, S. B., Woerman, A. L., Mordes, D. A., Watts, J. C., Rampersaud, R., Berry, D. B., et al. (2015). Evidence for alpha-synuclein prions causing multiple system atrophy in humans with parkinsonism. *Proc. Natl. Acad. Sci. U.S.A.* 112, E5308–E5317.

Ramirez-Alvarado, M., Kelly, J. W., and Dobson, C. M. (2010). *Protein Misfolding Diseases : Current and Emerging Principles and Therapies*. Hoboken, NJ: Wiley.

Rauch, J. N., Luna, G., Guzman, E., Audouard, M., Challis, C., Sibih, Y. E., et al. (2020). LRP1 is a master regulator of tau uptake and spread. *Nature* 580, 381–385. doi: 10.1038/s41586-020-2156-5

Rhee, S. W., Taylor, A. M., Tu, C. H., Cribbs, D. H., Cotman, C. W., and Jeon, N. L. (2005). Patterned cell culture inside microfluidic devices. *Lab Chip* 5, 102–107. doi: 10.1039/b403091e

Robertson, G., Bushell, T. J., and Zagnoni, M. (2014). Chemically induced synaptic activity between mixed primary hippocampal co-cultures in a microfluidic system. *Integr. Biol.* 6, 636–644. doi: 10.1039/c3ib40221e

Rodriguez-Villarreal, A. I., Arundell, M., Carmona, M., and Samitier, J. (2010). High flow rate microfluidic device for blood plasma separation using a range of temperatures. *Lab Chip* 10, 211–219. doi: 10.1039/b904531g

Ruiz, A., Joshi, P., Mastrangelo, R., Francolini, M., Verderio, C., and Matteoli, M. (2014). Testing Abeta toxicity on primary CNS cultures using drug-screening microfluidic chips. *Lab Chip* 14, 2860–2866. doi: 10.1039/c4lc00174e

Rushworth, J. V., Ahmed, A., Griffiths, H. H., Pollock, N. M., Hooper, N. M., and Millner, P. A. (2014). A label-free electrical impedimetric biosensor for the specific detection of Alzheimer's amyloid-beta oligomers. *Biosens. Bioelectron.* 56, 83–90. doi: 10.1016/j.bios.2013.12.036

Saar, K. L., Muller, T., Charmet, J., Challa, P. K., and Knowles, T. P. J. (2018). Enhancing the resolution of micro free flow electrophoresis through spatially controlled sample injection. *Anal. Chem.* 90, 8998–9005. doi: 10.1021/acs.analchem.8b01205

Saar, K. L., Yates, E. V., Muller, T., Saunier, S., Dobson, C. M., and Knowles, T. P. J. (2016). Automated *ex situ* assays of amyloid formation on a microfluidic platform. *Biophys. J.* 110, 555–560. doi: 10.1016/j.bpj.2015.11.3523

Saborio, G. P., Permanne, B., and Soto, C. (2001). Sensitive detection of pathological prion protein by cyclic amplification of protein misfolding. *Nature* 411, 810–813. doi: 10.1038/35081095

Sackmann, E. K., Fulton, A. L., and Beebe, D. J. (2014). The present and future role of microfluidics in biomedical research. *Nature* 507, 181–189. doi: 10.1038/nature13118

Saeed, S. M., and Fine, G. (1967). Thioflavin-T for amyloid detection. *Am. J. Clin. Pathol.* 47, 588–593.

Saijo, E., Groveman, B. R., Kraus, A., Metrick, M., Orru, C. D., Hughson, A. G., et al. (2019). Ultrasensitive RT-QuIC Seed Amplification Assays for Disease-Associated Tau, alpha-Synuclein, and Prion Aggregates. *Methods Mol. Biol.* 1873, 19–37. doi: 10.1007/978-1-4939-8820-4_2

Sano, K., Atarashi, R., Satoh, K., Ishibashi, D., Nakagaki, T., Iwasaki, Y., et al. (2018). Prion-like seeding of misfolded alpha-synuclein in the brains of dementia with lewy body patients in RT-QUIC. *Mol. Neurobiol.* 55, 3916–3930.

Saper, C. B., Wainer, B. H., and German, D. C. (1987). Axonal and transneuronal transport in the transmission of neurological disease: potential role in system degenerations, including Alzheimer's disease. *Neuroscience* 23, 389–398. doi: 10.1016/0306-4522(87)90063-7

Sardar Sinha, M., Ansell-Schultz, A., Civitelli, L., Hildesjo, C., Larsson, M., Lannfelt, L., et al. (2018). Alzheimer's disease pathology propagation by exosomes containing toxic amyloid-beta oligomers. *Acta Neuropathol.* 136, 41–56. doi: 10.1007/s00401-018-1868-1

Scheckel, C., and Aguzzi, A. (2018). Prions, prionoids and protein misfolding disorders. *Nat. Rev. Genet.* 19, 405–418. doi: 10.1038/s41576-018-0011-4

Scheidt, T., Lapinska, U., Kumita, J. R., Whiten, D. R., Klenerman, D., Wilson, M. R., et al. (2019). Secondary nucleation and elongation occur at different sites on Alzheimer's amyloid-beta aggregates. *Sci. Adv.* 5:eaau3112. doi: 10.1126/sciadv.aau3112

Schladitz, C., Vieira, E. P., Hermel, H., and Mohwald, H. (1999). Amyloid-beta-sheet formation at the air-water interface. *Biophys. J.* 77, 3305–3310. doi: 10.1016/s0006-3495(99)77161-4

Scialo, C., De Cecco, E., Manganotti, P., and Legname, G. (2019). Prion and Prion-Like protein strains: deciphering the molecular basis of heterogeneity in neurodegeneration. *Viruses* 11:261. doi: 10.3390/v11030261

Serafin, V., Gamella, M., Pedrero, M., Montero-Calle, A., Razzino, C. A., Yanez-Sedeno, P., et al. (2020). Enlightening the advancements in electrochemical bioanalysis for the diagnosis of Alzheimer's disease and other neurodegenerative disorders. *J. Pharm. Biomed. Anal.* 189, 113437. doi: 10.1016/j.jpba.2020.113437

Sethi, J., Van Bulck, M., Suhail, A., Safarzadeh, M., Perez-Castillo, A., and Pan, G. (2020). A label-free biosensor based on graphene and reduced graphene oxide dual-layer for electrochemical determination of beta-amyloid biomarkers. *Mikrochim. Acta* 187, 288.

Shah, R. K., and London, A. L. (1978). *Laminar Flow Forced Convection in Ducts : A Source Book for Compact Heat Exchanger Analytical Data*. New York, NY: Academic Press.

Shahnawaz, M., Mukherjee, A., Pritzkow, S., Mendez, N., Rabadia, P., Liu, X., et al. (2020). Discriminating alpha-synuclein strains in Parkinson's disease and multiple system atrophy. *Nature* 578, 273–277.

Shembekar, N., Chaipan, C., Utharala, R., and Merten, C. A. (2016). Droplet-based microfluidics in drug discovery, transcriptomics and high-throughput molecular genetics. *Lab Chip* 16, 1314–1331. doi: 10.1039/c6lc00249h

Shim, J. U., Cristobal, G., Link, D. R., Thorsen, T., Jia, Y., Piattelli, K., et al. (2007). Control and measurement of the phase behavior of aqueous solutions using microfluidics. *J. Am. Chem. Soc.* 129, 8825–8835.

Shin, W. S., Di, J., Murray, K. A., Sun, C., Li, B., Bitan, G., et al. (2019). Different amyloid-beta self-assemblies have distinct effects on intracellular Tau aggregation. *Front. Mol. Neurosci.* 12:268. doi: 10.3389/fnmol.2019.00268

Sigurdsson, E. M., Calero, M., and Gasset, M. (2012). *Amyloid Proteins : Methods and Protocols*. New York, NY: Humana Press.

Skinner, M., Grateau, G., and Kyle, R. A. (2005). *Amyloid and amyloidosis*. Boca Raton, Fl: CRC Press.

Smedler, E., Malmersjo, S., and Uhlen, P. (2014). Network analysis of time-lapse microscopy recordings. *Front. Neural Circuits* 8:111. doi: 10.3389/fncir.2014.00111

Song, H. L., Shim, S., Kim, D. H., Won, S. H., Joo, S., Kim, S., et al. (2014). beta-Amyloid is transmitted via neuronal connections along axonal membranes. *Ann. Neurol.* 75, 88–97. doi: 10.1002/ana.24029

Soto, C., Saborio, G. P., and Anderes, L. (2002). Cyclic amplification of protein misfolding: application to prion-related disorders and beyond. *Trends Neurosci.* 25, 390–394. doi: 10.1016/s0166-2236(02)02195-1

Surmeier, D. J., Obeso, J. A., and Halliday, G. M. (2017). Selective neuronal vulnerability in Parkinson disease. *Nat. Rev. Neurosci.* 18, 101–113. doi: 10.1038/nrn.2016.178

Tabeling, P. (2005). *Introduction to Microfluidics*. Oxford: Oxford University Press.

Takeda, S., Wegmann, S., Cho, H., Devos, S. L., Commins, C., Roe, A. D., et al. (2015). Neuronal uptake and propagation of a rare phosphorylated high-molecular-weight tau derived from Alzheimer's disease brain. *Nat. Commun.* 6:8490.

Taylor, A. M., Blurton-Jones, M., Rhee, S. W., Cribbs, D. H., Cotman, C. W., and Jeon, N. L. (2005). A microfluidic culture platform for CNS axonal injury, regeneration and transport. *Nat. Methods* 2, 599–605. doi: 10.1038/nmeth777

Taylor, A. M., and Jeon, N. L. (2010). Micro-scale and microfluidic devices for neurobiology. *Curr. Opin. Neurobiol.* 20, 640–647. doi: 10.1016/j.conb.2010.07.011

Taylor, A. M., Rhee, S. W., Tu, C. H., Cribbs, D. H., Cotman, C. W., and Jeon, N. L. (2003). Microfluidic multicompartment device for neuroscience research. *Langmuir* 19, 1551–1556. doi: 10.1021/la026417v

Teh, S. Y., Lin, R., Hung, L. H., and Lee, A. P. (2008). Droplet microfluidics. *Lab Chip* 8, 198–220.

Teller, S., Tahirbegi, I. B., Mir, M., Samitier, J., and Soriano, J. (2015). Magnetite-Amyloid-beta deteriorates activity and functional organization in an in vitro model for Alzheimer's disease. *Sci. Rep.* 5:17261.

Terakawa, M. S., Lin, Y., Kinoshita, M., Kanemura, S., Itoh, D., Sugiki, T., et al. (2018). Impact of membrane curvature on amyloid aggregation. *Biochim. Biophys. Acta Biomembr.* doi: 10.1016/j.bbamem.2018.04.012 [Epub ahead of print].

Toprakcioglu, Z., Challa, P., Xu, C., and Knowles, T. P. J. (2019). Label-free analysis of protein aggregation and phase behavior. *ACS Nano* 13, 13940–13948. doi: 10.1021/acsnano.9b05552

Tran, H. T., Chung, C. H., Iba, M., Zhang, B., Trojanowski, J. Q., Luk, K. C., et al. (2014). Alpha-synuclein immunotherapy blocks uptake and templated propagation of misfolded alpha-synuclein and neurodegeneration. *Cell Rep.* 7, 2054–2065. doi: 10.1016/j.celrep.2014.05.033

Tran, T. M., Cater, S., and Abate, A. R. (2014). Coaxial flow focusing in poly(dimethylsiloxane) microfluidic devices. *Biomicrofluidics* 8:016502. doi: 10.1063/1.4863576

Tu, P. H., Galvin, J. E., Baba, M., Giasson, B., Tomita, T., Leight, S., et al. (1998). Glial cytoplasmic inclusions in white matter oligodendrocytes of multiple system atrophy brains contain insoluble alpha-synuclein. *Ann. Neurol.* 44, 415–422. doi: 10.1002/ana.410440324

Uemura, N., Uemura, M. T., Lo, A., Bassil, F., Zhang, B., Luk, K. C., et al. (2019). Slow progressive accumulation of oligodendroglial alpha-synuclein (alpha-Syn) pathology in synthetic alpha-Syn fibril-induced mouse models of synucleinopathy. *J. Neuropathol. Exp. Neurol.* 78, 877–890. doi: 10.1093/jnen/nlz070

Uemura, N., Uemura, M. T., Luk, K. C., Lee, V. M., and Trojanowski, J. Q. (2020). Cell-to-cell transmission of tau and alpha-synuclein. *Trends Mol. Med.* doi: 10.1016/j.molmed.2020.03.012 [Epub ahead of print].

Urrea, L., Segura-Feliu, M., Masuda-Suzukake, M., Hervera, A., Pedraz, L., Garcia Aznar, J. M., et al. (2018). Involvement of cellular prion protein in alpha-synuclein transport in neurons. *Mol. Neurobiol.* 55, 1847–1860. doi: 10.1007/s12035-017-0451-4

Usenovic, M., Niroomand, S., Drolet, R. E., Yao, L., Gaspar, R. C., Hatcher, N. G., et al. (2015). Internalized Tau oligomers cause neurodegeneration by inducing accumulation of pathogenic Tau in human neurons derived from induced pluripotent stem cells. *J. Neurosci.* 35, 14234–14250. doi: 10.1523/jneurosci.1523-15.2015

Vanni, I., Pirisinu, L., Acevedo-Morantes, C., Kamali-Jamil, R., Rathod, V., Di Bari, M. A., et al. (2020). Isolation of infectious, non-fibrillar and oligomeric prions from a genetic prion disease. *Brain* 143, 1512–1524. doi: 10.1093/brain/awaa078

Vilette, D., Courte, J., Peyrin, J. M., Coudert, L., Schaeffer, L., Andreoletti, O., et al. (2018). Cellular mechanisms responsible for cell-to-cell spreading of prions. *Cell. Mol. Life Sci.* 75, 2557–2574. doi: 10.1007/s00018-018-2823-y

Volpicelli-Daley, L. A., Luk, K. C., Patel, T. P., Tanik, S. A., Riddle, D. M., Stieber, A., et al. (2011). Exogenous alpha-synuclein fibrils induce Lewy body pathology leading to synaptic dysfunction and neuron death. *Neuron* 72, 57–71. doi: 10.1016/j.neuron.2011.08.033

Wang, B., Underwood, R., Kamath, A., Britain, C., Mcferrin, M. B., Mclean, P. J., et al. (2018). 14-3-3 proteins reduce cell-to-cell transfer and propagation of pathogenic alpha-synuclein. *J. Neurosci.* 38, 8211–8232. doi: 10.1523/jneurosci.1134-18.2018

Watts, J. C., and Prusiner, S. B. (2018). beta-Amyloid Prions and the pathobiology of Alzheimer's disease. *Cold Spring Harb. Perspect. Med.* 8:a023507.

Wells, C., Brennan, S. E., Keon, M., and Saksena, N. K. (2019). Prionoid proteins in the pathogenesis of neurodegenerative diseases. *Front. Mol. Neurosci.* 12:271. doi: 10.3389/fnmol.2019.00271

Westergard, T., Jensen, B. K., Wen, X., Cai, J., Kropf, E., Iacovitti, L., et al. (2016). Cell-to-Cell transmission of Dipeptide Repeat Proteins Linked to C9orf72-ALS/FTD. *Cell Rep.* 17, 645–652. doi: 10.1016/j.celrep.2016.09.032

Whitesides, G. M., Ostuni, E., Takayama, S., Jiang, X., and Ingber, D. E. (2001). Soft lithography in biology and biochemistry. *Annu. Rev. Biomed. Eng.* 3, 335–373. doi: 10.1146/annurev.bioeng.3.1.335

Wilham, J. M., Orru, C. D., Bessen, R. A., Atarashi, R., Sano, K., Race, B., et al. (2010). Rapid end-point quantitation of prion seeding activity with sensitivity comparable to bioassays. *PLoS Pathog.* 6:e1001217. doi: 10.1371/journal.ppat.1008222

Winner, B., Jappelli, R., Maji, S. K., Desplats, P. A., Boyer, L., Aigner, S., et al. (2011). *In vivo* demonstration that alpha-synuclein oligomers are toxic. *Proc. Natl. Acad. Sci. U.S.A.* 108, 4194–4199.

Winston, C. N., Aulston, B., Rockenstein, E. M., Adame, A., Prikhodko, O., Dave, K. N., et al. (2019). Neuronal exosome-derived human Tau is toxic to recipient mouse neurons *in vivo*. *J. Alzheimers Dis.* 67, 541–553. doi: 10.3233/jad-180776

Woerman, A. L., Patel, S., Kazmi, S. A., Oehler, A., Lee, J., Mordes, D. A., et al. (2020). Kinetics of alpha-synuclein prions preceding neuropathological inclusions in multiple system atrophy. *PLoS Pathog.* 16:e1008222. doi: 10.1371/journal.ppat.1008222

Woerman, A. L., Watts, J. C., Aoyagi, A., Giles, K., Middleton, L. T., and Prusiner, S. B. (2018). alpha-Synuclein: multiple system atrophy prions. *Cold Spring Harb. Perspect. Med.* 8:a024588. doi: 10.1101/cshperspect.a024588

Wu, J. W., Herman, M., Liu, L., Simoes, S., Acker, C. M., Figueroa, H., et al. (2013). Small misfolded Tau species are internalized via bulk endocytosis and anterogradely and retrogradely transported in neurons. *J. Biol. Chem.* 288, 1856–1870. doi: 10.1074/jbc.m112.394528

Wu, J. W., Hussaini, S. A., Bastille, I. M., Rodriguez, G. A., Mrejeru, A., Rilett, K., et al. (2016). Neuronal activity enhances tau propagation and tau pathology *in vivo*. *Nat. Neurosci.* 19, 1085–1092. doi: 10.1038/nn.4328

Wurthner, F. (2020). Aggregation-Induced Emission (AIE): a historical perspective. *Angew. Chem. Int. Ed. Engl.* 9, 14192–14196. doi: 10.1002/anie.202007525

Xia, N., Zhou, B., Huang, N., Jiang, M., Zhang, J., and Liu, L. (2016). Visual and fluorescent assays for selective detection of beta-amyloid oligomers based on the inner filter effect of gold nanoparticles on the fluorescence of CdTe quantum dots. *Biosens. Bioelectron.* 85, 625–632. doi: 10.1016/j.bios.2016.05.066

Xu, Y., Martini-Stoica, H., and Zheng, H. (2016). A seeding based cellular assay of tauopathy. *Mol. Neurodegener.* 11:32.

Yakupova, E. I., Bobyleva, L. G., Vikhlyantsev, I. M., and Bobylev, A. G. (2019). Congo Red and amyloids: history and relationship. *Biosci. Rep.* 39:BSR20181415.

Yang, I. H., Gary, D., Malone, M., Dria, S., Houdayer, T., Belegu, V., et al. (2012). Axon myelination and electrical stimulation in a microfluidic, compartmentalized cell culture platform. *Neuromol. Med.* 14, 112–118. doi: 10.1007/s12017-012-8170-5

Yang, Y., Li, S., Zhang, Q., Kuang, Y., Qin, A., Gao, M., et al. (2019). An AIE-active theranostic probe for light-up detection of Abeta aggregates and protection of neuronal cells. *J. Mater. Chem. B* 7, 2434–2441. doi: 10.1039/c9tb00121b

Ylera, F., Lurz, R., Erdmann, V. A., and Furste, J. P. (2002). Selection of RNA aptamers to the Alzheimer's disease amyloid peptide. *Biochem. Biophys. Res. Commun.* 290, 1583–1588. doi: 10.1006/bbrc.2002.6354

Zeinabad, H. A., Zarrabian, A., Saboury, A. A., Alizadeh, A. M., and Falahati, M. (2016). Interaction of single and multi wall carbon nanotubes with the biological systems: tau protein and PC12 cells as targets. *Sci. Rep.* 6:26508.

Zhang, J. D., Mei, J., Hu, X. L., He, X. P., and Tian, H. (2016). Ratiometric Detection of beta-Amyloid and Discrimination from Lectins by a Supramolecular AIE Glyconanoparticle. *Small* 12, 6562–6567. doi: 10.1002/smll.201601470

Zhang, Y., Buell, A. K., Muller, T., De Genst, E., Benesch, J., Dobson, C. M., et al. (2016). Protein aggregate-ligand binding assays based on microfluidic diffusional separation. *Chembiochem* 17, 1920–1924. doi: 10.1002/cbic.201600384

Zhang, Y., Ren, B., Zhang, D., Liu, Y., Zhang, M., Zhao, C., et al. (2020). Design principles and fundamental understanding of biosensors for amyloid-beta detection. *J. Mater. Chem. B.* 8, 6179–6196. doi: 10.1039/D0TB00344A

Zhao, Y., Li, X., Yang, Y., Si, S., Deng, C., and Wu, H. (2020). A simple aptasensor for Abeta40 oligomers based on tunable mismatched base pairs of dsDNA and graphene oxide. *Biosens. Bioelectron.* 149:111840. doi: 10.1016/j.bios.2019.111840

Zheng, X., Liu, P., Yang, C., and Wu, X. (2020). Amyloid protein aggregation in diabetes mellitus accelerate intervertebral disc degeneration. *Med. Hypotheses* 141:109739. doi: 10.1016/j.mehy.2020.109739

Zhou, J., Meng, L., Ye, W., Wang, Q., Geng, S., and Sun, C. (2018). A sensitive detection assay based on signal amplification technology for Alzheimer's disease's early biomarker in exosome. *Anal. Chim. Acta* 1022, 124–130. doi: 10.1016/j.aca.2018.03.016

Zhou, Y., Dong, H., Liu, L., and Xu, M. (2015). Simple Colorimetric Detection of Amyloid beta-peptide (1-40) based on Aggregation of Gold Nanoparticles in the Presence of Copper Ions. *Small* 11, 2144–2149. doi: 10.1002/smll.201402593

Conflict of Interest: The authors declare that the research was conducted in the absence of any commercial or financial relationships that could be construed as a potential conflict of interest.

frontiers in Bioengineering and Biotechnology

ORIGINAL RESEARCH
published: 23 September 2020
doi: 10.3389/fbioe.2020.562953

Quantifying the Role of Lysine in Prion Replication by Nano-LC Mass Spectrometry and Bioassay

Christopher J. Silva, Melissa L. Erickson-Beltran and Irina C. Dynin*

Western Regional Research Center, United States Department of Agriculture, Agricultural Research Service, Albany, CA, United States

Prions propagate by a template driven process, inducing the normal cellular isoform (PrP^{C}) to adopt the prion (PrP^{Sc}) conformation. In PrP^{C}, the positions of lysines are highly conserved and strongly influence prion propagation. In this study, covalent modification was used to quantitate the role of lysines in the PrP^{Sc} template that drives prion replication. The ε-amino group of lysines in the PrP^{Sc} (hamster-adapted scrapie Sc237) template was acetylated by either acetic anhydride (Ac_2O) or the N-hydroxysuccinimide ester of acetic acid (Ac-NHS). The extent of lysine acetylation in PrP^{Sc} was quantitated by mass spectrometry or Western blot-based analysis. Identical samples were bioassayed to quantitate the loss of infectivity associated with lysine acetylation. The reduction of infectivity at the highest reagent concentration was approximately 90% (∼10-fold). Ten of the eleven prion lysines were acetylated to a greater extent (25−400-fold) than the observed loss of infectivity. Only one lysine, at position 220 (K_{220}), had a reactivity that is consistent with the loss of infectivity. Although lysines are highly conserved and play a crucial role in converting PrP^{C} into the PrP^{Sc} conformation, once that conformation is adopted, the lysines present in the PrP^{Sc} template play only a limited role in prion replication. In principle, this approach could be used to clarify the role of other amino acids in the replication of prions and other prion-like protein misfolding diseases.

Keywords: prion, mass spectrometry, Sc237, lysine, bioassay

OPEN ACCESS

Edited by:
Maria Dos Anjos Pires, University of Trás-os-Montes and Alto Douro, Portugal

Reviewed by:
Sumit Ghosh, The Research Institute at Nationwide Children's Hospital, United States
Rita Payan Carreira, University of Évora, Portugal

****Correspondence:***
Christopher J. Silva
christopher.silva@ars.usda.gov;
christopher.silva@usda.gov

Specialty section:
This article was submitted to Biosafety and Biosecurity, a section of the journal Frontiers in Bioengineering and Biotechnology

Received: *17 May 2020*
Accepted: *24 August 2020*
Published: *23 September 2020*

Citation:
Silva CJ, Erickson-Beltran ML and Dynin IC (2020) Quantifying the Role of Lysine in Prion Replication by Nano-LC Mass Spectrometry and Bioassay. Front. Bioeng. Biotechnol. 8:562953. doi: 10.3389/fbioe.2020.562953

INTRODUCTION

Prions (PrP^{Sc}) are molecular pathogens, which propagate by inducing the normal cellular prion protein (PrP^{C}) to adopt the prion's conformation and, thereby, propagate an infection (Telling et al., 1996; Prusiner, 1998). This template-mediated process is stoichiometric as opposed to catalytic or enzymatically driven. If there is a mismatch between the primary amino acid sequence of the PrP^{Sc} template and the PrP^{C} substrate, then there can be a significant delay in the onset of disease. This delay is traditionally referred to as the species barrier (Pattison, 1965), even though it can occur when both PrP^{C} and PrP^{Sc} are from the same species (Supattapone et al., 1999).

The introduction or deletion of lysines has been shown to significantly affect prion replication in animals. Using transgenic mouse models, researchers showed that deletion of the three N-terminal

Abbreviations: PrP, prion protein; PrP^{Sc}, infectious PrP isoform; PrP^{C}, normal cellular PrP isoform; rPrP, recombinant PrP.

lysine groups severely impedes prion replication (Turnbaugh et al., 2012). Experimentally infected heterozygous sheep (glutamine/lysine at position 171) succumb to scrapie after a longer incubation period than homozygous (glutamine/glutamine at position 171) sheep (Greenlee et al., 2012). In goats, a lysine at position 222 (K_{222}) has also been associated with protection from scrapie infection (Vaccari et al., 2006; Bouzalas et al., 2010). Replacement of a glutamic acid at position 211 with a lysine in bovine PrP^C is associated with sporadic disease (Nicholson et al., 2008). These results demonstrate that lysines are crucial for conversion of PrP^C to PrP^{Sc}.

Analogous results have been observed in the susceptibility of human populations to Creutzfeldt-Jakob disease (CJD). Replacement of glutamic acid at position 196 or 200 with a lysine in PrP^C is associated with inherited CJD (Spudich et al., 1995; Peoc'h et al., 2000). In Japan, approximately 12% of the population expresses a PrP^C polymorphism, where the glutamic acid at position 219 is replaced by lysine (K_{219}) (Kitamoto and Tateishi, 1994). This polymorphism is associated with protection from sporadic CJD (Shibuya et al., 1998a,b), but not from iatrogenic CJD (dura matter transplant) (Ikawa et al., 2009) or from familial CJD (Furukawa et al., 1995; Seno et al., 2000). Again, these observations support the importance of lysine in the conversion of PrP^C to PrP^{Sc}. However, once the PrP^{Sc} template is formed, the role of lysines is unclear.

Covalent modification of some amino acids in the PrP^{Sc} template has been associated with a substantial reduction in infectivity. The loss of infectivity was measured using the well-established incubation time bioassay (Prusiner et al., 1980). Diethylpyrocarbonate (DEPC) reacts with histidines to produce the labile ethoxyformyl adduct (McKinley et al., 1981). When highly purified samples from hamsters infected with the Sc237 strain of hamster-adapted scrapie are reacted with DEPC, a reduction of infectivity of 1,000-fold is observed (McKinley et al., 1981). The infectivity lost to DEPC was restored by the reaction with the nucleophile hydroxylamine, which removes an added ethoxyformyl group to restore an intact histidine (McKinley et al., 1981). When DEPC was reacted with the Sc237 PrP^{Sc} in brain homogenates, however, there was no loss of infectivity, presumably due to the endogenous nucleophiles present in those homogenates (Prusiner et al., 1981). Another reagent, β-propiolactone, effectively inactivates viruses, by covalently modifying DNA and to a much lesser extent the lysine in proteins (Uittenbogaard et al., 2011). When it was used to inactivate prions it was partially successful (∼10-fold reduction) (Haig and Clarke, 1968). The extent of the covalent modification of the amino acids present in the PrP^{Sc} template was not determined in either of these experiments. These results indicate that covalent modification of the PrP^{Sc} template has the potential to impede prion replication.

Acetic anhydride (Ac_2O) and esters of N-hydroxysuccinimide have been used to study the structure of prions (Gong et al., 2011; Silva, 2012; Silva et al., 2016). The extent of this reaction is determined by the chemical environment of a given lysine in the PrP^{Sc} isoform and has been quantitated using Western-blot and mass spectrometry-based analysis (Gong et al., 2011; Silva, 2012; Silva et al., 2016). While these experiments demonstrated methods to quantitate covalent differences in the PrP^{Sc} template, there was no attempt to relate a loss of infectivity to the extent of the covalent modifications of PrP^{Sc}.

Prion replication is a template driven process (Wille and Requena, 2018; Spagnolli et al., 2019), where covalent differences between the PrP^{Sc} template and PrP^C may influence prion propagation (Supattapone et al., 1999). In principle, covalent modification of lysines in the PrP^{Sc} template may impede its replication, as has been observed when histidines were covalently modified (McKinley et al., 1981). Once the template, containing acetylated lysines, converts PrP^C into the prion isoform, the newly formed terminal portion of the template no longer contains acetylated lysines and future prion replication can continue unimpeded from this template with a new terminus. Since prion replication is a template driven and not an enzymatically driven process, the degree of covalent modification of an amino acid essential in prion replication directly determines the extent of the impediment to prion replication. The extent of this impediment can be quantitated by using bioassay to measure the survival time and relate it to an equivalent dilution (Prusiner et al., 1982). The difference between the calculated dilution and the unreacted starting material corresponds to the loss of template due to the acetylation of lysines in that template.

A combined mass spectrometry and antibody-based method was used to quantitate the extent to which the lysines present in the PrP^{Sc} template reacted with acetic anhydride or the acetyl ester of N-hydroxysuccinimide. In addition, rodent bioassay was used to quantify the effects of lysine acetylation on infectivity. These approaches provide insight into surface exposure of the lysines of the wild type Sc237 prion and their importance in prion replication. The results of this analysis are reported below.

EXPERIMENTAL SECTION

HPLC grade water was purchased from Burdick and Jackson (Honeywell Research Chemicals; Charlotte, NC, United States). Acetonitrile, HPLC grade, was purchased from Fisher Scientific (Waltham, MA, United States). Trypsin (porcine, sequencing grade, modified) was purchased from Promega (Madison, WI, United States). Chymotrypsin was purchased from Worthington Biochemical Corp. (Lakewood, NJ, United States). All other reagents were purchased from Sigma-Aldrich (St. Louis, MO, United States).

Production of Recombinant PrP

Recombinant PrP was obtained from plasmids expressing the hamster protein sequence [equivalent to the mature protein sequence (23-231) with an N-terminal methionine]. The plasmids were cloned into BL21 cells (Millipore Sigma; Burlington, MA, United States) and induced to over express hamster recombinant PrP by the addition of isopropyl β-D-1-thiogalactopyranoside (IPTG). The cells were pelleted and the inclusion bodies isolated from that pellet using standard molecular biology techniques (Sambrook et al., 1989).

Isolation of Recombinant PrP

The inclusion body pellet was suspended in 1 ml of denaturing buffer (6M GuCl, 100 mM sodium phosphate, 10 mM Tris, pH 8.0) and sonicated for 3 min. After sonication the suspension was centrifuged at 20,000 × *g* for 5 min to remove any insoluble material. The supernatant was applied to a 1 ml HIS-Select cartridge (Sigma, St. Louis, MO, United States) that had previously been stripped of nickel (II) ions and recharged with copper (II) ions according to the manufacturer's instructions. The denatured recombinant protein bound to the cartridge was renatured by the application of a 5-h linear gradient (0.04 ml/min) starting with 100% denaturing buffer and ending with 100% refolding buffer (100 mM sodium phosphate, 10 mM Tris, pH 8.0). After the gradient was completed the cartridge was washed for a further hour with refolding buffer at a flow rate of 0.05 ml/min. The refolded protein was eluted with 5 ml of 0.1 M EDTA and immediately dialyzed against 1L of 100 mM ammonium acetate (pH 4.5) overnight at room temperature, using a dialysis cassette (7000 MWCO; Thermo Fisher Scientific/Pierce). The next day the dialysis buffer was discarded and replaced with 1 L of fresh buffer and allowed to dialyze for an additional 2 h. Aliquots were lyophilized and quantitated by protein assay (Thermo Fisher Scientific/Pierce BCA) and UV/visible spectrophotometry (absorbance at 280 nm). All of the proteins contained an N-terminal methionine (Flinta et al., 1986). The molecular weight of the proteins predicted by the *Prnp* gene sequences matched that observed by mass spectrometric analysis.

The purified ^{15}N-labeled Syrian hamster rPrP (^{15}NSHarPrP) was analyzed by mass spectrometry. The mass spectrometry-based analysis revealed that the protein was uniformly labeled with ^{15}N (>99.7) and could be used, after digestion with trypsin or chymotrypsin, to produce the required internal standards. The analysis also indicated that it contained the expected N-terminal methionine (Flinta et al., 1986).

Reaction of Recombinant PrP With Ac_2O or Ac-NHS

Purified natural abundance rPrP was dissolved in one milliliter of reaction buffer (2% w/v octyl β-D-glucopyranoside; 50 mM sodium phosphate, pH 8.0), mixed and then centrifuged (20,000 × *g*; 20 min) to remove any aggregates. 90 μl aliquots of the supernatant were placed into ten microfuge tubes. A 10-μl aliquot of a 0, 1, 10, 50, or 100 mM solution of Ac-NHS or 0, 50, 100, 200, or 500 mM solution of Ac_2O was added to different tubes. The tubes were rotated at room temperature (21°C) for 15 min. After 15 min, 10 μl of a 1 M Tris solution (pH 8.0) was added, and the tubes were rotated for an additional 15 min at room temperature to quench the reaction. 900 μl of cold (−20°C) methanol was added, mixed, and stored in a −20°C freezer, overnight. The tubes were removed from the freezer and centrifuged (−11°C; 20,000 × *g*; 20 min). The supernatant was removed; the pellet resuspended in 500 μl of cold (−20°C) 85% methanol and centrifuged (−11°C; 20,000 × *g*; 20 min). The supernatant was removed, and the pellet was processed for mass spectrometry-based analysis.

Animal Handling

Animal experiments were carried out in accordance with the recommendations contained in the Guide for the Care and Use of Laboratory Animals of the National Institutes of Health. The procedures were governed by a protocol that was approved by the Institutional Animal Care and Use Committee of the United States Department of Agriculture, Agricultural Research Service, Albany, CA, United States (Protocol Number: P-10-3). All inoculations and euthanizations were performed under isoflurane anesthesia. LVG Syrian golden hamsters (*Mesocricetus auratus*) were obtained from a commercial vendor (Charles River Laboratories; Wilmington, MA, United States). The Sc237 strain of hamster-adapted scrapie was purchased from InPro Biotechnology (South San Francisco, CA, United States) and passaged once through LVG Syrian golden hamsters.

To minimize adverse impacts of the chemical reagents upon the hamsters, all Ac_2O and Ac-NHS reaction mixtures containing the Ac_2O or Ac-NHS reagents were diluted 1:10 with PBS prior to inoculation. No inoculated animal was observed to suffer any short-term ill effects from these inoculations. Each female LVG hamster (4 weeks old), was inoculated intracranially (*ic*) with 50 μl of either one of the brain homogenate (BH) dilutions, one of the dilutions of purified prions, or one of the ten diluted (1:10) reaction mixtures. Six hamsters were inoculated with 50 μl replicates of each sample. Eighty-four animals were inoculated in total. Details on the various inocula can be found in the following methods sections: *Ac-NHS reactions*, *Acetic anhydride (Ac_2O) reactions*, *Quantitation of loss of infectivity by bioassay*, and *Bioassay of Ac-NHS and Ac_2O reaction mixtures*. The animals were observed for clinical signs and were humanely euthanized when they were no longer able to feed or drink. The appearance of clinical signs and the date of humane euthanization were recorded.

Preparation of Samples

Brains were removed from euthanized hamsters in the terminal stages of a prion infection following inoculation (*ic*) with the Sc237 strain of hamster-adapted scrapie. A 10% homogenate (w/v) was prepared from these brains in sucrose buffer (0.32M sucrose in PBS) using an Omni GLH general laboratory homogenizer and disposable Omni Tip plastic generator probes (Omni International; Kennesaw, GA, United States). The homogenate was then centrifuged for 15 min (3,000 × *g*; 20°C), in an Eppendorf 5810R refrigerated centrifuge (Eppendorf; Hamburg, Germany), to remove large particles. The supernatant was retained as the brain homogenate (BH). Some of this homogenate was used as the substrate for the acetic anhydride (Ac_2O) reaction (*vide infra*) and some was used to obtain purified prions.

PrP^{Sc} was purified according to the methods of Bolton et al. (1991), with some minor modifications (Silva et al., 2011). Briefly, the brain homogenate was diluted with an equivalent volume of 20% w/v N-Lauroylsarcosine sodium salt and 19 mM sodium phosphate, pH 8.5, to yield two volumes of Sarkosyl homogenate. This was allowed to stand for 30 min at room temperature and then centrifuged for 18 min (16,000 × *g*; 20°C), in an

Eppendorf 5810R refrigerated centrifuge, to yield the clarified Sarkosyl homogenate. A portion of this clarified homogenate was diluted to 3 ml with buffer (10% w/v N-Lauroylsarcosine sodium salt, 9.5 mM sodium phosphate, pH 8.5) and transferred to an ultracentrifuge tube (4.2 ml, 16 mm × 38 mm). The contents of the tube were underlaid with 1 ml of 20% w/v sucrose and sealed. The sample in the sealed tube was centrifuged for 75 min at 150,000 × *g* (46,000 rpm, 20°C) with a floating Noryl spacer in a Beckman 70.1 Ti rotor (Beckman Coulter; Brea, CA, United States) to obtain the pellet of purified PrP^{Sc}. The supernatant was carefully removed and discarded. The pellet was resuspended in 200 μl of buffer (2% w/v octyl β-D-glucopyranoside, 50 mM phosphate buffer, pH 8.0) by brief sonication using closed tubes in a cup horn (four 45-s bursts; Misonix 3000 sonicator; Misonix; Farmingdale, NY, United States). The sonicated suspension of purified PrP^{Sc} was used as a substrate for the N-hydroxysuccinimide ester of acetic acid (Ac-NHS) reaction (*vide infra*).

β-Propiolactone Reactions

A 10% brain homogenate was prepared by homogenizing a brain (1 g) from a healthy uninfected hamster in 100 mM phosphate buffer (pH 8.0) containing 2% (w/v) octyl β-D-glucopyranoside. After homogenization the solution was centrifuged (20,000 × *g* for 15 min) to remove the suspended particles and yield the clarified brain homogenate. The pellet was discarded. The supernatant was retained and used for the listed reactions.

Nine aliquots of the clarified brain homogenate were apportioned into separate screw-cap microcentrifuge tubes. 10 μl of either a 0, 1, 10, 50, 100, 250, 500, or 1000 mM solution of β-propiolactone in DMSO or a 200 mM solution of Ac-NHS in DMSO was added to one of the 90 μl aliquots. The tubes were rotated at room temperature (21−22°C) for 15 min. After 15 min of reaction, 10 μl of a 1M solution of Tris (pH 8.0) was added to quench the reaction and rotated for an additional 15 min. The samples were precipitated with cold (−20°C) methanol. The pellet was isolated by centrifugation (20,000 × *g*; 20 min; −11°C). 100 μl of Laemmli buffer was added to the dried pellet and boiled for 10 min. A 10-μl aliquot of cooled sample was analyzed by Western blot (probed with 3F4 mAb).

Ac-NHS Reactions

Twenty individual samples of purified prions were prepared and combined. The combined suspension was aliquoted (180 μl) into twenty 1.5 ml screw cap microcentrifuge tubes. To eight of the forty tubes was added 20 μl of one of the following five concentrations of Ac-NHS in DMSO: 0, 10, 50, 100, or 200 mM. These were rotated for 15 min at room temperature. To quench the reaction, 20 μl of 1 M Tris pH 8.0 was added and the samples were again rotated for 15 min at room temperature.

From each Ac-NHS reaction, three aliquots (110 μl) were retained for mass spectrometry-based analysis, three aliquots were retained for Western blot-based analysis, and one aliquot of each set of Ac-NHS reactions was diluted 10x with PBS before inoculation (*ic*) into hamsters (see section "Bioassay of Ac-NHS and Ac_2O Reaction Mixtures" below). An aliquot (110 μl) of the unreacted starting material (0 mM Ac-NHS) was further diluted (10^{-2} and 10^{-4}) and used to prepare the bioassay calibration curve (see section "Quantitation of Loss of Infectivity by Bioassay" below).

Acetic Anhydride (Ac_2O) Reactions

A total of 3.2 ml of the BH were brought up to 4 ml of a solution of 2% octyl β-D-glucopyranoside, 50 mM sodium phosphate pH 8.0, solubilized for 10 min, and then centrifuged for 10 min, 20,000 × *g*, to remove large particles. The supernatant was removed to a new tube and aliquoted (180 μl) into twenty 1.5 ml screw cap microcentrifuge tubes. To each was added 20 μl of one of the following five concentrations of Ac_2O in DMSO: 0, 50, 100, 200, or 500 mM. These were rotated for 15 min at room temperature. To quench the reaction, 20 μl of 1 M Tris pH 8.0 was added and the samples were again rotated for 15 min at room temperature.

From each Ac_2O reaction, three aliquots (110 μl) were retained for mass spectrometry-based analysis (*vide infra*), three were retained for Western blot analysis (*vide infra*), and one aliquot was diluted 10x with PBS before inoculation (*ic*) into hamsters (*vide supra*) (see section "Bioassay of Ac-NHS and Ac_2O Reaction Mixtures" below). One aliquot (110 μl) of the unreacted starting material (0 mM Ac-NHS) was further diluted (10^{-2} and 10^{-4}) and used to prepare the bioassay calibration curve (see section "Quantitation of Loss of Infectivity by Bioassay" below).

Reduction, Alkylation, and Tryptic Cleavage of PrP Samples

The reaction mixtures were inactivated by addition of enough 8M guanidine hydrochloride (GuCl) to achieve a final concentration of 6 M. The solutions stood for 24 h at room temperature. The denatured proteins were precipitated with ice-cold methanol (85% methanol plus 15% protein solution) and centrifuged for 20 min at 20,000 × *g* for 20 min in a cold rotor (−11°C) with an Eppendorf Model 5417R centrifuge (Eppendorf; Hamburg, Germany). The pellets resulting from the methanol precipitation were dissolved in a 10 μl solution (0.01% octyl β-D-glucopyranoside, 1 pmol/μl methionine, and 8% acetonitrile) and sonicated for 5 min. After sonication (Cole-Parmer model 8892; Vernon Hills, IL, United States), a 10 μl solution containing the appropriate internal standard (18 fmol/μl in 0.01% octyl β-D-glucopyranoside, 1 pmol/μl methionine, and 8% acetonitrile) was added. The 20 μl solution was sonicated for an additional 5 min and then 10 μl of a solution of 10 mM dithiothreitol (DTT) in buffer A (25 mM ammonium bicarbonate, 0.01% octyl β-D-glucopyranoside, 1 pmol/μl methionine, and 8% acetonitrile; pH 8.0) was added to the mixture and allowed to react for 1 h at 37°C. After the reaction mixture cooled to room temperature, 40 μl of a solution of 10 mM iodoacetamide in buffer A was added to the mixture and allowed to stand in the dark at room temperature for 1h. The excess iodoacetamide was quenched by the addition of DTT (20 μl of 10 mM DTT in buffer A). The reduced and alkylated proteins were subjected to proteolysis with added trypsin (1 μg trypsin/10 μl water) or chymotrypsin (500 ng chymotrypsin/10 μl of a 20 mM $CaCl_2$ solution). The trypsin digestion proceeded at 37°C for 16 h. The

chymotrypsin reaction proceeded at 30°C for 18 h, followed by the addition of 2.5 μl of 10% formic acid to stop the reaction. Samples were filtered through 10,000 molecular weight cutoff filters for 12 min at 14,000 × *g*. Samples were stored at −20°C until analyzed.

Quantitative Mass Spectrometry: Nanospray LCMSMS

An Applied Biosystems (Sciex; Framingham, MA, United States) Model 4000 Q-Trap instrument equipped with a nano-electrospray source was used to perform NanoLC-MS/MS. 6 ml aliquots of each digest (10.8 fmol internal standard) were loaded onto a C-18 trapping cartridge (PepMap, 5 μm, 100A, 300 μm i.d. × 5 mm, flow rate 15 μl/min; Thermo Fisher Scientific/Dionex; Sunnyvale, CA, United States). Salts were washed from the cartridge with a solution of acetic acid/acetonitrile/heptafluorobutyric acid/water (0.5/1/0.02/99). The salt-free bound peptides were eluted onto a reverse-phase column (Vydac Everest 238EV5.07515, 75 μm × 150 mm, flow rate 250 nL/min, Hichrom; Leicestershire, United Kingdom).

The solvents were delivered with an Applied Biosystems model Tempo nanoflow LC system (Sciex) with autosampler, column switching device, and nanoflow solvent delivery system. Samples were eluted from the column with a binary gradient (A, 0.5% acetic acid in water and B, 80% acetonitrile, 0.5% acetic acid). The flow rate was 250 nl/min with a 16-min linear gradient starting with 5% B and ending with 100% B. Elution with 100% B was held for 7 min followed by a return to 5% B over 4 min. The eluted samples were sprayed with non-coated spray tip (FS360-20-10-N-20-C12, New Objective Inc., Woburn, MA, United States) onto the Applied Biosystems source, Model Nanospray II.

The instrument response for the peptides **NKP**SKPKTNM (NKP), **PGG**WNTGGSR (PGG), and **QHT**VTTTTK (QHT) was optimized by a previously described method (Onisko et al., 2007). Briefly, a recombinant PrP digest (*vide supra*) or synthetic peptide (1 pmol/μl; 20 μl) dissolved in solvent (50/49.5/0.5; acetonitrile/water/acetic acid) was isocratically eluted from the reverse-phase column at a flow rate of 250 nL/min. The analyte signal was maximized by adjusting the source parameters (electrospray voltage, curtain gas and nebulizing gas settings, ion source heater temperature, declustering potential (DP), and nanospray tip positioning relative to the front plate orifice). The intensity of specified product ions was optimized by adjusting the Q2 offset voltage ["collision energy" (CE)] to yield optimal fragmentation. The mass settings for the three peptides are the following: NKPSKPKTNM [precursor ion m/z (z = 3) of 382.2, product ion of 226.1 (b_2-NH_3) or 590.3 (y_5)], PGGWNTGGSR [precursor ion m/z (z = 2) of 494.8, product ion of 891.5 (y_9)], and QHTVTTTTK [precursor ion m/z (z = 2) of 509.1, product ion of 751.4 (y_7)]. The optimal CEs for the peptides were determined to be 30 V for ions from NKPSKPKTNM and PGGWNTGGSR and 26 V for the ion from QHTVTTTTK. The optimal DPs for the b_2-NH_3 and y_5 ions from the peptide NKPSKPKTNM, the y9 ion from the peptide PGGWNTGGSR, and the y7 ion from the peptide QHTVTTTTK were determined to be 80, 90, 110, and 110 V, respectively. The mass spectrometer was operated in multiple reaction monitoring (MRM) mode, alternating between detection of the desired peptides and the appropriate internal standards.

The **NKP**SKPKTNM (NKP) peptide contains a methionine which can be oxidized (Silva et al., 2010, 2011, 2013). We determined that the peptide and its oxidized homolog are chromatographically separable. We employed our previously described method to quantitate the portion of the oxidized peptide (Silva et al., 2010, 2011, 2013). We determined that the oxidized peptide was found to be present in all of the samples and that the amount was consistently low (<5%). Therefore, we did not include it in any of our calculations. The peptide YRPVDQY does not contain a lysine and is unaffected by reaction with Ac_2O or Ac-NHS, so it was used to normalize samples digested with chymotrypsin.

Mass Spectrometry-Based Quantitation of Tryptic and Chymotryptic Peptides

Hamster PrP was digested with either trypsin or chymotrypsin using previously described conditions (Onisko et al., 2007). Trypsin digestion yields the lysine associated peptides **PGG**WNTGGSR (PGG), **QHT**VTTTTK (QHT), **GEN**FTETDIK (GEN), **VVE**QMCTTQYQK (VVE) and **ESQ**AYYDGR (ESQ). The optimized instrument response for the YPGQGSPGGNR, GEN, VVE, and ESQ peptides has been previously reported (Douma et al., 1998; Onisko et al., 2007; Silva et al., 2011). Chymotryptic digestion requires overnight digestion (30°C) for optimal results and yields the peptides **NKP**SKPKTNM (NKP) and YRPVDQY. The optimized instrument parameters for the peptide YRPVDQY have been previously reported (Sturm et al., 2012).

^{15}N-labeled rPrP was used as an internal standard. The isotopic purity of the uniformly labeled product was determined to be 99.7%. None of the peptides derived from ^{15}N-labeled rPrP interfered with the analysis of any other ^{15}N-labeled peptides or with any of the peptides derived from rPrP or PrP^{Sc} samples. The area ratios of the MRM transition signals from the tryptic peptides PGG (1.14 ± 0.03), QHT (0.22 ± 0.01), GEN (1.7 ± 0.07), VVE (0.084 ± 0.004), and ESQ (1.24 ± 0.03) peptides to YPGQGSPGGNR varied by less than 10% (n = 180). The area ratio of the MRM transition signals from the chymotryptic NKP (0.23 ± 0.02) to the YRPVDQY peptide also varied by less than 10% (n = 180). The YPGQGSPGGNR and YRPVDQY peptides do not contain lysines and are produced in proportion to the progenitor PrP protein, so they were used to normalize the MRM transition signals from the other tryptic or chymotryptic peptides, respectively, to the amount of PrP in the sample after trypsin or chymotrypsin digestion, respectively. Thus, normalizing labile peptide to an inert internal peptide is an effective means of correcting for the differences in the amount of PrP in each sample.

Western Blot

Protein gels were purchased from a commercial vendor (Thermo Fisher Scientific; Waltham, MA, United States) and used

according to the manufacturer's instructions. The primary antibody 3F4 (Covance; San Diego, CA, United States) and secondary antibody Anti-Mouse IgG (Fc specific)-AP (Sigma; St. Louis, MO, United States) were purchased. Blotting paper, membrane [polyvinylidene fluoride (PVDF)] and SDS−PAGE gels were presoaked in transfer buffer (25 mM Tris, 250 mM glycine in 15% methanol) for 10 min. The proteins were transferred from the gel to the PVDF membrane using a BIO-RAD *Trans*-Blot SD semi-dry transfer cell (50 min at 100 mA). After transfer, the PVDF membrane was placed into a square Petri dish (10 cm × 10 cm) and gently agitated in 20 ml of wash buffer (PBS + 0.05 Tween 20) for 5 min. After 5 min, the wash buffer was discarded, and the membrane was blocked (15 min in 10 ml of StartingBlock T20; Thermo Fisher Scientific/Pierce) with gentle agitation. The membrane was then incubated for 1 h at room temperature in 10 ml of blocking buffer with 1 μl of primary antibody (3F4; 2 mg/mL). After this incubation, the buffer was discarded, and 20 ml of wash buffer was added and gently agitated for 5 min. This was repeated three times with fresh wash buffer. 10 ml of blocking buffer with 10 μl of the secondary antibody was added and incubated at room temperature for 45 min. After incubation, the membrane was washed four times with wash buffer at 5-min intervals. The wash membrane was placed in 10 ml of a Sigma/FAST BCIP/NBT solution (1 tablet per 10 ml per manufacturer's instructions) and incubated at 37°C. After development, the blots were dried and scanned to obtain densitometry measurements.

Western Blot-Based Quantitation of Lysine at Position 110 (K_{110})

Five sets of dilutions (undiluted, 1:3.2, 1:10, 1:32, and 1:100) of a PrP 27-30 standard were prepared and each set was analyzed on a separate Western blot. The signal intensity, as measured by densitometry, was determined for the diglycosylated band of PrP 27-30 of each dilution (n = 5). The 10 kDa region in each lane was used as background and subtracted from the diglycosylated band in each lane. The relative signal intensity was calculated by normalizing the intensity of the signal (less background) from a dilution to that of the undiluted starting material (less background) for each blot. A calibration curve relating the normalized signal intensities of a dilution to the corresponding $\log_{10}$ of its experimental dilution was prepared.

Equivalent amounts of the reaction mixtures for Ac_2O (0, 5, 10, 20, and 50 mM) with BH and Ac-NHS (0, 1, 5, 10, and 20 mM) with purified prions were analyzed (n = 3) on separate Western blots. The calibration curve (*vide supra*) was used to relate the observed normalized signal intensity of the diglycosylated band of each PrP^{Sc} sample (*vide supra*) to a log dilution. This data was used to determine the relative extent of the reaction of K_{110} with Ac_2O or Ac-NHS.

Densitometry

Densitometry measurements were made using the AlphaEaseFC version 4.0.0 software (Alpha Innotech/Genetic Technologies, Inc., Miami, FL, United States) with black having a value of 255 and white having a value of 0. The statistical analysis was performed with Microsoft Excel.

Quantitation of Loss of Infectivity by Bioassay

Dilutions of BH or purified PrP^{Sc} preparations, derived from the brains of prion-infected hamsters, were used to prepare calibration curves relating survival times to their corresponding $\log_{10}$ dilutions. Two sets (BH or purified prions) of three dilutions (10^{-1}, 10^{-3}, or 10^{-5}) were inoculated (*ic*) into an animal (10^{-3} and 10^{-5} dilutions of 0 mM Ac-NHS and Ac_2O × 6 animals per dilution = 24 animals). The survival times were recorded and used to prepare the calibration curves for the BH and the purified preparations.

Bioassay of Ac-NHS and Ac_2O Reaction Mixtures

The prions contained in the BH were reacted with one of five final concentrations (0, 5, 10, 20, and 50 mM) of Ac_2O. Each reaction mixture was diluted 1:10 in phosphate buffered saline (PBS); a 50 μl aliquot of a dilution was injected (*ic*) into a hamster (5 reaction mixtures × 6 animals per reaction mixture = 30 animals). The animals were observed for the presentation of clinical signs of advanced prion disease, then humanely euthanized. The time from the date of the inoculation to the date of humane euthanization, the survival time, was determined for each set of inoculated reaction mixtures. The bioassay calibration curves for the BH were used to relate those observed survival times to their corresponding $\log_{10}$ dilutions.

Aliquots of the purified prions were reacted with five different final concentrations (0, 1, 5, 10, or 20 mM) of Ac-NHS. Again, each reaction mixture was diluted 1:10; a 50 μl aliquot of a dilution was injected (ic) into a hamster (5 reaction mixtures × 6 animals per reaction mixture = 30 animals). The observed survival times were recorded and used to calculate the corresponding $\log_{10}$ dilutions, based on the purified prion calibration curves.

Confirming the Presence on Prions in Infected Animals

A portion of the brain (∼50 mg) from two of the six animals in each set was removed and homogenized in 300 μl of PBS. The homogenate was clarified and divided into two portions. One was treated with proteinase K (50 μg/ml; 37°C; 1 h) and the other was not. The prions in the samples were inactivated by the addition of 3 volumes of 8M guanidine hydrochloride (GuCl) (Prusiner et al., 1993). The solutions were mixed and allowed to stand for 24 h at room temperature. The GuCl solutions were individually precipitated with cold (−20°C) aqueous methanol (85% methanol). The resulting pellets were suspended in Laemmli buffer, boiled (10 min) and then analyzed by Western blot (3F4 primary antibody) to confirm the presence of prions in that animal's brain.

These samples were tested for the presence of prions by Western blot (3F4 primary antibody). The resulting Western

blot analysis (data not shown) showed that these samples were indistinguishable from Sc237 controls. In addition, each animal displayed clinical signs that were consistent with being infected with the Sc237 strain of hamster-adapted scrapie.

Statistical Analysis

The bioassay and the mass spectrometry data were statistically analyzed. The unpaired Student's *t*-test was used to compare the relative peptide quantitation data from specific chemical reactions to the measured loss of infectivity of inoculated reaction mixtures. It was also used to compare the relative peptide quantitation data from specific chemical reactions to other chemical reactions. Linear least squares regression was used to prepare the bioassay calibration curves and the curves measuring the relationship between the extent of the reaction of individual peptides *v*. the concentration of the reagents. This analysis yielded the slope and intercept of those linear equations. *p*-Values for linear regression were determined using standard statistical methods[1]. The slopes of the regression lines derived from linear regression analysis were compared using a *t*-test[2]. Excel was used to perform all calculations.

Safety Considerations

All prion-containing samples were manipulated in a dedicated biosafety level 2 (BSL-2) laboratory, which was certified and inspected by the Animal and Plant Health Inspection Service (APHIS[3]) using procedures outlined in the Biosafety in Microbiological and Biomedical Laboratories, fifth edition[4]. The infectious prions were inactivated before removal from the BL2 laboratory (Prusiner et al., 1993). Acetonitrile is hazardous and was manipulated in a dedicated chemical safety hood.

RESULTS

Acetic Anhydride (Ac_2O) and Ac-NHS Were Selected to React With the Lysines of Prion Template

Acetic anhydride, Ac-NHS, diethylpyrocarbonate, and β-propiolactone have been used to covalently modify prions (Haig and Clarke, 1968; Gong et al., 2011; Silva, 2012; Silva et al., 2016). The diethylpyrocarbonate (DEPC) reagent was inhibited by the endogenous nucleophiles present in the brain homogenate (McKinley et al., 1981; Prusiner et al., 1981). β-propiolactone has been used to inactivate viruses and shown to react with lysines (Uittenbogaard et al., 2011). β-Propiolactone was evaluated to determine if its reactivity was influenced by external nucleophiles.

β-propiolactone has been previously shown to partially inactivate prions (Haig and Clarke, 1968). We assessed β-propiolactone's ability to covalently modify PrP^C's lysines by measuring the extent of propionation of lysine 110 (K_{110}). Each of nine supernatant samples from uninfected hamster brain homogenate were reacted with one of eight different concentrations of β-propiolactone or one concentration of Ac-NHS. The reaction mixtures were analyzed by Western blot, using the 3F4 mAb (**Figure 1**), and the resulting signals were quantified by densitometry. The signal intensity for each β-propiolactone reaction (**Figure 1**, lanes 2-8), relative to the unreacted starting material (**Figure 1**, lane 1), varied by only 6% (1.04 ± 0.06). The signal intensity for the Ac-NHS reaction (**Figure 1**, lane 9) was the same as background. This indicates that β-propiolactone reacts preferentially with molecules in the brain homogenate other than lysines in PrP^C and therefore was not suitable to assess the effect of lysine acetylation on prion inactivation.

Quantitation of Tryptic and Chymotryptic Peptides Can Be Related to the Acetylation of Lysine at Position 23, 24, 27, 101, 104, 106, 185, 194, 204, or 220 (K_{23}, K_{24}, K_{27}, K_{101}, K_{104}, K_{106}, K_{185}, K_{194}, K_{204}, and K_{220})

Acetylation of the ε-amino group of lysine precludes its cleavage by trypsin. Acetylation of K_{27}, K_{185}, K_{194}, or K_{220} which precede the peptide **PGG**WNTGGSR (PGG), **QHT**VTTTTK (QHT), **GEN**FTETDIK (GEN), or **ESQ**AYYDGR (ESQ) would prevent that peptide from being produced by trypsin digestion (**Figure 2**). Acetylation of K_{194}, K_{204}, or K_{220} which terminates QHT, GEN, or **VVE**QMCTTQYQK (VVE), would also prevent that peptide from being produced by tryptic cleavage. Therefore, the extent of the acetylation of K_{27}, K_{185}, K_{194}, K_{204}, or K_{220} can be quantitated by determining the amount of each peptide present after trypsin digestion relative to its abundance in a corresponding trypsin digest of unreacted starting material. K_{101}, K_{104}, and K_{106} are contained in the chymotryptic **NKP**SKPKTNM (NKP) peptide; acetylation of any one of these lysines results in the peptide being undetectable by our mass spectrometry-based method. Thus, a mass spectrometry-based analysis can be used to relate the extent of acetylation of a specific lysine to the loss of signal from a defined tryptic or chymotryptic peptide.

Western Blot Was Used to Quantitate the Acetylation of K_{110}

A Western blot, probed with the 3F4 antibody, was be used to quantitate the extent of acetylation of K_{110} (**Figure 3**). A calibration curve relating the relative signal intensity from a Western blot to the corresponding dilution was prepared. The resulting curve (**Figure 4**) was linear with an excellent correlation coefficient ($R^2 = 0.972$, $p < 0.01$). This curve was used to calculate the $\log_{10}$ dilution corresponding to the ratio of the

[1]http://www.real-statistics.com/regression/hypothesis-testing-significance-regression-line-slope/

[2]http://www.real-statistics.com/regression/hypothesis-testing-significance-regression-line-slope/comparing-slopes-two-independent-samples/

[3]https://www.aphis.usda.gov/aphis/resources/permits

[4]www.cdc.gov/biosafety/publications/bmbl5

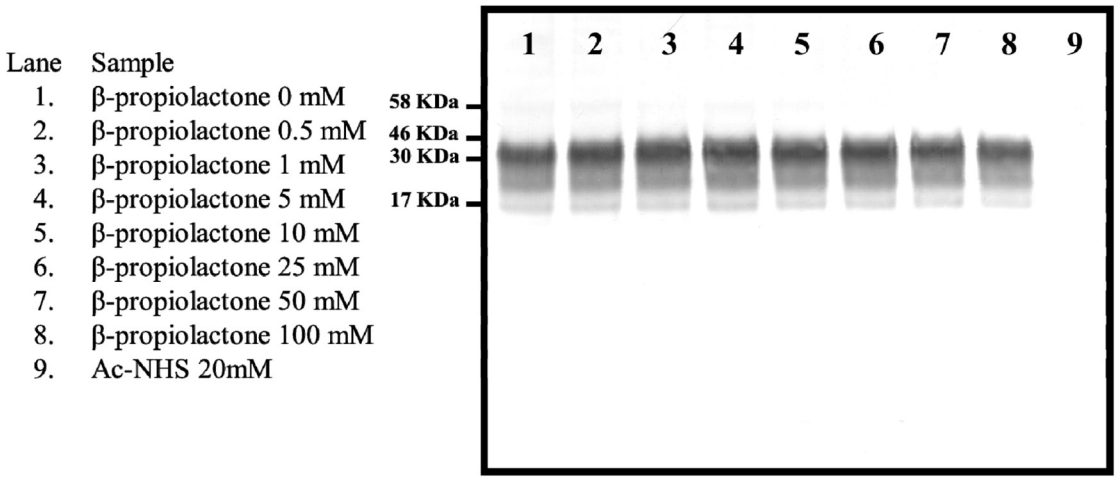

FIGURE 1 | Western blot showing the intensity of the signal from the reaction of various concentrations of β-propiolactone or Ac-NHS (20 mM) with the PrP^C present in a 10% brain homogenate from an uninfected hamster. The Western blot was probed with the 3F4 mAb.

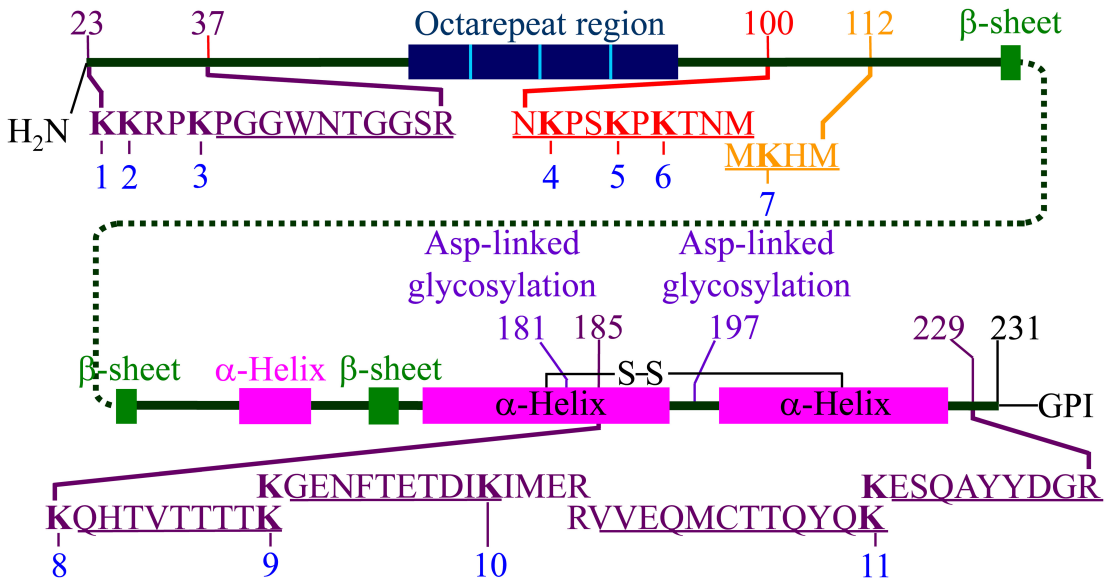

FIGURE 2 | Representation of hamster PrP^C including the locations of secondary structures and the position of the 11 lysine residues. The locations of the five tryptic peptides (**PGG**WNTGGSR, **QHT**VTTTTK, **GEN**FTETDIK, **VVE**QMCTTQYQK, and **ESQ**AYYDGR) are indicated. The locations of the chymotryptic peptide (**NKP**SKPKTNM) and the 3F4 mAb epitope (**MKH**M) are also indicated. Adapted from Silva et al. (2016). The locations of the secondary structure motifs are based on the NMR structure (1B10 in PDB) (James et al., 1997).

observed signal intensity to that of unreacted starting material for each reaction set.

The Lysines of rPrP React Equally Well With Either Ac_2O or Ac-NHS

Syrian hamster rPrP was reacted with five concentrations of Ac_2O or Ac-NHS. The reduction of the normalized MRM transition signal (log_{10}) of these peptides corresponds to the extent of lysine acetylation at positions 23, 24, 27, 185, 194, 204, and 220 (K_{23}, K_{24}, K_{27}, K_{185}, K_{194}, K_{204}, and K_{220}). The log_{10} of the normalized MRM transition signal for each of the five peptides after reaction with each concentration of Ac_2O or Ac-NHS was determined (**Figures 5**, **6**). Linear regression was used to calculate the slope, intercept, R^2, and *p*-value for the relationship between reagent concentration and the normalized MRM transition signal intensity (log_{10}) for each peptide. The data is summarized in **Tables 1A**, **2A**. The slopes from the regression were statistically compared and no significant differences were observed between the slopes for any of the peptides reacted with Ac_2O ($p > 0.66$) or Ac-NHS ($p > 0.57$) (**Tables 1B**, **2B**). No differences ($p > 0.62$) were observed when the slope of each peptide reacted with Ac_2O

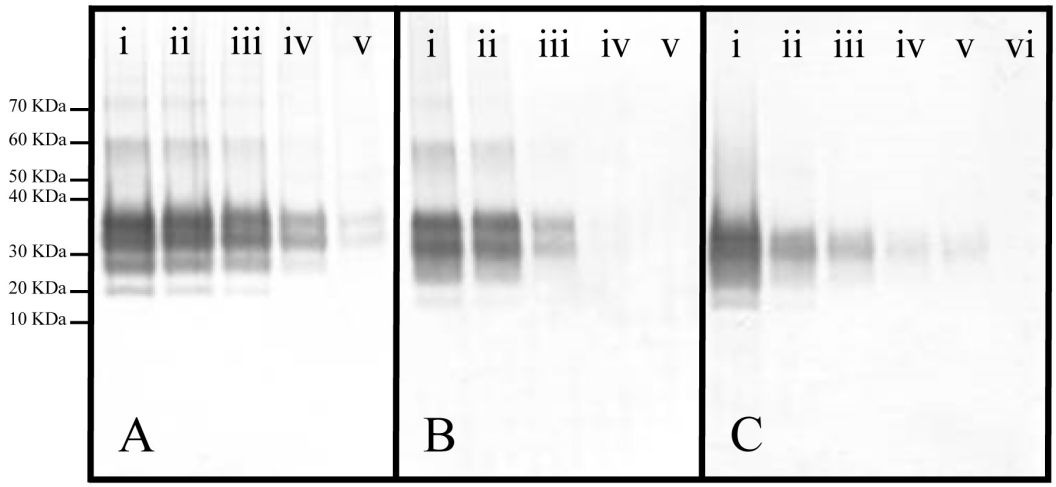

FIGURE 3 | Representative Western blots of panels **(A)** Ac_2O or **(B)** Ac-NHS reaction mixtures and **(C)** a dilution series of PrP 27-30 (primary mAb, 3F4). **(A)** Equal aliquots of a brain homogenate (BH) were reacted with either 0 (i), 5 (ii), 10 (iii), 20 (iv), or 50 mM (v) Ac_2O (*vide supra*). **(B)** Aliquots of purified PrP^{Sc} were reacted with either 0 (i), 1 (ii), 5 (iii), 10 (iv), or 20 (v) mM Ac-NHS. **(C)** PrP 27-30 was undiluted (i) or diluted 1:3.2 (ii), 1:10 (iii), 1:32 (iv), 1:100 (v), or 1:320 (vi).

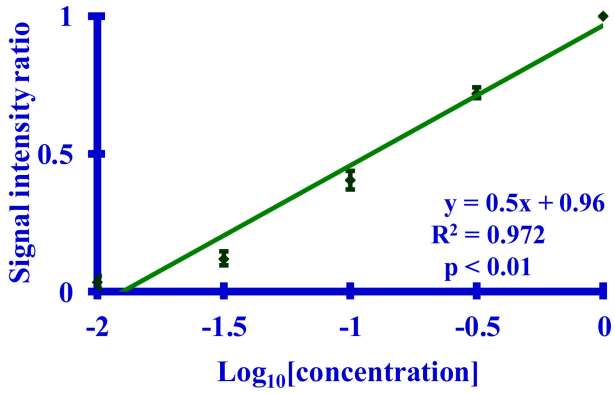

FIGURE 4 | A graph of a Western blot-based relationship between the calculated signal intensity ratio derived from the binding of the 3F4 mAb to its **MKH**M epitope and the corresponding dilution of PrP 27-30. The primary mAb was 3F4. The calculated signal intensity is the ratio of the signal from a dilution to the undiluted starting material, as measured by densitometry. Five dilutions (n = 5 per dilution) of PrP 27-30 (undiluted, 1:3.2, 1:10, 1:32, or 1:100) were used.

was compared to the slope of same peptide reacted with Ac-NHS (**Table 3A**). No significant difference ($p > 0.25$) was observed between the reaction of a given lysine with either Ac_2O or Ac-NHS at the 1, 5, or 10 mM concentrations (**Table 3B**). These results indicate that at the same concentration, both Ac_2O and Ac-NHS react indiscriminately with the lysines in rPrP.

Calibration Curves From the Bioassay

The observed incubation time of a prion disease can be related to the concentration of the prion inoculum (Prusiner et al., 1982). Calibration curves relating hamster incubation times to dilutions of prion-containing brain homogenate (BH) or purified prions were prepared. The calibration curves relating the survival times to the dilution of infectivity are linear with excellent correlation coefficients ($R^2 > 0.995$, $p < 0.05$) (**Figure 7**). The animals injected with purified preparations have noticeably shorter survival times than do those inoculated with comparable dilutions of BH, which is an expected consequence of using purified prions (Sajnani et al., 2012). These curves allow the calculation of the reduction of infectivity associated with lysine acetylation in BH or purified preparations from the observed survival times.

Comparing Lysine Acetylation in PrP^{Sc} After Reaction With Ac_2O or Ac-NHS

The normalized MRM transition signals (log_{10}) for the five other tryptic and one chymotryptic peptides were determined for each reaction sample. The log_{10}-based reduction of infectivity was derived from the bioassays. These values are reported in **Figures 8**, **9**. Linear regression was used to calculate the slope, intercept, R^2, and p-value for the relationship between reagent concentration and the log_{10} loss of infectivity of the normalized MRM transition signal for each peptide (**Tables 4A**, **5A**). When the slopes of the linear regression of the peptides were statistically compared (t-test, **Tables 4B**, **5B**), significant differences were found among the peptides (**Tables 4B**, **5B**). These tables show that PrP^{Sc}'s lysines, unlike those of rPrP, react differently, depending on the reagent used and, presumably, their chemical environment (Silva, 2012; Silva et al., 2016).

The PrP^{Sc} in BH is acetylated to a different extent with Ac_2O than is the purified PrP^{Sc} by Ac-NHS. At the highest concentration of the reagents (**Table 6**), the lysines associated with the peptides PGG ($p < 0.01$; K_{23}, K_{24}, and K_{27}), MKH ($p < 0.01$; K_{110}), QHT ($p < 0.03$; K_{185}), and GEN ($p < 0.01$; K_{194} and K_{204}) were acetylated to a significantly lesser extent by Ac_2O in the BH than by Ac-NHS in the purified preparation.

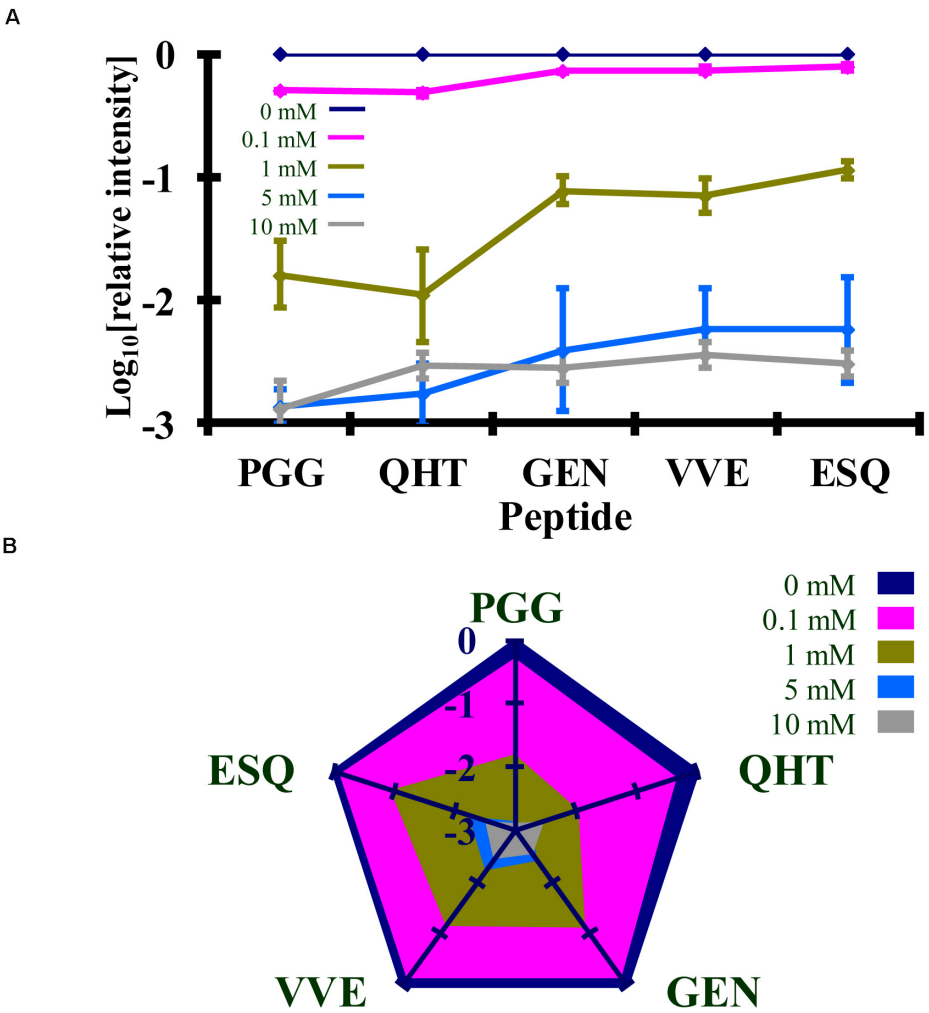

FIGURE 5 | Comparison of the changes in the $\log_{10}$ of the normalized MRM transition signals from five tryptic peptides (**PGG**WNTGGSR, **QHT**VTTTTK, **GEN**FTETDIK, **VVE**QMCTTQYQK, and **ESQ**AYYDGR) after the reaction of rPrP with Ac_2O. **(A)** Graphical representation of the data. **(B)** Radar plots of this data. Each rPrP reaction was performed in duplicate. The locations of the peptides may be found in **Figure 2**.

Other peptides, NKP ($p > 0.95$; K_{101}, K_{104}, or K_{106}), VVE ($p > 0.27$; K_{220}), and ESQ ($p > 0.77$; K_{220}), show no significant differences in the degree of acetylation in either BH or purified PrP^{Sc} at the highest concentration of the reagents. This suggests that K_{101}, K_{104}, K_{106}, and K_{220} share a chemical environment that is not influenced by the molecules present in BH. In contrast, the chemical environments of K_{23}, K_{24}, K_{27}, K_{111}, K_{185}, K_{194}, and K_{204} were more strongly influenced by the molecules present in BH.

Reaction of Ac_2O in BH or Ac-NHS With Purified Prions Results in a Similar Loss of Infectivity

The results of the bioassay of the reaction mixtures are summarized in **Figures 8**, **9** (Inf). The reactions using the three highest concentrations of Ac-NHS reagent (5, 10, 20 mM) show no statistical difference from the reactions using the three highest concentrations (10, 20, and 50 mM) of the Ac_2O reagent ($p > 0.89$, $p > 0.21$, $p > 0.97$, **Table 6**). At the highest concentration of either reagent, the loss of infectivity is approximately 10-fold.

Loss of Infectivity Is Associated With Acetylation of K_{220} in PrP^{Sc}

The slopes of the linear regression of the peptides were statistically compared to that of infectivity (*t*-test, **Tables 4B**, **5B**). This analysis showed that of the seven peptides, only the MKH, VVE, and ESQ peptides showed a *p*-Value that precludes the rejection of the null hypothesis when compared to infectivity (Inf) after reaction with Ac-NHS and Ac_2O. At each concentration of the Ac_2O reagent, the extent of the reaction ($\log_{10}$) of the MKH peptide is significantly different from that of the $\log_{10}$ loss of infectivity (Inf, unpaired Student's *t*-test, $p < 0.05$, **Table 4C**). The normalized MRM transition signal

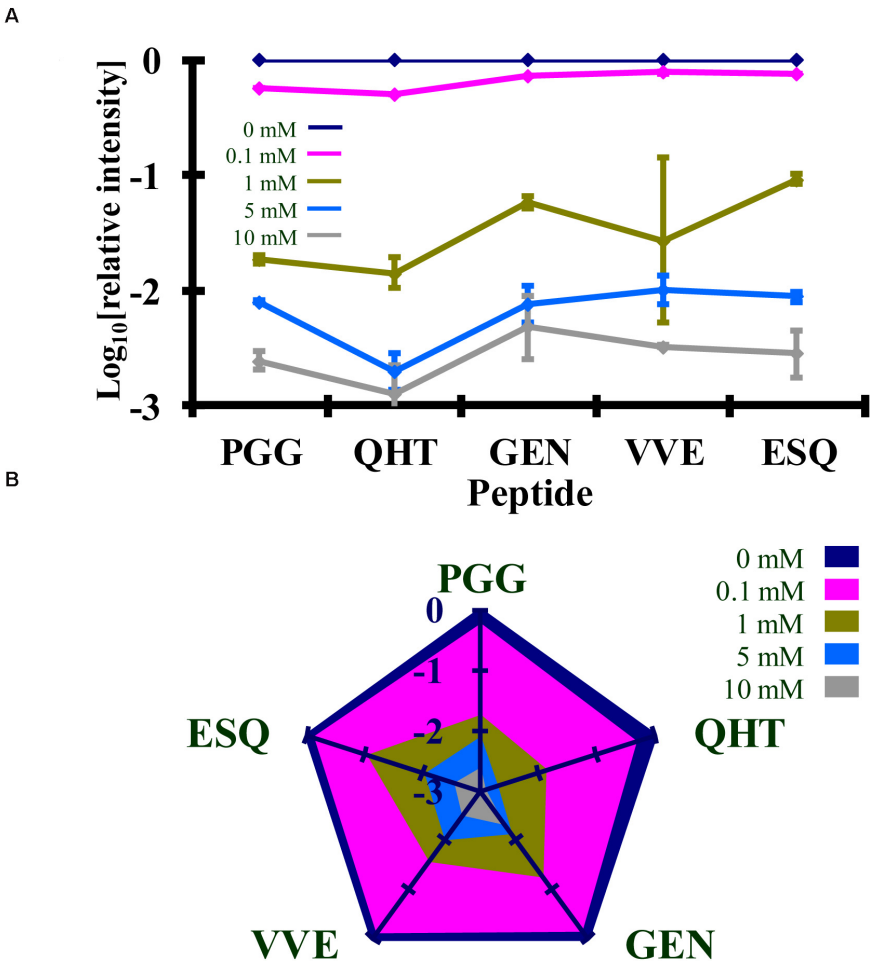

FIGURE 6 | Comparison of the changes in the $\log_{10}$ of the normalized MRM transition signals from five tryptic peptides (**PGG**WNTGGSR, **QHT**VTTTTK, **GEN**FTETDIK, **VVE**QMCTTQYQK, and **ESQ**AYYDGR) after the reaction of rPrP with Ac-NHS. **(A)** Graphical representation of the data. **(B)** Radar plots of this data. Each rPrP reaction was performed in duplicate. The locations of the peptides may be found in **Figure 2**.

($\log_{10}$) from the peptides VVE and ESQ show no significant difference ($p > 0.3$) when compared to the loss of infectivity at the highest concentration of the Ac_2O (**Table 4C**) or Ac-NHS (**Table 5C**). Furthermore, there is no significant difference ($p > 0.3$) between the slopes derived from the linear regression of the loss of infectivity and the normalized MRM transition signal ($\log_{10}$) for the peptides VVE and ESQ (**Tables 4B**, **5B**). These lines of evidence are true only for the VVE and ESQ peptides. Since the VVE and ESQ peptides are derived from the tryptic cleavage of K_{220}, the loss of signal from these peptides is the result of the acetylation of K_{220}. This indicates that the extent of acetylation of K_{220} is associated with the observed reduction in infectivity, although an accumulation of effects from the acetylation of the other lysines cannot be excluded.

Role of N-Terminal Lysines (K_{23}, K_{24}, and K_{27}) in Prion Replication

The reaction of the N-terminal lysines (K_{23}, K_{24}, and K_{27}) is noticeably different in BH than with purified Sc237 PrP^{Sc}. In contrast, the N-terminal lysines of rPrP are readily acetylated with either reagent at all concentrations. This is also true when purified PrP^{Sc} is reacted with Ac-NHS. When PrP^{Sc} in BH is reacted with Ac_2O, the N-terminal lysines are acetylated to a significantly ($p < 0.05$) lesser extent. These results suggest that the N-terminal region is bound to molecules present in BH, but absent in the purified preparation. In any event, once PrP^{Sc} is purified, the interfering molecules are presumably sufficiently removed and the N-terminal lysines are available to react, as can be seen when the purified samples are reacted with Ac-NHS.

DISCUSSION

The physicochemical properties of Ac_2O and Ac-NHS permit two independent measures of lysine reactivity. Ac_2O is more polar (logP of 0.47 vs. −0.57) than Ac-NHS and is more soluble in water (250 mM vs. 30 mM) than Ac-NHS.

TABLE 1 | Summary of statistical data for the reaction of rPrP with Ac_2O.

A					
Ac_20	**PGG**	**QHT**	**GEN**	**WE**	**ESQ**
Slope	−0.3	−0.2	−0.3	−0.2	−0.3
Intercept	−0.7	−0.8	−0.4	−0.4	−0.4
R^2 *p*-value	0.691	0.569	0.785	0.792	0.832
	$p < 0.01$	$p < 0.05$	$p < 0.01$	$p < 0.01$	$p < 0.01$

B					
***t*-test**	**PGG**	**QHT**	**GEN**	**WE**	**ESQ**
PGG	—	$p > 0.66$	$p > 0.84$	$p > 0.69$	$p > 0.82$
QHT		—	$p > 0.76$	$p > 0.88$	$p > 0.75$
GEN			—	$p > 0.82$	$p > 0.99$
VVE				—	$p > 0.82$
ESQ					—

(A) *Table of regression data (slope, intercept, R^2, p-value) for normalized MRM transition signals (log_{10}) of each peptide v. the Ac_2O concentration.* ***(B)*** *Summary of t-tests comparing the slopes of the linear regression of each peptide v. a different peptide. $p < 0.05$ indicate statistical significance. Each reaction was performed on PrP in duplicate. The locations of the peptides may be found in* ***Figure 2****.*

TABLE 2 | Summary of statistical data for the reaction of rPrP with Ac-NHS.

A					
Ac-NHS	**PGG**	**QHT**	**GEN**	**WE**	**ESQ**
Slope	−0.2	−0.3	−0.2	−0.2	−0.2
Intercept	−0.6	−0.7	−0.5	−0.5	−0.4
R^2	0.714	0.702	0.762	0.699	0.867
p-value	$p < 0.01$	$p < 0.01$	$p < 0.01$	$p < 0.01$	$p < 0.01$

B					
***t*-test**	**PGG**	**QHT**	**GEN**	**WE**	**ESQ**
PGG	–	$p > 0.65$	$p > 0.92$	$p > 0.96$	$p > 0.75$
QHT		–	$p > 0.57$	$p > 0.63$	$p > 0.81$
GEN			–	$p > 0.95$	$p > 0.64$
VVE				–	$p > 0.72$
ESQ					–

(A) *Table of regression data (slope, intercept, R^2, p-value) for normalized MRM transition signals (log_{10}) of each peptide v. the Ac-NHS concentration.* ***(B)*** *Summary of t-tests comparing the slopes of the linear regression of each peptide v. a different peptide. $p < 0.05$ indicate statistical significance. Each reaction was performed on PrP in duplicate. The locations of the peptides may be found in* ***Figure 2****.*

Since brain homogenate (BH) has higher concentrations of nucleophiles
than the purified material, a correspondingly higher concentration of acetylating reagent (50 mM vs. 20 mM) would be required to compensate for their presence. Thus, the more water-soluble reagent, Ac_2O, was used to react with prions in BH, while the less soluble reagent, Ac-NHS, was used to react with purified prions. Since these two reagents acetylate the lysines in rPrP equally (*vide infra*), they can be used to provide two independent measures

TABLE 3 | Statistical analysis of the comparison of the changes in the MRM transition signals (log_{10}) from five tryptic peptides (**PGG**WNTGGSR, **QHT**VTTTTK, **GEN**FTETDIK, **VVE**QMCTTQYQK, and **ESQ**AYYDGR) after the reaction of Ac_2O with rPrP.

A					
***t*-test**	**PGG**	**QHT**	**GEN**	**VVE**	**ESQ**
p-value	$p > 0.62$	$p > 0.69$	$p > 0.63$	$p > 0.85$	$p > 0.94$

B					
***t*-test**	**PGG**	**QHT**	**GEN**	**VVE**	**ESQ**
0.1 mM	$p < 0.02$	$p > 0.46$	$p > 0.85$	$p > 0.51$	$p > 0.61$
1 mM	$p > 0.95$	$p > 0.98$	$p > 0.87$	$p > 0.70$	$p > 0.89$
5 mM	$p > 0.79$	$p > 0.76$	$p > 0.33$	$p > 0.56$	$p > 0.27$
10 mM	$p > 0.41$	$p > 0.74$	$p > 0.97$	$p > 0.83$	$p > 0.94$

(A) *The slopes of the normalized MRM transition signals (log_{10}) of each peptide after reaction with five concentrations of Ac_2O v. the same concentrations of Ac-NHS were compared by a t-test.* ***(B)*** *Unpaired Student's t-test comparing the normalized MRM transition signal (log_{10}) of each peptide reacted with the same concentration of Ac_2O or Ac-NHS. $p < 0.05$ indicate statistical significance. The locations of the peptides may be found in* ***Figure 2****.*

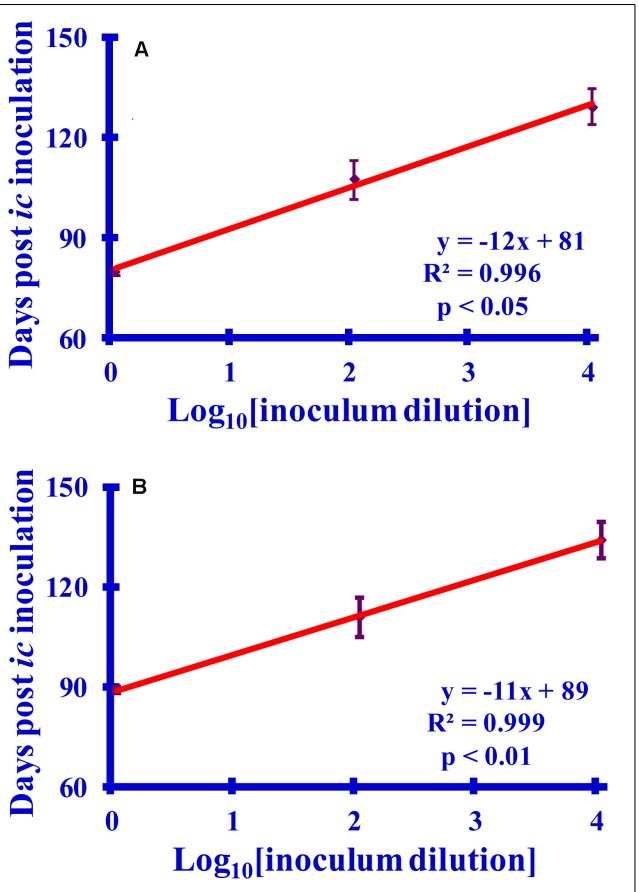

FIGURE 7 | Graphs relating the survival times to log_{10} dilutions (10×, 1000×, or 100,000×) of **(A)** purified PrP^{Sc} or **(B)** PrP^{Sc}-infected brain homogenate (BH). The survival times (6 hamsters per set) are recorded as days post-inoculation. For consistency with the reactions, which are diluted 1:10 prior to inoculation, the dilutions are reported relative to a 1:10 dilution of the starting sample.

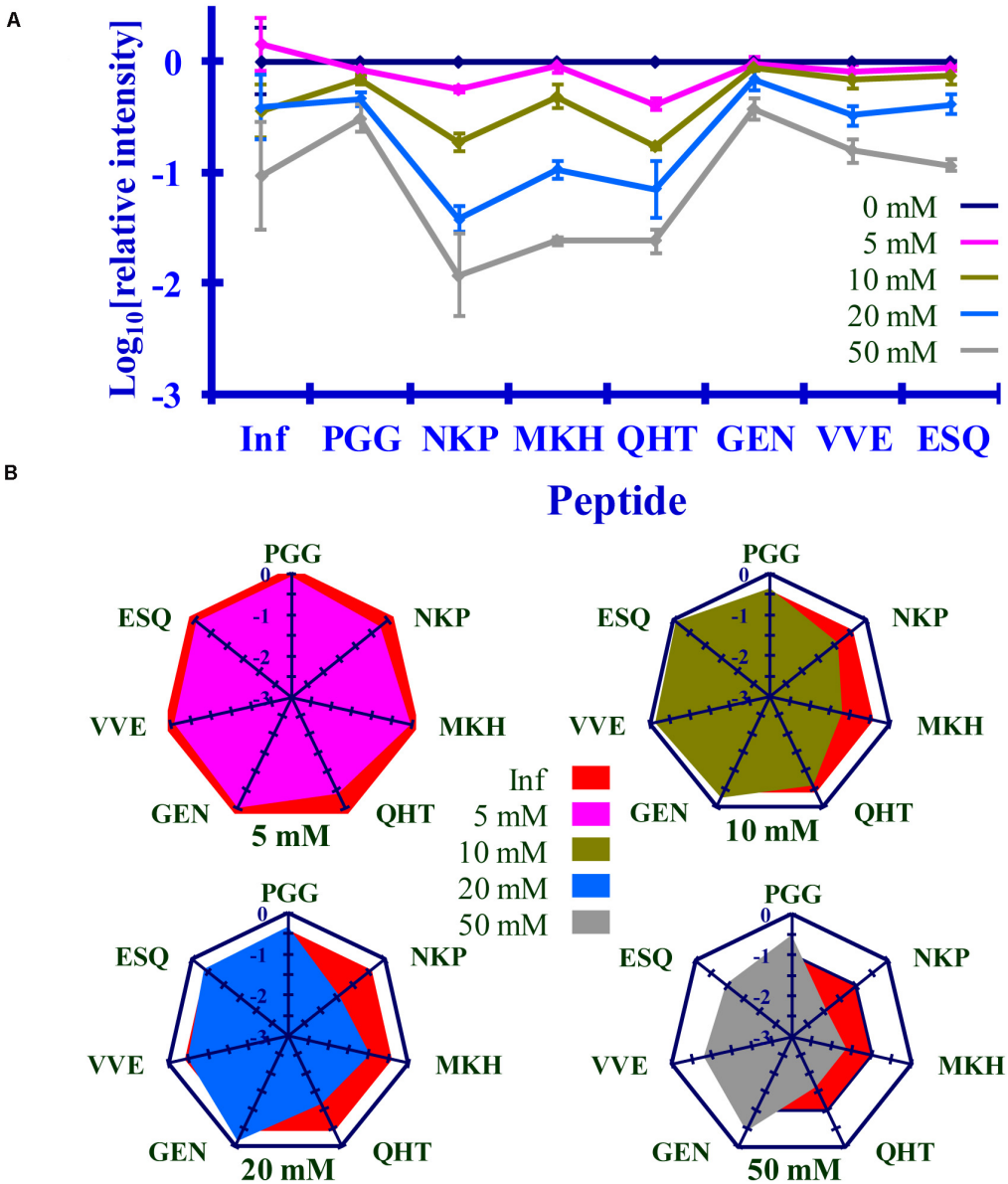

FIGURE 8 | Comparison of the changes in infectivity (Inf) (log_{10}) to the normalized MRM transition signals (log_{10}) of five tryptic peptides (**PGG**WNTGGSR, **QHT**VTTTTK, **GEN**FTETDIK, **VVE**QMCTTQYQK, and **ESQ**AYYDGR), one chymotryptic peptide (**NKP**SKPKTNM), and the 3F4 epitope (**MKH**M) after the reaction of Ac_2O with PrP^{Sc}-infected brain homogenate. **(A)** Graphical summary of this data. **(B)** Radar plots of this data. Each PrP^{Sc} reaction was performed in triplicate. Hamster bioassay (n = 6 per reagent concentration) was used to measure the infectivity. The locations of the peptides may be found in **Figure 2**.

of the effect of lysine acetylation on the infectivity of the prion template.

The sequence **MKH**M (MKH) spans the epitope of the 3F4 monoclonal antibody (mAb) which contains K_{110} (Kascsak et al., 1987; **Figure 2**). Other work demonstrated that acetylation of K_{110} by the N-hydroxysuccinimide ester of acetic acid (Ac-NHS) prevents the binding of 3F4 to this epitope (Silva, 2012). This results in the absence of a signal, since the primary antibody is no longer able to bind to the epitope. This permits the quantitation of K_{110} acetylation using Western blot in place of mass spectrometry. In principle, this approach can be used with other amino acid/mAb combinations, which extends the utility of the many anti-PrP mAbs.

Even though PrP^{C}'s lysines are conserved and strongly influence the propagation, once they are part of the PrP^{Sc} template their role in prion propagation is limited. When the PrP^{Sc}'s lysines are acetylated the loss of infectivity is approximately 10-fold. This is substantially less than the 1,000-fold loss of infectivity when DEPC is used to ethoxyformylate the histidines of purified Sc237 prions (McKinley et al., 1981). This loss of infectivity from the ethoxyformylation of histidines is reversed by the addition of hydroxylamine (McKinley et al.,

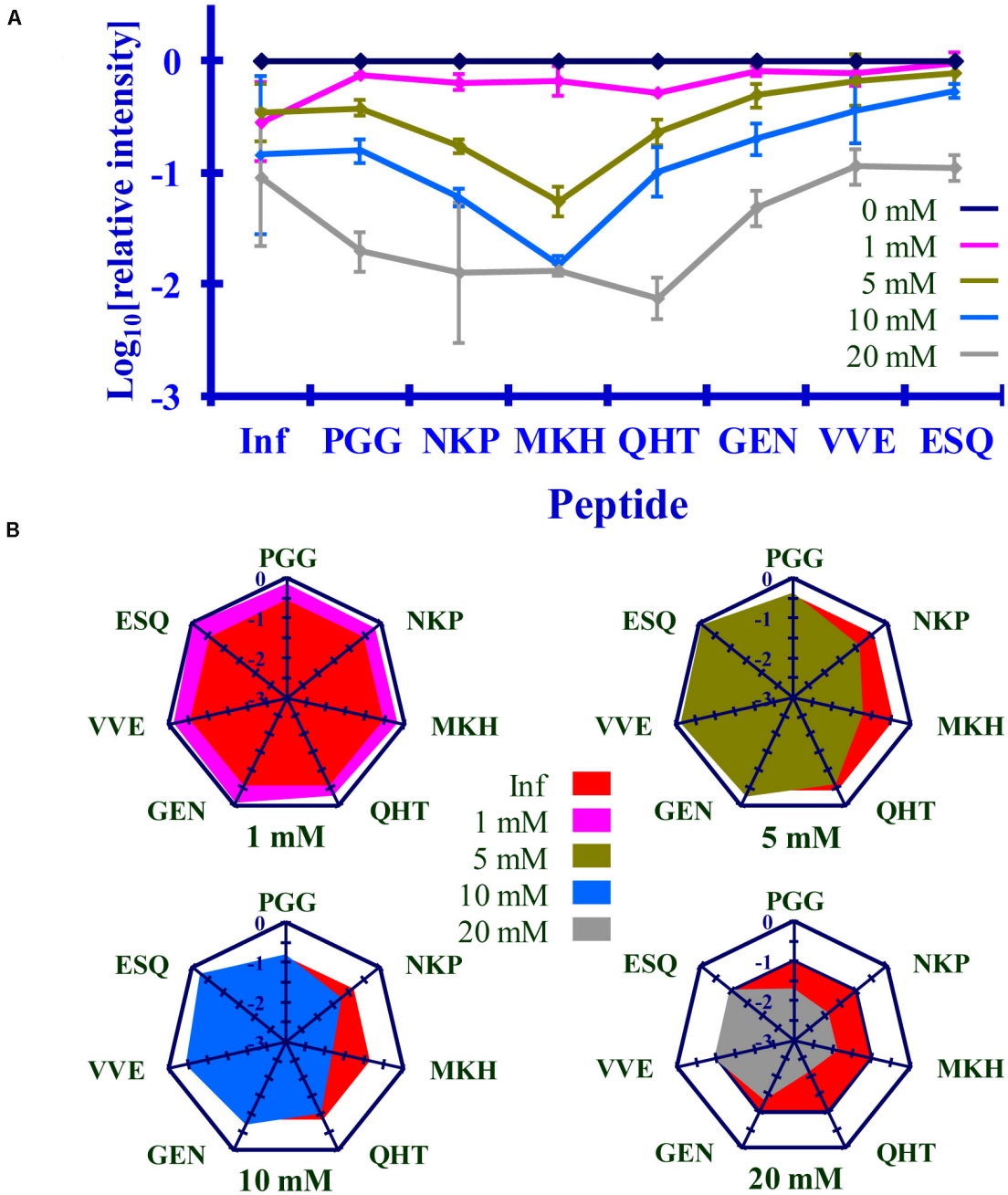

FIGURE 9 | Comparison of the changes in infectivity (Inf) (log_{10}) to the normalized MRM transition signals (log_{10}) of five tryptic peptides (PGGWNTGGSR, QHTVTTTTK, GENFTETDIK, VVEQMCTTQYQK, and ESQAYYDGR), one chymotryptic peptide (NKPSKPKTNM), and the 3F4 epitope (MKHM) after the reaction of Ac-NHS with purified PrP^{Sc}. **(A)** Graphical representation of this data. **(B)** Radar plots comparing changes in infectivity with the extent of the reaction of each peptide at the four Ac-NHS concentrations (1, 5, 10, or 20 mM). Each PrP^{Sc} reaction was performed in triplicate. Hamster bioassay (n = 6 per reagent concentration) was used to measure the infectivity. The locations of the peptides may be found in **Figure 2**.

1981), which suggests that the loss of infectivity is not due to a perturbation of the PrP^{Sc} template.

In the Spagnolli et al., model, histidines are largely on the outer surface of the β-solenoid (Spagnolli et al., 2019). The proteinase K digestion used to purify those prions results in the removal of the histidines at positions 61, 69, 77, and 85. The five remaining histidines (positions 96, 111, 140, 177, and 187) reside in the PK-resistant core, PrP 27-30 (Oesch et al., 1985). It is therefore likely that DEPC reacts with a histidine on the surface of the Sc237 prion and that amino acids on the outer surface of a β-solenoid can play a significant role in prion replication.

TABLE 4 | Summary of statistical data for the reaction of Ac_2O with PrP^{Sc}-infected brain homogenate.

A

Ac_2O	Inf	PGG	NKP	MKH	QHT	GEN	VVE	ESQ
Slope	−0.02	−0.01	−0.04	−0.03	−0.03	−0.01	−0.02	−0.02
Intercept	0.04	−0.06	−0.23	0	−0.31	0	−0.05	0.01
R^2	0.923	0.968	0.938	0.963	0.915	0.985	0.973	0.993
p-value	$p < 0.03$	$p < 0.01$	$p < 0.02$	$p < 0.01$	$p < 0.03$	$p < 0.01$	$p < 0.01$	$p < 0.01$

B

Ac_2O	Inf	PGG	NKP	MKH	QHT	GEN	VVE	ESQ
Inf	–	$p > 0.07$	$p > 0.15$	$p > 0.13$	$p > 0.38$	$p < 0.05$	$p > 0.36$	$p > 0.65$
PGG		–	$p < 0.02$	$p < 0.01$	$p < 0.03$	$p > 0.58$	$p > 0.05$	$p < 0.01$
NKP			–	$p > 0.7$	$p > 0.47$	$p < 0.02$	$p < 0.05$	$p > 0.06$
MKH				–	$p > 0.62$	$p < 0.01$	$p < 0.02$	$p < 0.03$
QHT					–	$p < 0.03$	$p > 0.1$	$p > 0.17$
GEN						–	$p < 0.02$	$p < 0.01$
VVE							–	$p > 0.23$
ESQ								–

C

Inf	PGG	NKP	MKH	QHT	GEN	VVE	ESQ
5 mM	$p > 0.05$	$p < 0.01$	$p < 0.05$	$p < 0.01$	$p > 0.15$	$p < 0.05$	$p > 0.05$
10 mM	$p < 0.05$	$p < 0.05$	$p < 0.01$	$p < 0.05$	$p < 0.01$	$p < 0.05$	$p < 0.05$
20 mM	$p > 0.56$	$p < 0.01$	$p < 0.01$	$p < 0.05$	$p > 0.05$	$p > 0.60$	$p > 0.85$
50 mM	$p > 0.10$	$p < 0.05$	$p < 0.01$	$p < 0.05$	$p > 0.05$	$p > 0.60$	$p > 0.94$

(A) *Table of linear regression data (slope, intercept, R^2, p-value) relating the change in infectivity (Inf) or the normalized MRM transition signals (log_{10}) of listed peptides for each concentration of Ac_2O.* ***(B)*** *t-test comparing the slopes of the linear regression from infectivity (Inf) v. the normalized MRM transition signal (log_{10}) of each listed peptide and the normalized MRM transition signal (log_{10}) of each peptide v. another peptide.* ***(C)*** *Unpaired Student's t-test comparison of the infectivity to the normalized MRM transition signal (log_{10}) of a peptide at a specific reagent concentration. $p < 0.05$ indicate statistical significance. Each PrP^{Sc} reaction was performed in triplicate. Hamster bioassay (n = 6 per reagent concentration) was used to measure the infectivity. The locations of the peptides may be found in* ***Figure 2****.*

Unlike lysines, histidines bind divalent metals such as copper (Hasnain et al., 2001; Jackson et al., 2001). This suggests that the disproportionate loss of infectivity (1000-fold) associated with histidine ethoxyformylation may be the result of the interference with the binding of a cofactor, such as a divalent cation.

K_{220} resides in the C-terminus of PrP^{Sc}, which is much more resistant to denaturation (Kocisko et al., 1996; Vazquez-Fernandez et al., 2012). Reaction of recombinant hamster PrP with the reagents showed that K_{220} is not intrinsically less resistant to reaction relative to the other lysines (*vide supra*) in the native PrP conformation. This suggests that, in the prion conformation, K_{220} resides in a chemical environment that prevents the reagents from reacting with it. In other hamster strains K_{220} is more susceptible to reaction, which supports the idea that its prion strain-dependent chemical environment influences the reactivity of K_{220} (Silva et al., 2016). Thus, the lack of reactivity of K_{220} in the Sc237 prion conformation is a feature of that conformation. When K_{220} does react, however, it is likely that the loss of infectivity results from the disruption of the C-terminal structure of Sc237.

In the recent Spagnolli et al. (2019) model of murine PrP 27-30 PrP^{Sc}, lysines K_{23}, K_{24}, and K_{27} are not included in the model, as they are digested by proteinase K to produce PrP27-30. In this murine model, lysines homologous to K_{101}, K_{104}, K_{106}, K_{110}, K_{185}, K_{194}, K_{204}, and K_{220} of hamster PrP are on the outer surface of a β-solenoid. Of these lysines, the one equivalent to K_{220} is part of a salt bridge on the outer surface. This suggests a possible explanation for the lower reactivity of K_{220}, even if it locates on the outer surface of the β-solenoid. An alternate possibility is that the murine β-solenoid model does not accurately model the Sc237 prion structure and that K_{220} projects into the β-solenoid, which could explain its lack of reactivity. In either case, significant disruption of the Sc237 C-terminal structural region would be expected to impede prion propagation.

In other strains of purified hamster-adapted scrapie (139H, Dy, 22AH, and 22CH), the N-terminal lysines are also less reactive (Silva et al., 2016). DNA and RNA are known to bind to the N-terminal region of PrP (Weiss et al., 1997; Gabus et al., 2001a,b) and the presence of nucleic acids is reduced, but not eliminated, during prion purification (Diringer et al., 1997), so it is possible that

TABLE 5 | Summary of statistical data for the reaction of Ac-NHS with purified PrP^{Sc}.

A

Ac-NHS	Inf	PGG	NKP	MKH	QHT	GEN	VVE	ESQ
Slope	−0.04	−0.08	−0.09	−0.09	−0.1	−0.06	−0.04	−0.05
Intercept	−0.27	0.01	−0.15	−0.36	−0.08	−0.01	−0.01	0.08
R^2	0.77	0.999	0.964	0.754	0.99	0.997	0.989	0.953
p-value	$p < 0.05$	$p < 0.01$	$p < 0.01$	$p < 0.06$	$p < 0.01$	$p < 0.01$	$p < 0.01$	$p < 0.01$

B

Ac-NHS	Inf	PGG	NKP	MKH	QHT	GEN	VVE	ESQ
Inf	–	$p < 0.03$	$p < 0.03$	$p > 0.18$	$p < 0.01$	$p > 0.14$	$p > 0.81$	$p > 0.76$
PGG		–	$p > 0.4$	$p > 0.74$	$p < 0.04$	$p < 0.01$	$p < 0.01$	$p < 0.01$
NKP			–	$p > 0.97$	$p > 0.56$	$p < 0.04$	$p < 0.01$	$p < 0.01$
MKH				–	$p > 0.85$	$p > 0.4$	$p > 0.17$	$p > 0.19$
QHT					–	$p < 0.01$	$p < 0.01$	$p < 0.01$
GEN						–	$p < 0.01$	$p < 0.03$
VVE							–	$p > 0.85$
ESQ								–

C

Inf	PGG	NKP	MKH	QHT	GEN	VVE	ESQ
1 mM	$p < 0.05$	$p > 0.05$	$p < 0.05$	$p > 0.13$	$p < 0.05$	$p < 0.05$	$p < 0.05$
5 mM	$p > 0.70$	$p < 0.05$	$p > 0.23$	$p > 0.20$	$p > 0.24$	$p > 0.15$	$p < 0.05$
10 mM	$p > 0.91$	$p > 0.23$	$p > 0.65$	$p > 0.63$	$p > 0.65$	$p > 0.26$	$p > 0.10$
20 mM	$p < 0.01$	$p > 0.05$	$p < 0.05$	$p < 0.01$	$p > 0.05$	$p > 0.62$	$p > 0.57$

(A) *Table of linear regression data (slope, intercept, R^2, p-value) relating the change in infectivity (Inf) or the normalized MRM transition signals (log_{10}) of the listed peptides for each concentration of Ac-NHS.* ***(B)*** *t-test comparing the slopes of the linear regression from infectivity (Inf) v. the normalized MRM transition signal (log_{10}) of each listed peptide and the normalized MRM transition signal (log_{10}) of each peptide v. another peptide.* ***(C)*** *Unpaired Student's t-test comparison of the infectivity to the normalized MRM transition signal (log_{10}) of a peptide at a specific reagent concentration. $p < 0.05$ indicate statistical significance. Each PrP^{Sc} reaction was performed in triplicate. The infectivity was measured by hamster bioassay (n = 6 per reagent concentration). The locations of the peptides may be found in* ***Figure 2****.*

TABLE 6 | Unpaired Student's *t*-tests comparing the infectivity (Inf) (log_{10}), the normalized MRM transition signals (log_{10}) of five tryptic peptides (**PGG**WNTGGSR, **QHT**VTTTTK, **GEN**FTETDIK, **VVE**QMCTTQYQK, and **ESQ**AYYDGR), one chymotryptic peptide (**NKP**SKPKTNM), and the normalized Western blot signal from 3F4 epitope (**MKH**M) after the reaction of purified PrP^{Sc} with Ac-NHS and PrP^{Sc}-infected brain homogenate with Ac_2O.

t-test	Inf	PGG	NKP	MKH	QHT	GEN	WE	ESQ
1	$p < 0.01$	$p > 0.24$	$p > 0.28$	$p < 0.03$	$p > 0.07$	$p > 0.12$	$p > 0.82$	$p > 0.61$
2	$p > 0.89$	$p < 0.01$	$p > 0.47$	$p < 0.01$	$p > 0.18$	$p < 0.04$	$p > 0.93$	$p > 0.78$
3	$p > 0.21$	$p < 0.01$	$p > 0.09$	$p < 0.01$	$p > 0.47$	$p < 0.01$	$p > 0.80$	$p > 0.12$
4	$p > 0.97$	$p < 0.01$	$p > 0.95$	$p < 0.01$	$p < 0.03$	$p < 0.01$	$p > 0.27$	$p > 0.77$

Row 1: The compared values were from the reactions with 1 mM Ac-NHS and 5 mM Ac_2O. Row 2: The compared values were from the reactions with 5 mM Ac-NHS and 10 mM Ac_2O. Row 3: The compared values were from the reactions with 10 mM Ac-NHS and 20 mM Ac_2O. Row 4: The compared values were from the reactions with 20 mM Ac-NHS and 50 mM Ac_2O. $p < 0.05$ indicate statistical significance. Each PrP^{Sc} reaction was performed in triplicate. Hamster bioassay (n = 6 per reagent concentration) was used to measure infectivity. The locations of the peptides may be found in ***Figure 2****.*

higher concentrations of these molecules are responsible for this effect.

Experiments with transgenic mice expressing PrP^{C} devoid of the N-terminal lysines have shown that the presence of these lysines in PrP^{C} is crucial for the conversion of PrP^{C} to PrP^{Sc} (Turnbaugh et al., 2012). By contrast, our results show that the extent of acetylation of K_{23}, K_{24}, and K_{27} in PrP^{Sc} is statistically different (unpaired Student's *t*-test; $p < 0.05$) from that of infectivity, which suggests that these lysines, when in the prion conformation, do not significantly influence prion replication. Our results are consistent with known properties of PrP 27−30, which, despite missing approximately 70 amino acids from its N-terminus, remains infectious. Our results and those of the transgenic mice appear to be contradictory. However, N-terminal lysines may have a significant role in facilitating the conformational conversion of PrP^{C} to PrP^{Sc}, whereas once PrP^{Sc} is formed they no longer play a significant role. The molecules preventing the reaction

of these lysines with Ac_2O in BH may be associated with this transformation.

We showed that mass spectrometry can be used to quantitate the role of lysines in prion replication. Mass spectrometry-based analysis could be used to quantitate the covalent modification of other amino acids in PrP^{Sc}, such as methionine (Silva et al., 2010, 2013) or tyrosine (Gong et al., 2011). Quantitating those covalent modifications would indicate their relative surface exposure, which would provide useful structural information. Thus, this approach can be applied to determining the importance of other amino acids in prion replication and their relative surface exposure in the prion conformation.

This approach could be applied to other protein misfolding diseases, such as Alzheimer's Disease (AD), Amyotrophic Lateral Sclerosis (ALS), and Parkinson's Disease (PD), which have prion-like features (Jucker and Walker, 2013; Grad and Cashman, 2014; Giles et al., 2017). For instance, the differences in incubation periods of acetylated amyloid β, tau, or α-synuclein, could be measured by an analogous bioassay (Giles et al., 2017). In this way covalent modification could be an important means of obtaining important conformational information after the misfolded proteins are denatured (Silva, 2014).

CONCLUSION

We have demonstrated that lysines play a limited role in prion propagation, once the PrP^{Sc} template is formed. This implies that acetylating lysines does not substantially perturb the PrP^{Sc} structure, which provides insight into the PrP^{Sc} structure and can be used to refine structural models and infer the structural differences that define prion strains.

DATA AVAILABILITY STATEMENT

The raw data supporting the conclusions of this article will be made available by the authors, without undue reservation.

ETHICS STATEMENT

The animal study was reviewed and approved by the procedures were governed by a protocol that was approved by the Institutional Animal Care and Use Committee of the United States Department of Agriculture, Agricultural Research Service, Albany, CA, United States.

AUTHOR CONTRIBUTIONS

CS designed the study and wrote the manuscript. CS, ID, and ME-B performed the experiments and analyzed and interpreted the data. CS and ME-B critically revised the manuscript. All authors contributed to the article and approved the submitted version.

FUNDING

This study was funded by the United States Department of Agriculture, Agricultural Research Service (CRIS 2030-32000-010-00D).

REFERENCES

Bolton, D. C., Rudelli, R. D., Currie, J. R., and Bendheim, P. E. (1991). Copurification of Sp33-37 and scrapie agent from hamster brain prior to detectable histopathology and clinical disease. *J. Gen. Virol.* 72(Pt 12), 2905–2913. doi: 10.1099/0022-1317-72-12-2905

Bouzalas, I. G., Dovas, C. I., Banos, G., Papanastasopoulou, M., Kritas, S., Oevermann, A., et al. (2010). Caprine PRNP polymorphisms at codons 171, 211, 222 and 240 in a Greek herd and their association with classical scrapie. *J. Gen. Virol.* 91, 1629–1634. doi: 10.1099/vir.0.017350-0

Diringer, H., Beekes, M., Ozel, M., Simon, D., Queck, I., Cardone, F., et al. (1997). Highly infectious purified preparations of disease-specific amyloid of transmissible spongiform encephalopathies are not devoid of nucleic acids of viral size. *Intervirology* 40, 238–246. doi: 10.1159/000150553

Douma, M. D., Kerr, G. M., Brown, R. S., Keller, B. O., and Oleschuk, R. D. (1998). Mass spectrometric detection of proteins in non-aqueous media - The case of prion proteins in biodiesel. *Can. J. Chem.* 86, 774–781. doi: 10.1139/v08-083

Flinta, C., Persson, B., Jornvall, H., and von Heijne, G. (1986). Sequence determinants of cytosolic N-terminal protein processing. *Eur. J. Biochem.* 154, 193–196. doi: 10.1111/j.1432-1033.1986.tb09378.x

Furukawa, H., Kitamoto, T., Tanaka, Y., and Tateishi, J. (1995). New variant prion protein in a Japanese family with Gerstmann-Straussler syndrome. *Brain Res. Mol. Brain. Res.* 30, 385–388. doi: 10.1016/0169-328x(95)00034-p

Gabus, C., Auxilien, S., Pechoux, C., Dormont, D., Swietnicki, W., Morillas, M., et al. (2001a). The prion protein has DNA strand transfer properties similar to retroviral nucleocapsid protein. *J. Mol. Biol.* 307, 1011–1021. doi: 10.1006/jmbi.2001.4544

Gabus, C., Derrington, E., Leblanc, P., Chnaiderman, J., Dormont, D., Swietnicki, W., et al. (2001b). The prion protein has RNA binding and chaperoning properties characteristic of nucleocapsid protein NCP7 of HIV-1. *J. Biol. Chem.* 276, 19301–19309. doi: 10.1074/jbc.M009754200

Giles, K., Woerman, A. L., Berry, D. B., and Prusiner, S. B. (2017). Bioassays and inactivation of prions. *Cold Spring Harb. Perspect. Biol.* 9:a023499. doi: 10.1101/cshperspect.a023499

Gong, B., Ramos, A., Vazquez-Fernandez, E., Silva, C. J., Alonso, J., Liu, Z., et al. (2011). Probing structural differences between PrP(C) and PrP(Sc) by surface nitration and acetylation: evidence of conformational change in the C-terminus. *Biochemistry* 50, 4963–4972. doi: 10.1021/bi102073j

Grad, L. I, and Cashman, N. R. (2014). Prion-like activity of Cu/Zn superoxide dismutase: implications for amyotrophic lateral sclerosis. *Prion* 8, 33–41. doi: 10.4161/pri.27602

Greenlee, J. J., Zhang, X., Nicholson, E. M., Kunkle, R. A., and Hamir, A. N. (2012). Prolonged incubation time in sheep with prion protein containing lysine at position 171. *J. Vet. Diagn. Invest.* 24, 554–558. doi: 10.1177/1040638712440993

Haig, D. A., and Clarke, M. C. (1968). The effect of beta-propiolactone on the scrapie agent. *J. Gen. Virol.* 3, 281–283. doi: 10.1099/0022-1317-3-2-281

Hasnain, S. S., Murphy, L. M., Strange, R. W., Grossmann, J. G., Clarke, A. R., Jackson, G. S., et al. (2001). XAFS study of the high-affinity copper-binding site of human PrP(91-231) and its low-resolution structure in solution. *J. Mol. Biol.* 311, 467–473. doi: 10.1006/jmbi.2001.4795

Ikawa, M., Yoneda, M., Matsunaga, A., Nakagawa, H., Kazama-Suzuki, A., Miyashita, N., et al. (2009). Unique clinicopathological features and PrP profiles in the first autopsied case of dura mater graft-associated Creutzfeldt-Jakob disease with codon 219 lysine allele observed in Japanese population. *J. Neurol. Sci.* 285, 265–267. doi: 10.1016/j.jns.2009.07.019

Jackson, G. S., Murray, I., Hosszu, L. L., Gibbs, N., Waltho, J. P., Clarke, A. R., et al. (2001). Location and properties of metal-binding sites on the human prion protein. *Proc. Natl. Acad. Sci. U.S.A.* 98, 8531–8535. doi: 10.1073/pnas.151038498

James, T. L., Liu, H., Ulyanov, N. B., Farr-Jones, S., Zhang, H., Donne, D. G., et al. (1997). Solution structure of a 142-residue recombinant prion protein corresponding to the infectious fragment of the scrapie isoform. *Proc. Natl. Acad. Sci. U.S.A.* 94, 10086–10091. doi: 10.1073/pnas.94.19.10086

Jucker, M., and Walker, L. C. (2013). Self-propagation of pathogenic protein aggregates in neurodegenerative diseases. *Nature* 501, 45–51. doi: 10.1038/nature12481

Kascsak, R. J., Rubenstein, R., Merz, P. A., Tonna-DeMasi, M., Fersko, R., Carp, R. I., et al. (1987). Mouse polyclonal and monoclonal antibody to scrapie-associated fibril proteins. *J. Virol.* 61, 3688–3693. doi: 10.1128/JVI.61.12.3688-3693.1987

Kitamoto, T., and Tateishi, J. (1994). Human prion diseases with variant prion protein. *Philos. Trans. R. Soc. Lond. B Biol. Sci.* 343, 391–398. doi: 10.1098/rstb.1994.0034

Kocisko, D. A., Lansbury, P. T. Jr., and Caughey, B. (1996). Partial unfolding and refolding of scrapie-associated prion protein: evidence for a critical 16-kDa C-terminal domain. *Biochemistry* 35, 13434–13442. doi: 10.1021/bi9610562

McKinley, M. P., Masiarz, F. R., and Prusiner, S. B. (1981). Reversible chemical modification of the scrapie agent. *Science* 214, 1259–1261. doi: 10.1126/science.6795721

Nicholson, E. M., Brunelle, B. W., Richt, J. A., Kehrli, M. E. Jr., and Greenlee, J. J. (2008). Identification of a heritable polymorphism in bovine PRNP associated with genetic transmissible spongiform encephalopathy: evidence of heritable BSE. *PLoS One* 3:e2912. doi: 10.1371/journal.pone.0002912

Oesch, B., Westaway, D., Walchli, M., McKinley, M. P., Kent, S. B., Aebersold, R., et al. (1985). A cellular gene encodes scrapie PrP 27-30 protein. *Cell* 40, 735–746. doi: 10.1016/0092-8674(85)90333-2

Onisko, B., Dynin, I., Requena, J. R., Silva, C. J., Erickson, M., and Carter, J. M. (2007). Mass spectrometric detection of attomole amounts of the prion protein by nanoLC/MS/MAm, S. *J. Soc. Mass Spectrom.* 18, 1070–1079. doi: 10.1016/j.jasms.2007.03.009

Pattison, I. H. (1965). "Experiments with scrapie with special reference to the nature of the agent and the pathology of the disease," in *Slow, Latent and Temperate Virus Infections (NINDB Monograph 2)*, eds C. J. Gajdusek, C. J. Gibbs, and M. P. Alpers (Washington DC: U.S. Government Printing Office), 249–257.

Peoc'h, K., Manivet, P., Beaudry, P., Attane, F., Besson, G., Hannequin, D., et al. (2000). Identification of three novel mutations (E196K, V203I, E211Q) in the prion protein gene (PRNP) in inherited prion diseases with Creutzfeldt-Jakob disease phenotype. *Hum. Mutat.* 15:482. doi: 10.1002/(sici)1098-1004(200005)15:5<482::aid-humu16>3.0.co;2-1

Prusiner, S. B. (1998). Prions. *Proc. Natl. Acad. Sci. U.S.A.* 95, 13363–13383. doi: 10.1073/pnas.95.23.13363

Prusiner, S. B., Cochran, S. P., Groth, D. F., Downey, D. E., Bowman, K. A., and Martinez, H. M. (1982). Measurement of the scrapie agent using an incubation time interval assay. *Ann. Neurol.* 11, 353–358. doi: 10.1002/ana.410110406

Prusiner, S. B., Groth, D., Serban, A., Stahl, N., and Gabizon, R. (1993). Attempts to restore scrapie prion infectivity after exposure to protein denaturants. *Proc. Natl. Acad. Sci. U.S.A.* 90, 2793–2797. doi: 10.1073/pnas.90.7.2793

Prusiner, S. B., Groth, D. F., Cochran, S. P., Masiarz, F. R., McKinley, M. P., and Martinez, H. M. (1980). Molecular properties, partial purification, and assay by incubation period measurements of the hamster scrapie agent. *Biochemistry* 19, 4883–4891. doi: 10.1021/bi00562a028

Prusiner, S. B., McKinley, M. P., Groth, D. F., Bowman, K. A., Mock, N. I., Cochran, S. P., et al. (1981). Scrapie agent contains a hydrophobic protein. *Proc. Natl. Acad. Sci. U.S.A.* 78, 6675–6679. doi: 10.1073/pnas.78.11.6675

Sajnani, G., Silva, C. J., Ramos, A., Pastrana, M. A., Onisko, B. C., Erickson, M. L., et al. (2012). PK-sensitive PrP is infectious and shares basic structural features with PK-resistant PrP. *PLoS Pathog.* 8:e1002547. doi: 10.1371/journal.ppat.1002547

Sambrook, J., Fritsch, E. F., and Maniatis, T. (1989). *Molecular Cloning. A Laboratory Manual*. Cold Spring Harbor, NY: Cold Spring Harbor Laboratory Press.

Seno, H., Tashiro, H., Ishino, H., Inagaki, T., Nagasaki, M., and Morikawa, S. (2000). New haplotype of familial Creutzfeldt-Jakob disease with a codon 200 mutation and a codon 219 polymorphism of the prion protein gene in a Japanese family. *Acta Neuropathol.* 99, 125–130. doi: 10.1007/pl00007415

Shibuya, S., Higuchi, J., Shin, R. W., Tateishi, J., and Kitamoto, T. (1998a). Codon 219 Lys allele of PRNP is not found in sporadic Creutzfeldt-Jakob disease. *Ann. Neurol.* 43, 826–828. doi: 10.1002/ana.410430618

Shibuya, S., Higuchi, J., Shin, R. W., Tateishi, J., and Kitamoto, T. (1998b). Protective prion protein polymorphisms against sporadic Creutzfeldt-Jakob disease. *Lancet* 351:419. doi: 10.1016/S0140-6736(05)78358-6

Silva, C. J. (2012). Using small molecule reagents to selectively modify epitopes based on their conformation. *Prion* 6, 163–173. doi: 10.4161/pri.18795

Silva, C. J. (2014). Applying the tools of chemistry (mass spectrometry and covalent modification by small molecule reagents) to the detection of prions and the study of their structure. *Prion* 8, 42–50. doi: 10.4161/pri.27891

Silva, C. J., Dynin, I., Erickson, M. L., Requena, J. R., Balachandran, A., Hui, C., et al. (2013). Oxidation of methionine 216 in sheep and elk prion protein is highly dependent upon the amino acid at position 218 but is not important for prion propagation. *Biochemistry* 52, 2139–2147. doi: 10.1021/bi3016795

Silva, C. J., Erickson-Beltran, M. L., and Dynin, I. C. (2016). Covalent surface modification of prions: a mass spectrometry-based means of detecting distinctive structural features of prion strains. *Biochemistry* 55, 894–902. doi: 10.1021/acs.biochem.5b01068

Silva, C. J., Onisko, B. C., Dynin, I., Erickson, M. L., Requena, J. R., and Carter, J. M. (2011). Utility of mass spectrometry in the diagnosis of prion diseases. *Anal. Chem.* 83, 1609–1615. doi: 10.1021/ac102527w

Silva, C. J., Onisko, B. C., Dynin, I., Erickson, M. L., Vensel, W. H., Requena, J. R., et al. (2010). Assessing the role of oxidized methionine at position 213 in the formation of prions in hamsters. *Biochemistry* 49, 1854–1861. doi: 10.1021/bi901850n

Spagnolli, G., Rigoli, M., Orioli, S., Sevillano, A. M., Faccioli, P., Wille, H., et al. (2019). Full atomistic model of prion structure and conversion. *PLoS Pathog.* 15:e1007864. doi: 10.1371/journal.ppat.1007864

Spudich, S., Mastrianni, J. A., Wrensch, M., Gabizon, R., Meiner, Z., Kahana, I., et al. (1995). Complete penetrance of Creutzfeldt-Jakob disease in Libyan Jews carrying the E200K mutation in the prion protein gene. *Mol. Med.* 1, 607–613. doi: 10.1007/bf03401601

Sturm, R., Sheynkman, G., Booth, C., Smith, L. M., Pedersen, J. A., and Li, L. (2012). Absolute quantification of prion protein (90-231) using stable isotope-labeled chymotryptic peptide standards in a LC-MRM AQUA workflow. *J. Am. Soc. Mass Spectrom.* 23, 1522–1533. doi: 10.1007/s13361-012-0411-1

Supattapone, S., Bosque, P., Muramoto, T., Wille, H., Aagaard, C., Peretz, D., et al. (1999). Prion protein of 106 residues creates an artifical transmission barrier for prion replication in transgenic mice. *Cell* 96, 869–878. doi: 10.1016/s0092-8674(00)80596-6

Telling, G. C., Parchi, P., DeArmond, S. J., Cortelli, P., Montagna, P., Gabizon, R., et al. (1996). Evidence for the conformation of the pathologic isoform of the prion protein enciphering and propagating prion diversity. *Science* 274, 2079–2082. doi: 10.1126/science.274.5295.2079

Turnbaugh, J. A., Unterberger, U., Saa, P., Massignan, T., Fluharty, B. R., Bowman, F. P., et al. (2012). The N-terminal, polybasic region of PrP(C) dictates the efficiency of prion propagation by binding to PrP(Sc). *J. Neurosci.* 32, 8817–8830. doi: 10.1523/JNEUROSCI.1103-12.2012

Uittenbogaard, J. P., Zomer, B., Hoogerhout, P., and Metz, B. (2011). Reactions of beta-propiolactone with nucleobase analogues, nucleosides, and peptides: implications for the inactivation of viruses. *J. Biol. Chem.* 286, 36198–36214. doi: 10.1074/jbc.M111.279232

Vaccari, G., Di Bari, M. A., Morelli, L., Nonno, R., Chiappini, B., Antonucci, G., et al. (2006). Identification of an allelic variant of the goat PrP gene associated with resistance to scrapie. *J. Gen. Virol.* 87, 1395–1402. doi: 10.1099/vir.0.81485-0

Vazquez-Fernandez, E., Alonso, J., Pastrana, M. A., Ramos, A., Stitz, L., Vidal, E., et al. (2012). Structural organization of mammalian prions as probed by limited proteolysis. *PLoS One* 7:e50111. doi: 10.1371/journal.pone.0050111

Weiss, S., Proske, D., Neumann, M., Groschup, M. H., Kretzschmar, H. A., Famulok, M., et al. (1997). RNA aptamers specifically interact with the prion protein PrP. *J. Virol.* 71, 8790–8797. doi: 10.1128/JVI.71.11.8790-8797.1997

Wille, H., and Requena, J. R. (2018). The structure of PrP(Sc) prions. *Pathogens* 7:20. doi: 10.3390/pathogens7010020

Conflict of Interest: The authors declare that the research was conducted in the absence of any commercial or financial relationships that could be construed as a potential conflict of interest.

frontiers in Bioengineering and Biotechnology

ORIGINAL RESEARCH
published: 06 October 2020
doi: 10.3389/fbioe.2020.590501

Modeling PrP^{Sc} Generation Through Deformed Templating

Giovanni Spagnolli[1,2†], Marta Rigoli[1†], Giovanni Novi Inverardi[1], Yaiza B. Codeseira[3], Emiliano Biasini[1,2*] and Jesús R. Requena[3*]*

[1] Department of Cellular, Computational and Integrative Biology, Centre for Integrative Biology, University of Trento, Trento, Italy, [2] Dulbecco Telethon Institute, University of Trento, Trento, Italy, [3] CIMUS Biomedical Research Institute, University of Santiago de Compostela-IDIS, Santiago de Compostela, Spain

OPEN ACCESS

Edited by:
Maria José Saavedra, Universidade de Trás-os-Montes e Alto Douro, Portugal

Reviewed by:
Dana Mitzel, Agricultural Research Service, United States Department of Agriculture, United States
Ilia V. Baskakov, University of Maryland, Baltimore, United States

***Correspondence:**
Giovanni Spagnolli
giovanni.spagnolli@unitn.it
Emiliano Biasini
emiliano.biasini@unitn.it; biasinie@gmail.com
Jesús R. Requena
jesus.requena@usc.es

† These authors have contributed equally to this work

Specialty section:
This article was submitted to Biosafety and Biosecurity, a section of the journal Frontiers in Bioengineering and Biotechnology

Received: *01 August 2020*
Accepted: *14 September 2020*
Published: *06 October 2020*

Citation:
Spagnolli G, Rigoli M, Novi Inverardi G, Codeseira YB, Biasini E and Requena JR (2020) Modeling PrP^{Sc} Generation Through Deformed Templating. Front. Bioeng. Biotechnol. 8:590501. doi: 10.3389/fbioe.2020.590501

Deformed templating is the process by which self-replicating protein conformations with a given cross-β folding pattern can seed formation of an alternative self-replicating state with different cross-β folding pattern. In particular, uninfectious but propagative PrP amyloid can transform into a *bona fide* infectious conformer, PrP^{Sc} through deformed templating. The process can take many rounds of replication (if taking place *in vitro*) or even several passages of the evolving PrP conformers through successive brains if *in vivo*, through experimental transmission. In all cases, deformed templating involves a forced conversion in which there is a mismatch between the template and the substrate and/or the templating environment, typically a recombinant PrP amyloid, adept at converting recombinant PrP under denaturing conditions (e.g., presence of chaotropic agents), encountering a glycosylated, GPI-anchored PrP^{C} substrate under physiological conversion conditions. Deformed templating is characterized by emergence of intermediate conformers that exhibit biochemical characteristics that are intermediate between those of the initial PrP amyloid and the final PrP^{Sc} conformers. Here, we took advantage of the recent elucidation of the structure of a PrP amyloid by cryo-EM and the availability of a physically plausible atomistic model of PrP^{Sc} that we have recently proposed. Using modeling and Molecular Dynamics (MD) approaches, we built a complete molecular modelization of deformed templating, including an atomistic model of a glycosylated intermediate conformer and a modified model of PrP^{Sc}. Among other unanticipated outcomes, our results show that fully glycosylated PrP can be stacked in-register, and how 4-rung β-solenoid (4RβS) PrP architectures can share key structural motifs with parallel-in register intermolecular sheet (PIRIBS) PrP amyloids. Our results shed light on the mechanisms of prion replication.

Keywords: deformed templating, PrP^{Sc}, PrP^{Sc} structure, PrP amyloid, 4RβS, PIRIBS, molecular dynamics

INTRODUCTION

Generation of the first synthetic prions in 2004 was a feat that changed the field of prion research (Legname et al., 2004). Synthetic prions were a logical corollary of the prion hypothesis that had been proposed about 20 years earlier by Stanley Prusiner (Prusiner, 1982). If mammalian prions were but a conformational variant of the mammalian protein PrP^{C}, it followed that it would

(and should) be possible to generate such conformation *in vitro*. However, the exact conditions, and co-factors needed to produce such transformation in the test tube were not obvious, and thus numerous attempts to produce recombinant prions failed. Legname, Baskakov, and cols. reasoned that given that PrP^{Sc} often appeared in the form of amyloid fibrils (Merz et al., 1981; DeArmond et al., 1985), converting recombinant PrP (recPrP) into amyloid fibers *in vitro* would be the most likely strategy to succeed. It should be noted that at the time there was a controversy as to whether the amyloid nature of PrP^{Sc} fibers was an intrinsic feature of the infectious prionic agent or just an epiphenomenon (Prusiner, 1998). In other words, these researchers reasoned that even if the amyloid they prepared was not the infectious agent *per se*, PrP amyloid preps would likely contain the infectious conformation even if as a minor component (Legname et al., 2004). Their success in unequivocally transmitting prion disease to a group of mice using PrP amyloids generated from recombinant protein and a set of simple chemicals alone, and thus completely free of any nucleic acid, was the definitive experimental proof of the prion hypothesis (Legname et al., 2004). However, this result was not exempt of controversy: the animals used in the experiment were transgenic mice expressing a truncated version of PrP, MoPrP 89–230, in large quantities (∼16x the expression seen in wt animals). This led some critics to argue that perhaps the PrP amyloid prep had not actually produced a prion disease, but rather, accelerated spontaneous development of a genetic form of neurodegeneration induced by overexpression of an aberrant form of PrP.

These objections were definitively laid to rest a few years later when Ma and cols. generated a $recPrP^{Sc}$ capable of infecting wild type mice with an attack rate of 100% and incubation times similar to those typical of brain-derived PrP^{Sc} (Wang et al., 2010). These authors used a modified version of protein misfolding cyclic amplification (PMCA), involving addition of co-factors to the conversion mixture, to generate their $recPrP^{Sc}$, rather than simple amyloid fibrillization (Wang et al., 2010). The term $recPrP^{Sc}$ aptly expresses the fact that their conformation is believed to be the same or virtually the same as that of brain PrP^{Sc}, i.e., the mammalian prion, whereas to describe the infectious conformer(s) prepared by Legname, Baskakov, and cols. the more conservative and generic "infectious PrP amyloid" is preferable. More recently, numerous $recPrP^{Sc}$ preps have been described (Piro et al., 2011; Deleault et al., 2012; Fernández-Borges et al., 2018; Eraña et al., 2019), generated by different PMCA-based methods and relying on different sets of co-factors. $Rec\text{-}PrP^{Sc}$ has in fact become a very promising material for structural studies, as it opens infinite possibilities of labeling, including with stable isotopes for solid state NMR (ssNMR) studies (Sevillano et al., 2018; Martín-Pastor et al., 2020). Preliminary studies suggest that all these infectious $recPrP^{Sc}$ variants are structurally similar *inter se* but different from the simpler PrP amyloid preps obtained by shaking recPrP under denaturing conditions (Tycko et al., 2010; Baskakov et al., 2019). One obvious difference is the extension of the β-sheet-rich core, which in PrP^{Sc} typically spans from ∼89 to 230 (mouse numbering), whereas in simpler PrP amyloids it spans only from ∼160/170 to 230 (Bocharova et al., 2005; Lu et al., 2007; Smirnovas et al., 2009, 2011; Tycko et al., 2010). This in turn results in larger Proteinase K (PK) resistant cores in infectious $recPrP^{Sc}$ conformers as compared with classic PrP amyloid (Bocharova et al., 2005; Lu et al., 2007; Smirnovas et al., 2009, 2011).

Shortly after the accomplishment of prion disease transmission with recPrP amyloids, Baskakov and associates made an unexpected discovery: while wt Syrian hamsters (Sha) inoculated with recombinant ShaPrP amyloid did not develop any clinical signs of prion disease, some of them accumulated abnormally folded forms of PrP, and inoculation of their brain homogenates to wt animals in a second passage induced a full-fledged prion disease (Makarava et al., 2010). These authors have prepared over time different variants of PrP amyloid, all behaving in a similar fashion, with a silent propagative phase followed by emergence of clinical disease in second or even third passage (Makarava et al., 2011, 2012, 2015, 2016; Makarava and Baskakov, 2012; Klimova et al., 2015). These studies have revealed that under most experimental conditions, upon first passage, a propagative, misfolded PrP species emerges that exhibits a peculiar, atypical pattern of PK-resistance. Namely, its main PK-resistant core spans from a position around ∼160 to the C-terminus and excludes the epitope recognized by antibody 3F4 (109–112) but includes the epitope of antibody SAF-84 (160–170). Such PK-resistant core is also characteristic of the PrP amyloid used for inoculation, and its size is related to the span of the PrP amyloid β-sheet-rich core already mentioned. The atypical, propagative PK-resistant PrP conformer is mostly monoglycosylated, although small fractions of diglycosylated and non-glycosylated conformer are also seen. With successive passages, classic PrP^{Sc} starts to emerge, eventually outcompeting the atypical propagative PK-resistant PrP conformer (Makarava et al., 2011, 2012, 2015, 2016; Makarava and Baskakov, 2012; Klimova et al., 2015). Careful experiments were carried out to discriminate between two possibilities: (a) minute amounts of PrP^{Sc} are present from the beginning in the first passage or (b) the atypical, propagative PK-resistant PrP conformer precedes PrP^{Sc}, which originates by a slow and progressive conversion of the former into the latter conformer. Baskakov and colleagues ruled out experimentally the first possibility, for example, with extremely sensitive PMCA-based analyses that would have detected even a small handful of PrP^{Sc} molecules (Makarava and Baskakov, 2012; Makarava et al., 2012). Therefore, they coined the term "deformed templating" to refer to the second process, which they demonstrated to be taking place (Makarava and Baskakov, 2012; Makarava et al., 2012). Furthermore, these authors proposed a wider application of the term, which was defined as defined as a process by which self-replicating protein conformational states with a given cross-β folding pattern can seed formation of an alternative self-replicating state with different cross-β folding pattern. Of note, deformed templating also explains seeding of amyloid fibrils (presumably non-infectious) by PrP^{Sc} in real time quacking-induced conversion (RT-QulC) assays, which could be viewed as the opposite process.

Very recently, Wang et al. (2020) used cryo-electron microscopy and reconstruction techniques to decipher the structure of classic recombinant PrP fibers and used the

experimental data to build an atomic structural model of this PrP conformer. On the other hand, we have built in the past an atomic model of PrP^{Sc} which is also based on cryo-EM data, albeit of much lower resolution (Vázquez-Fernández et al., 2016) and incorporates all other available experimental structural constraints (Spagnolli et al., 2019). Our model is the only one compatible with the most recent low-resolution experimental constraints and it is stable when challenged with plain MD simulations (Spagnolli et al., 2019). We reasoned that these two models offer a starting and a final point that could be used to build and test a molecular model of deformed templating.

We therefore employed a set of bioinformatic tools and approaches to develop a molecular mechanism of deformed templating. We present here our results.

MATERIALS AND METHODS

Modeling the Glycosylated PK-res PrP Candidate

The atomic coordinates for the human PrP amyloid characterized by Wang et al. (2020) were retrieved from PDB 6LNI (containing five PrP monomers arranged as a parallel-in-register-β-sheet). Protein topology was generated in Gromacs 2018 (Van Der Spoel et al., 2005) using Amber99SB-ILDN forcefield (Lindorff-Larsen et al., 2010). Asparagines N_{181} and N_{197} of each PrP monomer were glycosylated. The glycosylation procedure was carried out using doGlycans (Danne et al., 2017), a python-based tool that generates carbohydrate structure of glycoproteins, provided the carbohydrates sequence and the protein structure as input. The glycans employed are composed by four *N*-acetylglucosamines, 3 mannoses, 2 galactoses, 1 fucose, and 2 sialic acids ($GlcNAc_4Man_3Gal_2FucNeuNAc_2$) (Baskakov, 2017). The structure of the glycosylated fibril was visually inspected and torsional angles of the carbohydrates were adjusted to avoid extensive overlap between the sugar chains. The resulting structure was solvated in water (TIP3P) and ions (NaCl) at physiological concentration (150 mM). The solvated molecule was minimized using the steepest descent algorithm, in four steps. The first two steps were performed with position restraints on all protein atoms with force tolerance equal to 1000 kJ/(mol·nm) and then 500 kJ/(mol·nm), while the 3rd and the 4th steps were executed without restraints, with the same aforementioned tolerance values. The absence of steric clashes was evaluated using the Clashes/Contact Tool in UCSF Chimera. To generate the glycosylated decamer, two fully glycosylated pentamers were stacked. The system was then energy minimized following the aforementioned protocol.

Building the Deformed-Templating-Compatible-4-Rung β-Solenoid (4RβS) Mouse PrP^{Sc} Model

The stretch consisting of residues 181–208 (human numbering), retrieved from PDB 6LNI, was used as a template to build each rung of the 4RβS model. The threading scheme was obtained by considering different experimental constraints: PK cleavage sites, indicating residues likely excluded from the resistant core of the protein, mass spectrometry studies, revealing the presence of a disulfide bond between the two cysteines of PrP sequence, and the solvent exposure of the glycosylated side-chains that must be capable of accommodating the bulky glycans (Spagnolli et al., 2019). Residue numbering was switched to the mouse sequence and, in the different rungs, the amino acids were swapped to the target ones, to match the proper threading, using UCSF Chimera (Pettersen et al., 2004). Side-chains rotamers were retrieved from the Dunbrack's library. Protein loops were built using MODELLER (Sali and Blundell, 1993). Protein topology was generated in Gromacs using Amber99SB-ILDN forcefield and the resulting structure was solvated in water (TIP3P) and ions (NaCl) at physiological concentration (150 mM). The system was then energy minimized using the steepest descent algorithm with position restraints (force constant of 10000 $kJ{\cdot}mol^{-1}{\cdot}nm^{-2}$) on no-hydrogen atoms of backbone residues involved β-strands formation. A subsequent step of energy minimization was performed by removing the position restraints from all-atoms (a force tolerance of 200 $kJ{\cdot}mol^{-1}{\cdot}nm^{-1}$ was set for energy minimizations). At the end of this step, Ramachandran outliers and low-probability rotamers were corrected using Coot (Emsley et al., 2010). The absence of steric clashes was evaluated using the Clashes/Contact Tool in UCSF Chimera. 4RβS tetramer was built by stacking four monomers in a head-to-tail fashion followed by the previously reported energy minimization and refinement protocol. The glycosylated deformed-templating-compatible-4RβS tetramer was build using the same procedure employed to construct the glycosylated recPrP amyloid.

Molecular Dynamics Simulations and Analysis

The following protocol was employed for the glycosylated PrP amyloid, the non-glycosylated PrP amyloid and the 4RβS PrP^{Sc} model: the energy minimized system was subjected to 1 ns of NVT equilibration at 300 K by employing the V-rescale thermostat (Bussi et al., 2007). Then, NPT equilibration was performed by employing the V-rescale thermostat and the Perrinello-Rahman barostat (Parrinello and Rahman, 1981) at 300 K and 1 Bar for 1 additional ns. These two steps were carried out using positional restraints, with force constant of 1000 $kJ/(mol{\cdot}nm^2)$, on no-hydrogen atoms. Subsequently, 20 ns of molecular dynamics simulations (300 K, 1 Bar) were performed by introducing distance restraints between backbone atoms (amide H and O) involved in hydrogen bonding for β-strands formation (for more details, see Spagnolli et al., 2019). At the end, distance restraints were removed and the trajectory was extended to additional 100 ns of plain MD. This procedure was repeated three times for the three starting structure, yielding three independents 100 ns trajectories each. The simulations were performed using Gromacs 2018. Trajectories were then analyzed with VMD 1.9.2 (Humphrey et al., 1996), in particular, RMSD was computed using the "RMSD Trajectory Tool," while the β-strand content was evaluated with the "Timeline Tool." Graphs and images were generated with Matplotlib (Hunter, 2007) and UCSF Chimera, respectively.

RESULTS

Building of an Atypical Propagative PK-Resistant PrP Candidate

As noted by Baskakov and associates, the PK fragmentation pattern of the atypical, propagative PK-resistant PrP conformer that appears at the beginning of the deformed templating process is essentially identical to that of the original PrP amyloid inoculated (Makarava et al., 2012). This suggests that their architectures are likely to be very similar. However, one major difference between the two is that the atypical, propagative PK-resistant PrP conformer is glycosylated (mostly mono-glycosylated) and displays a GPI-anchor. Therefore, we first aimed at building a glycosylated version of the recombinant PrP amyloid whose architecture has recently been elucidated by Wang et al. (2020). For this, we generated a $GlcNAc_4Man_3Gal2FucNeuNAc_2$ glycan (**Supplementary Figure S1**), which is representative both in size, complexity and branching, of the most abundant glycans found in PrP^C and PrP^{Sc} (Rudd et al., 1999, 2001; Pettersen et al., 2004) and attached two of them *in silice* to the PrP amyloid model of Wang and colleagues (PDB 6LNI) at asparagines N_{181} and N_{197}. Based on prior considerations (Terruzzi et al., 2020) we expected that it would be very difficult to stack more than two monomers of such putative conformer because of steric clashes; however, to our surprise, we were able to easily stack a pentamer of the diglycosylated structure, without any steric clashes (**Figure 1**).

Molecular Dynamics Simulation of the Stability of the PIRIBS Atypical Propagative PK-Resistant PrP Candidate

We next performed MD simulations to evaluate the stability of the glycosylated PK-resistant PrP candidate. This PIRIBS structure (constituted by five diglycosylated subunits) was subjected to three independents 100 ns molecular dynamics simulations. The stability of the model was then measured in terms of root mean squared deviation of atomic position from the initial state (RMSD) and β-strand content. For the entire length of the simulations, the average RMSD of the protein lies below 2 Å and the average percentage of β-strands remains greater than 60% (**Figure 2A**). These results indicate a significant stability of the model, and are comparable to those obtained for the non-glycosylated PrP amyloid (**Supplementary Figure S2A**).

Building of a Modified 4RβS Atomic Model of PrP^{Sc}, Compatible With Deformed Templating

Having solved the structure of a possible atypical propagative PK-resistant PrP conformer, we set out to model the core of the deformed templating process, i.e., transition from this early intermediate to a *bona fide* PrP^{Sc} conformer. We noticed that the cross-section of the PrP amyloid described by Wang et al. (2020) features an approximately triangular core spanning approximately N_{181} to R_{208} (**Figures 3A,B**). Such triangular core surface is relatively compatible with the triangular cross-section of our 4RβS PrP^{Sc} structural model (Spagnolli et al., 2019), therefore we built a modified version of PrP^{Sc} by using the architecture of this region to template the four rungs. The residues 170–180 (human numbering) at the N-terminal part of the triangular core are rearranged to form a loop, while the residues at the C-terminal side (209–231) are remodeled into a loop and two β-strands in the target 4RβS structure (**Figure 3C**). The rest of the 4RβS was built by considering the same experimental constraints employed to construct our previously proposed PrP^{Sc} model (Spagnolli et al., 2019). Due to poor availability of experimental constraints of human PrP^{Sc}, we built the deformed-templating-compatible PrP^{Sc} model based on the mouse sequence. Importantly, the triangular core defined by residues 181–208, in the human sequence, and 180–207, in mouse one, share 100% identity. The resulting model (**Figure 4**), resembles our previously proposed one in many features: residues forming the inner core (T_{106}-A_{114}, Y_{127}-L_{129}, N_{142}-Y_{149}, and T_{215}-Y_{224}) are structurally conserved in the two putative PrP^{Sc} conformation (namely, residues pointing inward, or outward the hydrophobic regions are the same in both models); furthermore, important interactions are also

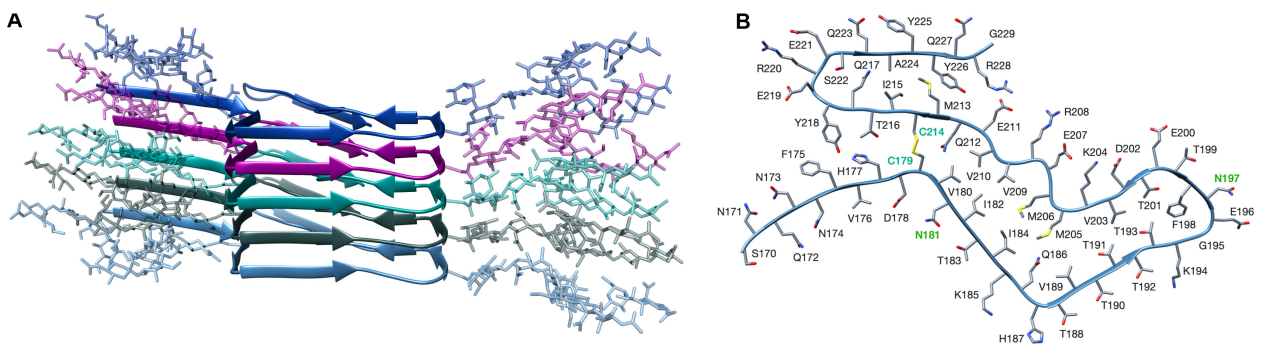

FIGURE 1 | Structural model of a fully glycosylated human PrP amyloid. **(A)** The structure of the PrP amyloid is represented as a cartoon, each of the monomer is depicted in different colors. Glycans are shown with sticks representation and colors matching the one of the linked PrP monomer. No steric clashes are present in the structure. **(B)** Top view of a single PrP amyloid monomer, cysteine labels are depicted in cyan, showing the disulfide bond between C_{179} and C_{214}. Labels of glycosylated asparagines (N_{181} and N_{197}) are shown in green. The structure of the non-glycosylated human PrP amyloid was retrieved from PDB 6LNI.

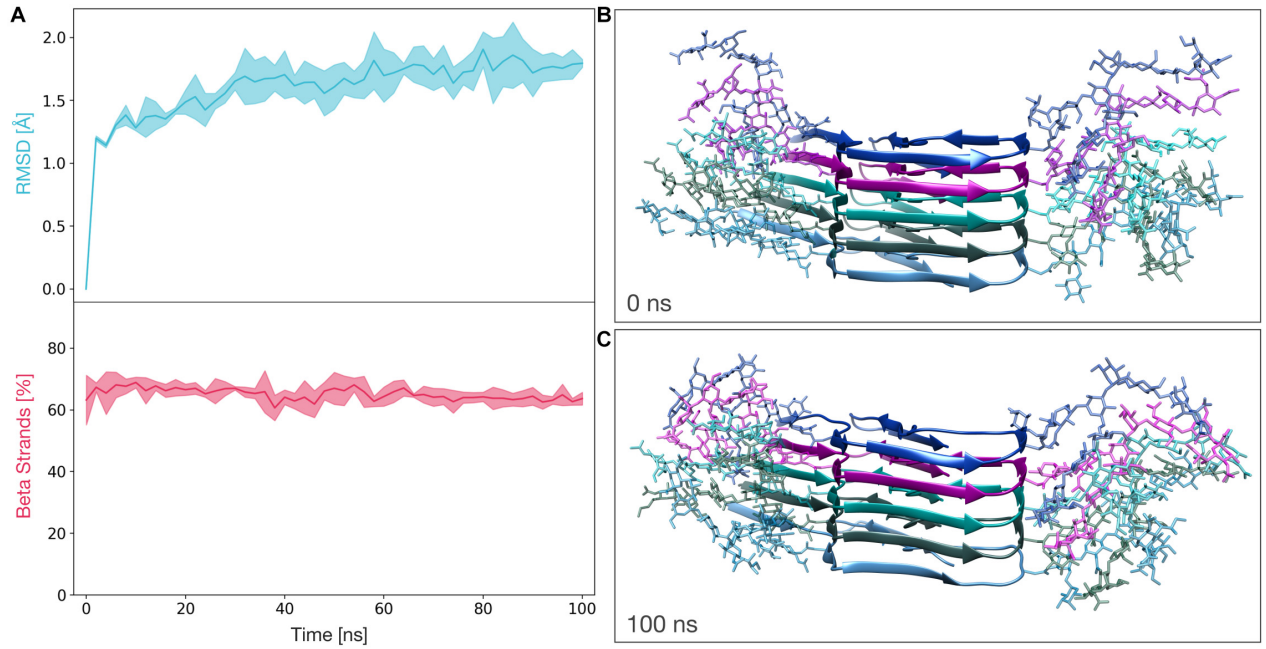

FIGURE 2 | Molecular Dynamics simulations of the fully glycosylated PrP amyloid. **(A)** The graphs show the RMSD (above) and percentage of β-strands (below) as a function of the simulation time. The line and the filled curve indicate the mean and the standard deviation, respectively, computed on the three performed simulations of 100 ns each. **(B)** Representative snapshot extracted at the beginning of the MD simulations (t = 0 ns). **(C)** Representative snapshot extracted at the end of the MD simulations (t = 100 ns).

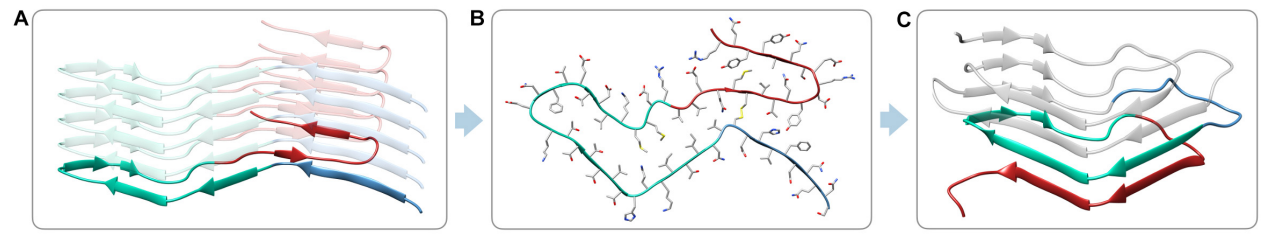

FIGURE 3 | Building a deformed-templated-compatible 4RβS PrP^{Sc}. Different stretches of PrP residues are depicted in different colors, based on the conformation displayed in the target 4RβS structure. The triangular core (N_{181}-R_{208}, human numbering) is depicted in aquamarine, the sequence at its N-terminus (S_{170}-V_{180}) is depicted in blue and the structure at its C-terminus (V_{209} to end) is depicted in red. **(A)** Representation of the colored sequences in a lateral view of recPrP. **(B)** Top view of the PrP monomer in the PIRIBS conformation with side-chains represented as sticks. **(C)** 4RβS model compatible with deformed templating.

shared between the two conformations, such as the buried salt-bridge between R_{147} and D_{166}. Despite these common characteristics, the two models also display notable differences, such as the overall shape of the β-solenoid, the orientation of particular residues composing the resistant core (T_{94}-N_{99}, Q_{167}-Y_{168}, and Q_{185}-H_{186}) and the stretch composed of residues 198–201 that is excluded by the central part of the triangular core, with residues 203–206, occupying that region (methionines pointing inward). The two models do not exclude each other, and in fact the differences in solenoid shapes and threadings might constitute a molecular basis for strain differences. However, discussion of this possibility lies beyond the scope of this study.

Then, we built a tetrameric stack of diglycosylated 4RβS units (**Supplementary Figure S3**), showing a looser packing of glycans in this architecture, compared to the PIRIBS conformation.

Molecular Dynamics Simulation of the Modified, Deformed Templating-Compatible, 4RβS Atomic Model of PrP^{Sc}

We next subjected a tetrameric model of the deformed templating-compatible 4RβS to the same MD protocol we employed in Spagnolli et al. (2019). The stability of this structure was also assessed by computing the RMSD and the β-strands content along the trajectories. The average RMSD at the end of the simulation resulted to be ∼4 Å, while the average percentage of β-strands remains above 40% for the entire length of the

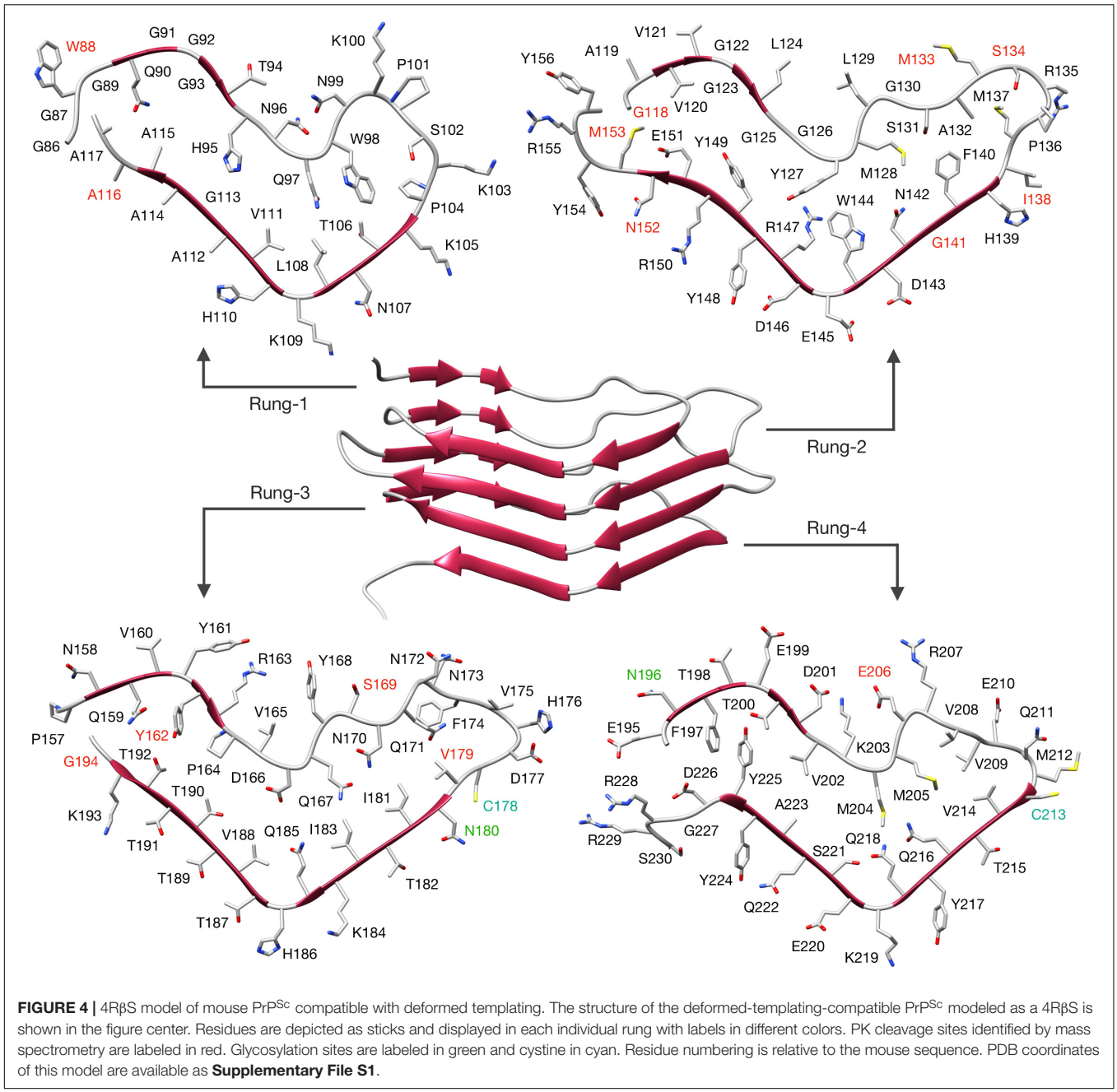

FIGURE 4 | 4RβS model of mouse PrP^{Sc} compatible with deformed templating. The structure of the deformed-templating-compatible PrP^{Sc} modeled as a 4RβS is shown in the figure center. Residues are depicted as sticks and displayed in each individual rung with labels in different colors. PK cleavage sites identified by mass spectrometry are labeled in red. Glycosylation sites are labeled in green and cystine in cyan. Residue numbering is relative to the mouse sequence. PDB coordinates of this model are available as **Supplementary File S1**.

simulations. These results show that the stability of this structure is comparable to the one observed in our previously proposed tetrameric model (**Figure 5** and ref 28).

Modeling Transition From the PIRIBS Atypical Propagative PK-Resistant PrP Intermediate to *Bona Fide* PrP^{Sc}

Finally, we elaborated a model of the transition between the PIRIBS atypical propagative PK-resistant PrP intermediate to *bona fide* PrP^{Sc}. In the proposed mechanism, the triangular core of the PIRIBS architecture, defined by residues 180–207 (mouse numbering), plays the fundamental role of templating the formation of the β-solenoid rungs. The deformed templating begins with the structural rearrangement of the C-terminus of the fibril-end PrP monomer. In this conformational change, residues 182–192 of the triangular core engage hydrogen bonds with residues 215–225, resulting in the formation of two new β-strands. This structure now displays a C-terminal surface that is indistinguishable from the C-terminal rung (rung 4) of 4RβS, as residues 196–230 are now forming a complete rung 4. This active end is now capable of starting the templating of a 4RβS PrP^{Sc}, that is achieved by a mechanism in which each rung templates the formation of the following one (as described in

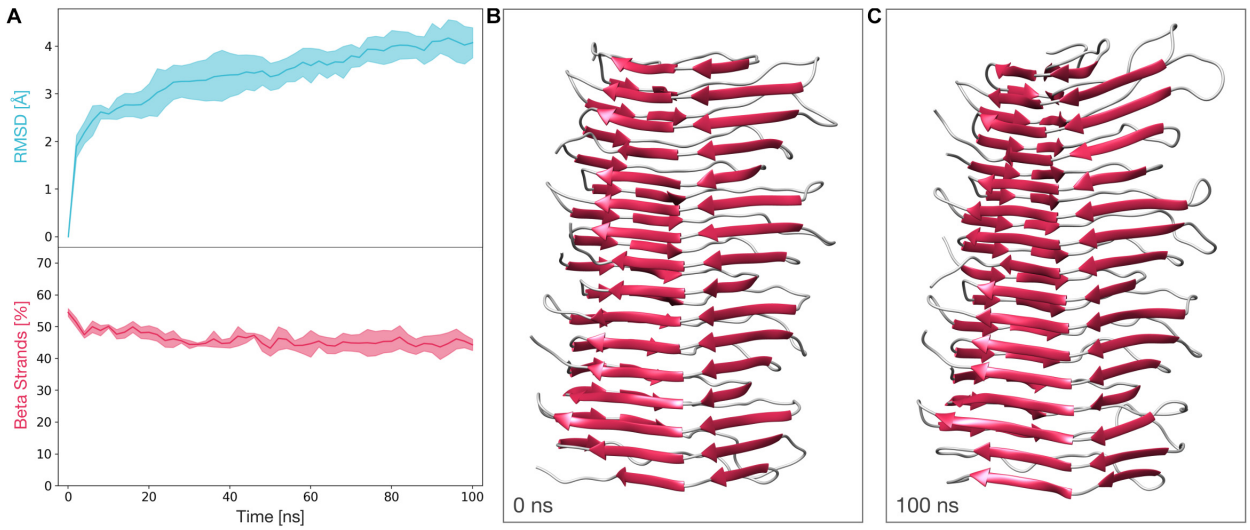

FIGURE 5 | Molecular dynamics simulations of the deformed templating-compatible 4RβS model of PrP^{Sc}. **(A)** The graphs show the RMSD (above) and percentage of β-strands (below) as a function of the simulation time. The line and the filled curve indicate the mean and the standard deviation, respectively, computed on the three performed simulations of 100 ns each. These results are compatible with the stability observed of the 4RβS model introduced in our previous work (Vázquez-Fernández et al., 2016). **(B)** Representative snapshot extracted at the beginning of the MD simulations (t = 0 ns). **(C)** Representative snapshot extracted at the end of the MD simulations (t = 100 ns).

28). A representation of the transition from the PIRIBS PrP intermediate (**Figure 6A**) to 4RβS PrP^{Sc} (**Figure 6D**) is shown in **Figure 6**.

DISCUSSION

Deformed templating, the process by which a classic PrP amyloid propagating in a brain or by PMCA eventually generates *bona fide* PrP^{Sc}, is in our opinion of central importance in prion biochemistry. Templated propagation is the core of prion biology, and while substantial progress has been made to understand and model it at the molecular level (Spagnolli et al., 2019; Terruzzi et al., 2020), a complete understanding of it will not be achieved until a full experimental model of PrP^{Sc} is available. And while such an understanding is not achieved, critical issues of practical importance such as transmission barriers and the identification of PrP^{Sc}-aimed therapies will be impossible. In this context, deformed templating provides an important constraint for the structure of PrP^{Sc} and the molecular process of its propagation: the structure and the process must be such that they are compatible with deformed templating. In other words, the structure of PrP^{Sc} must be such that with reasonable strains (deforming) it can be reached from a PrP amyloid as a starting point. And the fact that the structure of a PrP amyloid has been deciphered with a quasi-atomic resolution using cryo-EM offers a unique opportunity to challenge the PrP^{Sc} structural model, and the model of PrP^{Sc} propagation that we have proposed recently (Spagnolli et al., 2019).

Here, we provide a modelization of deformed templating that allows such challenging exercise and at the same time offers a plausible description of the process at the molecular level. As described in numerous studies from the Baskakov lab, the first step in deformed templating involves an intermediate PrP conformer with a pattern of PK-resistance that is strikingly similar to that of the original propagative PrP amyloid prepared *in vitro* and used to inoculate the experimental animals (Makarava and Baskakov, 2012; Makarava et al., 2012). In particular, the main PK-resistant fragment is C-terminal, spanning from ∼160 to 231. We reasoned that the most parsimonious explanation for this would be if the intermediate shares the same architecture as the initial amyloid: a PIRIBS one. However, it has been assumed in the past that such architecture does not allow stacking of the glycans (Baskakov and Katorcha, 2016; Baskakov et al., 2019). Still, we decided to explore this possibility, and to our surprise, a diglycosylated PrP amyloid core pentamer modeled from the structure recently solved by Wang et al. (2020) was stackable into a very stable PIRIBS (**Figures 1**, **2**). Furthermore, this pentamer could be extended to a decamer, showing the physical plausibility of longer glycoslylated assemblies (**Supplementary Figure S4**). Therefore, when a theoretically non-infectious PrP amyloid is inoculated into a brain (Makarava et al., 2011, 2012, 2015, 2016; Makarava and Baskakov, 2012; Klimova et al., 2015), some of the glycosylated PrP^{C} molecules (in particular the mono-glycosylated ones) of the host can be templated and incorporated into the amyloid seeds (**Figure 1**). Why are monoglycosylated PrP^{C} units incorporated preferentially over di- and non-glycosylated ones (Makarava et al., 2011, 2012, 2015, 2016; Makarava and Baskakov, 2012; Klimova et al., 2015)? One key characteristic of this first templating event is that the PrP^{C} substrate units possess a GPI-anchor, and in fact conversion is likely to take place while PrP^{C} is attached to a cell membrane, as has been documented for PrP^{C} to PrP^{Sc} conversion in general (Godsave et al., 2008). This

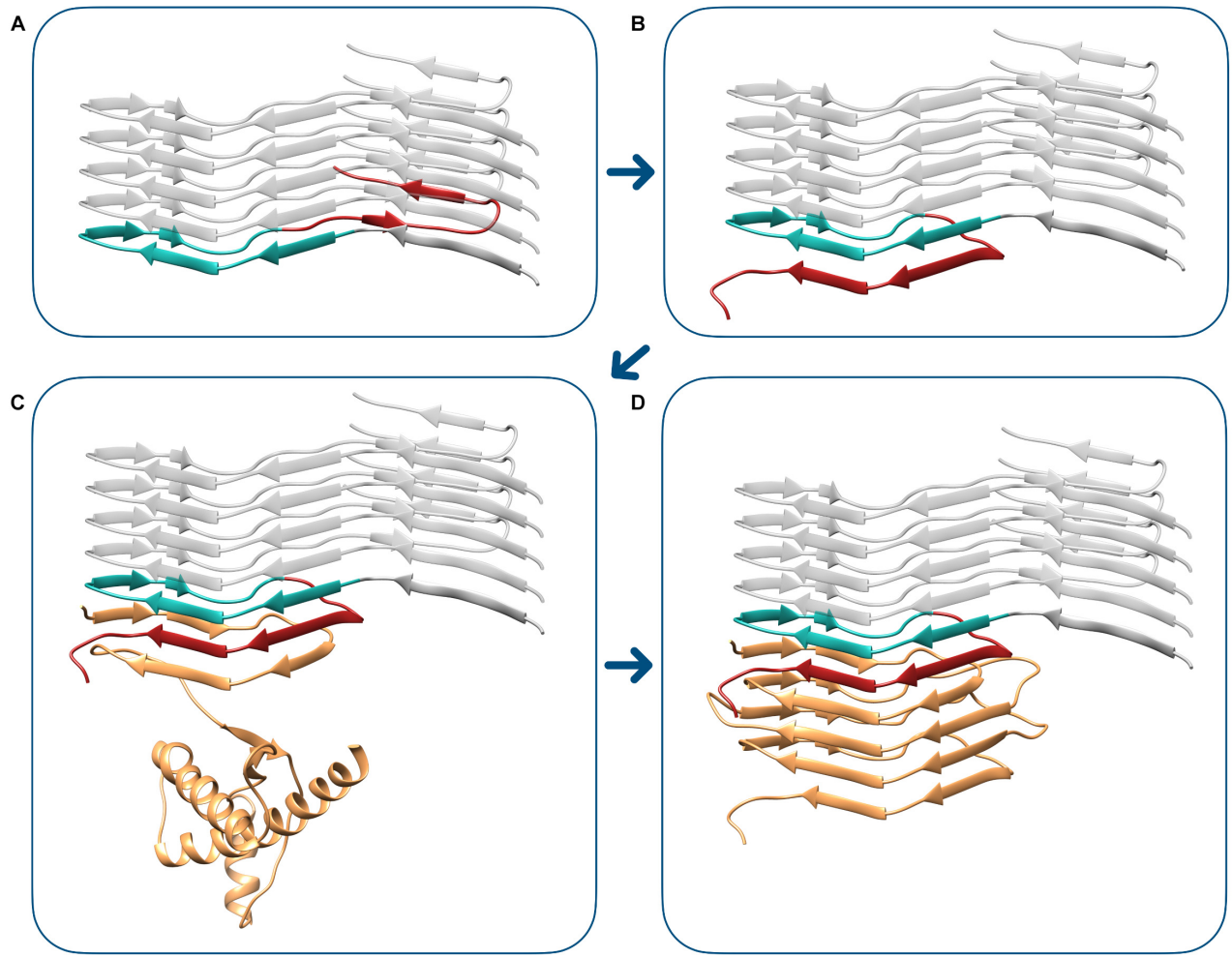

FIGURE 6 | Modeling transition from the PIRIBS atypical propagative PK-resistant PrP intermediate to 4RβS PrP^{Sc}. The deformed templating event begins with the conformational transition of the terminal PIRIBS monomer **(A)**, in which the C-terminal moiety (residues 208–230, mouse numbering), depicted in red, rearranges to engage intramolecular contacts with the central triangular core (residues 180–207), represented in aquamarine. This event generates an active-end, compatible with the propagation of the 4RβS architecture **(B)**. This terminal surface is now capable of templating the conversion of the unstructured region of PrP^{C} (depicted in orange), leading to the formation of the first rung of the β-solenoid, composed by residues 89–115 **(C)**. The completion of the conversion into 4RβS PrP^{Sc} **(D)** finally occurs by the sequential templating events of the subsequent rungs, as we have previously described (Vázquez-Fernández et al., 2016).

likely imposes constraints to the templating process, which must necessarily involve a partial/total unfolding of the C-terminal helices of PrP^{C}. It is conceivable that while the two glycans can be well-accommodated in the final product, their joint presence might sterically hamper the process of approximation, attachment and templated refolding of a partially unfolded, membrane-attached PrP^{C} subunit. Thus, incorporation of non-glycosylated and monoglycosylated PrP^{C} units might be favored over incorporation of diglycosylated PrP^{C} units (Makarava et al., 2011, 2012, 2015, 2016; Makarava and Baskakov, 2012; Klimova et al., 2015). The low proportion of non-glycosylated subunits in the final oligomer would merely reflect their scarcity. Another fact that needs to be considered is that a portion of glycans (Rudd et al., 1999, 2001) are tri- and tetra-antennary, this is, bulkier than the model di-antennary glycan that we have used for the modeling. Incorporation of a diglycosylated PrP subunit with two of these bulkier than average glycans might therefore be less favorable. Finally, the presence of charged sialic acid in some glycan units adds ionic constrains that might also be an important factor in selective recruitment of monoglycosylated PrP^{C}.

It should be noted that this first templating step, which involves the C-terminal region of PrP^{C}, is very different from the second one, involving transition from the glycosylated propagative PK-resistant PrP intermediate to *bona fide* PrP^{Sc}: in that case, conversion very likely begins at the flexible/intrinsically unfolded ∼90–120 segment of PrP^{C} (Spagnolli et al., 2019), already posed to be templated by any β-sheet-rich mold it encounters (from the perspective of the final main PK-resistant, β-sheet-rich core, the "N-terminus"). This segment of PrP^{C} is far apart from the glycans, which are much less likely to exert steric hindrances at the beginning of the conversion process, and therefore a

selection of monoglycosylated over diglycosylated substrate PrP^C units.

According to our model, this second conversion step involves two sub-steps: first the C-terminus of the PrP unit at the amyloid templating edge (196–230) must rearrange (deform) to form a "PrP^{Sc} templating surface." For this they have to engage in heterologous (i.e., non-PIRIBS) interactions and bonding for the first time. Once this sub-step is completed, the stage is set for the flexible "N-terminal" (∼90–120) stretch of a PrP^C substrate unit to be templated into *bona fide* PrP^{Sc} (**Figure 6**). Why is this intermediate rearrangement necessary, as opposed to a direct heterologous interaction of the "N-terminal" (∼90–120) stretch of an incoming PrP^C unit with the amyloid core of the atypical intermediate, or even the inoculum amyloid? We cannot provide an answer at this point, but the reason likely involves steric and energetic considerations.

We have based our modeling scheme on the human and murine sequences of PrP because our point of view is that deformed templating is a general process in PrP^{Sc} propagation. However, with minor changes it can be applied to ShaPrP, which was used in the majority of studies of the Baskakov lab. Furthermore, our modeling assumes that *bona fide* PrP^{Sc} is a 4RβS. Very substantial experimental evidence supports this view (Govaerts et al., 2004; Wille et al., 2009; Vázquez-Fernández et al., 2016; Wille and Requena, 2018; Spagnolli et al., 2019). However, an alternative PIRIBS model of PrP^{Sc} exists (Groveman et al., 2014). According to this model, PrP^{Sc} shares to some extent the C-terminal β-sheet-rich core of PrP amyloids, but the core extends with additional β-strands/loops up to position ∼90. While we currently do not support that model, we acknowledge that the matter is far from settled (Baskakov et al., 2019) and will not be until at least some ssNMR-based structural constraints become available. Therefore, we will briefly discuss our modeling-based findings in the context of that model. First of all, given that the propagative atypical intermediate we propose has a PIRIBS architecture, it is fully compatible with the model proposed by Groveman et al. (2014), although rearrangement of the tertiary structure and threading of some β-strands and connecting coils is necessary, as there are differences between the Groveman model and the structure of the PrP amyloid as deciphered by Wang et al. (2020). Once the glycosylated propagative atypical intermediate is formed, extension of the β-sheet-rich core in the same plane (perpendicular to the axis of growth of the stack) can take place easily. However, it has to proceed without any templating; rather, it would consist of a local rearrangement of the ∼90–170 flexible tails to collapse into each other to form additional β-sheets. The presence of cofactors such as lipids, polysaccharides, or polynucleotides acting as scaffolds/chemical chaperones, known to be critical for generation of *bona fide* PrP^{Sc} *in vitro* (Wang et al., 2010; Deleault et al., 2012; Eraña et al., 2019) would assist this non-templated, self-organizative process, until a definitive PrP^{Sc} templating surface is formed. Glycan stacking would not hamper the process, as shown by our modeling (**Figures 1**, **2**). However, sufficient space must be allocated to both glycan stacks, and therefore any "glycan cleft" in the putative PrP^{Sc} PIRIBS model must be sufficiently wide to allow it. Nevertheless, it should be underscored that the 4RβS architecture makes incorporation of diglycosylated units simpler, since the distance between respective glycosylated residues is 19.2 Å instead of 4.8 Å, providing much more room.

CONCLUSION

(1) We have modeled deformed templating, demonstrating how a simple PrP amyloid, with very low intrinsic infectivity, can evolve to adopt a *bona fide* PrP^{Sc} conformation. (2) We have found that a fully glycosylated PIRIBS amyloid stack is possible and stable; we propose that the atypical propagative intermediate that emerges initially during the deformed templating process is in fact a glycosylated PIRIBS amyloid. (3) We propose that such intermediate undergoes a conformational transition, whose nature we hypothesize at the atomistic level, to generate a PrP^{Sc} templating surface. (4) The constraints imposed by the necessity to allow for a deformed templating-based generation starting from a PIRIBS amyloid have led us to build a modified version of our previous 4RβS model of PrP^{Sc}. (5) However, we acknowledge that deformed templating can be also modeled if PrP^{Sc} had a PIRIBS architecture; this is possible given that stacking of glycans in a PIRIBS is, as mentioned, possible. (6) Deformed templating blurs the categories of infectious vs. non-infectious PrP amyloids, possibly expanding and modulating the prion concept (Requena, 2020); in particular, we hypothesize that in the classic experiment by Legname, Baskakov and colleagues (Legname et al., 2004), deformed templating may have played a role in allowing a simple PrP amyloid to behave as a prion.

DATA AVAILABILITY STATEMENT

The raw data supporting the conclusions of this article will be made available by the authors, without undue reservation.

AUTHOR CONTRIBUTIONS

JR, EB, and GS designed the study. GS, MR, and GNI designed and carried out modeling and MD studies and analyzed the data. GS, MR, YC, EB, and JR integrated the data into a theoretical framework and elaborated conclusions. JR and GS wrote the manuscript. All authors revised and contributed to the final version of the manuscript.

FUNDING

This work has received financial support from the Spanish Ministry of Industry and Competitiveness (grant BFU2017-86692-P, partially established with EU-ERDF funds); the Galician Regional Government (grants ED431B 2017/19 and ED431G), Centro Singular de Investigación de Galicia, accreditation 2019–2022, partially supported by the European Union [European Regional Development Fund (ERDF) 2019/02] and Fondazione Telethon (TCP14009). EB was an assistant Telethon scientist at the Dulbecco Telethon Institute. YC was a pre-doctoral fellow of the Galician Regional Government.

SUPPLEMENTARY MATERIAL

The Supplementary Material for this article can be found online at: https://www.frontiersin.org/articles/10.3389/fbioe.2020.590501/full#supplementary-material

Supplementary Figure 1 | Scheme of the model glycan. Both N181 and N197 of the glycosylated PrP amyloid are linked to this type of complex glycan. Different shapes in the figure represents different types of sugar moieties as described in the legend. The connectivity types between sugars is reported above (or below) the lines linking the shapes.

Supplementary Figure 2 | Molecular Dynamics simulations of the non-glycosylated PrP amyloid. **(A)** The graphs show the RMSD (above) and percentage of β-strands (below) as a function of the simulation time. The line and the filled curve indicate the mean and the standard deviation, respectively, computed on the three performed simulations of 100 ns each. Structure for the simulations is retrieved from PDB 6LNI. **(B)** Representative snapshot extracted at the beginning of the MD simulations (t = 0 ns). **(C)** Representative snapshot extracted at the end of the MD simulations (t = 100 ns).

Supplementary Figure 3 | Glycosylated structure of the deformed templating-compatible 4RβS model. The structure of the PrP^{Sc} 4RβS model is represented as a cartoon, each of the monomer is depicted in different colors. Glycans are shown with sticks representation and colors matching the one of the linked PrP monomer. In the 4RβS model the glycans are more spaced compared to the PIRIBS one (19.2 vs. 4.8 Å, as a distance between glycosylated residues). Thus, the 4RβS model can, in principle, accommodate fully glycosylated PrP^{Sc} monomers by introducing less strain compared to a PIRIBS PrP amyloid.

Supplementary Figure 4 | Structure of a fully glycosylated decamer of PrP amyloid. The energy minimized decamer of recombinant PrP amyloid is represented as a cartoon, different colors are used to depict the monomers constituting the fibril. Carbohydrates are shown with sticks representation and colors matching the one of the attached PrP monomer.

REFERENCES

Baskakov, I. V. (2017). Limited understanding of the functional diversity of N-linked glycans as a major gap of prion biology. *Prion* 11, 82–88. doi: 10.1080/19336896.2017.1301338

Baskakov, I. V., Caughey, B., Requena, J. R., Sevillano, A. M., Surewicz, W. K., and Wille, H. (2019). The prion 2018 round tables (I): the structure of PrP^{Sc}. *Prion* 13, 46–52. doi: 10.1080/19336896.2019.1569450

Baskakov, I. V., and Katorcha, E. (2016). Multifaceted role of sialylation in prion diseases. *Front. Neurosci.* 10:358. doi: 10.3389/fnins.2016.00358

Bocharova, O. V., Breydo, L., Salnikov, V. V., Gill, A. C., and Baskakov, I. V. (2005). Synthetic prions generated in vitro are similar to a newly identified subpopulation of PrP^{Sc} from sporadic Creutzfeldt-Jakob Disease. *Protein Sci.* 14, 1222–1232. doi: 10.1110/ps.041186605

Bussi, G., Donadio, D., and Parrinello, M. (2007). Canonical sampling through velocity rescaling. *J. Chem. Phys.* 126:014101. doi: 10.1063/1.2408420

Danne, R., Poojari, C., Martinez-Seara, H., Rissanen, S., Lolicato, F., Róg, T., et al. (2017). DoGlycans–tools for preparing carbohydrate structures for atomistic simulations of glycoproteins, glycolipids, and carbohydrate polymers for GROMACS. *J. Chem. Inf. Model.* 57, 2401–2406. doi: 10.1021/acs.jcim.7b00237

DeArmond, S. J., McKinley, M. P., Barry, R. A., Braunfeld, M. B., McColloch, J. R., and Prusiner, S. B. (1985). Identification of prion amyloid filaments in scrapie-infected brain. *Cell* 41, 221–235. doi: 10.1016/0092-8674(85)90076-5

Deleault, N. R., Piro, J. R., Walsh, D. J., Wang, F., Ma, J., Geoghegan, J. C., et al. (2012). Isolation of phosphatidylethanolamine as a solitary cofactor for prion formation in the absence of nucleic acids. *Proc. Natl. Acad. Sci. U.S.A.* 109, 8546–8551. doi: 10.1073/pnas.1204498109

Emsley, P., Lohkamp, B., Scott, W. G., and Cowtan, K. (2010). Features and development of Coot. *Acta Crystallogr. D Biol. Crystallogr.* 66(Pt 4), 486–501. doi: 10.1107/S0907444910007493

Eraña, H., Charco, J. M., Di Bari, M. A., Díaz-Domínguez, C. M., López-Moreno, R., Vidal, E., et al. (2019). Development of a new largely scalable in vitro prion propagation method for the production of infectious recombinant prions for high resolution structural studies. *PLoS Pathog.* 15:e1008117. doi: 10.1371/journal.ppat.1008117

Fernández-Borges, N., Di Bari, M. A., Eraña, H., Sánchez-Martín, M., Pirisinu, L., Parra, B., et al. (2018). Cofactors influence the biological properties of infectious recombinant prions. *Acta Neuropathol.* 135, 179–199. doi: 10.1007/s00401-017-1782-y

Godsave, S. F., Wille, H., Kujala, P., Latawiec, D., DeArmond, S. J., Serban, A., et al. (2008). Cryo-immunogold electron microscopy for prions: toward identification of a conversion site. Version 2. *J. Neurosci.* 28, 12489–12499. doi: 10.1523/JNEUROSCI.4474-08.2008

Govaerts, C., Wille, H., Prusiner, S. B., and Cohen, F. E. (2004). Evidence for assembly of prions with left-handed beta-helices into trimers. *Proc. Natl. Acad. Sci. U.S.A.* 101, 8342–8347. doi: 10.1073/pnas.0402254101

Groveman, B. R., Dolan, M. A., Taubner, L. M., Kraus, A., Wickner, R. B., and Caughey, B. (2014). Parallel in-register intermolecular β-sheet architectures for prion-seeded prion protein (PrP) amyloids. *J. Biol. Chem.* 289, 24129–24142. doi: 10.1074/jbc.M114.578344

Humphrey, W., Dalke, A., and Schulten, K. (1996). VMD: visual molecular dynamics. *J. Mol. Graph.* 14, 33–38. doi: 10.1016/0263-7855(96)00018-5

Hunter, J. D. (2007). Matplotlib: a 2D graphics environment. *Comput. Sci. Eng.* 9, 90–95. doi: 10.1109/MCSE.2007.55

Klimova, N., Makarava, N., and Baskakov, I. V. (2015). The diversity and relationship of prion protein self-replicating states. *Virus Res.* 207, 113–119. doi: 10.1016/j.virusres.2014.10.002

Legname, G., Baskakov, I. V., Nguyen, H. O., Riesner, D., Cohen, F. E., DeArmond, S. J., et al. (2004). Synthetic mammalian prions. *Science* 305, 673–676. doi: 10.1126/science.1100195

Lindorff-Larsen, K., Piana, S., Palmo, K., Maragakis, P., Klepeis, J. L., Dror, R. O., et al. (2010). Improved side-chain torsion potentials for the Amber ff99SB protein force field. *Proteins* 78, 1950–1958. doi: 10.1002/prot.22711

Lu, X., Wintrode, P. L., and Surewicz, W. K. (2007). Beta-sheet core of human prion protein amyloid fibrils as determined by hydrogen/deuterium exchange. *Proc. Natl. Acad. Sci. U.S.A.* 104, 1510–1515. doi: 10.1073/pnas.0608447104

Makarava, N., and Baskakov, I. V. (2012). Genesis of transmissible protein states via deformed templating. *Prion* 6, 252–255. doi: 10.4161/pri.19930

Makarava, N., Kovacs, G. G., Bocharova, O., Savtchenko, R., Alexeeva, I., Budka, H., et al. (2010). Recombinant prion protein induces a new transmissible prion disease in wild-type animals. *Acta Neuropathol.* 119, 177–187. doi: 10.1007/s00401-009-0633-x

Makarava, N., Kovacs, G. G., Savtchenko, R., Alexeeva, I., Budka, H., Rohwer, R. G., et al. (2011). Genesis of mammalian prions: from non-infectious amyloid fibrils to a transmissible prion disease. *PLoS Pathog.* 7:e1002419. doi: 10.1371/journal.ppat.1002419

Makarava, N., Kovacs, G. G., Savtchenko, R., Alexeeva, I., Ostapchenko, V. G., Budka, H., et al. (2012). A new mechanism for transmissible prion diseases. Version 2. *J. Neurosci.* 32, 7345–7355. doi: 10.1523/JNEUROSCI.6351-11.2012

Makarava, N., Savtchenko, R., Alexeeva, I., Rohwer, R. G., and Baskakov, I. V. (2016). New molecular insight into mechanism of evolution of mammalian synthetic prions. *Am. J. Pathol.* 186, 1006–1014. doi: 10.1016/j.ajpath.2015.11.013

Makarava, N., Savtchenko, R., and Baskakov, I. V. (2015). Two alternative pathways for generating transmissible prion disease de novo. *Acta Neuropathol. Commun.* 3:69. doi: 10.1186/s40478-015-0248-5

Martín-Pastor, M., Codeseira, Y. B., Spagnolli, G., Eraña, H., Fernández, L. C., Bravo, S., et al. (2020). Structural features of an infectious recombinant PrP^{Sc} prion using solid state NMR. *bioRxiv*

Merz, P. A., Somerville, R. A., Wisniewski, H. M., and Iqbal, K. (1981). Abnormal fibrils from scrapie-infected brain. *Acta Neuropathol.* 54, 63–74. doi: 10.1007/BF00691333

Parrinello, M., and Rahman, A. (1981). Polymorphic transitions in single crystals: a new molecular dynamics method. *J. Appl. Phys.* 52:7182. doi: 10.1063/1.328693

Pettersen, E. F., Goddard, T. D., Huang, C. C., Couch, G. S., Greenblatt, D. M., Meng, E. C., et al. (2004). UCSF Chimera–a visualization system for exploratory research and analysis. *J. Comput. Chem.* 25, 1605–1612. doi: 10.1002/jcc.20084

Piro, J. R., Wang, F., Walsh, D. J., Rees, J. R., Ma, J., and Supattapone, S. (2011). Seeding specificity and ultrastructural characteristics of infectious recombinant prions. *Biochemistry* 50, 7111–7116. doi: 10.1021/bi200786p

Prusiner, S. B. (1982). Novel proteinaceous infectious particles cause scrapie. *Science* 216, 136–144. doi: 10.1126/science.6801762

Prusiner, S. B. (1998). Prions. *Proc. Natl. Acad. Sci. U.S.A.* 95, 13363–13383. doi: 10.1073/pnas.95.23.13363

Requena, J. R. (2020). The protean prion protein. *PLoS Biol.* 18:e3000754. doi: 10.1371/journal.pbio.3000754

Rudd, P. M., Endo, T., Colominas, C., Groth, D., Wheeler, S. F., Harvey, D. J., et al. (1999). Glycosylation differences between the normal and pathogenic prion protein isoforms. *Proc. Natl. Acad. Sci. U.S.A.* 96, 13044–13049. doi: 10.1073/pnas.96.23.13044

Rudd, P. M., Wormald, M. R., Wing, D. R., Prusiner, S. B., and Dwek, R. A. (2001). Prion glycoprotein: structure, dynamics, and roles for the sugars. *Biochemistry* 40, 3759–3766. doi: 10.1021/bi002625f

Sali, A., and Blundell, T. L. (1993). Comparative protein modelling by satisfaction of spatial restraints. *J. Mol. Biol.* 234, 779–815. doi: 10.1006/jmbi.1993.1626

Sevillano, A. M., Fernández-Borges, N., Younas, N., Wang, F., Elezgarai, S., Bravo, S., et al. (2018). Recombinant PrP^{Sc} shares structural features with brain-derived PrPSc: insights from limited proteolysis. *PLoS Pathog.* 14:e1006797. doi: 10.1371/journal.ppat.1006797

Smirnovas, V., Baron, G. S., Offerdahl, D. K., Raymond, G. J., Caughey, B., and Surewicz, W. K. (2011). Structural organization of brain-derived mammalian prions examined by hydrogen-deuterium exchange. *Nat. Struct. Mol. Biol.* 18, 504–506. doi: 10.1038/nsmb.2035

Smirnovas, V., Kim, J. I., Lu, X., Atarashi, R., Caughey, B., and Surewicz, W. K. (2009). Distinct structures of scrapie prion protein (PrP^{Sc})-seeded versus spontaneous recombinant prion protein fibrils revealed by hydrogen/deuterium exchange. *J. Biol. Chem.* 284, 24233–24241. doi: 10.1074/jbc.M109.036558

Spagnolli, G., Rigoli, M., Orioli, S., Sevillano, A. M., Faccioli, P., Wille, H., et al. (2019). Full atomistic model of prion structure and conversion. *PLoS Pathog.* 15:e1007864. doi: 10.1371/journal.ppat.1007864

Terruzzi, L., Spagnolli, G., Boldrini, A., Requena, J. R., Biasini, E., and Faccioli, P. (2020). All-atom simulation of the HET-s prion replication. *bioRxiv*

Tycko, R., Savtchenko, R., Ostapchenko, V. G., Makarava, N., and Baskakov, I. V. (2010). The α-helical C-terminal domain of full-length recombinant PrP converts to an in-register parallel β-sheet structure in PrP fibrils: evidence from solid state nuclear magnetic resonance. *Biochemistry* 49, 9488–9497. doi: 10.1021/bi1013134

Van Der Spoel, D., Lindhal, E., Hess, B., Groenhof, G., Mark, A. E., and Berendsen, H. J. C. (2005). GROMACS: fast, flexible, and free. *J. Comput. Chem.* 26, 1701–1718. doi: 10.1002/jcc.20291

Vázquez-Fernández, E., Vos, M. R., Afanasyev, P., Cebey, L., Sevillano, A. M., Vidal, E., et al. (2016). The structural architecture of an infectious mammalian prion using electron ryomicroscopy. *PLoS Pathog.* 12:e1005835. doi: 10.1371/journal.ppat.1005835

Wang, F., Wang, X., Yuan, C. G., and Ma, J. (2010). Generating a prion with bacterially expressed recombinant prion protein. *Science* 327, 1132–1135. doi: 10.1126/science.1183748

Wang, L. Q., Zhao, K., Yuan, H. Y., Wang, Q., Guan, Z., Tao, J., et al. (2020). Cryo-EM structure of an amyloid fibril formed by full-length human prion protein. *Nat. Struct. Mol. Biol.* 27, 598–602. doi: 10.1038/s41594-020-0441-5

Wille, H., Bian, W., McDonald, M., Kendall, A., Colby, D. W., Bloch, L., et al. (2009). Natural and synthetic prion structure from X-ray fiber diffraction. *Proc. Natl. Acad. Sci. U.S.A.* 106, 16990–16995. doi: 10.1073/pnas.0909006106

Wille, H., and Requena, J. R. (2018). The structure of PrP^{Sc} Prions. *Pathogens* 7:20. doi: 10.3390/pathogens7010020

Conflict of Interest: The authors declare that the research was conducted in the absence of any commercial or financial relationships that could be construed as a potential conflict of interest.

frontiers in Bioengineering and Biotechnology

ORIGINAL RESEARCH
published: 16 October 2020
doi: 10.3389/fbioe.2020.588947

Inhibition of α-Synuclein Aggregation and Mature Fibril Disassembling With a Minimalistic Compound, ZPDm

Samuel Peña-Díaz[1,2†], Jordi Pujols[1,2†], Francisca Pinheiro[1,2], Jaime Santos[1,2], Irantzu Pallarés[1,2], Susanna Navarro[1,2], María Conde-Gimenez[3], Jesús García[4], Xavier Salvatella[4,5], Esther Dalfó[6,7], Javier Sancho[3] and Salvador Ventura[1,2,5]*

[1] Institut de Biotecnologia i Biomedicina, Universitat Autònoma de Barcelona, Barcelona, Spain, [2] Departament de Bioquímica i Biologia Molecular, Universitat Autònoma de Barcelona, Barcelona, Spain, [3] Department of Biochemistry and Molecular and Cell Biology, Institute for Biocomputation and Physics of Complex Systems (BIFI), University of Zaragoza, and Aragon Institute for Health Research (IIS Aragon), Zaragoza, Spain, [4] Institute for Research in Biomedicine (IRB Barcelona), The Barcelona Institute of Science and Technology, Barcelona, Spain, [5] ICREA, Barcelona, Spain, [6] Medicine, M2, Universitat Autònoma de Barcelona (UAB), Barcelona, Spain, [7] Faculty of Medicine, University of Vic-Central University of Catalonia (UVic-UCC), Barcelona, Spain

OPEN ACCESS

Edited by:
Jesus R. Requena,
University of Santiago de Compostela, Spain

Reviewed by:
Eva Zerovnik,
Institut Jožef Stefan (IJS), Slovenia
Joaquín Castilla,
CIC bioGUNE, Spain

***Correspondence:**
Salvador Ventura
Salvador.Ventura@uab.cat;
salvador.ventura@uab.es

[†] These authors have contributed equally to this work

Specialty section:
This article was submitted to Biosafety and Biosecurity, a section of the journal Frontiers in Bioengineering and Biotechnology

Received: 29 July 2020
Accepted: 22 September 2020
Published: 16 October 2020

Citation:
Peña-Díaz S, Pujols J, Pinheiro F, Santos J, Pallarés I, Navarro S, Conde-Gimenez M, García J, Salvatella X, Dalfó E, Sancho J and Ventura S (2020) Inhibition of α-Synuclein Aggregation and Mature Fibril Disassembling With a Minimalistic Compound, ZPDm. Front. Bioeng. Biotechnol. 8:588947. doi: 10.3389/fbioe.2020.588947

Synucleinopathies are a group of disorders characterized by the accumulation of α-Synuclein amyloid inclusions in the brain. Preventing α-Synuclein aggregation is challenging because of the disordered nature of the protein and the stochastic nature of fibrillogenesis, but, at the same time, it is a promising approach for therapeutic intervention in these pathologies. A high-throughput screening initiative allowed us to discover ZPDm, the smallest active molecule in a library of more than 14.000 compounds. Although the ZPDm structure is highly related to that of the previously described ZPD-2 aggregation inhibitor, we show here that their mechanisms of action are entirely different. ZPDm inhibits the aggregation of wild-type, A30P, and H50Q α-Synuclein variants *in vitro* and interferes with α-Synuclein seeded aggregation in protein misfolding cyclic amplification assays. However, ZPDm distinctive feature is its strong potency to dismantle preformed α-Synuclein amyloid fibrils. Studies in a *Caenorhabditis elegans* model of Parkinson's Disease, prove that these *in vitro* properties are translated into a significant reduction in the accumulation of α-Synuclein inclusions in ZPDm treated animals. Together with previous data, the present work illustrates how different chemical groups on top of a common molecular scaffold can result in divergent but complementary anti-amyloid activities.

Keywords: α-synuclein, protein aggregation, amyloid inhibitor, Parkinson's disease, synucleinopathies, small molecules

INTRODUCTION

Parkinson's disease (PD) is an incurable disorder that affects around 0.3% of the population and more than 1% of people over 60 years of age (4% over 80 years), being the second most prevalent neurodegenerative disease worldwide (Nussbaum and Ellis, 2003; Dexter and Jenner, 2013; Kalia and Lang, 2015). Together with Dementia with Lewy Bodies (DLB) and Multiple System Atrophy (MSA), PD is part of a group of human disorders known

as synucleinopathies (Spillantini et al., 1998a,b; Fanciulli and Wenning, 2015). Intracellular proteinaceous inclusions constitute the main culprit of neuronal damage and disease progression in the synucleinopathies, although the aggregates accumulate in different cell types and affect distinct brain regions depending on the disease (Fellner et al., 2011; Luk et al., 2012). These abnormal protein deposits are mostly composed of aggregated α-synuclein (α-Syn). In the particular case of PD, α-Syn aggregation occurs in the dopaminergic neurons of *substantia nigra pars compacta*. As a consequence, PD suffering patients display reduced dopamine levels, which results in the archetypic motor and non-motor symptoms of the disease (Spillantini et al., 1997). Indeed, single-point mutations and multiplications of the gene that encodes for α-Syn (*SNCA*) (Singleton et al., 2003; Ibanez et al., 2004) have been related to familial cases of PD with early-onset (Polymeropoulos et al., 1997), thus reinforcing the connection between α -Syn and PD.

α-Syn is an intrinsically disordered protein highly expressed in the brain and associated with vesicle trafficking in healthy conditions (Bendor et al., 2013). In pathological situations, α-Syn aggregates into oligomers and amyloid fibrils that compromise cellular homeostasis, exert toxicity and ultimately lead to neuronal death (Serpell et al., 2000). Remarkably, diffusible aggregated species can be internalized by healthy neighboring neurons, where they seed the aggregation of soluble α-Syn molecules, a mechanism that has been compared with the templated conformational conversion occurring in prion diseases (Hansen et al., 2011). As it occurs in prions, α-Syn assemblies can present diverse structural arrangements, forming strains (Li et al., 2018) that differ in their aggregation properties (Bousset et al., 2013), and target distinct brain regions and cell types (Lau et al., 2020).

Many of the current therapeutic approaches for PD aim to reduce the neuronal load of aggregated α-Syn, either by targeting the α-Syn polypeptide directly or through indirect approaches such as the stimulation of degradation pathways (Spencer et al., 2009; Decressac et al., 2013; Xilouri et al., 2013) and gene silencing (Faustini et al., 2018; Kantor et al., 2018; Lassot et al., 2018; Zharikov et al., 2019). Among them, the identification of small compounds that might act as chemical chaperones blocking the aggregation and propagation of α-Syn or, in the best-case scenario, dismantling α-Syn mature aggregates into non-toxic species is receiving increasing attention. However, the disordered nature of α-Syn, together with the multiplicity of conformationally different species that populate the aggregation process, imposes significant difficulties for the rational design of effective α-Syn binders. For this reason, high-throughput screening (HTS) of large chemical libraries has become a significant focus of research in the hunt for disease-modifying lead compounds (Silva et al., 2011).

To analyze the inhibitory potential of a chemical library with more than 14,000 chemically diverse structures, we optimized a robust HTS screening protocol (Pujols et al., 2017) based on Thioflavin-T (Th-T) fluorescence, light-scattering measurements and Transmission Electron Microscopy (TEM). This pipeline was used to discover and characterize small molecules that act as potent inhibitors of α-Syn amyloid formation, such as SynuClean-D (SC-D) (Pujols et al., 2018) and ZPD-2 (Pena-Diaz et al., 2019). In the present work, we present and characterize ZPDm (**Figure 1**), a novel molecule identified in the primary HTS screen. ZPDm was the smallest compound in the library displaying a significant inhibitory potency at a substoichiometric concentration. ZPDm prevents the aggregation of *wild type* α-Syn and the familial A30P and H50Q variants. The molecule acts preferentially at the late stages of the polymerization reaction, suggesting that it targets preferentially ordered aggregates. Indeed, ZPDm is highly effective at disaggregating the mature α-Syn fibrils of different strains. To the best of our knowledge, it constitutes the minimal synthetic molecule that *co*njugates inhibitory and α-Syn fibril disrupting activity in the same chemical scaffold. These *in vitro* activities are translated into the ability to reduce significantly α-Syn aggregation in a well-established *Caenorhabditis elegans* (*C. elegans*) model of PD.

MATERIALS AND METHODS

Protein Expression and Purification

WT α-Syn and its variants (H50Q and A30P) were expressed and purified as previously described (Pujols et al., 2017); the obtained protein was lyophilised and kept at -80°C until its use.

In vitro Aggregation of α-Syn

Lyophilised α-Syn was carefully resuspended in sterile PBS 1X and filtered through 0.22 μm membrane to discard small aggregates. Aggregation was performed at 70 μM of α-Syn (WT, H50Q or A30P) in a sealed 96-well plate, in a total volume of 150 μL. 40 μM Th-T in PBS 1X, a 1/8" diameter Teflon polyball (*Polysciences Europe GmbH, Eppelheim, Germany*) and 100 μM ZPDm, (trifluoromethyl)benzene or DMSO (in control samples)

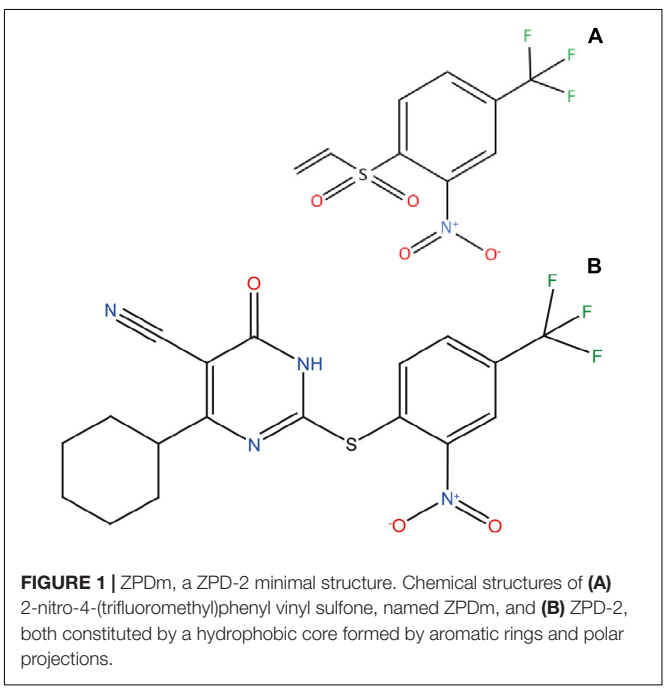

FIGURE 1 | ZPDm, a ZPD-2 minimal structure. Chemical structures of **(A)** 2-nitro-4-(trifluoromethyl)phenyl vinyl sulfone, named ZPDm, and **(B)** ZPD-2, both constituted by a hydrophobic core formed by aromatic rings and polar projections.

were also added to each well. The plate was incubated at 37°C and 100 rpm fixed in an orbital shaker Max-Q 4000 (Thermo Fisher Scientific, Waltham, Massachusetts, United States). Every 2 h, Th-T fluorescence was measured in a Victor3.0 Multilabel Reader (PerkinElmer, Waltham, Massachusetts, United States), exciting through a 430–450 nm filter and collecting emission signal with a 480–510 filter. Each assay was done in triplicate and the values of the kinetic fitted according to the following equation:

$$\propto = 1 - \frac{1}{k_b(e^{k_a t - 1}) + 1} \quad (1)$$

where k_b and k_a constitute the homogeneous nucleation rate constant and the autocatalytic rate constant, respectively (Crespo et al., 2016).

ZPDm was added at different concentrations in the titration assays (200, 150, 100, 75, and 50 μM). In time-dependent assays, 7 independent aggregation reactions were prepared simultaneously and incubated as aforementioned in a 96-well plate as triplicates. 100 μM of ZPDm were added at different time points after the reaction had begun (4, 8, 12, 16, 20, and 24 h). In all cases α-Syn concentration was constant at 70 μM. An equivalent volume of DMSO was added to the control sample at the beginning of the reaction.

For the study of the disaggregation assays, α-Syn 70 μM was incubated in a 96-well plate as previously described for 2 days and Th-T fluorescence measured. Then, ZPDm was added to a final concentration of 100 μM. The plate was incubated for an additional 24 h and Th-T fluorescence was measured.

Strains were generated as previously described (Bousset et al., 2013; Peelaerts et al., 2015; Li et al., 2018; Carija et al., 2019). Briefly, α-Syn was resuspended in PBS 1X and dialysed for 24 h in a 1:1,000 (v/v) ratio with either buffer B (50 mM Tris-HCl pH 7.0) or buffer C (50 mM Tris-HCl pH 7.0, 150 mM NaCl). Dialysed samples were filtered through 0.22 μm membranes and incubated at 70 μM for 2 days as described above. ZPDm was added to a final concentration of 100 μM and plates incubated for additional 24 h. Then, Th-T fluorescence was measured.

Light-Scattering

80 μL of end-point aggregates were collected, placed into a quartz cuvette and analyzed in a Cary Eclipse Fluorescence Spectrophotometer (Agilent, Santa Clara, CA, United States) by exciting at 300 and 340 nm and 90^o collecting between 280 and 360 nm.

Transmission Electron Microscopy (TEM)

End-point α-Syn aggregates were collected and Diluted 1/10 (v/v) in PBS 1X. Diluted samples were gently sonicated for 5 min and 5 μL of the resultant sample were placed on a carbon-coated copper grid for 5 min. Using a filter paper, the grids were dried to remove the excess of sample and washed twice with miliQ water. Finally, 5 μL of 2% (w/v) uranyl acetate were added and left incubate for 2 min. As previously indicated, the excess of uranyl acetate was removed, and grids were left to air-dry for 10 min. Images were obtained using a Transmission Electron Microscopy Jeol 1400 (Peabody, MA, United States) operating at an accelerating voltage of 120 kV. A minimum of 30 fields were screened per sample, in order to collect representative images.

Protein Misfolding Cyclic Amplification (PMCA)

PMCA protocol was performed as previously described (Herva et al., 2014). Briefly, α-Syn was resuspended in Conversion Buffer (PBS 1X, 1% Triton X-100, 150 mM NaCl) to a final concentration of 90 μM and supplemented with Complete Protease Inhibitor Mixture (Roche Applied Science, Penzberg, Germany). 60 μL of this solution were loaded into 200 μL PCR tubes containing 1.0 mm silica beads (Biospec Products, Bartlesville, OK, United States). α-Syn was then exposed to 24 h cycles of 30 s sonication and 30 min of incubation at 37°C, using a Misonix 4000 sonicator, at 70% power. The incubated sample was recovered after each 24 h cycle and 1 μL was added to a new PCR tube containing fresh α-Syn at 90 μM. In the case of ZPDm treated samples, the compound was added to the fresh sample in each step to a final concentration of 128 μM, which corresponds to the 0.7:1 α-Syn:ZPDm ratio of the previous aggregation assays. Untreated samples were prepared adding the same concentration of DMSO (0.26%) present in the treated mixtures. This process was repeated for 5 days. All the reactions were made in triplicate.

Ten microliter of aggregated samples at the end of each cycle were diluted 1:10 with 90 μL of PBS 1X, 40 μM Th-T. Th-T fluorescence emission was measured in a Cary Eclipse Fluorescence Spectrophotometer (Agilent, Santa Clara, CA, United States), by exciting the samples at 445 nm and collecting the emission signal between 460 and 600 nm.

Proteinase K Digestion

18 μL of PMCA-aggregated α-Syn were incubated with 6 μL of Proteinase K (5 μg/mL as final concentration) for 30 min at 37°C. Then, 8 μL of loading buffer containing 1% β-mercaptoethanol was added and the sample was incubated 10 min at 95°C for PK inactivation. Finally, 7 μL of the samples were loaded into a Tricine-SDS-PAGE gel. Unstained Protein Standard markers (Thermo Fisher Scientific, Waltham, MA, United States) were used as a reference. Gels were stained with Blue safe.

Nuclear Magnetic Resonance (NMR)

^{15}N-labeled human WT α-Syn was expressed in *E. coli BL21 DE3* strains. Cells were grown in LB medium until the optical density (OD) at 600 nm reached a level of 0.6. Cultures were then centrifuged at 3,000 rpm for 15 min and the obtained pellets resuspended in 1 L of minimal medium: 768 mL of miliQ water with 1 mL of ampicillin 100 mg/mL, 100 μL $CaCl_2$ 1M, 2 mL $MgSO_4$ 2 M, 20 mL glucose 20%, 10 mL vitamins 100x (Sigma-Aldrich, Darmstadt, Germany), 200 mL salts M9 and 1 g $^{15}NH_4$ (Cambridge Isotope Laboratories, Inc., Tewksbury, MA, United States). Cells were incubated for 1 h at 250 rpm and 37°C. Finally, 1 mM IPTG was added to induce protein expression for 4 h. Protein was purified as previously described (Pujols et al., 2017).

Caenorhabditis Elegans Assays

Maintenance

Animals synchronization was carried out by bleaching and overnight hatching in M9 (3 g/L KH_2PO_4, 6 g/L Na_2HPO_4, 5 g/L NaCl, 1 M $MgSO_4$) buffer. Thus, nematodes were cultured at 20°C on growth media plates (NGM) containing 1 mM $CaCl_2$, 1 mM $MgSO_4$, 5 μg/mL cholesterol, 250 M KH_2PO_4 pH 6.0, 17 g/L Agar, 3 g/L NaCl. Plates were previously seeded with *E. coli OP50* strain. Nematodes were maintained using standard protocols (Brenner, 1974).

Strains

Strain NL5901, *unc-119(ed3) III; pkIs2386* [*Punc-54*::α-*SYN*::*YFP; unc-119(+)*] was obtained from the *C. elegans* Genetic Center (CGC). For the α-Syn induced dopaminergic degeneration analysis, strain UA196 (Harrington et al., 2012), gifted generously by the laboratory of Dr. Guy Caldwell (Department of Biological Science, The University of Alabama, Tuscaloosa, United States), was used; [*sid-1(pk3321); baIn33* [*Pdat-1*::*sid-1, Pmyo-2*::*mCherry*]; *baIn11* [*Pdat-1*::α-*SYN; Pdat-1*::*GFP*]). In the main text, this strain was named *Pdat-1*::*GFP; Pdat-1*::α *-SYN*.

ZPDm Administration

After cooling, the autoclaved NGM agar medium (1 mM $CaCl_2$, 1 mM $MgSO_4$, 5 μg/mL cholesterol, 250 M KH_2PO_4 pH 6.0, 17 g/L Agar, 3 g/L NaCl) was enriched with 100 μM of a stock solution of 4 mM ZPDm in 0.2% DMSO to a final concentration of 10 μM. After 2 days, plates were seeded with 250 μL of *E. coli OP50* with 10 μM of ZPDm. Nematodes were placed on the plates at larval stages L4 and exposed either to ZPDm or DMSO (controls) for 7 days. Daily transfer was done to avoid cross progeny.

Aggregate Quantification

The number of cellular inclusions was quantified as previously described (van Ham et al., 2008; Munoz-Lobato et al., 2014). Briefly, NL5901 (*Punc-54*::α-*SYN*::*YFP*) worms were age-synchronized and left overnight to hatch. Nematodes in phase L1 were cultured and grown into individual NGM plates seeded with *E. coli* OP50. When animals reached L4 developmental stage, they were transferred onto either ZPDm treated plates or DMSO treated plates (negative control). Every day, animals were transferred into a new plate to avoid cross contamination. At stage L4+7, the aggregates in the anterior part of every single animal were counted. For each experiment, thirty 7-days old nematodes per treatment were analyzed using a Nikon Eclipse E800 epifluorescence microscope equipped with an Endow GFP HYQ filter cube (Chroma Technology Corp., Bellows Falls, Vermont United States) and each experiment was carried out in triplicate. Inclusions could be described as discrete bright structures, with edges distinguishable from surrounding fluorescence. ImageJ software was used for measuring the number of cellular aggregates considering the area dimensions. For the quantification of α-syn aggregates in *C. elegans* one single image was taken from each animal. However, every image contained among 30–45 stacks (1 μm) that allowed to detect aggregates that are at different positions.

Microscopy and Imaging

Animals were placed in a 1 mM solution of sodium azide and mounted with a coverslip on a 4% agarose pad. Animals were visualized with a Nikon Eclipse E800 epifluorescence microscope. The system acquires a series of frames at specific *Z*-axis position (focal plane) using a *Z*-axis motor device. Animals were examined at 100 × magnification to examine α-Syn induced DA cell death and at 40× to examine α-Syn apparent aggregate.

Statistical Analysis

All graphs were generated with GraphPad Prism 6.0 software (GraphPad Software Inc., La Jolla, CA, United States). Data were analyzed by two-way ANOVA Tukey test using SPSS software version 20.0 (*IBM Analytics, Armonk, NY, United States*) and *t*-test using GraphPad software version 6.0 (GraphPad Software Inc., La Jolla, CA, United States). All data are shown as means and standard error of mean (SEM). $P < 0.05$ was considered statistically significant. In the graphs *, **, and *** indicate $p < 0.05$, $p < 0.01$, and $p < 0.001$, respectively.

RESULTS

ZPDm Inhibits α-Synuclein Aggregation *in vitro*

ZPDm is a molecule that was initially identified as a positive hit in the HTS performed by our lab back in 2017 on top of the HitFinder^{TM} chemical library from Maybridge (Pujols et al., 2017). Although they were found independently, structurally, ZPDm is a minimalistic version of ZPD-2 (Pena-Diaz et al., 2019) with a reduced MW, LogP, and TPSA, which, in principle, would increase its drug-likeness (**Figure 1** and **Table 1**). Still, ZPDm implements the generic physicochemical properties common to most of the published inhibitors of α-Syn aggregation, namely, a planar hydrophobic core formed by aromatic rings that interact with apolar exposed regions in α-syn assemblies. This core is frequently coated with polar projections that interfere with hydrophobic packing and disrupt intermolecular hydrogen

TABLE 1 | SwissADME predicted properties of ZPDm and ZPD-2.

	ZPDm	ZPD-2
Molecular weight (g/mol)	281.21	424.4
Heavy atoms	18	29
Aromatic heavy atoms	6	12
H-bond acceptors	7	8
H-bond donors	0	1
TPSA (Å^2)	88.34	140.66
Log $P_{O/W}$	2.42	3.9
Solubility (mg/mL)	9.28E-02	1.94E-03
GI absorption	High	Low
Drug-like (Lipinski)	0 violations	0 violations
Drug-like (Veber)	0 violations	1 violations
Drug-like (Egan)	0 violations	2 violations
Leadlikeness	0 violations	2 violations

bonds; they difficult elongation and, eventually, might promote fibril disassembly (Pujols et al., 2020). A benzene ring constitutes the hydrophobic moiety of ZPDm, connected to three polar groups—vinyl sulfone, nitro, and trifluoromethyl – in carbon positions 1, 2, and 4, respectively. Remarkably, the ZPD-2 chemical structure displays the same functional groups in carbons 1, 2, and 4 of the primary phenyl ring. However, the vinyl sulfone is substituted by a sulfide group that extends the molecule to incorporate additional aromatic moieties, which we previously assumed to be critical for its activity (Pena-Diaz et al., 2020). Thus, ZPDm can be considered as a building block for the synthesis of the more complex ZPD-2 molecule. Considering these structural differences, we performed a set of orthogonal experiments to contrast if, as ZPD-2, ZPDm might turn to be a lead compound with significant α-Syn anti-aggregational activity.

The incubation of 70 μM α-Syn with 100 μM ZPDm inhibited the protein aggregation, decreasing the final Th-T fluorescence signal by 60% compared to control untreated samples (**Figure 2A**). Fitting of the kinetic data to a typical sigmoidal nucleation-polymerization reaction revealed that ZPDm diminishes the primary nucleation rate constant by eightfold (k_b = 0.0034), relative to the control reaction

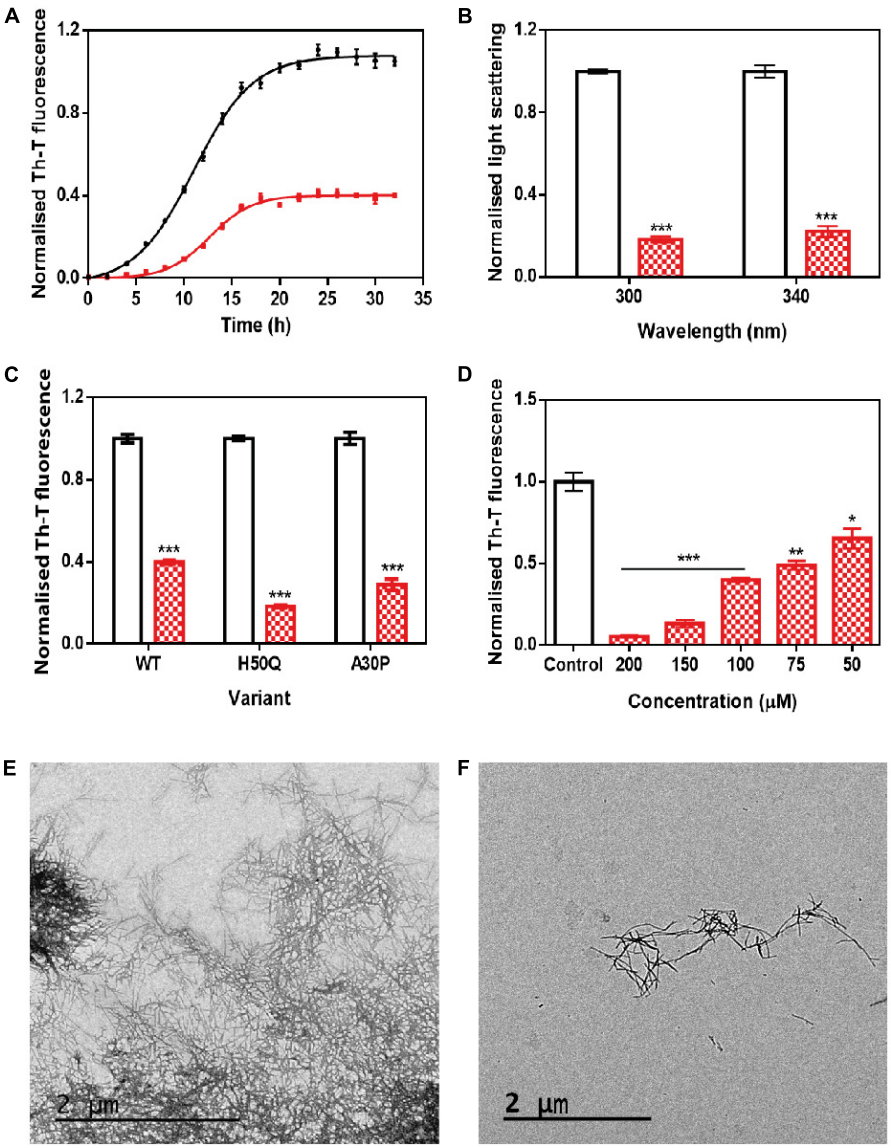

FIGURE 2 | *In vitro* analysis of the capacity of ZPDm to inhibit α-Syn aggregation. **(A)** α-Syn aggregation kinetics in the absence (black) and presence (red) of 100 μM of ZPDm followed by Th-T fluorescence. **(B)** Light-scattering measurements at 300 and 340 nm, in the absence (white) and presence (red) of ZPDm. **(C)** H50Q and A30P α-Syn variants aggregation in the absence (white) and presence (blue) of ZPDm. **(D)** Inhibition of α-Syn aggregation with different concentrations of ZPDm. **(E,F)** Representative TEM images in the absence **(E)** and presence **(F)** of ZPDm. Th-T fluorescence is plotted as normalized means. Final points were obtained at 48 h. Error bars are represented as SE of mean values; $*p < 0.05$, $**p < 0.01$, and $***p < 0.001$. ZPDm prevents the aggregation of WT, A30P, and H50Q α-Syn variants *in vitro*, even at substoichiometric ratios.

(k_b = 0.0275), at the expenses of a slightly higher autocatalytic rate constant, with k_a of 0.449 and 0.323 h^{-1} for ZPDm treated and untreated samples, respectively. This results in t_0 and $t_{1/2}$ being increased by 4 and 2 h, respectively, in the compound's presence. Light-scattering measurements at 300 and 340 nm at the end of the reaction reported a decrease of 81 and 78% in the dispersed light (**Figure 2B**) in the presence of ZPDm, respectively, consistent with a reduction of the total aggregated material. The visual inspection of α-Syn samples by TEM corroborated a reduction in the number of amyloid fibrils per field in the presence of ZPDm (**Figure 2F**), compared to untreated samples (**Figure 2E**). A titration assay in which we incubated 70 μM α-Syn in the presence of decreasing amounts of ZPDm indicated a dose-dependent inhibition, with a statistically significant activity at a substoichiometric concentration of 50 μM, at which ZPDm still reduces the Th-T signal at the end of the reaction by 35% (**Figure 2D**).

We further examined if ZPDm was able to prevent the aggregation of two mutants of α-Syn, H50Q, and A30P, which have been associated with familial PD (Kruger et al., 1998; Appel-Cresswell et al., 2013). The incubation of these α-Syn variants with ZPDm reduced Th-T fluorescence at the end of the reaction by 81 and 71% for H50Q and A30P, respectively (**Figure 2C**).

ZPDm, ZPD-2, and SC-D and other positive hits in the library, share a common property, the presence of a trifluoromethyl group connected to an aromatic ring. We hypothesized that perhaps we were in front of the minimal inhibitory unit, which might be very useful for future Structure Activity Relationship (SAR) studies. Therefore, we synthesized the (trifluoromethyl)benzene moiety and assessed its anti-aggregational potential (**Supplementary Figure S1**). Both kinetic data using Th-T and light scattering measurements converged to indicate that this molecule is devoid of any activity, suggesting that it might be necessary, but not sufficient to endorse ZPDm with the above-described anti-aggregation properties.

ZPDm Prevents α-Syn Aggregation in Protein Misfolding Cyclic Amplification Assays

We used protein-misfolding cyclic amplification (PMCA) to test the inhibitory capacity of ZPDm under continuous seeding conditions. Based on the nucleation-dependent polymerization model for prion replication, PMCA is a technique that forces aggregation to happen by seeding soluble α-Syn with preformed fibrils (Jung et al., 2017). After the first round of fibril elongation, aggregates are sonicated and used as seeds for the second cycle of PMCA. A representative sample from each cycle is then treated with proteinase K (PK) and analyzed by SDS-PAGE, to evidence fibril formation, since in contrast to soluble α-Syn, the fibrils are significantly resistant to proteolysis. Using this protocol, PK-resistant species could be observed already in the 1st cycle of PMCA in untreated samples, with a maximum of PK resistance at the 4th cycle (**Figure 3A**). Th-T fluorescence measurements of the same samples indicated that this protection correlates with the presence of amyloid-like assemblies (**Figure 3C**). In contrast, in the presence of ZPDm, PK-resistant species are absent until the 3rd cycle, and they never reach the levels of the control samples, although certain adaptation of misfolded α-Syn to ZPDm seems to occur in cycles 4th and 5th (**Figure 3B**). The Th-T fluorescence signal is negligible in the two first PMCA cycles and significantly lower than that of control samples at any considered cycle (**Figure 3C**).

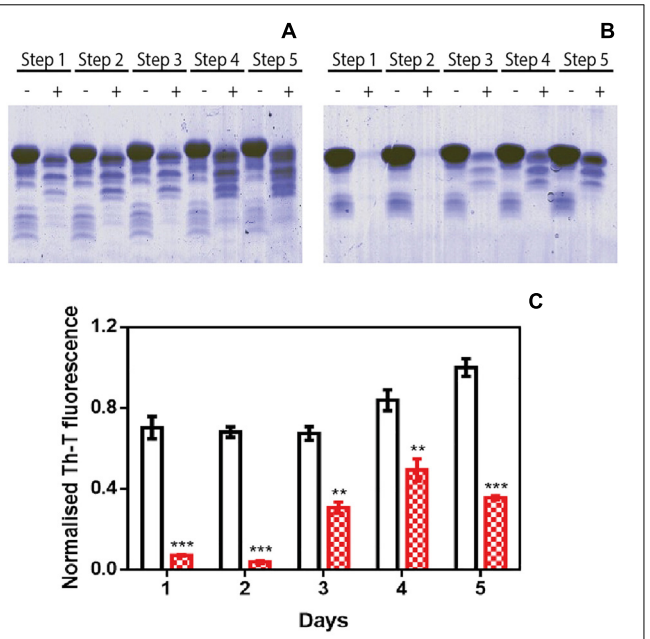

FIGURE 3 | Inhibitory activity of ZPDm in PMCA assays. **(A,B)** Bis/Tris SDS-PAGE gels of PMCA samples in the absence **(A)** and presence **(B)** of ZPDm, before (–) and after (+) PK digestion. **(C)** Th-T fluorescence of different PMCA cycles in samples treated (red) and untreated (white) with ZPDm. Th-T fluorescence is plotted as normalized means. Error bars are represented as SE of mean values; $^{**}p < 0.01$ and $^{***}p < 0.001$. ZPDm anti-aggregation activity results in delayed formation of PK-resistant and Th-T positive amyloid structures.

ZPDm Exhibits Amyloid Disaggregation Activity *in vitro*

ZPD-2 does not interact with soluble and monomeric α-Syn and, therefore, is not expected to interfere with the protein's functional state. Nuclear Magnetic Resonance ^{1}H-^{15}N HSQC spectra of N^{15} labeled α-Syn in the presence and absence of ZPDm, indicates that this is also the case for this smaller molecule since we could not identify any perturbations in chemical shifts or peak intensities in the spectra **(Supplementary Figure S2)**.

To address the time window in which ZPDm remains active, we set up an experiment in which a constant amount of ZPDm was added to different aggregation reactions at different time intervals after the reaction has begun (**Figure 4A**). To our surprise, the respective Th-T signals indicated that the anti-amyloid activity increased as the reaction progressed, which is in stark contrast with the behavior of ZPD-2, which was mostly active when added at the early stages of the reaction and inactive when added at the plateau phase (Pena-Diaz et al., 2019). The time-dependent activity profile of ZPDm can only be explained

if this compound recognizes the Th-T positive aggregated species and exerts an intense fibril disruption activity. To confirm this extent, α-Syn mature fibrils were incubated for 24 h with ZPDm. The Th-T fluorescence analysis revealed that treated samples suffered a signal reduction of 74% (**Figure 4B**). This data was supported by TEM images, which illustrated the disruption of large fibrillar clusters into shorter fibrils or amorphous aggregates (**Figures 4C,D**).

We assessed if this amyloid-disrupting activity was independent of the conformational properties of the mature fibrils, by aggregating α-Syn in 50 mM Tris–HCl pH 7.0 in the absence or presence of 150 mM NaCl, which generates two different strains, known as strain B and C, respectively (Bousset et al., 2013; Carija et al., 2019). As shown in **Figure 4**, the addition of ZPDm to the mature fibrils of these strains promoted a significant decrease in the amount of amyloid-like material as monitored both by Th-T fluorescence and TEM 24 h after the addition of the molecule (**Figure 5**). These data suggest that in contrast to ZPD-2, insensitive to preformed amyloid fibrils, ZPDm is endorsed with a generic and potent disaggregation activity.

ZPDm Decreases the Formation of α-Syn Aggregates in a *C. elegans* Model of PD

We decided to test if the ZPDm *in vitro* activity can be translated *in vivo* to a simple animal model of PD. To do so, we employed the well-described strain NL5901 of *C. elegans*. In this strain, α-Syn is fused to Yellow Fluorescence Protein (YFP) and expressed under the control of *the unc-54* promoter, transgene *pkIs2386 [Punc-54::α-SYN::YFP]* (Hamamichi et al., 2008; van Ham et al., 2008), generating protein inclusions in body wall muscle cells. ZPDm was administered in the food at 10 μM final concentration to animals at the L4 stage, and they were examined 7 days later, 9 days after hatching (L4+7). These aged worms are intended to mimic aged PD patients. We used epifluorescence microscopy to visualize the fluorescent aggregates. The images demonstrated that ZPDm reduced the formation of muscular inclusions by 43% (**Figure 6A**), with an average of 20.2 ± 2.13 apparent α-Syn aggregates in treated worms (**Figure 6C**) compared with the 35.2 ± 3.04 observed in control samples (**Figure 6B**).

DISCUSSION

The identification of small compounds that may abrogate the process of protein aggregation in neurodegenerative disorders is attracting increasing interest, both in academia and industry (Pujols et al., 2020).

The lack of structural information about the intermediate species that populate the reaction, and the intrinsically disordered nature of many of the proteins behind these diseases, has made it challenging to use of structure-guided drug design for amyloid inhibitors. Only recently, the high-resolution structures of the fibrils formed by proteins connected to different amyloidosis have allowed the rational design of peptides that interfere with the growth or seeding of the fibrils (Seidler et al., 2018; Saelices et al., 2019; Sangwan et al., 2020). However, because peptides usually display poor pharmacokinetics, which should be significantly optimized before they become drugs, small molecules are still the preferred option for the treatment of the diseases caused by the aggregation of proteins within the brain.

The screening of large chemical libraries in the search for α-Syn aggregation inhibitors has provided potent molecules like anle138b (Wagner et al., 2013), BIOD303 (Moree et al., 2015), SynuClean-D (Pujols et al., 2018), 582032 (Toth et al., 2019) or the collection of compounds recently reported by Kurnik et al. (2018). All these molecules display two or more aromatic rings in their structures, a property that is shared by active polyphenols like curcumin (Pandey et al., 2008), EGCG (Bieschke et al., 2010), and baicalein (Jiang et al., 2010), repurposed inhibitors like Fasudil (Tatenhorst et al., 2016), and LMTM (Schwab et al., 2017) or compounds generated by rational design like NPT100-18A (Wrasidlo et al., 2016). Usually, the aromatic rings form a planar hydrophobic core that is thought to interact with apolar exposed regions in α-Syn or its assemblies. However, despite the presence of multiple aromatic groups is recurrent in natural α-Syn aggregation inhibitors and many of the reported screening efforts result in the identification of this kind of molecules, several natural compounds exhibiting a single aromatic ring have been shown to act as α-Syn aggregation modulators (**Supplementary Figure S3**), including scyllo-inositol, gallic acid, dopamine, safranal and caffeic acid (Herrera et al., 2008; Di Giovanni et al., 2010; Liu et al., 2014; Ibrahim and McLaurin, 2016; Save et al., 2019).

We recently used a robust high-throughput screening pipeline to uncover molecules able to modulate α-Syn fibrillation (Pujols et al., 2017). Among the active compounds, we searched for a small compound bearing a single aromatic ring. We identified ZPDm, which, interestingly enough, is a minimal version of ZPD-2, a potent inhibitor identified in the same library (Pena-Diaz et al., 2019), with half of its heavy aromatic atoms. This opened an opportunity to approach a comparative SAR for these molecules.

ZPDm reduces the *in vitro* aggregation of WT α-Syn and the protein's A30P and H50Q familial variants in a 60%, or higher, at a 0.7:1 (protein: ZPDm) ratio. This activity was orthogonally confirmed by light-scattering and TEM. Moreover, the inhibitory activity of ZPDm reduced the number of PK-resistant and Th-T positive species in PMCA assays, thus interfering with α-Syn templated seeding and/or aggregates amplification (Herva et al., 2014). It should be explored whether adaptation of α-Syn to ZPDm at late PMCA stages might translate in some resistance to the molecule during aggregates propagation.

Solution NMR measurements indicated that ZPDm was not interacting with soluble α-Syn monomers, and, therefore, it is not expected to impact the physiological function of the protein. Moreover, the addition of ZPDm at different time points of the aggregation reaction suggested that ZPDm is mainly active at the latest stages of the aggregation and indeed, further analysis demonstrated that the molecule is capable of disassembling mature α-Syn amyloid fibrils generated under different solution conditions, conceptually similar to the α-Syn strains observed in different synucleinopathies (Bousset et al., 2013; Peelaerts et al., 2015). Importantly, these features translate into a significant reduction in the number of

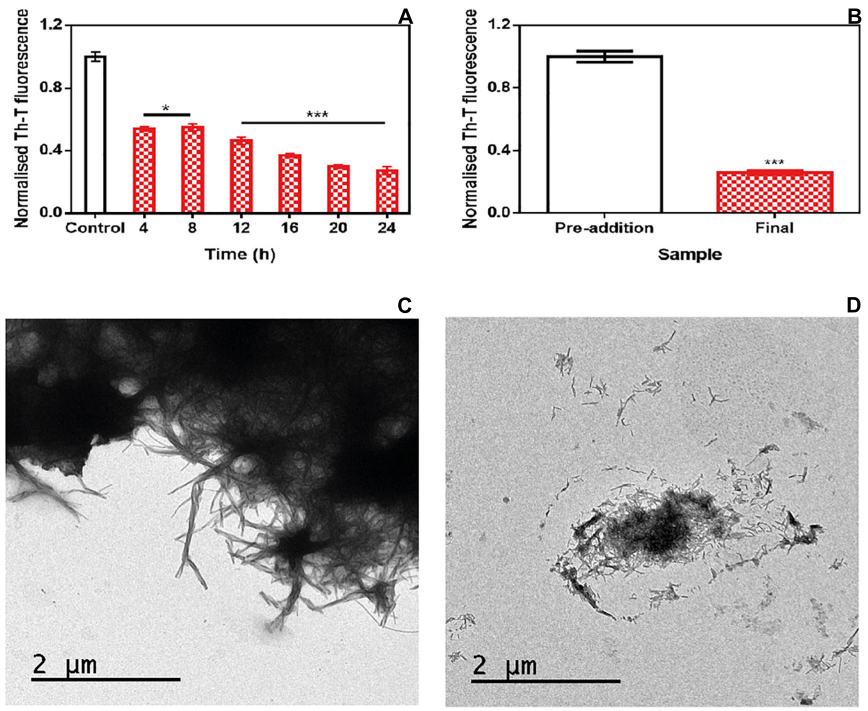

FIGURE 4 | Disaggregational activity of ZPDm. **(A)** Th-T fluorescence of α-Syn end-point aggregates after the addition of ZPDm at different time points during the aggregation kinetics. **(B)** Th-T fluorescence assay before and 24 h after the addition of ZPDm to mature α-Syn fibrils. **(C,D)** Representative TEM images in the absence **(C)** and presence **(D)** of ZPDm. Th-T fluorescence is plotted as normalized means. Error bars are represented as SE of mean values; $^{*}p < 0.05$ and $^{***}p < 0.001$. ZPDm inhibitory capacity increases with the reaction progress, indicating that the compound may interact with aggregated structures and disentangle them.

apparent aggregates in the muscular cell wall of a *C. elegans* model of PD when the compound is added in the food at a concentration of 10 uM; whether this i*n vivo* anti-aggregational effect results in animal phenotypic benefits should be further explored.

The above-described results illustrate how despite ZPD-2 and ZPDm share a significant part of their chemical structure and both are effective α-Syn aggregation inhibitors, their mechanism of action differs significantly, with ZPD-2 acting preferentially at the early stages of the fibrillation and becoming inactive once the polymerization has advanced significantly, being devoid of detectable fibril disrupting activity.

In contrast, ZPDm is more effective at later stages and behaves as a robust disaggregating agent. The fact that (trifluoromethyl)benzene is an inactive molecule indicates that the bulk of the structure shared by ZPD-2 and ZPDm acts as a building block and that the particular chemistry and spatial disposition of the groups that decorate this moiety are responsible for the different mode of action of these compounds. For instance, the (trifluoromethyl)benzene contains the aromatic ring common to the vast majority of small active compounds. However, it lacks a strong hydrogen bond donor/acceptor, which is another characteristic common to many of these molecules (**Supplementary Figure S3**). Therefore, our data suggest that these are the minimum requirements for an active α-Syn aggregation inhibitor. The aromatic rings would allow interactions with hydrophobic regions, and the polar groups might disrupt the abundant short inter-strand hydrogen bonds that contribute to the amyloid structure's sustainment. Indeed, despite their different size, the number of hydrogen bonds acceptors in ZPD-2 and ZPDm is fairly similar (**Table 1**). Despite speculative, the preferential affinity for early-stage aggregates exhibited by ZPD-2 could be explained by its extended aromatic core and higher Log $P_{O/W}$, which might facilitate interactions with exposed hydrophobic patches in oligomers and small aggregates. In contrast, the compact structure of ZPDm might allow targeting defined binding pockets at the ends of amyloid fibrils, interfering with fibril elongation, and eventually disrupting pre-formed non-covalent interactions.

From a pharmacokinetic point of view, ZPDm is predicted to be more soluble than ZPD-2, to exhibit a higher gastrointestinal absorption and better drug-likeness (**Table 1**). ZPDm is also predicted to be a better lead compound from a medicinal chemistry perspective than ZPD-2 (**Table 1**).

To the best of our knowledge, the only other active molecule with a single aromatic ring derived from the screening of a large chemical library is the compound 576755 (Toth et al., 2019), which in addition to a benzene ring, displays the expected hydrogen bonds acceptors/donors (**Supplementary Figure S3**). 576755 is a potent aggregation inhibitor that acts at the oligomerization stage both *in vitro* and *in cells*. However,

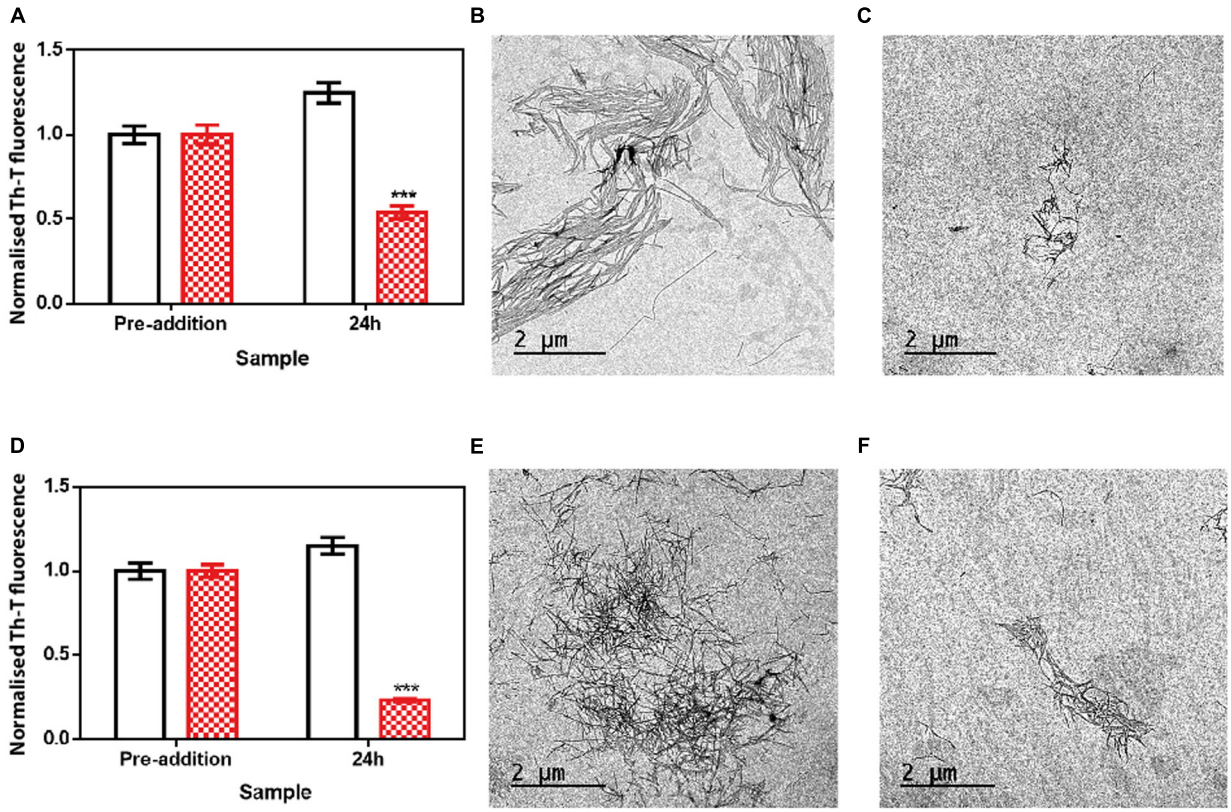

FIGURE 5 | Disaggregational effect of ZPDm in preformed fibrils of two different strains. **(A)** Strain B aggregates disaggregation in the presence (red) and absence (white) of ZPDm as monitored by Th-T fluorescence. **(B,C)** Representative TEM images of untreated **(B)** and ZPDm treated **(C)** samples. **(D)** Strain C aggregates disaggregation in presence (red) and absence (white) of ZPDm as monitored by Th-T fluorescence. **(E,F)** Representative TEM images of untreated **(E)** and ZPDm treated **(F)** samples. Data are shown as means, and error bars are shown as the SE of means; ***$p < 0.001$. The disaggregational ability of ZPDm is also observed in two morphologically different α-Syn strains.

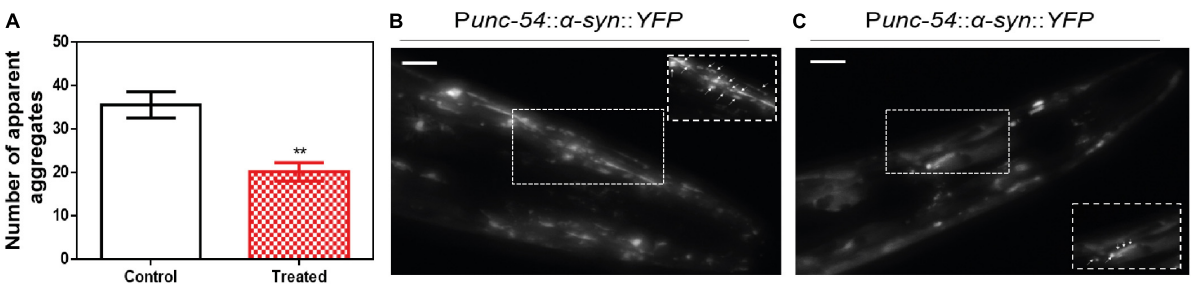

FIGURE 6 | Inhibition of α-Syn inclusions formation in a *C. elegans* model. **(A)** Quantification of α-Syn muscle inclusions per area in NL5901 worms in the absence (white) and presence of ZPDm (red). **(B,C)** Representative images of apparent α-Syn muscle aggregates obtained by epifluorescence microscopy of NL5901 worms treated without **(B)** and with ZPDm **(C)**. (Scale bars, 10 µm). Between 40 and 50 animals were analyzed per condition. Aggregates are indicated by white arrows. Data are shown as means, and error bars are shown as the SE of means; **$p < 0.01$. NL5901 *C. elegans* strain forms visible accumulations of aggregated α-Syn that are reduced when ZPDm is administered.

it was identified in a screening for compounds that interact with monomeric α-Syn, and therefore, is not expected to have fibril disrupting activity. Indeed, it did not impact fibril transmission (Toth et al., 2019), consistent with its activity and being complementary to that of ZPDm, a fibril anti-propagating agent in PMCA assays.

Overall, here we describe a new small molecule with the potential to be converted into a lead compound and, perhaps more importantly, together with previous data, envision a way to design minimal aromatic molecules with different α-Syn anti-aggregational activities rationally. Because ZPD-2 and ZPDm function on the same target but have complementary activity, it

will be interesting to test if a combination of them can have a synergic effect that overpasses the individual molecules' potential.

DATA AVAILABILITY STATEMENT

All datasets presented in this study are included in the article/**Supplementary Material**.

AUTHOR CONTRIBUTIONS

SV designed the research. SP-D, JP, FP, JST, SN, MC-G, JSC, JG, and ED performed the research. SP-D, JP, IP, XS, JSC, ED, and SV analyzed the data. SP-D, JP, and SV wrote the manuscript. All authors contributed to the article and approved the submitted version.

FUNDING

SV was supported by the Ministerio de Economía y Competitividad (MINECO) (BIO2016-78310-R), the ICREA (ICREA-Academia 2015), and the Fundación La Marató de TV3 (Ref. 20144330). JSC was supported by the MINECO (BFU2016-78232-P) and the Gobierno de Aragón (E45_17R). ED was supported by the Instituto de Salud Carlos III (PH613883/ERDF/ESF). JG and XS were supported by the MINECO (BIO2015-70092-R) and the European Research Council (Contract 648201).

ACKNOWLEDGMENTS

We thank the Infraestructura Científica y Técnica Singular NMR facility at Centres Científics i Tecnològics de la Universitat de Barcelona for help with NMR, the Servei de Microscòpia at Universitat Autònoma de Barcelona for their help with TEM, and Anna Villar-Pique for help with plasmid construction.

SUPPLEMENTARY MATERIAL

The Supplementary Material for this article can be found online at: https://www.frontiersin.org/articles/10.3389/fbioe.2020.588947/full#supplementary-material

Supplementary Figure 1 | Inhibitory capacity of (trifluoromethyl)benzene. **(A)** Chemical structures of (trifluoromethyl)benzene, (left) and ZPDm (right). **(B)** α-Syn aggregation kinetics in the absence (black) and presence (green) of 100 μM of (trifluoromethyl)benzene followed by Th-T fluorescence. **(C)** Light-scattering measurements at 300 and 340 nm, in the absence (white) and presence (green) of (trifluoromethyl)benzene.

Supplementary Figure 2 | NMR analysis of ZPDm lack ofinteraction with monomeric α-Syn. ^{1}H-^{15}N HSQC NMR spectra of 15N-labeled α-Syn (70 μM) in the presence **(A)** and in the absence **(B)** ofZPDm (100 μM). The superposition of the two NMR spectra is shown in **(C)**.

Supplementary Figure 3 | Chemical structures of different α-Syn aggregation inhibitors with asingle aromatic ring. Chemical structures of **(A)** scyllo-inositol, **(B)** gallic acid, **(C)** dopamine, **(D)** epinephrine, **(E)** norepinephrine, **(F)** thymoquinone, **(G)** safranal, **(H)** caffeic acid, **(I)** ferulic acid, **(J)** protocathecuic acid, **(K)** tyrosol, and **(L)** 576755.

REFERENCES

Appel-Cresswell, S., Vilarino-Guell, C., Encarnacion, M., Sherman, H., Yu, I., Shah, B., et al. (2013). Alpha-synuclein p.*H50Q*, a novel pathogenic mutation for Parkinson's disease. *Mov Disord.* 28, 811–813. doi: 10.1002/mds.25421

Bendor, J. T., Logan, T. P., and Edwards, R. H. (2013). The function of alpha-synuclein. *Neuron* 79, 1044–1066. doi: 10.1016/j.neuron.2013.09.004

Bieschke, J., Russ, J., Friedrich, R. P., Ehrnhoefer, D. E., Wobst, H., Neugebauer, K., et al. (2010). EGCG remodels mature alpha-synuclein and amyloid-beta fibrils and reduces cellular toxicity. *Proc. Natl. Acad. Sci. U.S.A.* 107, 7710–7715. doi: 10.1073/pnas.0910723107

Brenner, S. (1974). The genetics of *Caenorhabditis elegans*. *Genetics* 77, 71–94.

Bousset, L., Pieri, L., Ruiz-Arlandis, G., Gath, J., Jensen, P. H., Habenstein, B., et al. (2013). Structural and functional characterization of two alpha-synuclein strains. *Nat. Commun.* 4:2575. doi: 10.1038/ncomms3575

Carija, A., Pinheiro, F., Pujols, J., Bras, I. C., Lazaro, D. F., Santambrogio, C., et al. (2019). Biasing the native alpha-synuclein conformational ensemble towards compact states abolishes aggregation and neurotoxicity. *Redox Biol.* 22:101135. doi: 10.1016/j.redox.2019.101135

Crespo, R., Villar-Alvarez, E., Taboada, P., Rocha, F. A., Damas, A. M., and Martins, P. M. (2016). What Can the Kinetics of Amyloid Fibril Formation Tell about Off-pathway Aggregation? *J. Biol. Chem.* 291, 2018–2032. doi: 10.1074/jbc.M115.699348

Decressac, M., Mattsson, B., Weikop, P., Lundblad, M., Jakobsson, J., and Bjorklund, A. (2013). TFEB-mediated autophagy rescues midbrain dopamine neurons from alpha-synuclein toxicity. *Proc. Natl. Acad. Sci. U.S.A.* 110, E1817–E1826. doi: 10.1073/pnas.1305623110

Dexter, D. T., and Jenner, P. (2013). Parkinson disease: from pathology to molecular disease mechanisms. *Free Radic. Biol. Med.* 62, 132–144. doi: 10.1016/j.freeradbiomed.2013.01.018

Di Giovanni, S., Eleuteri, S., Paleologou, K. E., Yin, G., Zweckstetter, M., Carrupt, P. A., et al. (2010). Entacapone and tolcapone, two catechol O-methyltransferase inhibitors, block fibril formation of alpha-synuclein and beta-amyloid and protect against amyloid-induced toxicity. *J. Biol. Chem.* 285, 14941–14954. doi: 10.1074/jbc.M109.080390

Fanciulli, A., and Wenning, G. K. (2015). Multiple-system atrophy. *N. Engl. J. Med.* 372, 249–263. doi: 10.1056/NEJMra1311488

Faustini, G., Longhena, F., Varanita, T., Bubacco, L., Pizzi, M., Missale, C., et al. (2018). Synapsin III deficiency hampers alpha-synuclein aggregation, striatal synaptic damage and nigral cell loss in an AAV-based mouse model of Parkinson's disease. *Acta Neuropathol.* 136, 621–639. doi: 10.1007/s00401-018-1892-1

Fellner, L., Jellinger, K. A., Wenning, G. K., and Stefanova, N. (2011). Glial dysfunction in the pathogenesis of alpha-synucleinopathies: emerging concepts. *Acta Neuropathol.* 121, 675–693. doi: 10.1007/s00401-011-0833-z

Hamamichi, S., Rivas, R. N., Knight, A. L., Cao, S., Caldwell, K. A., and Caldwell, G. A. (2008). Hypothesis-based RNAi screening identifies neuroprotective genes in a Parkinson's disease model. *Proc. Natl. Acad. Sci. U.S.A.* 105, 728–733. doi: 10.1073/pnas.0711018105

Harrington, A. J., Yacoubian, T. A., Slone, S. R., Caldwell, K. A., and Caldwell, G. A. (2012). Functional analysis of VPS41-mediated neuroprotection in *Caenorhabditis elegans* and mammalian models of Parkinson's disease. *J. Neurosci.* 32, 2142–2153. doi: 10.1523/jneurosci.2606-11.2012

Hansen, C., Angot, E., Bergstrom, A. L., Steiner, J. A., Pieri, L., Paul, G., et al. (2011). alpha-Synuclein propagates from mouse brain to grafted dopaminergic neurons and seeds aggregation in cultured human cells. *J. Clin. Invest.* 121, 715–725. doi: 10.1172/JCI43366

Herrera, F. E., Chesi, A., Paleologou, K. E., Schmid, A., Munoz, A., Vendruscolo, M., et al. (2008). Inhibition of alpha-synuclein fibrillization by dopamine is mediated by interactions with five C-terminal residues and with E83 in the NAC region. *PLoS One* 3:e3394. doi: 10.1371/journal.pone.0003394

Herva, M. E., Zibaee, S., Fraser, G., Barker, R. A., Goedert, M., and Spillantini, M. G. (2014). Anti-amyloid compounds inhibit alpha-synuclein aggregation induced by protein misfolding cyclic amplification (PMCA). *J. Biol. Chem.* 289, 11897–11905. doi: 10.1074/jbc.M113.542340

Ibanez, P., Bonnet, A. M., Debarges, B., Lohmann, E., Tison, F., Pollak, P., et al. (2004). Causal relation between alpha-synuclein gene duplication and familial Parkinson's disease. *Lancet* 364, 1169–1171. doi: 10.1016/S0140-6736(04)17104-3

Ibrahim, T., and McLaurin, J. (2016). alpha-Synuclein aggregation, seeding and inhibition by scyllo-inositol. *Biochem. Biophys. Res. Commun.* 469, 529–534. doi: 10.1016/j.bbrc.2015.12.043

Jiang, M., Porat-Shliom, Y., Pei, Z., Cheng, Y., Xiang, L., Sommers, K., et al. (2010). Baicalein reduces E46K alpha-synuclein aggregation in vitro and protects cells against E46K alpha-synuclein toxicity in cell models of familiar Parkinsonism. *J. Neurochem.* 114, 419–429. doi: 10.1111/j.1471-4159.2010.06752.x

Jung, B. C., Lim, Y. J., Bae, E. J., Lee, J. S., Choi, M. S., Lee, M. K., et al. (2017). Amplification of distinct alpha-synuclein fibril conformers through protein misfolding cyclic amplification. *Exp. Mol. Med.* 49:e314. doi: 10.1038/emm.2017.1

Kalia, L. V., and Lang, A. E. (2015). Parkinson's disease. *Lancet* 386, 896–912. doi: 10.1016/S0140-6736(14)61393-3

Kantor, B., Tagliafierro, L., Gu, J., Zamora, M. E., Ilich, E., Grenier, C., et al. (2018). Downregulation of SNCA expression by targeted editing of DNA methylation: a potential strategy for precision therapy in PD. *Mol. Ther.* 26, 2638–2649. doi: 10.1016/j.ymthe.2018.08.019

Kruger, R., Kuhn, W., Muller, T., Woitalla, D., Graeber, M., Kosel, S., et al. (1998). Ala30Pro mutation in the gene encoding alpha-synuclein in Parkinson's disease. *Nat. Genet.* 18, 106–108. doi: 10.1038/ng0298-106

Kurnik, M., Sahin, C., Andersen, C. B., Lorenzen, N., Giehm, L., Mohammad-Beigi, H., et al. (2018). Potent alpha-synuclein aggregation inhibitors, identified by high-throughput screening, mainly target the monomeric state. *Cell Chem. Biol.* 25, 1389.e9–1402.e9. doi: 10.1016/j.chembiol.2018.08.005

Lassot, I., Mora, S., Lesage, S., Zieba, B. A., Coque, E., Condroyer, C., et al. (2018). The E3 Ubiquitin Ligases TRIM17 and TRIM41 Modulate alpha-Synuclein Expression by Regulating ZSCAN21. *Cell Rep.* 25, 2484.e9–2496.e9. doi: 10.1016/j.celrep.2018.11.002

Lau, A., So, R. W. L., Lau, H. H. C., Sang, J. C., Ruiz-Riquelme, A., Fleck, S. C., et al. (2020). alpha-Synuclein strains target distinct brain regions and cell types. *Nat. Neurosci.* 23, 21–31. doi: 10.1038/s41593-019-0541-x

Li, B., Ge, P., Murray, K. A., Sheth, P., Zhang, M., Nair, G., et al. (2018). Cryo-EM of full-length alpha-synuclein reveals fibril polymorphs with a common structural kernel. *Nat. Commun.* 9:3609. doi: 10.1038/s41467-018-05971-2

Liu, Y., Carver, J. A., Calabrese, A. N., and Pukala, T. L. (2014). Gallic acid interacts with alpha-synuclein to prevent the structural collapse necessary for its aggregation. *Biochim. Biophys. Acta* 1844, 1481–1485. doi: 10.1016/j.bbapap.2014.04.013

Luk, K. C., Kehm, V., Carroll, J., Zhang, B., O'Brien, P., Trojanowski, J. Q., et al. (2012). Pathological alpha-synuclein transmission initiates Parkinson-like neurodegeneration in nontransgenic mice. *Science* 338, 949–953. doi: 10.1126/science.1227157

Moree, B., Yin, G., Lazaro, D. F., Munari, F., Strohaker, T., Giller, K., et al. (2015). Small molecules detected by second-harmonic generation modulate the conformation of monomeric alpha-synuclein and reduce its aggregation in cells. *J. Biol. Chem.* 290, 27582–27593. doi: 10.1074/jbc.M114.636027

Munoz-Lobato, F., Rodriguez-Palero, M. J., Naranjo-Galindo, F. J., Shephard, F., Gaffney, C. J., Szewczyk, N. J., et al. (2014). Protective role of DNJ-27/ERdj5 in *Caenorhabditis elegans* models of human neurodegenerative diseases. *Antioxid. Redox Signal.* 20, 217–235. doi: 10.1089/ars.2012.5051

Nussbaum, R. L., and Ellis, C. E. (2003). Alzheimer's disease and Parkinson's disease. *N. Engl. J. Med.* 348, 1356–1364. doi: 10.1056/NEJM2003ra020003

Pandey, N., Strider, J., Nolan, W. C., Yan, S. X., and Galvin, J. E. (2008). Curcumin inhibits aggregation of alpha-synuclein. *Acta Neuropathol.* 115, 479–489. doi: 10.1007/s00401-007-0332-4

Peelaerts, W., Bousset, L., Van der Perren, A., Moskalyuk, A., Pulizzi, R., Giugliano, M., et al. (2015). alpha-Synuclein strains cause distinct synucleinopathies after local and systemic administration. *Nature* 522, 340–344. doi: 10.1038/nature14547

Pena-Diaz, S., Pujols, J., Conde-Gimenez, M., Carija, A., Dalfo, E., Garcia, J., et al. (2019). ZPD-2, a small compound that inhibits alpha-synuclein amyloid aggregation and its seeded polymerization. *Front. Mol. Neurosci.* 12:306. doi: 10.3389/fnmol.2019.00306

Pena-Diaz, S., Pujols, J., and Ventura, S. (2020). Small molecules to prevent the neurodegeneration caused by alpha-synuclein aggregation. *Neural Regen. Res.* 15, 2260–2261. doi: 10.4103/1673-5374.284993

Polymeropoulos, M. H., Lavedan, C., Leroy, E., Ide, S. E., Dehejia, A., Dutra, A., et al. (1997). Mutation in the alpha-synuclein gene identified in families with Parkinson's disease. *Science* 276, 2045–2047. doi: 10.1126/science.276.5321.2045

Pujols, J., Pena-Diaz, S., Conde-Gimenez, M., Pinheiro, F., Navarro, S., Sancho, J., et al. (2017). High-throughput screening methodology to identify alpha-synuclein aggregation inhibitors. *Int. J. Mol. Sci.* 18:478. doi: 10.3390/ijms18030478

Pujols, J., Pena-Diaz, S., Lazaro, D. F., Peccati, F., Pinheiro, F., Gonzalez, D., et al. (2018). Small molecule inhibits alpha-synuclein aggregation, disrupts amyloid fibrils, and prevents degeneration of dopaminergic neurons. *Proc. Natl. Acad. Sci. U.S.A.* 115, 10481–10486. doi: 10.1073/pnas.1804198115

Pujols, J., Pena-Diaz, S., Pallares, I., and Ventura, S. (2020). Chemical chaperones as novel drugs for Parkinson's Disease. *Trends Mol. Med.* 26, 408–421. doi: 10.1016/j.molmed.2020.01.005

Saelices, L., Nguyen, B. A., Chung, K., Wang, Y., Ortega, A., Lee, J. H., et al. (2019). A pair of peptides inhibits seeding of the hormone transporter transthyretin into amyloid fibrils. *J. Biol. Chem.* 294, 6130–6141. doi: 10.1074/jbc.RA118.005257

Sangwan, S., Sahay, S., Murray, K. A., Morgan, S., Guenther, E. L., Jiang, L., et al. (2020). Inhibition of synucleinopathic seeding by rationally designed inhibitors. *eLife* 9:e46775. doi: 10.7554/eLife.46775

Save, S. S., Rachineni, K., Hosur, R. V., and Choudhary, S. (2019). Natural compound safranal driven inhibition and dis-aggregation of alpha-synuclein fibrils. *Int. J. Biol. Macromol.* 141, 585–595. doi: 10.1016/j.ijbiomac.2019.09.053

Schwab, K., Frahm, S., Horsley, D., Rickard, J. E., Melis, V., Goatman, E. A., et al. (2017). A protein aggregation inhibitor, leuco-methylthioninium Bis(Hydromethanesulfonate), decreases alpha-synuclein inclusions in a transgenic mouse model of synucleinopathy. *Front. Mol. Neurosci.* 10:447. doi: 10.3389/fnmol.2017.00447

Seidler, P. M., Boyer, D. R., Rodriguez, J. A., Sawaya, M. R., Cascio, D., Murray, K., et al. (2018). Structure-based inhibitors of tau aggregation. *Nat. Chem.* 10, 170–176. doi: 10.1038/nchem.2889

Serpell, L. C., Berriman, J., Jakes, R., Goedert, M., and Crowther, R. A. (2000). Fiber diffraction of synthetic alpha-synuclein filaments shows amyloid-like cross-beta conformation. *Proc. Natl. Acad. Sci. U.S.A.* 97, 4897–4902. doi: 10.1073/pnas.97.9.4897

Silva, B., Einarsdóttir, O., Fink, A. L., and Uversky, V. (2011). Modulating α-synuclein misfolding and fibrillation in vitro by agrochemicals. *Res. Rep, Biol.* 2011, 43–56. doi: 10.2147/RRB.S16448

Singleton, A. B., Farrer, M., Johnson, J., Singleton, A., Hague, S., Kachergus, J., et al. (2003). alpha-Synuclein locus triplication causes Parkinson's disease. *Science* 302:841. doi: 10.1126/science.1090278

Spencer, B., Potkar, R., Trejo, M., Rockenstein, E., Patrick, C., Gindi, R., et al. (2009). Beclin 1 gene transfer activates autophagy and ameliorates the neurodegenerative pathology in alpha-synuclein models of Parkinson's and Lewy body diseases. *J. Neurosci.* 29, 13578–13588. doi: 10.1523/JNEUROSCI.4390-09.2009

Spillantini, M. G., Crowther, R. A., Jakes, R., Cairns, N. J., Lantos, P. L., and Goedert, M. (1998a). Filamentous alpha-synuclein inclusions link multiple system atrophy with Parkinson's disease and dementia with Lewy bodies. *Neurosci. Lett.* 251, 205–208. doi: 10.1016/s0304-3940(98)00504-7

Spillantini, M. G., Crowther, R. A., Jakes, R., Hasegawa, M., and Goedert, M. (1998b). alpha-Synuclein in filamentous inclusions of Lewy bodies from Parkinson's disease and dementia with lewy bodies. *Proc. Natl. Acad. Sci. U.S.A.* 95, 6469–6473. doi: 10.1073/pnas.95.11.6469

Spillantini, M. G., Schmidt, M. L., Lee, V. M., Trojanowski, J. Q., Jakes, R., and Goedert, M. (1997). Alpha-synuclein in Lewy bodies. *Nature* 388, 839–840. doi: 10.1038/42166

Tatenhorst, L., Eckermann, K., Dambeck, V., Fonseca-Ornelas, L., Walle, H., Lopes da Fonseca, T., et al. (2016). Fasudil attenuates aggregation of alpha-synuclein in models of Parkinson's disease. *Acta Neuropathol. Commun.* 4:39. doi: 10.1186/s40478-016-0310-y

Toth, G., Neumann, T., Berthet, A., Masliah, E., Spencer, B., Tao, J., et al. (2019). Novel Small molecules targeting the intrinsically disordered structural ensemble of alpha-synuclein protect against diverse alpha-synuclein mediated dysfunctions. *Sci. Rep.* 9:16947. doi: 10.1038/s41598-019-52598-4

van Ham, T. J., Thijssen, K. L., Breitling, R., Hofstra, R. M., Plasterk, R. H., and Nollen, E. A. (2008). *C. elegans* model identifies genetic modifiers of alpha-synuclein inclusion formation during aging. *PLoS Genet.* 4:e1000027. doi: 10.1371/journal.pgen.1000027

Wagner, J., Ryazanov, S., Leonov, A., Levin, J., Shi, S., Schmidt, F., et al. (2013). Anle138b: a novel oligomer modulator for disease-modifying therapy of neurodegenerative diseases such as prion and Parkinson's disease. *Acta Neuropathol.* 125, 795–813. doi: 10.1007/s00401-013-1114-9

Wrasidlo, W., Tsigelny, I. F., Price, D. L., Dutta, G., Rockenstein, E., Schwarz, T. C., et al. (2016). A de novo compound targeting alpha-synuclein improves deficits in models of Parkinson's disease. *Brain* 139(Pt 12), 3217–3236. doi: 10.1093/brain/aww238

Xilouri, M., Brekk, O. R., Landeck, N., Pitychoutis, P. M., Papasilekas, T., Papadopoulou-Daifoti, Z., et al. (2013). Boosting chaperone-mediated autophagy in vivo mitigates alpha-synuclein-induced neurodegeneration. *Brain* 136(Pt 7), 2130–2146. doi: 10.1093/brain/awt131

Zharikov, A., Bai, Q., De Miranda, B. R., Van Laar, A., Greenamyre, J. T., and Burton, E. A. (2019). Long-term RNAi knockdown of alpha-synuclein in the adult rat substantia nigra without neurodegeneration. *Neurobiol. Dis.* 125, 146–153. doi: 10.1016/j.nbd.2019.01.004

Conflict of Interest: The authors declare that the research was conducted in the absence of any commercial or financial relationships that could be construed as a potential conflict of interest.

frontiers in Bioengineering and Biotechnology

REVIEW
published: 20 October 2020
doi: 10.3389/fbioe.2020.585896

Challenges and Advances in Antemortem Diagnosis of Human Transmissible Spongiform Encephalopathies

Lucas M. Ascari[1], Stephanie C. Rocha[1], Priscila B. Gonçalves[1], Tuane C. R. G. Vieira[2] and Yraima Cordeiro[1]**

[1] Faculty of Pharmacy, Pharmaceutical Biotechnology Department, Federal University of Rio de Janeiro, Rio de Janeiro, Brazil, [2] Institute of Medical Biochemistry Leopoldo de Meis, National Institute of Science and Technology for Structural Biology and Bioimaging, Federal University of Rio de Janeiro, Rio de Janeiro, Brazil

Transmissible spongiform encephalopathies (TSEs), also known as prion diseases, arise from the structural conversion of the monomeric, cellular prion protein (PrP^{C}) into its multimeric scrapie form (PrP^{Sc}). These pathologies comprise a group of intractable, rapidly evolving neurodegenerative diseases. Currently, a definitive diagnosis of TSE relies on the detection of PrP^{Sc} and/or the identification of pathognomonic histological features in brain tissue samples, which are usually obtained postmortem or, in rare cases, by brain biopsy (antemortem). Over the past two decades, several paraclinical tests for antemortem diagnosis have been developed to preclude the need for brain samples. Some of these alternative methods have been validated and can provide a probable diagnosis when combined with clinical evaluation. Paraclinical tests include *in vitro* cell-free conversion techniques, such as the real-time quaking-induced conversion (RT-QuIC), as well as immunoassays, electroencephalography (EEG), and brain bioimaging methods, such as magnetic resonance imaging (MRI), whose importance has increased over the years. PrP^{Sc} is the main biomarker in TSEs, and the RT-QuIC assay stands out for its ability to detect PrP^{Sc} in cerebrospinal fluid (CSF), olfactory mucosa, and dermatome skin samples with high sensitivity and specificity. Other biochemical biomarkers are the proteins 14-3-3, tau, neuron-specific enolase (NSE), astroglial protein S100B, α-synuclein, and neurofilament light chain protein (NFL), but they are not specific for TSEs. This paper reviews the techniques employed for definite diagnosis, as well as the clinical and paraclinical methods for possible and probable diagnosis, both those in use currently and those no longer employed. We also discuss current criteria, challenges, and perspectives for TSE diagnosis. An early and accurate diagnosis may allow earlier implementation of strategies to delay or stop disease progression.

Keywords: prion diseases, prion protein, diagnostic, cell-free conversion assay, neurodegenerative disease

OPEN ACCESS

Edited by:
Jesus R. Requena, University of Santiago de Compostela, Spain

Reviewed by:
Wenquan Zou, Case Western Reserve University, United States
Franc Llorens, Center for Biomedical Research on Neurodegenerative Diseases (CIBERNED), Spain

****Correspondence:***
Tuane C. R. G. Vieira
tuane@bioqmed.ufrj.br
Yraima Cordeiro
yraima@pharma.ufrj.br; yraimacordeiro@gmail.com

Specialty section:
This article was submitted to Biosafety and Biosecurity, a section of the journal Frontiers in Bioengineering and Biotechnology

Received: *21 July 2020*
Accepted: *28 September 2020*
Published: *20 October 2020*

Citation:
Ascari LM, Rocha SC, Gonçalves PB, Vieira TCRG and Cordeiro Y (2020) Challenges and Advances in Antemortem Diagnosis of Human Transmissible Spongiform Encephalopathies. Front. Bioeng. Biotechnol. 8:585896. doi: 10.3389/fbioe.2020.585896

PRION DISEASES

Prion diseases, also known as transmissible spongiform encephalopathies (TSEs), are a rare group of infectious, fatal neurodegenerative diseases caused by the deposition of misfolded prion protein particles in the brain (Prusiner, 1998; Scheckel and Aguzzi, 2018). The term "prion" was originally coined in 1982 by Stanley Prusiner to define the proteinaceous infectious particles that cause TSEs

(Prusiner, 1982). The hallmark event in all TSEs is the conversion of the monomeric cellular prion protein (PrP^{C}) into abnormally folded multimers, collectively termed prion scrapie (PrP^{Sc}), which accumulate in the brain and display toxic and aggregation-prone properties (Prusiner, 1998; Requena and Wille, 2017; Baral et al., 2019).

These diseases progress slowly, with a long latency period prior to the manifestation of symptoms, which include ataxia, myoclonus, progressive dementia, depression, and general malaise. In contrast with other progressive neurodegenerative diseases, the period between the onset of symptoms and the TSE patient's death is usually up to 1 year, making them rapidly progressive dementias (Prusiner and Hsiao, 1994; Chesebro, 2003; Wadsworth et al., 2003). Treatment for human TSEs remains symptomatic and supportive, as no cure is available to date (Geschwind, 2015; Forloni et al., 2019).

Transmissible spongiform encephalopathies are unique in medicine since they can have three origins: spontaneous (sporadic), genetic (familial), and acquired (infectious/transmitted). Human TSEs encompass diseases such as Kuru, Creutzfeldt–Jakob disease (CJD), Gerstmann–Sträussler–Scheinker syndrome (GSS), and fatal familial insomnia (FFI) (Zanusso et al., 2016; Ironside et al., 2017). Among human TSE cases, 80% to 95% are sporadic CJD (sCJD), 10% to 15% are genetic (often familial), and less than 1% are acquired (Geschwind, 2015). These diseases affect approximately 1–2 people per million worldwide annually (Chen and Dong, 2016). The human TSEs described above are summarized in **Table 1**.

Creutzfeldt–Jakob disease, the most common human prion disease worldwide, occurs mainly in the form of sporadic CJD (sCJD), which was first described in 1920 by German neurologist Hans Gerhard Creutzfeldt in a 23-year-old woman who had experienced fluctuating neuropsychological symptoms since adolescence. Shortly afterward, Alfons Maria Jakob described five other cases between 1921 and 1923, which he found to be similar to Creutzfeldt's case (Iwasaki, 2017; Tee et al., 2018). There is no known genetic etiology of sCJD, nor are there known links between cases that are suggestive of an acquired disease; the assumption is, therefore, that cases of sCJD arise spontaneously (Ironside et al., 2017).

In 1987, a study described a prion disease in United Kingdom cattle named bovine spongiform encephalopathy (BSE) (Wells et al., 1987). Subsequently, in the 1990s, scientific and public attention was drawn to the appearance in the United Kingdom of a new human prion disease called variant CJD (vCJD), which was caused by the ingestion of meat from BSE-affected cattle (Will et al., 1996). In the late 1990s and early 2000s, some groups pointed to blood as a source of the scrapie agent, which at the time led to restrictions on blood transfusion in the United Kingdom as a way to prevent human-to-human transmission of vCJD (Turner and Ironside, 1998; Hunter et al., 2002; Llewelyn et al., 2004). A more recent study has shown that prion transmission in sheep via blood transfusion is indeed very efficient (Andréoletti et al., 2012).

Prior to the emergence of BSE, there were numerous reports of iatrogenic CJD (iCJD) cases in different countries in the 1970s and 1980s. These transmissions occurred via one of the following routes: treatment with human cadaver-derived growth hormone or gonadotropin, dura mater graft or corneal graft transplantation, and medical operations with neurosurgical instruments or depth electrodes (Will, 2003). Conventional sterilization protocols are ineffective in eradicating the PrP^{Sc} content in surgical instruments, and the methods recommended by the World Health Organization (WHO) are damaging to metal instruments and not practical for routine application (Thomas et al., 2013).

Despite the rarity of TSEs, these diseases represent a significant concern, not only because of their puzzling etiological aspects but also because of their considerable threat to public health. The development of non-invasive diagnostic methods for the early stages of TSEs is crucial in order to enable (*i*) the prevention of PrP^{Sc} spread, (*ii*) the implementation of potential therapies during earlier stages of the disease, and (*iii*) improvement in patient well-being. The development and validation of diagnostic methods for the detection at a preclinical stage are essential.

THE PRION PROTEIN

Mature PrP^{C} is a 208-residue protein constitutively found on the surface of many cells, particularly neurons (Peggion et al., 2017). Before reaching the cell surface, a 253-residue precursor of PrP^{C} undergoes some post-translational modifications: the excision of a 22-residue segment at the N-terminus and a 23-residue segment at the C-terminus, the establishment of a disulfide bond between cysteine residues 179 and 214, and the attachment of a glycosylphosphatidylinositol (GPI) anchor to the C-terminus (Prusiner, 1991). Recent findings have suggested that PrP^{C} plays a central role in a variety of neurodegenerative diseases and could be a common therapeutic target for these disorders (Ayers and Prusiner, 2020; Corbett et al., 2020).

The structure of PrP^{C} consists of an intrinsically unfolded N-terminal domain (residues 23–124) and a globular C-terminal domain (residues 125–230). The latter comprises three α-helices and a small, two-stranded β-sheet (Riek et al., 1996; Zahn et al., 2000; Requena and Wille, 2017) (**Figure 1A**). There are two glycosylation sites at asparagine residues 181 and 197, such that PrP^{C} exists in diglycosylated, monoglycosylated, and non-glycosylated forms (Prusiner, 1991). Despite its high conservation in mammals, the human PrP gene (*PRNP*) has over 40 deleterious mutations and a few polymorphisms (**Figure 1B**). The polymorphism at codon 129 (rs1799990) draws particular attention because it influences disease susceptibility and phenotype (Kim M. O. et al., 2018). Nearly 55% of the world population are homozygous for methionine (MM), while 9% are homozygous for valine (VV) and 36% are heterozygous (MV). The most common allele, M129, has a frequency of 97.5% in East Asians, 76% in South Asians, 67.5% in Europeans, 64.7% in Africans, and 59.4% in Hispanic Americans with Native ancestry (The 1000 Genomes Project Consortium, 2012).

While PrP^{C} has a predominantly α-helical structure, PrP^{Sc} consists of β-sheet-rich multimeric assemblies (Prusiner, 1998).

TABLE 1 | Transmissible spongiform encephalopathies (TSEs).

Disease	Form	Etiology	Clinical aspects	Incidence
Creutzfeldt–Jakob disease (CJD)	Sporadic (sCJD)	Either wild-type PrP^{C} converts spontaneously to PrP^{Sc}, or a somatic mutation in the PrP gene (*PRNP*) renders PrP^{C} more susceptible to misfolding.	Rapidly progressive cognitive impairment with behavioral and visual disturbances, pyramidal and extrapyramidal signs, ataxia, and myoclonus.	The most common form of CJD (85%), with an annual incidence of 1.5 per million people. It generally occurs in late middle age (mean age of 67 years). Short survival post-diagnosis (about 4 months).
	Genetic (gCJD)	An inherited mutation in *PRNP* renders PrP^{C} more susceptible to misfolding.	Usually similar to sporadic CJD.	The frequency is estimated at 10%–15% of all forms of CJD. Those affected tend to be in their middle age when symptoms first arise.
	Iatrogenic (iCJD)	Human-to-human transmission occurs via cadaver-derived pituitary hormones, dura mater transplant, cornea transplant, neurosurgical instruments, or depth electrodes.	Usually similar to sporadic CJD.	Rare. The first case was reported in 1974 in a patient who had received a corneal transplant from a CJD-positive donor. Over 450 cases have been reported.
	Variant (vCJD)	Ingestion of meat from BSE-affected cattle provides exogenous PrP^{Sc} seed.	Psychiatric and sensory symptoms, ataxia, involuntary movements, and progressive cognitive impairment.	Rare. It was first reported in 1996 in the United Kingdom, where it reached epidemic proportions between the mid-1980s and 1996. In fact, most people who have developed vCJD have lived in the United Kingdom.
Fatal insomnia	Sporadic	Wild-type PrP^{C} converts spontaneously to PrP^{Sc} in patients lacking a genetic basis for this phenotype.	Cognitive decline, ataxia, psychiatric signs, and insomnia.	Rare. Twenty-five typical cases have been reported.
	Genetic (FFI)	Inherited D178N mutation coupled with the M129 genotype in *PRNP* renders PrP^{C} more susceptible to misfolding.	Insomnia, dysautonomia, ataxia, myoclonus, and epileptic seizures.	Rare. At least 70 families, 198 members of these families, and other 18 unrelated individuals are known to carry the D178N-129M allele (D178N mutation coupled with the M129 genotype).
Variably protease-sensitive prionopathy (VPSPr)	Sporadic	The abnormal PrP displays unusual biochemical properties. There are no mutations in *PRNP* and no risk factors for the development of acquired CJD.	Cognitive decline, psychiatric symptoms, and ataxia.	Rare. First described in 2008, with 11 cases identified in the United States.
Gerstmann–Sträussler–Scheinker syndrome (GSS)	Genetic	Inherited mutation in *PRNP* renders PrP^{C} more susceptible to misfolding. P102L is the most common mutation.	Slowly progressive ataxia with cognitive decline and parkinsonism later in the disease course.	Rare. First described in an Austrian family in 1936.
PrP systemic amyloidosis	Genetic	Premature termination of PrP caused by an inherent stop codon mutation renders PrP^{C} more susceptible to misfolding.	Sensory and/or sensorimotor autonomic neuropathy.	Rare. Reported in three families.

References: Diack et al. (2014); Geschwind (2015); Zanusso et al. (2016); Ironside et al. (2017); Ritchie and Ironside (2017); Whitechurch et al. (2017); Cracco et al. (2018); Tee et al. (2018); Tesar et al. (2019); Uttley et al. (2020).

Experimental evidence combined with computational approaches suggests that PrP^{Sc} consists of β-strands and relatively short turns and/or loops that form a β-solenoid architecture with a hydrophobic β-sheet core (Wasmer et al., 2008; Smirnovas et al., 2011; Spagnolli et al., 2019). A remarkable property of the PrP^{Sc} particles is that they are self-propagating—i.e., they act like seeds/nuclei and induce the refolding of PrP^{C} units, which are then integrated into PrP^{Sc} multimers. Thus, PrP^{Sc} particles grow by a nucleation process (Chiti and Dobson, 2006; Caughey et al., 2009; Cobb and Surewicz, 2009) (**Figure 2**). The pathogenic scrapie agent can spread from cell to cell and can transfer to a new host through the mechanisms outlined earlier (Acquatella-Tran Van Ba et al., 2013; Kraus et al., 2013).

PrP^{Sc} particles are not homogenous structures. Indeed, they can adopt different conformations. An intriguing consequence of this fact is that these distinct PrP^{Sc} species can be associated with different clinical characteristics of TSEs, including the latency period, brain damage pattern, and symptomatology. The concept of the prion strain has, therefore, been defined to represent this structural, biochemical, and neuropathological diversity (Aguzzi et al., 2007; Rossi et al., 2019). Some groups have even reported the artificial production of prion strains *in vitro,* and the infectivity and pathogenicity in animal models of these scrapie agents generated *de novo* (Colby and Prusiner, 2011; Kim C. et al., 2018). Notably, the diversity of PrP primary sequences and PrP^{Sc} conformations (strains) greatly affects the susceptibility of an organism to PrP^{Sc} from another organism, especially if these organisms belong to different species. It is thus common to talk about a species barrier or strain barrier for prion diseases (Scott et al., 2005; Sharma et al., 2016; Igel-Egalon et al., 2018).

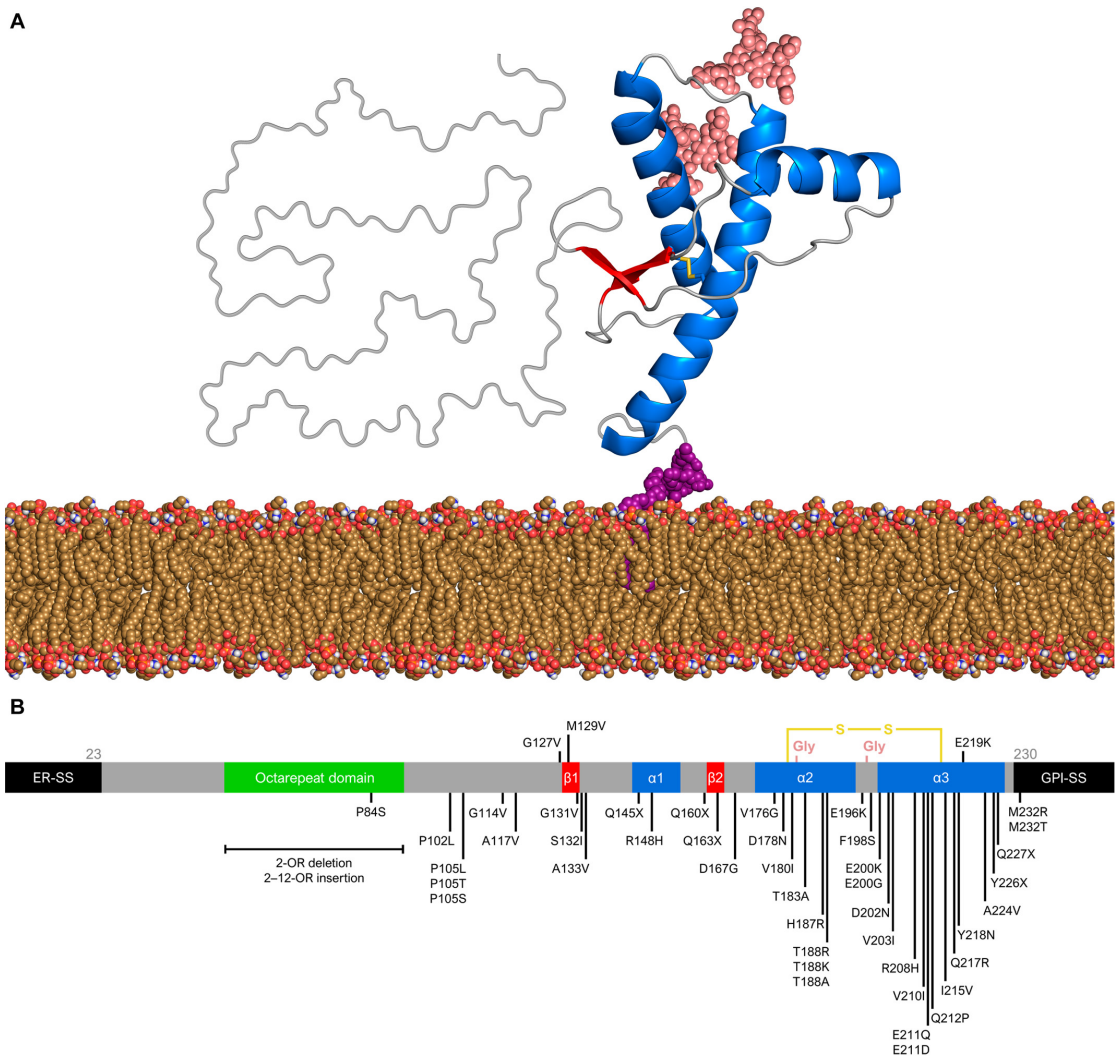

FIGURE 1 | Prion protein structure and genetic variation. **(A)** Diglycosylated, full-length human PrP^{C} ($huPrP^{23-230}$) attached to the membrane (yellow brown) by a GPI anchor (purple). The globular C-terminal domain comprises three α-helices (blue) and two small β-strands (red), while the N-terminal is intrinsically flexible. Turns and random coils are represented in gray, and the glycosides are shown in salmon. A disulfide bond (yellow) connects the α-helices 2 and 3. The globular domain structure was determined by nuclear magnetic resonance (PDB code 1QLX). **(B)** Schematic of human PrP primary structure, with disease-associated mutations (below) and polymorphisms (above). Deleterious mutations include missense and nonsense changes, as well as octarepeat insertions and deletions. The octarepeat domain (green) is a copper-binding segment of 4–5 contiguous repeats of the sequence PHGGGWGQ. The 22-residue endoplasmic reticulum signal sequence (ER-SS) and 23-residue GPI signal sequence (GPI-SS) at the ends are shown in black. The other portions are colored as in panel **(A)**.

A distinguishing feature between PrP^{C} and PrP^{Sc} is that the former has total protease sensitivity, whereas the latter generally has a protease-resistant core comprising the ∼90–230 region; hence, PrP^{C} and PrP^{Sc} are also referred to as sensitive PrP (^{sen}PrP) and resistant PrP (^{res}PrP), respectively (Prusiner, 1998; Caughey, 2000). Different strain-related PrP^{Sc} species can also have particular proteolytic digestion profiles, as they may differ in the length of their protease-resistant core (Bessen et al., 1995; Zou et al., 2003; Kobayashi et al., 2011; Kushnirov et al., 2020). Distinguishing between native PrP^{C} and infectious PrP^{Sc} based on their different biochemical properties is considered the "gold standard" approach for TSE diagnosis (Lukan et al., 2013; Haley and Richt, 2017). However, such an approach to discern different prion strains has yet to be exploited for diagnostic purposes.

DIAGNOSTIC APPROACHES FOR PRION DISEASES

At present, the definite diagnosis for TSEs is obtained via at least one of the following options: (*i*) identification of pathognomonic histological features in brain tissue sections, (*ii*) detection of ^{res}PrP by immunohistochemical staining of brain tissue sections, or (*iii*) detection of ^{res}PrP by immunoblotting of brain homogenate. Clinical evaluation and paraclinical tests only

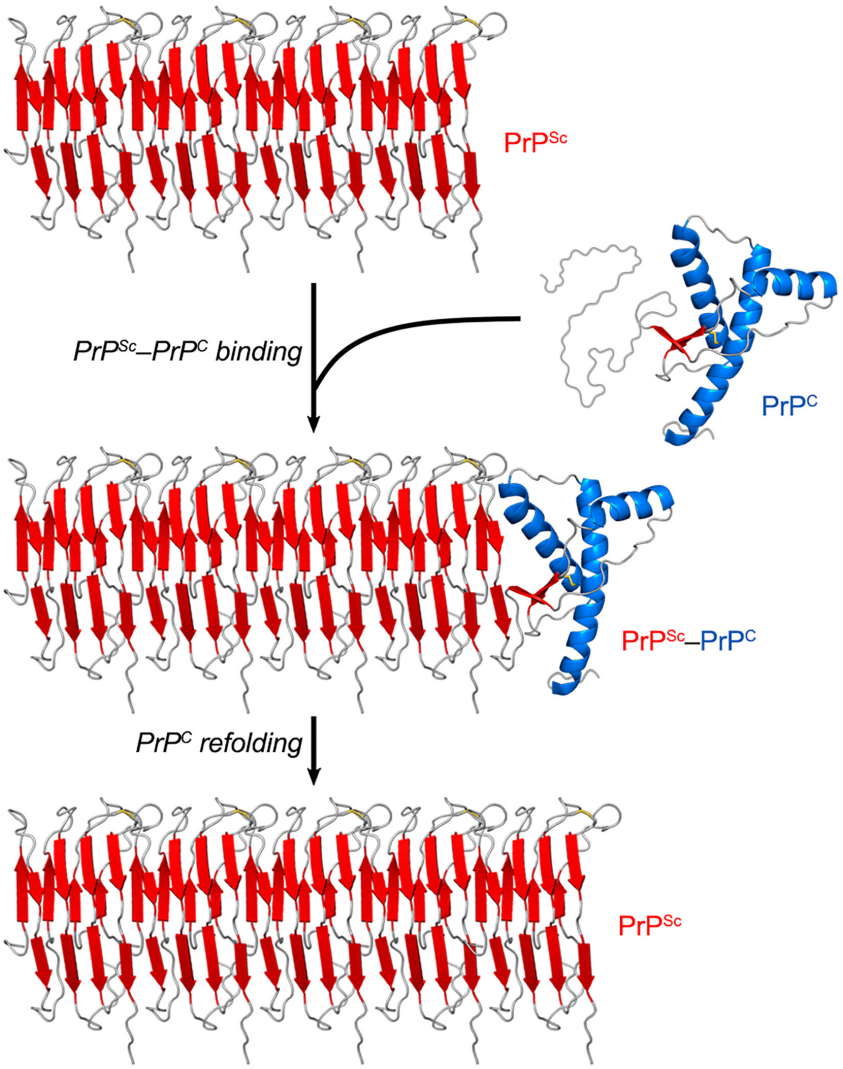

FIGURE 2 | PrP^{Sc} amplification from PrP^{C}. PrP^{Sc} particles grow by a nucleation process. A unit of PrP^{C} forms a complex with PrP^{Sc}, and the latter induces the refolding of the former into a β-sheet-rich structure which then becomes part of the PrP^{Sc} multimer. In this self-propagating process, the PrP^{Sc} particles act like seeds/nuclei, with PrP^{C} serving as a substrate. The secondary structures are colored as follows: α-helices in blue, β-strands in red, and unstructured portions in gray. The atomistic model of PrP^{Sc} was constructed by combining experimental data and molecular dynamics simulations (Spagnolli et al., 2019).

lead to a classification as possible or probable (Brown et al., 2003; CDC's Diagnostic Criteria for Creutzfeldt–Jakob Disease (CJD), 2018). In the following sections, we will discuss the currently validated tests for definite, possible, and probable diagnosis, as well as other tests.

At this point, it is important to note two key terms in medical diagnosis: sensitivity and specificity. Sensitivity is the ability of a test to correctly identify true positive cases of the disease, whereas specificity is the ability of a test to identify true negative cases of the disease correctly. A high-sensitivity test produces more true positive results than false-negative results, while a high-specificity test produces more true negative results than false-positive results. The ultimate goal for diagnostic testing is to obtain sensitivity and specificity values as close to 100% as possible (Feinstein, 1975).

Brain Tissue Examination

Transmissible spongiform encephalopathy patients' brain tissue is characterized by vacuolization (spongiosis), neuronal death, dendritic and synaptic loss, astrogliosis, and ^{res}PrP deposition. These features are most prominent in the cerebral and cerebellar cortexes. Vacuolization can be observed by histopathological examination. The vacuoles may, in fact, be an artifact generated by tissue processing (fixation, paraffin embedding, and staining). Apoptotic neurons can be identified by staining nuclei with DAPI (4′,6-diamidino-2-phenylindole) and/or immunochemical staining of caspase-3. Dendritic and synaptic loss can be revealed by Golgi silver staining. While astrogliosis is not specific to this group of diseases, it is consistently present and can be detected through immunochemical staining of glial fibrillary acidic protein (GFAP) (Aguzzi et al., 2001; Soto and Satani, 2011).

However, these examinations have some drawbacks. Since tissue segments may have been collected from unaffected areas of the brain, these analyses offer limited diagnostic sensitivity and may well lead to false-negative results (Soto, 2004; Safar et al., 2005).

Immunohistochemical staining of brain tissue sections is a validated technique for detecting PrP^{Sc} in the brains of TSE-affected patients. To selectively stain for $^{res}PrP^{Sc}$, brain tissue sections are previously subjected to limited proteolysis by proteinase K (PK) to eliminate the ^{sen}PrP content (Bendheim et al., 1984; Parchi et al., 1999, 2012; Gambetti et al., 2003). This technique allows for higher diagnostic sensitivity than the brain tissue staining techniques mentioned above since it directly probes the etiological agent behind TSEs (Safar et al., 2005). However, the enzymatic pre-treatment does represent a significant drawback in terms of diagnostic sensitivity, since the PrP^{Sc} content may have varying degrees of resistance to proteolysis depending on the prion strain. Indeed, there have been reports of strain-associated PrP^{Sc} particles so poorly protease-resistant that they have been termed sensitive PrP^{Sc} ($^{sen}PrP^{Sc}$) (Safar et al., 2005; Pastrana et al., 2006; Sajnani et al., 2012). Limited proteolysis can thus result in digestion of a significant part of the whole PrP^{Sc} content, underestimating the total level of PrP^{Sc} in the brain (Safar et al., 2005).

One way to circumvent the limitations of the immunohistochemical examination is to skip the PK pre-treatment step and to perform conformation-dependent immunoassays (CDIs) using brain homogenate. CDIs markedly increase diagnostic sensitivity since they detect PrP^{Sc} species regardless of their protease resistance level (Safar et al., 1998, 2005; Kim et al., 2011, 2012). CDIs employ antibodies that recognize conformational epitopes rather than linear epitopes and are therefore selective for PrP^{Sc} over PrP^{C} (Kascsak et al., 1987; Bellon et al., 2003). Many conformational antibodies with selectivity for PrP^{Sc} have already been produced (Saijo et al., 2016). However, CDIs have not been tested in large cohorts and are thus not yet used in routine diagnostics or screening.

Another validated technique that is extensively used for diagnosis is Western blotting (immunoblotting) of brain homogenate, which also employs a pre-treatment with PK to digest the PrP^{C} content. This technique is particularly important because it provides information on several aspects of PrP^{Sc}: its degree of proteolytic resistance, the size of the protease-resistant cores, and the ratio between the three different PrP glycoforms (un-, mono-, and diglycosylated). These features are correlated with the properties of individual strains as well as disease genotypes and phenotypes. The electrophoretic migration of the unglycosylated PK-resistant core is used to define two PrP^{Sc} types in cases of CJD: type 1, characterized by a ∼21-kDa band, and type 2, characterized by a ∼19-kDa band (Parchi et al., 1999). CJD subtypes are then categorized by codon 129 polymorphism and PrP^{Sc} type as MM1, MM2, MV1, MV2, VV1, and VV2. Type-1 PrP^{Sc} is mostly correlated with the 129 MM genotype, while type-2 PrP^{Sc} is generally correlated with the 129VV and 129MV genotypes; therefore, the most frequent subtypes are MM1, VV2, and MV2 (Parchi et al., 1999; Zerr et al., 2000b). With respect to PrP glycoforms, samples from sCJD patients predominantly contain the monoglycosylated band (Bendheim et al., 1984; Parchi et al., 1999, 2012; Gambetti et al., 2003). Meanwhile, FFI and vCJD are characterized by type-2 PrP^{Sc} and abundance of the diglycosylated band (Hill et al., 1997; Rossi et al., 1998).

Brain tissue examination is frequently performed postmortem, but brain biopsies provide an option for antemortem investigation. However, brain biopsies can lead to false-negative results since TSE pathology is variably distributed in the brain, and small samples may not contain pathognomonic histological features and/or detectable levels of PrP^{Sc}. Because of their invasiveness, brain biopsies are very uncomfortable for the patients and can cause severe complications, including brain abscesses and hemorrhaging. Furthermore, the medical instruments used in neurosurgery must be appropriately discarded or subjected to WHO-recommended cleaning methods. Therefore, brain tissue examination is generally performed only postmortem (Brown et al., 2003).

Neuropsychiatric Clinical Evaluation

The degeneration of certain areas of the brain, probably caused by PrP conversion and aggregation or by lack of functional PrP^{C}, leads to the development of clinical signs that motivate patients to seek medical attention. Depending on their symptoms, a number of assessments of sCJD patients are possible. These include the cognitive or Heidenhain form of CJD, which accounts for the largest number of sCJD cases and is characterized by cognitive decline, cortical visual disturbances (involvement of the occipital cortex), mild psychiatric symptoms, and myoclonus. Cases can also be classified as ataxic or Brownell-Oppenheimer, a form that is characterized by cerebellar ataxia, cognitive decline, mood changes, and myoclonus at later stages, or as non-CJD phenotypes or Stern, characterized by presenile dementia, ataxia, and sleep disturbance (related to degeneration of the thalamus) (Puoti et al., 2012; Fragoso et al., 2017).

Gerstmann–Sträussler–Scheinker syndrome patients predominantly present cerebellar clinical features, progressive ataxia, incoordination, and late dementia. FFI patients' main symptoms include sleep-related issues (insomnia, sleep-related dyspnea, sleep-related involuntary movements), and less frequently ataxia and psychiatric symptoms. Behavioral and psychiatric symptoms (excluding sleep disturbance) are also found in vCJD patients, along with persistent painful sensory symptoms, ataxia, myoclonus, and later dementia (Fragoso et al., 2017; Wu et al., 2018).

However, none of these signs alone are enough to diagnose prion diseases definitively. Subacute encephalopathy can be a consequence of infectious, inflammatory, autoimmune, or other causes, leading to diseases that should have their differential diagnosis because they are mostly treatable, unlike TSEs (Annus et al., 2016; Fragoso et al., 2017). For example, Hashimoto's encephalopathy is a treatable disorder that results in cognitive decline, myoclonus, ataxia, and neuropsychiatric signs (Murray, 2011), similar to TSEs.

To determine a possible or probable TSE diagnosis, clinical symptoms must be consistent with paraclinical tests, which can include magnetic resonance imaging (MRI), electroencephalography (EEG), and CSF analysis (Soto, 2004;

Araújo, 2013). However, this combination of clinical evaluation and paraclinical tests is insufficient for a definite TSE diagnosis, since biochemical and imaging alterations are not specific to the various TSE cases, as they are also present in other neurodegenerative conditions.

In vitro Cell-Free PrP Conversion Assays

Based on the self-replicating ability of PrP^{Sc}, a cell-free conversion assay called protein misfolding cyclic amplification (PMCA) was published at the beginning of the 2000s (Saborio et al., 2001). This technique consists of mixing PBS-diluted healthy brain homogenate and scrapie-infected brain homogenate (at a much higher dilution) in microtubes and then performing repeated cycles of incubation with orbital shaking at 37°C and sonication. Healthy and scrapie-infected brain homogenates are sources of PrP^{C}/^{sen}PrP (the reaction substrate) and PrP^{Sc}/^{res}PrP (the infectious seed), respectively. The incubation step allows aggregate growth, while the sonication step fragments these aggregates into smaller particles, which can act as seeds in the following incubation step. The reaction products are subjected to PK treatment and then to Western blotting to reveal their final ^{res}PrP content. The result is an exponential increase in the amount of ^{res}PrP per cycle (Saborio et al., 2001) (**Figure 3**).

The PMCA assay was later improved by optimizing brain homogenate preparation, medium composition, and sonication method, as well as by developing an automated option for the incubation–sonication step (Castilla et al., 2004; Saá et al., 2005) (**Table 2** and **Figure 3**). These modifications allowed simultaneous runs of multiple samples with enhanced amplification efficiency (Castilla et al., 2005). The improved PMCA assay was shown to have very high sensitivity, as it significantly amplified as little as 10^{-18} g of PrP^{Sc} (equivalent to a 10^{12}-fold dilution of SHB), as well as high specificity, as it never generated any detectable ^{res}PrP in the absence of scrapie-infected brain homogenate inoculum, even after hundreds of PMCA cycles (Saá et al., 2006). When applied to human brain samples (collected either postmortem or by brain biopsy), PrP^{Sc} from sCJD and vCJD patients has been successfully amplified by PMCA (Soto et al., 2005; Jones et al., 2007; Oshita et al., 2016).

A simpler and less expensive version of PMCA, called rPrP-PMCA, was developed by replacing PrP^{C} from brain or cell homogenate with bacterially expressed, folded recombinant ^{sen}PrP ($^{sen}rPrP$) (**Table 2**). The substrate concentration could thus be more accurately and efficiently defined in rPrP-PMCA than in classical PMCA (Atarashi et al., 2007). In the same year, another cell-free conversion technique, the amyloid seeding assay (ASA), was published (Colby et al., 2007). This cell-free conversion technique consists of loading a multiwell microplate with (*i*) guanidine-denatured $^{sen}rPrP$, (*ii*) PrP^{Sc} partially purified from scrapie-infected brain homogenate, (*iii*) guanidine, and (*iv*) thioflavin T (ThT). The latter component is a probe that emits fluorescence when it binds to amyloid structures. The mixture is incubated with continuous linear shaking at 37°C in a plate reader, which measures ThT fluorescence emission throughout the reaction, thus revealing the kinetics of aggregate formation (Colby et al., 2007) (**Table 2**).

Protein misfolding cyclic amplification (and its variation, rPrP-PMCA) and ASA have important differences. While it is challenging to deliver sound energy evenly to samples during sonication, lateral shaking subjects samples to the same motion, making ASA more practical and reproducible than the PMCA assays (Colby et al., 2007). The ASA technique is also faster and much more suitable for high-throughput investigations than PMCA since ASA relies on simple, automated, real-time, and fluorescence-based read-outs rather than time-consuming, immunoblotting-based read-outs (Colby et al., 2007). However, ASA has the disadvantage of frequently producing false-positive results, probably because of the presence of guanidine, a chaotropic agent, in the reaction medium (Colby et al., 2007).

A more refined cell-free conversion assay, the quaking-induced conversion (QuIC), was published more recently than the above techniques (Atarashi et al., 2008). The QuIC assay consists of loading microtubes with folded $^{sen}rPrP$ and highly diluted scrapie-infected brain homogenate and then incubating the mixture at a controlled temperature with alternating cycles of orbital shaking and rest. The intermittent shaking results in separate aggregate fragmentation (seed formation) and aggregate growth phases, speeding up the conversion process. The read-out is performed by PK digestion and Western blotting, as in the PMCA assay (**Table 2**). The QuIC technique had high sensitivity, successfully amplifying as little as 10^{-16} g of PrP^{Sc} from brain homogenate, while also achieving high specificity, as it generated either no PK-resistant band or atypical, low molecular weight PK-resistant bands (Atarashi et al., 2008). The QuIC assay detected PrP^{Sc} with high sensitivity in brain homogenates from animals and humans and CSF samples from animals (Atarashi et al., 2008; Orrú et al., 2009).

The QuIC assay was then combined with the ASA read-out method to create the most sophisticated technique currently available for amplifying PrP^{Sc} *in vitro*, namely the real-time quaking-induced conversion (RT-QuIC) (Wilham et al., 2010). RT-QuIC differs from its predecessor in several steps. First, instead of microtubes, the conversion medium is supplemented with ThT and loaded into multiwell microplates. It is then incubated at 42°C with alternating cycles of double orbital shaking and rest and analyzed using real-time ThT fluorescence measurements rather than immunoblotting (**Table 2** and **Figure 4**). The RT-QuIC technique is the fastest, most straightforward, most practical, least expensive, and most suitable cell-free conversion assay for high-throughput surveys. The RT-QuIC assay detected PrP^{Sc} at levels between $\sim 10^{-15}$ g and 10^{-13} g in brain homogenate, nasal fluids, and CSF from different animal species with high specificity (Wilham et al., 2010).

In the last decade, numerous studies have reported the detection of PrP^{Sc} in non-brain samples from human TSE patients by PMCA and especially RT-QuIC, as summarized in **Table 3**. The PMCA assay has been used to amplify PrP^{Sc} with high sensitivity and specificity from human samples such as blood (Lacroux et al., 2014; Bougard et al., 2016; Concha-Marambio et al., 2016) and urine (Moda et al., 2014). These studies used homogenates from the following biological materials as substrate sources: healthy human brain (Soto et al., 2005), human platelets (Jones et al., 2007), human PrP^{C}-expressing transgenic mouse

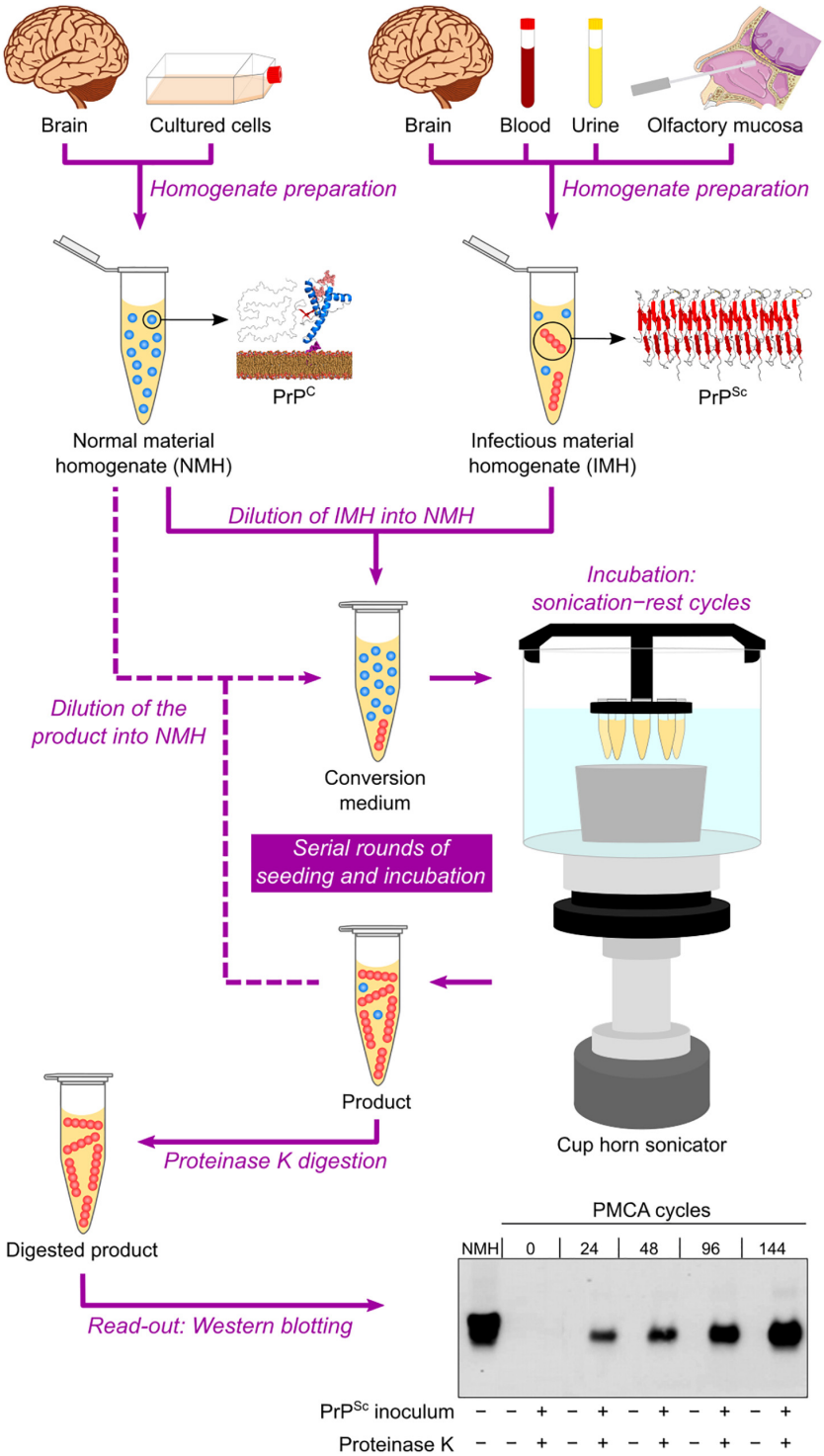

FIGURE 3 | Protein misfolding cyclic amplification (PMCA) in automated fashion. Normal material homogenate (NMH), a source of PrP^{C} (substrate), is prepared from brain sections or cultured cells. Suspected infectious material homogenate (IMH), a possible source of PrP^{Sc} (seed), is prepared from brain sections, blood, urine, or olfactory mucosa brushings. Suspected IMH is diluted into NMH, and the resulting mixture is incubated with alternating cycles of sonication and rest. Subsequent rounds can be performed by diluting the product of the previous round into fresh NMH and repeating the incubation step. As a result, the amount of PrP^{Sc} is amplified after several sonication–rest cycles and even more after serial rounds of seeding and incubation. The products from different cycles and rounds are treated with proteinase K to eliminate PrP^{C} and then subjected to Western blotting to reveal the growing amount of ^{res}PrP. This result indicates a positive TSE diagnosis. The Western blot shown is republished with permission of American Society for Biochemistry and Molecular Biology, from Ultra-efficient replication of infectious prions by automated protein misfolding cyclic amplification, Saá, Castilla, and Soto, 281, 46, 2006; permission conveyed through Copyright Clearance Center, Inc.

TABLE 2 | *In vitro* cell-free PrP conversion assays.

Assay	Medium composition	Substrate	Container	Motion	Temperature	Sonication	Read-out
PMCA	Buffer system: $H_2PO_4^-$, HPO_4^{2-}; Counterions: Na^+, Cl^-, K^+; Chelating agent: EDTA; Surfactants: Triton X-100, (SDS); Protease inhibitors	PrP^C from brain or cell homogenate	Microtubes	Manual: orbital shaking (450 rpm); Automated: stationary	37°C	Manual or automated	PK treatment and Western blotting
rPrP-PMCA	Buffer system: $H_2PO_4^-$, HPO_4^{2-}; Counterions: Na^+, Cl^-, K^+; Surfactants: Triton X-100, SDS	Bacterially expressed, folded ^{sen}rPrP	Microtubes	Stationary	37°C	Automated	PK treatment and Western blotting
ASA	Buffer system: $H_2PO_4^-$, HPO_4^{2-}; Counterions: Na^+, Cl^-, K^+; Chaotropic agent: guanidine; Fluorescent probe: ThT	Bacterially expressed, unfolded ^{sen}rPrP	Multiwell microplate	Linear shaking	37°C	None	ThT fluorescence (real-time)
QuIC	Buffer system: $H_2PO_4^-$, HPO_4^{2-}; Counterions: Na^+, Cl^-; Surfactants: Triton X-100, SDS	Bacterially expressed, folded ^{sen}rPrP	Microtubes	Cycles of 1-min orbital shaking (1500 rpm) and 1-min rest	37–55°C	None	PK treatment and Western blotting
RT-QuIC	Buffer system: $H_2PO_4^-$, HPO_4^{2-}; Counterions: Na^+, Cl^-; Chelating agent: EDTA; Surfactant: SDS; Fluorescent probe: ThT	Bacterially expressed, folded ^{sen}rPrP	Multiwell microplate	Cycles of 1-min double orbital shaking (700 rpm) and 1-min rest	42–55°C	None	ThT fluorescence (real-time)

ASA, amyloid seeding assay; EDTA, ethylenediaminetetraacetate; PK, proteinase K; PMCA, protein misfolding cyclic amplification; PrP^C, cellular prion protein; QuiC, quaking-induced conversion; rPrP-PMCA, recombinant prion protein–protein misfolding cyclic amplification; RT-QuIC, real-time quaking-induced conversion; SDS, sodium dodecyl sulfate; ^{sen}rPrP, sensitive recombinant prion protein; ThT, thioflavin T.

brain (Jones et al., 2007; Lacroux et al., 2014; Moda et al., 2014; Bougard et al., 2016; Concha-Marambio et al., 2016), and human PrP^C-expressing 293F cells (Oshita et al., 2016). Another study has demonstrated that a CDI can be used as a read-out for PMCA to allow the detection of supposed $^{sen}PrP^{Sc}$ species (Jones et al., 2007).

Several studies have reported the high-sensitivity and high-specificity amplification of ^{res}PrP using RT-QuIC with different human samples, including brain homogenate (Atarashi et al., 2011; Peden et al., 2012), CSF (Atarashi et al., 2011; McGuire et al., 2012, 2016; Sano et al., 2013; Orrú et al., 2014; Cramm et al., 2015, 2016; Hermann et al., 2018; Rudge et al., 2018), olfactory mucosa (Orrú et al., 2014; Bongianni et al., 2017; Fiorini et al., 2020), and dermatome skin (Orrú et al., 2017). Another study coupled immunoprecipitation of PrP^{Sc} from human plasma with RT-QuIC, thus avoiding interference from plasma components and increasing sensitivity up to 10^{-18} g of PrP^{Sc} (Orrú et al., 2011).

Since it is common practice to collect CSF samples from patients with suspected CJD in order to rule out other diseases, this bodily fluid is highly valuable for diagnosis (Chitravas et al., 2011). A second-generation RT-QuIC assay (with small modifications in the protocol) has been developed specifically to enhance sensitivity in CSF analyses and shorten reaction times (Orrú et al., 2015a). It was designated as improved RT-QuIC for CSF (IQ-CSF). Subsequent work achieved high-sensitivity diagnosis from human CSF samples by using IQ-CSF (Groveman et al., 2016; Bongianni et al., 2017; Foutz et al., 2017; Franceschini et al., 2017; Abu-Rumeileh et al., 2019; Fiorini et al., 2020).

Some studies have shown that bank voles (BV) have a uniquely weak species/strain barrier for prion transmission, as they are susceptible to multiple PrP^{Sc} strains from a wide range of species, including humans, sheep, deer, and hamsters (Nonno et al., 2006; Agrimi et al., 2008; Di Bari et al., 2008, 2013). Another study has shown that BV PrP^C-expressing mice are susceptible to many prion strains from eight different species, including humans (Watts et al., 2014). Collectively, these data indicated that BV PrP^C was a universal substrate for conversion into PrP^{Sc}, thus circumventing the need for suitable ^{sen}PrP substrates (with different sequences) to identify distinct prion types using RT-QuIC and PMCA.

RT-QuIC reactions using BV ^{sen}rPrP as substrate have been able to detect multiple human prion strains with high sensitivity in human samples including brain homogenate (Orrú et al., 2015b), olfactory mucosa (Redaelli et al., 2017), and dermatome skin samples (Orrú et al., 2017). These studies observed the generation of BV ^{res}PrP species with different PK-resistance profiles, though without any clear correlation between the proteolytic digestion profiles and the different strains used as seed. Similarly, PMCA reactions using BV brain homogenate successfully amplified PrP^{Sc} from human olfactory mucosa samples, although the original glycoform ratio and the electrophoretic migration of the unglycosylated PK-resistant core of prion strains were not maintained (Redaelli et al., 2017). Even though the use of BV ^{sen}PrP cannot provide valuable information on prion strains, this substrate does simplify and lower the cost of routine application of RT-QuIC and PMCA for TSE diagnosis.

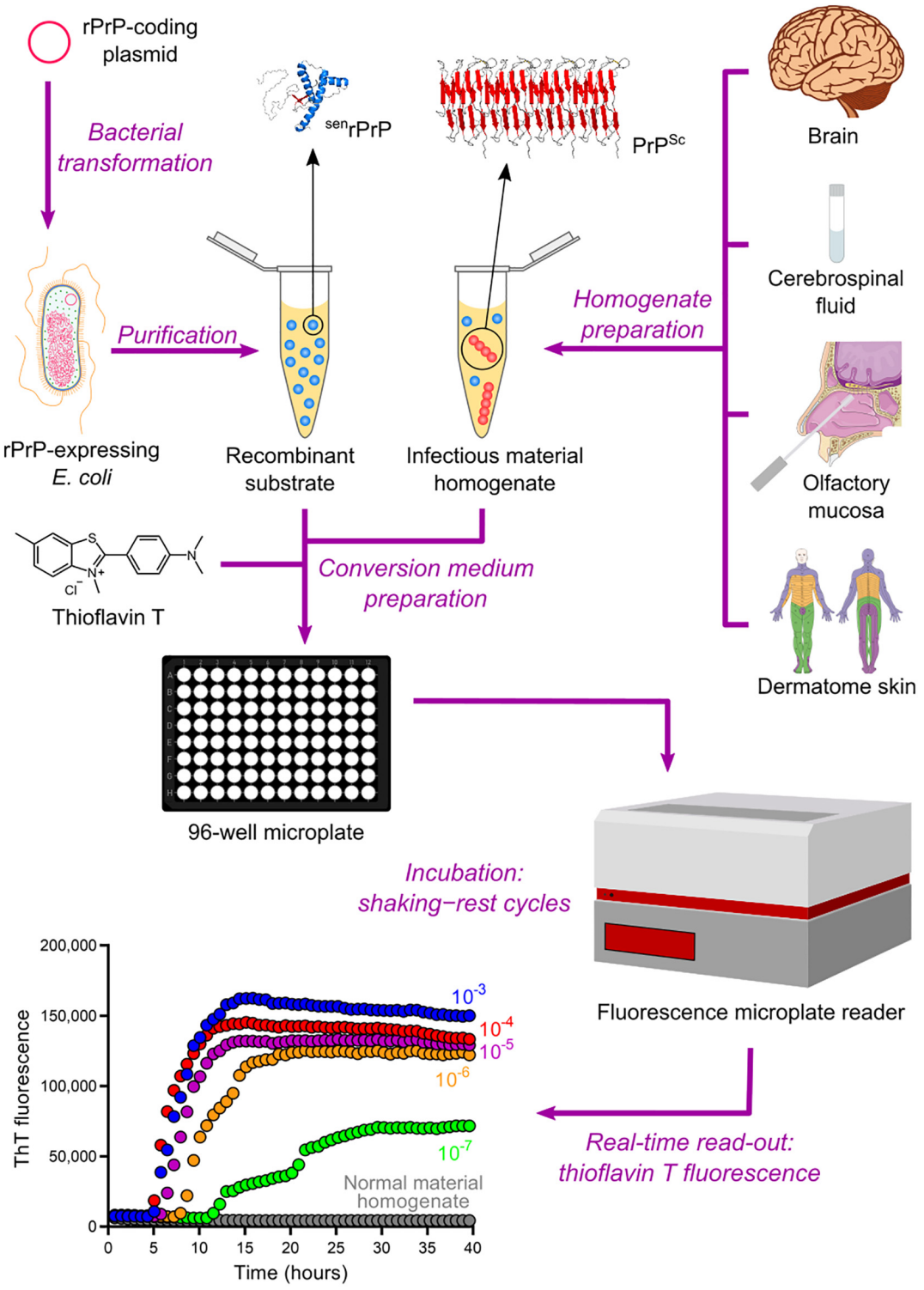

FIGURE 4 | Real-time quaking-induced conversion (RT-QuIC). Recombinant PrP (rPrP) is expressed heterologously in *E. coli* and purified as folded protease-sensitive rPrP (^{sen}rPrP), the substrate for RT-QuIC. Suspected infectious material homogenate, a possible source of PrP^{Sc} (seed), is prepared from brain sections, cerebrospinal fluid, olfactory mucosa brushings, and dermatome skin sections. High dilutions of a test sample are mixed with ^{sen}rPrP, buffer, and thioflavin T (a fluorescent amyloid probe) to produce the conversion medium, which is loaded into a multiwell microplate and then incubated with alternating cycles of shaking and rest in a fluorescence microplate reader. This equipment records thioflavin T fluorescence emission throughout the incubation, thus revealing the kinetics of aggregate formation. A sigmoidal growth in thioflavin T fluorescence indicates a positive TSE diagnosis. The use of normal material homogenate does not lead to any increase in thioflavin T fluorescence, indicating that no conversion is happening. The positive result shown was obtained with brain homogenate from a patient with GSS.

An important study has reported the detection of PrP^{Sc} in skin samples of prion-infected rodents by PMCA and RT-QuIC at a preclinical stage of disease. Hamsters infected with 263K scrapie strain, which displayed clinical signs from 10 weeks post inoculation (wpi), were positively diagnosed at 2 wpi by PMCA and 3 wpi by RT-QuIC. Human PrP^{C}-expressing mice infected with sCJD agent, which showed clinical signs at 24 wpi, were positively diagnosed at 4 wpi by PMCA and 20 wpi by RT-QuIC (Wang et al., 2019). These findings additionally highlight the enormous potential of *in vitro* cell-free PrP conversion assays for an early TSE diagnosis.

Protein misfolding cyclic amplification and RT-QuIC have important differences in terms of their end products. When PMCA products were inoculated intraperitoneally in wild-type hamsters, these animals developed the same disease pattern as hamsters inoculated with infectious brain material did, demonstrating that infectivity could also be amplified by PMCA (Saá et al., 2006). Conversely, when RT-QuIC products were inoculated intracerebrally in wild-type hamsters, their brains showed very low seeding activity but no histopathological changes, while Western blotting detected no ^{res}PrP. This result indicated that RT-QuIC-generated ^{res}PrP was neither infectious nor pathogenic, suggesting that RT-QuIC is much less biohazardous than PMCA for routine use (Groveman et al., 2017). In another study, sCJD-seeded RT-QuIC products inoculated intracerebrally in mice overexpressing human PrP^{C} elicited neither clinical signs of disease nor astrogliosis (Raymond et al., 2020). In fact, PMCA products are more similar to brain-derived PrP^{Sc}, while the ^{res}PrP species produced by RT-QuIC have shorter PK-resistant cores (McGuire et al., 2012; Groveman et al., 2015, 2017; Kraus et al., 2015), which may explain why PMCA and RT-QuIC end products are distinct in terms of infectivity. Thus, the methodological simplicity and biosafety of RT-QuIC over PMCA is probably the reason why RT-QuIC was

TABLE 3 | Performance of PMCA and RT-QuIC for PrP^{Sc} detectionin non-brain samples from human patients with TSEs.

Study	Assay	Body Fluid	Sensitivity	Specificity
Atarashi et al., 2011	RT-QuIC	CSF	80% (sCJD)	100%
McGuire et al., 2012	RT-QuIC	CSF	87% (sCJD)	100%
Sano et al., 2013	RT-QuIC	CSF	83% (gCJD), 90% (GSS), 83% (FFI)	NP
Orrú et al., 2014	RT-QuIC	Olfactory mucosa	97% (sCJD), 100% (gCJD)	100%
	RT-QuIC	CSF	79% (sCJD), 50% (gCJD)	100%
Moda et al., 2014	PMCA	Urine	93% (vCJD)	100%
Orrú et al., 2015a	IQ-CSF	CSF	96% (sCJD)	100%
Cramm et al., 2016	RT-QuIC	CSF	80% (sCJD), 100% (gCJD), 57% (FFI)	99%
Bougard et al., 2016	PMCA	Plasma	100% (vCJD)	100%
McGuire et al., 2016	RT-QuIC	CSF	86%–100% (sCJD)	100%
Concha-Marambio et al., 2016	PMCA	Blood	100% (vCJD)	100%
Foutz et al., 2017	IQ-CSF	CSF	92%–95% (sCJD), 93%–100% (gCJD)	99–100%
Bongianni et al., 2017	RT-QuIC	Olfactory mucosa	97% (sCJD), 75% (gCJD/GSS)	100%
	RT-QuIC	CSF	72% (sCJD), 57% (gCJD/GSS)	NP
	IQ-CSF	CSF	86% (sCJD), 50% (gCJD)	100%
	RT-QuIC + IQ-CSF	CSF	95% (sCJD), 71% (gCJD/GSS)	100%
	RT-QuIC + IQ-CSF	Olfactory mucosa + CSF	100% (sCJD), 75% (gCJD/GSS)	100%
Groveman et al., 2016	RT-QuIC	CSF	73% (sCJD)	100%
	IQ-CSF	CSF	94% (sCJD)	100%
Franceschini et al., 2017	IQ-CSF	CSF	92% (sCJD), 100% (gCJD), 100% (iCJD), 25% (vCJD), 33% (GSS), 0% (FFI), 100% (VPSPr)	100%
Redaelli et al., 2017	PMCA	Olfactory mucosa	100% (FFI)	100%
	RT-QuIC	Olfactory mucosa	100% (FFI/sCJD/iCJD)	100%
Orrú et al., 2017	RT-QuIC	Dermatome skin	88%–94% (sCJD)	100%
Rudge et al., 2018	RT-QuIC	CSF	89% (sCJD)	100%
Hermann et al., 2018	RT-QuIC	CSF	89% (sCJD)	100%
Abu-Rumeileh et al., 2019	RT-QuIC	CSF	83% (sCJD), 86% (gCJD)	100%
	IQ-CSF	CSF	97% (sCJD), 100% (gCJD)	100%
Metrick et al., 2019	RT-QuIC	Olfactory mucosa	100% (sCJD)	100%
Fiorini et al., 2020	RT-QuIC	Olfactory mucosa	91% (sCJD)	100%
	IQ-CSF	CSF	96% (sCJD)	100%
	RT-QuIC + IQ-CSF	Olfactory mucosa + CSF	100% (sCJD)	100%

Abbreviations: CJD, Creutzfeldt–Jakob disease; CSF, cerebrospinal fluid; FFI, fatal familial insomnia; gCJD, genetic Creutzfeldt–Jakob disease;GSS, Gerstmann–Sträussler–Scheinker syndrome; iCJD, iatrogenic Creutzfeldt–Jakob disease; IQ-CSF, improved RT-QuIC for CSF (2nd generation); NP, not performed; PMCA, protein misfolding cyclic amplification; RT-QuIC, real-time quaking-induced conversion; sCJD, sporadic Creutzfeldt–Jakob disease; vCJD, variant Creutzfeldt–Jakob disease.

the most employed assay for TSE diagnosis in robust studies published in the 2010s (**Table 3**).

A recent study has shown that the replacement of chloride anions with less hydrated bromide anions in the RT-QuIC medium significantly increased sensitivity and specificity for PrP^{Sc} amplification in brain and olfactory mucosa samples from sCJD patients (Metrick et al., 2019). This important finding may enable the RT-QuIC technique to be even more refined and distinguished in the years to come.

The RT-QuIC assay was first offered clinically in 2015 in the United States and became part of the Centers for Disease Control and Prevention (CDC) criteria in 2018. Currently, RT-QuIC, in combination with other techniques, characterizes TSE diagnosis only as probable, not definitive (CDC's Diagnostic Criteria for Creutzfeldt–Jakob Disease (CJD), 2018). Outstandingly, two studies have reported sCJD diagnosis with 100% sensitivity and 100% specificity by combining RT-QuIC analysis of olfactory mucosa samples and IQ-CSF (Bongianni et al., 2017; Fiorini et al., 2020). Two other studies have shown that the association of IQ-CSF with other techniques—such as MRI, EEG, and 14-3-3 detection (discussed below)—resulted in sCJD diagnosis with at least 97% sensitivity and 99% specificity (Hermann et al., 2018; Rudge et al., 2018). Therefore, it is very plausible that a definitive antemortem diagnosis can be obtained by the combination of RT-QuIC testing of at least two biological samples with analyses by other available techniques.

Surrogate Biomarkers

Although PrP^{Sc} is the most specific biochemical marker in TSEs, it is not the sole one. Surrogate biomarkers have been studied for both differential diagnosis and prognosis, especially in CJD cases. The search for biomarkers capable of predicting disease onset is especially important for patients with genetic forms, as well as for the inclusion of patients in clinical trials. Other proteins exploited for TSE diagnosis are 14-3-3 proteins, tau, neuron-specific enolase (NSE), astroglial protein S100B, α-synuclein, and neurofilament light chain protein (NFL) (**Table 4**). Among these, CSF 14-3-3 is a biomarker already considered in current guidelines (CDC's Diagnostic Criteria for Creutzfeldt–Jakob Disease (CJD), 2018).

14-3-3 proteins are indicators of neuronal cell loss and can be detected in CSF samples by immunoblotting (Hsich et al., 1996), capture assay (Peoc'h et al., 2001), or enzyme-linked immunosorbent assay (ELISA) (Kenney et al., 2000). Measurement of CSF 14-3-3 has sensitivity values of 53%–100% for sCJD, 0%–97% for genetic prion diseases (gCJD, GSS, and FFI), 60%–70% for iCJD, and 45%–58% for vCJD. Numerous features account for these highly variable values: disease form (sCJD, gCJD, vCJD, iCJD, GSS, FFI), disease subtype (MM1, MM2, MV1, MV2, VV1, VV2), patient's age, disease duration, and method used for quantification (Zerr et al., 2000b; Van Everbroeck et al., 2003; Collins et al., 2006; Gmitterová et al., 2009). Specificity values range from 27% to 100% since 14-3-3 elevation is not specific for TSEs. Acute neurological events (e.g., encephalitis, stroke, and epileptic seizures), brain tumor, and other neurodegenerative diseases also result in neuronal death, leading to an increase in 14-3-3 (Chohan et al., 2010; Stoeck et al., 2012). However, sensitivity and specificity have been shown to increase with disease duration in sCJD (Chohan et al., 2010).

An increase in CSF tau is typically an indicator of neuronal death associated with Alzheimer's disease and can be measured by ELISA (Jensen et al., 1995). However, CSF tau levels are also increased in CJD and therefore have been extensively used for TSE diagnosis (Otto et al., 1997; Bahl et al., 2009; Stoeck et al., 2012; Abu-Rumeileh et al., 2019). Measurement of CSF tau has sensitivity values of 75%–100% for sCJD, 0%–86% for genetic prion diseases (gCJD, GSS, and FFI), 53% for iCJD, and 24%–80% for vCJD, while specificity values range from 49% to 100%. Similarly to 14-3-3, tau sensitivity is limited by disease form and subtype, patient's age, and disease progression, while specificity is restricted by overlap with other diseases (Van Everbroeck et al., 2003; Hamlin et al., 2012; Stoeck et al., 2012; Cohen et al., 2016). CSF tau levels—along with information on patient's age, sex, and codon 129 polymorphism—has been recently used to build the first prognostic model to predict the survival time of sCJD individuals with moderate to good accuracy (Llorens et al., 2020a).

The detection of elevated levels of the proteins NSE and S100B in CSF samples from CJD patients have also been reported (Zerr et al., 1995; Beaudry et al., 1999; Aksamit et al., 2001; Bahl et al., 2009; Ladogana et al., 2009). Measurement of CSF NSE and S100B has respective sensitivity values of 79%–85% and 65%–94% for sCJD, 0%–64% and 20%–87% for genetic prion diseases (gCJD, GSS, and FFI), and 52% and 78% for vCJD, while specificity values are 83–92% for NSE and 76%–90% for S100B. The combination of two or three biomarkers among 14-3-3, tau, NSE, and S100B significantly increased specificity, but at the cost of reduced sensitivity (Aksamit et al., 2001; Bahl et al., 2009; Chohan et al., 2010). However, in relation to 14-3-3 and tau, NSE and S100B alone showed no particular advantage and, therefore, have been much less explored for TSE diagnosis.

More recent studies reported that sCJD patients' CSF also contains high levels of α-synuclein (Llorens et al., 2017, 2018; Kruse et al., 2018; Schmitz et al., 2019). Measurement of this protein had a sensitivity of 86%–98% and a specificity of 91%–98%, which are consistently high values in comparison to those of 14-3-3, tau, NSE, and S100B. These findings highlight α-synuclein as a very accurate surrogate biomarker in TSEs, but further studies are still necessary to reinforce the diagnostic utility of this protein.

Transmissible spongiform encephalopathy patients present elevated NFL in CSF as a result of neuroaxonal degeneration (Steinacker et al., 2016; Abu-Rumeileh et al., 2018, 2019). Measurement of CSF NFL has a sensitivity of 86%–97% for different TSE forms (sCJD, gCJD, and GSS) and specificity of 43%–95%. Increased tau and NFL levels can also be detected in TSE patients' serum or plasma (Steinacker et al., 2016; Thompson et al., 2018, 2020). In sCJD and gCJD patients, measurement of blood tau and NFL has a respective sensitivity of 57%–91% and 93%–100% and specificity of 83–97% and 57%–100%. Blood tau and CSF tau display no significant difference in sensitivity and specificity, while blood NFL is slightly more accurate than CSF NFL.

TABLE 4 | Surrogate biomarkers of prion diseases.

Biomarker	Body fluid	Detection method	Sensitivity	Specificity	References
14-3-3	CSF	Western blotting, capture assay, ELISA	53%–100% (sCJD), 0%–97% (gCJD/FFI/GSS), 60%–75% (iCJD), 45%–58% (vCJD)	27%–100%	Hsich et al. (1996), Zerr et al. (1998, 2000a,b), Beaudry et al. (1999); Kenney et al. (2000), Lemstra et al. (2000); Aksamit et al. (2001), Green et al. (2001, 2002), Peoc'h et al. (2001); Otto et al. (2002), Geschwind et al. (2003); Van Everbroeck et al. (2003), Collins et al. (2006), Sanchez-Juan et al. (2006, 2007), Bahl et al. (2009), Gmitterová et al. (2009); Ladogana et al. (2009), Chohan et al. (2010); Stoeck et al. (2012), Sano et al. (2013); Schmitz et al. (2016), Hermann et al. (2018); Abu-Rumeileh et al. (2019), Llorens et al. (2020b)
tau	CSF	ELISA	75%–100% (sCJD), 0%–86% (gCJD/FFI/GSS), 53% (iCJD), 24%–80% (vCJD)	49%–100%	Otto et al. (1997, 2002), Green et al. (2001); Van Everbroeck et al. (2003), Sanchez-Juan et al. (2006, 2007), Bahl et al. (2009); Ladogana et al. (2009), Chohan et al. (2010); Hamlin et al. (2012), Stoeck et al. (2012); Sano et al. (2013), Steinacker et al. (2016), Abu-Rumeileh et al. (2018, 2019)
	Serum/Plasma	Simoa	57%–91% (sCJD/gCJD)	83%–97%	Steinacker et al. (2016), Thompson et al. (2018, 2020)
NSE	CSF	ELISA, TRACE	79%–85% (sCJD), 64% (gCJD), 52% (vCJD), 0% (GSS/FFI)	83%–92%	Zerr et al. (1995); Beaudry et al. (1999), Aksamit et al. (2001); Green et al. (2001), Bahl et al. (2009); Ladogana et al. (2009)
S100B	CSF	ELISA	65%–94% (sCJD), 87% (gCJD), 78% (vCJD), 50% (GSS), 20% (FFI)	76%–90%	Beaudry et al. (1999); Green et al. (2001), Ladogana et al. (2009); Chohan et al. (2010)
	Serum	ECL	78%–84% (sCJD/gCJD)	63%–81%	Otto et al. (1998); Steinacker et al. (2016)
α-Synuclein	CSF	ECL, ELISA	86%–98% (sCJD)	91%–98%	Llorens et al. (2017, 2018), Kruse et al. (2018); Schmitz et al. (2019)
NFL	CSF	ELISA	86%–97% (CJD/GSS)	43%–95%	Steinacker et al. (2016), Abu-Rumeileh et al. (2018, 2019)
	Serum/plasma	Simoa	93%–100% (sCJD/gCJD)	57%–100%	Steinacker et al. (2016), Thompson et al. (2018, 2020)

CJD, Creutzfeldt–Jakob disease; ECL, electrochemiluminescence-based assays; ELISA, enzyme-linked immunosorbent assay; FFI, fatal familial insomnia; gCJD, genetic Creutzfeldt–Jakob disease; GSS, Gerstmann–Sträussler–Scheinker syndrome; iCJD, iatrogenic Creutzfeldt–Jakob disease; NFL, neurofilament light chain protein; NSE, neuron-specific enolase; sCJD, sporadic Creutzfeldt–Jakob disease; Simoa, single molecule array; TRACE, time-resolved amplified cryptate emission; vCJD, variant Creutzfeldt–Jakob disease.

Since serum and plasma samples are more easily obtained than CSF samples, these blood biomarkers also represent very useful tools for TSE diagnosis. Blood tau and NFL levels also increase in other neurological diseases and correlate with worsening of symptoms (Weydt et al., 2016; Mielke et al., 2017; Foiani et al., 2018), but they are generally higher in CJD patients (Thompson et al., 2020). Furthermore, blood tau concentration correlates with disease progression in sCJD patients and, thus, can be used to predict survival time (Thompson et al., 2018; Staffaroni et al., 2019). The analysis of plasma from patients carrying *PRNP* mutations associated with slowly progressive disease showed that NFL levels increase before the onset of symptoms (2 years before), suggesting that it may constitute a prodromal marker (Thompson et al., 2020). However, this interesting line of research will require additional studies with other populations.

Total PrP (t-PrP) has recently arisen as another potential biomarker. Since the concentration of t-PrP in CSF decreases as disease progresses (Villar-Piqué et al., 2019), it has been suggested as a pharmacodynamic biomarker (Minikel et al., 2019; Vallabh et al., 2019). CSF t-PrP concentration has been shown to be stable during 2 years of follow up, but none of the patients tested developed disease during the time frame of the research (Vallabh et al., 2020). The time point at which t-PrP levels start to decline and PrP^{Sc} levels start to increase in CSF is still unknown. Therefore, unveiling these events is of paramount importance for understanding disease progression. Additionally, elevated t-PrP levels have been detected in the plasma of sCJD and genetic TSE patients as a probable consequence of blood-brain barrier impairment (Llorens et al., 2020c). In this study, plasma t-PrP correlated with CSF biomarkers of neuronal death, but not with CSF t-PrP.

The diversity of TSE forms and subtypes poses a great challenge for defining a qualitative and quantitative standard for all the surrogate biomarkers reviewed here. As none of these approaches can undoubtedly distinguish human prion diseases from other neurological disorders, all these biomarkers should be analyzed with caution and always in combination with other methods, such as clinical evaluation, bioimaging (MRI) analysis, and EEG assessment (Hamlin et al., 2012).

Electroencephalography (EEG)

Transmissible spongiform encephalopathy diagnoses can be supported by the appearance of periodic sharp wave complexes (PSWCs)—typical bilateral periodic discharges with a frequency

of 0.5 to 2 per second—in EEG output. However, EEG findings alone are not specific for CJD, since PSWCs have been reported in patients with Alzheimer's disease, vascular dementia, Lewy body disease, and voltage-gated potassium channel complex antibodies (VGKC-cAbs) encephalitis (Wieser et al., 2006; Savard et al., 2016). PSWCs are found in 60% to 70% of sCJD patients and 75% of fCJD patients, while they are rarely found in GSS and FFI cases and never in vCJD cases. The use of benzodiazepines for epilepsy has been shown to mask EEG findings. PSWCs appear months after the symptoms have started, and patients tend to recover a few weeks after their appearance. Meanwhile, bilateral frontal intermittent rhythmical delta activity (FIRDA) and a slowing of EEG background activity have been recorded in the early stages of CJD (Hansen et al., 1998; Manix et al., 2015). The absence of PSWC in EEG data does not exclude a diagnosis of sCJD, and typical EEG findings may not be observed in the terminal stage of the disease. Patients with CJD can also exhibit diffuse, non-specific slow EEG background patterns, which can also be observed in encephalopathy of various neurodegenerative diseases other than CJD. Hence, the diagnosis of sCJD should depend on a combination of EEG with MRI, CSF analysis, and clinical findings (Kwon and Kwon, 2019).

Bioimaging

Neuroimaging tests are an accessible and non-invasive diagnostic tool for TSEs (Ortega-Cubero et al., 2013). Some neuroimaging techniques to help clinical neurologists provide a definite diagnosis have been extensively evaluated. In particular, CJD diagnosis has employed MRI, computed tomography (CT), radionuclide techniques using positron emission tomography (PET), and single-photon emission tomography (SPECT) with different radiopharmaceuticals (Caobelli et al., 2015). In clinical practice, the probable diagnosis of TSEs relies on clinical features combined with the results of at least one paraclinical test (EEG, CSF analysis, and/or MRI abnormalities).

Diffusion-weighted imaging (DWI), fluid-attenuated inversion recovery (FLAIR), and apparent diffusion coefficient (ADC) are MRI sequences used to image the brain. High-intensity patterns in FLAIR, hyperintensity signals in DWI (the most sensitive sequence), and restricted diffusion in the ADC map gray matter regions give a positive predictive value for TSEs, with sensitivity and specificity values of 80% for detecting CJD (Gibson et al., 2018). CJD diagnostic criteria by bioimaging includes the presence of abnormal signal in the caudate and putamen, and MRI signal hyperintensities in the cortex of at least two lobes, excluding the frontal lobes on DWI and FLAIR for sCJD (Zerr et al., 2009; Bizzi et al., 2020). A recent study included a new criterion (index test) for diffusion MRI for the diagnosis of sCJD, being at least one positive brain region in addition to the current criteria (Bizzi et al., 2020). Analysis of diffusion MRI including the index test from ∼1,400 patients with suspected sCJD was superior to that of current standard criteria and comparable to second generation RT-QuIC (Bizzi et al., 2020).

Between 57% and 80% of sCJD patients show hyperintensity in the basal ganglia or cortex, with some also showing hyperintensity in the thalamus. MRI results are usually normal in patients with GSS and FFI, though some FFI patients show increased quantitative ADC and myoinositol in the thalamus. Quantitative MRI changes were also reported for FFI, characterized by increased mean diffusivity in the thalamus and cerebellum resultant from volumetric and diffusion tensor imaging (DTI) changes in the patient's brain (Grau-Rivera et al., 2017). In 90% of cases, vCJD shows a pulvinar sign in which the posterior third of the thalamus has a higher signal than other basal ganglia (Manix et al., 2015; Fragoso et al., 2017). MRI signal changes are correlated with disease duration and with the degree of spongiosis (Eisenmenger et al., 2016). The strict application of diagnostic criteria and careful interpretation of MRI output remain the most recommended approach to *in vivo* diagnosis of sCJD (Fragoso et al., 2017). In the context of clinical suspicion of TSEs, however, CT does remain useful as a first-line test to exclude other diagnoses that may have similar clinical features (Letourneau-Guillon et al., 2012).

Positron emission tomography (PET) is not a paraclinical test included in the guidelines for TSE diagnosis, but it has recently been tested with a small group of patients. CJD patients showed hypometabolism in the frontal and parietal cortex using [18F] fluoro-2-deoxy-D-glucose (FDG-PET), suggesting a correlation between clinical results and PET findings (Renard et al., 2017). In a different group of patients, hypermetabolism was observed in the limbic and mesolimbic systems (Mente et al., 2017). Hypometabolism in brain regions is consistent with neuropathology, but it is not an exclusive characteristic of prion diseases (Higuchi et al., 2000).

Amyloid tracers may also be used with PET to diagnose neurodegenerative diseases, but the selectivity of these tracers remains a topic of discussion and requires improvement. Therefore, this technique is still limited for the differential diagnosis of these diseases, though it has yet to be explored in detail in living patients.

Immunoassays

Immunoassays exploit the structural differences between PrP^{C} and PrP^{Sc} and rely on the specific interaction of monoclonal antibodies (mAbs) with PrP^{Sc} (Lukan et al., 2013). Although with potential application in diagnosis, immunoassays developed for analyzing body fluids, such as blood, CSF, or urine, have certain limitations. Unlike diagnostic studies using *in vitro* cell-free PrP conversion assays, reports of immunoassays have been restricted to blood samples not endogenously infected with PrP^{Sc} or from symptomatic vCJD patients. Almost all blood-based immunoassays developed to date rely on the detection of PrP^{Sc}. The major issue in blood detection systems is an extremely small amount of PrP^{Sc} combined with a high background PrP^{C} concentration (Abdel-Haq, 2015). For this reason, a PrP^{Sc} enrichment step is usually required in these assays (Lukan et al., 2013). The solid-state binding matrix assay relies on the selective adsorption of PrP^{Sc}, thus, no PK pre-treatment of samples is required in this assay (Properzi and Pocchiari, 2013), being also adapted for urine assessment (Luk et al., 2016). This approach has led to the establishment of a prototype blood test for the diagnosis of vCJD with high

sensitivity and specificity (Edgeworth et al., 2011), and was shown to be more efficient than immunoprecipitation with antibodies for detecting PrP^{Sc} in human whole blood spiked with high dilutions of vCJD-infected brain homogenate (Abdel-Haq, 2015). Although initially promising, this test failed to identify patients with sCJD or other TSEs (Edgeworth et al., 2011) and asymptomatic vCJD individuals (Jackson et al., 2014; Abdel-Haq, 2015). In summary, all these approaches present severe limitations regarding efficient detection of PrP^{Sc} in a variety of body fluids and tissues, being not recommended for routine diagnosis of human TSEs.

GUIDELINES FOR DIAGNOSIS

The WHO prepared a report in 1998, updated in 2003, defining the diagnostic criteria for CJD. However, much research has been carried out in the intervening years, and new diagnostic tools have been developed and tested with great success. The Centers for Disease Control and Prevention (CDC), an agency of the United States Department of Health and Human Services, updated the clinical diagnostic criteria for sCJD to include MRI brain scans and RT-QuIC analysis for the probable diagnosis of sCJD (**Table 5**).

The diagnosis of iCJD was defined as a progressive cerebellar syndrome in a patient treated with pituitary hormone receptor derived from human cadavers; or in a patient diagnosed with sporadic CJD with a recognized exposure risk—e.g., previous neurosurgery with dura mater graft. Genetic CJD is classified as definite or probable CJD plus definite or probable CJD in a first-degree relative; and/or neuropsychiatric disorder plus disease-specific PrP gene mutation (Brown et al., 2003; CDC's Diagnostic Criteria for Creutzfeldt–Jakob Disease (CJD), 2018).

One characteristic that distinguishes vCJD from sCJD is its prominent tropism for lymphoid organs, such as the tonsils. The analysis of PrP extracted from amygdala biopsy tissue appears to provide a sensitive and specific method for the diagnosis of vCJD in the appropriate clinical context (Araújo, 2013). However, due to the invasive nature of this test, it should only be performed in patients who meet the clinical criteria for vCJD, but where MRI data lacks the characteristic pulmonary sign. The detection of 14-3-3 protein in the CSF is not a sensitive marker for vCJD (Araújo, 2013). Definitive cases are diagnosed by visualization of amyloid plaques surrounded by vacuoles in both the cerebellum and cerebrum, called florid plaques, and by PrP deposition shown by immunohistochemistry (CDC's Diagnostic Criteria for Creutzfeldt–Jakob Disease (CJD), 2018). Suspected cases are identified based on the age of onset of the disease (<50 years), psychiatric symptoms (such as frank pain and/or dysesthesia), neurologic signs (at least two of the following: poor coordination, myoclonus, chorea, hyperreflexia, or visual signs), duration of illness of over 6 months, and no history for iCJD or gCJD.

Because of its genetic character, the diagnosis of GSS is limited to the demonstration of mutations in the *PRNP* gene. This seems to be a sensitive and highly specific way to diagnose GSS, but neuropathology, although less used in practice, can also be useful in a postmortem scenario (Araújo, 2013).

Finally, the diagnosis of FFI is first suggested by rapidly progressive cognitive impairment (dementia), along with changes in behavior or mood, ataxia, and sleep disorders. Additional diagnosis may include a sleep study. Given its etiology, genetic testing confirms the diagnosis (Wu et al., 2018).

CHALLENGES

Human prion diseases are rare, with an annual incidence of around 1–2 cases per million individuals worldwide, and around five cases per million after age 65 (Holman et al., 2010). These diseases are very intriguing and can have a quite distinct clinical

TABLE 5 | Current guidelines for sCJD diagnosis.

Diagnostic	Signals and symptoms	
	***WHO, 2003**	****CDC, 2018**
Possible	Progressive dementia; **AND** at least two of the following four clinical features: myoclonus, cerebellar or visual disturbance, pyramidal/extrapyramidal dysfunction, akinetic mutism; **AND** unknown or atypical EEG; **AND** disease duration less than two years.	Progressive dementia; **AND** at least two of the following four clinical features: myoclonus, cerebellar or visual disturbance, pyramidal/extrapyramidal dysfunction, akinetic mutism; **AND** no positive result for any of the four tests that would classify a case as "probable"; **AND** disease duration less than two years; **AND** no alternative diagnosis from routine investigations.
Probable	Progressive dementia; **AND** at least two of the following four clinical features: myoclonus, cerebellar or visual disorder, pyramidal/extrapyramidal dysfunction, akinetic mutism; **AND** typical EEG regardless of disease duration; **AND/OR** positive CSF 14-3-3 assay **and** disease duration to death less than two years; **AND** no alternative diagnosis from routine investigations.	Neuropsychiatric disorder **and** positive RT-QuIC in CSF or other samples; **OR** rapidly progressive dementia **and** at least two of the following four clinical features: myoclonus, cerebellar or visual disorder, pyramidal/extrapyramidal dysfunction, akinetic mutism; **AND** a positive result on at least one of the following tests: typical EEG regardless of disease duration, positive CSF 14-3-3 assay with disease duration less than two years, high signal in caudate/putamen on MRI brain scan or at least two cortical regions (temporal, parietal, occipital) either on DWI or FLAIR; **AND** no alternative diagnosis from routine investigations.
Definite	Neuropathological confirmation; **AND/OR** detection of ^{res}PrP by immunochemistry **or** immunoblotting; **AND/OR** observation of PrP^{Sc} fibrils.	Neuropathological confirmation; **AND/OR** detection of ^{res}PrP by immunochemistry **or** immunoblotting; **AND/OR** observation of PrP^{Sc} fibrils.

**Reference: Brown et al. (2003). ***Reference: CDC's Diagnostic Criteria for Creutzfeldt-Jakob Disease (CJD), 2018.*

presentation and causes (sporadic, inherited, and acquired). This heterogeneity poses challenges for diagnoses. Interestingly, all prion diseases involve the conversion and aggregation of PrP^{C} into its pathological form, PrP^{Sc}. Therefore, it is no wonder that the detection of PrP^{Sc} is used as the gold standard for a definite diagnosis.

The detection of PrP^{Sc} in patient samples is traditionally performed by neuropathological inspection of brain tissue, which is a criterion for a definite diagnosis (Brown et al., 2003). However, this assessment is done most often postmortem due to the invasiveness of tissue collection. Clinical and paraclinical antemortem evaluations are not considered sufficient to define the final diagnosis. However, with continued technological advances, there has been a marked improvement in several tests in recent years, contributing to the interpretation of cases.

The last decade has seen the development of the RT-QuIC assay, which can now detect the presence of PrP^{Sc}. This technique has several advantages, including:

(1) It can be used on more accessible samples, such as CSF;
(2) It exhibits high sensitivity and specificity, making other biochemical tests obsolete;
(3) It can detect PrP^{Sc} in samples from different types of TSEs;
(4) It involves a relatively simple method, employing materials and equipment that are more accessible and easier to maintain;
(5) A growing number of centers around the world have independently tested, validated, and used this technique to investigate large cohorts of patients;
(6) It is being adapted for the diagnosis of other neurodegenerative diseases, such as Parkinson's disease, tauopathies, and others.

Given these advantages, the CDC has included RT-QuIC as a parameter to characterize TSE diagnosis as probable (CDC's Diagnostic Criteria for Creutzfeldt–Jakob Disease (CJD), 2018). WHO guidelines do not yet include this parameter and should be updated to encourage its implementation in more facilities that can carry out these tests. The combination of (*i*) clinical evaluation, (*ii*) RT-QuIC analyses of two biological samples, and (*iii*) testing with at least one other technique—such as MRI, EEG, or 14-3-3 detection—should be considered internationally for a definite antemortem diagnosis, given that such combinations have provided diagnoses with 100% or nearly 100% sensitivity and specificity (Bongianni et al., 2017; Hermann et al., 2018; Rudge et al., 2018; Fiorini et al., 2020).

Furthermore, the RT-QuIC assay has been adapted in the last few years for detecting α-synuclein aggregates/fibrils and tau filaments in biological samples (Ferreira and Caughey, 2020). Therefore, the growth in RT-QuIC-based TSE diagnosis would certainly pave the way for RT-QuIC utilization in the early diagnosis of other neurodegenerative disorders, such as synucleinopathies (e.g., Parkinson's disease and dementia with Lewy bodies) and tauopathies (e.g., Alzheimer's disease and chronic traumatic encephalopathy.

Even with all the advances achieved to date in TSE diagnosis, most patients present the first typical clinical signs of the disease very late, when the degeneration is already quite advanced and irreversible. Regular clinical evaluation is only initiated at this point, resulting in therapeutic options that are, at best, symptomatic. Therefore, a significant challenge is to further increase the sensitivity and accuracy of testing to allow early antemortem diagnosis and to relate the findings to the progression of the disease. Another challenge is to obtain a diagnosis at pre-symptomatic stages of genetic forms of TSEs, which would require the combination of genotyping and the examination of samples using the assays discussed in this review. If an early diagnosis can be achieved, this opens the door to novel therapeutic strategies being tested and used successfully in the future.

AUTHOR CONTRIBUTIONS

YC, TCRGV, and LMA contributed to the conception and design of the study. SCR wrote the first draft of the manuscript. TCRGV, YC, LMA, and PBG wrote sections of the manuscript. LMA produced all figures. All authors contributed to the manuscript revision and read and approved the submitted version.

FUNDING

This study was financed in part by the Coordenação de Aperfeiçoamento de Pessoal de Nível Superior - Brasil (CAPES) - Finance Code 001; by Fundação de Amparo à Pesquisa do Estado do Rio de Janeiro (FAPERJ); and by the Conselho Nacional de Desenvolvimento Científico e Tecnológico (CNPq).

ACKNOWLEDGMENTS

We thank Natalia C. Ferreira for providing an RT-QuIC result and Pierluigi Gambetti for providing the brain samples used in this assay.

REFERENCES

Abdel-Haq, H. (2015). Factors intrinsic and extrinsic to blood hamper the development of a routine blood test for human prion diseases. *J. Gen. Virol.* 96, 479–493. doi: 10.1099/vir.0.070979-0

Abu-Rumeileh, S., Baiardi, S., Polischi, B., Mammana, A., Franceschini, A., Green, A., et al. (2019). Diagnostic value of surrogate CSF biomarkers for Creutzfeldt–Jakob disease in the era of RT-QuIC. *J. Neurol.* 266, 3136–3143. doi: 10.1007/s00415-019-09537-0

Abu-Rumeileh, S., Capellari, S., Stanzani-Maserati, M., Polischi, B., Martinelli, P., Caroppo, P., et al. (2018). The CSF neurofilament light signature in rapidly progressive neurodegenerative dementias. *Alzheimer's Res. Ther.* 10:3. doi: 10.1186/s13195-017-0331-1

Acquatella-Tran Van Ba, I., Imberdis, T., and Perrier, V. (2013). From prion diseases to prion-like propagation mechanisms of neurodegenerative diseases. *Int. J. Cell Biol.* 2013:975832. doi: 10.1155/2013/975832

Agrimi, U., Nonno, R., Dell'Omo, G., Di Bari, M. A., Conte, M., Chiappini, B., et al. (2008). Prion protein amino acid determinants of differential susceptibility and

molecular feature of prion strains in mice and voles. *PLoS Pathog.* 4:e1000113. doi: 10.1371/journal.ppat.1000113

Aguzzi, A., Glatzel, M., Montrasio, F., Prinz, M., and Heppner, F. L. (2001). Interventional strategies against prion diseases. *Nat. Rev. Neurosci.* 2, 745–749. doi: 10.1038/35094590

Aguzzi, A., Heikenwalder, M., and Polymenidou, M. (2007). Insights into prion strains and neurotoxicity. *Nat. Rev. Mol. Cell Biol.* 8, 552–561. doi: 10.1038/nrm2204

Aksamit, A. J., Preissner, C. M., and Homburger, H. A. (2001). Quantitation of 14-3-3 and neuron-specific enolase proteins in CSF in Creutzfeldt-Jakob disease. *Neurology* 57, 728–730. doi: 10.1212/WNL.57.4.728

Andréoletti, O., Litaise, C., Simmons, H., Corbière, F., Lugan, S., Costes, P., et al. (2012). Highly efficient prion transmission by blood transfusion. *PLoS Pathog.* 8:e1002782. doi: 10.1371/journal.ppat.1002782

Annus, Á, Csáti, A., and Vécsei, L. (2016). Prion diseases: new considerations. *Clin. Neurol. Neurosurg.* 150, 125–132. doi: 10.1016/j.clineuro.2016.09.006

Araújo, A. Q. C. (2013). Doenças priônicas. *Arq. Neuropsiquiatr.* 71, 731–737. doi: 10.1590/0004-282X201301461

Atarashi, R., Moore, R. A., Sim, V. L., Hughson, A. G., Dorward, D. W., Onwubiko, H. A., et al. (2007). Ultrasensitive detection of scrapie prion protein using seeded conversion of recombinant prion protein. *Nat. Methods* 4, 645–650. doi: 10.1038/nmeth1066

Atarashi, R., Satoh, K., Sano, K., Fuse, T., Yamaguchi, N., Ishibashi, D., et al. (2011). Ultrasensitive human prion detection in cerebrospinal fluid by real-time quaking-induced conversion. *Nat. Med.* 17, 175–178. doi: 10.1038/nm.2294

Atarashi, R., Wilham, J. M., Christensen, L., Hughson, A. G., Moore, R. A., Johnson, L. M., et al. (2008). Simplified ultrasensitive prion detection by recombinant PrP conversion with shaking. *Nat. Methods* 5, 211–212. doi: 10.1038/nmeth0308-211

Ayers, J. I., and Prusiner, S. B. (2020). Prion protein — mediator of toxicity in multiple proteinopathies. *Nat. Rev. Neurol.* 16, 187–188. doi: 10.1038/s41582-020-0332-8

Bahl, J. M. C., Heegaard, N. H. H., Falkenhorst, G., Laursen, H., Høgenhaven, H., Mølbak, K., et al. (2009). The diagnostic efficiency of biomarkers in sporadic Creutzfeldt-Jakob disease compared to Alzheimer's disease. *Neurobiol. Aging* 30, 1834–1841. doi: 10.1016/j.neurobiolaging.2008.01.013

Baral, P. K., Yin, J., Aguzzi, A., and James, M. N. G. (2019). Transition of the prion protein from a structured cellular form (PrPC) to the infectious scrapie agent (PrPSc). *Protein Sci.* 28, 2055–2063. doi: 10.1002/pro.3735

Beaudry, P., Cohen, P., Brandel, J. P., Delasnerie-Laupрêtre, N., Richard, S., Launay, J. M., et al. (1999). 14-3-3 Protein, neuron-specific enolase, and S-100 protein in cerebrospinal fluid of patients with Creutzfeldt-Jakob disease. *Dement. Geriatr. Cogn. Disord.* 10, 40–46. doi: 10.1159/000017095

Bellon, A., Seyfert-Brandt, W., Lang, W., Baron, H., Gröner, A., and Vey, M. (2003). Improved conformation-dependent immunoassay: suitability for human prion detection with enhanced sensitivity. *J. Gen. Virol.* 84, 1921–1925. doi: 10.1099/vir.0.18996-0

Bendheim, P. E., Barry, R. A., Dearmond, S. J., Stites, D. P., and Prusiner, S. B. (1984). Antibodies to a scrapie prion protein. *Nature* 310, 418–421. doi: 10.1038/310418a0

Bessen, R. A., Kocisko, D. A., Raymond, G. J., Nandan, S., Lansbury, P. T., and Caughey, B. (1995). Non-genetic propagation of strain-specific properties of scrapie prion protein. *Nature* 375, 698–700. doi: 10.1038/375698a0

Bizzi, A., Pascuzzo, R., Blevins, J., Grisoli, M., Lodi, R., Moscatelli, M. E. M., et al. (2020). Evaluation of a new criterion for detecting prion disease with diffusion magnetic resonance Imaging. *JAMA Neurol.* 77, 1–9. doi: 10.1001/jamaneurol.2020.1319

Bongianni, M., Orrù, C., Groveman, B. R., Sacchetto, L., Fiorini, M., Tonoli, G., et al. (2017). Diagnosis of human prion disease using real-time quaking-induced conversion testing of olfactory mucosa and cerebrospinal fluid samples. *JAMA Neurol.* 74, 155–162. doi: 10.1001/jamaneurol.2016.4614

Bougard, D., Brandel, J. P., Bélondrade, M., Béringue, V., Segarra, C., Fleury, H., et al. (2016). Detection of prions in the plasma of presymptomatic and symptomatic patients with variant Creutzfeldt-Jakob disease. *Sci. Transl. Med.* 8:370ra182. doi: 10.1126/scitranslmed.aag1257

Brown, P., Brunk, C., Budka, H., Cervenakova, L., Collie, D., Green, A., et al. (2003). *). WHO Manual for Surveillance of Human Transmissible Spongiform Encephalopathies, Including Variant Creutzfeldt-Jakob Disease*. Geneva: World Health Organization.

Caobelli, F., Cobelli, M., Pizzocaro, C., Pavia, M., Magnaldi, S., and Guerra, U. P. (2015). The role of neuroimaging in evaluating patients affected by creutzfeldt-jakob disease: a systematic review of the literature. *J. Neuroimaging* 25, 2–13. doi: 10.1111/jon.12098

Castilla, J., Saá, P., and Soto, C. (2004). "Cyclic Amplification of Prion Protein Misfolding," in *Techniques in Prion Research*, eds S. Lehmann and J. Grassi (Basel: Birkhäuser), 198–213. doi: 10.1007/978-3-0348-7949-1_14

Castilla, J., Saá, P., and Soto, C. (2005). Detection of prions in blood. *Nat. Med.* 11, 982–985. doi: 10.1038/nm1286

Caughey, B. (2000). Formation of protease-resistant prion protein in cell-free systems. *Curr. Issues Mol. Biol.* 2, 95–101.

Caughey, B., Baron, G. S., Chesebro, B., and Jeffrey, M. (2009). Getting a grip on prions: oligomers, amyloids, and pathological membrane interactions. *Annu. Rev. Biochem.* 78, 177–204. doi: 10.1146/annurev.biochem.78.082907.145410

CDC's Diagnostic Criteria for Creutzfeldt–Jakob Disease (CJD) (2018). *Centers Dis. Control Prev*. Available online at: https://www.cdc.gov/prions/cjd/diagnostic-criteria.html (accessed September 22, 2020).

Chen, C., and Dong, X. P. (2016). Epidemiological characteristics of human prion diseases. *Infect. Dis. Poverty* 5:47. doi: 10.1186/s40249-016-0143-8

Chesebro, B. (2003). Introduction to the transmissible spongiform encephalopathies or prion diseases. *Br. Med. Bull.* 66, 1–20. doi: 10.1093/bmb/dg66.001

Chiti, F., and Dobson, C. M. (2006). Protein misfolding, functional amyloid, and human disease. *Annu. Rev. Biochem.* 75, 333–366. doi: 10.1146/annurev.biochem.75.101304.123901

Chitravas, N., Jung, R. S., Kofskey, D. M., Blevins, J. E., Gambetti, P., Leigh, R. J., et al. (2011). Treatable neurological disorders misdiagnosed as Creutzfeldt-Jakob disease. *Ann. Neurol.* 70, 437–444. doi: 10.1002/ana.22454

Chohan, G., Pennington, C., Mackenzie, J. M., Andrews, M., Everington, D., Will, R. G., et al. (2010). The role of cerebrospinal fluid 14-3-3 and other proteins in the diagnosis of sporadic Creutzfeldt-Jakob disease in the UK: a 10-year review. *J. Neurol. Neurosurg. Psychiatry* 81, 1243–1248. doi: 10.1136/jnnp.2009.197962

Cobb, N. J., and Surewicz, W. K. (2009). Prion diseases and their biochemical mechanisms. *Biochemistry* 48, 2574–2585. doi: 10.1021/bi900108v

Cohen, O. S., Chapman, J., Korczyn, A. D., Warman-Alaluf, N., Nitsan, Z., Appel, S., et al. (2016). CSF tau correlates with CJD disease severity and cognitive decline. *Acta Neurol. Scand.* 133, 119–123. doi: 10.1111/ane.12441

Colby, D. W., and Prusiner, S. B. (2011). De novo generation of prion strains. *Nat. Rev. Microbiol.* 9, 771–777. doi: 10.1038/nrmicro2650

Colby, D. W., Zhang, Q., Wang, S., Groth, D., Legname, G., Riesner, D., et al. (2007). Prion detection by an amyloid seeding assay. *Proc. Natl. Acad. Sci. U.S.A.* 104, 20914–20919. doi: 10.1073/pnas.0710152105

Collins, S. J., Sanchez-Juan, P., Masters, C. L., Klug, G. M., Van Duijn, C., Poleggi, A., et al. (2006). Determinants of diagnostic investigation sensitivities across the clinical spectrum of sporadic Creutzfeldt-Jakob disease. *Brain* 129, 2278–2287. doi: 10.1093/brain/awl159

Concha-Marambio, L., Pritzkow, S., Moda, F., Tagliavini, F., Ironside, J. W., Schulz, P. E., et al. (2016). Detection of prions in blood from patients with variant Creutzfeldt-Jakob disease. *Sci. Transl. Med.* 8:370ra183. doi: 10.1126/scitranslmed.aaf6188

Corbett, G. T., Wang, Z., Hong, W., Colom-Cadena, M., Rose, J., Liao, M., et al. (2020). PrP is a central player in toxicity mediated by soluble aggregates of neurodegeneration-causing proteins. *Acta Neuropathol.* 139, 503–526. doi: 10.1007/s00401-019-02114-9

Cracco, L., Appleby, B. S., and Gambetti, P. (2018). Fatal familial insomnia and sporadic fatal insomnia. *Handb. Clin. Neurol.* 153, 271–299. doi: 10.1016/B978-0-444-63945-5.00015-5

Cramm, M., Schmitz, M., Karch, A., Mitrova, E., Kuhn, F., Schroeder, B., et al. (2016). Stability and reproducibility underscore utility of RT-QuIC for diagnosis of Creutzfeldt-Jakob Disease. *Mol. Neurobiol.* 53, 1896–1904. doi: 10.1007/s12035-015-9133-2

Cramm, M., Schmitz, M., Karch, A., Zafar, S., Varges, D., Mitrova, E., et al. (2015). Characteristic CSF prion seeding efficiency in humans with prion diseases. *Mol. Neurobiol.* 51, 396–405. doi: 10.1007/s12035-014-8709-6

Di Bari, M. A., Chianini, F., Vaccari, G., Esposito, E., Conte, M., Eaton, S. L., et al. (2008). The bank vole (Myodes glareolus) as a sensitive bioassay for sheep scrapie. *J. Gen. Virol.* 89, 2975–2985. doi: 10.1099/vir.0.2008/005520-0

Di Bari, M. A., Nonno, R., Castilla, J., D'Agostino, C., Pirisinu, L., Riccardi, G., et al. (2013). Chronic wasting disease in bank voles: characterisation of the shortest incubation time model for prion diseases. *PLoS Pathog.* 9:e1003219. doi: 10.1371/journal.ppat.1003219

Diack, A. B., Ritchie, D. L., Peden, A. H., Brown, D., Boyle, A., Morabito, L., et al. (2014). Variably protease-sensitive prionopathy, a unique prion variant with inefficient transmission properties. *Emerg. Infect. Dis.* 20, 1969–1979. doi: 10.3201/eid2012.140214

Edgeworth, J. A., Farmer, M., Sicilia, A., Tavares, P., Beck, J., Campbell, T., et al. (2011). Detection of prion infection in variant Creutzfeldt-Jakob disease: a blood-based assay. *Lancet* 377, 487–493. doi: 10.1016/S0140-6736(10)62308-2

Eisenmenger, L., Porter, M. C., Carswell, C. J., Thompson, A., Mead, S., Rudge, P., et al. (2016). Evolution of diffusion-weighted magnetic resonance imaging signal abnormality in sporadic Creutzfeldt-jakob disease, with histopathological correlation. *JAMA Neurol.* 73, 76–84. doi: 10.1001/jamaneurol.2015.3159

Feinstein, A. R. (1975). XXXI. On the sensitivity, specificity, and discrimination of diagnostic tests. *Clin. Pharmacol. Ther.* 17, 104–116. doi: 10.1002/cpt1975171104

Ferreira, N. D. C., and Caughey, B. (2020). Proteopathic seed amplification assays for neurodegenerative disorders. *Clin. Lab. Med.* 40, 257–270. doi: 10.1016/j.cll.2020.04.002

Fiorini, M., Iselle, G., Perra, D., Bongianni, M., Capaldi, S., Sacchetto, L., et al. (2020). High diagnostic accuracy of RT-QuIC assay in a prospective study of patients with suspected sCJD. *Int. J. Mol. Sci.* 21:880. doi: 10.3390/ijms21030880

Foiani, M. S., Woollacott, I. O. C., Heller, C., Bocchetta, M., Heslegrave, A., Dick, K. M., et al. (2018). Plasma tau is increased in frontotemporal dementia. *J. Neurol. Neurosurg. Psychiatry* 89, 804–807. doi: 10.1136/jnnp-2017-317260

Forloni, G., Roiter, I., and Tagliavini, F. (2019). Clinical trials of prion disease therapeutics. *Curr. Opin. Pharmacol.* 44, 53–60. doi: 10.1016/j.coph.2019.04.019

Foutz, A., Appleby, B. S., Hamlin, C., Liu, X., Yang, S., Cohen, Y., et al. (2017). Diagnostic and prognostic value of human prion detection in cerebrospinal fluid. *Ann. Neurol.* 81, 79–92. doi: 10.1002/ana.24833

Fragoso, D. C., Gonçalves Filho, A. L., da, M., Pacheco, F. T., Barros, B. R., Littig, I. A., et al. (2017). Imaging of Creutzfeldt-Jakob disease: imaging patterns and their differential diagnosis. *Radiographics* 37, 234–257. doi: 10.1148/rg.2017160075

Franceschini, A., Baiardi, S., Hughson, A. G., McKenzie, N., Moda, F., Rossi, M., et al. (2017). High diagnostic value of second generation CSF RT-QuIC across the wide spectrum of CJD prions. *Sci. Rep.* 7:10655. doi: 10.1038/s41598-017-10922-w

Gambetti, P., Kong, Q., Zou, W., Parchi, P., and Chen, S. G. (2003). Sporadic and familial CJD: classification and characterisation. *Br. Med. Bull.* 66, 213–239. doi: 10.1093/bmb/66.1.213

Geschwind, M. D. (2015). Prion Diseases. *Contin. Lifelong Learn. Neurol.* 21, 1612–1638. doi: 10.1212/CON.0000000000000251

Geschwind, M. D., Martindale, J., Miller, D., DeArmond, S. J., Uyehara-Lock, J., Gaskin, D., et al. (2003). Challenging the clinical utility of the 14-3-3 protein for the diagnosis of sporadic Creutzfeldt-Jakob disease. *Arch. Neurol.* 60, 813–816. doi: 10.1001/archneur.60.6.813

Gibson, L. M., Chappell, F. M., Summers, D., Collie, D. A., Sellar, R., Best, J., et al. (2018). Post-mortem magnetic resonance imaging in patients with suspected prion disease: pathological confirmation, sensitivity, specificity and observer reliability. A national registry. *PLoS One* 13:e0201434. doi: 10.1371/journal.pone.0201434

Gmitterová, K., Heinemann, U., Bodemer, M., Krasnianski, A., Meissner, B., Kretzschmar, H. A., et al. (2009). 14-3-3 CSF levels in sporadic Creutzfeldt-Jakob disease differ across molecular subtypes. *Neurobiol. Aging* 30, 1842–1850. doi: 10.1016/j.neurobiolaging.2008.01.007

Grau-Rivera, O., Calvo, A., Bargalló, N., Monté, G. C., Nos, C., Lladó, A., et al. (2017). Quantitative magnetic resonance abnormalities in creutzfeldt-jakob disease and fatal insomnia. *J. Alzheimer's Dis.* 55, 431–443. doi: 10.3233/JAD-160750

Green, A. J. E., Ramljak, S., Müller, W. E. G., Knight, R. S. G., and Schröder, H. C. (2002). 14-3-3 in the cerebrospinal fluid of patients with variant and sporadic Creutzfeldt-Jakob disease measured using capture assay able to detect low levels of 14-3-3 protein. *Neurosci. Lett.* 324, 57–60. doi: 10.1016/S0304-3940(02)00172-6

Green, A. J. E., Thompson, E. J., Stewart, G. E., Zeidler, M., McKenzie, J. M., MacLeod, M. A., et al. (2001). Use of 14-3-3 and other brain-specific proteins in CSF in the diagnosis of variant Creutzfeldt-Jakob disease. *J. Neurol. Neurosurg. Psychiatry* 70, 744–748. doi: 10.1136/jnnp.70.6.744

Groveman, B. R., Kraus, A., Raymond, L. D., Dolan, M. A., Anson, K. J., Dorward, D. W., et al. (2015). Charge neutralization of the central lysine cluster in prion protein (PrP) promotes PrPSc-Like folding of recombinant PrP amyloids. *J. Biol. Chem.* 290, 1119–1128. doi: 10.1074/jbc.M114.619627

Groveman, B. R., Orrú, C. D., Hughson, A. G., Bongianni, M., Fiorini, M., Imperiale, D., et al. (2016). Extended and direct evaluation of RT-QuIC assays for Creutzfeldt-Jakob disease diagnosis. *Ann. Clin. Transl. Neurol.* 4, 139–144. doi: 10.1002/acn3.378

Groveman, B. R., Raymond, G. J., Campbell, K. J., Race, B., Raymond, L. D., Hughson, A. G., et al. (2017). Role of the central lysine cluster and scrapie templating in the transmissibility of synthetic prion protein aggregates. *PLoS Pathog.* 13:e1006623. doi: 10.1371/journal.ppat.1006623

Haley, N. J., and Richt, J. A. (2017). Evolution of diagnostic tests for chronic wasting disease, a naturally occurring prion disease of cervids. *Pathogens* 6:35. doi: 10.3390/pathogens6030035

Hamlin, C., Puoti, G., Berri, S., Sting, E., Harris, C., Cohen, M., et al. (2012). A comparison of tau and 14-3-3 protein in the diagnosis of Creutzfeldt-Jakob disease. *Neurology* 79, 547–552. doi: 10.1212/WNL.0b013e318263565f

Hansen, H. C., Zschocke, S., Stürenburg, H. J., and Kunze, K. (1998). Clinical changes and EEG patterns preceding the onset of periodic sharp wave complexes in Creutzfeldt-Jakob disease. *Acta Neurol. Scand.* 97, 99–106. doi: 10.1111/j.1600-0404.1998.tb00617.x

Hermann, P., Laux, M., Glatzel, M., Matschke, J., Knipper, T., Goebel, S., et al. (2018). Validation and utilization of amended diagnostic criteria in Creutzfeldt-Jakob disease surveillance. *Neurology* 91, e331–e338. doi: 10.1212/WNL.0000000000005860

Higuchi, M., Tashiro, M., Arai, H., Okamura, N., Hara, S., Higuchi, S., et al. (2000). Glucose hypometabolism and neuropathological correlates in brains of dementia with Lewy bodies. *Exp. Neurol.* 162, 247–256. doi: 10.1006/exnr.2000.7342

Hill, A. F., Desbruslais, M., Joiner, S., Sidle, K. C. L., Gowland, I., Collinge, J., et al. (1997). The same prion strain causes vCJD and BSE. *Nature* 389, 448–450. doi: 10.1038/38925

Holman, R. C., Belay, E. D., Christensen, K. Y., Maddox, R. A., Minino, A. M., Folkema, A. M., et al. (2010). Human prion diseases in the United States. *PLoS One* 5:e8521. doi: 10.1371/journal.pone.0008521

Hsich, G., Kenney, K., Gibbs, C. J., Lee, K. H., and Harrington, M. G. (1996). The 14-3-3 brain protein in cerebrospinal fluid as a marker for transmissible spongiform encephalopathies. *N. Engl. J. Med.* 335, 924–930. doi: 10.1056/NEJM199609263351303

Hunter, N., Foster, J., Chong, A., McCutcheon, S., Parnham, D., Eaton, S., et al. (2002). Transmission of prion diseases by blood transfusion. *J. Gen. Virol.* 83, 2897–2905. doi: 10.1099/0022-1317-83-11-2897

Igel-Egalon, A., Béringue, V., Rezaei, H., and Sibille, P. (2018). Prion strains and transmission barrier phenomena. *Pathogens* 7:5. doi: 10.3390/pathogens7010005

Ironside, J. W., Ritchie, D. L., and Head, M. W. (2017). Prion diseases. *Handb. Clin. Neurol.* 145, 393–403. doi: 10.1016/B978-0-12-802395-2.00028-6

Iwasaki, Y. (2017). Creutzfeldt-Jakob disease. *Neuropathology* 37, 174–188. doi: 10.1111/neup.12355

Jackson, G. S., Burk-Rafel, J., Edgeworth, J. A., Sicilia, A., Abdilahi, S., Korteweg, J., et al. (2014). Population screening for variant Creutzfeldt-Jakob disease using a novel blood test: diagnostic accuracy and feasibility study. *JAMA Neurol.* 71, 421–428. doi: 10.1001/jamaneurol.2013.6001

Jensen, M., Basun, H., and Lannfelt, L. (1995). Increased cerebrospinal fluid tau in patients with Alzheimer's disease. *Neurosci. Lett.* 186, 189–191. doi: 10.1016/0304-3940(95)11297-A

Jones, M., Peden, A. H., Prowse, C. V., Gröner, A., Manson, J. C., Turner, M. L., et al. (2007). In vitro amplification and detection of variant Creutzfeldt-Jakob disease PrPSc. *J. Pathol.* 213, 21–26. doi: 10.1002/path.2204

Kascsak, R. J., Rubenstein, R., Merz, P. A., Tonna-DeMasi, M., Fersko, R., Carp, R. I., et al. (1987). Mouse polyclonal and monoclonal antibody to scrapie-associated fibril proteins. *J. Virol.* 61, 3688–3693. doi: 10.1128/jvi.61.12.3688-3693.1987

Kenney, K., Brechtel, C., Takahashi, H., Kurohara, K., Anderson, P., and Gibbs, C. J. (2000). An enzyme-linked immunosorbent assay to quantify 14-3-3 proteins in the cerebrospinal fluid of suspected Creutzfeldt-Jakob disease patients. *Ann. Neurol.* 48, 395–398. doi: 10.1002/1531-8249(200009)48:3<395::AID-ANA18<3.0.CO;2-A

Kim, C., Haldiman, T., Cohen, Y., Chen, W., Blevins, J., Sy, M. S., et al. (2011). Protease-sensitive conformers in broad spectrum of distinct prp sc structures in sporadic creutzfeldt-jakob disease are indicator of progression rate. *PLoS Pathog.* 7:e1002242. doi: 10.1371/journal.ppat.1002242

Kim, C., Haldiman, T., Surewicz, K., Cohen, Y., Chen, W., Blevins, J., et al. (2012). Small protease sensitive oligomers of PrPSc in distinct human prions determine conversion rate of PrPC. *PLoS Pathog.* 8:e1002835. doi: 10.1371/journal.ppat.1002835

Kim, C., Xiao, X., Chen, S., Haldiman, T., Smirnovas, V., Kofskey, D., et al. (2018). Artificial strain of human prions created in vitro. *Nat. Commun.* 9:2166. doi: 10.1038/s41467-018-04584-z

Kim, M. O., Takada, L. T., Wong, K., Forner, S. A., and Geschwind, M. D. (2018). Genetic PrP prion diseases. *Cold Spring Harb. Perspect. Biol.* 10:a033134. doi: 10.1101/cshperspect.a033134

Kobayashi, A., Mizukoshi, K., Iwasaki, Y., Miyata, H., Yoshida, Y., and Kitamoto, T. (2011). Co-occurrence of types 1 and 2 PrPres in sporadic Creutzfeldt-Jakob disease MM1. *Am. J. Pathol.* 178, 1309–1315. doi: 10.1016/j.ajpath.2010.11.069

Kraus, A., Anson, K. J., Raymond, L. D., Martens, C., Groveman, B. R., Dorward, D. W., et al. (2015). Prion protein prolines 102 and 105 and the surrounding lysine cluster impede amyloid formation. *J. Biol. Chem.* 290, 21510–21522. doi: 10.1074/jbc.M115.665844

Kraus, A., Groveman, B. R., and Caughey, B. (2013). Prions and the potential transmissibility of protein misfolding diseases. *Annu. Rev. Microbiol.* 67, 543–564. doi: 10.1146/annurev-micro-092412-155735

Kruse, N., Heslegrave, A., Gupta, V., Foiani, M., Villar-Piqué, A., Schmitz, M., et al. (2018). Interlaboratory validation of cerebrospinal fluid α-synuclein quantification in the diagnosis of sporadic Creutzfeldt-Jakob disease. *Alzheimer's Dement.* 10, 461–470. doi: 10.1016/j.dadm.2018.06.005

Kushnirov, V. V., Dergalev, A. A., and Alexandrov, A. I. (2020). Proteinase K resistant cores of prions and amyloids. *Prion* 14, 11–19. doi: 10.1080/19336896.2019.1704612

Kwon, G. T., and Kwon, M. S. (2019). Diagnostic challenge of rapidly progressing sporadic Creutzfeldt-Jakob disease. *BMJ Case Rep.* 12:e230535. doi: 10.1136/bcr-2019-230535

Lacroux, C., Comoy, E., Moudjou, M., Perret-Liaudet, A., Lugan, S., Litaise, C., et al. (2014). Preclinical detection of variant CJD and BSE prions in blood. *PLoS Pathog.* 10:e1004202. doi: 10.1371/journal.ppat.1004202

Ladogana, A., Sanchez-Juan, P., Mitrová, E., Green, A., Cuadrado-Corrales, N., Sánchez-Valle, R., et al. (2009). Cerebrospinal fluid biomarkers in human genetic transmissible spongiform encephalopathies. *J. Neurol.* 256, 1620–1628. doi: 10.1007/s00415-009-5163-x

Lemstra, A. W., Van Meegen, M. T., Vreyling, J. P., Meijerink, P. H. S., Jansen, G. H., Bulk, S., et al. (2000). 14-3-3 testing in diagnosing Creutzfeldt-Jakob disease: a prospective study in 112 patients. *Neurology* 55, 514–516. doi: 10.1212/WNL.55.4.514

Letourneau-Guillon, L., Wada, R., and Kucharczyk, W. (2012). Imaging of prion diseases. *J. Magn. Reson. Imaging* 35, 998–1012. doi: 10.1002/jmri.23504

Llewelyn, C. A., Hewitt, P. E., Knight, R. S. G., Amar, K., Cousens, S., MacKenzie, J., et al. (2004). Possible transmission of variant Creutzfeldt-Jakob disease by blood transfusion. *Lancet* 363, 417–421. doi: 10.1016/S0140-6736(04)15486-X

Llorens, F., Kruse, N., Karch, A., Schmitz, M., Zafar, S., Gotzmann, N., et al. (2018). Validation of α-Synuclein as a CSF biomarker for sporadic Creutzfeldt-Jakob disease. *Mol. Neurobiol.* 55, 2249–2257. doi: 10.1007/s12035-017-0479-5

Llorens, F., Kruse, N., Schmitz, M., Gotzmann, N., Golanska, E., Thüne, K., et al. (2017). Evaluation of α-synuclein as a novel cerebrospinal fluid biomarker in different forms of prion diseases. *Alzheimer's Dement.* 13, 710–719. doi: 10.1016/j.jalz.2016.09.013

Llorens, F., Rübsamen, N., Hermann, P., Schmitz, M., Villar-Piqué, A., Goebel, S., et al. (2020a). A prognostic model for overall survival in sporadic Creutzfeldt-Jakob disease. *Alzheimer's Dement.* 16, 1438–1447. doi: 10.1002/alz.12133

Llorens, F., Villar-Piqué, A., Hermann, P., Schmitz, M., Goebel, S., Waniek, K., et al. (2020b). Cerebrospinal fluid non-phosphorylated tau in the differential diagnosis of Creutzfeldt–Jakob disease: a comparative prospective study with 14-3-3. *J. Neurol.* 267, 543–550. doi: 10.1007/s00415-019-09610-8

Llorens, F., Villar-Piqué, A., Schmitz, M., Diaz-Lucena, D., Wohlhage, M., Hermann, P., et al. (2020c). Plasma total prion protein as a potential biomarker for neurodegenerative dementia: diagnostic accuracy in the spectrum of prion diseases. *Neuropathol. Appl. Neurobiol.* 46, 240–254. doi: 10.1111/nan.12573

Luk, C., Jones, S., Thomas, C., Fox, N. C., and Tze, H. (2016). Prospective diagnosis of sporadic CJD by the detection of abnormal PrP in patient urine. *JAMA Neurol.* 73, 1454–1460. doi: 10.1001/jamaneurol.2016.3733

Lukan, A., Vranac, T., and Èurin Šerbec, V. (2013). TSE diagnostics: recent advances in immunoassaying prions. *Clin. Dev. Immunol.* 2013:360604. doi: 10.1155/2013/360604

Manix, M., Kalakoti, P., Henry, M., Thakur, J., Menger, R., Guthikonda, B., et al. (2015). Creutzfeldt-Jakob disease: updated diagnostic criteria, treatment algorithm, and the utility of brain biopsy. *Neurosurg. Focus* 39:E2. doi: 10.3171/2015.8.FOCUS15328

McGuire, L. I., Peden, A. H., Orrú, C. D., Wilham, J. M., Appleford, N. E., Mallinson, G., et al. (2012). Real time quaking-induced conversion analysis of cerebrospinal fluid in sporadic Creutzfeldt-Jakob disease. *Ann. Neurol.* 72, 278–285. doi: 10.1002/ana.23589

McGuire, L. I., Poleggi, A., Poggiolini, I., Suardi, S., Grznarova, K., Shi, S., et al. (2016). Cerebrospinal fluid real-time quaking-induced conversion is a robust and reliable test for sporadic creutzfeldt-jakob disease: an international study. *Ann. Neurol.* 80, 160–165. doi: 10.1002/ana.24679

Mente, K. P., O'Donnell, J. K., Jones, S. E., Cohen, M. L., Thompson, N. R., Bizzi, A., et al. (2017). Fluorodeoxyglucose positron emission tomography (FDG-PET) correlation of histopathology and MRI in prion disease. *Alzheimer Dis. Assoc. Disord.* 31, 1–7. doi: 10.1097/WAD.0000000000000188

Metrick, M. A., do Carmo Ferreira, N., Saijo, E., Hughson, A. G., Kraus, A., Orrú, C., et al. (2019). Million-fold sensitivity enhancement in proteopathic seed amplification assays for biospecimens by Hofmeister ion comparisons. *Proc. Natl. Acad. Sci. U.S.A.* 116, 23029–23039. doi: 10.1073/pnas.1909322116

Mielke, M. M., Hagen, C. E., Wennberg, A. M. V., Airey, D. C., Savica, R., Knopman, D. S., et al. (2017). Association of plasma total tau level with cognitive decline and risk of mild cognitive impairment or dementia in the Mayo Clinic study on aging. *JAMA Neurol.* 74, 1073–1080. doi: 10.1001/jamaneurol.2017.1359

Minikel, E. V., Kuhn, E., Cocco, A. R., Vallabh, S. M., Hartigan, C. R., Reidenbach, A. G., et al. (2019). Domain-specific quantification of prion protein in cerebrospinal fluid by targeted mass spectrometry. *Mol. Cell. Proteomics* 18, 2388–2400. doi: 10.1074/mcp.RA119.001702

Moda, F., Gambetti, P., Notari, S., Concha-Marambio, L., Catania, M., Park, K.-W., et al. (2014). Prions in the urine of patients with variant Creutzfeldt–Jakob Disease. *N. Engl. J. Med.* 371, 530–539. doi: 10.1056/NEJMoa1404401

Murray, K. (2011). Creutzfeldt-jacob disease mimics, or how to sort out the subacute encephalopathy patient. *Pract. Neurol.* 11, 19–28. doi: 10.1136/pgmj.2010.235721rep

Nonno, R., Di Bari, M. A., Cardone, F., Vaccari, G., Fazzi, P., Dell'Omo, G., et al. (2006). Efficient transmission and characterization of Creutzfeldt-Jakob disease strains in bank voles. *PLoS Pathog.* 2:e12. doi: 10.1371/journal.ppat.0020012

Orrú, C. D., Bongianni, M., Tonoli, G., Ferrari, S., Hughson, A. G., Groveman, B. R., et al. (2014). A test for Creutzfeldt–Jakob Disease using nasal brushings. *N. Engl. J. Med.* 371, 519–529. doi: 10.1056/nejmoa1315200

Orrú, C. D., Groveman, B. R., Hughson, A. G., Zanusso, G., Coulthart, M. B., and Caughey, B. (2015a). Rapid and sensitive RT-QuIC detection of human creutzfeldt-jakob disease using cerebrospinal fluid. *mBio* 6:e02451-14. doi: 10.1128/mBio.02451-14

Orrú, C. D., Groveman, B. R., Raymond, L. D., Hughson, A. G., Nonno, R., Zou, W., et al. (2015b). Bank vole prion protein as an apparently universal substrate for RT-QuIC-Based Detection and discrimination of prion strains. *PLoS Pathog.* 11:e1004983. doi: 10.1371/journal.ppat.1004983

Orrú, C. D., Wilham, J. M., Hughson, A. G., Raymond, L. D., McNally, K. L., Bossers, A., et al. (2009). Human variant Creutzfeldt-Jakob disease and sheep scrapie PrPres detection using seeded conversion of recombinant prion protein. *Protein Eng. Des. Sel.* 22, 515–521. doi: 10.1093/protein/gzp031

Orrú, C. D., Wilham, J. M., Raymond, L. D., Kuhn, F., Schroeder, B., Raeber, A. J., et al. (2011). Prion disease blood test using immunoprecipitation and improved quaking-induced conversion. *mBio* 2:e00078-11. doi: 10.1128/mBio.00078-11

Orrú, C. D., Yuan, J., Appleby, B. S., Li, B., Li, Y., Winner, D., et al. (2017). Prion seeding activity and infectivity in skin samples from patients with sporadic Creutzfeldt-Jakob disease. *Sci. Transl. Med.* 9:eaam7785. doi: 10.1126/scitranslmed.aam7785

Ortega-Cubero, S., Luquín, M. R., Domínguez, I., Arbizu, J., Pagola, I., Carmona-Abellán, M. M., et al. (2013). Structural and functional neuroimaging in human prion diseases. *Neurología* 28, 299–308. doi: 10.1016/j.nrleng.2011.03.012

Oshita, M., Yokoyama, T., Takei, Y., Takeuchi, A., Ironside, J. W., Kitamoto, T., et al. (2016). Efficient propagation of variant Creutzfeldt-Jakob disease prion protein using the cell-protein misfolding cyclic amplification technique with samples containing plasma and heparin. *Transfusion* 56, 223–230. doi: 10.1111/trf.13279

Otto, M., Wiltfang, J., Cepek, L., Neumann, M., Mollenhauer, B., Steinacker, P., et al. (2002). Tau protein and 14-3-3 protein in the differential diagnosis of Creutzfeldt-Jakob disease. *Neurology* 58, 192–197. doi: 10.1212/WNL.58.2.192

Otto, M., Wiltfang, J., Schütz, E., Zerr, I., Otto, A., Pfahlberg, A., et al. (1998). Diagnosis of Creutzfeldt-Jakob disease by measurement of S100 protein in serum: prospective case-control study. *Br. Med. J.* 316, 577–582. doi: 10.1136/bmj.316.7131.577

Otto, M., Wiltfang, J., Tumani, H., Zerr, I., Lantsch, M., Kornhuber, J., et al. (1997). Elevated levels of tau-protein in cerebrospinal fluid of patients with Creutzfeldt-Jakob disease. *Neurosci. Lett.* 225, 210–212. doi: 10.1016/S0304-3940(97)00215-2

Parchi, P., De Boni, L., Saverioni, D., Cohen, M. L., Ferrer, I., Gambetti, P., et al. (2012). Consensus classification of human prion disease histotypes allows reliable identification of molecular subtypes: an inter-rater study among surveillance centres in Europe and USA. *Acta Neuropathol.* 124, 517–529. doi: 10.1007/s00401-012-1002-8

Parchi, P., Giese, A., Capellari, S., Brown, P., Schulz-Schaeffer, W., Windl, O., et al. (1999). Classification of sporadic Creutzfeldt-Jakob disease based on molecular and phenotypic analysis of 300 subjects. *Ann. Neurol.* 46, 224–233. doi: 10.1002/1531-8249(199908)46:2<224::AID-ANA12<3.0.CO;2-W

Pastrana, M. A., Sajnani, G., Onisko, B., Castilla, J., Morales, R., Soto, C., et al. (2006). Isolation and characterization of a proteinase K-sensitive PrPSc fraction. *Biochemistry* 45, 15710–15717. doi: 10.1021/bi0615442

Peden, A. H., McGuire, L. I., Appleford, N. E. J., Mallinson, G., Wilham, J. M., Orrú, C. D., et al. (2012). Sensitive and specific detection of sporadic Creutzfeldt-Jakob disease brain prion protein using real-time quaking-induced conversion. *J. Gen. Virol.* 93, 438–449. doi: 10.1099/vir.0.033365-0

Peggion, C., Bertoli, A., and Sorgato, M. C. (2017). Almost a century of prion protein(s): from pathology to physiology, and back to pathology. *Biochem. Biophys. Res. Commun.* 483, 1148–1155. doi: 10.1016/j.bbrc.2016.07.118

Peoc'h, K., Schröder, H. C., Laplanche, J. L., Ramljak, S., and Müller, W. E. G. (2001). Determination of 14-3-3 protein levels in cerebrospinal fluid from Creutzfeldt-Jakob patients by a highly sensitive capture assay. *Neurosci. Lett.* 301, 167–170. doi: 10.1016/S0304-3940(01)01619-6

Properzi, F., and Pocchiari, M. (2013). Identification of misfolded proteins in body fluids for the diagnosis of prion diseases. *Int. J. Cell Biol.* 2013:839329. doi: 10.1155/2013/839329

Prusiner, S. (1982). Novel proteinaceous infectious particles cause scrapie. *Science* 216, 136–144. doi: 10.1126/science.6801762

Prusiner, S. B. (1991). Molecular biology of prion diseases. *Science* 252, 1515–1522. doi: 10.1126/science.1675487

Prusiner, S. B. (1998). Prions. *Proc. Natl. Acad. Sci. U.S.A.* 95, 13363–13383. doi: 10.1073/pnas.95.23.13363

Prusiner, S. B., and Hsiao, K. K. (1994). Human prion diseases. *Ann. Neurol.* 35, 385–395. doi: 10.1002/ana.410350404

Puoti, G., Bizzi, A., Forloni, G., Safar, J. G., Tagliavini, F., and Gambetti, P. (2012). Sporadic human prion diseases: molecular insights and diagnosis. *Lancet Neurol.* 11, 618–628. doi: 10.1016/S1474-4422(12)70063-7

Raymond, G. J., Race, B., Orrú, C. D., Raymond, L. D., Bongianni, M., Fiorini, M., et al. (2020). Transmission of CJD from nasal brushings but not spinal fluid or RT-QuIC product. *Ann. Clin. Transl. Neurol.* 7, 932–944. doi: 10.1002/acn3.51057

Redaelli, V., Bistaffa, E., Zanusso, G., Salzano, G., Sacchetto, L., Rossi, M., et al. (2017). Detection of prion seeding activity in the olfactory mucosa of patients with Fatal Familial Insomnia. *Sci. Rep.* 7, 1–8. doi: 10.1038/srep46269

Renard, D., Castelnovo, G., Collombier, L., Thouvenot, E., and Boudousq, V. (2017). FDG-PET in Creutzfeldt-Jakob disease: analysis of clinical-PET correlation. *Prion* 11, 440–453. doi: 10.1080/19336896.2017.1387348

Requena, J. R., and Wille, H. (2017). The Structure of the Infectious Prion Protein and Its Propagation. *Prog. Mol. Biol. Transl. Sci.* 150, 341–359. doi: 10.1016/bs.pmbts.2017.06.009

Riek, R., Hornemann, S., Wider, G., Billeter, M., Glockshuber, R., and Wüthrich, K. (1996). NMR structure of the mouse prion protein domain PrP(121–231). *Nature* 382, 180–182. doi: 10.1038/382180a0

Ritchie, D. L., and Ironside, J. W. (2017). Neuropathology of Human Prion Diseases. *Prog. Mol. Biol. Transl. Sci.* 150, 319–339. doi: 10.1016/bs.pmbts.2017.06.011

Rossi, G., Macchi, G., Porro, M., Giaccone, G., Bugiani, M., Scarpini, E., et al. (1998). Fatal familial insomnia: genetic, neuropathologic, and biochemical study of a patient from a new Italian kindred. *Neurology* 50, 688–692. doi: 10.1212/WNL.50.3.688

Rossi, M., Baiardi, S., and Parchi, P. (2019). Understanding prion strains: evidence from studies of the disease forms affecting humans. *Viruses* 11:309. doi: 10.3390/v11040309

Rudge, P., Hyare, H., Green, A., Collinge, J., and Mead, S. (2018). Imaging and CSF analyses effectively distinguish CJD from its mimics. *J. Neurol. Neurosurg. Psychiatry* 89, 461–466. doi: 10.1136/jnnp-2017-316853

Saá, P., Castilla, J., and Soto, C. (2005). Cyclic amplification of protein misfolding and aggregation. *Methods Mol. Biol.* 2005, 53–65. doi: 10.1385/1-59259-874-9:053

Saá, P., Castilla, J., and Soto, C. (2006). Ultra-efficient replication of infectious prions by automated protein misfolding cyclic amplification. *J. Biol. Chem.* 281, 35245–35252. doi: 10.1074/jbc.M603964200

Saborio, G. P., Permanne, B., and Soto, C. (2001). Sensitive detection of pathological prion protein by cyclic amplification of protein misfolding. *Nature* 411, 810–813. doi: 10.1038/35081095

Safar, J., Geschwind, M., Deering, C., Didorenko, S., Sattavat, M., Sanchez, H., et al. (2005). Diagnosis of human prion disease. *Proc. Natl. Acad. Sci. U.S.A.* 102, 3501–3506. doi: 10.1073/pnas.0409651102

Safar, J., Wille, H., Itri, V., Groth, D., Serban, H., Torchia, M., et al. (1998). Eight prion strains have PrPSc molecules with different conformations. *Nat. Med.* 4, 1157–1165. doi: 10.1038/2654

Saijo, E., Hughson, A. G., Raymond, G. J., Suzuki, A., Horiuchi, M., and Caughey, B. (2016). PrP Sc -specific antibody reveals c-terminal conformational differences between prion strains. *J. Virol.* 90, 4905–4913. doi: 10.1128/jvi.00088-16

Sajnani, G., Silva, C. J., Ramos, A., Pastrana, M. A., Onisko, B. C., Erickson, M. L., et al. (2012). PK-sensitive PrPSc is infectious and shares basic structural features with PK-resistant PrPSc. *PLoS Pathog.* 8:e1002547. doi: 10.1371/journal.ppat.1002547

Sanchez-Juan, P., Green, A., Ladogana, A., Cuadrado-Corrales, N., Sáanchez-Valle, R., Mitrováa, E., et al. (2006). CSF tests in the differential diagnosis of Creutzfeldt-Jakob disease. *Neurology* 67, 637–643. doi: 10.1212/01.wnl.0000230159.67128.00

Sanchez-Juan, P., Sánchez-Valle, R., Green, A., Ladogana, A., Cuadrado-Corrales, N., Mitrová, E., et al. (2007). Influence of timing on CSF tests value for Creutzfeldt-Jakob disease diagnosis. *J. Neurol.* 254, 901–906. doi: 10.1007/s00415-006-0472-9

Sano, K., Satoh, K., Atarashi, R., Takashima, H., Iwasaki, Y., Yoshida, M., et al. (2013). Early detection of abnormal prion protein in genetic human prion diseases now possible using real-time QUIC assay. *PLoS One* 8:e54915. doi: 10.1371/journal.pone.0054915

Savard, M., Irani, S. R., Guillemette, A., Gosselin-Lefebvre, S., Geschwind, M., Jansen, G. H., et al. (2016). Creutzfeldt-Jakob disease-like periodic sharp wave complexes in voltage-gated potassium channel-complex antibodies

encephalitis: a case report. *J. Clin. Neurophysiol.* 33, e1–e4. doi: 10.1097/WNP.0000000000000171

Scheckel, C., and Aguzzi, A. (2018). Prions, prionoids and protein misfolding disorders. *Nat. Rev. Genet.* 19, 405–418. doi: 10.1038/s41576-018-0011-4

Schmitz, M., Ebert, E., Stoeck, K., Karch, A., Collins, S., Calero, M., et al. (2016). Validation of 14-3-3 protein as a marker in sporadic Creutzfeldt-Jakob Disease Diagnostic. *Mol. Neurobiol.* 53, 2189–2199. doi: 10.1007/s12035-015-9167-5

Schmitz, M., Villar-Piqué, A., Llorens, F., Gmitterová, K., Hermann, P., Varges, D., et al. (2019). Cerebrospinal fluid total and phosphorylated α-synuclein in patients with Creutzfeldt–Jakob Disease and synucleinopathy. *Mol. Neurobiol.* 56, 3476–3483. doi: 10.1007/s12035-018-1313-4

Scott, M. R., Peretz, D., Nguyen, H.-O. B., DeArmond, S. J., and Prusiner, S. B. (2005). Transmission barriers for bovine, ovine, and human prions in transgenic mice. *J. Virol.* 79, 5259–5271. doi: 10.1128/jvi.79.9.5259-5271.2005

Sharma, A., Bruce, K. L., Chen, B., Gyoneva, S., Behrens, S. H., Bommarius, A. S., et al. (2016). Contributions of the prion protein sequence, strain, and environment to the species barrier. *J. Biol. Chem.* 291, 1277–1288. doi: 10.1074/jbc.M115.684100

Smirnovas, V., Baron, G. S., Offerdahl, D. K., Raymond, G. J., Caughey, B., and Surewicz, W. K. (2011). Structural organization of brain-derived mammalian prions examined by hydrogen-deuterium exchange. *Nat. Struct. Mol. Biol.* 18, 504–506. doi: 10.1038/nsmb.2035

Soto, C. (2004). Diagnosing prion diseases: needs, challenges and hopes. *Nat. Rev. Microbiol.* 2, 809–819. doi: 10.1038/nrmicro1003

Soto, C., Anderes, L., Suardi, S., Cardone, F., Castilla, J., Frossard, M. J., et al. (2005). Pre-symptomatic detection of prions by cyclic amplification of protein misfolding. *FEBS Lett.* 579, 638–642. doi: 10.1016/j.febslet.2004.12.035

Soto, C., and Satani, N. (2011). The intricate mechanisms of neurodegeneration in prion diseases. *Trends Mol. Med.* 17, 14–24. doi: 10.1016/j.molmed.2010.09.001

Spagnolli, G., Rigoli, M., Orioli, S., Sevillano, A. M., Faccioli, P., Wille, H., et al. (2019). Full atomistic model of prion structure and conversion. *PLoS Pathog.* 15:e1007864. doi: 10.1371/journal.ppat.1007864

Staffaroni, A. M., Kramer, A. O., Casey, M., Kang, H., Rojas, J. C., Orrú, C. D., et al. (2019). Association of blood and cerebrospinal fluid tau level and other biomarkers with survival time in sporadic Creutzfeldt-Jakob Disease. *JAMA Neurol.* 76, 969–977. doi: 10.1001/jamaneurol.2019.1071

Steinacker, P., Blennow, K., Halbgebauer, S., Shi, S., Ruf, V., Oeckl, P., et al. (2016). Neurofilaments in blood and CSF for diagnosis and prediction of onset in Creutzfeldt-Jakob disease. *Sci. Rep.* 6:38737. doi: 10.1038/srep38737

Stoeck, K., Sanchez-Juan, P., Gawinecka, J., Green, A., Ladogana, A., Pocchiari, M., et al. (2012). Cerebrospinal fluid biomarker supported diagnosis of Creutzfeldt-Jakob disease and rapid dementias: a longitudinal multicentre study over 10 years. *Brain* 135, 3051–3061. doi: 10.1093/brain/aws238

Tee, B. L., Longoria Ibarrola, E. M., and Geschwind, M. D. (2018). Prion Diseases. *Neurol. Clin.* 36, 865–897. doi: 10.1016/j.ncl.2018.07.005

Tesar, A., Matej, R., Kukal, J., Johanidesova, S., Rektorova, I., Vyhnalek, M., et al. (2019). Clinical variability in P102L Gerstmann–Sträussler–Scheinker syndrome. *Ann. Neurol.* 86, 643–652. doi: 10.1002/ana.25579

The 1000 Genomes Project Consortium (2012). An integrated map of genetic variation from 1,092 human genomes. *Nature* 491, 56–65. doi: 10.1038/nature11632

Thomas, J. G., Chenoweth, C. E., and Sullivan, S. E. (2013). Iatrogenic Creutzfeldt-Jakob disease via surgical instruments. *J. Clin. Neurosci.* 20, 1207–1212. doi: 10.1016/j.jocn.2013.01.007

Thompson, A., Anastasiadis, P., Druyeh, R., Whitworth, I., Nayak, A., Nihat, A., et al. (2020). Evaluation of plasma tau and neurofilament light chain biomarkers in a 12-year clinical cohort of human prion diseases. *medRxiv* [Preprint]. doi: 10.1101/2020.07.27.20157594

Thompson, A. G. B., Luk, C., Heslegrave, A. J., Zetterberg, H., Mead, S. H., Collinge, J., et al. (2018). Neurofilament light chain and tau concentrations are markedly increased in the serum of patients with sporadic Creutzfeldt-Jakob disease, and tau correlates with rate of disease progression. *J. Neurol. Neurosurg. Psychiatry* 89, 955–961. doi: 10.1136/jnnp-2017-317793

Turner, M. L., and Ironside, J. W. (1998). New-variant Creutzfeldt-Jakob disease: the risk of transmission by blood transfusion. *Blood Rev.* 12, 255–268. doi: 10.1016/S0268-960X(98)90007-8

Uttley, L., Carroll, C., Wong, R., Hilton, D. A., and Stevenson, M. (2020). Creutzfeldt-Jakob disease: a systematic review of global incidence, prevalence, infectivity, and incubation. *Lancet Infect. Dis.* 20, e2–e10. doi: 10.1016/S1473-3099(19)30615-2

Vallabh, S. M., Minikel, E. V., Williams, V. J., Carlyle, B. C., McManus, A. J., Wennick, C. D., et al. (2020). Cerebrospinal fluid and plasma biomarkers in individuals at risk for genetic prion disease. *BMC Med.* 18:140. doi: 10.1186/s12916-020-01608-8

Vallabh, S. M., Nobuhara, C. K., Llorens, F., Zerr, I., Parchi, P., Capellari, S., et al. (2019). Prion protein quantification in human cerebrospinal fluid as a tool for prion disease drug development. *Proc. Natl. Acad. Sci. U.S.A.* 116, 7793–7798. doi: 10.1073/pnas.1901947116

Van Everbroeck, B., Quoilin, S., Boons, J., Martin, J. J., and Cras, P. (2003). A prospective study of CSF markers in 250 patients with possible Creutzfeldt-Jakob disease. *J. Neurol. Neurosurg. Psychiatry* 74, 1210–1214. doi: 10.1136/jnnp.74.9.1210

Villar-Piqué, A., Schmitz, M., Lachmann, I., Karch, A., Calero, O., Stehmann, C., et al. (2019). Cerebrospinal fluid total prion protein in the spectrum of prion diseases. *Mol. Neurobiol.* 56, 2811–2821. doi: 10.1007/s12035-018-1251-1

Wadsworth, J., Hill, A., Beck, J., and Collinge, J. (2003). Molecular and clinical classification of human prion disease. *Br. Med. Bull.* 66, 241–254. doi: 10.1093/bmb/dg66.241

Wang, Z., Manca, M., Foutz, A., Camacho, M. V., Raymond, G. J., Race, B., et al. (2019). Early preclinical detection of prions in the skin of prion-infected animals. *Nat. Commun.* 10:247. doi: 10.1038/s41467-018-08130-9

Wasmer, C., Lange, A., Van Melckebeke, H., Siemer, A. B., Riek, R., and Meier, B. H. (2008). Amyloid fibrils of the HET-s(218-289) prion form a β solenoid with a triangular hydrophobic core. *Science* 319, 1523–1526. doi: 10.1126/science.1151839

Watts, J. C., Giles, K., Patel, S., Oehler, A., DeArmond, S. J., and Prusiner, S. B. (2014). Evidence That Bank Vole PrP Is a Universal Acceptor for Prions. *PLoS Pathog.* 10:e1003990. doi: 10.1371/journal.ppat.1003990

Wells, G. A., Scott, A. C., Johnson, C. T., Gunning, R. F., Hancock, R. D., Jeffrey, M., et al. (1987). A novel progressive spongiform encephalopathy in cattle. *Vet. Rec.* 121, 419–420. doi: 10.1136/vr.121.18.419

Weydt, P., Oeckl, P., Huss, A., Müller, K., Volk, A. E., Kuhle, J., et al. (2016). Neurofilament levels as biomarkers in asymptomatic and symptomatic familial amyotrophic lateral sclerosis. *Ann. Neurol.* 79, 152–158. doi: 10.1002/ana.24552

Whitechurch, B. C., Welton, J. M., Collins, S. J., and Lawson, V. A. (2017). Clinical Aspects of Alzheimer ' s Disease Chapter 13 Prion Diseases. *Adv. Neurobiol.* 15, 335–364. doi: 10.1007/978-3-319-57193-5

Wieser, H. G., Schindler, K., and Zumsteg, D. (2006). EEG in Creutzfeldt-Jakob disease. *Clin. Neurophysiol.* 117, 935–951. doi: 10.1016/j.clinph.2005.12.007

Wilham, J. M., Orrú, C. D., Bessen, R. A., Atarashi, R., Sano, K., Race, B., et al. (2010). Rapid end-point quantitation of prion seeding activity with sensitivity comparable to bioassays. *PLoS Pathog.* 6:e1001217. doi: 10.1371/journal.ppat.1001217

Will, R., Ironside, J., Zeidler, M., Estibeiro, K., Cousens, S., Smith, P., et al. (1996). A new variant of Creutzfeldt-Jakob disease in the UK. *Lancet* 347, 921–925. doi: 10.1016/S0140-6736(96)91412-9

Will, R. G. (2003). Acquired prion disease: iatrogenic CJD, variant CJD, kuru. *Br. Med. Bull.* 66, 255–265. doi: 10.1093/bmb/66.1.255

Wu, L. Y., Zhan, S. Q., Huang, Z. Y., Zhang, B., Wang, T., Liu, C. F., et al. (2018). Expert consensus on clinical diagnostic criteria for fatal familial insomnia. *Chin. Med. J. Engl.* 131, 1613–1617. doi: 10.4103/0366-6999.235115

Zahn, R., Liu, A., Lührs, T., Riek, R., von Schroetter, C., López García, F., et al. (2000). NMR solution structure of the human prion protein. *Proc. Natl. Acad. Sci. U.S.A.* 97, 145–150. doi: 10.1073/pnas.97.1.145

Zanusso, G., Monaco, S., Pocchiari, M., and Caughey, B. (2016). Advanced tests for early and accurate diagnosis of Creutzfeldt-Jakob disease. *Nat. Rev. Neurol.* 12, 325–333. doi: 10.1038/nrneurol.2016.65

Zerr, I., Bodemer, M., Gefeller, O., Otto, M., Poser, S., Wiltfang, J., et al. (1998). Detection of 14-3-3 protein in the cerebrospinal fluid supports the diagnosis of Creutzfeldt-Jakob disease. *Ann. Neurol.* 43, 32–40. doi: 10.1002/ana.410430109

Zerr, I., Bodemer, M., Räcker, S., Grosche, S., Poser, S., Weber, T., et al. (1995). Cerebrospinal fluid concentration of neuron-specific enolase in diagnosis of Creutzfeldt-Jakob disease. *Lancet* 345, 1609–1610. doi: 10.1016/S0140-6736(95)90118-3

Zerr, I., Kallenberg, K., Summers, D. M., Romero, C., Taratuto, A., Heinemann, U., et al. (2009). Updated clinical diagnostic criteria for sporadic Creutzfeldt-Jakob disease. *Brain* 132, 2659–2668. doi: 10.1093/brain/awp191

Zerr, I., Pocchiari, M., Collins, S., Brandel, J. P., De Pedro Cuesta, J., Knight, R. S. G., et al. (2000a). Analysis of EEG and CSF 14-3-3 proteins as aids to the diagnosis of Creutzfeldt-Jakob disease. *Neurology* 55, 811–815. doi: 10.1212/WNL.55.6.811

Zerr, I., Schulz-Schaeffer, W. J., Giese, A., Bodemer, M., Schröter, A., Henkel, K., et al. (2000b). Current clinical diagnosis in Creutzfeldt-Jakob disease: identification of uncommon variants. *Ann. Neurol.* 48, 323–329. doi: 10.1002/1531-8249(200009)48:3<323::AID-ANA6<3.0.CO;2-5

Zou, W. Q., Capellari, S., Parchi, P., Sy, M. S., Gambetti, P., and Chen, S. G. (2003). Identification of novel proteinase k-resistant c-terminal fragments of PrP in Creutzfeldt-Jakob Disease. *J. Biol. Chem.* 278, 40429–40436. doi: 10.1074/jbc.M308550200

Conflict of Interest: The authors declare that the research was conducted in the absence of any commercial or financial relationships that could be construed as a potential conflict of interest.

frontiers in Bioengineering and Biotechnology

ORIGINAL RESEARCH
published: 29 October 2020
doi: 10.3389/fbioe.2020.589182

A Novel, Reliable and Highly Versatile Method to Evaluate Different Prion Decontamination Procedures

Hasier Eraña[1,2†], Miguel Ángel Pérez-Castro[1†], Sandra García-Martínez[1,2], Jorge M. Charco[1,2], Rafael López-Moreno[1], Carlos M. Díaz-Dominguez[1], Tomás Barrio[1], Ezequiel González-Miranda[1,2] and Joaquín Castilla[1,3]*

[1] Center for Cooperative Research in Biosciences (CIC bioGUNE), Basque Research and Technology Alliance (BRTA), Bizkaia Technology Park, Derio, Spain, [2] Atlas Molecular Pharma S. L., Bizkaia Technology Park, Derio, Spain, [3] IKERBASQUE, Basque Foundation for Science, Bilbao, Spain

OPEN ACCESS

Edited by:
Maria Dos Anjos Pires, University of Trás-os-Montes and Alto Douro, Portugal

Reviewed by:
Sumit Ghosh, The Research Institute at Nationwide Children's Hospital, United States
Zohre Kurt, Middle East Technical University, Turkey

***Correspondence:**
Joaquín Castilla
castilla@joaquincastilla.com

† These authors have contributed equally to this work

Specialty section:
This article was submitted to Biosafety and Biosecurity, a section of the journal Frontiers in Bioengineering and Biotechnology

Received: *30 July 2020*
Accepted: *14 October 2020*
Published: *29 October 2020*

Citation:
Eraña H, Pérez-Castro MÁ, García-Martínez S, Charco JM, López-Moreno R, Díaz-Dominguez CM, Barrio T, González-Miranda E and Castilla J (2020) A Novel, Reliable and Highly Versatile Method to Evaluate Different Prion Decontamination Procedures. Front. Bioeng. Biotechnol. 8:589182. doi: 10.3389/fbioe.2020.589182

Transmissible spongiform encephalopathies (TSEs) are a group of invariably fatal neurodegenerative disorders. The causal agent is an aberrantly folded isoform (PrP^{Sc} or prion) of the endogenous prion protein (PrP^{C}) which is neurotoxic and amyloidogenic and induces misfolding of its physiological counterpart. The intrinsic physical characteristics of these infectious proteinaceous pathogens makes them highly resistant to the vast majority of physicochemical decontamination procedures used typically for standard disinfection. This means prions are highly persistent in contaminated tissues, the environment (surfaces) and, of great concern, on medical and surgical instruments. Traditionally, decontamination procedures for prions are tested on natural isolates coming from the brain of infected individuals with an associated high heterogeneity resulting in highly variable results. Using our novel ability to produce highly infectious recombinant prions *in vitro* we adapted the system to enable recovery of infectious prions from contaminated materials. This method is easy to perform and, importantly, results in highly reproducible propagation *in vitro*. It exploits the adherence of infectious prion protein to beads of different materials allowing accurate and repeatable assessment of the efficacy of disinfectants of differing physicochemical natures to eliminate infectious prions. This method is technically easy, requires only a small shaker and a standard biochemical technique and could be performed in any laboratory.

Keywords: transmissible spongiform encephalopathy, prion, decontamination, PMSA, *in vitro* propagation

INTRODUCTION

Transmissible spongiform encephalopathies (TSEs) or prion diseases are a group of invariably fatal neurodegenerative disorders that affect humans and a wide variety of mammals (Aguzzi and Calella, 2009). The main event in prion pathogenesis is the conformational conversion of the cellular prion protein (PrP^{C}) into a pathological conformer (PrP^{Sc}) (Prusiner, 1982a). These two isoforms differ only in their three-dimensional structures and also functionally in that the pathological isoform is both neurotoxic and able to induce conformation change of the normal cellular counterpart, PrP^{C}, to the pathological isoform, PrP^{Sc} (Edgeworth et al., 2010). The latter, upon misfolding, contains a higher content of β-sheets and this makes it prone to aggregation, insolubility and partial

resistance to treatment with proteases (Kocisko et al., 1994; Saborio et al., 2001). For many decades the resistance of pathogenic prions to standard decontamination procedures attracted the attention of part of the scientific community due to the public health implications.

Transmissibility of scrapie was first demonstrated in 1936 (Cuille and Chelle, 1936) and subsequent studies focused on identifying the causative agent, which was believed initially to be a virus. However, this led to the discovery of the prion protein and the extraordinary resistance of pathogenic prions to inactivation. The first recognition of this was prior to the knowledge that prions were responsible for TSEs when part of a Scottish sheep flock suffered from scrapie after being given a vaccine against louping ill virus prepared from sheep brain homogenates treated previously with 0.35% formalin (Gordon, 1946; Giles et al., 2017). Further studies demonstrated that the scrapie agent in sheep brain was active after treatment with up to 40% formalin (Stamp et al., 1959; Pattison, 1965) and could withstand extreme temperatures (Stamp et al., 1959; Pattison and Millson, 1961) and UV irradiation (Alper et al., 1967) also, suggesting it might be devoid of nucleic acid. Nuclease digestion repeatedly failed to inactivate the infectious agent (Prusiner et al., 1978; Prusiner et al., 1980b) as well as most other procedures targeting nucleic acids. Therefore, treatments that modify amino acid residues were then tested to assess if they could inactivate prions. Initially, proteinase K and trypsin (Hunter and Millson, 1967; Prusiner et al., 1981b) were shown to reduce the titer of the scrapie agent in a concentration-dependent manner. Some chemical modifications also inactivated the scrapie agent, including treatment with diethyl pyrocarbonate (Prusiner et al., 1980a), butanedione and phenylmethylsulfonyl fluoride (PMSF) (Prusiner, 1982b). Although weak chaotropic agents failed to inactivate scrapie, strong chaotropic agents such as thiocyanate, guanidinium, and trichloroacetate are effective (Prusiner et al., 1981a). Similarly, exposure to high concentration of denaturants, like urea, decreased prion infectivity (Hunter, 1969) as did treatment with SDS or phenol (Prusiner et al., 1980a), all of which supported the "protein only" hypothesis.

The resistance of prions to conventional methods of pathogen decontamination (Taylor, 2000) leads to persistence in the environment and increased risk of transmission including to other mammalian species. While many prion diseases are apparently not transmissible to humans, bovine spongiform encephalopathy (BSE) provides a perfect example of prion zoonosis and highlights the hazard posed by prions to humans (Pattison, 1998). This novel form of human prion disease, known as variant Creutzfeldt-Jakob disease (vCJD), which was directly related to BSE-contaminated meat consumption, became the first zoonotic human prion disease (Pattison, 1998; Scott et al., 1999) and give rise to an unprecedented health and food crisis that highlighted the risk of deficient decontamination of prions. However, vCJD is not the only acquired prion disease in humans. Iatrogenic CJD (iCJD) refers to the transmission of prions via inadvertent medical exposure, emphasizing that efficient prion decontamination processes are necessary to avoid transmission to health care providers and patients (Gibbs et al., 1969; Duffy et al., 1974; Simpson et al., 1996; el Hachimi et al., 1997; Brown and Farrell, 2015; Bonda et al., 2016).

Despite traditional protocols being ineffective against prion infectivity (Taylor, 2000), the World Health Organization (WHO) and the Centre for Disease Control and Prevention (CDC) of the United States of America published guidelines for prion decontamination for commonly used instruments (WHO, 1999; CDC, 2019). The advice was to incinerate all instruments after single use but as this was not feasible the WHO suggested procedures for both heat-resistant and heat-sensitive instruments. However, efficient protocols are not practical for routine decontamination and proved to be damaging to several surgical devices. On the contrary, those that are harmless for the instrumentation barely eliminate prions (Sehulster, 2004; Brown et al., 2005). Therefore, novel decontamination methods capable of abolishing prion infectivity and allowing the reuse of expensive, heat-sensitive medical devices remain elusive (Crotti, 2020).

To assess the efficacy of prion decontamination/inactivation procedures accurate, reliable evaluation methods are required and these have, traditionally, used prion-infected brain homogenates of different species (Tateishi et al., 1988; Peretz et al., 2006). Although some of these procedures were evaluated using cell culture (Supattapone et al., 2001), bioassays were an unavoidable step to evaluate decontamination in terms of prion infectivity. Prions retain their infectivity *in vivo* when bound to metal surfaces (Zobeley et al., 1999; Flechsig et al., 2001) so research has focused primarily on novel decontamination procedures to ensure the safety of stainless steel medical instruments (Fichet et al., 2004). Contaminated steel wires have been widely used to model the contamination of surgical material and have achieved more representative results than whole brain homogenates, cell cultures (Edgeworth et al., 2011) or *in vitro* methods such as Real-time quaking-induced conversion (RT-QuIC) (Hughson et al., 2016). As *in vitro* prion propagation methods become more reliable, with respect to recombinant prion infectivity, bioassay is considered increasingly unnecessary thereby paving the way for prion decontamination assessment methodologies based exclusively on prion-contaminated steel wires and *in vitro* protocols (Belondrade et al., 2016; Mori et al., 2016). Methods using infected brain homogenates can be inaccurate as, in most cases, wet homogenates are employed despite clear evidence that dehydration can increase the persistence of infectious prions in the environment (Yuan et al., 2018). Although assays based on steel wires addressed this issue, these methods can only evaluate the effect of different decontaminants or procedures on prions attached to steel surfaces and do not reproduce the effects of different surface materials on the infectivity of adhered prions nor the efficacy of any decontamination procedure.

In the present study, we exploit PMSA (Protein Misfolding Shaking Amplification), a novel technique for propagation of infectious recombinant prion *in vitro* (Erana et al., 2019), and the ability of recombinant prions to bind to surfaces comprised of different materials to establish an affordable method to evaluate prion-specific decontaminants. Contrary to conventional decontaminant assessment methodologies using

brain homogenates, PMSA reduces variability by using highly reproducible recombinant infectious prions. Beads of different materials, representing some of the common surfaces in clinical or laboratory settings, were investigated for their ability to adsorb prions, and PMSA was adapted to propagate the adsorbed prions. This allowed us to measure the efficacy of disinfectants with different distinct physicochemical properties to abolish prion propagation capacity from a diverse range of materials' surfaces as proof of concept for this novel assay without the requirement for expensive specialist equipment.

MATERIALS AND METHODS

Generation of Prion-Coated Beads

We used a prion strain, obtained in previous experiments [termed *L-seeded-PMSA (1)* in (Erana et al., 2019) and abbreviated as Sst01], derived from the mammalian strain CWD-Vole109I and propagated *in vitro* by Protein Misfolding Cyclic Amplification (PMCA) using a substrate of recombinant bank vole I109 PrP (rec-VoPrP) complemented with dextran sulfate (Fernández-Borges et al., 2017a). It was adapted to the PMSA methodology by serial passaging ensuring it retained its strain properties which included biochemical features and *in vivo* and *in vitro* propagation (Erana et al., 2019). Four different types of beads; glass (BioSpec Products Inc.), zirconia/silica (BioSpec Products Inc.), stainless steel (Luis Aparicio S.L.), all (1 mm), and PTFE (Teflon®, 2 mm) (Luis Aparicio S.L.), were coated with the chosen recombinant prion. Prior to coating, the beads were rinsed by vortexing three times with phosphate buffered saline (PBS), each lasting at least 4 h with intense shaking (700 rpm), to eliminate impurities or dust from their surfaces that could influence the efficiency of prion adsorption. After a final rinse with sterile water the beads were dried completely in a stove (42°C) overnight. For the coating, approximately 1 ml of the *Sst01* inoculum was added to each 2 ml tube containing approximately 500 mm^2 of beads. The tubes were placed on a mixer and incubated for 1–2 h with gentle agitation (40 rpm) at room temperature (20–25°C). Subsequently, the supernatant was removed and the beads subjected to 24 h PMSA using 800 µl of fresh rec-VoPrP substrate in 2 ml tubes as described below. After PMSA, the supernatant was removed and the beads rinsed by vortexing twice with PBS and twice with sterile water and dried completely in a stove (42°C) overnight prior to being stored at room temperature. Each batch of prion-coated beads was always tested before their use to ensure proper coating and reproducibility of the results in terms of propagation capacity of prions adhered to beads. For that, at least four beads of the recently coated batch were used as seeds in four different 24 h PMSA reactions using 800 µl of fresh rec-VoPrP substrate in 2 ml tubes as described below. The samples were afterward digested with proteinase K, submitted to electrophoresis and total protein staining in order to monitor the presence of rec-PrP^{res}. Only those batches of prion-coated beads able to give rise to rec-PrP^{res} in all the replicates were considered valid for the decontamination assays, to ensure reproducibility of the methodology.

Decontamination of Prion-Coated Beads

Beads coated with infectious prions were subjected to different procedures commonly used for decontamination of equipment, materials and surfaces (**Table 1**). To assess the effectiveness of temperature-based decontamination protocols, the coated beads were subjected to autoclaving for 20 min either at 121°C, the traditional temperature but insufficient for complete prion inactivation, or at 134°C, effective for prion decontamination according to WHO recommendations (WHO, 1999). Similarly, to assess the effect of ultraviolet irradiation coated beads were exposed to direct UV light at 254 nm for 1 h with orbital shaking to achieve complete exposure. For the evaluation of chemical disinfection procedures, the beads were submerged in the following solutions for 1 h and subjected to gentle agitation at room temperature: commercial bleach (37% chlorine) (Henkel); sodium hydroxide (NaOH) 1N (Fisher Scientific); Virkon™ at 1% (Zotal); and a mixture of sodium dodecyl sulfate (SDS) 1% (Sigma-Aldrich) and acetic acid (AcO) 0.5% (Thermo Fisher Scientific). In addition, a set of beads was treated with PBS as a negative control. In all cases, after the decontamination procedure the beads were rinsed by vortexing twice with PBS and twice with distilled water.

To investigate whether addition of detergents could improve the efficiency of prion inactivation, prion-coated Teflon® beads were treated for 1 h with bleach or NaOH solutions, both

TABLE 1 | Physicochemical decontamination treatments selected to evaluate the novel assay developed for the assessment of potential prion inactivation procedures.

Type	Decontaminant	Conditions	References
Physical	Autoclave at 121°C	Exposition of the beads to 121°C for 20 min.	Known to be insufficient for prion inactivation (WHO, 1999).
	Autoclave at 134°C	Exposition of the beads to 134°C for 20 min.	Recommended for decontamination of prions (WHO, 1999).
	UV	Exposition of the beads to a UV (254 nm) lamp for 1 h.	Known to be insufficient for prion inactivation (Bellinger-Kawahara et al., 1987).
Chemical	Bleach	Incubation of the beads in commercial bleach (approximately 37 g hypochlorite per L) for 1 h with gentle shaking.	Recommended for decontamination of prions (WHO, 1999).
	NaOH	Incubation of the beads in 1 N NaOH solution for 1 h with gentle shaking.	Recommended for decontamination of prions (WHO, 1999).
	Virkon™	Incubation of the beads in 1% Virkon™ solution for 1 h with gentle shaking.	Commonly used virucidal agent. Effect on prions unknown.
	AcO-SDS	Incubation of the beads in a solution with 2% SDS detergent together 1% AcOH at room temperature for 1 h with gentle shaking.	Partially effective against prions (Peretz et al., 2006).

containing 1% Triton-X-100 (Sigma-Aldrich) and subjected to mild shaking. Under the same PMSA conditions (see below), using 1 and 2 beads with reaction times of 1, 2, and 4 h and their respective positive and negative controls, the presence or absence of rec-PrP^{res} propagation was evaluated by proteinase K digestion, electrophoresis and total protein staining.

Preparation and Purification of Recombinant PrP for the PMSA Substrate

The bacterial expression of bank vole I109 recombinant prion protein (rec-VoPrP) was achieved using a pOPIN E expression vector prepared using standard molecular biology procedures, as described previously (Elezgarai et al., 2017; Fernández-Borges et al., 2017a; Fernández-Borges et al., 2017b). Briefly, the oligonucleotides 5′ AGGAGATATACCATGAAGAAGCGGCCAAAGCCTGG 3′ and 5′ GTGATGGTGATGTTTGGAACTTCTCCCTTCGTAGTA 3′ (Sigma-Aldrich) were used to amplify the target sequence, i.e., the ORF of the *PRNP* gene from bank vole I109, from genomic DNA. The pOPIN E vector was digested with *Nco*I and *Pme*I (Fermentas) restriction enzymes, and the insert was introduced into the vector by homologous recombination using the In-Fusion cloning method. The final construct was transformed in *E. coli* Rosetta (DE3) competent bacteria using standard molecular biology procedures, and the expression of the protein of interest was induced upon addition of isopropyl β-D-1-thiogalactopyranoside (IPTG) at 1 mM (Gold BioTechnology) to the LB broth (Pronadisa) used for culture. The bacterial pellet obtained from each liter of culture, after centrifugation was resuspended in 50 ml of lysis buffer containing 50 mM Tris-HCl (Fisher Scientific), 5 mM EDTA (Sigma-Aldrich), 1% Triton X-100 (Sigma-Aldrich), 1 mM PMSF (Sigma-Aldrich) and 100 μg/ml lysozyme (Sigma-Aldrich), and then incubated with 100 U/ml DNase (Sigma-Aldrich) and 20 mM $MgCl_2$ (Sigma-Aldrich) for 30 min with stirring at 200 rpm at room temperature. The resultant lysate was centrifuged at 8,500 *g* and 4°C for 1 h, and the resulting pellet, containing bacterial inclusion bodies, was resuspended in 50 ml of washing buffer [20 mM Tris-HCl, 150 mM NaCl (Sigma-Aldrich), 1 mM EDTA, 1% Sarkosyl (Sigma-Aldrich)]. After an additional centrifugation at 8,500 *g* at 4°C for 1 h, the new pellet was dissolved in 6 ml of inclusion buffer [20 mM Tris-HCl, 0.5 M NaCl and 6 M GdnHCl (Sigma-Aldrich)] and incubated overnight at 37°C with stirring to break down inclusion bodies and solubilize the recombinant protein. A final centrifugation at 8,500 *g*, at 4°C for 1 h and filtration thought a 0.20 μm-pore membrane (Corning) were performed prior to purification. At this point, the first fraction of 10 μl was collected to monitor the process, which is called the Lysis fraction. Although the recombinant protein did not contain a His-tag, the purification step was performed using a histidine affinity column coupled to Aktä FPLC equipment (GE Healthcare), taking advantage of the natural His residues present in the octapeptide repeat region of PrP. The affinity column was first equilibrated with 10 column volumes (CV) of Binding buffer [20 mM Tris-HCl, 500 mM NaCl, 5 mM imidazole (Sigma-Aldrich) and 2 M GdnHCl], then the lysate obtained from the bacterial pellet was loaded into the column, collecting the second 10 μl fraction, the Loading fraction, from the flow through. Once loaded, the column was washed with 15 CV of Binding buffer, from which the next 10 μl fraction was collected, the Washing fraction. Finally, the protein was eluted in 30 ml of elution buffer containing 20 mM Tris-HCl, 500 mM NaCl, 500 mM imidazole and 2 M GdnHCl, from which the final fraction, named Elution was taken, and then completely denatured by addition of GdnHCl to a final concentration of 6 M. The four fractions collected during the purification process were precipitated by adding an equivalent to the 85% of the volume of sample of ice-cold methanol, incubation for 30 min at −20°C and centrifugation at maximum speed for 20 min at room temperature. After drying all the methanol from the precipitated samples, these were resuspended in loading buffer (NuPage 4X, Invitrogen) diluted 1:3 (v:v) in PBS and submitted to electrophoresis and total protein staining (**Supplementary Figure 1**). The final concentration of the protein was adjusted to 25 mg/ml, using the absorbance at 280 nm measured with a NanoDrop™ (Thermo Fisher Scientific), by concentrating the eluted solution using 10 kDa centrifugal filter units (Millipore), aliquoted and stored at −80°C until required. The stability of the protein has been evaluated in terms of its capacity to sustain prion propagation efficiency using serially diluted seeds. According to this internal tests, the protein stored at −80 or −20°C, without further thawing and freezing cycles maintains the *in vitro* propagation capacity for at least 1 year, although may keep sufficient quality for propagation likely indefinitely. At lower storage temperatures, such as or 4°C, the propagation capacity decays with time, but we have determined that it is suitable for PMSA at least for 1 month.

Preparation of PMSA Substrate

For the substrate, the prepared rec-VoPrP protein was thawed, diluted 1:5 in PBS (Fisher Scientific) and dialyzed against PBS (1 L for 100 μl of protein) for 1 h. The dialyzed protein was then diluted 1:10 in conversion buffer (CB) containing 0.15 M NaCl and 1% Triton X-100 and complemented with 0.5% dextran sulfate 6,500–10,000 kDa (Sigma-Aldrich). In contrast to the purified protein, which is conserved at 6 M of GdnHCl, substrates are devoid of denaturants and show shorter half-life. For this study they were used immediately after the first thawing, keeping the conveniently aliquoted substrate at −80°C for about a month. In such storage conditions, substrates have been found to have maximum propagation efficiency up to 1 year after preparation at least. The same substrates conserved at 4°C, without freezing have been found to be stable and show the same propagation efficiency for 4 days maximum.

Protein Misfolding Shaking Amplification (PMSA)

The PMSA protocol used was based on that published previously (Erana et al., 2019) with slight modifications to optimize it for bead-adsorbed prions. Briefly, prion-coated beads of different materials (1 or 5 for glass beads, zirconia/silica beads

and stainless steel beads, and 1 or 2 for PTFE beads) were placed in clean, labeled 2 ml tubes (Fisher Scientific) after the decontamination procedures (see above). Fresh substrate (500 μl) was added to each tube and they were subjected to a single PMSA round at 39°C and 700 rpm shaking. The duration of the *in vitro* propagation was determined for each set of conditions (type of surface and number of beads) using prion-coated beads not subjected to any decontamination procedure to allow discrimination between weak and strong decontamination procedures. Moreover, it was used to prove that the efficiency of the propagation was linearly dependent upon the number of beads and the duration of the PMSA. Thus, three durations (**t1**; time at which propagation is still undetectable, **t2**; time at which propagation is detectable but has not reached plateau and **t3**; time at which prion propagation has reached plateau) were selected for each setting: 1 h, 2 h, and ≥ 4 h for reactions containing a single bead of any material or 2 PTFE beads (due to their larger size). Additional timings included: 30 min, 1 h, and ≥ 2 h for reactions containing 5 Zirconia/silica or stainless steel beads, and 15 min, 30 min, and ≥ 2 h for reactions containing five glass beads. Each reaction was performed in triplicate and was accompanied by two positive controls (i.e., non-decontaminated prion-loaded beads at the shortest and the longest times used) and one negative control (i.e., non-loaded beads at the longest time used) to check for cross-contamination or spontaneous misfolding. The use of distinct amounts of beads and different reaction times was selected because it could help to establish a scale for the different decontamination treatments, revealing weak disinfectants as opposed to strong ones. Presumably, the weak disinfectants would be able to reduce propagation with the lowest amount of beads and at the shortest reaction times, while the stronger ones should be able to inhibit prion propagation in all conditions. To evaluate the effect of the different decontamination treatments on prion propagation, just intermediate (t2) and longest (t3) PMSA reaction times were taken into consideration, since t1, a time point in which propagation should not be detected, was included as a control for the process to check that the propagation kinetics were the expected ones for each type of bead. In all cases, positive controls (prion-coated beads not subjected to any decontamination procedure that were washed in the same way than the treated ones) for t1 and t3 were included and negative controls (uncoated beads of the same type) were also included for t3 to evaluate cross-contamination or spontaneous misfolding.

Proteinase K Digestion and Total Protein Staining

The PMSA-derived products were digested with proteinase K (Roche) and subjected to electrophoresis and staining of total protein to assess the presence of proteinase K-resistant misfolded PrP (rec-PrP^{res}) in each sample. Briefly, 400 μl of each PMSA product were transferred to 1.5 ml Eppendorf tubes and proteinase K added to a final concentration of 25 μg/ml. The tubes were incubated at 42°C for 1 h and then centrifuged at 19,000 *g* at 4°C for 15 min. The supernatant was discarded carefully without disturbing the pellet and the pellet was washed with 500 μl of PBS and centrifuged again at 19,000 *g* for 5 min at 4°C. After removing all the PBS, the pellet was resuspended in 15 μl of loading buffer NuPage 4X (Invitrogen) diluted in PBS; at this point samples could be stored at −20°C until required. For electrophoresis, digested samples, together with non-digested controls, were boiled at 100°C for 10 min and loaded in 4–12% acrylamide gels (Invitrogen) for 1 h 20 min at 70 V for 10 min at 110 V for the next 10 min and 150 V for 1 h. The gel was then transferred to a glass bucket and total protein stained using BlueSafe (NzyTech) for at least 1 h at room temperature with gentle rocking.

Statistical Analysis of Prion Decontamination Studies

A grouped analysis using a two-way ANOVA with Bonferroni's post-test was performed to assess the effect of each decontaminant in different materials based on detection or absence of proteinase K-resistant misfolded recombinant PrP, comparing with absence of decontaminant (control situation). GraphPad Prism 5® software was used for statistical analyses. No measurement was excluded for statistical analysis. For all analyses, $p \leq 0.05$ was considered significant. Data displayed in **Tables 2**, **3** represent mean ± SD, excluding those cases for which the SD was 0. Statistically significant differences are also indicated in **Tables 2**, **3** with the following symbols: $^{\times}p < 0.05$, $^{\times\times}p < 0.01$, and $^{\sim}p < 0.001$.

RESULTS

Development of a New Method for Recombinant Prion Propagation *in vitro* Based on Coated Beads Used as Seed

All prion-coated beads made of different materials were able to give rise to Proteinase K-resistant misfolded recombinant PrP (rec-PrP^{res}) upon PMSA and showed the same electrophoretic mobility pattern and PK-resistant fragments (∼16, 9, and 2 kDa) as the original Sst01 (**Figure 1**). The same beads not coated with rec- PrP^{res} were unable to generate these products after PMSA as denoted by electrophoresis. In some cases small molecular weight fragments were present and most likely represented spontaneous formation of amorphous PrP aggregates from the substrate. This can also be observed in unseeded reactions in the absence of beads.

Characterization of the Propagation Capacity of Each Type of Coated Bead by PMSA

The propagation capacity of each type of prion-coated bead was examined at different PMSA reaction times and results are summarized in **Figure 2** (raw data available at **Supplementary Figure 2**). The most readily amplified rec-PrP was that adsorbed to zirconia-silica beads, for which rec-PrP^{res} was detected at 30 min reaction time with either 1 or 5 coated beads. Prion-coated glass beads gave the next most rapid result, 1 bead gave rise to rec-PrP^{res} at 2 h and 5 beads as early as 30 min. Steel beads showed a similar time scale, propagating as early as 2 h

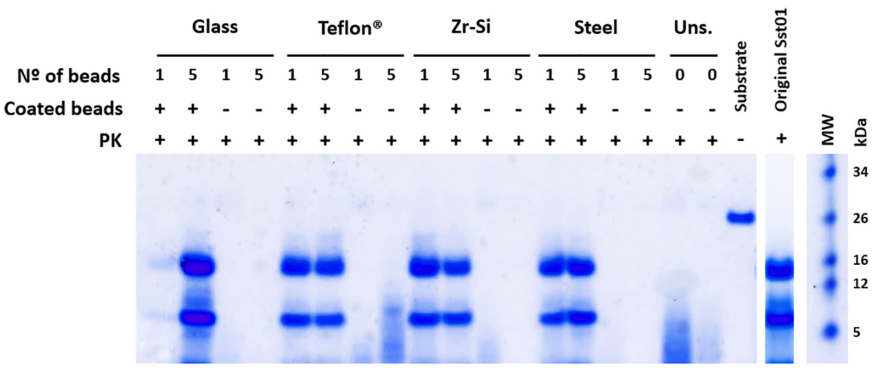

FIGURE 1 | Efficient recombinant prion propagation by PMSA using different prion-coated beads as seed. Electrophoresis and total protein staining of the PMSA products obtained, using either 1 or 5 recombinant prion-coated beads of different materials as seeds, showing rec-PrP^{res} after treatment with Proteinase K (PK). Prion-coated beads of glass, zirconia/silica, stainless steel and Teflon® were used as seeds and the same beads without prion coating were also submitted to the same process as controls of cross-contamination or spontaneous rec-PrP^{res} formation. Unseeded (Uns.) reactions without beads and without any seeding were also used for this purpose. All prion-coated beads were able to give rise to rec-PrP^{res}, showing the same electrophoretic patterns as the original Sst01 strain with predominant ~16 and ~9 kDa fragments. No cross-contamination or spontaneous formation of rec-PrP^{res} was detected in any of the unseeded reactions either with or without beads. A sample of the substrate rec-PrP without PK digestion is also shown as reference for the size of the undigested rec-PrP. MW, Molecular weight marker.

for 1 bead and within 1 h for 5 coated beads. Finally, Teflon® beads induced the formation of detectable amounts of rec-PrP^{res} at 2 h irrespective of using 1 or 2 beads. These results allowed determination of a rec-PrP^{res} PMSA propagation time window for each type of bead where (1) propagation is not observed (as a control of the sensitivity of the process), (2) propagation is first detected (the time point at which propagation is detectable but not maximal) and 3) the shortest time in which propagation reached the maximum capacity or plateau. Thus, t1, t2, and t3, respectively, were established for each type of bead, dependent on their ability to propagate rec-PrP^{res} by PMSA and these time points were used to determine the success or otherwise of each decontamination treatment applied to the prion-coated beads of various material.

Development of an Assay to Evaluate the Effect of Potential Prion Decontamination Procedures

To validate this assay, a panel of physicochemical decontamination procedures was selected and subjected to it. The different treatments were chosen based on WHO recommendations, previous reports or on treatments commonly used for prion decontamination in laboratories working on TSE (summarized in **Table 1**). To assess the effect of the treatments on the propagation capacity of prions, beads of each type were used after decontamination to seed PMSA reactions with different durations as determined in the previous section. The results corresponding to all beads and decontamination treatments are summarized in **Table 2** and visually represented in **Figure 3**, although only different reaction times were considered given the identical results obtained with 1 or 5 beads (2 in the case of Teflon®) for the selected time points (raw data available at **Supplementary Figure 2**). Original electrophoresis gels of representative experiments are also shown as examples of the result readouts (**Figure 4**).

Complete decontamination (0 out of 6 replicates positive for rec-PrP^{res} at t3) of adhered rec-PrP^{res} was achieved after treatment of steel beads with bleach, NaOH or in the autoclave, either at 121 or 134°C for 20 min. It was also achieved after treating zirconia-silica beads with bleach and Teflon® beads with Virkon™. In all the other cases prion inactivation was incomplete but bleach was the most effective decontaminant for most type of beads followed by autoclaving at 134°C. Prions adsorbed to glass beads, with two positive tubes at t3, and Teflon® beads, with 4 out of 6 positive tubes, resisted inactivation by bleach, most likely due to the physical properties of the bead material. As expected, UV treatment showed no effect on prion inactivation causing slight reduction of prion propagation at t2 for zirconia-silica, steel and Teflon® beads. Similarly, acidic SDS treatment also showed little effect reducing prion propagation at t2, but not achieving complete inactivation in any case. Surprisingly, Virkon™, a well-known virucidal agent showed some effect on prion propagation capacity at t2 for all the types of beads, providing total prion inactivation in the case of Teflon® beads. Finally, the treatment with 1N NaOH showed lower prion inactivation capacity than expected for zirconia-silica, glass and Teflon® beads, inhibiting propagation in few replicates just at t2 and suggesting that the effect of the decontaminant treatment is highly dependent on the treated surface material.

Combination of Decontamination Treatments With Non-ionic Surfactants Can Improve Prion Inactivation Efficiency in Hydrophobic Surfaces

The unexpectedly low prion inactivation capacity showed by bleach and NaOH treatments for some of the surface materials used such as Teflon®, prompted us to investigate whether it was due to hydrophobicity or surface tension that could avoid proper contact between the decontaminants and the

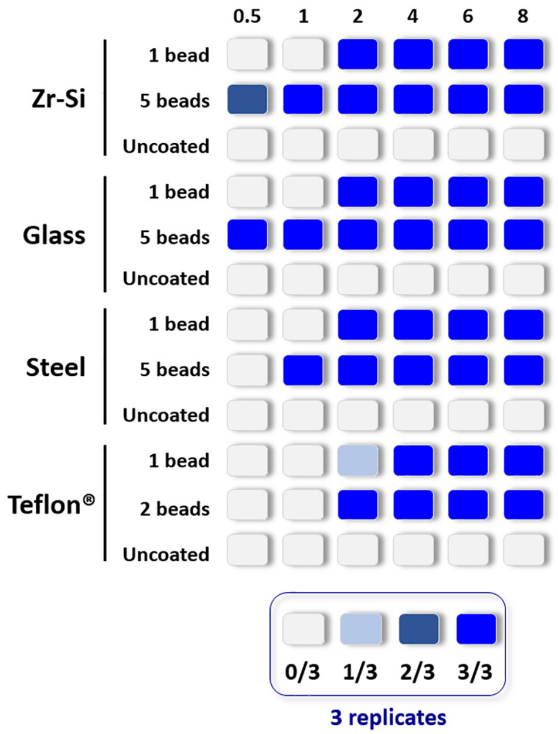

FIGURE 2 | Representation of the propagation capacity of each type of prion-coated bead at different PMSA reaction times. In order to characterize the propagation kinetics of each prion-coated bead type and determine the best propagation time window for evaluation of decontamination treatments, either 1 or 5 prion-coated beads were used as seeds (except for Teflon® beads for which 1 or 2 beads were used) and triplicate samples submitted to PMSA from 30 min to 8 h. The maximum number of uncoated beads of each type were also used in the same conditions as controls for cross contamination or spontaneous rec-PrP^{res} generation. The figure represents with different shades of blue the number of replicate tubes in which rec-PrP^{res} was detected for each PMSA time as indicated in the legend. Rec-PrP^{res} was detected for zirconia-silica (Zr-Si) and glass beads as early as 30 min when using 5 beads while the prion-coated steel beads required 1 h and the 2 prion-coated Teflon® beads 2 h. When a single bead of each type was used 3 out of 3 replicates showed detectable rec-PrP^{res} at 2 h except for the Teflon® bead that required 4 h to reach the same result.

prions adsorbed to the surface of this material. For that, 1% Triton-X-100, a non-ionic detergent, was added to the original treatments with commercial bleach and 1N NaOH. The results summarized in **Table 3** clearly demonstrate that the addition of Triton-X-100 greatly improved the inactivation of prions coating Teflon® beads treated with bleach or NaOH, achieving complete decontamination.

DISCUSSION

Protein misfolding shaking amplification (PMSA) has been already shown to propagate recombinant bona fide prions in a simple but highly efficient and robust way (Erana et al., 2019). Requiring a minimum of laboratory equipment, a shaker with speed and temperature control, the scalability and the robustness of the system makes it highly versatile as it is able to generate large amounts of recombinant prions and perform high-throughput screenings of potential prion decontamination procedures or anti-prion drugs. Taking advantage of the ability of recombinant prions to adsorb on to the surface of beads of different materials and the exceptional sensitivity of PMSA to detect their presence, we have developed a method capable of assessing the prion inactivation capacity of distinct physicochemical treatments. Using decontaminants recommended by the WHO or CDC (WHO, 1999; CDC, 2019), along with other treatments known to have little effect or no effect on prion inactivation, we have validated this novel method for this purpose.

Although most published studies on prion decontaminants rely on bioassays to evaluate their efficacy, in terms of infectivity (Taylor, 2000), some *in vitro* (Fichet et al., 2004; Belondrade et al., 2016, 2020; Hughson et al., 2016; Mori et al., 2016; Gough et al., 2017) and *ex vivo* (Edgeworth et al., 2011; Botsios et al., 2015) methodologies have been used to assess the efficacy of treatments and methods based on highly sensitive *in vitro* prion propagation systems have been considered most successful. However, decontamination treatments applied on samples with low prion titers or using model systems with not enough sensitivity for prion detection can dangerously overestimate prion elimination capacity of a treatment (Giles et al., 2017).

TABLE 2 | Summary of the results obtained for rec-PrP^{res} propagation in PMSA from the different prion-coated beads treated with the chosen different decontamination procedures.

	Autoclave 121°C		Autoclave 134°C		UV		NaOH		Bleach		Virkon™		AcO-SDS	
Material	**t2**	**t3**	**t2**	**t3**	**t2**	**t3**	**t2**	**t3**	**t2**	**t3**	**t2**	**t3**	**t2**	**t3**
Glass	6/6	6/6	0/6$^{\sim}$	4/6 (±0.52)	6/6	6/6	4/6 (±0.52)	6/6	0/6$^{\sim}$	2/6$^{\sim}$ (±0.52)	3/6$^{\times}$ (±0.55)	6/6	2/6$^{\sim}$ (±0.52)	6/6
Zr-Si	6/6	6/6	5/6 (±0.41)	6/6	5/6 (±0.41)	6/6	3/6$^{\times}$ (±0.55)	6/6	0/6$^{\sim}$	0/6$^{\sim}$	5/6 (±0.41)	6/6	5/6 (±0.41)	6/6
Steel	0/6$^{\sim}$	0/6$^{\sim}$	0/6$^{\sim}$	0/6$^{\sim}$	5/6 (±0.41)	6/6	0/6$^{\sim}$	0/6$^{\sim}$	0/6$^{\sim}$	0/6$^{\sim}$	2/6 (±0.52)	6/6	4/6 (±0.52)	6/6
Teflon®	3/6 (±0.55)	6/6	0/6$^{\sim}$ (±0.55)	2/6$^{\sim}$ (±0.52)	3/6 (±0.55)	6/6	3/6 (±0.55)	6/6	1/6$^{\times}$ (±0.41)	5/6 (±0.41)	0/6$^{\sim}$	0/6$^{\sim}$	3/6 (±0.55)	6/6

Number of replicate tubes subjected to PMSA showing rec-PrP^{res} by electrophoresis and total protein staining/total number of replicates. Presence of rec-PrP^{res} indicates incomplete inactivation of the rec-PrP^{res} adsorbed to the surface of the beads. t2 refers to the shortest PMSA reaction time in which rec-PrP^{res} was detected in the absence of any decontamination treatment but propagation has not reach a plateau, and t3 refers to the shortest PMSA reaction time in which rec-PrP^{res} signal was considered to have reached plateau which is considered to be the maximum propagation limit.

The numbers in parenthesis show the mean ± SD, excluding those cases for which SD was 0. Statistically significant differences with respect to untreated controls are also indicated with the following symbols: $^{\times}p < 0.05$, $^{\times\times}p < 0.01$, and $^{\sim}p < 0.001$.

TABLE 3 | Summary of the results obtained for rec-PrP^{res} propagation in PMSA from the prion-coated Teflon® beads treated with NaOH and bleach with Triton X-100 added.

	NaOH		NaOH + Triton X-100		Bleach		Bleach + Triton X-100	
Material	**t2**	**t3**	**t2**	**t3**	**t2**	**t3**	**t2**	**t3**
Teflon®	3/6 (± 0.55)	6/6	0/6$^{\sim}$	0/6$^{\sim}$	1/6$^{\times}$ (±0.41)	5/6 (±0.41)	0/6$^{\sim}$	0/6$^{\sim}$

Number of replicate tubes subjected to PMSA showing rec-PrP^{res} by electrophoresis and total protein staining/total number of replicate tubes is represented for each treatment. Presence of rec-PrP^{res} indicates incomplete inactivation of the seeds adsorbed to the surface of the beads. t2 refers to the shortest PMSA reaction time in which rec-PrP^{res} can be detected in the absence of a decontamination treatment but propagation has not reach a plateau, and t3 refers to the shortest PMSA reaction time in which the rec-PrP^{res} signal reached plateau, which is considered to be the maximum propagation limit.
The numbers in parenthesis show the mean ± SD, excluding those cases for which SD was 0. Statistically significant differences with respect to untreated controls are also indicated with the following symbols: $^{\times}p < 0.05$, $^{\times\times}p < 0.01$, and $^{\sim}p < 0.001$.

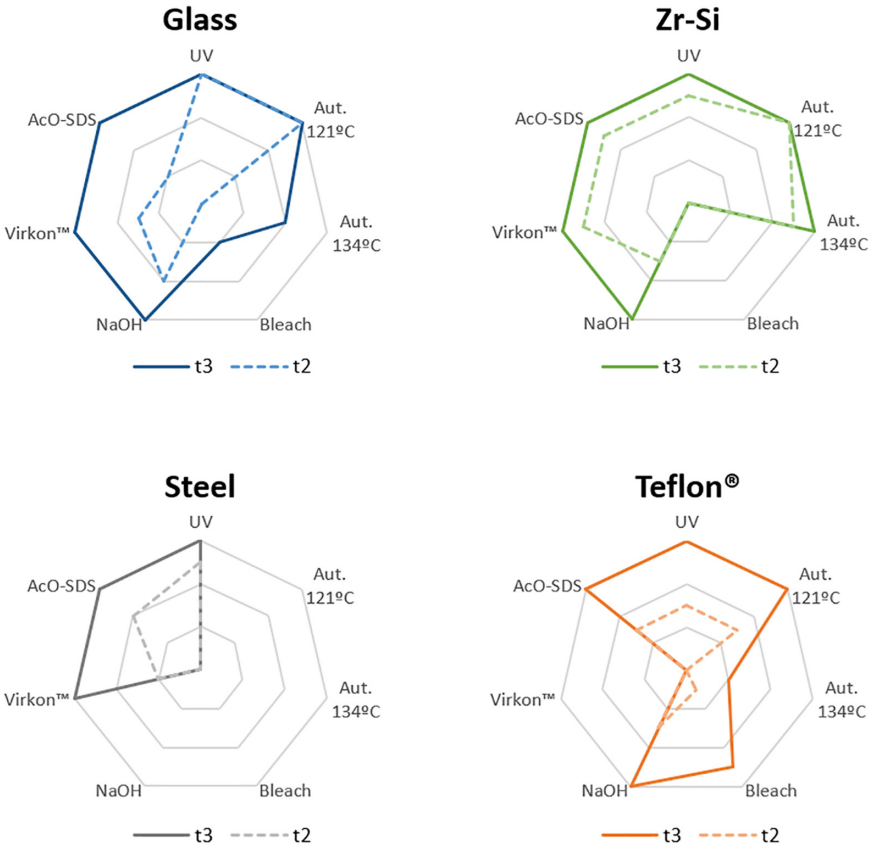

FIGURE 3 | Graphical representation of the results obtained for rec-PrP^{res} propagation in PMSA from the different prion-coated beads treated with the chosen different decontamination procedures. Radar charts represent the number of replicate tubes subjected to PMSA showing rec-PrP^{res} by electrophoresis and total protein staining. Colored lines represent the presence of rec-PrP^{res}, which indicates incomplete inactivation of the rec-PrP^{res} adsorbed to the surface of the beads. t2 (dotted lines) refers to the shortest PMSA reaction time in which rec-PrP^{res} was detected in the absence of any decontamination treatment but propagation has not reach a *plateau*, and t3 (solid lines) refers to the shortest PMSA reaction time in which rec-PrP^{res} signal reached *plateau* which is considered to be the maximum propagation limit. Each axes of the radar chart represent one of the decontamination treatment used that are detailed in **Table 1** (autoclave at 121°C, at 134°C, NaOH, bleach, Virkon^{TM} and AcO-SDS treatment). The plots of the results of **Table 2**, show clearly that prions adsorbed to steel beads are the ones more easily eliminated by most of the treatments used, and also that bleach and autoclave at 134°C are the most effective for decontamination of prions from most of the surface materials tested, with the exception of Teflon® beads highly susceptible to the treatment with Virkon^{TM}.

Despite the reported success of highly sensitive *in vitro* methods, without bioassay they cannot guarantee complete absence of infectious capacity and only provide an approximation based on assessment of propagation capacity for which only minute amounts of infectious prions are required. Therefore, although initial studies on different decontamination procedures were mostly performed through treatment of prion-containing brain homogenates and inoculation in model animals, the improvement of *ex vivo* and *in vitro* models is starting to gain importance. Apart from the obvious benefits in terms of cost,

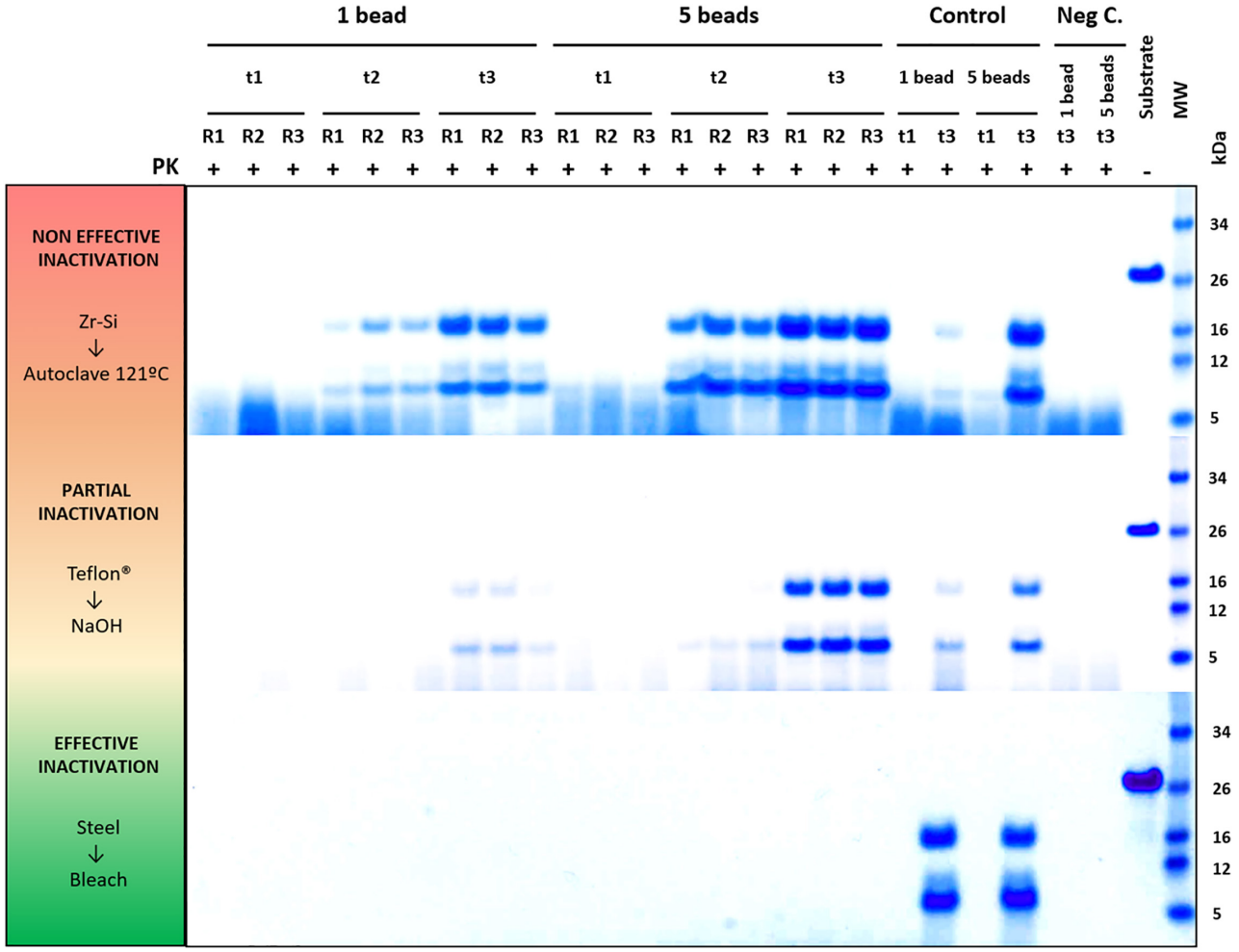

FIGURE 4 | Representative decontamination treatment evaluation experiments showing examples of a non-efficient, partially efficient and completely efficient treatment for prion decontamination. Electrophoresis and total protein staining of the Proteinase K (PK)-digested PMSA products of three representative experiments are shown as examples of decontamination treatment evaluation by PMSA. Three replicates (R1, R2, and R3) of either 1 or 5 prion-coated zirconia-silica (Zr-Si) beads treated by autoclaving at 121°C for 20 min and submitted to a PMSA round at three time points (t1, t2, and t3), serve as an example of a non-effective inactivation treatment, since rec-PrP^{res} with the characteristic ∼16 kDa predominant band could be detected in all replicates at t2 and t3. Samples at t1 were negative which, being a time point chosen as a control of the process, indicates that the propagation kinetics were as expected. Positive control samples (Control), performed with untreated prion-coated beads of the same type at t1 and t3 demonstrate that the PMSA allowed propagation as expected, and negative controls (Neg C.), performed using non-coated beads of the same time show there was no cross contamination or spontaneous generation during the process. A sample of substrate, not digested with PK, was also included to facilitate size comparisons. As an example of a partially effective treatment, the experiment performed using Teflon® beads treated with 1N NaOH for 1 h is shown. Finally, an example of a completely effective inactivation, the experiment carried out with prion-coated steel beads treated with commercial bleach for 1 h is shown. MW, Molecular weight marker.

turnaround time and animal welfare of the *in vitro* techniques, the availability of permissive animal models for each prion strain under analysis is also a significant limitation of the bioassay. Giles and collaborators highlighted the importance of evaluating the efficacy of a decontamination treatment for a particular prion strain by showing that bovine spongiform encephalopathy (BSE) prions are 1,000-fold more resistant to inactivation than the mouse-adapted BSE strain 301V, and up to a million-fold more resistant than some other strains examined (Giles et al., 2008). However, *in vitro* methods for evaluation of decontamination efficacy allow using as many different strains as desired thereby increasing their versatility as shown by Hughson et al. using RT-QuIC to examine the efficacy of decontaminants against five different prion strains concurrently (Hughson et al., 2016). For our PMSA-based method we chose a recombinant prion derived from bank voles, the infectivity of which was determined previously along with its biochemical characteristics (Erana et al., 2019). Specifically, its high PK-resistance is noteworthy [resistant to more than 1,000 μg/ml of PK which is equivalent or even higher than BSE, 1,000 μg/ml of PK but as whole brain extract, while the recombinant prion contains only dextran (Masujin et al., 2008)], indicating a highly packed amyloid core that, theoretically, will confer exceptional resistance to decontamination treatments. Therefore, using experimentally

obtained recombinant prions to provide consistency to this novel method, although not directly related to natural mammalian-derived strains, is offset by using recombinant prions showing the most resistance to destruction. Although only Sst01 prions were used in this study, we have already generated several distinct rec-PrP^{res} isoforms showing different characteristics, using recombinant PrP from several mammalian species. All these recombinant prion conformers could be used together in the assay, providing exceptional robustness and reliability and therefore safely representative of less stable tissue-derived prions.

A critical advantage of this novel assay is the use of dried beads of different materials as prions can be adsorbed to the surfaces of many different materials that have been washed and dried. This approach has been used previously, principally by coating steel wires with prions by incubation with brain homogenates from affected animals. These prion-coated steel wires have been used to assess the efficacy of prion inactivation or elimination treatments by determining infectivity *in vivo* (Peretz et al., 2006; Giles et al., 2008; Berberidou et al., 2013) and by other criteria by *ex vivo* (Edgeworth et al., 2011) and *in vitro* (Fichet et al., 2004; Belondrade et al., 2016; Mori et al., 2016; Belondrade et al., 2020) methodologies also. Limited studies have been performed using other materials, mainly metallic or oxidized surfaces such as titanium (Berberidou et al., 2013), aluminum oxide and silicon dioxide (Jacobson et al., 2013), and non-metallic materials such as bricks (Gough et al., 2017) or farm soil (Sohn et al., 2019). These data, together with the results presented here, clearly demonstrate the relevance of the material prions are attached to with respect to the variability in efficacy of decontaminants, highlighting differences even between metallic surfaces such as steel and titanium (Berberidou et al., 2013). However, the ability to use prion-coated materials for assessment of decontaminant procedures after washing and drying allows greater representation of the real situations where prions could be found. Dehydration may promote and increase in prion resistance to inactivation or elimination (Yuan et al., 2018), so the use of brain homogenates or prions recovered from contaminated surfaces in solvents for the evaluation of decontamination may significantly overestimate their efficacy. The novel method presented here is the first reported that examines several radically different surface materials mimicking the real-life scenario including exposure to being washed and dried previously to replicate what effect this may have on adhered prions. The major weaknesses of decontaminant assessment methodologies based exclusively on *in vitro* prion propagation is the lack of direct comparison with confirmatory *in vivo* assays as correlation between rec-PrP^{res} detection and prion infectivity would be ideal. The primary aim of this study was to report a low-cost, easy and fast assay that could be used as a pre-screening assay to evaluate many different decontamination treatments and bioassay would only be required for those treatments that are successful on *in vitro* prion propagation. However, in our extensive experience with *in vitro* prion propagation methods, we have never observed infectivity in bioassay from a recombinant seed that had been unable to give rise to rec-PrP^{res} after being submitted to PMSA, suggesting a good correlation between *in vitro* propagation capacity and *in vivo* infectivity. Although, the possibility of a sample retaining infectivity *in vivo* despite being undetectable by PMSA propagation cannot be excluded completely, this has been addressed previously by others who showed good correlation as long as the *in vitro* amplification technique was highly sensitive (Lee et al., 2000; Belondrade et al., 2020). Therefore, given the data, we consider our novel system will have excellent correlation with rec-PrP^{res} detection by bioassay.

Our main goal was to develop an assay to assess potential prion decontamination treatments, not the evaluation of decontaminants *per se*. However, the results obtained with the treatments chosen and used as proof of concept for this methodology are noteworthy. The use of an autoclave at 121°C and UV irradiation were selected because they have been proven to be inefficient for prion inactivation (Alper et al., 1967; WHO, 1999; Taylor, 2000) and our results support this. Exposure to UV light did not reduce prion propagation capacity at t3 for any of the materials tested and, except for prions adsorbed to steel beads, autoclaving at 121°C showed little, if any, effect. The fact that prion-coated steel beads could be inactivated completely by this procedure could be due to a more significant reduction in propagative units than for other materials, it is possible that the steel beads already contained lower initial amount of prions or that the temperature resulted more effective eliminating prions from this surface due to its higher thermal conductivity, since a reduction in infectivity at 121°C have also been reported for brain homogenates (Prusiner, 1984; Ernst and Race, 1993). In fact, autoclave at 121°C has been previously reported as partially efficient for the decontamination of prion-coated metal wires, evaluated by PMCA (Belondrade et al., 2016). Whether this increased reduction of prions adsorbed to steel beads in comparison with the rest is a result of a lower load of prions, unlikely according to preliminary propagation experiments, or a different mechanism of prion-surface interaction cannot be explained at present. On the contrary, the autoclave at 134°C, bleach and NaOH treatments were chosen due to their efficacy, according to the WHO, and, as such, they are used routinely in research laboratories working with prions (WHO, 1999). Surprisingly, the autoclave method was only partially effective for most of the materials examined, being especially ineffective for zirconia-silica and glass beads, which may have the most irregular or porous surfaces among the materials used, suggesting some degree of protection for prions adsorbed to such materials. This partial decontamination by autoclaving at 134°C has also been reported for other systems based on steel wires and bioassay, revealing the importance of humidity during the process (Fichet et al., 2004) and which could explain our results. NaOH and bleach are the most popular and widely used chemical decontaminants and bleach was the most effective decontaminant agent for prions by our assay. However, striking differences were found depending on the bead materials used. In the case of steel beads, decontamination was complete in agreement with previous results obtained *in vitro* and *in vivo* with brain homogenates and steel wires (Fichet et al., 2004; Lemmer et al., 2008; Hughson et al., 2016), although for other materials results can differ as demonstrate by the work of Gough et al. in which NaOH and free chlorine were unable to decontaminate

prions on the surface of bricks (Gough et al., 2017). Therefore, we can assume that the characteristics of materials such as zirconia-silica, glass or Teflon® can limit the effectiveness of bleach and NaOH treatments either by protecting prions inside the pores of a coarse surface or hindering proper contact between the decontaminant solution and the prions due, for example, to hydrophobicity. The results obtained for Teflon® beads with Virkon™, a well-known virucidal with abundant peroxides and surfactants with unknown effect on prions, and acidic SDS treatment, proved partially effective (Peretz et al., 2006), resulted in similar or even better results than bleach and NaOH. This prompted us to investigate whether it was due to hydrophobicity or surface tension that was hindering proper contact between the decontaminants and the prions adsorbed to the surface of this material. The presence of Triton-X-100 in the bleach or NaOH solutions greatly improved their prion elimination capacity, indicating the importance of the properties of each material with bound prions when assessing decontamination treatments. The presence of a non-ionic surfactant probably facilitates the access of the decontaminants to the highly hydrophobic surface of the bead, although other mechanisms cannot be ruled out.

Overall, we present a novel PMSA method to assess prion decontamination or inactivation procedures suitable for examining prions bound to different materials' surfaces that is easy to perform in any laboratory using minimum equipment and biosafety conditions. By using known effective, partially effective or ineffective treatments, we have validated this method with previous results. Furthermore, as previous results were obtained mainly by treatment of brain homogenates or prions bound to steel wires, we have provided novel data and new insights with respect to the decontamination of surface adsorbed prions, revealing the relevance that different surface materials and their possibly distinct interactions with prions influence significantly the efficacy of different prion decontamination treatments. Combinations of different treatments that increase their efficacy are actually recommended (WHO, 1999) and when used have reduced the risk of iatrogenic transmission of prion disorders almost completely. However, in order to find a universal decontamination treatment effective for any kind of prion strain bound to any surface, assessment methods such as the novel one presented here are required given the continued threat to public health posed by extremely persistent prions.

DATA AVAILABILITY STATEMENT

All datasets generated for this study are included in the article/**Supplementary Material**, further inquiries can be directed to the corresponding author.

AUTHOR CONTRIBUTIONS

HE, MP-C, SG-M, and JC contributed to the conception and design of the study. MP-C, SG-M, JMC, EG-M, RL-M, CD-D, and TB performed the experiments, interpreted the results, and designed figures and tables. HE, MP-C, and TB wrote the first draft of the manuscript. JC was responsible for funding acquisition. All authors contributed to manuscript revision, read, and approved the submitted version.

FUNDING

This work was supported financially by Spanish grant awarded to JC (AGL2015-65046-C2-1-R) by MINECO/FEDER, as well as an Interreg (POCTEFA EFA148/16) grant awarded to JC by FEDER. Therefore this project was co-funded by the European Regional Developement Fund. The funders had no role in study design, data collection and analysis, decision to publish, or preparation of the manuscript.

ACKNOWLEDGMENTS

We want to acknowledge the excellent technical assistance of Patricia Piñeiro and thank Dr. Mark P. Dagleish for useful discussion and advice. We also thank MINECO for the Severo Ochoa Excellence Accreditation (SEV-2016-0644) to the CIC bioGUNE.

SUPPLEMENTARY MATERIAL

The Supplementary Material for this article can be found online at: https://www.frontiersin.org/articles/10.3389/fbioe.2020.589182/full#supplementary-material

REFERENCES

Aguzzi, A., and Calella, A. M. (2009). Prions: protein aggregation and infectious diseases. *Physiol. Rev.* 89, 1105–1152. doi: 10.1152/physrev.00006.2009

Alper, T., Cramp, W. A., Haig, D. A., and Clarke, M. C. (1967). Does the agent of scrapie replicate without nucleic acid? *Nature* 214, 764–766. doi: 10.1038/214764a0

Bellinger-Kawahara, C., Cleaver, J. E., Diener, T. O., and Prusiner, S. B. (1987). Purified scrapie prions resist inactivation by UV irradiation. *J. Virol.* 61, 159–166.

Belondrade, M., Jas-Duval, C., Nicot, S., Bruyere-Ostells, L., Mayran, C., Herzog, L., et al. (2020). Correlation between bioassay and protein misfolding cyclic amplification for variant creutzfeldt-jakob disease decontamination studies. *mSphere* 5:e00649-19. doi: 10.1128/mSphere.00649-19

Belondrade, M., Nicot, S., Beringue, V., Coste, J., Lehmann, S., and Bougard, D. (2016). Rapid and highly sensitive detection of variant creutzfeldt-jakob disease abnormal prion protein on steel surfaces by protein misfolding cyclic amplification: application to prion decontamination studies. *PLoS One* 11:e0146833. doi: 10.1371/journal.pone.0146833

Berberidou, C., Xanthopoulos, K., Paspaltsis, I., Lourbopoulos, A., Polyzoidou, E., Sklaviadis, T., et al. (2013). Homogenous photocatalytic decontamination of prion infected stainless steel and titanium surfaces. *Prion* 7, 488–495. doi: 10.4161/pri.27180

Bonda, D. J., Manjila, S., Mehndiratta, P., Khan, F., Miller, B. R., Onwuzulike, K., et al. (2016). Human prion diseases: surgical lessons learned from iatrogenic prion transmission. *Neurosurg. Focus* 41:E10. doi: 10.3171/2016.5.FOCUS15126

Botsios, S., Tittman, S., and Manuelidis, L. (2015). Rapid chemical decontamination of infectious CJD and scrapie particles parallels

treatments known to disrupt microbes and biofilms. *Virulence* 6, 787–801. doi: 10.1080/21505594.2015.1098804

Brown, P., and Farrell, M. (2015). A practical approach to avoiding iatrogenic Creutzfeldt-Jakob disease (CJD) from invasive instruments. *Infect. Control Hosp. Epidemiol.* 36, 844–848. doi: 10.1017/ice.2015.53

Brown, S. A., Merritt, K., Woods, T. O., and Busick, D. N. (2005). Effects on instruments of the World Health Organization–recommended protocols for decontamination after possible exposure to transmissible spongiform encephalopathy-contaminated tissue. *J. Biomed. Mater. Res. B Appl. Biomater.* 72, 186–190. doi: 10.1002/jbm.b.30125

CDC (2019). *CJD Infection Control [Online]*. Atlanta: Centers for Disease Control and Prevention.

Crotti, N. (2020). *Case Medical Lands Patent for Prion-Decontamination Formula [Online]*. Available: https://www.medicaldesignandoutsourcing.com/case-medical-lands-patent-for-prion-decontamination-formula/ (accessed June, 20 2020).

Cuille, J., and Chelle, P. (1936). La maladie dite tremblante du mouton est-elle inoculable? *CR Acad. Sci.* 203, 1552–1554.

Duffy, P., Wolf, J., Collins, G., DeVoe, A. G., Streeten, B., and Cowen, D. (1974). Letter: possible person-to-person transmission of Creutzfeldt-Jakob disease. *N. Engl. J. Med.* 290, 692–693. doi: 10.1056/nejm197403212901220

Edgeworth, J. A., Gros, N., Alden, J., Joiner, S., Wadsworth, J. D., Linehan, J., et al. (2010). Spontaneous generation of mammalian prions. *Proc. Natl. Acad. Sci. U.S.A.* 107, 14402–14406. doi: 10.1073/pnas.1004036107

Edgeworth, J. A., Sicilia, A., Linehan, J., Brandner, S., Jackson, G. S., and Collinge, J. (2011). A standardized comparison of commercially available prion decontamination reagents using the standard steel-binding assay. *J. Gen. Virol.* 92(Pt 3), 718–726. doi: 10.1099/vir.0.027201-0

el Hachimi, K. H., Chaunu, M. P., Cervenakova, L., Brown, P., and Foncin, J. F. (1997). Putative neurosurgical transmission of Creutzfeldt-Jakob disease with analysis of donor and recipient: agent strains. *C. R. Acad. Sci. III* 320, 319–328. doi: 10.1016/s0764-4469(97)82774-6

Elezgarai, S. R., Fernández-Borges, N., Erana, H., Sevillano, A., Moreno, J., Harrathi, C., et al. (2017). Generation of a new infectious recombinant prion: a model to understand Gerstmann–Sträussler–Scheinker syndrome. *Sci. Rep.* 7:9584. doi: 10.1038/s41598-017-09489-3

Erana, H., Charco, J. M., Di Bari, M. A., Diaz-Dominguez, C. M., Lopez-Moreno, R., Vidal, E., et al. (2019). Development of a new largely scalable in vitro prion propagation method for the production of infectious recombinant prions for high resolution structural studies. *PLoS Pathog.* 15:e1008117. doi: 10.1371/journal.ppat.1008117

Ernst, D. R., and Race, R. E. (1993). Comparative analysis of scrapie agent inactivation methods. *J. Virol. Methods* 41, 193–201. doi: 10.1016/0166-0934(93)90126-c

Fernández-Borges, N., Di Bari, M. A., Erana, H., Sanchez-Martin, M., Pirisinu, L., Parra, B., et al. (2017a). Cofactors influence the biological properties of infectious recombinant prions. *Acta Neuropathol.* 135, 179–199. doi: 10.1007/s00401-017-1782-y

Fernández-Borges, N., Erana, H., Elezgarai, S. R., Harrathi, C., Venegas, V., and Castilla, J. (2017b). "A quick method to evaluate the effect of the amino acid sequence in the misfolding proneness of the prion protein," in *Prions: Methods and Protocols*, ed. V. A. Lawson (Cham: Springer).

Fichet, G., Comoy, E., Duval, C., Antloga, K., Dehen, C., Charbonnier, A., et al. (2004). Novel methods for disinfection of prion-contaminated medical devices. *Lancet* 364, 521–526. doi: 10.1016/S0140673604168104

Flechsig, E., Hegyi, I., Enari, M., Schwarz, P., Collinge, J., and Weissmann, C. (2001). Transmission of scrapie by steel-surface-bound prions. *Mol. Med.* 7, 679–684. doi: 10.1007/bf03401958

Gibbs, C. J. Jr., Gajdusek, D. C., and Alpers, M. P. (1969). Attempts to transmit subacute and chronic neurological diseases to animals. *Int. Arch. Allergy Appl. Immunol.* 36(Suppl.), 519–552. doi: 10.1007/978-1-4613-3988-5_24

Giles, K., Glidden, D. V., Beckwith, R., Seoanes, R., Peretz, D., DeArmond, S. J., et al. (2008). Resistance of bovine spongiform encephalopathy (BSE) prions to inactivation. *PLoS Pathog.* 4:e1000206. doi: 10.1371/journal.ppat.1000206

Giles, K., Woerman, A. L., Berry, D. B., and Prusiner, S. B. (2017). Bioassays and inactivation of prions. *Cold Spring Harb. Perspect. Biol.* 9:a023499. doi: 10.1101/cshperspect.a023499

Gordon, W. S. (1946). Advances in veterinary research. *Vet. Rec.* 58, 516–525.

Gough, K. C., Baker, C. A., and Maddison, B. C. (2017). An in vitro model for assessing effective scrapie decontamination. *Vet. Microbiol.* 207, 138–142. doi: 10.1016/j.vetmic.2017.05.018

Hughson, A. G., Race, B., Kraus, A., Sangare, L. R., Robins, L., Groveman, B. R., et al. (2016). Inactivation of prions and amyloid seeds with hypochlorous acid. *PLoS Pathog.* 12:e1005914. doi: 10.1371/journal.ppat.1005914

Hunter, G. D. (1969). The size and intracellular location of the scrapie agent. *Biochem. J.* 114, 22–23.

Hunter, G. D., and Millson, G. C. (1967). Attempts to release the scrapie agent from tissue debris. *J. Comp. Pathol.* 77, 301–307. doi: 10.1016/0021-9975(67)90039-4

Jacobson, K. H., Kuech, T. R., and Pedersen, J. A. (2013). Attachment of pathogenic prion protein to model oxide surfaces. *Environ. Sci. Technol.* 47, 6925–6934. doi: 10.1021/es3045899

Kocisko, D. A., Come, J. H., Priola, S. A., Chesebro, B., Raymond, G. J., Lansbury, P. T., et al. (1994). Cell-free formation of protease-resistant prion protein. *Nature* 370, 471–474. doi: 10.1038/370471a0

Lee, D. C., Stenland, C. J., Hartwell, R. C., Ford, E. K., Cai, K., Miller, J. L., et al. (2000). Monitoring plasma processing steps with a sensitive Western blot assay for the detection of the prion protein. *J. Virol. Methods* 84, 77–89. doi: 10.1016/s0166-0934(99)00135-4

Lemmer, K., Mielke, M., Kratzel, C., Joncic, M., Oezel, M., Pauli, G., et al. (2008). Decontamination of surgical instruments from prions. II. In vivo findings with a model system for testing the removal of scrapie infectivity from steel surfaces. *J. Gen. Virol.* 89(Pt 1), 348–358. doi: 10.1099/vir.0.83396-0

Masujin, K., Shu, Y., Yamakawa, Y., Hagiwara, K., Sata, T., Matsuura, Y., et al. (2008). Biological and biochemical characterization of L-type-like bovine spongiform encephalopathy (BSE) detected in Japanese black beef cattle. *Prion* 2, 123–128. doi: 10.4161/pri.2.3.7437

Mori, T., Atarashi, R., Furukawa, K., Takatsuki, H., Satoh, K., Sano, K., et al. (2016). A direct assessment of human prion adhered to steel wire using real-time quaking-induced conversion. *Sci. Rep.* 6:24993. doi: 10.1038/srep24993

Pattison, I. H. (1965). Resistance of the scrapie agent to formalin. *J. Comp. Pathol.* 75, 159–164. doi: 10.1016/0021-9975(65)90006-x

Pattison, I. H., and Millson, G. C. (1961). Further experimental observations on scrapie. *J. Comp. Pathol.* 71, 350–359. doi: 10.1016/s0368-1742(61)80040-4

Pattison, J. (1998). The emergence of bovine spongiform encephalopathy and related diseases. *Emerg. Infect. Dis.* 4, 390–394. doi: 10.3201/eid0403.980311

Peretz, D., Supattapone, S., Giles, K., Vergara, J., Freyman, Y., Lessard, P., et al. (2006). Inactivation of prions by acidic sodium dodecyl sulfate. *J. Virol.* 80, 322–331. doi: 10.1128/JVI.80.1.322-331.2006

Prusiner, S. B. (1982a). Novel proteinaceous infectious particles cause scrapie. *Science* 216, 136–144. doi: 10.1126/science.6801762

Prusiner, S. B. (1982b). Research on scrapie. *Lancet* 2, 494–495. doi: 10.1016/s0140-6736(82)90519-0

Prusiner, S. B. (1984). Prions: novel infectious pathogens. *Adv. Virus Res.* 29, 1–56. doi: 10.1016/s0065-3527(08)60404-2

Prusiner, S. B., Groth, D. F., Cochran, S. P., Masiarz, F. R., McKinley, M. P., and Martinez, H. M. (1980a). Molecular properties, partial purification, and assay by incubation period measurements of the hamster scrapie agent. *Biochemistry* 19, 4883–4891. doi: 10.1021/bi00562a028

Prusiner, S. B., Groth, D. F., Cochran, S. P., McKinley, M. P., and Masiarz, F. R. (1980b). Gel electrophoresis and glass permeation chromatography of the hamster scrapie agent after enzymatic digestion and detergent extraction. *Biochemistry* 19, 4892–4898. doi: 10.1021/bi00562a029

Prusiner, S. B., Groth, D. F., McKinley, M. P., Cochran, S. P., Bowman, K. A., and Kasper, K. C. (1981a). Thiocyanate and hydroxyl ions inactivate the scrapie agent. *Proc. Natl. Acad. Sci. U.S.A.* 78, 4606–4610. doi: 10.1073/pnas.78.7.4606

Prusiner, S. B., Hadlow, W. J., Garfin, D. E., Cochran, S. P., Baringer, J. R., Race, R. E., et al. (1978). Partial purification and evidence for multiple molecular forms of the scrapie agent. *Biochemistry* 17, 4993–4999. doi: 10.1021/bi00616a021

Prusiner, S. B., McKinley, M. P., Groth, D. F., Bowman, K. A., Mock, N. I., Cochran, S. P., et al. (1981b). Scrapie agent contains a hydrophobic protein. *Proc. Natl. Acad. Sci. U.S.A.* 78, 6675–6679. doi: 10.1073/pnas.78.11.6675

Saborio, G. P., Permanne, B., and Soto, C. (2001). Sensitive detection of pathological prion protein by cyclic amplification of protein misfolding. *Nature* 411, 810–813. doi: 10.1038/35081095

Scott, M. R., Will, R., Ironside, J., Nguyen, H. O., Tremblay, P., DeArmond, S. J., et al. (1999). Compelling transgenetic evidence for transmission of bovine spongiform encephalopathy prions to humans. *Proc. Natl. Acad. Sci. U.S.A.* 96, 15137–15142. doi: 10.1073/pnas.96.26.15137

Sehulster, L. M. (2004). Prion inactivation and medical instrument reprocessing: challenges facing healthcare facilities. *Infect. Control Hosp. Epidemiol.* 25, 276–279. doi: 10.1086/502391

Simpson, D. A., Masters, C. L., Ohlrich, G., Purdie, G., Stuart, G., and Tannenberg, A. E. (1996). Iatrogenic Creutzfeldt-Jakob disease and its neurosurgical implications. *J. Clin. Neurosci.* 3, 118–123. doi: 10.1016/s0967-5868(96)90003-x

Sohn, H. J., Park, K. J., Roh, I. S., Kim, H. J., Park, H. C., and Kang, H. E. (2019). Sodium hydroxide treatment effectively inhibits PrP(CWD) replication in farm soil. *Prion* 13, 137–140. doi: 10.1080/19336896.2019.1617623

Stamp, J. T., Brotherston, J. G., Zlotnik, I., Mackay, J. M., and Smith, W. (1959). Further studies on scrapie. *J. Comp. Pathol.* 69, 268–280. doi: 10.1016/s0368-1742(59)80026-6

Supattapone, S., Wille, H., Uyechi, L., Safar, J., Tremblay, P., Szoka, F. C., et al. (2001). Branched polyamines cure prion-infected neuroblastoma cells. *J. Virol.* 75, 3453–3461. doi: 10.1128/JVI.75.7.3453-3461.2001

Tateishi, J., Tashima, T., and Kitamoto, T. (1988). Inactivation of the Creutzfeldt-Jakob disease agent. *Ann. Neurol.* 24, 466–466. doi: 10.1002/ana.410240325

Taylor, D. M. (2000). Inactivation of transmissible degenerative encephalopathy agents: a review. *Vet. J.* 159, 10–17. doi: 10.1053/tvjl.1999.0406

WHO (1999). *WHO Infection Control Guidelines for Transmissible Spongiform Encephalopathies*. Geneva: World Health Organization [WHO].

Yuan, Q., Telling, G., Bartelt-Hunt, S. L., and Bartz, J. C. (2018). Dehydration of prions on environmentally relevant surfaces protects them from inactivation by freezing and thawing. *J. Virol.* 92:e02191-17. doi: 10.1128/JVI.02191-17

Zobeley, E., Flechsig, E., Cozzio, A., Enari, M., and Weissmann, C. (1999). Infectivity of scrapie prions bound to a stainless steel surface. *Mol. Med.* 5, 240–243.

Conflict of Interest: HE, JMC, SG-M, and EG-M were employed by the commercial company ATLAS Molecular Pharma SL. This does not alter our adherence to all Frontiers policies on sharing data and materials.

The remaining authors declare that the research was conducted in the absence of any commercial or financial relationships that could be construed as a potential conflict of interest.

frontiers in Bioengineering and Biotechnology

BRIEF RESEARCH REPORT
published: 19 November 2020
doi: 10.3389/fbioe.2020.586890

Optimization of the Real-Time Quaking-Induced Conversion Assay for Prion Disease Diagnosis

*Inga Zerr[1], Maria Cramm[1], Susana Margarida da Silva Correia[1], Saima Zafar[1,2], Anna Villar-Piqué[1,3,4], Franc Llorens[1,3,4] and Matthias Schmitz[1]**

[1] Department of Neurology, German Center for Neurodegenerative Diseases (DZNE), University Medical Center Göttingen, Göttingen, Germany, [2] Biomedical Engineering and Sciences Department, School of Mechanical and Manufacturing Engineering, National University of Sciences and Technology, Islamabad, Pakistan, [3] Bellvitge Biomedical Research Institute, Hospitalet de Llobregat, Barcelona, Spain, [4] Center for Networked Biomedical Research on Neurodegenerative Diseases, Institute of Health Carlos III, Hospitalet de Llobregat, Barcelona, Spain

The real-time quaking-induced conversion (RT-QuIC) assay is a highly reproducible and robust methodology exhibiting an excellent pre-mortem diagnostic accuracy for prion diseases. However, the protocols might be time-consuming and improvement of the detection technology is needed. In the present study, we investigated the influence of a pre-analytical cerebrospinal fluid (CSF) treatment with proteinase K (PK) on the kinetic of the RT-QuIC signal response. For this purpose, we added PK at different concentrations in RT-QuIC reactions seeded with Creutzfeldt–Jakob disease (sCJD) CSF. We observed that a mild pre-analytical PK treatment of CSF samples resulted in an increased seeding efficiency of the RT-QuIC reaction. Quantitative seeding parameters, such as a higher area under the curve (AUC) value or a shorter lag phase indicated a higher conversion efficiency after treatment. The diagnostic accuracy resulting from 2 μg/ml PK treatment was analyzed in a retrospective study, where we obtained a sensitivity of 89%. Additionally, we analyzed the agreement with the previously established standard RT-QuIC protocol without PK treatment in a prospective study. Here, we found an overall agreement of 94% to 96%. A Cohen's kappa of 0.9036 (95% CI: 0.8114–0.9958) indicates an almost perfect agreement between both protocols. In conclusion, the outcome of our study can be used for a further optimization of the RT-QuIC assay in particular for a reduction of the testing time.

Keywords: cerebrospinal fluid, Creutzfeldt-Jakob disease, diagnostic test, prion protein, real-time quaking-induced conversion

OPEN ACCESS

Edited by:
Maria Dos Anjos Pires, University of Trás-os-Montes and Alto Douro, Portugal

Reviewed by:
Rita Payan Carreira, University of Evora, Portugal
Bruno Jorge Antunes Colaço, University of Trás-os-Montes and Alto Douro, Portugal

****Correspondence:***
Matthias Schmitz
matthias.schmitz@med.uni-goettingen.de

Specialty section:
This article was submitted to Biosafety and Biosecurity, a section of the journal Frontiers in Bioengineering and Biotechnology

Received: *24 July 2020*
Accepted: *07 October 2020*
Published: *19 November 2020*

Citation:
Zerr I, Cramm M, da Silva Correia SM, Zafar S, Villar-Piqué A, Llorens F and Schmitz M (2020) Optimization of the Real-Time Quaking-Induced Conversion Assay for Prion Disease Diagnosis. Front. Bioeng. Biotechnol. 8:586890. doi: 10.3389/fbioe.2020.586890

INTRODUCTION

The pre-mortal diagnostic criteria of Creutzfeldt–Jakob disease (sCJD) include clinical examinations combined with magnetic resonance imaging (MRI) of the brain, electroencephalography (EEG), and laboratory analysis of cerebrospinal fluid (CSF; WHO, 1998, 2003; Zerr et al., 2009). Surrogate biomarkers such as 14-3-3, tau, alpha synuclein, etc. were applied for pre-mortem diagnosis (Zerr et al., 1998; Llorens et al., 2016, 2017; Schmitz et al., 2016c,d, 2019). A major innovation in prion disease diagnostic was the development of *in vitro* protein misfolding cyclic amplification (PMCA) assays. These include the PMCA (Saborio et al., 2001),

the amyloid seeding assay (ASTA; Colby et al., 2007), the quaking-induced conversion (QuIC; Atarashi et al., 2008), and the real-time quaking-induced conversion (RT-QuIC; Atarashi et al., 2011; McGuire et al., 2012; Orru et al., 2014; Schmitz et al., 2016a,b). Atarashi et al. (2011) firstly used the RT-QuIC to amplify minuscule amounts of a PrP^{Sc} seed in CSF from patients with prion disease. Afterward, a high specificity of approximately 100%, robustness, and high reproducibility of the RT-QuIC had been demonstrated by several groups (McGuire et al., 2012, 2016; Sano et al., 2013; Cramm et al., 2015, 2016). The sensitivity of the RT-QuIC depends on the kind of prion disease (Sano et al., 2013; Cramm et al., 2015); for sCJD, it varies between 80% and 95%. Other confounding factors are the composition of the study cohort or the type of recombinant PrP^{C} (hamster, hamster–sheep, human, bank vole, etc.; Orru et al., 2015; Candelise et al., 2017).

Recently, a suggestion has been made to amend the criteria by adding the PrP^{Sc} detection by RT-QuIC (Hermann et al., 2018). Therefore, a further optimization of the RT-QuIC by reducing the average testing time of 80 h would be beneficial.

In the present study, we analyzed the influence of a mild pre-analytical proteinase K (PK) treatment of CSF samples (sCJD and controls) on the PrP conversion efficiency in the RT-QuIC as defined by quantitative seeding parameters, such as the lag phase or the area under the curve (AUC). After selection of a PK concentration, we performed a retrospective study to define the sensitivity and a prospective study to compare the accordance of the RT-QuIC with and without pre-analytical PK treatment.

MATERIALS AND METHODS

Ethics Statement

The studies involving human CSF samples were reviewed and approved by the local Ethics Committee of the University Medicine Göttingen, Von Siebold-Str. 37075 Göttingen, No. 24/8/12. All samples were analyzed blinded for at least personal data.

Patients

We performed a retrospective study including 65 sCJD patients [35 patients with codon 129 homozygous methionine genotype (MM), 15 heterozygous MV, and 15 VV cases] as well as 20 control subjects without prion disease. All sCJD cases were diagnosed as probable cases according to diagnostic consensus criteria; 20 were confirmed by autopsy (WHO, 1998, 2003; Zerr et al., 2009). From them, we used four sCJD MM cases for studying the influence of PK incubation and deactivation steps on RT-QuIC signal response.

The control group included patients either healthy or with clinically defined alternative diagnosis such as Alzheimer's disease, alpha synucleinopathies, or psychiatric disorders (psychosis, bipolar disorder, and schizophrenia). Additionally, we included a prospective cohort that consisted of 35 RT-QuIC positive cases (suspected sCJD cases) and 51 cases exhibiting a negative RT-QuIC seeding response (suspected controls). These samples were collected during diagnostic routine without any further characterization.

RT-QuIC Analysis

We conducted the RT-QuIC analysis according to an established protocol (Schmitz et al., 2016b, 2018). Each sample was run in triplicates. Briefly, 85 µl of RT-QuIC buffer [162 mM phosphate buffer (pH 6.9), 170 mM sodium chloride, 1 mM ethylenediaminetetraacetic acid (EDTA), 10 µM Thioflavin-T (Th-T), and 0.1 mg/ml recPrP] was seeded with 15 µl of CSF (total volume of 100 µl). For RT-QuIC analysis, we used the BMG OPTIMA FLUOStar plate reader. Reactions were run at 42°C for 80 h with intermittent shaking cycles [1-min double orbital shaking at the highest speed (600 rpm)] followed by 1-min incubation. Every 30 min, fluorescence was measured at 450-nm excitation and 480-nm emission.

Pre-analytical PK Treatment

Cerebrospinal fluid samples were subjected to a mild pre-analytical treatment with PK in a range of 0–6 µg/ml. After adding PK, samples were incubated for 30 min at 37°C. Subsequently, PK was deactivated by heating at 65°C for 30 min.

Coomassie Brilliant Blue Staining

Acrylamide gels (12%) were fixed in a solution containing 50% methanol and 10% glacial acetic acid for 1 h. After 1 h, solution was exchanged. Staining with 1% Coomassie brilliant blue R-250, 50% methanol, and 10% glacial acetic occurred for 20 min with gentle agitation. Destaining in 40% methanol and 10% glacial acetic acid solution was carried out until the gel background was fully transparent destained. Finally, gels were stored at RT in 5% glacial acetic acid solution.

Statistical Analysis

Agreement between the standard and the modified protocol was measured with the Cohen's kappa statistics, available in the vcd R package (Meyer et al., 2020). Then, measures of seeding efficiency were calculated for each individual sample defined by relative area under the curve (rel. AUC) and lag phase (time to 50% signal increase). Multiple comparisons data were analyzed by one-way ANOVA followed by Dunn's *Post hoc* test. Two groups (normally distributed) were compared using the Student's *t* test, while for non-normally distributed values, we considered the Mann–Whitney *U* test as appropriate. All analyses were conducted by using GraphPad Prism 8.

RESULTS

Influence of Serial Pre-analytical PK Treatments on the RT-QuIC Seeding Response

We performed a mild pre-analytical treatment of CSF samples with PK (2 µg/ml). After adding PK, samples were incubated for 30 min at 37°C. Subsequently, PK was deactivated by heating at 65°C for 30 min.

The incubation step for 30 min at RT or at 37°C alone or in combination with the incubation of 30 min at 65°C (without PK)

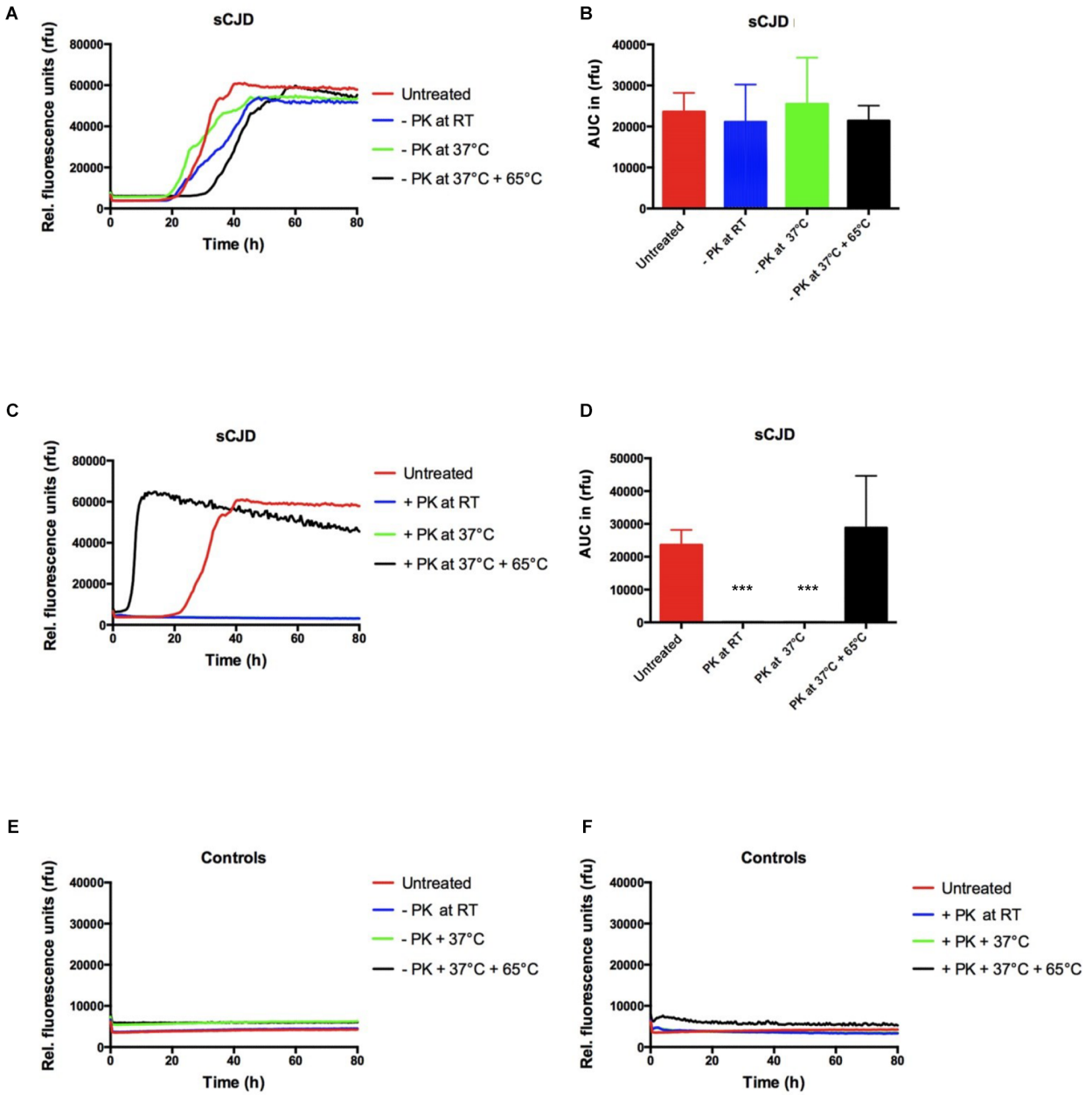

FIGURE 1 | Influence of PK incubation and deactivation steps on the RT-QuIC signal response. **(A,B)** All incubation and deactivation steps without PK (addition of water instead of PK) had no effect on the seeding kinetic and the AUC values in sCJD (MM; $n = 4$) seeded RT-QuIC reactions. **(C,D)** PK treatment (2 mg/ml) requires a deactivation step (30 min at 65°C); otherwise, no seeding reaction is observable when incubating with PK at room temperature (RT) or at 37°C. **(E,F)** In control-seeded reactions ($n = 4$), neither the incubation of 30 min at RT or at 37°C nor the deactivation for 30 min at 65°C exhibited a significant influence on the signal response independently from PK treatment. p values: <0.001 as extremely significant (***).

exhibited a non-significant effect on signal response compared to untreated reactions (**Figures 1A,B**).

In PK-treated reactions, the deactivation step is required; otherwise, all sCJD (MM) seeded reactions showed a negative seeding response comparable to controls (**Figures 1C,D**). In control seeded reactions, none of the conditions had changed the seeding kinetics (**Figures 1E,F**).

Subsequently, 20 well-characterized CSF samples from sCJD (MM) patients and 20 controls without prion disease were treated with different PK concentrations (0–6 μg/ml). After PK treatment, samples were subjected to RT-QuIC analysis using the standard protocol (Cramm et al., 2016; Schmitz et al., 2016b, 2018), which included recombinant hamster–sheep as substrate. The signal-kinetic in the RT-QuIC reaction was measured in

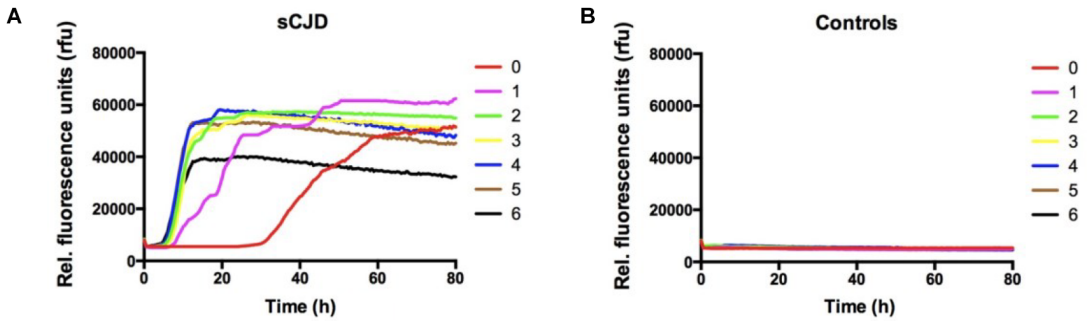

C

PK in µg/ml	0	1	2	3	4	5	6
sCJD	17/20 (85%)	16/20* (80%)	19/20* (95%)	19/20* (95%)	15/20* (75%)	15/20* (75%)	12/20* (60%)
Controls	0/20 (100%)	0/20* (100%)	0/20* (100%)	3/20* (85%)	3/20* (85%)	4/20* (80%)	2/20* (90%)

*Running time terminated at 40 h

FIGURE 2 | Influence of different amounts of PK on the RT-QuIC seeding response. **(A,B)** RT-QuIC reactions seeded either with sCJD MM or with control CSF were treated with different amounts of PK (0–6 µg/ml). The kinetics of positive RT-QuIC signaling responses indicated that treatment with PK influences the conversion efficiency of PrP in comparison to untreated reactions. **(C)** Accuracy of the RT-QuIC before and after PK treatment suggested a pre-treatment with 2 µg/ml PK as most suitable for a reliable diagnostic. For simplification, we displayed the means of all positive sCJD and negative control seeded reactions per group at each point in time and not the false-positive or -negative reactions.

dependency from the PK concentration (0–6 µg/ml). It indicated a significant increase of the conversion efficiency of reactions, seeded with sCJD CSF after PK treatment (**Figures 2A,B**). To define the optimal assay conditions for the sCJD diagnosis, we validated the correctly classified sCJD and control cases. Interestingly, the pre-analytical PK treatment of CSF samples in a concentration of 2 µg/ml revealed the best diagnostic accuracy; 19/20 sCJD cases and 0/20 control cases showed over a duration of 40 h testing time a positive RT-QuIC signal response (**Figure 2C**). The use of higher PK amounts and longer testing times may result in false-positive RT-QuIC reactions (**Figure 2C**).

Pre-analytical PK Treatment (2 µg/ml) Significantly Reduced the Lag Phase and the Testing Time of the RT-QuIC

The impact of a pre-analytical CSF treatment with 2 µg/ml PK on the total protein amount and the quantitative seeding parameters (such as lag phase and AUC) was now analyzed more in detail.

At first, we compared the total protein amount in sCJD MM CSF samples before and after PK treatment (2 µg/ml) by gel electrophoresis followed by *Coomassie Brilliant Blue* staining. Quantification of band intensities occurred by *Image Lab* software. Interestingly, we observed total protein amounts up to 50% decreased after PK treatment (**Supplementary Figures 1A,B**).

Next, we calculated quantitative seeding parameters of untreated in comparison to PK (2 µg/ml)-treated RT-QuIC reactions seeded with sCJD MM CSF. The obtained data indicated that RT-QuIC reactions pre-analytically exposed to PK revealed a significantly shorter lag phase, which decreased from more than 30 h (untreated) to 6–9 h on average as well as an increased AUC value after PK treatment (**Figures 3A–C**), while controls remained on a baseline level (**Figure 3D**).

Determination of the Sensitivity After PK Treatment in a Retrospective Study

The sensitivity of RT-QuIC after pre-analytical treatment with PK was analyzed in a retrospective study. The cohort consisted of 65 sCJD patients (35 MM, 15 MV, and 15 VV). After pre-analytical exposure to 2 µg/ml PK, samples were

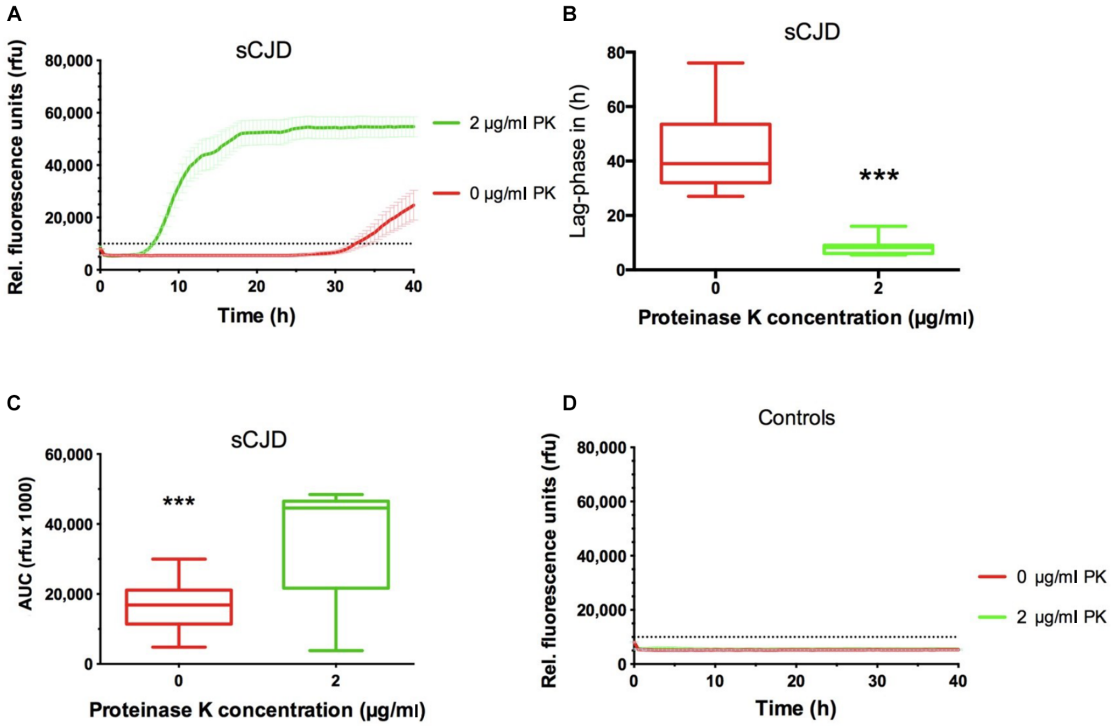

E

sCJD genotype	MM	MV	VV	In total
Sensitivity	32/35 (91%)	13/15 (87%)	13/15 (87%)	58/65 (89%)

FIGURE 3 | Optimization of the CSF RT-QuIC. **(A)** RT-QuIC reactions terminated at 40 h and seeded with sCJD MM CSF (n = 20) were treated with 2 µg/ml of PK, which increased the conversion efficiency of PrP significantly as indicated by a shorter lag phase **(B)** and a higher relative area under the curve (AUC) value **(C)**. Non-prion disease controls (n = 20) remained negative **(D)**. **(E)** In a retrospective study, we analyzed the sensitivity of the RT-QuIC after PK (2 µg/ml) treatment in different sCJD codon 129 MV genotypes showing an average sensitivity of 89% for all sCJD codon 129 MV genotypes. RT-QuIC responses were measured in rfu over a period of 40 h. Displayed are means ± SEM (standard error of the mean) at each point in time. p values: <0.001 as extremely significant (***).

analyzed via RT-QuIC for 40 h. The sensitivities varied between different sCJD codon 129 MV genotypes between 87% and 91%, while the average sensitivity for all sCJD genotype was 89% (**Figure 3E**).

Examination of the Agreement Between Optimized and Standard RT-QuIC

To determine the analytical agreement of the optimized RT-QuIC (with PK 2 µg/ml) and the standard RT-QuIC, a prospective study on a patient cohort consisting of 35 samples with a positive RT-QuIC response as well as 51 samples exhibiting a negative standard RT-QuIC response was performed. PK-treated and untreated samples were analyzed in parallel on the same plate. Interestingly, we obtained an agreement of 94% for the RT-QuIC positively classified cases and 96% for all CSF samples exhibiting a negative RT-QuIC signal response (**Table 1**). In addition, we calculated the Cohen's kappa value to determine the agreement between the standard and the optimized RT-QuIC protocol. Interestingly, we obtained a value of 0.9036 (95% CI: 0.8114–0.9958), which indicates an almost perfect agreement between both protocols.

DISCUSSION

Until now, several *in vitro* protein misfolding amplification systems, such as the RT-QuIC, have been established

TABLE 1 | In a prospective study, we analyzed the agreement of untreated (standard) and PK (2 μg/ml)-treated (optimized) RT-QuIC reactions.

Prospective study	Untreated	2 μg/ml PK treated	Agreement in %
RT-QuIC positive reactions	35	33	94%
RT-QuIC negative reactions	51	49	96%

We selected CSF samples with positive or negative signal response in the standard RT-QuIC and analyzed them in parallel in the optimized RT-QuIC.

providing relevant improvements in prion disease diagnostics and prion research (Atarashi et al., 2011; McGuire et al., 2012; Sano et al., 2013; Cramm et al., 2015, 2016). The standard diagnostic RT-QuIC protocol for the analysis of sCJD CSF (with recombinant hamster–sheep PrP^C as a substrate) exhibited a total assay duration for testing of 80 h (Cramm et al., 2015, 2016; Schmitz et al., 2016a,b, 2018). The lag phase of a positive RT-QuIC reaction lasts 30–40 h in average with accuracy between 80 and 85% and a specificity of almost 100% (Cramm et al., 2016). In the present study, we intend to modify the RT-QuIC standard protocol to reduce the lag phase and the testing time of the RT-QuIC.

Optimization of sCJD RT-QuIC by a Pre-analytical PK Treatment

In an initial study, we included a mild PK treatment of CSF in the pre-analytical protocol. Afterward, CSF samples were subjected to the standard RT-QuIC analysis (Cramm et al., 2016; Schmitz et al., 2016b, 2018). To elucidate the optimal amount of PK, we performed a serial dilution from 0 to 6 μg/ml of PK. All PK concentrations ≥2 μg/ml reduced the lag phase significantly. However, the diagnostic accuracy of the optimized RT-QuIC depended on the amount of PK. The usage of ≥3 μg/ml of PK resulted in a significant decrease of the specificity by creating false-positive RT-QuIC signals, as revealed by control RT-QuIC reactions (CSF without prion disease). A 2 μg/ml PK treatment provided the best diagnostic accuracy and allowed a reduction of the testing time from 80 to 40 h. Under these conditions, the PrP conversion process is accelerated, as indicated by a reduced lag phase and an increase of AUC values compared to the standard protocol without PK treatment. A potential reason may be that PK treatment resulted in a decrease of total protein amounts of more than 50%. Lower protein levels may affect the PrP^C–PrP^{Res} interaction in the RT-QuIC, which most likely promotes the conversion efficiency. Alternatively, it could be that PK partially digests external parts of PrP^{Res} species. This way, inner beta strands may become more exposed, displaying a higher seeding capacity.

To examine the application to all sCJD codon 129 MV genotypes and define the diagnostic sensitivity, a retrospective study was performed by analyzing 65 confirmed sCJD cases. Here, we obtained an average sensitivity for all genotypes of 89%. This is an increase compared to the standard RT-QuIC protocol (Cramm et al., 2016; Schmitz et al., 2016b, 2018), whereas the number of samples was lower.

In addition, we investigated the agreement of the new protocol (with PK) to the previous standard protocol in a prospective study. The accordance between both protocols varied between 94 and 96% with a Cohen's kappa of 0.9036 (95% CI: 0.8114–0.9958), which indicates an almost perfect agreement between both protocols. For four CSF samples, where we do not have any follow-up information, both protocols disagreed. One explanation may be an increase of sensitivity of the RT-QuIC after PK treatment. However, to finally elucidate this issue, a retrospective study on a higher number of well-characterized samples (e.g., >200 sCJD samples, consisting of typical and atypical sCJD cases as well as >100 neurological controls) is recommended.

Besides the standard or first generations of the RT-QuIC, a few studies successfully applied a so termed second generation of the RT-QuIC assay. In the second generation of the RT-QuIC, a truncated Syrian hamster recombinant PrP substrate (amino acids 90–231) and some modifications [incubations at 55°C instead of 42°C, and the addition of 0.002% sodium dodecyl sulfate (SDS)] of the standard RT-QuIC protocol have been used (Foutz et al., 2017; Franceschini et al., 2017; Groveman et al., 2017). In contrast to the full-length recombinant PrP substrate, the use of truncated recombinant PrP as a substrate contributed to an acceleration of the RT-QuIC seeding response and an increase of the conversion efficiency. The lag phase (less than 20 h) and the detection times (2-day reduction in average detection time) were significantly reduced in the second generation of the RT-QuIC (Foutz et al., 2017; Franceschini et al., 2017; Groveman et al., 2017), which is comparable to the optimized protocol with PK treatment. Moreover, the sensitivity of the RT-QuIC could be increased (up 94%, 113 CJD cases were tested) without loss of specificity (100%; Foutz et al., 2017; Franceschini et al., 2017; Groveman et al., 2017; Thompson and Mead, 2019).

In summary, our study provides an alternative to the originally as second generation described RT-QuIC for a further optimization of this test. The pre-analytical treatment of CSF with PK helps to reduce the testing time by increasing the conversion efficiency indicated by a shorter lag phase, higher AUC values, and an increase of the sensitivity.

DATA AVAILABILITY STATEMENT

All datasets presented in this study are included in the article/**Supplementary Material**.

ETHICS STATEMENT

The studies involving human participants were reviewed and approved by local ethics committee in Göttingen (No. 24/8/12). The patients/participants provided their written informed consent to participate in this study.

AUTHOR CONTRIBUTIONS

IZ and MS conceived the study. MC and SC performed experiments. IZ, MC, FL, and MS analyzed and interpreted data. IZ and MS drafted the manuscript. SZ, AV-P, and FL critically revised the manuscript. All authors read and approved the final manuscript version.

FUNDING

The project was supported by the German Academic Exchange Service (DAAD) project 57421248, by the Alzheimer Forschung Initiative (AFI) project 17022, and the Instituto de Salud Carlos III (Grant PI19/00144).

SUPPLEMENTARY MATERIAL

The Supplementary Material for this article can be found online at: https://www.frontiersin.org/articles/10.3389/fbioe.2020.586890/full#supplementary-material

Supplementary Figure 1 | Decrease of total protein amounts after treatment with PK 2 μg/ml **(A)** CSF samples from sCJD MM patients either treated with PK or untreated were stained with Coomassie brilliant blue. **(B)** Densitometric analysis via Image Lab indicated a decrease of total protein amount after treatment with PK.

REFERENCES

Atarashi, R., Satoh, K., Sano, K., Fuse, T., Yamaguchi, N., Ishibashi, D., et al. (2011). Ultrasensitive human prion detection in cerebrospinal fluid by real-time quaking-induced conversion. *Nat. Med.* 17, 175–178. doi: 10.1038/nm.2294

Atarashi, R., Wilham, J. M., Christensen, L., Hughson, A. G., Moore, R. A., Johnson, L. M., et al. (2008). Simplified ultrasensitive prion detection by recombinant PrP conversion with shaking. *Nat. Methods* 5, 211–212. doi: 10.1038/nmeth0308-211

Candelise, N., Schmitz, M., Da Silva, Correia, S. M., Arora, A. S., Villar-Pique, A., et al. (2017). Applications of the real-time quaking-induced conversion assay in diagnosis, prion strain-typing, drug pre-screening and other amyloidopathies. *Expert Rev. Mol. Diagn.* 17, 897–904. doi: 10.1080/14737159.2017.1368389

Colby, D. W., Zhang, Q., Wang, S., Groth, D., Legname, G., Riesner, D., et al. (2007). Prion detection by an amyloid seeding assay. *Proc. Natl. Acad. Sci. U S A.* 104, 20914–20919. doi: 10.1073/pnas.0710152105

Cramm, M., Schmitz, M., Karch, A., Mitrova, E., Kuhn, F., Schroeder, B., et al. (2016). Stability and Reproducibility Underscore Utility of RT-QuIC for Diagnosis of Creutzfeldt-Jakob Disease. *Mol. Neurobiol.* 53, 1896–1904. doi: 10.1007/s12035-015-9133-2

Cramm, M., Schmitz, M., Karch, A., Zafar, S., Varges, D., Mitrova, E., et al. (2015). Characteristic CSF prion seeding efficiency in humans with prion diseases. *Mol. Neurobiol.* 51, 396–405. doi: 10.1007/s12035-014-8709-6

Foutz, A., Appleby, B. S., Hamlin, C., Liu, X., Yang, S., Cohen, Y., et al. (2017). Diagnostic and prognostic value of human prion detection in cerebrospinal fluid. *Ann. Neurol.* 81, 79–92. doi: 10.1002/ana.24833

Franceschini, A., Baiardi, S., Hughson, A. G., Mckenzie, N., Moda, F., Rossi, M., et al. (2017). High diagnostic value of second generation CSF RT-QuIC across the wide spectrum of CJD prions. *Sci. Rep.* 7:10655.

Groveman, B. R., Orru, C. D., Hughson, A. G., Bongianni, M., Fiorini, M., Imperiale, D., et al. (2017). Extended and direct evaluation of RT-QuIC assays for Creutzfeldt-Jakob disease diagnosis. *Ann. Clin. Transl. Neurol.* 4, 139–144. doi: 10.1002/acn3.378

Hermann, P., Laux, M., Glatzel, M., Matschke, J., Knipper, T., Goebel, S., et al. (2018). Validation and utilization of amended diagnostic criteria in Creutzfeldt-Jakob disease surveillance. *Neurology* 91:e331–e338.

Llorens, F., Kruse, N., Schmitz, M., Gotzmann, N., Golanska, E., Thune, K., et al. (2017). Evaluation of alpha-synuclein as a novel cerebrospinal fluid biomarker in different forms of prion diseases. *Alzheimers Dement* 13, 710–719. doi: 10.1016/j.jalz.2016.09.013

Llorens, F., Schmitz, M., Karch, A., Cramm, M., Lange, P., Gherib, K., et al. (2016). Comparative analysis of cerebrospinal fluid biomarkers in the differential diagnosis of neurodegenerative dementia. *Alzheimers Dement* 12, 577–589. doi: 10.1016/j.jalz.2015.10.009

McGuire, L. I., Peden, A. H., Orru, C. D., Wilham, J. M., Appleford, N. E., Mallinson, G., et al. (2012). Real time quaking-induced conversion analysis of cerebrospinal fluid in sporadic Creutzfeldt-Jakob disease. *Ann. Neurol.* 72, 278–285. doi: 10.1002/ana.23589

McGuire, L. I., Poleggi, A., Poggiolini, I., Suardi, S., Grznarova, K., Shi, S., et al. (2016). Cerebrospinal fluid real-time quaking-induced conversion is a robust and reliable test for sporadic Creutzfeldt-Jakob disease: An international study. *Ann. Neurol.* 80, 160–165. doi: 10.1002/ana.24679

Meyer, D., Zeileis, A., and Hornik, K. (2020). *vcd: Visualizing Categorical Data R package version 1.4-7*.

Orru, C. D., Bongianni, M., Tonoli, G., Ferrari, S., Hughson, A. G., Groveman, B. R., et al. (2014). A test for Creutzfeldt-Jakob disease using nasal brushings. *N. Engl. J. Med.* 371, 519–529. doi: 10.1056/nejmoa1315200

Orru, C. D., Groveman, B. R., Hughson, A. G., Zanusso, G., Coulthart, M. B., and Caughey, B. (2015). Rapid and sensitive RT-QuIC detection of human Creutzfeldt-Jakob disease using cerebrospinal fluid. *MBio* 6, 2451–2414e. doi: 10.1128/mBio.02451-14

Saborio, G. P., Permanne, B., and Soto, C. (2001). Sensitive detection of pathological prion protein by cyclic amplification of protein misfolding. *Nature* 411, 810–813. doi: 10.1038/35081095

Sano, K., Satoh, K., Atarashi, R., Takashima, H., Iwasaki, Y., Yoshida, M., et al. (2013). Early detection of abnormal prion protein in genetic human prion diseases now possible using real-time QUIC assay. *PLoS One* 8:e54915. doi: 10.1371/journal.pone.0054915

Schmitz, M., Candelise, N., Llorens, F., and Zerr, I. (2018). Amplification and Detection of Minuscule Amounts of Misfolded Prion Protein by Using the Real-Time Quaking-Induced Conversion. *Methods Mol. Biol.* 1779, 257–263. doi: 10.1007/978-1-4939-7816-8_16

Schmitz, M., Cramm, M., Llorens, F., Candelise, N., Muller-Cramm, D., Varges, D., et al. (2016a). Application of an in vitro-amplification assay as a novel pre-screening test for compounds inhibiting the aggregation of prion protein scrapie. *Sci. Rep.* 6:28711.

Schmitz, M., Cramm, M., Llorens, F., Muller-Cramm, D., Collins, S., Atarashi, R., et al. (2016b). The real-time quaking-induced conversion assay for detection of human prion disease and study of other protein misfolding diseases. *Nat. Protoc.* 11, 2233–2242. doi: 10.1038/nprot.2016.120

Schmitz, M., Ebert, E., Stoeck, K., Karch, A., Collins, S., Calero, M., et al. (2016c). Validation of 14-3-3 Protein as a Marker in Sporadic Creutzfeldt-Jakob Disease Diagnostic. *Mol. Neurobiol.* 53, 2189–2199.

Schmitz, M., Llorens, F., Pracht, A., Thom, T., Correia, A., Zafar, S., et al. (2016d). Regulation of human cerebrospinal fluid malate dehydrogenase 1 in sporadic Creutzfeldt-Jakob disease patients. *Aging (Albany NY)* 8, 2927–2935. doi: 10.18632/aging.101101

Schmitz, M., Villar-Pique, A., Llorens, F., Gmitterova, K., Hermann, P., Varges, D., et al. (2019). Cerebrospinal Fluid Total and Phosphorylated alpha-Synuclein in Patients with Creutzfeldt-Jakob Disease and Synucleinopathy. *Mol Neurobiol* 56, 3476–3483. doi: 10.1007/s12035-018-1313-4

Thompson, A. G. B., and Mead, S. H. (2019). Review: Fluid biomarkers in the human prion diseases. *Mol Cell Neurosci* 97, 81–92. doi: 10.1016/j.mcn.2018.12.003

WHO (1998). Human transmissible spongiform encephalopathies. *Wkly Epidemiol Rec* 73, 361–365.

WHO (2003). *WHO Manual for Surveillance of human transmissible spongiform encephalopathies including variant Creutzfeldt-Jakob disease. Communicable disease surveillance and response World Health Organisation*. Genova: World Health Organisation, 51–59.

Zerr, I., Bodemer, M., Gefeller, O., Otto, M., Poser, S., Wiltfang, J., et al. (1998). Detection of 14-3-3 protein in the cerebrospinal fluid supports the diagnosis of Creutzfeldt-Jakob disease. *Ann. Neurol.* 43, 32–40. doi: 10.1002/ana.410430109

Zerr, I., Kallenberg, K., Summers, D. M., Romero, C., Taratuto, A., Heinemann, U., et al. (2009). Updated clinical diagnostic criteria for sporadic Creutzfeldt-Jakob disease. *Brain* 132, 2659–2668.

Conflict of Interest: The authors declare that the research was conducted in the absence of any commercial or financial relationships that could be construed as a potential conflict of interest.

frontiers in Bioengineering and Biotechnology

REVIEW
published: 01 December 2020
doi: 10.3389/fbioe.2020.591024

Improving the Predictive Value of Prion Inactivation Validation Methods to Minimize the Risks of Iatrogenic Transmission With Medical Instruments

*Mohammed Moudjou[1], Johan Castille[2], Bruno Passet[2], Laetitia Herzog[1], Fabienne Reine[1], Jean-Luc Vilotte[2], Human Rezaei[1], Vincent Béringue[1] and Angélique Igel-Egalon[1,3]**

[1] Université Paris Saclay, INRAE, UVSQ, VIM, Jouy-en-Josas, France, [2] Université Paris Saclay, INRAE, AgroParisTech, GABI, Jouy-en-Josas, France, [3] FB.INT'L, Montigny-le-Bretonneux, France

OPEN ACCESS

Edited by:
Jesus R. Requena, University of Santiago de Compostela, Spain

Reviewed by:
Rodrigo Morales, University of Texas Health Science Center at Houston, United States
Jason C. Bartz, Creighton University, United States

***Correspondence:**
Angélique Igel-Egalon
angelique.egalon@inrae.fr

Specialty section:
This article was submitted to Biosafety and Biosecurity, a section of the journal Frontiers in Bioengineering and Biotechnology

Received: *03 August 2020*
Accepted: *05 November 2020*
Published: *01 December 2020*

Citation:
Moudjou M, Castille J, Passet B, Herzog L, Reine F, Vilotte J-L, Rezaei H, Béringue V and Igel-Egalon A (2020) Improving the Predictive Value of Prion Inactivation Validation Methods to Minimize the Risks of Iatrogenic Transmission With Medical Instruments. Front. Bioeng. Biotechnol. 8:591024. doi: 10.3389/fbioe.2020.591024

Prions are pathogenic infectious agents responsible for fatal, incurable neurodegenerative diseases in animals and humans. Prions are composed exclusively of an aggregated and misfolded form (PrP^{Sc}) of the cellular prion protein (PrP^{C}). During the propagation of the disease, PrP^{Sc} recruits and misfolds PrP^{C} into further PrP^{Sc}. In human, iatrogenic prion transmission has occurred with incompletely sterilized medical material because of the unusual resistance of prions to inactivation. Most commercial prion disinfectants validated against the historical, well-characterized laboratory strain of 263K hamster prions were recently shown to be ineffective against variant Creutzfeldt-Jakob disease human prions. These observations and previous reports support the view that any inactivation method must be validated against the prions for which they are intended to be used. Strain-specific variations in PrP^{Sc} physico-chemical properties and conformation are likely to explain the strain-specific efficacy of inactivation methods. Animal bioassays have long been used as gold standards to validate prion inactivation methods, by measuring reduction of prion infectivity. Cell-free assays such as the real-time quaking-induced conversion (RT-QuIC) assay and the protein misfolding cyclic amplification (PMCA) assay have emerged as attractive alternatives. They exploit the seeding capacities of PrP^{Sc} to exponentially amplify minute amounts of prions in biospecimens. European and certain national medicine agencies recently implemented their guidelines for prion inactivation of non-disposable medical material; they encourage or request the use of human prions and cell-free assays to improve the predictive value of the validation methods. In this review, we discuss the methodological and technical issues regarding the choice of (i) the cell-free assay, (ii) the human prion strain type, (iii) the prion-containing biological material. We also introduce a new optimized substrate for high-throughput PMCA amplification of human prions bound on steel wires, as translational model for prion-contaminated instruments.

Keywords: prion, sporadic CJD, amplification, PMCA, surface, decontamination

INTRODUCTION

Transmissible spongiform encephalopathies (TSE) or prion diseases are fatal, uncurable neurodegenerative diseases affecting animals and humans (Collinge, 2001). TSE include scrapie in sheep and goats, bovine spongiform encephalopathy (BSE), chronic wasting disease in cervids and Creutzfeldt-Jakob disease (CJD) in humans. Intra- and inter-species TSE transmission has recurrently occurred in animals and humans via medical and dietary settings. BSE has occurred as an epidemic in cattle and has propagated in human under the form of variant CJD (vCJD). Other dietary exposure in human includes kuru epidemic among Fore people of Papua New Guinea due to funerary cannibalism. Iatrogenic CJD forms are related to the use of contaminated cadaver-extracted human growth hormone and dura mater or to insufficiently sterilized contaminated brain surgery material. The most common forms of CJD are inherited or sporadic.

Transmissible spongiform encephalopathies are caused by prions. Prions are unconventional pathogens exclusively composed of an aggregated and misfolded form (PrP^{Sc}) of the cellular prion protein (PrP^{C}). During the disease pathogenesis, PrP^{Sc} recruits PrP^{C} and induces its misfolding into further PrP^{Sc}. This replicative self-templating process is at the origin of prion infectious nature (Prusiner, 1982). Biochemically, PrP^{Sc} and PrP^{C} properties strongly differ. PrP^{Sc} is β-sheet rich, contains a protease-resistant core and is prone to aggregation, while PrP^{C} is α-helix rich, protease-sensitive and monomeric (Colby and Prusiner, 2011).

Susceptible mammals, including laboratory species, stably propagate structurally distinct PrP^{Sc} assemblies known as prion strains. Prion strains differ biochemically at the level of PrP^{Sc} tertiary and quaternary structures. Phenotypically, prion strains encode unique stereotypical biological traits including the time course to disease, neuropathological features and tropism for specific brain regions or lymphoid organs (Bruce, 2003; Collinge and Clarke, 2007; Beringue et al., 2008b; Weissmann et al., 2011). Co-propagation of strains has been observed, notably in CJD (Cassard et al., 2020) and sheep scrapie (Le Dur et al., 2017; Huor et al., 2019). PrP^{Sc} structural polymorphism is mostly considered as between strain polymorphism. However, experimental evidence supports the view for further structural diversity and co-propagation of PrP^{Sc} assemblies within specific prion populations and strains (Igel-Egalon et al., 2019a).

While human TSE remain relatively rare, they constitute a critical public health concern. First, the disease incubation period is long, asymptomatic, without impact on most biological constants. Early diagnosis of the disease is lacking. Medical, non-disposable instruments may thus be used on individuals incubating silently the disease and potentially be reused. Second, while prions are neurotropic agents, they can replicate extraneurally at significant levels, markedly increasing the range of medical acts that can transmit the disease iatrogenically. Third, prions are highly resistant to common inactivation methods as compared to viruses or bacteria. Since 1999, the World Health Organization guidelines and their national counterparts recommend procedures, which include immersion of non-disposable surgical instruments in 1M sodium hydroxide (NaOH) or 20,000 ppm sodium hypochlorite (2% NaOCl) for 1h, followed by porous autoclaving at 134°C for 18 min (WHO, 1999; DGS, 2011). To circumvent the limits imposed by these methods (e.g., instrument corrosion), the French Medicine Agency (ANSM), for example, recommend since 2011 a list of commercial methods validated for their efficacy to inactivate prions according to a standardized protocol (Ansm, 2011). The validation studies were exclusively based on the inactivation of laboratory prion strains, including as primary model with short incubation time and high infectivity titer hamster-adapted scrapie 263K (or Sc237) prions (Kimberlin and Walker, 1977), as model relevant to BSE/vCJD, mouse-derived BSE prions (Bruce et al., 1994; Lasmezas et al., 1996) or Fukuoka-1 prions derived from the mouse adaptation of human, inherited Gerstmann-Sträussler-Scheinker (GSS) syndrome (Tateishi et al., 1979) as model relevant to human TSE. The inactivation of these prion strains was primarily tested by measuring residual infectivity in hamster or mouse bioassays. However, prion inactivation efficacy is strain-dependent. For example, sporadic CJD prions were shown to be 100,000-fold more resistant than hamster Sc237 prions to acidic SDS treatment (Peretz et al., 2006). The host species in which the strain is passaged can also impact the final efficacy. For example, cattle BSE prions were >1,000-fold more resistant to acidic SDS treatment than BSE-derived mouse 301V prions (Giles et al., 2008). Extended heating or steam sterilization by autoclaving similarly inactivated prions in a strain-dependent manner, BSE and BSE-derived sources being amongst the most resistant strains (Fernie et al., 2012; Marin-Moreno et al., 2019). Worryingly, most ANSM-validated disinfectants which totally inactivated 263K, mouse-BSE or Fukuoka-1 prions were subsequently shown to partially inactivate human vCJD prions (Belondrade et al., 2016; Bélondrade et al., 2020). Collectively, these observations strongly support the view that any inactivation method must be validated against the prions for which they are intended to be used.

The studies by Belondrade et al. (2016); Bélondrade et al. (2020) suggested that cell-free prion amplification assays may replace animal bioassays to quantify prion inactivation efficacy. The European and French Medicine agencies thus implemented their protocols to validate prion inactivation methods. They encourage or request the use of both human prions (or human-relevant prions) and highly sensitive cell-free prion amplification assays (Ansm, 2018; EMA, 2018). These assays measure prion concentration by limiting dilution titration, based on PrP^{Sc} seeding activity. Their sensitivity is equivalent or greater than animal bioassays which are measuring prion infectivity. Yet, they are not routinely used in inactivation methods. In this review, we discuss the methodological and technical issues raised by such implementations, with respect to the choice of the cell-free assay, the human prion strain type and the nature of the prion-containing biological material.

REPLACING ANIMAL BIOASSAYS BY CELL-FREE ASSAYS IN PRION INACTIVATION METHODS

Measuring prion concentration in a test sample has for long relied on measuring prion infectivity by bioassay in laboratory animals. Prion infectious titer can be obtained by endpoint dilution titration of the sample in bio-indicator animals or by using incubation time values once prion dose response curves have been established (Prusiner et al., 1980, 1982). Surrogately, cell-free assays estimate prion concentration by measuring prion self-converting activity. Among them, two ultrasensitive amplification assays deserve attention to their effectiveness to detect minute amounts of prions: the real-time quacking-induced conversion (RT-QuIC) assay (Atarashi et al., 2008; Wilham et al., 2010) and the protein misfolding cyclic amplification (PMCA) assay (Saborio et al., 2001; **Figure 1**). In essence a PrP^{Sc}-containing sample is mixed with a substrate containing normally folded, monomeric recombinant PrP (RT-QuIC) or brain PrP^{C} (PMCA). The conversion is favored and accelerated by cycles of shaking (RT-QuIC) or sonication (PMCA) and quiescent incubation. In the RT-QuIC assay, the conversion of recombinant PrP into amyloid aggregates is followed in real-time by incorporation of thioflavin T (ThT), an amyloid-sensitive fluorescent dye. In the PMCA assay, the conversion of PrP^{C} into PrP^{Sc} is assessed at the end of the reaction by biochemical purification and immunodetection of PrP^{Sc}. Both tests reach similar or greater sensitivities than those of the animal bioassays. Both have a wide range of fundamental and applied applications, including TSE diagnostic. Both have benefits and drawbacks that make them complementary techniques in the TSE field, as summarized in **Table 1**.

The RT-QuIC Assay

In the RT-QuIC assay, the ThT-positive amyloid assemblies formed by seeded recombinant PrP are poorly infectious (Groveman et al., 2017; Raymond et al., 2020). Manipulation of prion infectivity is thus limited to the seed, limiting biohazards in routine use of the assay. A limiting aspect of RT-QuIC is the possible self-polymerization of recombinant PrP in the absence of any seed. From a diagnostic viewpoint, RT-QuIC is particularly efficient at amplifying prion sub-infectious doses in sample biopsies from the skin (Orru et al., 2017), olfactory mucosa (Orru et al., 2014), urine, saliva (Henderson et al., 2015), blood (Elder et al., 2013), and CSF (McGuire et al., 2012). The second generation of RT-QuIC specially designed for prion detection in the CSF achieved >95% sensitivity and 100% specificity (Orru et al., 2015a), with a good interlaboratory reproducibility, thus opening new avenue for ante-mortem diagnosis of CJD (Rhoads et al., 2020). CSF-based RT-QuIC is now considered as the most powerful versatile technique for diagnosing CJD. It is recommended by the American Center for Disease Control and Prevention (CDC) since 2018. Following this pioneering work, similar CSF-based assays were successfully developed for other prion-like neurodegenerative diseases linked to protein misfolding. These RT-QuIC assays identify alpha-synuclein (Rossi et al., 2020) and Tau (Kraus et al., 2019; Saijo et al., 2020) seeding activity in CSF of patients with Lewy bodies or Parkinson's disease and Alzheimer's disease or frontotemporal lobar degeneration, respectively. Proof of concept has been obtained with TDP-43 in amyotrophic lateral sclerosis and frontotemporal lobar degeneration (Scialò et al., 2020).

Given the analytical sensitivity of the RT-QuIC assay and the clear correlation between seeding activity and infectivity in measuring prion concentration (Wilham et al., 2010), its potential to assess prion inactivation methods was assayed. There were discrepancies between the animal bioassay and the RT-QuIC assay. One disinfectant inactivating all measurable prion infectivity by bioassay was not able to eliminate all seeding activity by RT-QuIC (Hughson et al., 2016). In another study, the seeding activity of human CJD prions bound to stainless steel wires was measurable by RT-QuIC and completely removed after a 2 h-treatment with 1M NaOH (Mori et al., 2016), as expected. The reason for such discrepancies is unclear. Prion inactivation treatment may destroy prion infectivity without affecting all PrP seeding activity, given the high sensitivity of the assay. Alternatively, as the RT-QuIC generates amyloid fibers that are off-pathway to prion infectivity, treatment neutralizing these forms may not necessarily affect prion infectivity *per se*.

The PMCA Assay

As key feature, PMCA mirrors in an accelerated manner the prion replication process (Igel-Egalon et al., 2019b). The reaction products are highly infectious – with infectivity titers equivalent to those found in the brain at the terminal stage of the disease – and contain prions which generally retain the parental seed strain phenotype (Weber et al., 2007; Shikiya and Bartz, 2011; Moudjou et al., 2014). PMCA has been instrumental in identifying co-factors (Deleault et al., 2012a,b; Fernández-Borges et al., 2018), PrP domains (Burke et al., 2020a) or post-translational modifications (Moudjou et al., 2016; Burke et al., 2020b) involved in the prion replication process. It has also been instrumental in studying the diversification of PrP^{Sc} assemblies and their dynamic interactions (Igel-Egalon et al., 2019b).

The analytical sensitivities of the PMCA and RT-QuIC assays are generally equivalent. RT-QuIC is the method of choice to quantify the seeding activity of prions responsible for sporadic CJD (notably the most prevalent MM1 subtype), whereas PMCA is more performant at detecting vCJD prions (Moudjou et al., 2014; Camacho et al., 2019). PMCA has been incredibly good at detecting vCJD/BSE prions in blood from asymptomatic carriers, in small and large animal models and in human (Lacroux et al., 2014; Bougard et al., 2016; Concha-Marambio et al., 2016). Yet, the necessity to work with PrP^{C}-containing cell or brain substrate and the absence of real-time detection of the conversion process are major impediments to a diagnostic use. Several laboratories are working at substituting PrP^{C}-containing brain substrate with recombinant PrP (Fernández-Borges et al., 2018; Eraña et al., 2019).

With respect to prion inactivation methods, a strong correlation between animal bioassay and PMCA was found in two compelling studies testing several disinfectants or physical processes on 263K prions or vCJD prions bound on stainless steel

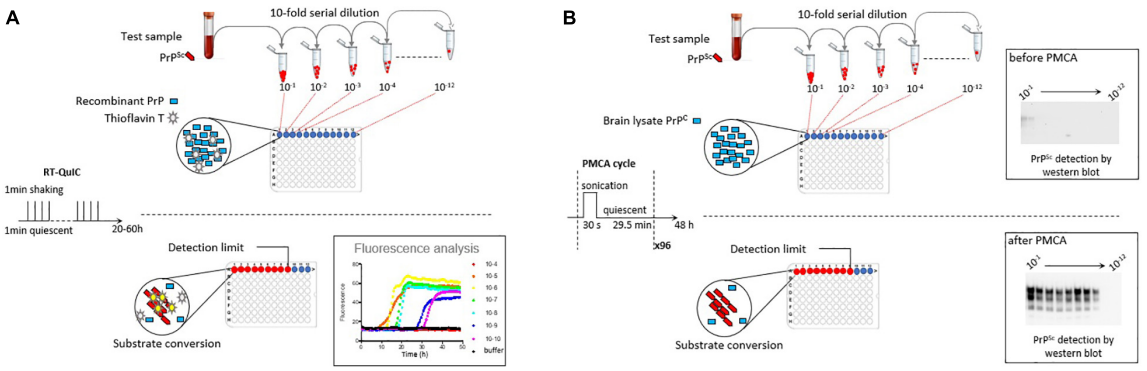

FIGURE 1 | Scheme summarizing the principles of the RT-QuIC and PMCA assays. **(A)** RT-QuIC is based on the polymerization of recombinant PrP protein by prions in the test sample. During iterative cycles of shaking and quiescent incubation, polymerization is monitored in real-time by the increase in Thioflavin T fluorescence. **(B)** PMCA is based on the bona fide conversion of brain PrP^{C} by prions in the test sample. Conversion is favored by iterative cycles of quiescent incubation and sonication. At the end of the reaction, the presence of abnormal PrP^{Sc} is analyzed by proteinase K digestion and western blot. In both methods, prion seeding activity in the test sample can be quantified by limiting dilution titration.

TABLE 1 | Benefits and drawbacks of the RT-QuIC and PMCA assays.

	RT-QuIC	PMCA
Substrate	Recombinant PrP	Cellular form of PrP
Protocol	Shaking/incubation	Sonication/incubation
Measure of prion concentration	PrP^{Sc} seeding activity	PrP^{Sc} seeding activity
Conversion products	Thioflavin T positive amyloid PrP	PrP^{Sc} assemblies
Pros	-Real time and direct readout -Low biohazard -Detection in bodily fluids, notably CSF -CSF-based diagnostic for CJD -Commercial substrate available -Universal substrate -Good inter-laboratory reproducibility of the second-generation RT-QuIC -Use in other neurodegenerative diseases	-Generation of bona fide prion infectivity -Prion strain typing -Detection of sub-infectious prion doses -Detection in bodily fluids, notably blood -Correlation between infectivity and seeding activity in inactivation tests
Cons	-Amplified product poorly infectious -Discrepancies between infectivity and seeding activity in inactivation tests	-Indirect readout (immunoblot) -No universal substrate -Strains refractory to amplification -Biohazardous method -No commercial substrate -Limited inter-laboratory reproducibility -Use of cofactors required for certain strains
Application	Diagnostic	Research use

wires (Pritzkow et al., 2011; Belondrade et al., 2016; Bélondrade et al., 2020). PMCA thus emerged as a potent tool to evaluate the degree of effectiveness of prion inactivation methods, at least with certain human and laboratory strains.

FINDING THE RIGHT PRION STRAIN IN THE RIGHT SHAPE TO STANDARDIZE PRION INACTIVATION METHODS

Human Prion Strains

The choice of the "right" human prion strain to implement the validation of prion inactivation methods is a conundrum:

1. None of the human prion strains have been studied as deeply as hamster 263K with respect to pathogenesis, infectivity titers and response to inactivating treatments by bioassay;
2. The use and relevance of human prions adapted to wild-type laboratory animals must be studied on a case-by-case basis. For example, mouse-adapted Fukuoka-1 prions were not able to propagate on back-passage to transgenic mice expressing human PrP, suggesting loss of parental CJD transmission characteristics (Giles et al., 2017). Oppositely, sporadic CJD prions propagated in bank voles with little or no species barrier, consistent with potential maintain of CJD transmission characteristics (Nonno et al., 2006). Early transmission studies indicated that non-human primates were susceptible to sporadic and vCJD prions (Gibbs et al., 1968; Lasmézas et al., 1996), providing a potential source of human-like prion infectivity. However, macaque and human PrP sequences

differ by nine amino acids, which were shown by transgenic modeling to create a substantial species barrier on transmission of sporadic CJD (Espinosa et al., 2019). Whether macaque-passaged prions retain *in fine* CJD parental properties remain to be determined. Seminal studies by transgenic modeling indicated that amino acid sequence identity between PrP^{Sc} and PrP^{C} usually abrogate the barrier to transmission between species (for review Moreno and Telling, 2017). Human prions did not escape the rule. Sporadic and vCJD prions propagate without species barrier in mice transgenic for human PrP, in the absence of mismatch at polymorphic codon 129 (Bishop et al., 2010; Beringue et al., 2012; Chapuis et al., 2016; Jaumain et al., 2016; Cassard et al., 2020). These models, – in the absence of cell models propagating human prions –, allow a relatively rapid, inexpensive, and large production of potentially biologically cloned and well-characterized *humanized* prions with respect to pathogenesis, strain type and infectivity titers. Oppositely, sporadic and vCJD reference reagents from the World Health Organization contain mixture of strains (Minor et al., 2004; Beringue et al., 2008a; Yull et al., 2009), which may complicate their use in decontamination protocols. It remains to be determined whether *humanized* prions exhibit similar resistance/sensitivity to inactivation as those that accumulate directly in the human brain. At least, they seem to share similar levels of infectivity (Beringue et al., 2008a; Halliez et al., 2014);

3. The pros and cons of assaying (human or *humanized*) sporadic or vCJD prions in inactivation trials must be weighed. While the number of clinical cases of vCJD has remained limited (∼235 cases worldwide), this disease is a key issue due to the large number of potential asymptomatic carriers (Gill et al., 2020), the large distribution of infectivity in the body (Douet et al., 2017) and the associated risks of secondary transmission, notably by blood transfusion or surgery (Peden et al., 2004). The disease is due to a unique prion strain type (classical BSE prions) (Diack et al., 2012). When testing heat sterilization methods, BSE/vCJD prions thermostability may increase the predictive value of the assay (Fernie et al., 2012; Marin-Moreno et al., 2019). Sporadic forms of CJD are more prevalent with approximately 1.5 cases per millions per year. The disease is heterogeneous, making the choice of the "right" strain a dilemma; nine sub-types of sporadic CJD are described according to the clinical and neuropathological characteristics of the disease in infected individuals, the polymorphism of the *PRNP* gene at codon 129 (MM, MV, or VV) and the electrophoretic profile of brain PrP^{Sc} (type 1 or type 2) (for review Zerr and Parchi, 2018). At least six distinct strain types are described according to their transmission properties in transgenic mice expressing human PrP. Starting from the most prevalent cases in the population, these strains are classified as MM1/MV1, VV2, MV2, VV1, cortical-MM2, thalamic-MM2 strains (Bishop et al., 2010; Moda et al., 2012; Chapuis et al., 2016; Jaumain et al., 2016; Cassard et al., 2020). Co-propagation of MM1 and VV2 strains has been observed in a significant proportion of sporadic CJD patients (Cassard et al., 2020).

Although direct assay of human prions in inactivation methods may sound highly relevant with respect to iatrogenic risk of prion transmission, it necessitates a thorough examination to ensure that the results obtained are of added value and that extrapolation to the human situation can be made.

Stainless Steel Wires as Model for Surgery Instruments

Prions and bacterial biofilms are a challenge to proper sterilization of non-disposable medical devices because of their high resistance to inactivation and binding affinity for steel surfaces. To date, six cases of iatrogenic CJD have been reported worldwide by contaminated surgical instruments or depth EEG electrodes (for review Bonda et al., 2016). Prion-contaminated stainless steel wires have become the gold standard to screen and validate prion inactivation methods for medical instruments. This translational model, which is used in most guidelines, came from the seminal work of Charles Weissmann and collaborators (Zobeley et al., 1999; Flechsig et al., 2001). In essence, wires are artificially contaminated in prion-containing brain macerates. To measure prion concentration pre- and post-disinfection, the wires are permanently implanted in the brain of bio-indicator animals and reduction in the disease attack rate is measured. The reduction factor is established by comparing the results obtained with endpoint titration of prions bound on steel wires. A prion-cell endpoint assay (Klohn et al., 2003) was adapted that offered greater sensitivity, practicability and rapidity than the animal bioassay (Edgeworth et al., 2009). However, its use is so far limited to mouse prions. A sensitive assay based on direct immunodetection of surface-bound prions was also reported and validated against human vCJD prions (Edgeworth et al., 2011b).

Key issues in the interpretation and overall validity of the results are the rate of prion adsorption, desorption and/or bio-activity (i.e., ability to initiate infection in the brain). With mouse or hamster prions, a contact of a few minutes between the infected brain homogenate and the wire was sufficient to transmit the disease with 100% attack rate (Flechsig et al., 2001; Giles et al., 2017). A transient insertion of contaminated wires in the brain for 5–30 min was sufficient to transmit the disease to laboratory animals with 100% attack rate, yet with delayed disease tempo (Flechsig et al., 2001; Yan et al., 2004). This suggested relatively rapid rate of adsorption and release/bio-activity. The information on prion fate once surface-adsorbed is relatively limited. Binding to soil fractions (montmorillonite) was reported to potentiate the disease transmission capacity of hamster 263K prions by oral route (Johnson et al., 2007). The opposite was found on binding to silty clay upon intracerebral inoculation (Saunders et al., 2011). In "standard" conditions, wires are contaminated for 1 h and permanently inserted in bio-indicator animals. To further circumvent these uncertainties and address the possibility that the decontamination procedures unbound prions from the wires without inactivating them, an additional study on the inactivation

potential of the method on desorbed material may be requested (Ansm, 2011, 2018).

Heterogeneity of Prion Assemblies

The brain tissue does not represent the more likely source of iatrogenic prion contamination, except during neurosurgical procedures. The use of sensitive animal bioassays with human PrP transgenic mice and/or cell-free assays allowed demonstrating that many tissues outside the brain contain substantial amounts of prions, thus markedly increasing the range of medical acts with non-disposable equipment that may transmit human TSE iatrogenically. This includes dentistry, organ transplant, blood transfusion, and surgery. In individuals infected with vCJD, at the symptomatic or pre-symptomatic stage, prions have been detected in a wider and more unexpected variety of peripheral tissues (Douet et al., 2017) than previously reported (Wadsworth et al., 2001). Those include bone marrow, kidney, salivary glands, skeletal muscle, pancreas, liver or heart in addition to tissue of the lymphoid system. In sporadic CJD, while prion distribution is more intense in the central and peripheral nervous systems, substantial amounts of prions have been found in the bone marrow (Huor et al., 2017), skin (Orru et al., 2017), kidney, lung, liver, adrenal glands (Takatsuki et al., 2016), and muscle (Peden et al., 2006; Rubenstein and Chang, 2013). Prions were also detected in biological fluids, notably blood, and urine of patients with sporadic and variant of CJD, often well before the onset of early clinical signs (Edgeworth et al., 2011a; Lacroux et al., 2014; Moda et al., 2014; Sawyer et al., 2015; Luk et al., 2016). Confirmed cases of iatrogenic transmission of vCJD by blood transfusion, and a probable case in a patient treated with coagulation factors VIII manufactured from plasma indicate that blood constitutes an effective source of iatrogenic contamination (Peden et al., 2004, 2010; Wroe et al., 2006). It was reported that the prion protein PrP^{C} is a major contaminant of the purified urinary-derived gonadotropins used in infertility treatment (Van Dorsselaer et al., 2011). These elements raise specifically the question of prion biosafety of blood, blood-derived products, and urine-derived drug products. Analytical technics for securing drug manufacturing process from blood and urine must be reconsidered and implemented as those securing medical instrumentation, as recently recommended by the European Medicines Agency **(EMA, 2018)**.

Prion presence in several tissues and bodily fluids raises the question of the most physiologically relevant PrP^{Sc} aggregates and of the best experimental approach for their inactivation. Most studies use brain macerates or microsomal brain fractions to contaminate steel wires or as spike for studying prion removal. Their high infectious titer compared to other extraneural tissues or fluids obviously increases the analytical sensitivity of the approach. However, PrP^{Sc} assemblies in bodily fluids or extraneural tissue may be of smaller size than in the brain. Compelling evidence indicate that different subassemblies with specific structural properties are co-accumulating in the brain at the disease terminal stage. These sub-assemblies harbor different size, different infectivity titer or seeding activity (for review Igel-Egalon et al., 2019a). Their capacity to bind steel wires or their retention properties may vary.

Further, the preparation of the spike or of the dilutions in the *ad hoc* experimental conditions may modify PrP^{Sc} assembly composition. In our previous work, we demonstrated that PrP^{Sc} assemblies have two levels of organization (Igel-Egalon et al., 2017). The first one is formed by the packing of oligomeric building blocks (called suPrP) into larger assemblies. In this organization, the cohesion forces are weak, as shown that rapid depolymerization following urea chaotropic treatment. The second level of organization is formed by suPrP itself. suPrP is a very stable oligomer between a dimer or a tetramer that resists >6–8 M urea. This study led us to conclude that PrP^{Sc} assemblies and their building blocks are in a highly dynamic equilibrium (Igel-Egalon et al., 2017, 2019a). A simple dilution of purified PrP^{Sc} assemblies was able to drive the equilibrium towards their depolymerization into suPrP. A dilution process may thus drive which PrP^{Sc} morphotype is submitted to the inactivation/retention process; in return PrP^{Sc} morphotype are likely to react to such process in a structural-dependent manner. To conciliate the advantage of using brain extract with the relevance of the model, one alternative could be the use of small PrP^{Sc} particles, obtained by fractionation experiments. We previously demonstrated that these assemblies have high specific infectivity values despite their small size (Tixador et al., 2010; Laferriere et al., 2013) and are relatively stable over time out of the conversion process (Igel-Egalon et al., 2019b).

As for the nature of the prion strain, these data collectively support the view that the retention/inactivation methods must be validated against the biological material for which they are intended to be used.

HUMAN PRION PMCA

PMCA Improvements and Putative Mechanisms of Prion Amplification

Efficient amplification of human prions by PMCA is strain dependent. It was initially believed that optimal amplification of human prion strains required absence of mismatch at codon 129 between the seed and the substrate. Thus, Jones et al. (2009) classified CJD subtypes in two distinct groups according to their "preference" for the *PRNP* genotype substrate. The first group, composed of vCJD, MM1, MM2, and MV1 sporadic prions, is preferentially amplified by the *PRNP*-129MM substrate. The second one, composed of VV1, VV2, and MV2 sporadic CJD prions, is more efficiently amplified by *PRNP*-129VV substrate. Despite this sequence compatibility, prions were not amplified to a degree of sensitivity sufficient for validating decontamination methods.

Other parameters can be adjusted to improve PMCA efficacy: (1) Obviously, the number of PMCA rounds can be increased. While it was initially suspected to increase the probability of de novo PrP^{Sc} formation in the absence of preexisting prions, carefully designed PMCA operating conditions suggested that spontaneous prion formation in PMCA reactions was rather a result of inadvertent cross-contamination (Cosseddu et al., 2011). Three to six rounds of PMCA are routinely used to amplify low amounts of human prions (Lacroux et al.,

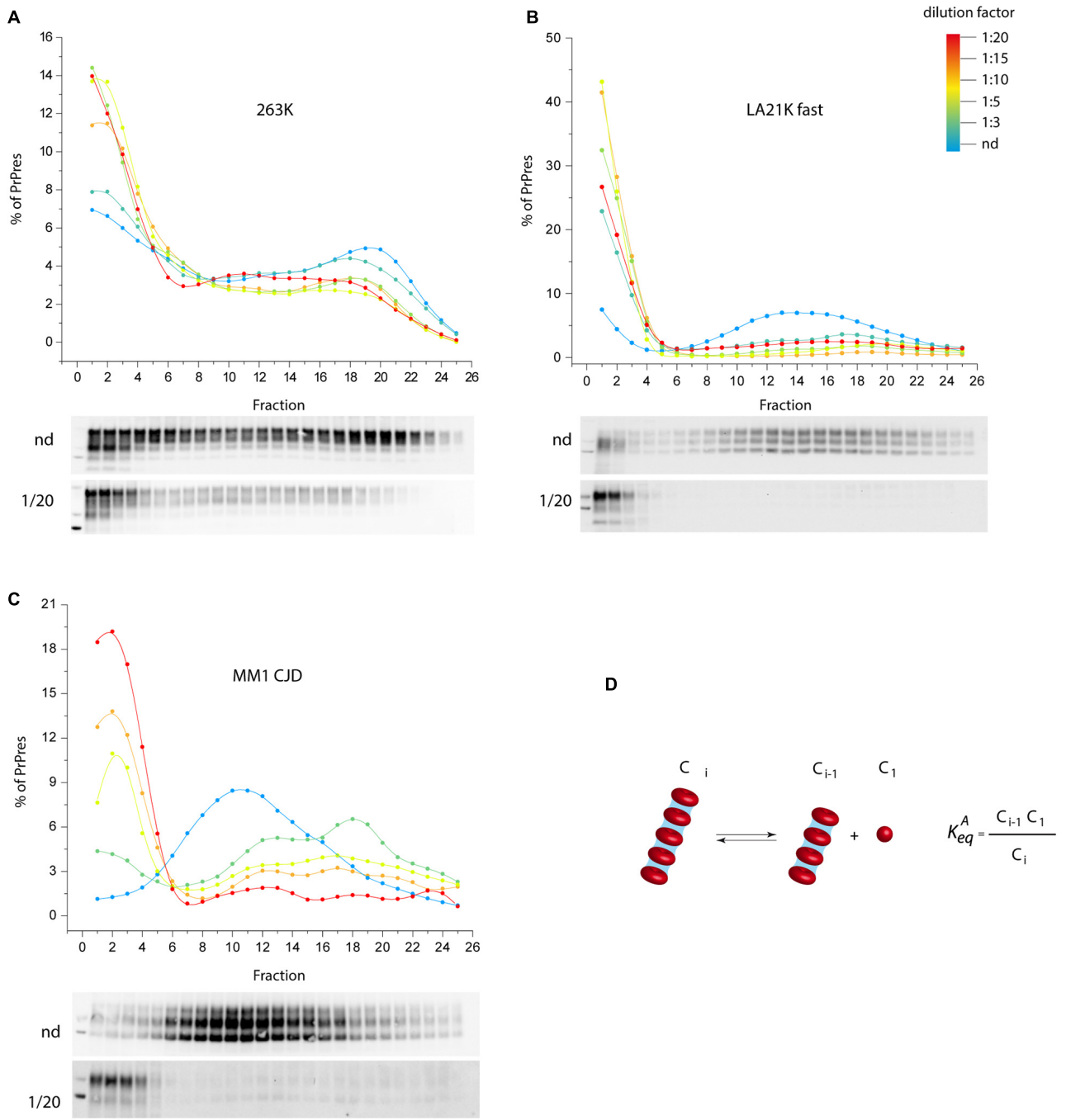

FIGURE 2 | The disassembling effect of PMCA buffer on PrP^{Sc} assemblies. **(A–C)** Twenty percent infected brain homogenate from hamster 263K prions (Kimberlin and Walker, 1977), sheep-derived LA21K *fast* (Le Dur et al., 2017), and *humanized* MM1 sporadic CJD prions (Beringue et al., 2008a) were directly diluted [not diluted (nd), 1:3, 1:5, 1:15, 1:20 from blue to red line] in a $PrP^{0/0}$ lysate made in PMCA buffer (thus in the absence of PrP^{C} substrate). After a 4 h-incubation at 4°C in the absence of sonication, PrP^{Sc} assemblies quaternary structure was investigated by sedimentation velocity fractionation (Tixador et al., 2010). The collected fractions (numbered from top to bottom of the gradient) were analyzed for PrP^{Sc} content by immunoblot. The graphs show the relative amount of PrP^{Sc} per fraction. Representative immunoblots are shown. For the three prion strains, dilution induced a disassembling process generating small PrP^{Sc} objects. **(D)** PrP^{Sc} assemblies (C_i) dilution in PMCA buffer tends to displace a detailed-balance toward the formation of smaller objects here termed C_1, which are assimilated to suPrP (Igel-Egalon et al., 2017).

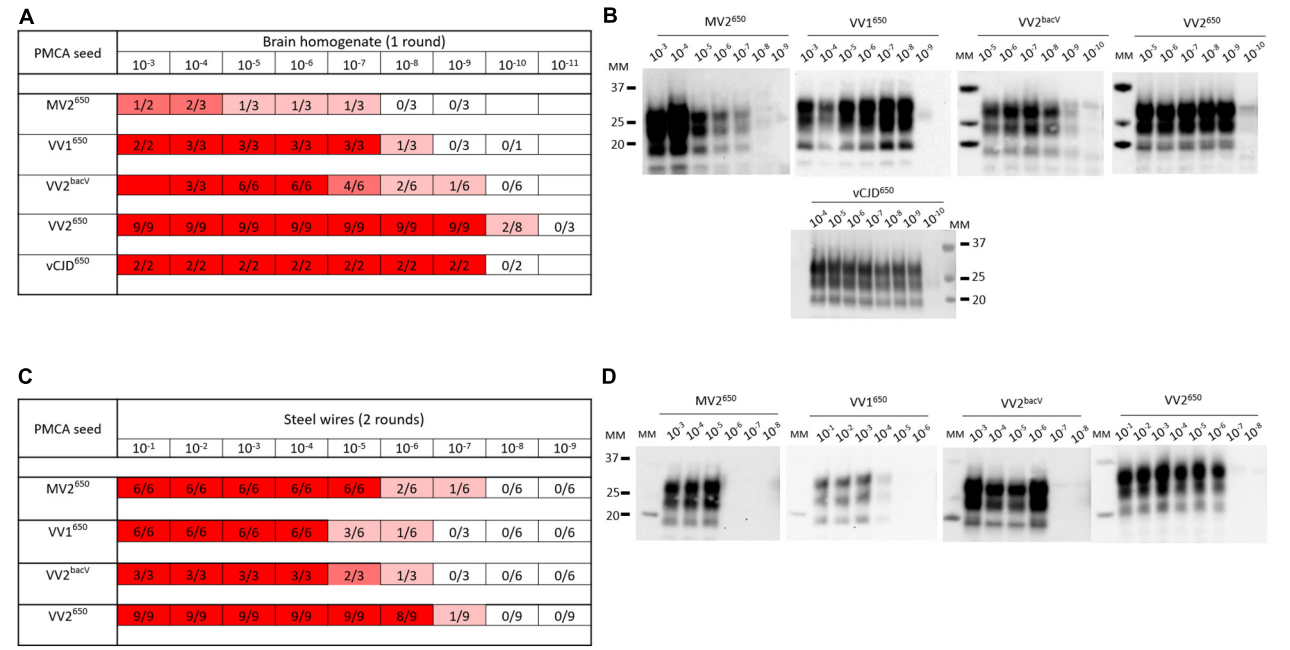

FIGURE 3 | PMCA detection of sporadic and variant CJD prions in suspension or bound to steel wires using BacV-derived human PrP substrate. Serial dilutions of *humanized* sporadic CJD subtypes and variant CJD (vCJD) prions passaged into human PrP mice [tg650 line (Met129 allele) or BacV line (Val129 allele)] were used in suspension **(A,B)** or bound to steel wires **(C,D)**. They were mixed with uninfected BacV brain homogenate and submitted to the mb-PMCA for one round **(A,B)** or two rounds **(C,D)** of 96 cycles of sonication/incubation for 48 h. The PMCA products were analyzed for PrP^{Sc} content by immunoblot. **(A,C)** Summary of the results obtained. The red boxes indicate the presence of PrP^{Sc} in PMCA products, the ratio in each box corresponds to the number of PrP^{Sc}-positive amplification products over the number of PMCA replicates performed. **(B,D)** Representative immunoblots (Sha31 anti-PrP antibody). MM, molecular weight markers.

2014; Bougard et al., 2016; Concha-Marambio et al., 2016; Cassard et al., 2020); (2) The PrP^{C} substrate can be optimized. The higher the PrP^{C} concentration, the higher the sensitivity achieved (Mays et al., 2009; Moudjou et al., 2014, 2016), which lends support for the use of brain from transgenic mice overexpressing PrP^{C}. Further, markedly improved sensitivities, including with human prions, were obtained when PMCA was performed with partially desialylated (Katorcha et al., 2015) or unglycosylated PrP^{C} (Nishina et al., 2006; Camacho et al., 2019) as substrate. The authors attribute this phenomenon to sialic acid electrostatic repulsion forces and the glycan steric hindrance that may interfere with the conversion of PrP^{C} by PrP^{Sc}. Whether this would work with all strains given their variable glycoform requirements (Khalili-Shirazi et al., 2005; Nishina et al., 2006) remains to be determined; (3) Conversion enhancers can be added to the PMCA reaction, including polyanions (Fernández-Borges et al., 2018), anionic lipids (Deleault et al., 2007), or dextran sulfate (Moudjou et al., 2016). Their mode of action on the conversion process remains poorly understood. Their impact on ionic strength, osmolarity, water molecule organization, PrP^{C} or assemblies stability may play a role in the replication/templating process; (4) Physical change in the PMCA environment such as the reaction volume or the addition of microbeads in the substrate affected significantly the amplification efficacy with respect to the dilution achieved (Gonzalez-Montalban et al., 2011; Johnson et al., 2012; Moudjou et al., 2014).

The commonly shared view that microbeads addition increases the fragmentation of the newly converted PrP^{Sc} assemblies during the sonication steps and therefore multiplies the number of templating interface for conversion was recently challenged. By using sedimentation velocity to explore the quaternary structure of prion assemblies, we found no evidence for fragmentation in PMCA conditions with beads (Igel-Egalon et al., 2019b). Alternative hypotheses such as beads serving as thermoacoustic convertor (Povey et al., 2011) and/or as multidirectional secondary source may be considered.

We propose an alternative model to prion fragmentation to explain prion amplification during PMCA, based on the existence of a detailed-balance between PrP^{Sc} assemblies and suPrP (Chyba et al., 2020). A perturbation in prion environment would shift the balance towards PrP^{Sc} assemblies depolymerization into suPrP, thus multiplying the number of templating interface. We experimentally investigated this by studying the impact on PrP^{Sc} assemblies size of diluting infected brain homogenate in PMCA buffer, out of a replicative context and without sonication. As shown in **Figures 2A–C**, a >1:3 dilution was sufficient to depolymerize PrP^{Sc} assemblies into smaller objects, indicating an equilibrium displacement (**Figure 2D**). This was observed for three different prion strains, suggesting a possible generic effect. This observation supports the view that the physico-chemical properties of the PMCA buffer are enough to disrupt PrP^{Sc} assemblies, suggesting therefore that PrP^{Sc} fragmentation does not occur during bead-PMCA reactions.

Despite these major improvements, certain prion types remain unamplifiable by PMCA or do not achieve degrees of amplification requested by the medicine agencies (6 Log_{10} of magnitude (Ansm, 2018)). The MM1 subtype remains the most difficult sporadic CJD subtype to amplify. At variance with RT-QuIC (Orru et al., 2015b), there is no universal PMCA substrate for human CJD prions.

A PMCA Substrate to Amplify With High Sensitivity Human Prion Strains Adsorbed on Steel Surface or in Suspension

With all the potential factors improving PMCA sensitivity in mind, we optimized a substrate to amplify human sporadic CJD prions. First, we designed a new transgenic mouse line homozygous at the locus transgene that overexpressed approximately five- to sixfold the valine allele at codon 129 of human PrP^C (BacV line) on a pure FVB/N PrP-knockout background (Passet et al., 2020). The transgene designed for targeting expression of human PrP in these mice is based on a large human BAC insert (the details of the transgenic mice will be published elsewhere). The brain of these mice was used as PrP^C substrate in PMCA reactions (see **Supplementary Material** for the methods section). To improve the sensitivity of the reaction, we added polymers of dextran, one teflon microbeads and worked with a reduced reaction volume, as previously described in our so-called mb-PMCA protocol (Moudjou et al., 2014, 2016). As seed, we used brain homogenates from *humanized* mice in which we isolated and phenotypically characterized different sporadic CJD subtypes (Jaumain et al., 2016). Those were serially diluted and submitted to one to three rounds of mb-PMCA reaction. *Humanized* MV2, VV1, VV2 sporadic CJD prions, and vCJD prions were used. Positive reactions were obtained for these *humanized* strain types up to the 10^{-7} (MV2 subtype) to 10^{-10} (VV2 subtype) dilution (**Figures 3A,B**). Noticeably, mismatch at codon 129 between seed and substrate was not detrimental as the highest levels of amplification were observed with sporadic CJD VV2 prions and vCJD prions serially passaged onto transgenic mice expressing human-PrP^C with Met at codon 129. The dynamic of amplification obtained with vCJD prions (limiting dilution at 10^{-9}) or VV2 (10^{-9} or 10^{-10} depending on the allele on which the subtype was propagated) offered an analytical sensitivity compatible with the validation of prion inactivation methods. In the case of vCJD prions, it was more sensitive than animal bioassays by at least two orders of magnitude (Douet et al., 2014; Halliez et al., 2014).

In the context of the risk evaluation associated with the decontamination of medical instruments, we further evaluated the effectiveness of the BacV-derived mb-PMCA substrate to detect human prions bound onto steel surface. Briefly, fine stainless steel wires were contaminated with serial dilutions of prion-containing brain homogenate (Zobeley et al., 1999; Flechsig et al., 2001) and added directly to the mb-PMCA reaction mix as seed. As summarized in **Figures 3C,D**, two rounds of PMCA were enough to detect bound prions up to the 10^{-6}–10^{-7} dilution. Again, these limiting dilution values were in the range required for appraisal of inactivation methods by using steel wire as translational model for medical instruments.

CONCLUSION

This mini-review addresses the questions raised by the implementations, by the competent authorities, of prionicidal product authorizations. Any validation procedure should be tested against prions for which the inactivant is intended to be used, suggesting that human or *humanized* prions should be used in fine. However, several pending questions are emerging, including the choice of the prion subtype and of the prion-containing biological matrix. Another operational aspect to consider is the high biohazard level to manipulate these agents as compared to laboratory 263K prions.

Given the correlation between PMCA and animal bioassay in measuring prion concentration bound on steel wires or in suspension, there is a proof of concept that this cell-free assay could complement and even replace animal bioassays. This would provide an economical and ethically sound method. Yet, certain human prion subtypes remain poorly amplifiable, limiting the potential relevance of the assay. Given the high-throughput, rapid format of the assay, the use of several prion subtypes may circumvent this. Animal bioassays using human or *humanized* prion are still considered as gold standard methods. These models and the PMCA assay are mostly manipulated in academic laboratories and not in Contract Research Organizations (CROs) that routinely perform studies for biocidal products authorizations. This may delay the time to market of these products.

AUTHOR CONTRIBUTIONS

VB, HR, and AI-E designed the study, analyzed the data and drafted the manuscript. J-LV, BP, JC, and VB designed the new mice line. AI-E, MM, LH, and FR performed the experiments. All authors gave their final approval of the submitted version.

FUNDING

This work was funded by the Fondation pour la Recherche Médicale (Equipe FRM DEQ20150331689).

SUPPLEMENTARY MATERIAL

The Supplementary Material for this article can be found online at: https://www.frontiersin.org/articles/10.3389/fbioe.2020.591024/full#supplementary-material

REFERENCES

Ansm (2011). *Protocole Standard Prion*. Saint-Denis: Ansm.

Ansm (2018). *Protocole Standard Prion. v2*. Saint-Denis: Ansm.

Atarashi, R., Wilham, J. M., Christensen, L., Hughson, A. G., Moore, R. A., Johnson, L. M., et al. (2008). Simplified ultrasensitive prion detection by recombinant PrP conversion with shaking. *Nat. Methods* 5, 211–212. doi: 10.1038/nmeth 0308-211

Bélondrade, M., Jas-Duval, C., Nicot, S., Bruyére-Ostells, L., Mayran C, Herzog, L., et al. (2020). Correlation between bioassay and protein misfoldingcyclic amplification for variant Creutzfeldt-Jakob disease decontamination studies. *mSphere* 5:e00649-19. doi: 10.1128/mSphere.00649-19

Belondrade, M., Nicot, S., Bèringue, V., Coste, J., Lehmann, S., and Bougard, D. (2016). Rapid and highly sensitive detection of variant creutzfeldt - jakob disease abnormal prion protein on steel surfaces by protein misfolding cyclic amplification: application to prion decontamination studies. *PLoS One* 11:e0146833. doi: 10.1371/journal.pone.0146833

Beringue, V., Herzog, L., Jaumain, E., Reine, F., Sibille, P., Le Dur, A., et al. (2012). Facilitated cross-species transmission of prions in extraneural tissue. *Science* 335, 472–475. doi: 10.1126/science.1215659

Beringue, V., Le Dur, A., Tixador, P., Reine, F., Lepourry, L., Perret-Liaudet, A., et al. (2008a). Prominent and persistent extraneural infection in human PrP transgenic mice infected with variant CJD. *PLoS One* 3:e1419. doi: 10.1371/journal.pone.0001419

Beringue, V., Vilotte, J. L., and Laude, H. (2008b). Prion agent diversity and species barrier. *Vet. Res.* 39:47. doi: 10.1051/vetres:2008024

Bishop, M. T., Will, R. G., and Manson, J. C. (2010). Defining sporadic Creutzfeldt-Jakob disease strains and their transmission properties. *Proc. Natl. Acad. Sci. U.S.A.* 107, 12005–12010. doi: 10.1073/pnas.1004688107

Bonda, D. J., Manjila, S., Mehndiratta, P., Khan, F., Miller, B. R., Onwuzulike, K., et al. (2016). Human prion diseases: surgical lessons learned from iatrogenic prion transmission. *Neurosurg. Focus* 41:E10.

Bougard, D., Brandel, J. P., Belondrade, M., Beringue, V., Segarra, C., Fleury, H., et al. (2016). Detection of prions in the plasma of presymptomatic and symptomatic patients with variant Creutzfeldt-Jakob disease. *Sci. Transl. Med.* 8:370ra182. doi: 10.1126/scitranslmed.aag1257

Bruce, M., Chree, A., Mcconnell, I., Foster, J., Pearson, G., and Fraser, H. (1994). Transmission of bovine spongiform encephalopathy and scrapie to mice: strain variation and the species barrier. *Philos. Trans. R. Soc. Lond. B Biol. Sci.* 343, 405–411. doi: 10.1098/rstb.1994.0036

Bruce, M. E. (2003). TSE strain variation. *Br. Med. Bull.* 66, 99–108. doi: 10.1093/bmb/66.1.99

Burke, C. M., Mark, K. M. K., Walsh, D. J., Noble, G. P., Steele, A. D., Diack, A. B., et al. (2020a). Identification of a homology-independent linchpin domain controlling mouse and bank vole prion protein conversion. *PLoS Pathog.* 16:e1008875. doi: 10.1371/journal.ppat.1008875

Burke, C. M., Walsh, D. J., Mark, K. M. K., Deleault, N. R., Nishina, K. A., Agrimi, U., et al. (2020b). Cofactor and glycosylation preferences for in vitro prion conversion are predominantly determined by strain conformation. *PLoS Pathog.* 16:e1008495. doi: 10.1371/journal.ppat.1008495

Camacho, M. V., Telling, G., Kong, Q., Gambetti, P., and Notari, S. (2019). Role of prion protein glycosylation in replication of human prions by protein misfolding cyclic amplification. *Lab. Invest.* 99, 1741–1748. doi: 10.1038/s41374-019-0282-1

Cassard, H., Huor, A., Espinosa, J. C., Douet, J. Y., Lugan, S., Aron, N., et al. (2020). Prions from sporadic creutzfeldt-jakob disease patients propagate as strain mixtures. *mBio* 11:e00393-20. doi: 10.1128/mBio.00393-20

Chapuis, J., Moudjou, M., Reine, F., Herzog, L., Jaumain, E., Chapuis, C., et al. (2016). Emergence of two prion subtypes in ovine PrP transgenic mice infected with human MM2-cortical Creutzfeldt-Jakob disease prions. *Acta Neuropathol. Commun.* 4, 2–15.

Chyba, M., Kotas, J., Beringue, V., Eblen, C., Igel-Egalon, A., Kravchenko, Y., et al. (2020). An alternative model to prion fragmentation based on the detailed balance between PrP^{Sc}and suPrP. *bioRxiv[Preprint]*.

Colby, D. W., and Prusiner, S. B. (2011). Prions. *Cold Spring Harb. Perspect. Biol.* 3:a006833.

Collinge, J. (2001). Prion diseases of humans and animals: their causes and molecular basis. *Annu. Rev. Neurosci.* 24, 519–550. doi: 10.1146/annurev.neuro.24.1.519

Collinge, J., and Clarke, A. R. (2007). A general model of prion strains and their pathogenicity. *Science* 318, 930–936. doi: 10.1126/science.1138718

Concha-Marambio, L., Pritzkow, S., Moda, F., Tagliavini, F., Ironside, J. W., Schulz, P. E., et al. (2016). Detection of prions in blood from patients with variant Creutzfeldt-Jakob disease. *Sci. Transl. Med.* 8:370ra183.

Cosseddu, G. M., Nonno, R., Vaccari, G., Bucalossi, C., Fernandez-Borges, N., Di Bari, M. A., et al. (2011). Ultra-efficient PrP(Sc) amplification highlights potentialities and pitfalls of PMCA technology. *PLoS Pathog.* 7:e1002370. doi: 10.1371/journal.ppat.1002370

Deleault, N. R., Harris, B. T., Rees, J. R., and Supattapone, S. (2007). Formation of native prions from minimal components in vitro. *Proc. Natl. Acad. Sci. U.S.A.* 104, 9741–9746. doi: 10.1073/pnas.0702662104

Deleault, N. R., Piro, J. R., Walsh, D. J., Wang, F., Ma, J., Geoghegan, J. C., et al. (2012a). Isolation of phosphatidylethanolamine as a solitary cofactor for prion formation in the absence of nucleic acids. *Proc. Natl. Acad. Sci. U.S.A.* 109, 8546–8551. doi: 10.1073/pnas.1204498109

Deleault, N. R., Walsh, D. J., Piro, J. R., Wang, F., Wang, X., Ma, J., et al. (2012b). Cofactor molecules maintain infectious conformation and restrict strain properties in purified prions. *Proc. Natl. Acad. Sci. U.S.A.* 109, E1938–E1946.

DGS (2011). *DGS/RI3/2011/449 du 1er décembre 2011 relative à l'actualisation des recommandations visant à réduire les risques de transmission d'agents transmissibles non conventionnels lors des actes invasifs*. Paris: F.M.O. Health.

Diack, A. B., Ritchie, D., Bishop, M., Pinion, V., Brandel, J. P., Haik, S., et al. (2012). Constant transmission properties of variant Creutzfeldt-Jakob disease in 5 countries. *Emerg. Infect. Dis.* 18, 1574–1579. doi: 10.3201/eid1810.120792

Douet, J. Y., Lacroux, C., Aron, N., Head, M. W., Lugan, S., Tillier, C., et al. (2017). Distribution and quantitative estimates of variant Creutzfeldt-Jakob disease prions in tissues of clinical and asymptomatic patients. *Emerg. Infect. Dis.* 23, 946–956. doi: 10.3201/eid2306.161734

Douet, J. Y., Zafar, S., Perret-Liaudet, A., Lacroux, C., Lugan, S., Aron, N., et al. (2014). Detection of infectivity in blood of persons with variant and sporadic Creutzfeldt-Jakob disease. *Emerg. Infect. Dis.* 20, 114–117. doi: 10.3201/eid2001.130353

Edgeworth, J. A., Farmer, M., Sicilia, A., Tavares, P., Beck, J., Campbell, T., et al. (2011a). Detection of prion infection in variant Creutzfeldt-Jakob disease: a blood-based assay. *Lancet* 377, 487–493. doi: 10.1016/s0140-6736(10)62308-2

Edgeworth, J. A., Jackson, G. S., Clarke, A. R., Weissmann, C., and Collinge, J. (2009). Highly sensitive, quantitative cell-based assay for prions adsorbed to solid surfaces. *Proc. Natl. Acad. Sci. U.S.A.* 106, 3479–3483. doi: 10.1073/pnas.0813342106

Edgeworth, J. A., Sicilia, A., Linehan, J., Brandner, S., Jackson, G. S., and Collinge, J. (2011b). A standardized comparison of commercially available prion decontamination reagents using the Standard Steel-Binding Assay. *J. Gen. Virol.* 92, 718–726. doi: 10.1099/vir.0.027201-0

Elder, A. M., Henderson, D. M., Nalls, A. V., Wilham, J. M., Caughey, B. W., Hoover, E. A., et al. (2013). In vitro detection of prionemia in TSE-infected cervids and hamsters. *PLoS One* 8:e80203. doi: 10.1371/journal.pone.0080203

EMA (2018). *CHMP position statement on Creutzfeldt-Jakob disease and plasma-derived and urine-derived medicinal products*. London: E.M. Agency.

Eraña, H., Charco, J. M., Di Bari, M. A., Díaz-Domínguez, C. M., López-Moreno, R., Vidal, E., et al. (2019). Development of a new largely scalable in vitro prion propagation method for the production of infectious recombinant prions for high resolution structural studies. *PLoS Pathog* 15:e1008117. doi: 10.1371/journal.ppat.1008117

Espinosa, J. C., Comoy, E. E., Marin-Moreno, A., Aguilar-Calvo, P., Birling, M.-C., Pitarch, J. L., et al. (2019). Transgenic mouse models expressing human and macaque prion protein exhibit similar prion susceptibility on a strain-dependent manner. *Sci. Rep.* 9:15699.

Fernández-Borges, N., Di Bari, M. A., Eraña, H., Sánchez-Martín, M., Pirisinu, L., Parra, B., et al. (2018). Cofactors influence the biological properties of infectious recombinant prions. *Acta Neuropathol.* 135, 179–199. doi: 10.1007/s00401-017-1782-y

Fernie, K., Hamilton, S., and Somerville, R. A. (2012). Limited efficacy of steam sterilization to inactivate vCJD infectivity. *J. Hosp. Infect.* 80, 46–51. doi: 10.1016/j.jhin.2011.09.004

Flechsig, E., Hegyi, I., Enari, M., Schwarz, P., Collinge, J., and Weissmann, C. (2001). Transmission of scrapie by steel-surface-bound prions. *Mol. Med.* 7, 679–684. doi: 10.1007/bf03401958

Gibbs, C.J. Jr, Gajdusek, D. C., Asher, D. M., Alpers, M. P., Beck, E., Daniel, P. M., et al. (1968). Creutzfeldt-Jakob disease (spongiform encephalopathy): transmission to the chimpanzee. *Science* 161, 388–389.

Giles, K., Glidden, D. V., Beckwith, R., Seoanes, R., Peretz, D., Dearmond, S. J., et al. (2008). Resistance of bovine spongiform encephalopathy (BSE) prions to inactivation. *PLoS Pathog.* 4:e1000206. doi: 10.1371/journal.ppat.1000206

Giles, K., Woerman, A. L., Berry, D. B., and Prusiner, S. B. (2017). Bioassays and Inactivation of Prions. *Cold Spring Harb. Perspect. Biol* 9:a023499. doi: 10.1101/cshperspect.a023499

Gill, O. N., Spencer, Y., Richard-Loendt, A., Kelly, C., Brown, D., Sinka, K., et al. (2020). Prevalence in Britain of abnormal prion protein in human appendices before and after exposure to the cattle BSE epizootic. *Acta Neuropathol.* 139, 965–976. doi: 10.1007/s00401-020-02153-7

Gonzalez-Montalban, N., Makarava, N., Ostapchenko, V. G., Savtchenk, R., Alexeeva, I., Rohwer, R. G., et al. (2011). Highly efficient protein misfolding cyclic amplification. *PLoS Pathog.* 7:e1001277. doi: 10.1371/journal.ppat.1001277

Groveman, B. R., Raymond, G. J., Campbell, K. J., Race, B., Raymond, L. D., Hughson, A. G., et al. (2017). Role of the central lysine cluster and scrapie templating in the transmissibility of synthetic prion protein aggregates. *PLoS Pathog.* 13:e1006623. doi: 10.1371/journal.ppat.1006623

Halliez, S., Reine, F., Herzog, L., Jaumain, E., Haik, S., Rezaei, H., et al. (2014). Accelerated, spleen-based titration of variant Creutzfeldt-Jakob disease infectivity in transgenic mice expressing human prion protein with sensitivity comparable to that of survival time bioassay. *J. Virol.* 88, 8678–8686. doi: 10.1128/jvi.01118-14

Henderson, D. M., Davenport, K. A., Haley, N. J., Denkers, N. D., Mathiason, C. K., and Hoover, E. A. (2015). Quantitative assessment of prion infectivity in tissues and body fluids by real-time quaking-induced conversion. *J. Gen. Virol.* 96, 210–219. doi: 10.1099/vir.0.069906-0

Hughson, A. G., Race, B., Kraus, A., Sangare, L. R., Robins, L., Groveman, B. R., et al. (2016). Inactivation of prions and amyloid seeds with hypochlorous acid. *PLoS Pathog.* 12:e1005914. doi: 10.1371/journal.ppat.1005914

Huor, A., Douet, J. Y., Lacroux, C., Lugan, S., Tillier, C., Aron, N., et al. (2017). Infectivity in bone marrow from sporadic CJD patients. *J. Pathol.* 243, 273–278. doi: 10.1002/path.4954

Huor, A., Espinosa, J. C., Vidal, E., Cassard, H., Douet, J. Y., Lugan, S., et al. (2019). The emergence of classical BSE from atypical/Nor98 scrapie. *Proc. Natl. Acad. Sci. U.S.A.* 116, 26853–26862. doi: 10.1073/pnas.1915737116

Igel-Egalon, A., Bohl, J., Moudjou, M., Herzog, L., Reine, F., Rezaei, H., et al. (2019a). Heterogeneity and architecture of pathological prion protein assemblies: time to revisit the molecular basis of the Prion replication process? *Viruses* 11:429. doi: 10.3390/v11050429

Igel-Egalon, A., Laferriere, F., Moudjou, M., Bohl, J., Mezache, M., Knapple, T., et al. (2019b). Early stage prion assembly involves two subpopulations with different quaternary structures and a secondary templating pathway. *Commun. Biol.* 2:363.

Igel-Egalon, A., Moudjou, M., Martin, D., Busley, A., Knapple, T., Herzog, L., et al. (2017). Reversible unfolding of infectious prion assemblies reveals the existence of an oligomeric elementary brick. *PLoS Pathog.* 13:e1006557. doi: 10.1371/journal.ppat.1006557

Jaumain, E., Quadrio, I., Herzog, L., Reine, F., Rezaei, H., Andreoletti, O., et al. (2016). Absence of evidence for a causal link between Bovine Spongiform encephalopathy strain variant L-BSE and known forms of sporadic Creutzfeldt-Jakob disease in human PrP Transgenic Mice. *J. Virol.* 90, 10867–10874. doi: 10.1128/jvi.01383-16

Johnson, C. J., Aiken, J. M., Mckenzie, D., Samuel, M. D., and Pedersen, J. A. (2012). Highly efficient amplification of chronic wasting disease agent by protein misfolding cyclic amplification with beads (PMCAb). *PLoS One* 7:e35383. doi: 10.1371/journal.pone.0035383

Johnson, C. J., Pedersen, J. A., Chappell, R. J., Mckenzie, D., and Aiken, J. M. (2007). Oral transmissibility of prion disease is enhanced by binding to soil particles. *PLoS Pathog* 3:e93. doi: 10.1371/journal.ppat.0030093

Jones, M., Peden, A. H., Yull, H., Wight, D., Bishop, M. T., Prowse, C. V., et al. (2009). Human platelets as a substrate source for the in vitro amplification of the abnormal prion protein (PrP) associated with variant Creutzfeldt-Jakob disease. *Transfusion* 49, 376–384. doi: 10.1111/j.1537-2995.2008.01954.x

Katorcha, E., Makarava, N., Savtchenko, R., and Baskakov, I. V. (2015). Sialylation of the prion protein glycans controls prion replication rate and glycoform ratio. *Sci. Rep.* 5:16912. doi: 10.1038/srep16912

Khalili-Shirazi, A., Summers, L., Linehan, J., Mallinson, G., Anstee, D., Hawke, S., et al. (2005). PrP glycoforms are associated in a strain-specific ratio in native PrPSc. *J. Gen. Virol.* 86, 2635–2644. doi: 10.1099/vir.0.80375-0

Kimberlin, R. H., and Walker, C. (1977). Characteristics of a short incubation model of scrapie in the golden hamster. *J. Gen. Virol.* 34, 295–304. doi: 10.1099/0022-1317-34-2-295

Klohn, P. C., Stoltze, L., Flechsig, E., Enari, M., and Weissmann, C. (2003). A quantitative, highly sensitive cell-based infectivity assay for mouse scrapie prions. *Proc. Natl. Acad. Sci. U.S.A.* 100, 11666–11671. doi: 10.1073/pnas.1834432100

Kraus, A., Saijo, E., Metrick, M. A. II, Newell, K., Sigurdson, C. J., Zanusso, G., et al. (2019). Seeding selectivity and ultrasensitive detection of tau aggregate conformers of Alzheimer disease. *Acta Neuropathol.* 137, 585–598. doi: 10.1007/s00401-018-1947-3

Lacroux, C., Comoy, E., Moudjou, M., Perret-Liaudet, A., Lugan, S., Litaise, C., et al. (2014). Preclinical Detection of Variant CJD and BSE prions in blood. *PLoS Pathog.* 10:e1004202. doi: 10.1371/journal.ppat.1004202

Laferriere, F., Tixador, P., Moudjou, M., Chapuis, J., Sibille, P., Herzog, L., et al. (2013). Quaternary structure of pathological prion protein as a determining factor of strain-specific prion replication dynamics. *PLoS Pathog.* 9:e1003702. doi: 10.1371/journal.ppat.1003702

Lasmezas, C. I., Deslys, J. P., Demaimay, R., Adjou, K. T., Hauw, J. J., and Dormont, D. (1996). Strain specific and common pathogenic events in murine models of scrapie and bovine spongiform encephalopathy. *J. Gen. Virol.* 77(Pt. 7), 1601–1609. doi: 10.1099/0022-1317-77-7-1601

Lasmézas, C. I., Deslys, J. P., Demaimay, R., Adjou, K. T., Lamoury, F., Dormont, D., et al. (1996). BSE transmission to macaques. *Nature* 381, 743–744. doi: 10.1038/381743a0

Le Dur, A., Lai, T. L., Stinnakre, M. G., Laisne, A., Chenais, N., Rakotobe, S., et al. (2017). Divergent prion strain evolution driven by PrPC expression level in transgenic mice. *Nat. Commun.* 8:14170.

Luk, C., Jones, S., Thomas, C., Fox, N. C., Mok, T. H., Mead, S., et al. (2016). Diagnosing sporadic Creutzfeldt-Jakob disease by the detection of abnormal prion protein in patient Urine. *JAMA Neurol.* 73, 1454–1460. doi: 10.1001/jamaneurol.2016.3733

Marin-Moreno, A., Aguilar-Calvo, P., Moudjou, M., Espinosa, J. C., Beringue, V., and Torres, J. M. (2019). Thermostability as a highly dependent prion strain feature. *Sci. Rep.* 9:11396.

Mays, C. E., Titlow, W., Seward, T., Telling, G. C., and Ryou, C. (2009). Enhancement of protein misfolding cyclic amplification by using concentrated cellular prion protein source. *Biochem. Biophys. Res. Commun.* 388, 306–310. doi: 10.1016/j.bbrc.2009.07.163

McGuire, L. I., Peden, A. H., Orru, C. D., Wilham, J. M., Appleford, N. E., Mallinson, G., et al. (2012). Real time quaking-induced conversion analysis of cerebrospinal fluid in sporadic Creutzfeldt-Jakob disease. *Ann. Neurol.* 72, 278–285. doi: 10.1002/ana.23589

Minor, P., Newham, J., Jones, N., Bergeron, C., Gregori, L., Asher, D., et al. (2004). Standards for the assay of Creutzfeldt-Jakob disease specimens. *J. Gen. Virol.* 85, 1777–1784.

Moda, F., Gambetti, P., Notari, S., Concha-Marambio, L., Catania, M., Park, K. W., et al. (2014). Prions in the urine of patients with variant Creutzfeldt-Jakob disease. *N. Engl. J. Med.* 371, 530–539.

Moda, F., Suardi, S., Di Fede, G., Indaco, A., Limido, L., Vimercati, C., et al. (2012). MM2-thalamic Creutzfeldt-Jakob disease: neuropathological, biochemical and transmission studies identify a distinctive prion strain. *Brain Pathol.* 22, 662–669. doi: 10.1111/j.1750-3639.2012.00572.x

Moreno, J. A., and Telling, G. C. (2017). Insights into mechanisms of transmission and pathogenesis from transgenic mouse models of Prion diseases. *Methods Mol. Biol.* 1658, 219–252. doi: 10.1007/978-1-4939-7244-9_16

Mori, T., Atarashi, R., Furukawa, K., Takatsuki, H., Satoh, K., Sano, K., et al. (2016). A direct assessment of human prion adhered to steel wire using real-time quaking-induced conversion. *Sci. Rep.* 6:24993.

Moudjou, M., Chapuis, J., Mekrouti, M., Reine, F., Herzog, L., Sibille, P., et al. (2016). Glycoform-independent prion conversion by highly efficient, cell-based, protein misfolding cyclic amplification. *Sci. Rep.* 6:29116.

Moudjou, M., Sibille, P., Fichet, G., Reine, F., Chapuis, J., Herzog, L., et al. (2014). Highly infectious prions generated by a single round of microplate-based protein misfolding cyclic amplification. *mBio* 5:e00829-13.

Nishina, K. A., Deleault, N. R., Mahal, S. P., Baskakov, I., Luhrs, T., Riek, R., et al. (2006). The stoichiometry of host PrPC glycoforms modulates the efficiency of PrPSc formation in vitro. *Biochemistry* 45, 14129–14139.

Nonno, R., Di Bari, M. A., Cardone, F., Vaccari, G., Fazzi, P., Dell'omo, G., et al. (2006). Efficient transmission and characterization of Creutzfeldt-Jakob disease strains in bank voles. *PLoS Pathog.* 2:e12. doi: 10.1371/journal.ppat.0020012

Orru, C. D., Bongianni, M., Tonoli, G., Ferrari, S., Hughson, A. G., Groveman, B. R., et al. (2014). A test for Creutzfeldt-Jakob disease using nasal brushings. *N. Engl. J. Med.* 371, 519–529. doi: 10.1056/nejmoa1315200

Orru, C. D., Groveman, B. R., Hughson, A. G., Zanusso, G., Coulthart, M. B., and Caughey, B. (2015a). Rapid and sensitive RT-QuIC detection of human Creutzfeldt-Jakob disease using cerebrospinal fluid. *mBio* 6, e002451-14. doi: 10.1128/mBio.02451-14

Orru, C. D., Groveman, B. R., Raymond, L. D., Hughson, A. G., Nonno, R., Zou, W., et al. (2015b). Bank vole prion protein as an apparently universal substrate for RT-QuIC-based detection and discrimination of prion strains. *PLoS Pathog.* 11:e1004983. doi: 10.1371/journal.ppat.1004983

Orru, C. D., Yuan, J., Appleby, B. S., Li, B., Li, Y., Winner, D., et al. (2017). Prion seeding activity and infectivity in skin samples from patients with sporadic Creutzfeldt-Jakob disease. *Sci. Transl. Med.* 9:eaam7785. doi: 10.1126/scitranslmed.aam7785

Passet, B., Castille, J., Makhzami, S., Truchet, S., Vaiman, A., Floriot, S., et al. (2020). The Prion-like protein Shadoo is involved in mouse embryonic and mammary development and differentiation. *Sci. Rep.* 10:6765.

Peden, A., Mccardle, L., Head, M. W., Love, S., Ward, H. J., Cousens, S. N., et al. (2010). Variant CJD infection in the spleen of a neurologically asymptomatic UK adult patient with haemophilia. *Haemophilia* 16, 296–304. doi: 10.1111/j.1365-2516.2009.02181.x

Peden, A. H., Head, M. W., Ritchie, D. L., Bell, J. E., and Ironside, J. W. (2004). Preclinical vCJD after blood transfusion in a PRNP codon 129 heterozygous patient. *Lancet* 364, 527–529. doi: 10.1016/s0140-6736(04)16811-6

Peden, A. H., Ritchie, D. L., Head, M. W., and Ironside, J. W. (2006). Detection and localization of PrPSc in the skeletal muscle of patients with variant, iatrogenic, and sporadic forms of Creutzfeldt-Jakob disease. *Am. J. Pathol.* 168, 927–935. doi: 10.2353/ajpath.2006.050788

Peretz, D., Supattapone, S., Giles, K., Vergara, J., Freyman, Y., Lessard, P., et al. (2006). Inactivation of prions by acidic sodium dodecyl sulfate. *J. Virol.* 80, 322–331. doi: 10.1128/jvi.80.1.322-331.2006

Povey, M. J. W., Moore, J. D., Braybrook, J., Simons, H., Belchamber, R., Raganathan, M., et al. (2011). Investigation of bovine serum albumin denaturation using ultrasonic spectroscopy. *Food Hydrocoll.* 25, 1233–1241. doi: 10.1016/j.foodhyd.2010.11.011

Pritzkow, S., Wagenfuhr, K., Daus, M. L., Boerner, S., Lemmer, K., Thomzig, A., et al. (2011). Quantitative detection and biological propagation of scrapie seeding activity in vitro facilitate use of prions as model pathogens for disinfection. *PLoS One* 6:e20384. doi: 10.1371/journal.pone.0020384

Prusiner, S. B. (1982). Novel proteinaceous infectious particles cause scrapie. *Science* 216, 136–144. doi: 10.1126/science.6801762

Prusiner, S. B., Cochran, S. P., Groth, D. F., Downey, D. E., Bowman, K. A., and Martinez, H. M. (1982). Measurement of the scrapie agent using an incubation time interval assay. *Ann. Neurol.* 11, 353–358. doi: 10.1002/ana.410110406

Prusiner, S. B., Groth, D. F., Cochran, S. P., Masiarz, F. R., Mckinley, M. P., and Martinez, H. M. (1980). Molecular properties, partial purification, and assay by incubation period measurements of the hamster scrapie agent. *Biochemistry* 19, 4883–4891. doi: 10.1021/bi00562a028

Raymond, G. J., Race, B., Orrú, C. D., Raymond, L. D., Bongianni, M., Fiorini, M., et al. (2020). Transmission of CJD from nasal brushings but not spinal fluid or RT-QuIC product. *Ann. Clin. Transl. Neurol.* 7, 932–944. doi: 10.1002/acn3.51057

Rhoads, D. D., Wrona, A., Foutz, A., Blevins, J., Glisic, K., Person, M., et al. (2020). Diagnosis of prion diseases by RT-QuIC results in improved surveillance. *Neurology* 95, e1017–e1026.

Rossi, M., Candelise, N., Baiardi, S., Capellari, S., Giannini, G., Orru, C. D., et al. (2020). Ultrasensitive RT-QuIC assay with high sensitivity and specificity for Lewy body-associated synucleinopathies. *Acta Neuropathol.* 140, 49–62. doi: 10.1007/s00401-020-02160-8

Rubenstein, R., and Chang, B. (2013). Re-assessment of PrP(Sc) distribution in sporadic and variant CJD. *PLoS One* 8:e66352. doi: 10.1371/journal.pone.0066352

Saborio, G. P., Permanne, B., and Soto, C. (2001). Sensitive detection of pathological prion protein by cyclic amplification of protein misfolding. *Nature* 411, 810–813. doi: 10.1038/35081095

Saijo, E., Metrick, M. A. II, Koga, S., Parchi, P., Litvan, I., Spina, S., et al. (2020). 4-Repeat tau seeds and templating subtypes as brain and CSF biomarkers of frontotemporal lobar degeneration. *Acta Neuropathol.* 139, 63–77. doi: 10.1007/s00401-019-02080-2

Saunders, S. E., Bartz, J. C., Vercauteren, K. C., and Bartelt-Hunt, S. L. (2011). An enzymatic treatment of soil-bound prions effectively inhibits replication. *Appl. Environ. Microbiol.* 77, 4313–4317. doi: 10.1128/aem.00421-11

Sawyer, E. B., Edgeworth, J. A., Thomas, C., Collinge, J., and Jackson, G. S. (2015). Preclinical detection of infectivity and disease-specific PrP in blood throughout the incubation period of prion disease. *Sci. Rep.* 5:17742.

Scialò, C., Tran, T. H., Salzano, G., Novi, G., Caponnetto, C., Chiò, A., et al. (2020). TDP-43 real time quaking induced conversion reaction optimization and detection of seeding activity in CSF of amyotrophic lateral sclerosis and frontotemporal dementia patients. *Brain Commun.* 2:fcaa142.

Shikiya, R. A., and Bartz, J. C. (2011). In vitro generation of high-titer prions. *J. Virol.* 85, 13439–13442. doi: 10.1128/jvi.06134-11

Takatsuki, H., Fuse, T., Nakagaki, T., Mori, T., Mihara, B., Takao, M., et al. (2016). Prion-seeding activity is widely distributed in tissues of sporadic Creutzfeldt-Jakob disease patients. *eBioMed.* 12, 150–155. doi: 10.1016/j.ebiom.2016.08.033

Tateishi, J., Ohta, M., Koga, M., Sato, Y., and Kuroiwa, Y. (1979). Transmission of chronic spongiform encephalopathy with kuru plaques from humans to small rodents. *Ann. Neurol.* 5, 581–584. doi: 10.1002/ana.410050616

Tixador, P., Herzog, L., Reine, F., Jaumain, E., Chapuis, J., Le Dur, A., et al. (2010). The physical relationship between infectivity and prion protein aggregates is strain-dependent. *PLoS Pathog.* 6:e1000859. doi: 10.1371/journal.ppat.1000859

Van Dorsselaer, A., Carapito, C., Delalande, F., Schaeffer-Reiss, C., Thierse, D., Diemer, H., et al. (2011). Detection of prion protein in urine-derived injectable fertility products by a targeted proteomic approach. *PLoS One* 6:e17815. doi: 10.1371/journal.pone.0017815

Wadsworth, J. D., Joiner, S., Hill, A. F., Campbell, T. A., Desbruslais, M., Luthert, P. J., et al. (2001). Tissue distribution of protease resistant prion protein in variant Creutzfeldt-Jakob disease using a highly sensitive immunoblotting assay. *Lancet* 358, 171–180. doi: 10.1016/s0140-6736(01)05403-4

Weber, P., Giese, A., Piening, N., Mitteregger, G., Thomzig, A., Beekes, M., et al. (2007). Generation of genuine prion infectivity by serial PMCA. *Vet Microbiol* 123, 346–357. doi: 10.1016/j.vetmic.2007.04.004

Weissmann, C., Li, J., Mahal, S. P., and Browning, S. (2011). Prions on the move. *EMBO Rep* 12, 1109–1117. doi: 10.1038/embor.2011.192

WHO (1999). "WHO infection control guidelines for transmissible spongiform encephalopathies," in *World Health Organization Emerging and Other Communicable Diseases*, ed. W.H. Organization (Geneva: WHO).

Wilham, J. M., Orru, C. D., Bessen, R. A., Atarashi, R., Sano, K., Race, B., et al. (2010). Rapid end-point quantitation of prion seeding activity with sensitivity comparable to bioassays. *PLoS Pathog.* 6:e1001217. doi: 10.1371/journal.ppat.1001217

Wroe, S. J., Pal, S., Siddique, D., Hyare, H., Macfarlane, R., Joiner, S., et al. (2006). Clinical presentation and pre-mortem diagnosis of variant Creutzfeldt-Jakob disease associated with blood transfusion: a case report. *Lancet* 368, 2061–2067. doi: 10.1016/s0140-6736(06)69835-8

Yan, Z. X., Stitz, L., Heeg, P., Pfaff, E., and Roth, K. (2004). Infectivity of prion protein bound to stainless steel wires: a model for testing decontamination

procedures for transmissible spongiform encephalopathies. *Infect. Control Hosp. Epidemiol.* 25, 280–283. doi: 10.1086/502392

Yull, H. M., Ironside, J. W., and Head, M. W. (2009). Further characterisation of the prion protein molecular types detectable in the NIBSC Creutzfeldt-Jakob disease brain reference materials. *Biologicals* 37, 210–215. doi: 10.1016/j.biologicals.2009.01.009

Zerr, I., and Parchi, P. (2018). Sporadic Creutzfeldt-Jakob disease. *Handb. Clin. Neurol.* 153, 155–174.

Zobeley, E., Flechsig, E., Cozzio, A., Enari, M., and Weissmann, C. (1999). Infectivity of scrapie prions bound to a stainless steel surface. *Mol. Med.* 5, 240–243. doi: 10.1007/bf03402121

Conflict of Interest: The authors declare that the research was conducted in the absence of any commercial or financial relationships that could be construed as a potential conflict of interest.

Advantages of publishing in Frontiers

OPEN ACCESS
Articles are free to read for greatest visibility and readership

FAST PUBLICATION
Around 90 days from submission to decision

HIGH QUALITY PEER-REVIEW
Rigorous, collaborative, and constructive peer-review

TRANSPARENT PEER-REVIEW
Editors and reviewers acknowledged by name on published articles

Frontiers
Avenue du Tribunal-Fédéral 34
1005 Lausanne | Switzerland

Visit us: www.frontiersin.org
Contact us: frontiersin.org/about/contact

REPRODUCIBILITY OF RESEARCH
Support open data and methods to enhance research reproducibility

DIGITAL PUBLISHING
Articles designed for optimal readership across devices

FOLLOW US
@frontiersin

IMPACT METRICS
Advanced article metrics track visibility across digital media

EXTENSIVE PROMOTION
Marketing and promotion of impactful research

LOOP RESEARCH NETWORK
Our network increases your article's readership